Proceedings of the 5th International Conference on Civil Engineering for Sustainable Development (ICCESD 2020), 7~9 February 2020, KUET, Khulna, Bangladesh (ISBN-978-984-34-8764-3)

A COMPARATIVE STUDY ON PERVIOUS CONCRETE AND A WAY TO REDUCE ITS PERMEABILITY

Jesika Rahman*[1] and Md. Jahidul Islam[2]

[1]Lecturer, Military Institute of Science and Technology, Bangladesh, e-mail: jesikarahman547@ce.mist.ac.bd
[2]Associate Professor, Military Institute of Science and Technology, Bangladesh, e-mail: mjislam@ce.mist.ac.bd

***Corresponding Author**

ABSTRACT

Pervious concrete (PC) is a highly porous concrete and one of the measures invented to address the environment related concerns like runoff and flash flood. Despite having many advantages, a concrete with a high void content can also be unfavorable when it comes to strength and serviceability requirements. For instance, when the fine aggregate gets washed down during a construction, a PC is formed instead of a conventional concrete (CC) and exhibits undesirable characteristics of a PC such as allowing seepage of water through the structure thereby deteriorating the reinforcements. This study presents a research programmed to evaluate the effect of decreasing the permeability of a PC with cement grout injection and compare the results with that of a PC without grout injection. Later, setting the reference concrete as the CC, these results were compared with it to identify the extent of improvement. The results obtained indicated that the void content and permeability were reduced (5.98% vs. 4.43% and 3.96mm/s vs. 1.99mm/s respectively) in the PC samples. Also, it was observed that these reduced parameters were still higher than that of the CC (3.41% and 0.73mm/sec). The study thus represents a probability of reducing the voids in a faulty concrete without having to reconstruct.

Keywords: *Pervious concrete, Grout injection, Permeability, Falling head permeability.*

1. INTRODUCTION

One of the unabating problems in concrete construction is the inadequate serviceability which often arises due to poor workmanship on site. Such a concrete, affected by improper workmanship and supervision, is termed as a poor quality or faulty concrete (Femi, 2014). A concrete is termed as a good or poor-quality basing on its performance and serviceability characteristics (Alam, Habib, Sheikh & Hasan, 2014). Water ingression in potentially vulnerable structures like swimming pool and basement is one of the performance issues regarding poor workmanship. Due to lack of proper proportioning and compaction by the workforce, voids, much greater than the maximum allowable of 4.5% (NPCA, 2012), are found to weaken the performance criteria as well as the serviceability (Barnes, 2013). A typical example of insufficient supervision is the formation of a highly porous concrete mix formed when the fine aggregates (FA) get washed down by rain on site. During such cases a structure becomes prone to water leakage by the permeable voids present in it and it is this fault that reduces service life of the structure as water moves in to deteriorate the reinforcement.

To reduce permeable voids in a structure by keeping it in functional stage is quite challenging and till date no such research has been made. In this paper such a case is studied and the porosity of a highly porous concrete is reduced by injecting cement grout into the hardened concrete.

In order to simulate a faulty concrete where water ingression remains a severe problem, three types of pervious concrete (PC) mix designs were prepared having different FA contents, namely 0%, 10% and 20% of the total aggregate. The aim of this study is to compare the rate of permeability, measured through Falling Head Method (FHM), of each of the PC samples with that of the CC samples. Later on, the PC samples were treated with cement grout injection and again tested for the rate of permeability to identify the degree of improvement.

2. METHODOLOGY

ASTM Type I Ordinary Portland Cement (OPC) was used as the binding material. The water to cement ratio (w/c) was kept to a constant of 0.4 throughout the study. Natural crushed stone as coarse aggregate complying to grading requirements by ASTM C33 (2018) size 67 (19.00 to 9.5mm) range and Sylhet sand as fine aggregate having a fineness modulus of 3.2 were used.

The PC samples were prepared according to ACI 211.3R-02 (2011) following a design void content of 15% which allows to maintain a minimum percolation rate of 0 inches per minute and consequently higher compressive strength. The CC samples were proportioned following ACI 211.1-91 (2002) specifications. Both the PC and CC were designed for a target strength of 3000 psi, Mix proportions of the various designs used in the study are summarized in Table 1 where PC0F=0% FA, PC10F=10% FA and PC20F= 20% FA. The conventional concrete is designated as NAC. The aggregates were used in saturated surface dry condition. The mix designs were used to cast cylinders having a diameter and height of 4 inch and 8 inches respectively. The casting was done according to ASTM C192 standard specifications (2016).

Table 1: Mix proportioning of concrete for 1.00 m^3

Sample	w/c ratio	Deign void content (%)	Mass of Cement (kg)	Mass of Water (kg)	Mass of Coarse Aggregate (kg)	Mass of Fine Aggregate (kg)
PC0F	0.4	15	362.4	145	1567	0
PC10F	0.4	15	334.5	133.8	1472	145
PC20F	0.4	15	292.7	117.1	1361	301
NAC	0.4	-	475	190	1005	626

Permeability of the hardened concrete samples aged at 28 days was measured using the FHM. The gap between the inner surface of the apparatus and concrete sample was filled so that movement of water was confined in the vertical direction only. The samples were saturated before the test in order to get rid of the air trapped inside the voids. The time t required by the water column to fall through a specified height was recorded and the rate of permeability K was determined using the equation (1) below derived from Darcy's law. Void content analysis was made on samples after 28 days of casting according to ASTM C642 (2013).

$$K = \frac{A_1 l}{A_2 t} \log\left(\frac{h_2}{h_1}\right) \tag{1}$$

The equation (1) uses cross-sectional areas of the sample and the tube as A1 and A2 respectively and the initial and final height of the water column in the graduated cylinder as h1 and h2 respectively. The length of the sample here is denoted as l. Figure 1 represents the apparatus used for this test.

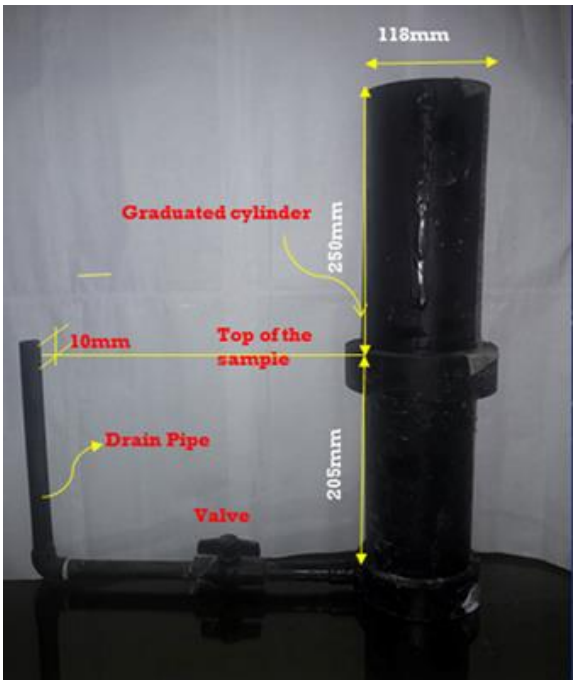

Figure 1 Falling Head Permeability Apparatus

To render the PC samples semi-pervious, the cylinders were injected with cement grout having a w/c ratio of 0.5. Before commencing the task, surface of the cylinders was cleaned to remove the adhering dust and impurities and applied two coats of a waterproofing solution: Nitobond EP, to seal the outer surface in order to contain the grout inside. Nitobond EP is a two-component solvent-free epoxy resin as a concrete bonding agent from FOSROC complying with ASTM C881 standards. This resin is basically used for binding wet cement with existing concrete surfaces and is found to be an excellent sealant to stop fluids inside from percolating out of the concrete. The cement grout was then injected in the PC samples with the help of a dual cartridge gun.

3. RESULTS AND DISCUSSIONS

A comparison made on compressive strengths of the PC samples represented (Fig. 2) indicates that there appears no particular trend in gaining or loosing compressive strength in the grout injected samples. However, there is a trend within the untreated samples showing that as the percentage of

fines increased so did the compressive strength. The cement flows in to fill the voids in the fresh state but once it hardens it shrinks and does not form the required bond with the honeycombed matrix. This refers to the fact that cement grout did not impart any notable changes in strength of the PC samples.

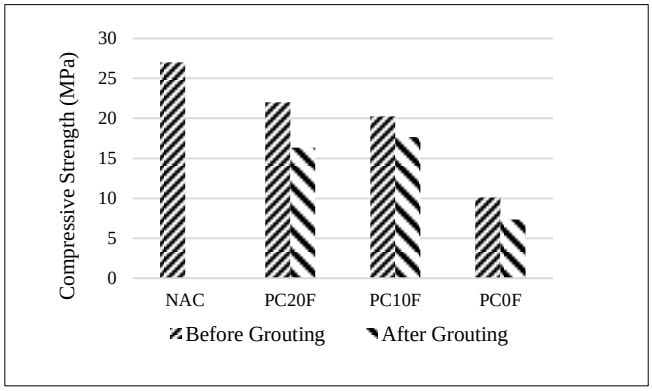

Figure 2: Effect of cement grout injection on compressive strength of PC samples

The following figures 3 and 4 represent the results obtained for the rate of permeability tested on samples before and after grout injection. It shows that, before the samples were injected, both the rate of permeability and void content is highest in PC0F and lowest in NAC. The results are then compared with that of PC samples injected with cement grout and it is seen that the rate of permeability decreased to about 50% in PC10F and 38% in PC20F whereas the void content reduced by 26% in PC10F and 4% for PC20F. PC0F samples were too delicate as there was inadequate bond due to having no fine particles to provide the bulk and so pressure grouting was not attainable.

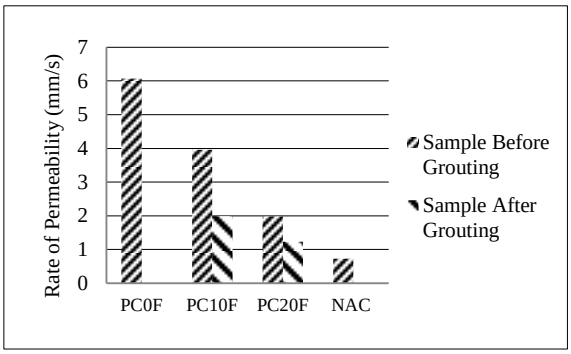

Figure 3: Rate of permeability in PC and CC samples

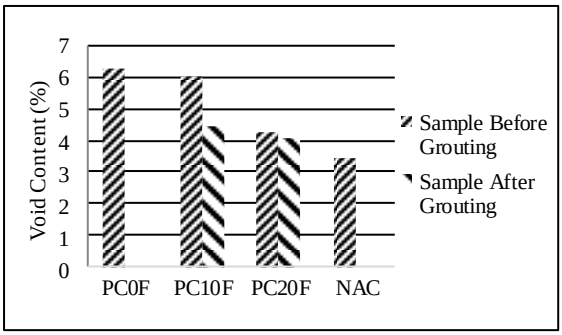

Figure 4: Void content in PC and CC samples

Hence it can be inferred that the void content and rate of permeability decreases with the increase in amount of fine aggregate in the mix. Inclusion of cement grout within the porous structure of PC samples did reduce the permeability and percentage of void content but it is still no match for the parameters that was found in the case of CC samples.

4. CONCLUSIONS

In this paper, effects of cement grout injection in a faulty concrete, as signified by its high porosity, is studied. Faulty concrete is modeled here as PC [Alam, #16]and the probability of a low cost renovation technique is evaluated. Three different mix designs were incorporated for the PC test specimens. Tests were carried out and changes in physical properties (compressive strength, rate of permeability and void content) of the samples were noted. A falling head apparatus was fabricated specifically for this research. Further, the properties tested for both grouted and un-grouted samples were compared with that of a control specimen (CC).

The results of this study conclude that when percentage of fine aggregate in the PC was lowest (0% of the total aggregate), both void content and rate of permeability was the highest and lowest when fine aggregate content was greatest (20% of the total aggregate). The cement grout injection facilitated a decrease of void content and permeability in the PC samples. These findings, when compared with that of the control specimen (CC), helped to identify the extent of reduction in voids and permeability in the grout injected PC samples.

REFERENCES

ACI 211.1-91, (2002) *Standard Practice for Selecting Proportions for Normal, Heavyweight, and Mass Concrete*. American Concrete Institute, Farmington Hills, MI, USA

ACI 211.3R-02 (2009) *Guide for Selecting Proportions for No-Slump Concrete*. American Concrete Institute, Farmington Hills, MI, USA

Alam, M. A., Habib, M. Z., Sheikh, M. R., & Hasan, A. A (2016). *Study on the Quality Control of Concrete Production in Dhaka City*. Journal of Mechanical and Civil Engineering (IOSR-JMCE), 3 (13), 89-98.

ASTM C33, (2018) *Standard Specification for Concrete Aggregates*. ASTM International, West Conshohocken, PA. www.astm.org

ASTM C192, (2016) Standard Practice for Making and Curing Concrete Test Specimens in the Laboratory, ASTM International, West Conshohocken, PA. www.astm.org

ASTM C642, (2013) in Standard Test Method for Density, Absorption, and Voids in Hardened Concrete, ASTM International, West Conshohocken, PA. www.astm.org

Barnes, R. A. (2013). Investigation of water ingress to concrete basements. Proceedings of the Institution of Civil Engineers-Forensic Engineering, 166(3), 107-115.

Femi, O. T. (2014). *Effects of faulty construction on building maintenance*. International Journal of Technology Enhancements and Emerging Engineering Research, 2(3), 2347-4289.

National Precast Concrete Association, (2012, December). Air Entrainment versus Air Entrapment. *Precast Solutions Magazine*. Retrieved December 8, 2018, from https://precast.org/2012/12/air-entrainment-versus-air-entrapment

Proceedings of the 5th International Conference on Civil Engineering for Sustainable Development (ICCESD 2020), 7~9 February 2020, KUET, Khulna, Bangladesh (ISBN-978-984-34-8764-3)

EXPERIMENTAL STUDY ON COMPRESSIVE STRENGTH AND FAILURE MODE OF GFRP WRAPPED CONCRETE CYLINDER

Md. Rezaul Islam*[1], Riyadul Hashem Riyad[2] and Pranta Roy[3]

[1]Post Graduate Student, MIST, Bangladesh, e-mail: rezaul_islam29@outlook.com
[2]Graduated Student, AUST, Bangladesh, e-mail: riyadhashem.aust@gmail.com
[3]Graduated Student, KUET, Bangladesh, e-mail: prantakuet2k13@gmail.com

***Corresponding Author**

ABSTRACT

Fiber-reinforced polymer (FRP) wrap has been established as an effective method of strengthening of concrete structures. GFRP (Glass Fiber Reinforced Polymer) is one type of FRP that is made of glass fibers in a polymeric matrix. In case of unsupported long column, buckling effect makes the column more vulnerable under compressive loading. To minimize this problem, wrapping of concrete column with GFRP composite jacketing could be a solution. There were three series of sample and each series consists of 4 cylindrical specimen having concrete mixing ratio 1:2:4, water-cement ratio was 0.5, curing period was 28 days where two specimens were unwrapped and rest two were wrapped with single layer GFRP jacketing with varying heights of 12 inches, 16 inches, 20 inches and diameter 4 inches for each series. The average compressive strength of unwrapped cylindrical specimens of series I, series II and series III were 9.923 MPa, 6.854 MPa, and 3.771 MPa respectively whereas for wrapped cylindrical that were 50.369 MPa, 45.635 MPa, and 27.783 MPa respectively. The increase in strength of wrapped specimens is 5 times for series I 7 times for series II and 7.5 timed for series III. Numerical average of strain of unwrapped and wrapped specimens of series I, II, III are 0.01225, 0.01255, 0.007 and 0.05255, 0.03185, 0.0339 respectively which shows due to lateral confinement variation of strain among unwrapped and wrapped specimens are too high. Failure of unwrapped specimens mostly happened due to shear fracture and compression failure, in contrast, wrapped specimen fails due to the rupture of GFRP jacketing. So, using glass fiber wrap is an effective way to minimize buckling, without increasing the self-weight of cylindrical specimens significantly

Keywords: *GFRPC jacketing, Wrapped and Unwrapped specimen, Failure pattern, Compressive (axial) loading, Retrofitting*

1. INTRODUCTION

A large number of old buildings in our country are considered as structurally unsafe and at risk of failure as they were constructed long ago using older design codes [BNBC 93] that does not meet the demand of new building design codes. Replacement of such deficient elements of those structures is a huge challenge and demands a substantial amount of time and resources. So external strengthening has now become a suitable alternative for these structures. The process of strengthening of older structures without destroying the existing structure is called retrofitting. Retrofitting is the maintenance, rehabilitation, and upgrading of existing structural members is one of the most suitable processes of the solution in case of structural problems. Wrapping of columns with fibers, especially with glass fiber is being done nowadays all over the world. Its major benefit is its high longitudinal tensile strength in the direction of the fibers. Other advantages include its non-corrosive behavior and thus is beneficial in coastal environments (Balendran, Rana, Maqsood, & Tang, 2002). Retrofitting with FRP materials is a technically sound and cost-effective repair technology and is now extensively being used in Bangladesh.

FRP composites have been used for decades since the early 1940s in the defense industry, in particular, the aeronautical and naval industries, as well as military applications (Bonacci & Maalej, 2001). During this time, it was recognized as having a high strength to weight ratio, non-corrosive, thus resistant to weather conditions and the corrosive effects of the sea and salt air (Masoud & Soudki, 2006). A composite material called Fiber-reinforced plastic (FRP) is made of polymer matrix reinforced with fibers. The fibers are usually glass (in fiberglass), carbon (in the carbon-fiber-reinforced polymer), aramid, or basalt (Hadi, 2007). Fibers are used in polymeric composite materials because of their high strength, high stiffness, and lightweight (Ameli, Ronagh, & Dux, 2007). The polymer matrix is usually a polyester, epoxy or vinyl ester resin, with its primary role to embed and bond the continuous fibers. It also provides a protective barrier to the fibers, preventing any surface damage during service life. The strength and ductility of the circular column increase significantly due to FRP wrapping. The FRP wrap did not increase the strength of square columns because of sharp corners. However, the square column with rounded corners exhibited higher strength and ductility compared with sharp corners. There are various types of FRP are currently being used all over the world, they are: Glass Fiber Reinforced Polymer (GFRP), Basalt Fiber Reinforced Polymer (BFRP), Aramid Fiber Reinforced Polymer (AFRP), Carbon Fiber Reinforced Polymer (CFRP) etc.

Glass fiber reinforced polymer (GFRP) is one kind of FRPs which is using glass fibers are the predominant reinforcing fiber in all forms. E-glass is the most commonly used fiber. It has high electrical insulating properties, good heat resistance, and has the lowest cost (Barghi, Azadbakht, & Hadad, 2012). S-glass fibers have higher heat resistance and about one-third higher tensile strength than e-glass. The specialty of glass fibers are resistant to the alkaline environment found in concrete but have a much higher cost. There are some advantages of GFRP which are: High Strength: GFRP has a very high strength to weight ratio and within a range between 10 to 30 GPa (Sugarman, 1967). Lightweight: of GFRP increase workability in case of maintenance, rehabilitation and upgrading of structural members, Resistance: GFRP resist outer surface of structure from acid rain, salts, and chemicals, Able to Mold Complex Shapes: GFRP can be molded in any shape or format because of this property. In this research, glass fiber was used as the main materials and other materials were used for preparing concrete. In this research, Nitowrap EP (GF) is used as GFRP for strengthening specimens to improve compressive strength and deformation characteristics. Cylindrical specimens were wrapped by Nitowrap GF conjunction with epoxy sealer cum primer, Nitowrap 30, and a high build epoxy saturant Nitowrap 410. Nitowrap (GF) type 1 was used and its major properties are: Weight of fiber - 920 g/m^2, Fiber orientation - Unidirectional, Tensile strength - 3400 N/mm^2.

2. METHODOLOGY

An experimental program was conducted to investigate the behavior and static response of cylindrical specimens (wrapped & unwrapped) by glass fiber under static loading. The specimen was categorized

into three series: Series I, Series II and Series III with varying heights of 12 inches, 16 inches, 20 inches and diameter 4 inches for each series. Every Series consists of 4 cylindrical specimens of which 2 specimens were unwrapped and 2 specimens were wrapped by single-layer glass fiber. Tinius Olsen universal testing machine was used during this experiment. This machine consists of a output device which shows the value of static loading and strain amount for corresponding loading.

2.1 Specimens Preparation

Concrete was prepared by using coarse aggregate (brick chips), fine aggregate (sand), binding materials (Portland cement) and water. The ratio of cement, sand and brick chips was maintained at 1:2:4, the water-cement ratio was 1:2 and curing period was 28 days. Concrete was prepared for making 12 cylindrical specimens. The same mixing ratio of concrete were maintained for all three series. The most widely used construction cement is Portland cement and in this research Crown Cement was used, silica sand was used as fine aggregates and uniformly graded brick chips were used as coarse aggregates.

2.1.1 Wrapping of Cylindrical Specimens

Cylindrical specimens of different Series I, II, III were wrapped by epoxy adhesive. Epoxy was prepared by mixing of nitowrap 410 hardener and nitowrap 410 base in a ratio of 1:2.

Figure 1: Wrapping of specimens

2.2 Experimental Setup

Wrapped and Unwrapped specimens of different series were tested using the Tinius Olsen universal testing machine shown in Figure 2. Specimens were positioned into the crosshead of Tinius Olsen universal testing machine. Data were collected up to the total failure of specimens. The strain data and static loading data from the universal testing machines were recorded using the data acquisition system and imported into an excel spreadsheet for critical analysis

Figure 2: Wrapped and Unwrapped specimens under static loading

3. RESULTS AND DISCUSSION

3.1 Figures and Graphs

From figure 3, Combined stress vs. strain graph of series I depicts that, unwrapped specimens strength capacity was 11.971 MPa (specimen I) and 7.875 MPa (specimen II) at the time of failure, whereas wrapped specimens strength capacity was 50.367 MPa (specimen I) and 50.372 MPa (specimen II) at the time of failure.

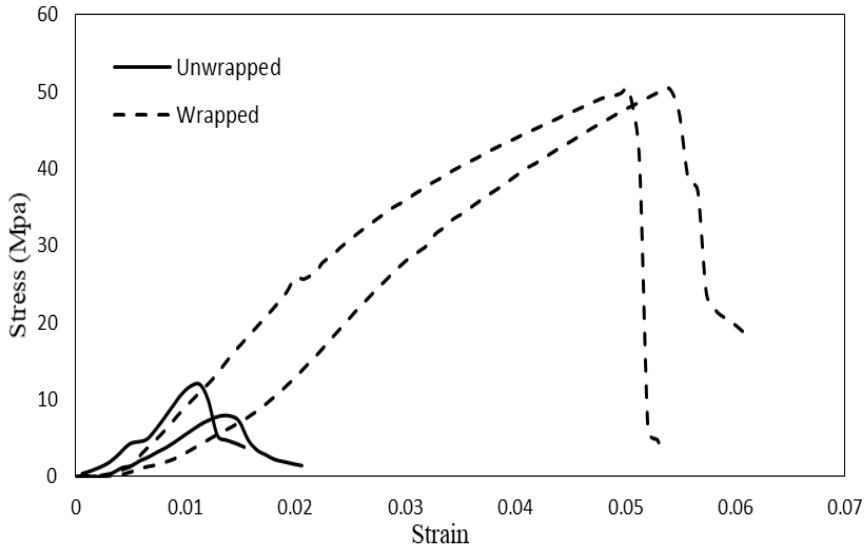

Figure 3: Combined stress vs. strain graph of (Series I) specimen

From figure 4, Combined stress vs. strain graph of series II depicts that, unwrapped specimens strength capacity was 7.227 MPa (specimen I) and 5.941 MPa (specimen II) at the time of failure, whereas wrapped specimens strength capacity was 47.797 MPa (specimen I) and 43.474 MPa (specimen II) at the time of failure.

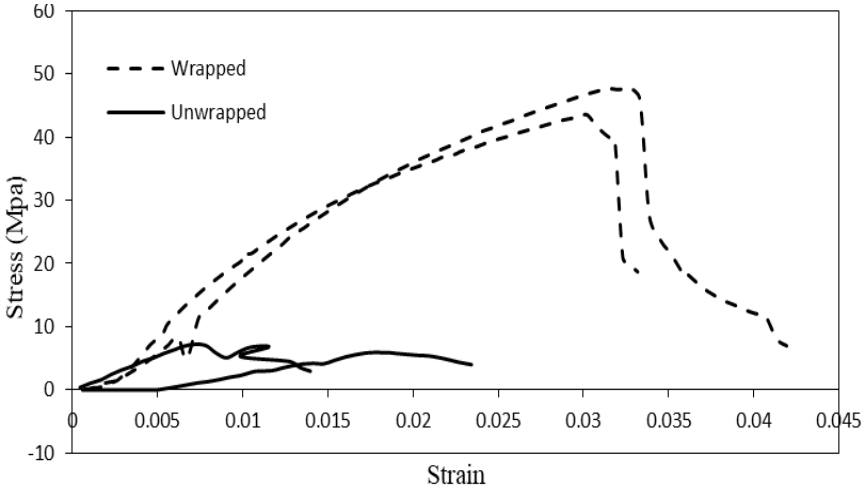

Figure 4: Combined stress vs. strain graph of (Series II) specimen

Figure 5 indicates, Combined stress vs. strain graph of series III depicts that, unwrapped specimens strength capacity was 4.298 MPa (specimen I) and 3.244 MPa (specimen II) at the time of failure, whereas wrapped specimens strength capacity was 25.259 MPa (specimen I) and 30.31 MPa (specimen II) at the time of failure.

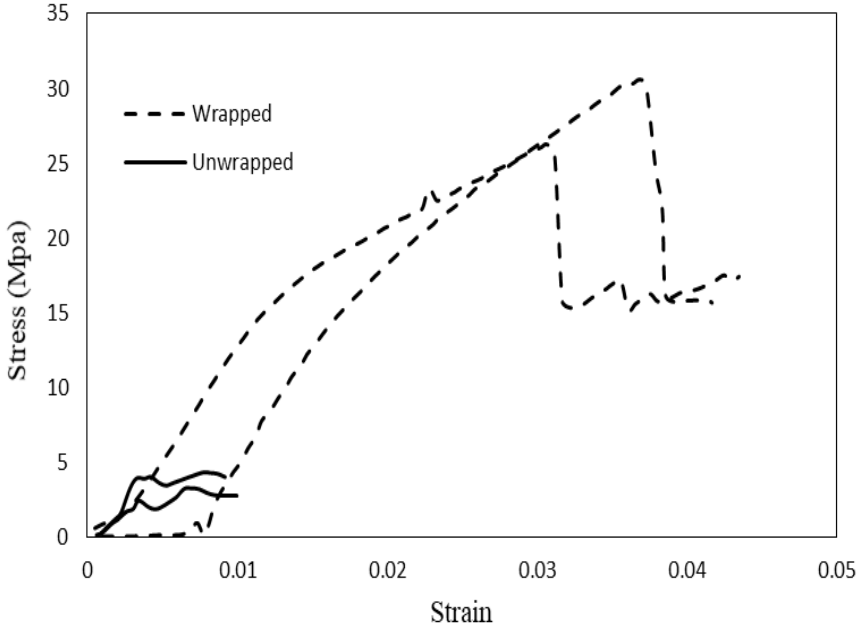

Figure 5: Combined stress vs. strain graph of (Series III) specimen

So, from all of these, it can clearly specify from the comparison of strength capacity of specimens that all of the wrapped specimens of Series I, II, III had more strength than all of the unwrapped specimens because of single layer wrapping of GFRP jacketing provide more strength to the wrapped specimens with negligible amount of increasing self-weight.

From the "stress vs. strain" curve (figure 6), it was observed that unwrapped specimen showed a

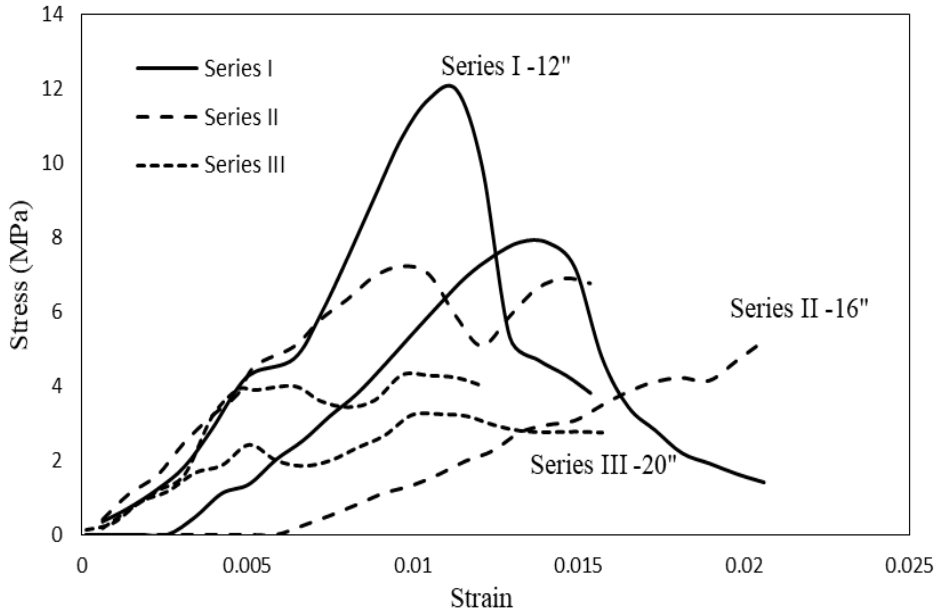

Figure 6: Combined stress vs. strain graph of unwrapped specimen

different curve pattern that doesn't match with the standard stress-strain curve. There are many reasons that were responsible for it and this was the casting of the specimen was from different batches, some specimen's end surface was not properly horizontal.

From Figure 7, wrapped specimen showed consistency and maintaining a slop of increasing strength with deflection due to confined with glass fiber. One or two sudden breakpoints were being noticed where load increases with no deflection and then sudden deflection occurred. It was because of failure in one or two string, or the bonding got lose in between the fiber and concrete surface.

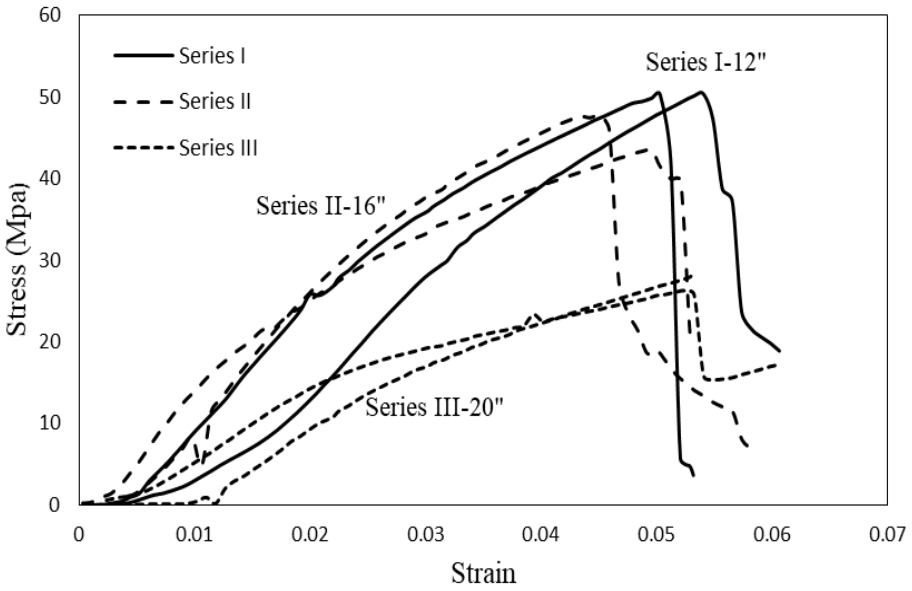

Figure 7: Combined stress vs. strain graph of wrapped specimen

3.2 Mode of Failure

Figure 8: Failure pattern of unwrapped cylindrical specimens.

Figure 9: Failure pattern of wrapped cylindrical specimens.

Figure 8 indicates, failure pattern of unwrapped specimens that failure was happened due to shear crack and compression failure. In some cases, it happened due to failure of weak concrete at top of the specimen. Whereas in figure 9, wrapped specimens failed due to failure of glass fiber confinement and all of these were compression failure. Specially, for Series III (height 20 inches) both wrapped and unwrapped specimens' failure also occurred due to buckling effect.

3.3 Tables

Table 1: Result of Unwrapped specimen

Type of Specimen	L/r ratio	Specimen Weight (Kg)	Load Max. (N)	Displacement (mm)	Strength (N/mm^2)	Average Strength (N/mm^2)	Strain
Unwrapped	12	4.99	97058	3.449	11.971	9.923	0.0113
		4.89	63852	4.035	7.875		0.0132
	16	6.49	58591	2.931	7.227	6.584	0.0072
		6.45	48168	7.259	5.941		0.0179
	20	8.31	26520	3.893	4.298	3.771	0.0076
		8.20	35108	3.535	3.244		0.0064

Table 2: Result of Wrapped specimen

Type of Specimen	L/r ratio	Specimen Weight (Kg)	Load Max. (N)	Displacement (mm)	Strength (N/mm^2)	Average Strength (N/mm^2)	Strain
Wrapped	12	5.22	408342	16.487	50.367	50.3695	0.0541
		5.21	408380	15.315	50.372		0.051
	16	6.54	387510	13.282	47.797	45.6355	0.0327
		7.02	352960	15.361	43.474		0.031
	20	8.35	212890	15.546	25.259	27.7837	0.0306
		8.59	249555	18.912	30.3084		0.0372

4. CONCLUSIONS

Lateral confinement of concrete with GFRP can significantly increase concrete strength and ductility. Because of lateral confinement, wrapped specimens have higher strength as specimens will fail when concrete and FRP both will be failed whereas unwrapped specimens will fail when concrete will fail. And, in case of ductility, FRP string will be strained when specimens are loaded but when load are releasing from specimens string will be back in their original position just like ductile materials. As a result, significant change in lateral strain as well as axial strain was observed in wrapped specimens than unwrapped specimens. In this experimental study, the uniaxial compressive strength capacity of cylindrical specimens for both unwrapped and wrapped by glass fiber are observed. From the test results and calculated strength values for Series I, II and III. it is clearly noticeable that after using glass fiber wrap self-weight of the specimen increased by 5% whereas strength capacity increased by 407%, 594% and 636% respectively. And, amount of strain increases for unwrapped column, because GFRP confinement helps concrete to carry more compressive load with being strained highly.Average value of strain of both unwrapped and wrapped specimens of series I,II,III are 0.01225, 0.01255, 0.007 and 0.05255, 0.03185, 0.0339 respectively. So, Considering slenderness ratio which is not vary with wrapped and unwrapped condition but vary with height of cylindrical specimens that increase with strength capacity decreases. This happens due to buckling effect of cylindrical specimens. This studies shows that buckling of cylindrical specimens can be minimized largely by using glass fiber wrap at the same time without increasing self-weight of cylindrical specimens significantly.

ACKNOWLEDGEMENTS

The authors express their sincere thanks to Prof. Dr. Md. Mahmudur Rahman, Prof. Dr. Sharmin Reza Chowdhury and Asst. Prof. Md. Mashfiqul Islam for their advice and providing the necessary facility for this research study.

REFERENCES

Ameli, M., Ronagh, H. R., & Dux, P. F. (2007). Behavior of FRP strengthened reinforced concrete beams under torsion. Journal of Composites for Construction. https://doi.org/10.1061/(ASCE)1090-0268(2007)11:2(192)

Balendran, R. V., Rana, T. M., Maqsood, T., & Tang, W. C. (2002). Application of FRP bars as reinforcement in civil engineering structures. Structural Survey. https://doi.org/10.1108/02630800210433837

Barghi, M., Azadbakht, M., & Hadad, M. (2012). Evaluating the ductility and shear behaviour of

carbon fibre reinforced polymer and glass fibre reinforced polymer reinforced concrete columns. Structural Design of Tall and Special Buildings. https://doi.org/10.1002/tal.590

Bonacci, J. F., & Maalej, M. (2001). Behavioral trends of RC beams strengthened with externally bonded FRP. Journal of Composites for Construction. https://doi.org/10.1061/(ASCE)1090-0268(2001)5:2(102)

Hadi, M. N. S. (2007). Behaviour of FRP strengthened concrete columns under eccentric compression loading. Composite Structures. https://doi.org/10.1016/j.compstruct.2005.06.007

Masoud, S., & Soudki, K. (2006). Evaluation of corrosion activity in FRP repaired RC beams. Cement and Concrete Composites. https://doi.org/10.1016/j.cemconcomp.2006.07.013

Sugarman, B. (1967). Strength of glass (a review). Journal of Materials Science. https://doi.org/10.1007/BF00555385

Proceedings of the 5th International Conference on Civil Engineering for Sustainable Development (ICCESD 2020), 7~9 February 2020, KUET, Khulna, Bangladesh (ISBN-978-984-34-8764-3)

ARTIFICIAL LIGHTWEIGHT AGGREGATE PRODUCTION USING RICE HUSK ASH

Md. Sajjad Hossain*[1] and Abu Zakir Morshed[2]

[1]Undergraduate Student, Department of Civil Engineering, Khulna University of Engineering & Technology, Khulna-9203, Bangladesh, e-mail: md.sazzad.ce15@gmail.com
[2]Professor, Department of Civil Engineering, Khulna University of Engineering & Technology, Khulna-9203, Bangladesh, e-mail: azmorshed@ce.kuet.ac.bd

***Corresponding Author**

ABSTRACT

The demand of construction materials is increasing nowadays due to the rapid growth of construction industry all over the world. Specially, the aggregates which are incorporated in concrete is collected from natural resources. But, it is known that natural resources are limited. Continuous collection indicate the depletion of these natural resources which would be threat for all lives on the earth. On the other hand, disposal of waste from industry is now major issue in case of sustainable development. To reduce the pollution from these industrial waste, recycling is introduced in many countries of the world. The better sustainable system largely depends on recycling and reducing of waste materials which generated from different types of industry. These waste materials can be utilized by using them in production of new materials like lightweight aggregates. The non-accessibility of natural lightweight aggregate and their demand are going up in worldwide, thus new alternatives on producing artificial aggregate should be developed. The world is tremendously inspired by innovative creation of alternative material in development industry as of late utilizing industrial by products, the huge scale use of these modern side-effects lessens ecological contamination and decreasing the scarcity of aggregates. Subsequently there is a requirement for, the generation of artificial aggregates, which meets present necessity of the industrial business. In this research work, lightweight aggregates was manufactured from industrial waste like rice husk ash and a binding material like cement. Cement and rice husk ash were mixed with respect to volume (1:5, 1:4 & 1:3) with water. The determination of unit weight, specific gravity & water absorption of artificial aggregate were carried out. Also, the aggregate crushing value (ACV) test and aggregate abrasion value test were performed. Different types of mixing ratio showed different values of unit weight, specific gravity, aggregate crushing value and aggregate abrasion value. Unit weight of artificial aggregates was calculated which ranges from 464 kg/m^3 to 850.6 kg/m^3 and the value of specific gravity was laid between 0.752 and 0.953. According to mixing ratio of cement and rice husk ash (1:3) showed the best result. Water-solid (w/s) ratio was observed 0.91, where solid represents the total amount of the cement and ash. The unit weight and specific gravity of artificial lightweight aggregate were found 850.6 kg/m^3 and 0.953, respectively. Water absorption of artificial aggregate was found 33.27%. Aggregate crushing value showed about 15.05% while aggregate abrasion value was found 37.2%. The artificial aggregate properties were compared to the natural aggregates of stone chips and first class brick chips, by which it was clear that the artificial aggregate which was produced from industrial waste of rice husk ash was lightweight. The compressive strength of concrete incorporated with artificial aggregates (1:3) were found 10.26 MPa and 11.34 MPa for the curing period of 7 days and 28 days, respectively. The compressive strength of Concrete incorporated with natural aggregates like stone chips was measured also in same curing period for reference sample. There are wide applications of artificial lightweight aggregate, for structural use, filling and block concrete, insulation purposes and many more. The concrete incorporating with artificial lightweight aggregate results in produce eco-friendly concrete.

Keywords: *Artificial lightweight aggregate, Rice husk ash, Physical properties, Mechanical properties, Compressive strength.*

1. INTRODUCTION

Concrete is a composite material which is used in various types of construction work (Kwek & Awang, 2018). The amount of natural aggregates which are used for production of concrete is about 8 to 12 million tons annually and aggregates take place about 70% of the total volume of concrete (Dash, Patro, & Rath, 2016). As a result, naturally available aggregates are decreasing sharply (B. Durga & M. Indira, 2016). Many researchers (Lura, Wyrzykowsky, Tang, & Lehmann, 2014) are incorporated with the industrial development in investigation of the maintainable artificial lightweight aggregate production as an alternative to natural aggregates. Researchers have produced artificial lightweight aggregate by using industrial waste like fly ash, palm oil fuel ash, paper sludge, water treatment sludge, wood dust, iron ore dust etc. These industrial wastes have a great negative impact on environment which is increasing in an alarming rate.

These days one of the serious issues that should be a worry is to limit and reusing waste materials from industry. The waste materials from industry can be utilized in manufacturing lightweight aggregates. Due to rapid growth of population in Bangladesh, large amount of rice is required for feeding the people. As a result, auto rice mill industry is growing very fast where rice is produced from paddy. During the production of rice, large quantity of rice husk ash is produced in the mill by incineration process of raw rice husk. According to estimation, currently 700 million tons rice is producing in the world. Approximately, 25 Kg rice husk ash is generated from the burning of 100 Kg rice husk (Singh, 2018). Bangladesh is an agricultural country, as a result rice husk ash is largely available in Bangladesh and consider as a renewable agriculture waste from auto rice mill. Rice husk ash contains large amount of silica than other plant residues. Generally, 78% rice and 20% raw rice husk is produced from paddy plant in the rice mill where remaining 2% consider as a lost product during the process. Combustion process in the boiler results in the production (1/5 to 1/4) of rice husk ash from rice husk (Singh, 2018). Rice husk ash consider as an industrial waste because of having no commercial value. Dispose of this ash create many problems in the surrounding environment because its degradation process takes enough time. Also, ash lead to pollution which may create health problems among the people. Rice husk ash can be used as a soil amendment or a filler. Rice husk ash particles can be absorbed large amount of water due to its porous microstructure. Its weight is very negligible compare to its volume, by which it can be considered as a lightweight. Rice husk ash is so fine that it can be served as a material of partial replacement of cement in the construction industry. Since researchers have conducted the manufacture of artificial aggregates by using different types of industrial waste, hence rice husk ash can also be used in production of artificial aggregates which overcome the shortage of natural aggregates as well as reuse of industrial waste.

Artificial aggregates take place in construction field greatly. In this condition, the present investigation on production of artificial coarse aggregate by using wastes has much significance. The accessibility of raw materials declines significantly which creates many problems in construction field all over the world. Also, deficiency of natural aggregates leads to need of artificial aggregates. The artificial lightweight aggregate has a wide application on construction work (Nor, et al., 2016). As a construction material, the use of artificial lightweight aggregate will provide economic advantages compare to normal aggregates in future (Arioz, et al., 2008).

The main focus of this research is placed on the manufacturing process of artificial lightweight aggregates by using rice husk ash collected from local source. To determine the physical and mechanical properties of artificial lightweight aggregate and compare with the relevant standards.

2. MATERIALS AND METHODS

Artificial lightweight aggregate production was involved basically collection of raw materials, paste of ash and cement, molds of different thickness & different sizes of wire mash for slicing the paste. The size of aggregates are depends on laboratory test, so aggregates were made of two sizes of 1/2"

and 3/4". Ordinary Portland cement was mixed with rice husk ash according to volume. Paste was placed in mould of 1'x1'x0.5" and 1'x1'x0.75". The paste was sliced by wire mashes into small pieces using hand pressure after casting to initial setting time. After hardening, aggregates kept in water chamber for curing.

2.1 Materials

The rice husk, also called rice hull, is the coating on a seed or grain of rice. It is formed from hard materials, including silica and lignin, to protect the seed during the growing season. Each kg of milled white rice results in roughly 0.28 kg of rice husk as a by-product of rice production during milling. Rice husk ash is the remaining by-product after combustion is done. The amount of carbon remaining in ash depends on the combustion performance (i.e., complete or incomplete combustion). Rice husk ash was collected from auto-rice mill industry, then it was sun-dried by spreading it on the floor. For production of artificial aggregate, some binder is needed to bond with rice husk ash and form a hard-solid block. Ordinary Portland cement was used as a binder.

2.2 Mould and Tools

Two wooden frame type moulds were used for artificial aggregate production. The moulds were 1ft x 1ft in size with top and bottom surface open having a depth of 1/2" and 3/4", respectively. Two different sizes of wire meshes having 1/2" square and 3/4" square opening were used for slicing the paste. Wire-mesh generally divided into number of small square blocks.

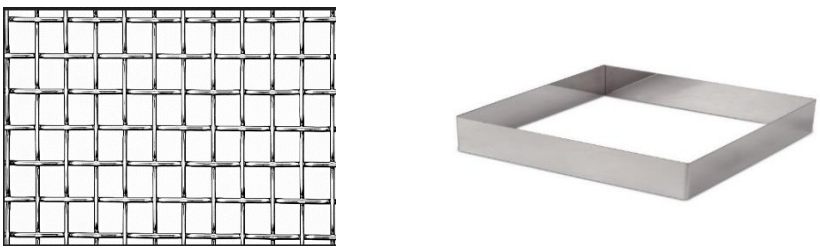

Figure 1: Wire Mesh and Mold

Figure 1 represents the picture of Wire mesh (Each square block of 1/2" & 3/4") and wood mold (1'x1'x1/2" & 1'x1'x3/4").

2.3 Specimen Preparation

Dry rice husk ash was stirred vigorously to break down any lumps or agglomerates. Then, Cement and rice husk ash were mixed with volume ratios 1:3, 1:4 & 1:5, respectively. After that, water was added the mix to produce a paste. Water & solid (W/S) ratio was 0.91 by mass. Solid was represented by the total mass of rice husk ash and cement. Two moulds were filled with paste and compacted properly to avoid void content. After placement of paste, moulds were kept for some times. Then, mould was removed from surrounding the paste and wire mash was used for slicing the paste before end of initial setting time (45 to 60 minutes). Hand pressure was applied in the wire mash which penetrated into the paste up to the bottom of the mould. As a result, paste was divided into number of small blocks. Then, it was allowed for hardening. After hardening, small blocks were collected and placed in water chamber for curing at 7 days. Then, aggregates were kept in room temperature for one day before performed laboratory test.

3. EXPERIMENTAL PROGRAMS

3.1 Physical Properties of Aggregate

Unit Weight of coarse aggregate was performed according to ASTM C29 test method in laboratory. Specific Gravity and Absorption of coarse aggregate was conducted in the laboratory according to ASTM C127 test method.

3.2 Mechanical Properties of Aggregate

The Los Angeles test was performed according to ASTM C535 to observe the resistance to degradation against abrasion and impact.

BS 812 test method was followed in the laboratory to conduct the Aggregate Crushing Value (ACV) test.

3.3 Concrete Mix Proportion

Design compressive strength of concrete (fc′) at 28 days was 20 Mpa. Ordinary portland cement was used as binder. River sand having fineness modulus of 2.60 was used as the fine aggregate. Mixing ratio of 1/2″ and 3/4″ artificial aggregate was 1:1 in the concrete mix. Water-cement ratio was 0.69. Target slump value of concrete was taken 75-100 mm and concrete mix ratio (by weight) was 1: 1.1: 1.87. All of the aggregates were presoaked in water and made saturated surface dry (SSD) condition before incorporating in the concrete mix.

3.4 Compressive Strength of Concrete

Cylindrical specimens (Diameter 4" & Height 8") were made to determine the compressive strength of concrete. Concrete was made incorporated with both Artificial aggregate and Natural aggregate (stone chips). For both types of specimen, curing period was 7 days and 28 days. After curing, compressive strength of both type of cylindrical specimen was determined and then comparison of compressive strength of concrete was done. Compressive strength of cylindrical concrete specimens was conducted according to ASTM C39.

Figure 2: Artificial Aggregate and Concrete Incorporated with Artificial Aggregate

Figure 2 shows the artificial aggregates after curing for 7 days in water and cylindrical specimens incorporated with artificial aggregate. Cylindrical specimens were cured for 7 days and 28 days in water to determine the compressive strength of concrete.

4. RESULTS AND DISCUSSIONS

Table 1: Physical Properties of Artificial Aggregate

Properties	1:3	1:4	1:5	**Brick Chips (1st Class)**	**Stone Chips**
Specific Gravity	0.953	0.897	0.752	1.95	2.55
Unit Weight (Kg/m^3)	850.6	630.5	464.0	991.3	1485
Water Absorption (%)	33.27	61.17	91.28	16.79	1.89

Table 1 shows the variation of specific gravity of artificial aggregate. Specific gravity is increasing significantly with mix proportion of increasing of binder and decreasing of rice husk ash. But, finally specific gravity of artificial aggregate (0.953) shows the lower value than the natural aggregate like

stone chips (2.55) and brick chips (1.95). According to other research (Kwek & Awang, 2018), lower value of specific gravity compared to natural aggregate can be considered as a lightweight aggregate. Table 1 illustrates the change in unit weight of artificial aggregates which ranges from 464 to 850.6 Kg/m^3. The 1:3 mixing ratio shows the highest (850.6 Kg/m^3) value of unit weight. Overall, the unit weight of artificial aggregate is comparatively lower rather than Brick chips (991.3 Kg/m^3) and natural aggregate of stone chips (1485 Kg/m^3). According to ACI code, there are three (3) types of lightweight aggregte based on unit weight. Among them, lightweight aggregate for insulation purposes should have unit weight less than 1000 Kg/m^3. This experiment values were satisfied these criterion.

Table 1 demonstrates the variation of percentage (%) of water absorption of artificial aggregate with change in mix ratio. Water absorption of coarse aggregate contributed mostly by open and close pore space of aggregate (Nor, et al., 2016). Cellulose structure of artificial aggregates lead to consume more water rather than normal coarse aggregates. According to ASTM C127 and ASTM C128 procedure, the water absorption of structural lightweight aggregate varies from 5% to more than 25% by mass of dry aggregate. The mix ratio of 1:3 shows the 33.27% of water absorption which relatively larger than brick chips (16.79%) and stone chips (1.89%). The deviation of water absorption percentage from standard value was occured due to high proportion of rice husk ash which was turnrd into large amount of void space in the aggregtae.

Table 2: Mechanical Properties of Artificial Aggregate

Properties	1:3	1:4	1:5	**Brick Chips (1st Class)**	**Stone Chips**
Crushing Value (%)	15.05	15.38	17.20	26.81	14.05
Abrasion Value (%)	37.20	43.70	45.80	33.10	16.20

Table 2 shows the variation of crushing value and abrasion value of artificial aggregate. For structural purposes, the recommended Aggregate crushing value (Equal to or not greater than) is 30% and Aggregate abrasion value (Equal to or not grated than) is 50%. Artificial aggregate (1:3) shows the crushing value of 15% and abrasion value of 37% which lies within the recommended limit.

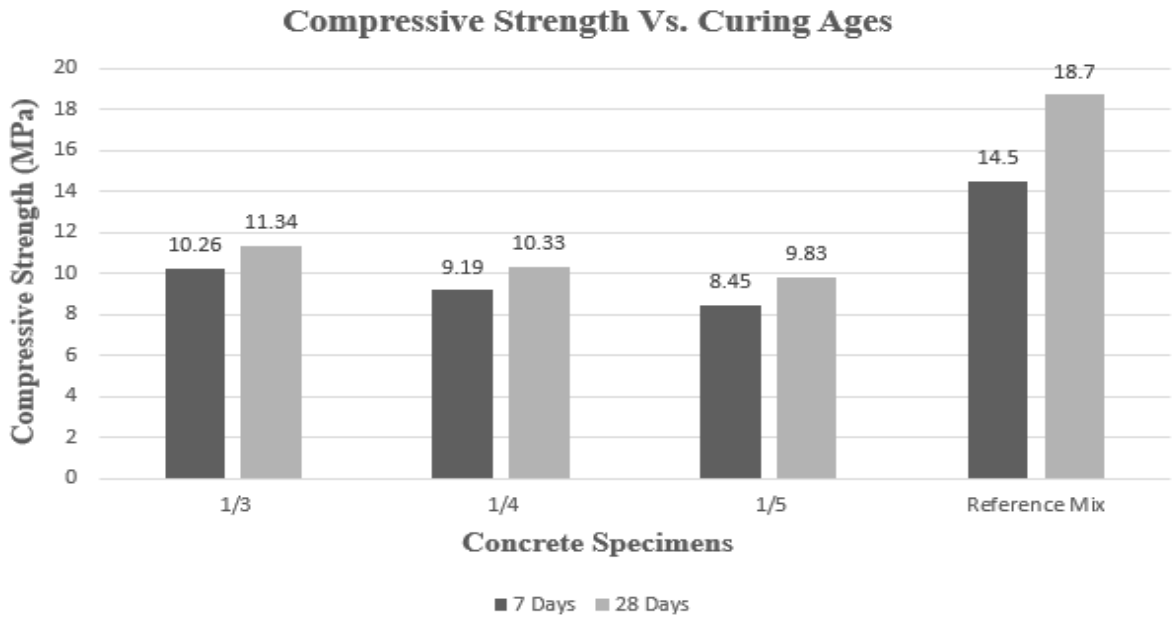

Figure 3: Compressive Strength of Concrete Specimens at Different Curing Periods

Figure 3 represents the compressive strength (MPa) of concrete specimens incorporated with artificial aggregate and reference mix (stone chips) at curing age of 7 days and 28 days. Among three (03) mix ratios, 1:3 shows the highest compressive strength of 10.26 MPa and 11.34 MPa for curing period of 7

days and 28 days, respectively. In case of artificial aggregates compressive strength increased very small amount (about 1.08 MPa) from 7 days to 28 days curing period while compressive strength of reference mix was rose up significantly (above 4 MPa). According to ACI code, lightweight concrete can be used in two (02) purposes based on their compressive strength at 28 days. Compressive strength equal or above 17 MPa can be considered as structural lightweight concrete and compressive strength less than 17 MPa can be considered as a non-structural lightweight concrete.

5. CONCLUSIONS

According to current study and result analysis, artificial lightweight aggregates can be manufactured from rice husk ash. The properties of artificial aggregate obtained compared with normal aggregates. Conclusions about this study can be stated as –

- According to other research study (Kwek & Awang, 2018), lower value of specific gravity of artificial aggregates compared to natural aggregates indicates it can be served as a lightweight coarse aggregate material.
- Water absorption (%) of artificial lightweight aggregate is deviated slightly from ASTM C 127 and ASTM C 128 standard value where recommended value is within 25%.
- ACI code recommends the density of lightweight concrete generally lies between 500 and 1850 Kg/m^3. In this experiment, the density of concrete incorporated with artificial aggregate was obtained 1383 Kg/m^3 which satisfies the practical range stated in the ACI code.
- According to ACI code, if compressive strength of lightweight concrete at 28 days is less than 17 MPa then it can be considered as a non-structural lightweight concrete. Since the compressive strength of experimental lightweight concrete (11.34 MPa) is less than this recommended value so this concrete can be served as a non-structural lightweight concrete.
- Considering low density and compressive strength of concrete based on ACI code, this type of artificial lightweight aggregate can be used in insulation purposes.
- Artificial lightweight aggregate used in construction can reduce the total construction cost which treat as alternate source of natural coarse aggregate.

ACKNOWLEDGEMENTS

The authors would like to acknowledge the IRRI Rice Knowledge Bank for providing research related useful information, Mahabub Brothers Auto Rice Mill for supplying raw materials and Khulna University of Engineering & Technology (KUET), Bangladesh for the laboratory facility and financial support.

REFERENCES

Arioz, O., Kilinc, K., Karasu, B., Kaya, G., Arslan, G., Tuncan, M., Kivrak, S. (2008). A Preliminary Research On The Properties of Lightweight Expanded Clay Aggregate . J. Aust. Ceram. Soc., 44, 23-30.

B.Durga, & M.Indira. (2016). Experimental Study on Various Effects of Partial Replacement of Fine Aggregate with Silica Sand in Cement Concrete and Cement Mortar. International Journal of Engineering Trends and Technology(IJETT), 33, 252-253.

Dash, M. K., Patro, S. K., & Rath, A. K. (2016). Sustainable use of industrial-waste as partial replacement of fine aggregate for preparation of concrete. International Journal of Sustainable Built Environment, 5, 484-516.

Kwek, S. Y., & Awang, H. (2018). Artificial lightweight aggregate from palm oil fuel ash (POFA) and water treatment waste . 14th International Conference on Concrete Engineering and Technology (pp. 1-5). Malaysia: IOP Publishing.

Lura, P., Wyrzykowsky, M., Tang, C., & Lehmann, E. (2014). Internal curing with lightweight aggregate produced from biomass-derived waste. Cement and Concrete Research, 59, 27-30.

Nor, A. M., Yahya, Z., Abdullah, M. A., Razak, R. A., Ekaputri, J. J., Faris, M., & Hamzah, H. N. (2016). A Review on the Manufacturing of Lightweight Aggregates Using Industrial By-Product . MATEC Web of Conferences 78, 01067 (pp. 1-5). Malaysia: IConGDM.

Singh, B. (2018). 13 - Rice husk ash. Waste and supplimentary cementitious materials in concrete, 418-422.

Proceedings of the 5th International Conference on Civil Engineering for Sustainable Development (ICCESD 2020), 7~9 February 2020, KUET, Khulna, Bangladesh (ISBN-978-984-34-8764-3)

AXIAL CAPACITY OF CIRCULAR AND NON-CIRCULAR CONCRETE COLUMNS CONFINED WITH JFRP AND CFRP UNDER CYCLIC LOADING

Tamanna Nabila Islam*[1], Riyadul Hashem Riyad[2] and Towsif Mahdi Nur[3]

[1]Transmission Line Engineer, Electricity Transmission Consultants (BD.) Ltd., Bangladesh, e-mail: tnabila.aust06@gmail.com
[2]Lecturer, European University of Bangladesh, Bangladesh, e-mail: riyadhashem.aust@gmail.com
[3]Student, Ahsanullah University of Science and Technology, Bangladesh, e-mail: towsifturzo@gmail.com

***Corresponding Author**

ABSTRACT

Strengthening of column is of greatest concern of a civil engineer as it carries the loads of slabs and beams and transfers them to the ground. The natural fibres are replacing the strengthening materials in the field of constructions due to their advantageous criteria such as no environmental hazards, human friendly, aesthetical and engineering properties. Among such Fibre Reinforced Polymers (FRPs), Carbon and Jute is commonly used for their high strength and durability. Here jute and carbon fibre reinforced polymer (JFRP & CFRP) were used as unidirectional and untreated fibres due to their abundant availability in our country. In this study jute and carbon fibre has reinforced the composites and the epoxy being the matrix material has strengthened the composite much more. Hand lay-up techniques were used to construct the composites. A total 18 specimens were tested varying shapes i.e. circular & non circular, i.e. square and rectangular and different constituent coarse aggregate i.e. bricks and stones, and no. of layers of JFRP and CFRP. Among them 6 columns of circular, square and rectangular were wrapped by CFRP and rest with JFRP. These columns were subjected to cyclic loading until it reaches the ultimate stress and fails so that stress strain curve is easy to attain by Kaleida graph with high definition (HD) images by digital HD camera. Such analysis is done to determine the effect of JFRP confinement to the cyclic loading capacity improvement and further increasing strength of columns and the failure patterns of JFRP and CFRP as well. The data and graphs that show the effect clearly that confined columns are strengthened by confinement and the more no of layers of FRP the more its strength. These unidirectional JFRP has given an adequate improved capacity of resisting cyclic loading to the columns and showed the effect of confinement. The procedure is made by the guidelines for the design and construction of externally bonded FRP systems for strengthening concrete columns (ACI 440.2R-08) and parameters came out same as JFRP confined columns. Such this study has made a clear visualization about strengthening the concrete columns by confining with FRPs

Keywords: JFRP, CFRP, Cyclic loading, Axial capacity, Failure pattern.

1. INTRODUCTION

In the field of construction, concrete has taken the significant position among all the available materials around the world. The durability of concrete generally depends on how it is reinforced and the reinforcing material. In order to strengthening the concrete composites besides steel, FRPs are also of great significance. Deterioration is the common incident of concrete composites nowadays. In order to resist the deterioration, retrofitting of the structure is very successful and demanding process in order to strengthening of structure. FRP has high stiffness and strength, high fatigue resistance, lower density, easy and rapid installation, high damping, little change in structural properties, which made it the most favourable material for retrofitting the concrete structure (Shrikant M. Harle, 2014). Moreover, it can be turned into shape, which is almost impossible with steels. Due to environmental issues, synthetic fibres should be replaced by the natural fibres, which are biodegradable, renewable and cost effective for fabrication (Spadea, G., &Bencardino, F. 1997). Natural fibres may have the durability, high strength, low cost, low density, good intensity over the synthetic fibres. Besides, it needs less skilled labor. It can cover up the irregularities in the shape of concrete surface and also can be installed on a curved shape. Overlapping can be done if required. Among the merits, there are some demerits too. Such as, relative cost is high and long run durability data is not available yet. The main demerit of associating the external strengthening material is the fire accidents and damages. However, damage of this material will only reduce the overall factor of safety but won't lead to structure collapse (Carneiro, R. J. D. F., &Melo, G. S. D. A. 2011). Besides, lack of approved data regarding design and analysis and inexperienced labors are the main deterring factors for this work.

In Bangladesh, jute is the mostly available and cheapest natural fibre among all. Moreover, it is of high strength. Some elementary features of Jute are such as, it has low pesticide and fertilizer needs and the cheapest vegetable fibre procured from the bast or skin of the plant's stem (Andrawes, B. 2017). The best source of jute in the world is the Bengal Delta Plain in the Ganges Delta, most of which is occupied by Bangladesh (Wikipedia). In this study the seismic behavior of jute fibre reinforced polymer (JFRP) wrapped concrete column under cyclic loading has been conducted. The analysis would also show the improved strength of FRP confined column over the casual one**.**

Objective of this study is to investigate the axial behavior of concrete column under cyclic loading and to evaluate the confining pressure distribution produced from brick aggregates and stone aggregate due to JFRP and CFRP confinement (Campione, G. (2013), Afifi, M. Z., Mohamed, H. M., Chaallal, O., &Benmokrane, B. (2014)). Researches regarding FRP have analyzed on the axial behavior of concrete columns with different FRP jacketing from different strength and durability perspective (Karthik, M. M., &Mander, J. B. (2010), Al-Salloum, Y. A., Al-Amri, G. S., Siddiqui, N. A., Almusallam, T. H., & Abbas, H. (2018)). The main purpose of this research is to investigate the seismic behavior enhancement of JFRP confined columns. Moreover, jute is in abundant quantity in Bangladesh, so it can be used as an engineering material in construction field for further enhancement of capacity.

2. METHODOLOGY

The main objective of this study is to investigate the enhancement of compressive strength capacity of confined composites in comparison to the unconfined columns. The variations were done by differentiating the aggregate types, shapes of specimen and the number of layers of wrapping. All the numerical data was compared to each other to attain the seismic load sustaining capacity of confined columns.

2.1Materials

2.1.1 Properties of Concrete

Stone and brick chips have been used as aggregate for casting of concrete. The average compressive strength of unconfined stone and brick plain concrete is 3000 psi (21 MPa) and 2600 psi (18 MPa) respectively. As cementing material, Portland Composite Cement was used.

2.1.2 Aggregates

Crushed stone and brick chips were used in the mixture of plain concrete. Different aggregate sizes were used such as 1 inch (25mm) passing and ¾ inch (19mm) retained and ¾ inch (19mm) passing and ½ inch (12.5mm) retained. Sylhet sand was used as fine aggregate.

2.1.3 Fibre sheets

The jute fibre sheet was named as Bangla Tossa Jute having a scientific name Corchorusolitorius. The fibre sheet (fig 1) was of 27 inches in length and 8 inches in width and weight of each jute fabric was 600 g/m^2. The fabric was limited to this length so that the uniformity in volume and fabrication could be maintained Carbon fibre Nitowrap EP (CF200) (fig 2) was used in this research. The fabrication was similar to the jute fabric in unidirectional form. The weight of each carbon fibre sheet was 200 g/m^2. The fibre sheet was of 20 inch in width and 0.0004 inch in thickness.

Figure 1: JFRP fabric

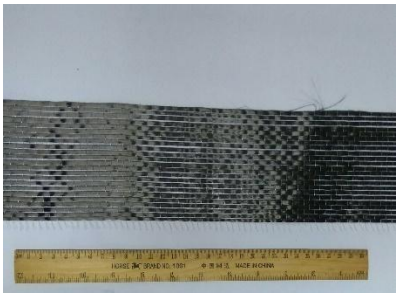

Figure 2: CFRP fabric

2.1.4 Epoxy Primer Coating

Nitowrap 410 was used in this experiment with the Base and Hardener ratio of 2:1 (ACI 440.2R-08).

2.2 Geometry of Column Specimen

A total 16 number of column specimens were casted. Among them 8 specimens were of stone chips and 8 were of brick chips. They were different in shapes such as circular and non- circular. Each category has one control specimen. 4 specimens were wrapped by CFRP and 8 were wrapped by JFRP. The dimension of all specimens was same in height of 12 inch. Circular specimen had diameter of 6 inch and the square having width of 6 inch.

2.3 Mix Design

Portland Composite Cement (PCC) was used for this experiment. The ratio of Cement, Fine aggregate and Coarse aggregate was 1:2:4. The water-cement ratio and Slump was 0.5 and 1inch respectively as per ACI 440.2R-08 standards.

2.4 Specimen Properties

2.4.1 Casting and Curing

A concrete mixture machine was used to mix the concrete and cast the specimen. The steel moulds were made in the laboratory as per standard size of the specimen of 1 feet height with 6 inches diameter. After casting the specimen were kept for 28 days under water to cure properly.

2.4.2 Wrapping process of the column specimen

Among all the specimens, 8 were wrapped with JFRP and 4 were wrapped with CFRP. At first the specimens were made clean with a brush or cloth. The fabric was wet lay-up with the epoxy as per the guidelines for the design and construction of externally bonded FRP systems for strengthening concrete columns (ACI 440.2R-08). It was then wrapped around the circumference of specimen and kept as it was for 24 hours. The epoxy was applied on to the FRP fabric by rolling brush gently. The mixture was applied right after mixing as it could be thicker with the time being. The circular and square

specimens were wrapped with 2 & 3 layers of JFRP and 1 single layer of CFRP. Both brick and stone chips were having the same procedure of wrapping. Due to the overlapping of jute fabric on the height of the specimen, it took much time to finish the wrapping. Overlapping was provided 2-4 inches. For 3 layers of JFRP, it took 6 days to complete the wrap. At first, the specimen was made clean then the epoxy was applied. The epoxy mixture was also applied on to the fabric using wet lay-up technique. Then it was wrapped around the circumference of the specimen. It was kept like this for next 24 hours. Again, the next day another portion of the height was wrapped with the JFRP fabric by overlapping the sheets. The overlap was of 2 inches. Similar procedure was followed for 2 layers of wrapping. In case of CFRP wrapping there was no need to give overlap as the fabric was cut into the size as per specimen height. Therefore, the epoxy was applied on to the fabric by wet lay-up technique and wrapped around the surface of the specimen. Then it was kept for 24 hours as like as the JFRP composites.

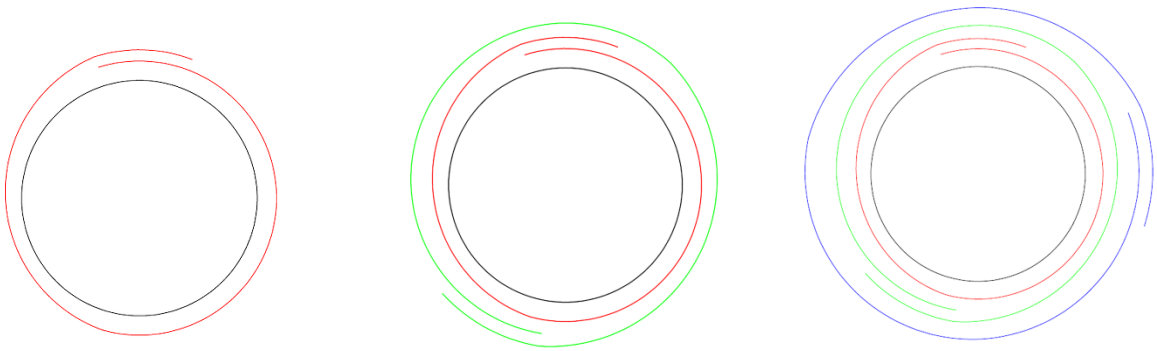

Figure 3: Top view of (a) Single wrap, (b) Double wrap, (c) Triple wrap

3. ILLUSTRATIONS

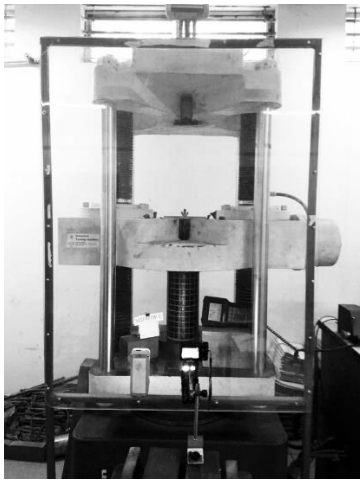

Figure 4: Experimental setup

3.1 Effect of Type of FRP

From the experimental investigation, it could be perceived that the axial stress of unconfined columns (fig 5) is relatively lower than the columns having confinement with FRP (fig 6). Also, the circular columns have the higher strength (fig 5 & fig 7) than that of square columns (fig 6 & fig 8).

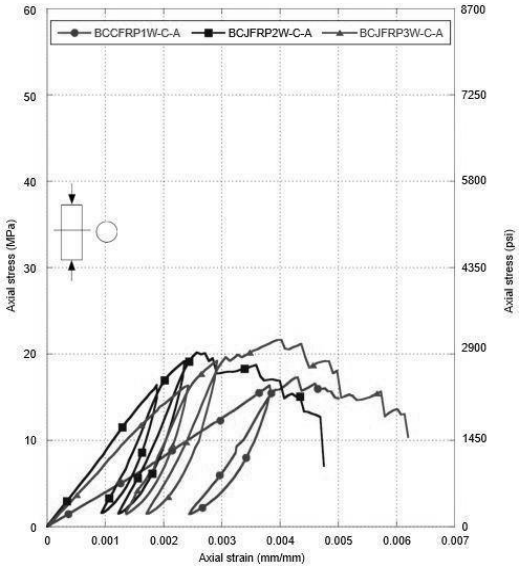

Figure 5: Evaluation of axial stress vs. axial strain behavior of BCCFRP1W-C, BCJFRP2W-C and BCJFRP3W-C concrete column under cyclic loading

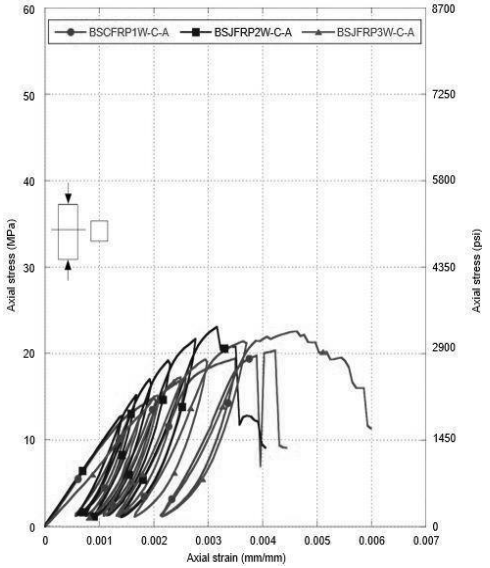

Figure 6: Evaluation of axial stress vs. axial strain behavior of BCCFRP1W-C, BCJFRP2W-C and BCJFRP3W-C concrete column under cyclic loading

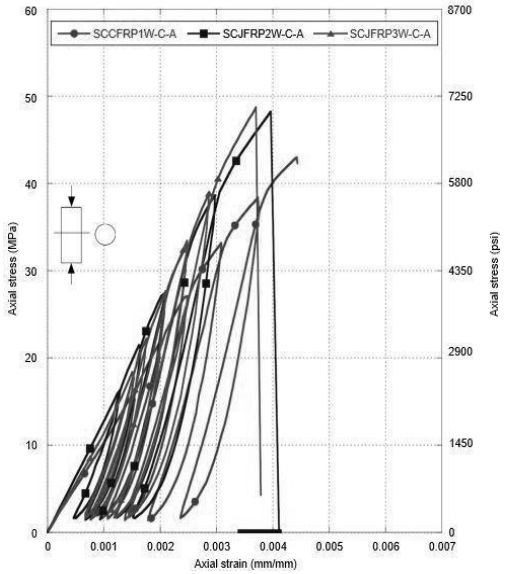

Figure 7: Evaluation of axial stress vs. axial strain behavior of SCCFRP1W-C, SCJFRP2W-C and SCJFRP3W-C concrete column under cyclic loading.

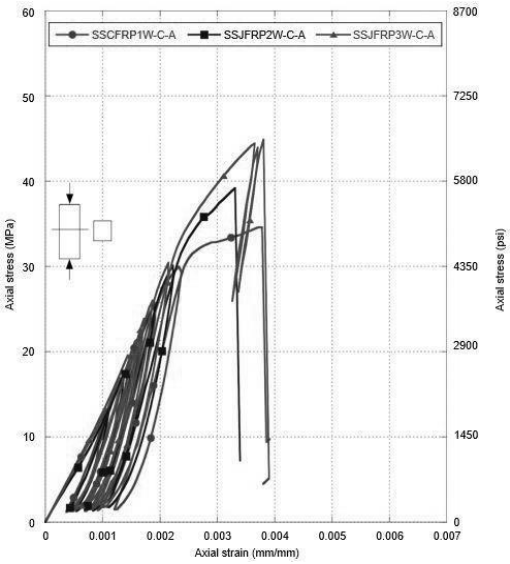

Figure 8: Evaluation of axial stress vs. axial strain behavior of SSCFRP1W-C, SSJFRP2W-C and SSJFRP3W-C concrete column under cyclic loading.

3.1Effect of No. of Layer of FRP

Generally, specimens confined with FRP show higher axial stress compared to unconfined specimen. From the experimental investigation it could be perceived that the axial stress of circular concrete columns (fig 9 & fig 11) as well as square columns (fig 10 & fig 12) confined with JFRP 2 layer are relatively lower than the concrete columns confined with JFRP 3 layer.

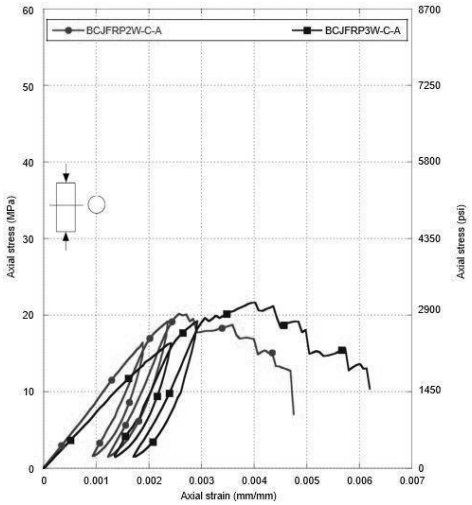

Figure 9: Evaluation of axial stress vs. axial strain behavior of BCJFRP2W-C and BCJFRP3W-C concrete column under cyclic loading

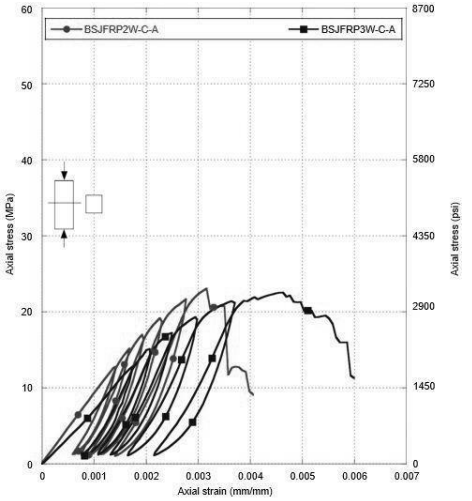

Figure 10: Evaluation of axial stress vs. axial strain behavior of BSJFRP2W-C and BSJFRP3W-C concrete column under cyclic loading

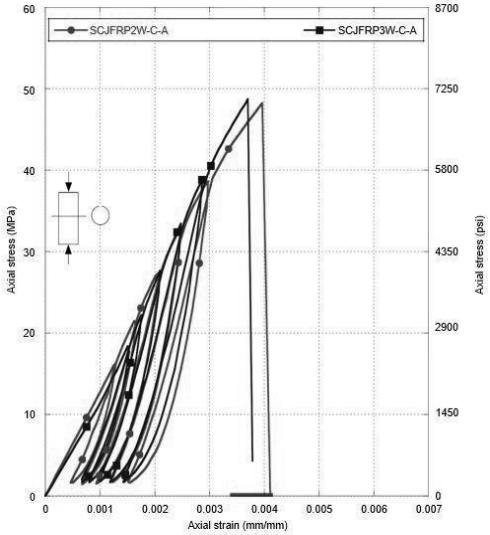

Figure 11: Evaluation of axial stress vs. axial strain behavior of SCJFRP2W-C and SCJFRP3W-C concrete column under cyclic loading

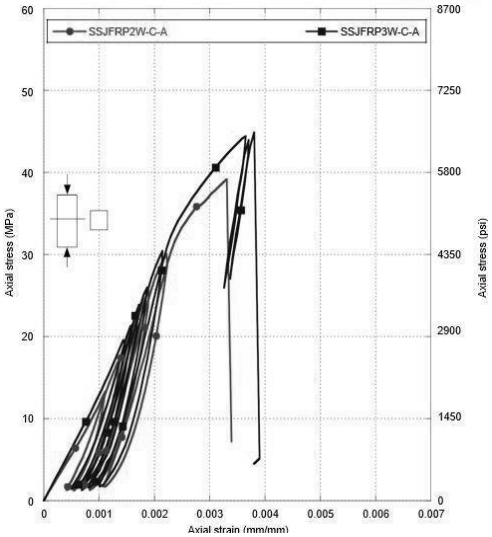

Figure 12: Evaluation of axial stress vs. axial strain behavior of SSJFRP2W-C and SSJFRP3W-C concrete column under cyclic loading.

3.2Effect of Coarse Aggregate (CA) Type

From the experimental investigation it could be perceived that the axial stress of concrete columns of stone chips in circular column is relatively higher than the concrete columns of brick chips (fig 13) and so as for the square columns (fig 14)**.**

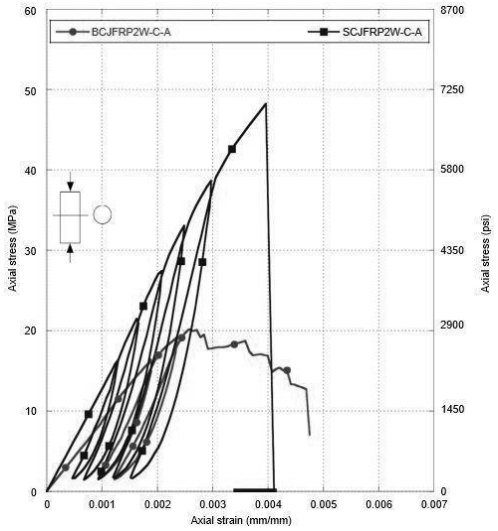

Figure 13: Evaluation of axial stress vs. axial strain behavior of BCJFRP2W-C and SCJFRP2W-C concrete column under cyclic loading.

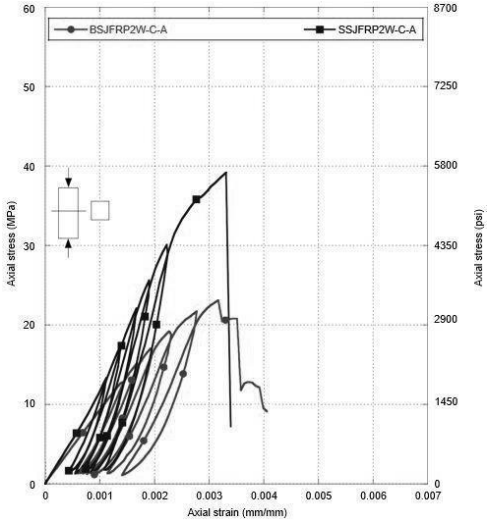

Figure 14: Evaluation of axial stress vs. axial strain behavior of BSJFRP2W-C and SSJFRP2W-C concrete column under cyclic loading.

3.3Result of Axial Compressive Test

Table 1: Summary of axial compressive test conducted on FRP wrapped concrete column under cyclic loading

CA type	Specimen Designation	Confinement type	No. of FRP layers	Max axial stress (MPa)	Axial strain at failure	Lateral strain at failure	Percentage increase on axial load carrying capacity
Brick	BCCON	-	-	12.13	0.002099	-	-
Brick	BCCFRP1W	CFRP	1	17.27	0.00431	0.01271	42.37%
Brick	BCJFRP2W-C	JFRP	2	20.19	0.00257	0.0002	66.45%
Brick	BCJFRP3W-C	JFRP	3	21.62	0.004024	0.00094	78.24%
Brick	BSCON	-	-	7.51	0.00233	-	-
Brick	BSCFRP1W-C	CFRP	1	20.34	0.004232	0.00642	170.84%
Brick	BSJFRP2W-C	JFRP	2	23.05	0.00316	0.00181	206.92%
Brick	BSJFRP3W-C	JFRP	3	22.55	0.00463	0.0009	200.27%
Stone	SCCON	-	-	18.19	0.003198	-	-
Stone	SCCFRP1W-C	CFRP	1	42.99	0.004423	0.00088	136.34%
Stone	SCJFRP2W-C	JFRP	2	48.23	0.00396	0.00198	165.15%
Stone	SCJFRP3W-C	JFRP	3	48.74	0.003699	0.00146	167.95%
Stone	SSCON	-	-	21.39	0.00533	-	-
Stone	SSCFRP1W-C	CFRP	1	34.59	0.00378	0.00254	61.61%
Stone	SSJFRP2W-C	JFRP	2	39.18	0.00331	0.00009	83.17%
Stone	SSJFRP3W-C	JFRP	3	44.87	0.0038	0.00179	109.77%

*CA: Coarse aggregate.

Here, in the aforementioned table it is clearly visible that the percentage increase on axial load carrying capacity is higher in confined columns than that of unconfined columns. Also, square columns showed greater strength than circular columns.

3.4Failure Pattern

The specimens were subjected to cyclic loading to investigate their axial capacity enhancement after wrapping. Most of the non-circular confined columns failed having corner edge failure (fig 16) whereas the circular confined columns had hoop tension failure (fig 15).

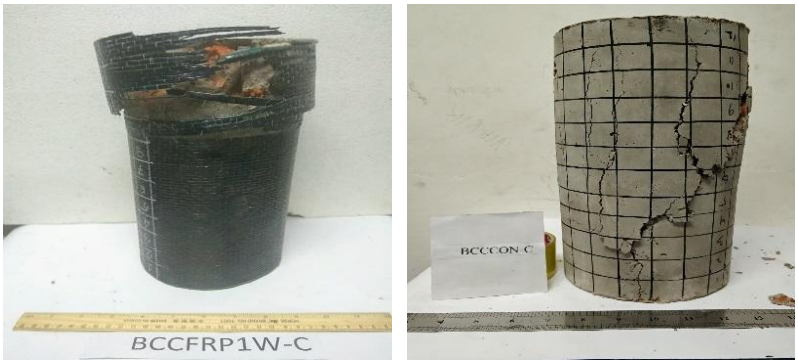

Figure 15: Hoop Tension Failure

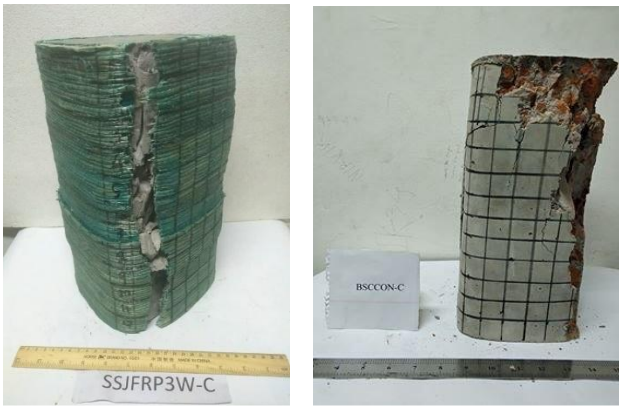

Figure 16: Corner Edge Failure

4. CONCLUSIONS

This study conducted following results

- Due to confinement with JFRP fabric the strength has enhanced significantly. The increase in ultimate compressive strength for single layer of CFRP in brick and stone chips concrete column are 42.37% (circular), 170.84% (non-circular) and 136.34% (circular), 61.61% (non-circular) respectively. For double layers of JFRP fabric in brick chips concrete column have increased by 66.45% (circular) and 206.92% (non-circular). Again, for triple layers of JFRP fabric in stone chips concrete columns have increased by 167.95% (circular) and 109.77% (non-circular).
- The study shows that for same double layer of JFRP fabric in different shape of columns (i.e. circular and non-circular) the ultimate strength increased by almost 100% more. Though the height of the specimens was same yet the result variation is noticeable.
- For same layers of JFRP fabric in different aggregate type concrete columns the strength of stone chips concrete columns shows higher strength capacity than that of brick chips concrete columns.

- JFRP confined columns behaved in a bi-linear manner connected by a nonlinear transition region, which is similar to the axial stress- axial strain response of CFRP confined columns.
- For same layers of JFRP fabric the axial compressive load resisting capacity in circular is higher than that of non-circular stone chips concrete columns under cyclic loading.
- In case of CFRP the performance of the columns under cyclic load was consistent. At the early stages of loading of the confined specimens, the noise related to micro cracking of concrete core was evident, indicating the start of stress transfer from the dilated concrete to the CFRP wrap.
- The failure was gradual. Most of the specimen had hoop tension failure while a few had corner edge failure. The failure of the wrap initiated away from the overlap region with an explosive sound.
- JFRP composites showed the potentiality as external reinforcement material. Moreover, the contact between the wrap and the concrete indicated that no de-bonding was created in the whole study.

On this note JFRP has made its place as an affordable effective reinforcement material in strengthening concrete columns.

ACKNOWLEDGEMENTS

The authors express their sincere thanks to Assistant Professor Md. Mashfiqul Islam, Professor Dr. Md. Mahmudur Rahman and Professor Dr. Sharmin Reza Chowdhury for their valuable advices and providing the necessary facilities for this research study.

REFERENCES

Lahlou, K., Lachemi, M., &Aïtcin, P. C. (1999). Confined high-strength concrete under dynamic compressive loading. Journal of Structural Engineering, 125(10), 1100-1108.

Chen, Q., &Andrawes, B. (2017). Cyclic Stress–Strain Behavior of Concrete Confined with NiTiNb-Shape Memory Alloy Spirals. Journal of Structural Engineering, 143(5), 04017008.

Carneiro, R. J. D. F., &Melo, G. S. D. A. (2011). Analytical Model for CFRP-Strengthened Prestressed Concrete Girders Subject to Cyclic Loading. Journal of Composites for Construction, 15(5), 871-874.

Spadea, G., &Bencardino, F. (1997). Behavior of fiber-reinforced concrete beams under cyclic loading. Journal of Structural Engineering, 123(5), 660-668.

Campione, G. (2013). Flexural and Shear Resistance of Steel Fiber–Reinforced Lightweight Concrete Beams. Journal of Structural Engineering, 140(4), 04013103.

Afifi, M. Z., Mohamed, H. M., Chaallal, O., &Benmokrane, B. (2014). Confinement model for concrete columns internally confined with carbon FRP spirals and hoops. Journal of Structural Engineering, 141(9), 04014219.

Karthik, M. M., &Mander, J. B. (2010). Stress-block parameters for unconfined and confined concrete based on a unified stress-strain model. Journal of Structural Engineering, 137(2), 270-273.

Al-Salloum, Y. A., Al-Amri, G. S., Siddiqui, N. A., Almusallam, T. H., & Abbas, H. (2018). Effectiveness of CFRP Strengthening in Improving Cyclic Compression Response of Slender RC Columns. Journal of Composites for Construction, 22(3), 04018009.

Shrikant M. Harle, "The Performance of Natural Fiber Reinforced Polymer Composites: Review", International Journal of Civil Engineering Research, 2014, Volume 5, PP. 285-288.

Proceedings of the 5th International Conference on Civil Engineering for Sustainable Development (ICCESD 2020), 7~9 February 2020, KUET, Khulna, Bangladesh (ISBN-978-984-34-8764-3)

NONLINEAR INELASTIC BEHAVIOR MODELING VIA BOUC-WEN MODEL FOR REAL-TIME CONTROL IMPLEMENTATIONS

Mohammad S. Miah*[1,2], Md Jihad Miah[3] and Ou Yaowen[4]

[1]Visiting Scientist, Technische Universität Dresden-TU Dresden, 01187 Dresden, Germany
[2]Associate Professor, International University of Business Agriculture and Technology, Dhaka 1230, Bangladesh, e-mail: mmshamim@iubat.edu
[3]Assistant Professor, University of Asia Pacific, Dhaka 1215, Bangladesh, e-mail: jihad.miah@uap-bd.edu
[4]Independent Researcher, e-mail: ywuomechaeng576@qq.com

***Corresponding Author**

ABSTRACT

Often structures are experiencing large inelastic type deformation due to extreme external loads such as earthquake, wind, blast, and fire. However, the magnitudes and intensity of any dynamic input loads play a pivotal role in destruction of structures. Therefore, it is crucial to deal with those types of extreme dynamic loads. Further complicacy is induced by the vibration mitigation and controlling devices, especially, the smart devices those are accompanied with highly nonlinear behavior such as electromagnetic/magnetorheological damper. Hence, appropriate modelling for the aforementioned type inelastic and hysteretic behavior is needed. In order to achieve this goal, herein a prototype single-degree-of-freedom (SDOF) nonlinear system is considered which is coupled with Bouc-Wen type element. A numerical investigation is performed by using MATLAB and SIMULINK. The motivation behind the selection of Bouc-Wen model is due to its versatility and applicability for nonlinear behavior modeling and the performance of the early mentioned model. The preliminary results show that the studied is capable of predicting nonlinear inelastic behavior quite accurately. Furthermore, it is worth mentioning here that the conceptual framework is expected to be implemented for real-time control implementations. In order to implement the framework in real-time, the SIMULINK is employed as computing tool to solve the nonlinear system and the restoring force is estimated thereafter. In contrary, the offline simulations are conducted via the use of MATLAB. Moreover, the online results (e.g. form SIMULINK) are compared with offline results, achieving a good match between the online and offline results. Future study is planned to extend the framework for multi-storey system with limited sensor information for real-time vibration control implementations.

Keywords: *Nonlinear inelastic response, Bouc-Wen model, Real-time control, Hysteresis, Nonlinear system.*

1. INTRODUCTION

The structures and infrastructures (e.g. building, bridges) are playing a pivotal role in the national economy all over the world. The aforementioned structures are not only providing shelter or point-to-point transportation network connectivity but also making daily-life effortless. Therefore, any interruption or severe damage to those structures may lead to usability problem including financial loss as well as human lives. The damage is typically induced by extreme dynamic loads such as earthquake. In order to minimize the damage of early mentioned structures, modern structures are equipped with energy dissipative devices such as passive, active, semi-active or hybrid control systems (Miah, 2015). However, almost all of the control devices demand an appropriate controlling strategy or algorithm (except passive systems) that assist the device to perform optimally. In order to be effective, the aforementioned algorithms and devices need to work in real-time (Miah et al., 2017) as often the hitting time of any dynamic loading is unknown. One-step further, the complicacy is induced by the complex nonlinear behavior of the adopted devices (e.g. active, semi-active). Therefore, it is essential to understand and predict their behavior precisely in real-time for optimal controlling performances. An experimental investigation of semi-active by using H-infinity robust control algorithm was performed by (Cetin et al., 2011). The previously mentioned author used a magnetorheological damper (MR) as a controlling device to mitigate the vibration of a 6 degree-of-freedom (DOF) system and significant reduction of overall response was reported. In (Miah et al., 2017) presented real-time experimental verification of a novel control scheme that was proposed in their preceding work (Miah et al., 2015).

The smart vibration controlling devices are linked to complex nonlinear behavior which can be modelled by various model (Bhowmik, 2011). The Bouc-Wen model is one of the most commonly used nonlinear model that is used to predict hysteretic type nonlinear behavior (Bouc, 1967) and (Wen, 1976). The efficacy of the aforementioned model has been verified by many models such as (Baber and Noori, 1985; Baber and Noori, 1986; Bhowmik, 2011; Charalampakis and Koumousis, 2008; Charalampakis and Koumousis, 2009; Kottari et al., 2014; Song and Der Kiureghian, 2006). However, in a recent study carried by (Miah et al., 2015) shows that the conventional Bouc-Wen model itself may not be capable of capturing the complex behavior of a new disc-type MR damper.

As the modeling of the hysteretic nonlinear behavior is an unavoidable part of real-time control implementation system coupled with smart vibration mitigating devices. In a nutshell, this study focused on real-time implementation for vibration mitigation and control. The rest of the paper is organized as follows: the immediate section covered the mathematical modeling, the next section contains numerical simulations and results, and finally the outcome is summarized in conclusion.

2. MATHEMATICAL FORMULATION

2.1 The Bouc-Wen Model

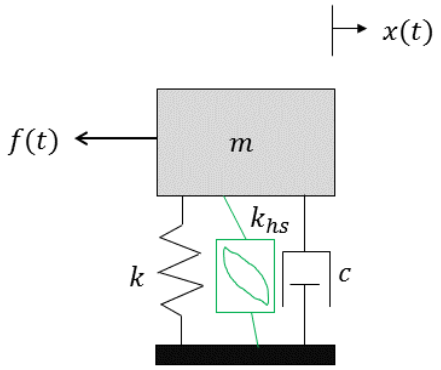

Figure 1: The structure with nonlinear element.

The numerical investigations are performed by considering a single-degree-of-freedom (SDOF) system, which is assumed to be attached to a nonlinear element. The sample structure linked with a nonlinear hysteretic type element is depicted in figure 1.

$$m\ddot{x} + c\dot{x} + \underbrace{\alpha k_i x + (1-\alpha)k_i z_{hs}}_{F_{non}} = f(t) \tag{1}$$

The restoring (nonlinear) force is denoted by F_{non} in the equation (1), m is the mass of the system, x represents the displacement, c is the damping coefficient, z_{hs} represents the hysteretic displacement. In order to make it clearer, the nonlinear restoring force is given by,

$$F_{non} = \frac{k_f}{k_i}\left(\frac{F_y}{x_y}\right)x + \left(1-\frac{k_f}{k_i}\right)\left(\frac{F_y}{x_y}\right)z_{hs} \tag{2}$$

where z_{hs} represents the hysteretic displacement, α is the ratio of the post-yield (k_f) to pre-yield (k_i), the pre-yield (k_i) stiffness is given by

$$k_i = \left(\frac{F_y}{x_y}\right) \tag{3}$$

where F_y is the yield force and x_y is the yield displacement. In equation (2), the term hysteretic displacement (z_{hs}) can be calculated via the equation given below,

$$z_{hs} = \theta \times \dot{x} - \beta \times |\dot{x}| \times |z_{hs}|^{(n-1)} \times z_{hs} - \gamma \times \dot{x} \times |z_{hs}|^n \tag{4}$$

where θ, β, γ and n are the dimensionless quantities, typically, all of those quantities are responsible for the behavior of the model. Hence, θ, β, γ and n requires appropriate tuning to obtain the optimal performance of the Bouc-Wen model.

2.2 The State-Space Formulation

A compact formulation is adopted for the offline implementations that are known as the state-space formulation (SSF). The main advantage of the SSF is that this formulation brings a second order differential equation (e.g. equation of motion) into a first order differential. As a result, it becomes much easier to solve and most importantly, one can get the response of the system only solving one equation called system/process equation. However, it needs to be mentioned that full-formulation of SSF contains two main equations: (i) system/process equation, shown in equation (5), (ii) observation/measurement equation, presented in equation (6). The process/system equation includes all of the information related to structure along with excitation/control force information. While the measurement equation deals with the desire measurement quantities such as displacement, velocity and acceleration. Designers have the freedom to formulate the measurement equation as per their problem specification and requirements.

Herein, the SDOF system has been re-formulated from the equation of motion by employing SSF as depicted below,

$$\dot{\chi} = A\chi + Bu \tag{5}$$

$$y = C\chi + Du \tag{6}$$

Assume the state variables are $\chi_1 = x$, $\dot{\chi}_1 = \dot{x} = \chi_2$, $\dot{\chi}_2 = \ddot{x}$, and $\chi_3 = z_{hs}$, hence the process equation can be written as,

$$\begin{Bmatrix} \dot{\chi}_1 \\ \dot{\chi}_2 \\ \dot{\chi}_3 \end{Bmatrix} = \begin{bmatrix} 0 & 1 & 0 \\ -\alpha k_i m^{-1} & -cm^{-1} & (1-\alpha)k_i \\ 0 & \theta & 0 \end{bmatrix} \begin{Bmatrix} \chi_1 \\ \chi_2 \\ \chi_3 \end{Bmatrix} + \begin{bmatrix} 0 \\ m^{-1} \\ 0 \end{bmatrix} f + \underbrace{\begin{bmatrix} 0 & 0 \\ 0 & 0 \\ -\beta & -\gamma \end{bmatrix} \begin{Bmatrix} |\chi_2| \times |\chi_3|^{(n-1)} \times \chi_3 \\ \chi_2 \times |\chi_3|^n \end{Bmatrix}}_{Due\ to\ the\ Cross\ Term} \tag{7}$$

And the accompanying measurement is defined as,

$$y = \begin{bmatrix} 1 & 0 & 0 \end{bmatrix} \begin{Bmatrix} \chi_1 \\ \chi_2 \\ \chi_3 \end{Bmatrix} \tag{8}$$

3. NUMERICAL EXAMPLES

3.1 The Offline Investigations

The offline simulations are performed via the use of MATLAB. To achieve the goal, the state space formulation is adopted for the problem implementations. It needs to be mentioned that the offline solutions via MATLAB or any comparable computing tools are very common and quite useful, as they only required the fundamentals of programing skills.

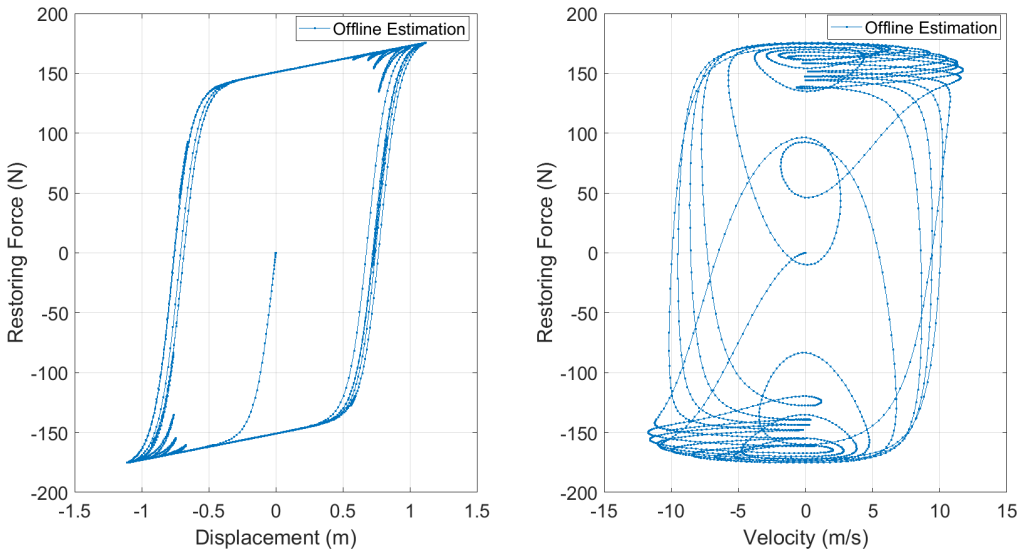

Figure 2: The offline results: restoring force versus displacement (left) and restoring force versus velocity (right).

In contrast, real-time implementations demand advanced computing tools (e.g. SIMULINK, dSPACE) as well as high computing power of the used computer such as parallel computing.

The outcome of the offline simulation is presented in figure 2. It can be observed from the early mentioned figure that the starting of the simulations/systems are moving to the steady-state conditions. Typically, displacement is smoother than the velocity as the later one is a time derivative of the displacement.

3.2 The Real-time Implementations

In order to investigate the real-time implementations herein, SIMULINK is employed as a real-time simulator tool along with MATLAB. An illustration of the SIMULINK model is furnished in figure 3. This implantation can be done via either MATLAB or SIMULINK independently or by using them both. In addition, the real-time implementations can be let it run for infinite time, while offline implementation is often done for a certain period due to cost-effectiveness analysis. In addition to those issues, real-time implementation also requires advanced knowledge of electro-mechanical. In other words, how the machine is going to behave or act with a real structure while they are built in different criterion.

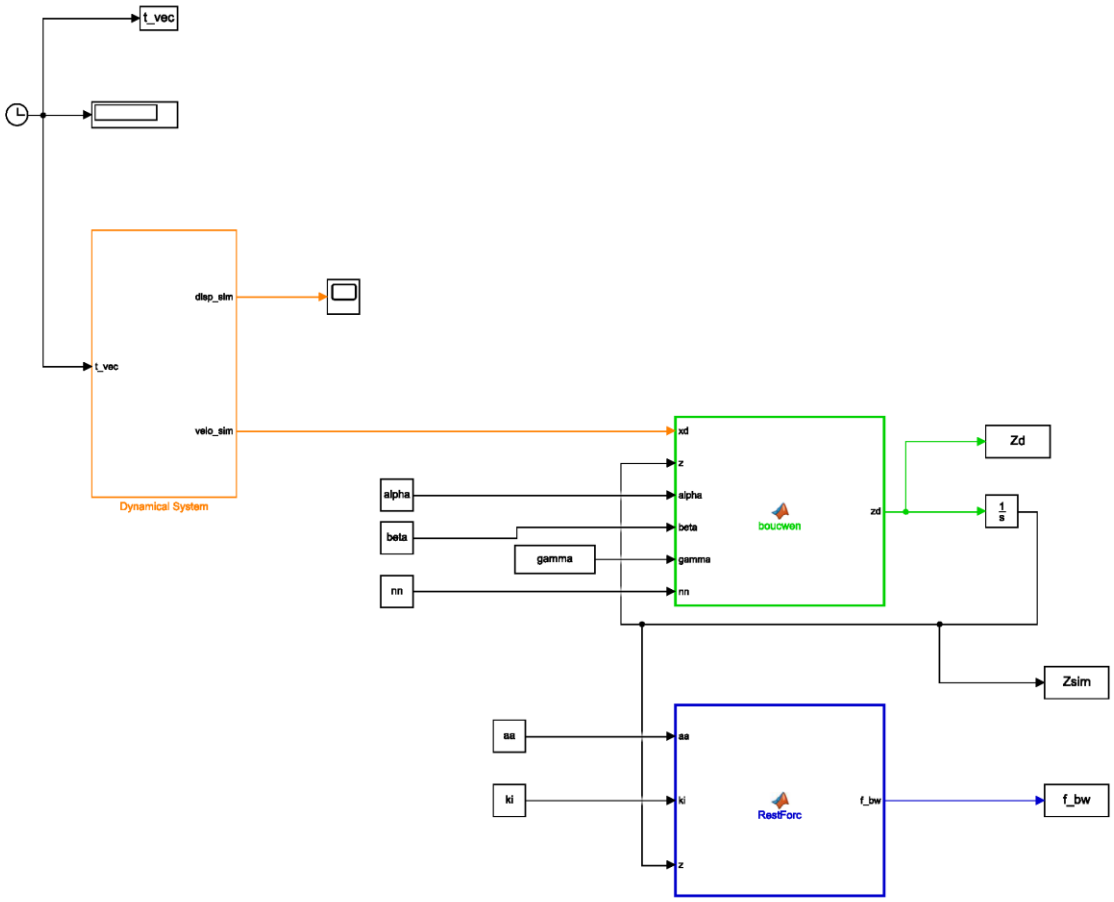

Figure 3: Illustrative model in SIMULINK.

In figure 4, it shows the sample results obtained from SIMULINK of the nonlinear model. This figure gives an idea how the system starts and goes into the steady-state level. However, it needs to be mentioned that the systems switching into steady state (see figure 4 (left)) situation fast, because the simulation is conducted for 5 seconds only (can be seen in figure 5).

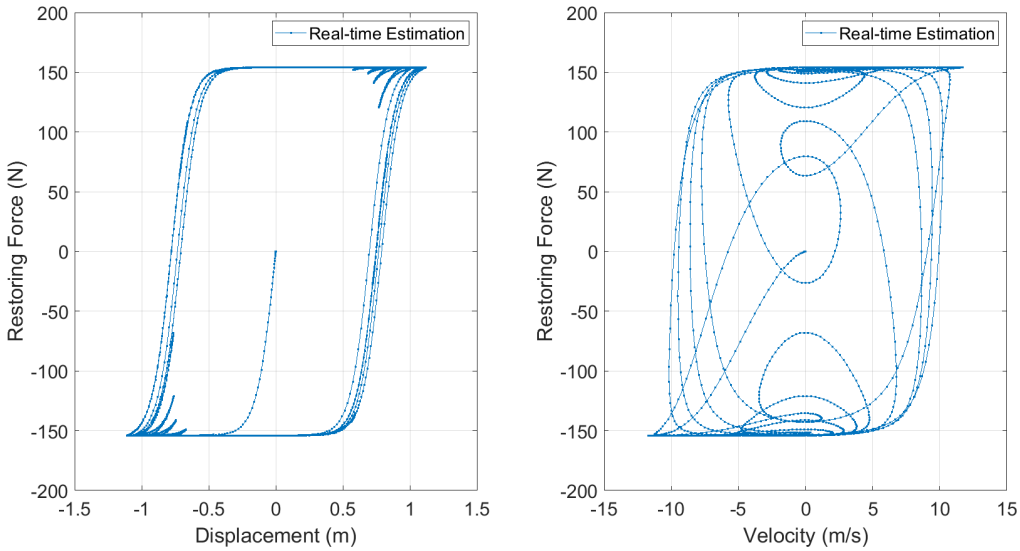

Figure 4: The real-time results: restoring force as a function of displacement (left) and velocity (right).

3.3 Results Comparison

For the comparison, the offline simulations are carried out by using MATLAB while the real-time simulations are performed via SIMULINK. In general, the offline simulation requires a longer time to complete the simulations in comparison to the real-time implementations e.g. SIMULINK. However, it also needs to be mentioned that this may not be true for all of the cases, as there will be many parameters those will control the overall simulation performance i.e., the complexity of the model itself, discretization, and ability of the used computer. The outcome of the offline and real-time results is compared in this section. Firstly, the displacement trajectory is compared in figure 5, it can be noticed that both the offline and real-time simulations results are almost identical.

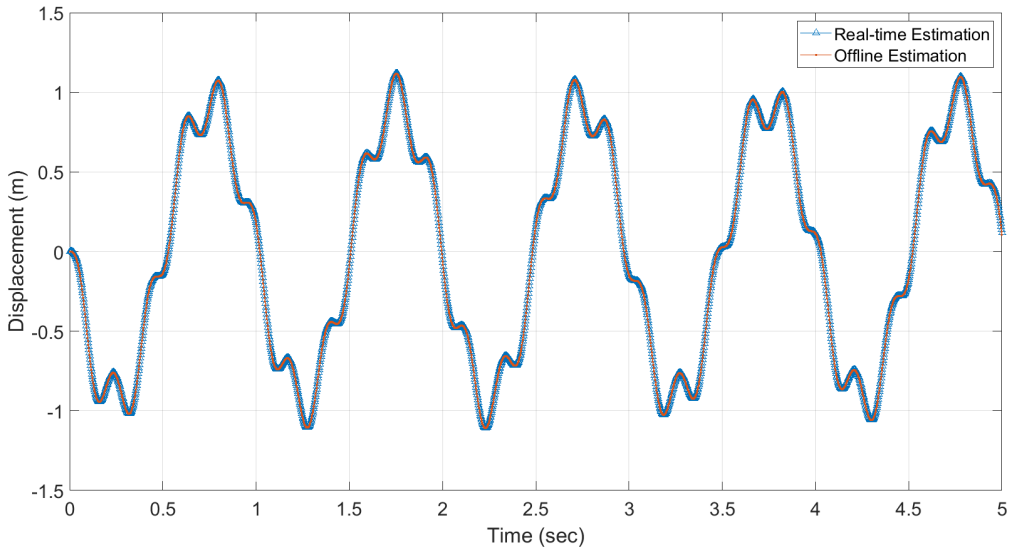

Figure 5: The full-time history of displacement.

However, even though, in the displacement trajectory, they agreed quite well that does not guarantee their hysteretic behavior with respect to the estimated restoring force. Moreover, this what can be seen in figure 6, where the restoring force hysteresis as a function of displacement is presented. In addition, it is even more visible in figure 7, where the restoring force hysteresis versus velocity is exhibited.

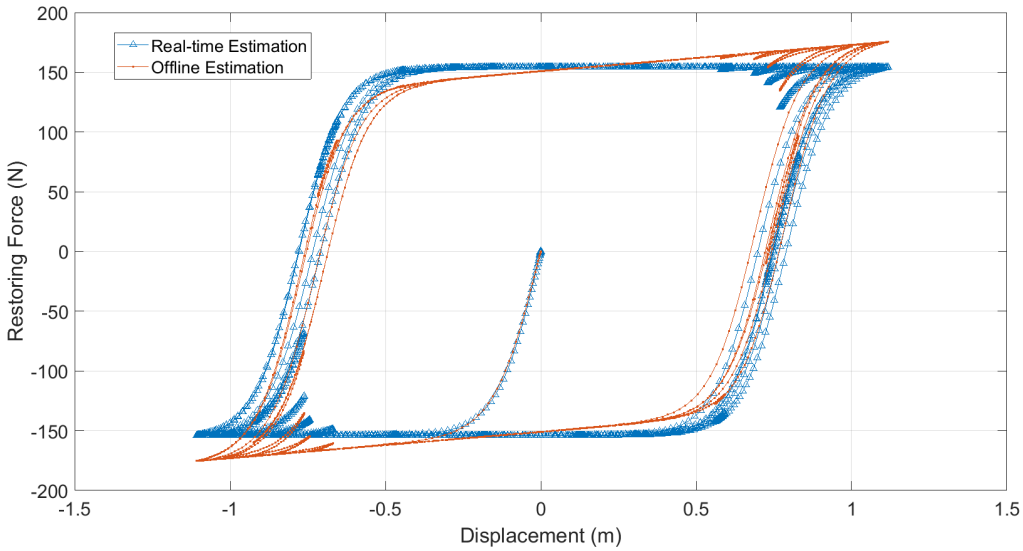

Figure 6: Restoring force hysteresis versus displacement..

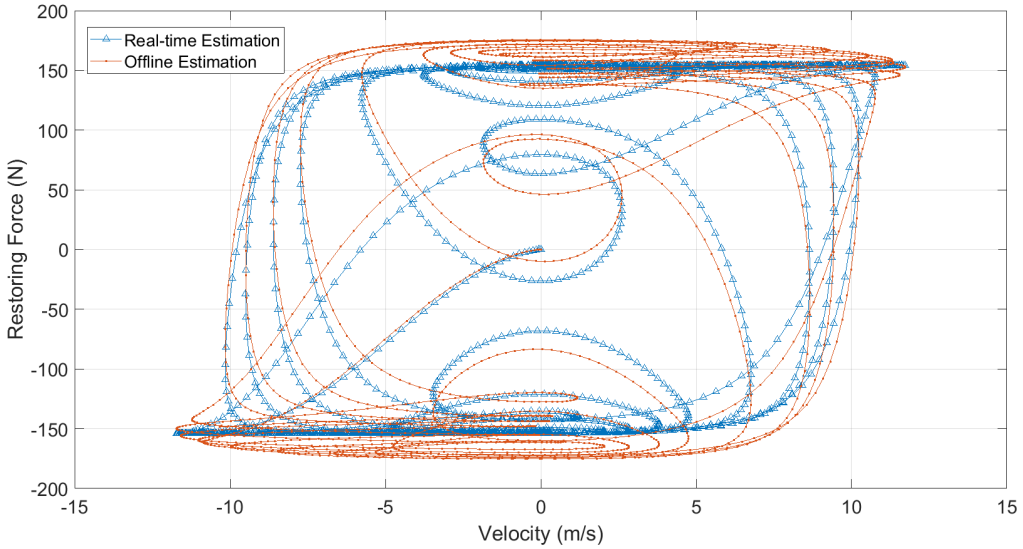

Figure 7: Evolution of restoring force hysteresis as a function of velocity.

Finally, the time-history of the restoring force is presented in figure 8. Moreover, from this figure, it can be clearly seen that indeed there is a little discrepancy between the offline and real-time estimation, especially, in the area of the peaks. In addition, this is what might be very important for the real-time implementations, as even such small error may create overall monitoring problem. Because the aforementioned error will then trigger the response of the systems.

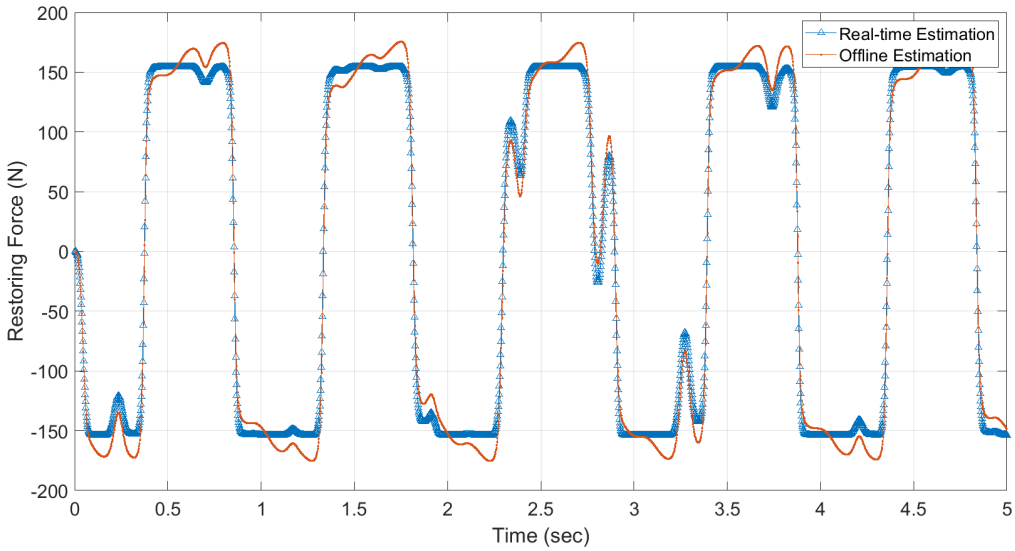

Figure 8: Time-history of the restoring force.

4. CONCLUSIONS

Present study investigates the possibility of real-time modeling of nonlinear behavior via the use of Bouc-Wen model. The preliminary results show the potential of real-time modeling of smart type materials e.g. magnetorheological fluid which later can be implemented for the real-time vibration mitigation and control applications. The real-time performance is compared with the offline response. In addition, the outcome shows that both options can be suitable for modeling nonlinear behavior. However, as modern devices are needed to be operated in real-time, hence, the real-time model is inevitable. In order to be optimal in terms of overall performance, further study is essential to optimize the parameters of the adopted nonlinear model for more complex type behavior.

ACKNOWLEDGEMENTS

The author would like to thank the fund provider the German Research Funding Organization, DFG. This work is sponsored by the grant number F-003661-553-A1G-1140901 of TU Dresden's Institutional Strategy, Technische Universität Dresden - TU Dresden, Dresden, Germany.

REFERENCES

Bouc, R. (1967). "Forced vibration of mechanical systems with hysteresis". Proceedings of the Fourth Conference on Nonlinear Oscillation. Prague, Czechoslovakia. 315.

Baber, T.T. and Noori, M.N. (1985). Random vibration of degrading pinching systems. *Journal of Engineering Mechanics*, *111*(8), 1010–1026.

Baber, T. T. and Noori, M. N. (1986). Modeling general hysteresis behaviour and random vibration applications. *Journal of Vibration, Acoustics, Stress, and Reliability in Design*, *108*(4), 411–420.

Bhowmik, S. (2011). *Modelling and Control of Magnetorheological Damper: Real-time implementation and experimental verification*, Technical University of Denmark, Lyngby, Denmark.

Charalampakis, A. E., Koumousis, V. K. (2008). On the response and dissipated energy of Bouc–Wen hysteretic model. *Journal of Sound and Vibration*, *309*(3–5), 887–895.

Charalampakis, A. E., Koumousis, V. K. (2009). A Bouc–Wen model compatible with plasticity postulates. *Journal of Sound and Vibration*, *322*(4–5), 954–968.

Kottari, A. K., Charalampakis, A. E., and Koumousis, V. K. (2014). A consistent degrading Bouc-Wen model. *Engineering Structures*, *60*(February), 235–240.

Miah, M. S., Chatzi, E. N., Dertimanis, V. K., and Weber, F. (2017) Real-time experimental validation of a novel semi-active control scheme for vibration mitigation, *Structural Control Health Monitoring*, 24: e1878.

Miah, M. S., Chatzi, E. N., and Weber, F. (2013). Semi-active control of structural systems with uncertainties using an unscented Kalman filter, *Research and Applications in Structural Engineering, Mechanics and Computation*, Edited by Alphose Zingoni, CRC Press, 61-66.

Miah, M. S. (2015). *Semi-active control for magnetorheological dampers via coupling of system identification methods*. ETH-Zürich, Zurich, Switzerland, 22776.

Miah, M. S., Chatzi, E. N., and Weber, F. (2014). MR Damper based Vibration Mitigation using a Bouc-Wen Model and a Nonlinear Observer. In J. Rodellar, A. Güemes, and F. Pozo (Eds.), Sixth World Conference on Structural Control and Monitoring, Barcelona, Spain, 1185–1194.

Miah, M. S., Chatzi, E. N., Dertimanis, V. K., and Weber, F. (2015). Nonlinear modeling of a rotational MR damper via an enhanced Bouc–Wen model. *Smart Materials and Structures*, *24*(10), 105020.

Song, J., and Der Kiureghian, A. (2006). Generalized Bouc–Wen model for highly asymmetric hysteresis. *Journal of Engineering Mechanics*, *132*(6), 610–618.

Wen, Y. K. (1976). Method for random vibration of hysteretic systems. *Journal of Engineering Mechanics, 102*(2), 249–263.

Proceedings of the 5th International Conference on Civil Engineering for Sustainable Development (ICCESD 2020), 7~9 February 2020, KUET, Khulna, Bangladesh (ISBN-978-984-34-8764-3)

MECHANICAL PROPERTIES OF HIGH-STRENGTH MORTAR MADE WITH INDUCTION FURNACE STEEL SLAG AS FINE AGGREGATE

Md Jihad Miah*[1], Mohammad S. Miah[1,2] and Md. Munir Hossain Patoary[3]

[1]Assistant Professor, University of Asia Pacific, Bangladesh, Email: jihad.miah@uap-bd.edu
[2]Visiting Scientist, Technische Universität Dresden-TU Dresden, 01187 Dresden, Germany, Email: mohammad_shamim.miah@tu-dresden.de & mshamim@uap-bd.edu
[3]Postgraduate Student, University of Asia Pacific, Department of Civil Engineering, Dhaka-1215, Bangladesh. E-mail: 3dcometdesign@gmail.com

***Corresponding Author**

ABSTRACT

Induction furnace steel slag as fine aggregate is a waste material produced during crushing the steel slag boulders to make coarse aggregate. Utilization of this waste as fine aggregate will reduce the demand for natural river sand (NRS) in the concrete construction works, and can play an important role in the sustainability of construction material in Bangladesh, as well as around the world. Within this context, this research work presents an experimental investigation on the physical and mechanical properties of high-strength mortar (HSM) made with three different replacement percentages (0%, 50% and 100%) of NRS by steel slag fine aggregate (SSFA). The cube specimens (50 mm x 50 mm x 50 mm) for compression and briquet specimens for tension tests are prepared at 7days, 14 days and 28 days. The failure mechanism of HSM under compression and tension is discussed as well. Furthermore, the dry density of mortar is also measured on the specimens that have been used for the compression test. The weight basis mix design with water to cement ratio of 0.3 and sand to cement ratio of 1.5 are used for all mortar mixes. The experimental results have shown that the compressive strength of mortar blocks made with SSFA is significantly higher as compared to mortar blocks made with 100% NRS. The average compressive strength of mortar tested at 28 days of 0%, 50% and 100% SSFA are, respectively, 49.6 MPa (7200 psi), 57.7 MPa (8370 psi) and 58.3 MPa (8450 psi). The compressive strength of mortar made with 100% SSFA at 7 days, 14 days and 28 days are on average 46%, 20% and 18%, respectively, higher than the mortar made with 100% NRS. The tensile strength of mortar is significantly higher for SSFA than NRS, which is 41% higher for mortar made with 100% SSFA than 100% NRS. This behavior could be attributed to higher surface texture, higher angularity and excellent surface roughness of SSFA than NRS. By contrast, the reduction in workability is observed for mortar containing SSFA than NRS due to higher angularity of SSFA and a bit higher temperature of fresh mortar at the time of placing. Moreover, it is shown that the density of mortar increases with the increased replacement percentage of NRS by SSFA, probably due to higher specific gravity (3.24 for SSFA and 2.56 for NRS) and better interlocking of cement paste with SSFA than NRS. Based on the results presented herein, it is demonstrated that SSFA can be used as a full replacement of NRS, which will not save money and energy, it will also solve the disposal problem, reduce the demand for natural fine aggregate.

Keywords: *Induction furnace steel slag, High-strength mortar, Compressive strength, Tensile strength, Density.*

1. INTRODUCTION

In South Asia, some countries like Bangladesh has very limited availability of natural aggregates due to geological features to build concrete structures and infrastructures. Therefore, the concrete industry mostly depends on burnt clay brick aggregate due to very limited availability of natural stones (Miah et al., 2019), which harms the environment (increases CO_2 in the air). Concrete is commonly used construction building materials in the globe, where fine aggregate has a significant role to provide strength and durability as well as the price of concrete. Typically, fine aggregate occupies about 20-30% of the total volume of concrete, and it is the second most important component of concrete after coarse aggregate since it helps to improve the various properties of concrete or mortar such as reducing the shrinkage, provide workability, volume stability, strength by filling the voids and durability to the concrete. Furthermore, fine aggregate is used to make brickwork, plastering, repairing work and retrofitting (e.g., ferrocement mortar).

In Bangladesh, natural river sand (NRS) as fine aggregate is mainly used which is limited, and the demand for sand is increasing due to the booming of the construction in Bangladesh. At the same time, the demand for other materials such as steel and iron are also increasing which increasing the waste materials as well. If this waste can be used in construction that will resolve the disposal problem, reduce the demand for new aggregates and reduce the cost and energy. This present study investigates the utilization of the induction steel slag as fine aggregate instead of NRS, which is the by-product of the steel manufacturing process. In the literature, it is shown that using this material has better mechanical properties, cost-effective and environment-friendly. The mechanical properties of concrete made with different replacement percentages (0%, 10%, 20%, 30%, 40%, 60%, 80% and 100%) of natural fine aggregate (NFA) by SSFA was investigated (Guo et al., 2019). The authors found that the compressive strength and toughness were higher for the concrete made with SSFA than the NFA. Another study showed that the incorporation of SSFA as a replacement of NFA improves the compressive strength and modulus of elasticity of concrete (Guo et al., 201). Though all the replacement percentage of NFA by SSFA has higher strength as compared to reference concrete, the optimum percentage of SSFA for the compressive strength of concrete is 20%. Moreover, the mechanical and microstructure of mortar made with four different replacement percentages (0%, 25%, 50%, 75% and 100%) of NFA by SSFA were investigated (Santamaría-Vicario et al., 2015). It was found that the compressive and flexural performance of mortar made with SSFA was increased with the replacement percentage of NFA. By contrast, a bit higher dry density of mortar made with SSFA was observed as compared to NFA. Similarly, it was observed that the incorporation of slag fine aggregate enhances the compressive, tensile and flexural strength of concrete (Devi and Gnanavel, 2014). Furthermore, it was found that the compressive and flexural strength of concrete increases with for all concrete mixes made with SSFA (Qasrawi et al., 2009).

Though a number of researchers found that the concrete made with SSFA has superior mechanical performances as compared to NFA, in Bangladesh, almost no investigation has been conducted yet on the physical and mechanical properties of high-strength mortar (HSM) made with induction furnace SSA as replacement of NRS. This HSM could be used in ferrocement technique and repairing work. Indeed, the mechanical properties of ferrocement mortar have a significant role to enhance the global performance of the retrofitted structure and the durability performance (corrosion) of ferrocement due to its lower net cover and higher surface area of the steel wire mesh. To do this end, comprehensive experimental studies are conducted on the possibility of using induction furnace steel slag as fine aggregate as a replacement of NRS. This research work aims to investigate the physical and mechanical (i.e., compressive and tensile strength) properties of HSM made with three different replacement percentages (0%, 50% and 100%) of NRS by SSFA.

2. EXPERIMENTAL INVESTIGATIONS

Two types of fine aggregates (Sylhet sand and SSFA) have been used in this study. Steel slag is a solid waste from the steel production industry. The steel slag chunks are collected from the local steel

manufacturing company. During crushing the steel chunk to make coarse aggregate, fine dust is produced as well which has been used as fine aggregate in this study. The image of steel slag chunks and steel slag fine aggregate are presented in Figure 1. Both fine aggregates (natural river sand known as Sylhet sand: NRS, and steel slag fine aggregate: SSFA) are tested for grading, specific gravity and absorption capacity as per ASTM C136 and ASTM C128 standards, respectively. The specific gravity, absorption capacity and fineness modulus are 3.24, 1.0 and 3.04 for SSFA, respectively, and 2.56, 3.1 and 2.86 for NRS, accordingly. The sieve analysis of SSFA and NRS is presented in Figure 2. The weight basis mix design with water to cement ratio of 0.3, sand to cement ratio of 1.5 and air content of 2% are used for all mortar mixes. Since the water to cement ratio is lower, superplasticizer as a chemical admixture is used (0.5% by mass of total cement) to provide the workability of fresh mortar. To investigate the effect of SSFA on HSM, three different replacement percentages (0, 50% and 100%) of NRS by SSFA are used. The cube specimens (50 mm x 50 mm x 50 mm) are made to perform the uniaxial compression test of mortar as per the ASTM C109 standard. While the briquette specimens are used for the tensile strength test of mortar as per the ASTM C307 standard. The evaluation of compressive and tensile strength of mortar was investigated at 7, 14 and 28 days. The dry density of mortar was also measured on the specimens that have been used for the compression test.

Figure 1: Steel slag chunks (left) and steel slag fine aggregate (right), respectively.

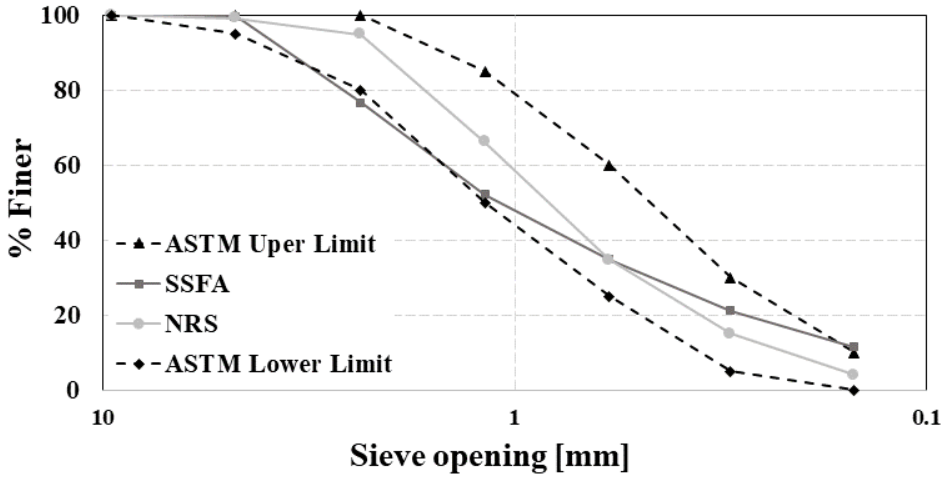

Figure 2: Grading curve of Sylhet sand (NRS) and SSFA, and comparison with the ASTM upper and lower limit.

3. EXPERIMENTAL RESULTS AND DISCUSSIONS

3.1 Physical properties of fine aggregates

The specific gravity of SSFA is higher than the NRS (3.24 for SSFA and 2.56 for NRS), which could be responsible for the higher percentage of Fe_2O_3 of steel slag since it is the by-product of the steel manufacturing process, and that could provide a higher density of mortar. By contrast, significant lower absorption capacity (1% for SSFA and 3.1 for SSFA) is observed for SSFA than NRS, which implies that the mortar made with SSFA will absorb less water which is good for those structures which are exposed to water like the exterior wall, roof, repairing/strengthening structural elements, etc. This lower absorption capacity will delay the time of corrosion of steel reinforcement/steel wire mesh of ferrocement (the surface area of steel wire mesh is quite high) due to lower penetration and absorption of water. The closer visual observation showed that SSFA is highly angular in shape, sharp edges and has a higher rough surface texture than NRS, resulting in better interlocking in the mix that provides higher strength.

3.2 Fresh mortar properties

The mortar made with SSFA has lower workability than the NRS. The slump values of mortar made with 0%, 50% and 100% SSFA are 23 mm, 19 mm and 13 mm respectively. This behavior could be due to higher angular in shape, sharp edges and rough surface texture of SSFA than NRS, resulting in the reduction of the mobility of fresh mortar due to better interlocking in the mix. Similar results are found in the literature (Devi and Gnanavel, 2014; Qasrawi et al., 2009). This could be also linked to the concrete temperature at the time of placing. It is observed that the temperature of the fresh mortar at the time of placement is a bit higher for SSFA than NRS.

3.3 Mechanical properties

The compressive strength of mortar made with three different replacement percentages of NRS (Sylhet sand) by SSFA was conducted at 7, 14 and 28 days and presented in Figure 3. For every data set, three cubic mortar blocks are performed and then the average value is calculated. It is seen that the mortar made with SSFA has higher compressive strength at all curing ages as compared to 100% NRS. None of the specimens showed lower compressive strength as compared to the mortar blocks made with 100% NRS. The average compressive strength of mortar tested at 28 days of 0%, 50% and 100% SSFA are, respectively, 49.6 MPa, 57.7 MPa and 58.3 MPa. The higher compressive strength of concrete made with SSFA could be attributed to higher strength, coarser particle, higher angularity and rough surface of SSFA than NRS, which provide stronger interfacial transition zone (ITZ) between SSFA and cement paste. Indeed, ITZ is the weakest path for the failure of mortar or concrete during mechanical loading. These results are consistent with the results available in the literature (Guo et al., 2019; Santamaría-Vicario et al., 2015; Qasrawi et al., 2009).

To better understanding the role of different percentages of SSFA on the compressive strength of mortar, normalized compressive strength is calculated by dividing the strength of cube made with 100% sand (0% NRS) and compared with the results found in the literature, see Figure 4. The experimental results showed that as the percentage of SSFA increased, the compressive strength of mortar increased. At 7 days, a significant strength increment is observed for 100% SSFA as compared to other ages. The compressive strength of mortar made with 100% SSFA at 7, 14 and 28 days are on average 46%, 20% and 18% respectively higher than the mortar made with 100% NRS. The analysis of fractured surfaces of mortar specimens after compressive strength tests (see Figure 5a-c) showed that the failure plane passes through the SSFA and cement mortar. This failure pattern confirmed the stronger ITZ between the aggregate and cement paste.

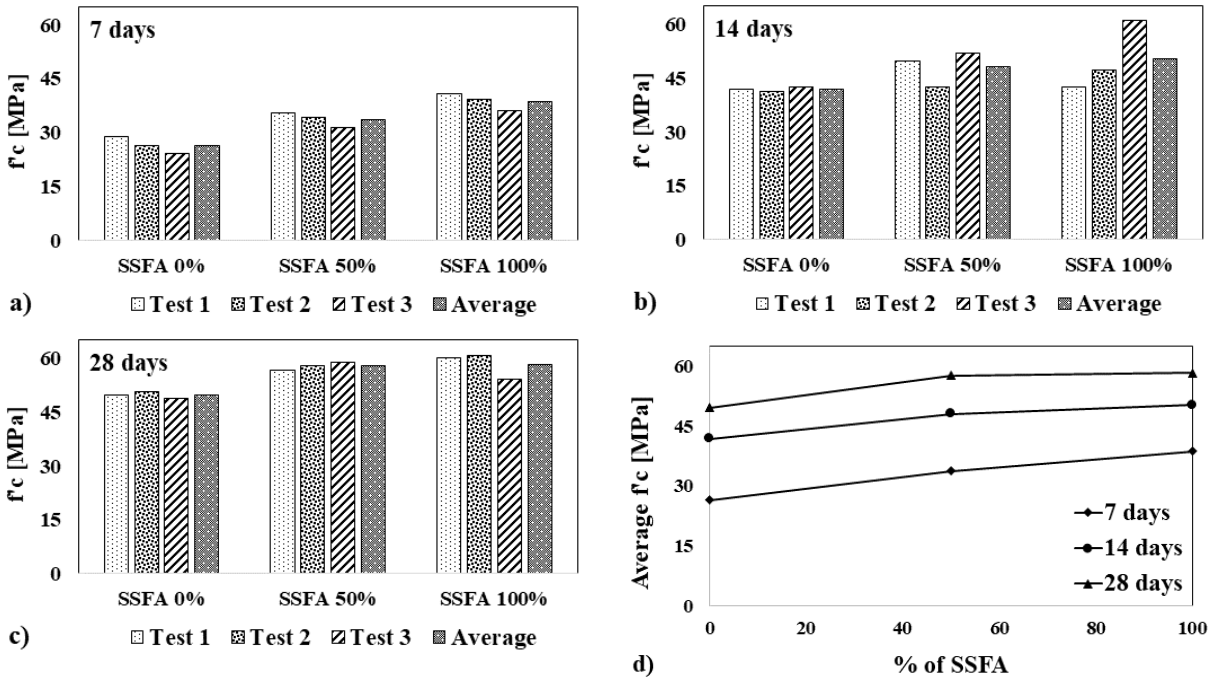

Figure 3: Compressive strength (f′c) of mortar conducted at 7, 14 and 28 days.

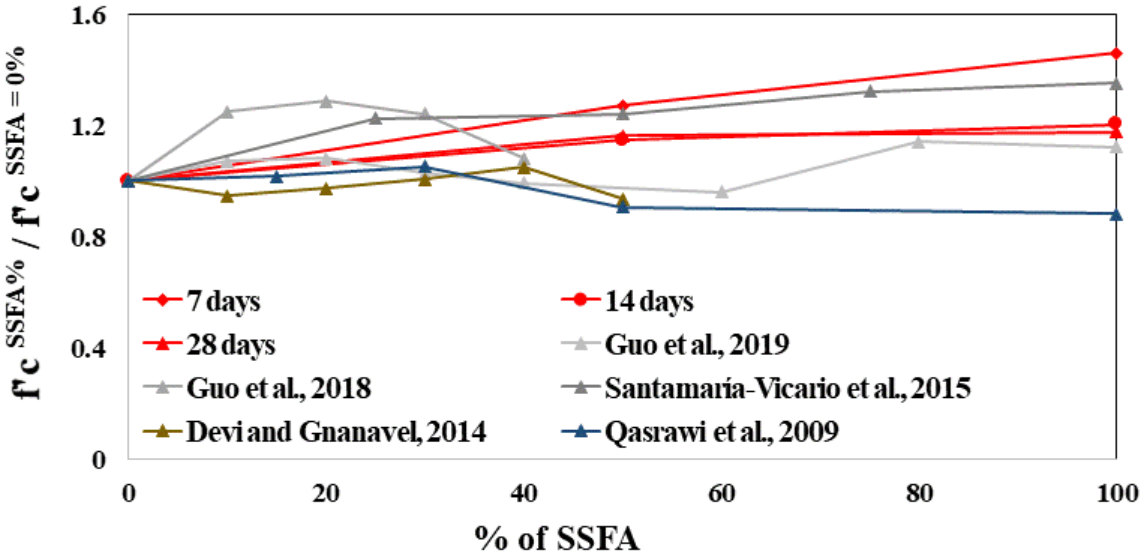

Figure 4: Normalized compressive strength of concrete mixes are compared with other results found in the literature.

It is observed that the experimental results are in good agreement with the results found in the literature. Most of the researchers found similarities with this experimental work. This high strength mortar made with SSFA provides a better future direction for the strengthening/repairing of the structures. In Bangladesh, ferrocement is commonly used for retrofitting due to available material and cost-effectiveness where the strength of the mortar plays an important role (Miah et al., 2019). Further, micro concrete or ultra-high performance concrete/mortar is needed to build highrise building, foundation and infrastructures where aggregates play a vital role in terms of strength and durability. Based on the results presented in this paper, this high strength mortar could be used in the ferrocement technique which will not provide higher strength, it will also provide better bonds among mortar, steel wear mesh and parent concrete.

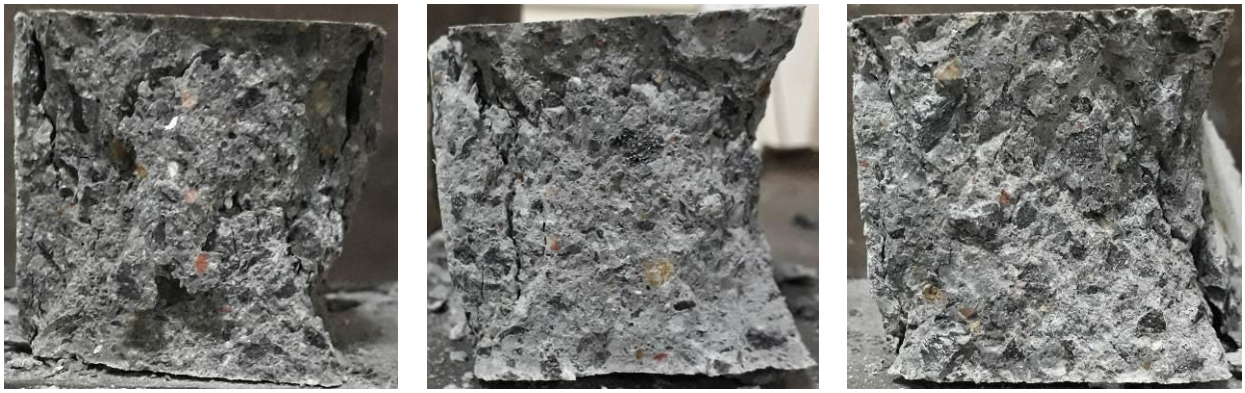

a) 0% SSFA for f'c test b) 50% SSFA for f'c test c) 100% SSFA for f'c test

d) 0% SSFA for f't test e) 100% SSFA for f't test

Figure 5: Fracture pattern of the cubes for compression (a-c) and briquette for tension (d-e) tests, respectively.

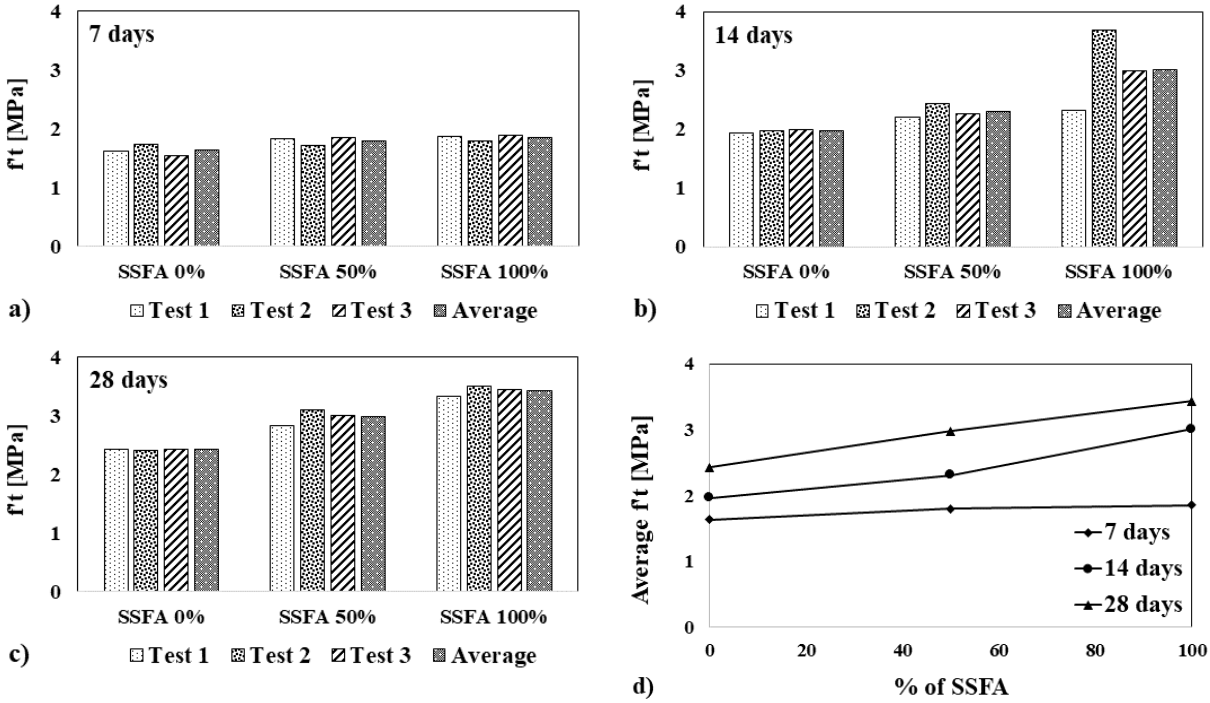

Figure 6: Tensile strength (f't) of mortar performed at 7, 14 and 28 days.

The tensile strength of mortar mixes made with different replacement percentages of NRS by SSFA is presented in Figure 6. It is seen that the tensile strength increases with the increasing percentage of

SSFA for all curing ages, which is in good agreement with the results of the compressive strength as discussed above. The tensile strength of mortar made with 0% SSFA, 50% SSFA and 100% SSFA are, respectively, 2.4 MPa, 3.0 MPa and 3.4 at 28 days, which increases the tensile strength up to 41% for the mortar when the NRS is fully replaced by SSFA. These results are consistent with the results available in the literature (Devi and Gnanavel, 2014; Qasrawi et al., 2009). As described briefly above, this higher tensile strength of mortar made with SSFA could be linked to higher strength, higher angularity and excellent surface roughness of SSFA than the NRS which ensured strong ITZ around the SSFA than the NRS. It is noted that the combined (cement mortar and aggregate) failure occurs for mortar made with SSFA (see Figure 5d-e). It is also seen that the mortar made with SSFA is more dense, less void, while some big voids are visible in mortar made with NRS, which allows lower mechanical load than SSFA mortar.

The dry density of mortar made with different replacement percentages of NRS by SSFA was measured at 7, 14 and 28 days and presented in Figure 7a-c. To better understand the effect of SSFA on dry density, Figure 7d is drawn with the average density as a function of % of SSFA. It is shown that the density of mortar is increased with the increasing replacement percentage of NRS by SSFA. The dry density of mortar made with 0% SSFA, 50% SSFA and 100% SSFA are, respectively, 2393 kg/m^3, 2572 kg/m^3 and 2809 kg/m^3 at 28 days. This higher density of mortar made with SSFA is directly linked with the higher specific gravity (3.24 for SSFA and 2.56 for NRS) and better interlocking of cement paste with SSFA than NRS. It should be noted that the compressive and tensile strength of mortar made with SSFA are significantly higher than NRS which increases the dry density of mortar. The higher density of concrete/mortar made with SSFA was also reported by other researchers in the literature (Santamaría-Vicario et al., 2015).

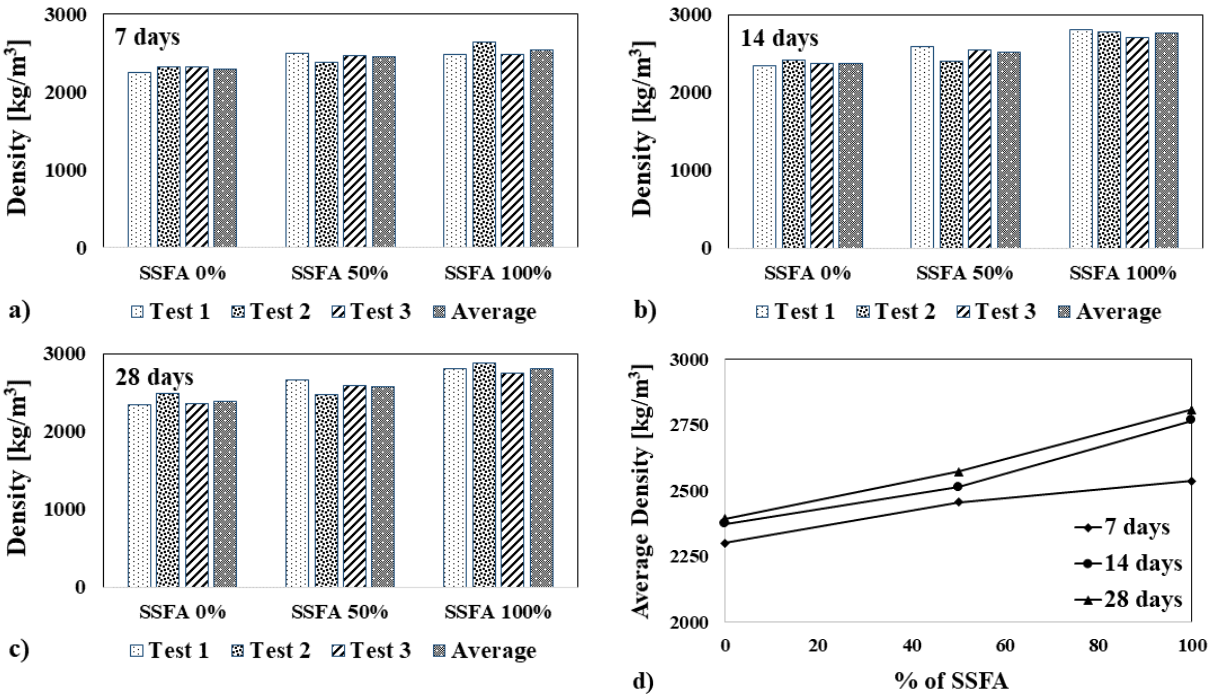

Figure 7: Dry density of mortar made with different replacement percentage of NRS by SSFA.

4. CONCLUSIONS

This paper investigates the physical and mechanical properties of mortar made with three different replacement percentage of NRS by SSFA. The cube specimens were made to perform compression tests and briquette specimens for the tensile test. The dry density of the mortar mixes was measured on the cube specimens which has been used for the compression test. Based on the results presented herein, the following conclusions can be drawn:

I. The compressive strength of mortar blocks made with SSFA is significantly higher as compared to mortar blocks made with 100% NRS. The compressive strength of mortar made with 100% SSFA at 7, 14 and 28 days are on average 46%, 20% and 18%, respectively, higher than the mortar made with 100% NRS.
II. The tensile strength of mortar is significantly higher for SSFA than NRS, which is about 41% higher for mortar made with 100% SSFA than 100% NRS.
III. Lower workability is noticed for the mortar made with SSFA than NRS, which could be attributed to the higher rough surface texture and better interlocking due to higher angularity of SSFA than NRS.
IV. The application of SSFA mortar could be more effective for the repairing work and the strengthening of the structures (e.g., ferrocement technique) since the strength of mortar is the key parameter that could enhance the global performance of the structures. Also, the mortar made with SSFA will prevent water penetration due to lower water absorption capacity of SSFA, which reduce corrosion and increase durability.

This study is limited to the evaluation of the compressive and tensile strength of the mortar. Other properties such as flexural strength and durability tests such as porosity, water absorption capacity and fire behavior of mortar need to be carried out. The outcome of this research project will encourage steel making industry to utilize the steel by-product in the concrete industry which are cost-effective and sustainable construction material since natural river sand is limited which is mostly extracted from the riverbed by dredging.

ACKNOWLEDGEMENTS

The authors acknowledge funding and facilities provided by the Institute for Energy, Environment, Research and Development (Ref: IEERD/AC/18) and Department of Civil Engineering, University of Asia Pacific to undertake this research study.

REFERENCES

Miah, M.J., Miah, M.S., Alam, W.B., Lo Monte, F., & Li, Y. (2019). Strengthening of RC beams by ferrocement made with unconventional concrete. *Magazine of Civil Engineering, 89*(5), 94-105.

Guo, Y., Xie, J., Zhao, J., & Zuo, K. (2019). Utilization of unprocessed steel slag as fine aggregate in normal- and high-strength concrete. *Construction and Building Materials, 204*, 41–49.

Guo, Y., Xie, J., Zheng, W., & Li, J. (2018). Effects of steel slag as fine aggregate on static and impact behaviours of concrete. *Construction and Building Materials, 192*, 194–201.

Santamaría-Vicario, I., Rodríguez, A., Gutiérrez-González, S., & Calderón, V. (2015). Design of masonry mortars fabricated concurrently with different steel slag aggregates. *Construction and Building Materials, 95*, 197–206.

Devi, V.S., & Gnanavel, B.K. (2014). Properties of concrete manufactured using steel slag. *Procedia Engineering, 97*, 95 – 104.

Qasrawi, H., Shalabi, F., & Asi, I. (2009). Use of low CaO unprocessed steel slag in concrete as fine aggregate. *Construction and Building Materials, 23*, 1118–1125.

ASTM C136/C136M-14. (2014). Standard Test Method for Sieve Analysis of Fine and Coarse Aggregates. *ASTM International, West Conshohocken*, PA, www.astm.org.

ASTM C128-15. (2015). Standard Test Method for Relative Density (Specific Gravity) and Absorption of Fine Aggregate. *ASTM International, West Conshohocken*, PA, www.astm.org.

ASTM C109/C109M-16a. (2016). Standard Test Method for Compressive Strength of Hydraulic Cement Mortars (Using 2-in. or [50-mm] Cube Specimens). *ASTM International, West Conshohocken*, PA, www.astm.org.

ASTM C307-18. (2018). Standard Test Method for Tensile Strength of Chemical-Resistant Mortar, Grouts, and Monolithic Surfacings. *ASTM International, West Conshohocken*, PA, www.astm.org.

Proceedings of the 5th International Conference on Civil Engineering for Sustainable Development (ICCESD 2020), 7~9 February 2020, KUET, Khulna, Bangladesh (ISBN-978-984-34-8764-3)

SEISMIC BEHAVIOR OF CONCRETE BRIDGE PIERS OF DIFFERENT DIMENSIONS

Ahmed Farhan Ahnaf Siddique*[1] and Tahsin Reza Hossain[2]

[1]Lecturer, Department of Civil Engineering, BUET, Bangladesh, e-mail: ahnafrcs2011@gmail.com
[2]Professor, Department of Civil Engineering, BUET, Bangladesh, e-mail: tahsin.hossain@gmail.com

***Corresponding Author**

ABSTRACT

Bridges are vital structures for a country, failure of any of them would be devastating. Situated at the northwestern end of the Indo-Australian plate, Bangladesh lies in a seismically active region where several destructive earthquakes have occurred historically and in recent times which is alarming for the bridge designers.

The local Code, BNBC (2017), is intended to aid building design. However, the available earthquake parameters in BNBC can be rationally applied to determine the seismic forces on bridges. The structural design and seismic performance evaluation of bridges of different pier heights located in high seismic zone of Bangladesh have been done following the AASHTO (2011, 2012) specifications in this study.

The contribution of earthquake forces decrease for bridges of higher pier heights as these bridges tend to have higher fundamental time periods compared to shorter pier bridges. Longer pier height bridges also have higher flexibility which increases its deflection capacity.

Bridges designed by the force based concept fails to determine the nonlinear behavior which is required to predict the performance of a bridge under different levels of seismic events.

In this research, concrete bridges of varying pier heights have been designed by the force based concept of which the performance targets were checked by nonlinear static pushover analysis. All the bridges studied in this research satisfied the performance criteria in response to different levels of earthquake. However, the change in pier heights highly affects the seismic base shear on the bridges as well as the displacement demands and capacities of the piers which implies the importance of appropriate knowledge and application of earthquake engineering and also the necessity of performance based design.

Keywords: *Earthquake; Bridge Design Codes; Pier Dimension; Flexibility; Pushover.*

1. INTRODUCTION

Bangladesh lies at the northwestern end of the Indo-Australian plate, which has been subjected to the long-term process of subduction between the plate margins of Indo-Australian and Eurasian plates. As a result, several devastating earthquakes have occurred in this region over the time and it has been marked as a seismically active region. Subsequently, considerations of seismic effects on structures became essential for structural engineers as well as the architects and the users. The increased number of occurrences of earthquake events in the recent times is so alarming for the engineers that it has drawn special attention and provisions for earthquake engineering (Indian Institute of Technology, Kanpur, 2002).

However, the design Code followed in Bangladesh, namely BNBC (2017), does not provide any guideline to the engineers regarding the design and construction of highway bridges as it mainly focuses on the design and construction of buildings. Alternatively, bridges are popularly designed following the specifications provided by AASHTO (2011, 2012).

The seismic force determining parameters used in AASHTO specifications are more suited for regions within and around the United States of America. The earthquake forces and all other related parameters should represent the earthquake events occurring in Bangladesh which is already available in the BNBC. Therefore, it is more rational to apply the BNBC to determine earthquake forces and follow the AASHTO guidelines to design a bridge in Bangladesh (Siddique, 2018).

The effect of earthquake on structures, especially as massive as a bridge, largely depends on the size and shape of the structure itself. Small structures are more affected, or shaken, by high frequency short and frequent waves. Whereas, large structures are more affected by long period or slow shaking (USGS, n.d.). Therefore, bridges with varying pier dimensions will affect its behavior under seismic events which is studied in this research. The bridges studied are two lane three span prestressed concrete I-girder bridges supported by intermediate piers on site class C located in Sylhet which is in seismic zone 4 according to BNBC.

Bridges are conventionally designed by linear static analysis, or the force-based design method which calculates the seismic force demands by equivalent static procedure, but it fails to determine the seismic behavior of the bridge under earthquake events. AASHTO clearly states the necessary methods of analysis for bridge design with respect to seismic design categories, seismic zonings and number of bridge spans to determine the seismic behavior of bridges under such events. Federal Highway Administration (2014) and Caltrans (2015) extensively describes the AASHTO guidelines for bridge design.

The current force-based design method has several shortcomings; the major limitation being that it cannot explicitly relate to the performance of the bridges as there are many uncertainties in achieving the expected level of performance. This method ignores the fact that displacement is more important than strength for inelastic structural components whereas it is the most direct reason that cause structural damages. In order to reduce the underlying uncertainties of force-based design method, researchers have developed the framework of performance based design (Zhang, 2015).

Therefore, whenever it is specified, undertaking the inelastic analysis of a bridge is more rational approach compared to the elastic analysis. In this research, pushover analysis method (nonlinear static procedure) have been followed to capture the inelastic behavior of structures under the action of seismic activity.

2. METHODOLOGY

The main focus of this study is to determine the seismic behavior of concrete bridges of varying pier dimensions designed as per AASHTO guidelines and considering the earthquake demand parameters of BNBC.

Piers are the interior supports of a bridge. The piers are designed for the loads that it requires to resist which includes the vertical loads coming from the dead and vehicular live loads along with the lateral loads coming from the seismic demand. Taly (1998) provided a detailed outline of the loads that are to be considered. The design forces shall be those determined for strength and extreme event limit states.

At the preliminary design stage, design strength interaction diagrams of trial sections are built and these are checked with the aforementioned design loads to be resisted. The loads were determined in accordance with the codes which has been reviewed extensively by Siddique (2018). However, this is the force-based design approach and it must be reviewed by performance evaluation later on.

In the performance-based approach, standard bridges, classified as "other bridges" by AASHTO, are designed with at least two hazard levels. At the lower hazard level, bridges are designed to achieve the target performance which is to remain essentially elastic for expected/serviceability earthquakes having a return period of 150 years. However, at the higher hazard level, collapse prevention of bridges must be assured for rare/maximum considered earthquakes having a return period of 2500 years. The performance requirements of bridges are shown in Table 2.1.

Table 2.1: Performance Requirements of Bridges for Different Hazard Levels

Bridge Operational Category	**Performance Requirement for Hazard Level**		
	Expected Earthquake	Design Earthquake	Maximum Considered Earthquake
Standard/Other	Immediate Occupancy	Collapse Prevention	Collapse Prevention
Essential	Immediate Occupancy	Immediate Occupancy	Collapse Prevention
Critical	Immediate Occupancy	Immediate Occupancy	Immediate Occupancy

The term "Immediate Occupancy" refers to the requirement that the bridge elements should remain essentially elastic immediately after the earthquake event. The term "Collapse Prevention" refers to the requirement that the bridge elements may sustain significant damage during the earthquake event and service may significantly disrupt, but life safety must be assured by collapse prevention. In such cases, the bridge may need to be replaced after a large earthquake.

2.1 Analysis Procedure to Determine Seismic Demand

Earthquake loads are given by the product of the elastic seismic response coefficient and the equivalent weight of the superstructure. The equivalent weight is a function of the actual weight and bridge configuration and is automatically included in both the single-mode and multimode methods of analysis. This is the equivalent static method to determine the earthquake loads according to BNBC. However, AASHTO provides a more detailed guideline about the seismic demand determination procedure which is discussed in this section. Minimum requirements for the selection of an analysis method to determine seismic demand may be taken as specified in Table 2.2 (AASHTO 2012).
Where, * = no seismic analysis required; UL = uniform load elastic method
SM = single-mode elastic method; MM = multimode elastic method
TH = time history method

Table 2.2: Minimum Analysis Requirements for Seismic Effects

Seismic Design Category	**Single-Span Bridges**	**Multispan Bridges**					
		Other Bridges		**Essential Bridges**		**Critical Bridges**	
		Regular	**Irregular**	**Regular**	**Irregular**	**Regular**	**Irregular**
A	No Seismic Analysis Required	*	*	*	*	*	*
B		SM/UL	SM	SM/UL	MM	MM	MM
C		SM/UL	MM	MM	MM	MM	TH
D		SM/UL	MM	MM	MM	TH	TH

However, multimode elastic method has been followed in this study. In order to do so, demand response spectrum have been developed as guided by BNBC, 2017. The considered seismic parameters have been provided in Table 2.3.

Table 2.3: Seismic Factors for Bridges Designed in Sylhet

Parameter	Description
Site class	SC
Soil factor, S	1.15
T_B	0.20 sec
T_C	0.60 sec
T_D	2.0 sec
Damping correction factor, η	1
Seismic zone coefficient, Z	0.36
Importance factor, I	1
Response modification factor, R	5

The Response spectrums have been developed based on these factors for expected earthquake (EE), design earthquake (DE), and maximum credible earthquake (MCE). Figure 2.1 shows the unmodified response spectrum for the bridge under consideration.

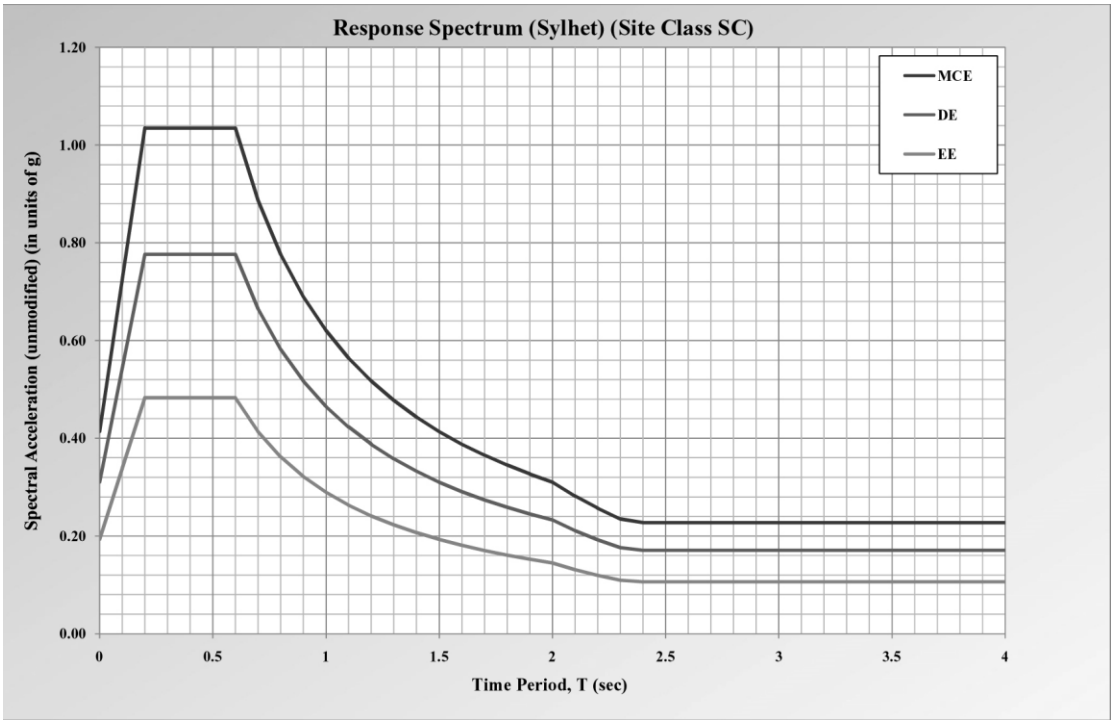

Figure 2.1: Unmodified Response Spectrum for SC Soil in Sylhet

The software runs a modal analysis to determine the time periods corresponding to the mode shapes of the bridge. Using these time periods, the software runs a response spectrum analysis to obtain the seismic forces. The unmodified response spectrum has been scaled according to the provisions of AASHTO.

2.1.1 Determination of Seismic Displacement Demand

The global seismic displacement demands were determined independently along two perpendicular axes, typically the longitudinal and transverse axes of the bridge. A combination of orthogonal seismic displacement demands shall be used to account for the directional uncertainty of earthquake motions and the simultaneous occurrences of earthquake forces in two perpendicular horizontal

directions (AASHTO, 2011). The seismic displacements resulting from analyses in the two perpendicular directions were combined to form two independent load cases as follows:

- Load Case 1: Obtained by adding 100 percent of the absolute value of the member seismic displacements resulting from the analysis in one of the perpendicular direction (longitudinal) to 30 percent of the absolute value of the corresponding member seismic displacements resulting from the analysis in the second perpendicular direction (transverse).
- Load Case 2: Obtained by adding 100 percent of the absolute value of the member seismic displacements resulting from the analysis in the second perpendicular direction (transverse) to 30 percent of the absolute value of the corresponding member seismic displacements resulting from the analysis in the first perpendicular direction (longitudinal).

The seismic demand displacements are obtained by running a response spectrum analysis for the demand response spectrum. The software generates demand displacements for X-direction and Y-direction using directional combination for a scale factor of 0.3. This is done to take into account the aforementioned directional load combinations.

2.2 Determination of Seismic Displacement Capacity

For piers, displacement capacity can be evaluated using a nonlinear static analysis procedure referred to as pushover analysis. Although it is recognized that force redistribution may occur as the displacement increases, particularly for frames with piers of different stiffness and strength, the objective of the capacity verification is to determine the maximum displacement capacity of each pier.

Nonlinear static procedure, or pushover analysis, is an incremental linear analysis method that captures the overall nonlinear behavior of the elements, including soil effects, by pushing them laterally to initiate plastic action. Each increment of loading pushes the frame laterally, through all possible stages, until the potential collapse mechanism is achieved. Because the analytical model used in the pushover analysis accounts for the redistribution of internal actions as components respond inelastically, pushover analysis is expected to provide a more realistic measure of behavior than may be obtained from elastic analysis procedures (AASHTO, 2011).

For the immediate occupancy criterion, the elastic displacement capacity is determined from the pushover curve obtained for "first hinge at limit state" bent failure criterion. The displacement capacity is the point on the curve after which the curve is no longer linear.

For the collapse prevention criterion, the ultimate displacement capacity of bent is determined from the pushover curve obtained for "pushover curve drop" bent failure criterion. The ultimate displacement capacity is determined as the displacement at which the base shear first drops from its absolute maximum in the pushover curve to a value 1% less than that maximum. The full pushover displacement is used if the base shear does not decrease 1% from the maximum.

2.3 Seismic Displacement Demand to Capacity Ratio for Bridges

The objective of the determination of the displacement demand and capacity is to check the performance of the bridge which is done by verifying that each bridge bent satisfies equation 2.1.

$$\Delta_D \leq \Delta_C \tag{2.1}$$

where,

Δ_D = displacement demand taken along the local principal axis of the ductile member.

Δ_C = displacement capacity taken along the local principal axis corresponding to Δ_D of the ductile member.

Therefore, the seismic displacement demand to capacity ratio must be less than 1 in order to satisfy the performance targets.

3. ANALYSIS, DESIGN, AND PERFORMANCE EVALUATION

The bridges considered are 350' long and 36' wide consisting of two 14' lanes located in Sylhet which lies in seismic zone 4 and seismic design category D. The bridge has 3 spans of lengths 100', 150', and 100' respectively. The bridge rests on abutments at its ends and is supported by intermediate bents in between. The superstructure consists of 8" thick deck slab laid on four 6' deep AASHTO type VI precast concrete I-girders which are simply supported at its bottom by abutments and bents. The bents consist of circular columns and 32'-6" long rectangular bent caps. The columns are assumed to be fixed supported at its base. The cross-sectional dimensions of bent caps and columns have been found through force-based design for each bridge. The bridge operational category is "Other" for the bridges. The performance targets of these bridges have been evaluated subsequently on the basis of BNBC and AASHTO guidelines as discussed before. The first, second, and third bridges consist of two 45', 55', and 65' long piers respectively in each bent. The fourth bridge consists of one 55' long pier in each bent. Modeling, analysis, design, and seismic performance evaluation of the bridges have been done using CSIBridge 19.2.0.

The following material properties have been used in this research.
Concrete strength for all members except girders, $f_c' = 4$ ksi
Modulus of elasticity of concrete for all members except girders, $E_c = 3605$ ksi
Concrete strength for girders, $f_c' = 6$ ksi
Modulus of elasticity of concrete for girders, $E_c = 4415$ ksi
Yield strength of reinforcing steel, $f_y = 60$ ksi
Modulus of elasticity of steel, $E_s = 29000$ ksi
Yield strength of prestressing steel tendons, $f_{py} = 243$ ksi
Ultimate strength of prestressing steel tendons, $f_{pu} = 270$ ksi
Modulus of elasticity of prestressing steel, $E_{ps} = 28500$ ksi

3.1 Bridge Consisting of Two 45' Long Columns Located in Sylhet

The forces due to dead load and design earthquake on each column base have been found to be **672.643 kips** and **67.91 kips** respectively. Design earthquake force on the column base is **10.1%** of the dead load coming on it.

The force-based design results show that the required circular column section is of **3'-6"** diameter with **2.76%** steel ratio which is provided using **39-#9** bars. The design is governed by extreme event I limit state. The lateral steel obtained from shear criterion does not govern over the minimum seismic criteria.

For this bridge, the results of performance evaluation through the determination of seismic displacement demands and capacities of the bents along with corresponding demand-capacity ratios have been provided in Table 3.1.

Table 3.1: Demand Capacity Ratios for 45' Long Column Bridge Located in Sylhet

Performance Target	Hazard Level	Direction	Demand (inches)	Capacity (inches)	Demand-Capacity Ratio
Immediate Occupancy	EE	Transverse	5.07"	5.68"	0.8929
Immediate Occupancy	EE	Longitudinal	5.11"	11.49"	0.4444
Collapse Prevention	MCE	Transverse	10.86"	11.17"	0.9722
Collapse Prevention	MCE	Longitudinal	10.94"	17.75"	0.6163

3.2 Bridge Consisting of Two 55' Long Columns Located in Sylhet

The forces due to dead load and design earthquake on each column base have been found to be **687.402 kips** and **50.832 kips** respectively. Design earthquake force on the column base is **7.4%** of the dead load coming on it.

The force based design results show that the required circular column section is of **3'-6"** diameter with **2.41%** steel ratio which is provided using **34-#9** bars. The design is governed by extreme event I limit state. The lateral steel obtained from shear criterion does not govern over the minimum seismic criteria.

For this bridge, the results of performance evaluation through the determination of seismic displacement demands and capacities of the bents along with corresponding demand-capacity ratios have been provided in Table 3.2.

Table 3.2: Demand Capacity Ratios for 55' Long Column Bridge Located in Sylhet

Performance Target	Hazard Level	Direction	Demand (inches)	Capacity (inches)	Demand-Capacity Ratio
Immediate Occupancy	EE	Transverse	6.81"	8.17"	0.8333
Immediate Occupancy	EE	Longitudinal	6.73"	17.71"	0.4019
Collapse Prevention	MCE	Transverse	14.58"	16.15"	0.9029
Collapse Prevention	MCE	Longitudinal	14.41"	26.47"	0.5445

3.3 Bridge Consisting of Two 65' Long Columns Located in Sylhet

The forces due to dead load and design earthquake on each column base have been found to be **719.847 kips** and **46.078 kips** respectively. Design earthquake force on the column base is **6.4%** of the dead load coming on it.

The force-based design results show that the required circular column section is of **3'-10"** diameter with **1.76%** steel ratio which is provided using **30-#9** bars. The design is governed by extreme event I limit state. The lateral steel obtained from shear criterion does not govern over the minimum seismic criteria.

For this bridge, the results of performance evaluation through the determination of seismic displacement demands and capacities of the bents along with corresponding demand-capacity ratios have been provided in Table 3.3.

Table 3.3: Demand Capacity Ratios for 65' Long Column Bridge Located in Sylhet

Performance Target	Hazard Level	Direction	Demand (inches)	Capacity (inches)	Demand-Capacity Ratio
Immediate Occupancy	EE	Transverse	9.45"	9.82"	0.9615
Immediate Occupancy	EE	Longitudinal	9.35"	20.24"	0.4617
Collapse Prevention	MCE	Transverse	20.24"	20.99"	0.9639
Collapse Prevention	MCE	Longitudinal	20.02"	34.38"	0.5822

3.4 Bridge Consisting of One 55' Long Columns Located in Sylhet

The forces due to dead load and design earthquake on each column base have been found to be **1347.21 kips** and **141.202 kips** respectively. Design earthquake force on the column base is **10.5%** of the dead load coming on it.

The force-based design results show that the required circular column section is of **4'-6"** diameter with **2.93%** steel ratio which is provided using **43-#11** bars. The design is governed by extreme event I limit state. The lateral steel obtained from shear criterion does not govern over the minimum seismic criteria.

For this bridge, the results of performance evaluation through the determination of seismic displacement demands and capacities of the bents along with corresponding demand-capacity ratios have been provided in Table 3.4.

Table 3.4: Demand Capacity Ratios for 55' Long Single Column Bridge Located in Sylhet

Performance Target	Hazard Level	Direction	Demand (inches)	Capacity (inches)	Demand-Capacity Ratio
Immediate Occupancy	EE	Transverse	8.04"	13.50"	0.5952
Immediate Occupancy	EE	Longitudinal	5.71"	13.29"	0.4293
Collapse Prevention	MCE	Transverse	17.21"	20.40"	0.8438
Collapse Prevention	MCE	Longitudinal	12.23"	20.11"	0.6079

4. CONCLUSIONS

The authors have found from this research that the contribution of earthquake forces increase for shorter height column bridges. This is because, due to the higher flexibility of longer column bridges, these tend to have higher fundamental time periods compared to shorter column bridges. The higher fundamental time periods results in a shift towards lower spectral acceleration in the seismic demand response spectrum which eventually leads to lower contribution of seismic forces. The fewer number of columns in a bent results in a much larger design column section. The larger column sections reduces the flexibility of the bridge and makes it stiffer. As a result, the contribution of earthquake forces on single column bent bridges are higher than that on multi-column bent bridges of same pier heights. However, the contribution of earthquake force may be considerably higher for bridges of different time periods.

The seismic displacement demand increases for longer column height bridges as the pier slenderness increases in such cases. Also, the moments and subsequently the deflections of the piers increase with longer dimensions of the piers. Similar to the displacement demand, the displacement capacity of bents also increases for longer column height bridges as well as for smaller column cross-sections and higher steel ratios which is due to the increased flexibility possessed by such bents.

Both single column bent and multi-column bent prestressed concrete I-girder bridges, properly designed for seismic forces, satisfy the seismic performance targets. However, the demand capacity ratios change for different selections of combination of column section and steel ratio. Therefore, it is necessary to evaluate the performance of a bridge prior to finalizing the design.

This research can be further extended in the following fields:

- The AASHTO (2011, 2012) specifications recommend the consideration of liquefaction assessment of subsoil which has not been done in this study. The performance of bridges subjected to liquefaction of subsoil can be studied.
- The column base have been assumed to be fixed at its bottom in this research. However, the soil-structure interaction between piles that support the columns can be researched. Piles are likely to induce additional deflection to the bents.
- All the columns for both bents of the bridges considered in this study have the same height. Bridges having columns of varying heights may be studied.
- The bridges studied in this study consist 3 spans of certain lengths. The number of spans and their lengths can be varied in further researches.

REFERENCES

AASHTO (2011). *Guide Specifications for LRFD Seismic Bridge Design*. American Association of State Highway and Transportation Officials, Washington, D.C.

AASHTO (2012). *LRFD Bridge Design Specifications*. American Association of State Highway and Transportation Officials, Washington, D.C.

BNBC (2017). *Bangladesh National Building Code*. Ministry of Works, Bangladesh.

Caltrans (2015). *Bridge Design Practice, 4th Edition*. California Department of Transportation.

Federal Highway Administration (2014). *LRFD Seismic Analysis and Design of Bridges, Reference Manual, NHI course no. 130093 and 130093A*. National Highway Institute, U.S. Department of Transportation.

Indian Institute of Technology, Kanpur (2002). *Earthquake Tips*. Building Materials and Technology Promotion Council, New Delhi, India.

Siddique, A. F. A. (2018). *Seismic Performance Evaluation of Concrete Bridges*. Bangladesh University of Engineering and Technology, Dhaka.

Taly, N. (1998). *Design of Modern Highway Bridges*. McGraw-Hill.

USGS. (n.d.). Retrieved from https://earthquake.usgs.gov/learn/topics/buildings-eqs.php

Zhang, Q. (2015). Performance *Based Design and Evaluation of Reinforced Concrete Bridges*. University of British Columbia, Okanagan.

Proceedings of the 5th International Conference on Civil Engineering for Sustainable Development (ICCESD 2020), 7~9 February 2020, KUET, Khulna, Bangladesh (ISBN-978-984-34-8764-3)

STRUCTURAL STRENGTH AND BEHAVIOR OF PROFILED STEEL SHEET- CONCRETE COMPOSITE SLAB

S. M. Zahurul Islam*[1] Bulbul Ahmed[2], Abu Sayed Md. Mahbub[3], Md. Jayed Siddique[4] and Shah Alam[5]

[1]Professor, Department of Civil Engineering, Rajshahi University of Engineering and Technology, Rajshahi-6204, Bangladesh, e-mail: zahurul90@gmail.com
[2]Assistant Professor, Department of Civil Engineering, Rajshahi University of Engineering and Technology, Rajshahi-6204, Bangladesh
[3,4,5]Student, Department of Civil Engineering, Rajshahi University of Engineering and Technology, Rajshahi-6204, Bangladesh

***Corresponding Author**

ABSTRACT

Profiled Steel Sheet-Concrete Composite Slabs (PSSCCSs) are getting emerging importance for the construction industry for different purposes. The composite slabs can be performed as form work during construction. These composite slabs systems can be efficiently used as a permanent deck scaffolding. The local buckling of the slab is reduced by profile steel sheet. The slab thickness is reduced and the total construction cost of construction is lower than the normal slab construction. The main objective of this research is to measure the behavior of structure and strength of PSSCCSs. Three different types of PSSCCSs are prepared for experimental investigations. Type I: PSSCCS with studs; Type-II: PSSCCS with minimum reinforcement and Type-III: PSSCCS without reinforcement are considered for this research. A series of laboratory tests were conducted on PSSCCS. Static load is applied on each PSSCCS during laboratory test. The composite slabs are placed over supporting roller hinge supports and load is applied incrementally on universal testing machine. The ultimate capacity, failure modes, and the stress-strain behavior of PSSCCS are observed. From the test result, the load carrying capacity of Type-II slabs is two times of Type-III slabs. Type-I slab showed the maximum load carrying capacity and it is three times of the Type-III slabs. The experimental test results are validated by the analytical results. The analytical results have very good agreement with experimental results and this analytical model can predict properly the structural behavior and the load carrying capacity of composite slabs. This composite slab system may suitable to minimize cost and to provide an increase in stiffness and strength. The research also comprised the study of the strength of composite slab using various thickness of profile sheet. It is an advanced composite slab system made of a profile steel sheet which can be effectively used in high rise building.

Keywords: *Composite slab, Steel deck, Compressive strength, Strength behaviour.*

1. INTRODUCTION

Profiled Steel Sheet-Concrete Composite Slabs (PSSCCS) are very demanding for modern construction industry. The application of this slab systemvery simple. The construction period is very faster. Structurally this slab system is light weight. Construction formwork is minimized by the steel profile sheet and hence the total construction cost of the slab system is comparatively lower than the normal sab system. For the construction of high rise building this slab system are using widely. Steel cold-formed plates with a reduced thickness can be efficiently used as permanent deck scaffolding for concrete slabs. The main benefit of these structural systems is to make the construction speedy as they do not require the standard scaffolding and propping systems (Calixto and Lavall 1998). The system is well accepted by the construction industry due to the many advantages over other types of floor systems (Andrade 2004; Makelainen and Sum 1999; Stanislava 2015). Profiled steel deck performs some major roles that act as a permanent formwork during the concrete casting and also act as tensile reinforcement after the concrete become hardened (Chen 2003; Veljkovic 1998; Porter and Ekberg 1971). Wright et al. (1987) conducted more than 200 tests on composite slab specimens including studs and intermediate stiffeners with trapezoidal profile deck. Crisinel and Marimon (2004) developed a simplified design method to measure ultimate capacity of composite slabs. Leon and Rassati (2013) conducted experimental test of three specimens of continuous composite concrete slabs tested under two-point loading system at each span up to failure. These research works indicate that the analysis of the composite slab behavior is highly complex (Marimuthu et al. 2006). However, no research works have been done by other researchers to compare the structural behavior of three different types of steel profile composite slabs. The main objective of our work is to determine structural strength and behavior of PSSCCS and to compare the load carrying capacity between different three different types of steel profile composite slabs including studs, minimum reinforcement and without reinforcement. The results of the research offered in this paper are a contribution to new experimental findings on the mechanical behavior of composite slabs, and on the analysis of the bonding behavior of composite profile slabs by using three different types of composite slabs. The experiemntal test results are validated by proposed analytical results. The proposed analytical model is capable to predict the behavior and the load carrying capacity of composite slabs.

2. MATERIALS AND METHODOLOGY

Locally available corrugated galvanized steel profile sheet is used. Both surface of the steel sheet is galvanized during manufacturing to protect from corrosion. In Fig. 1, the corrugated galvanized profile steel sheet is presented. These steel decks present heights ranging from 38 up to 90 mm with thickness varying from 0.76 to 1.5 mm. The main purpose of this geometry of the steel profile sheet is to increase the concrete to steel deck interlock resistance in the bottom profile corrugations for the three-dimensional state of stress present in the deck. The detail specification of trapezoidal steel profile is presented in Fig. 2. The height of the deck, slope of deck and width of sheet rib is described in this figure (see. Fig. 2).

Fig. 1:Trapezoidal steel profile decking sheet

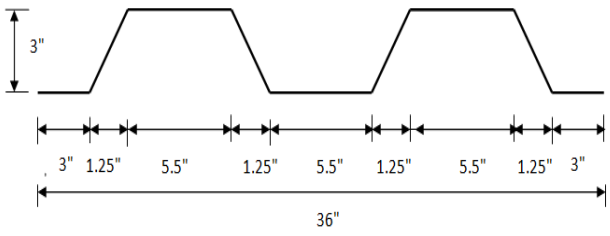

Fig. 2: Specification of trapezoidal steel profile decking sheet

Concrete mix is prepared by OPC cement, coarse aggregate and coarse sand with fresh water. The FM of coarse sand and coarse aggregate is 2.86 and 5.50 respectively. Concrete mix proportion is used in the mixture 1:2:4. Water-Cement ratio is 0.50 for the mix for making the mixture workable. Concrete mixture is prepared in the laboratory shown in Fig. 3. The well graded coarse aggregate and coarse sand is used in the concrete mix. The cement and water contents are higher in lightweight concrete because of the absorption of water by the aggregate. Lightweight concrete is commonly used because the obvious advantage of (typically) 25% weight saving can provide economic benefit for the overall design of the composite slab (Rackham et al. 2009). Workability is measured by slum test which is presented in Fig. 4.

Fig. 3: Concrete mixture (M20)

Fig. 4: Slum value test of M20 grade concrete

3. PREPARATION OF COMPOSITE SLABS

The composite slab specimens are constructed with 4 inch nominal depth 24 inch width and 36 inch span. The thickness of the concrete above the flange is 1 inch while depth of the profiled steel deck is 3 inch. All composite slab specimens are cast with full support on the plain surface concrete flooring in the Composite Testing Laboratory. Steel-decking surface is well cleaned before casting of the concrete. PSSCCSs are casted for measuring the structural strength. Total three types of PSSCCS slabs are made to test the axial load. Type-I: PSSCCS is prepared by welded the studs with the steel deck. The studs are 3.5 inch in length and ½inch diameter (see Fig. 5). Studs are placed @ 6inch c/c along the steel profile sheet. Studs fixed in a single line at a butt joint in the decking do not provide sufficient anchorage for the decking to contribute to the transverse reinforcement (see Fig. 6). In this slab minimum steel re-bars are used. Type-II: PSSCCS has steel deck with minimum reinforcement. Mild steel mesh reinforcement is used as shrinkage and temperature control reinforcements as specified in the ASCE (1985) specification and Type-III: PSSCCS are prepared using no reinforcement in which only concrete is placed over the steel profile deck. The slabs are tested after 28 days curing period. Once shear studs and transverse reinforecment are provided, the concrete mixute is pured to cast the slabs (Fig. 7).

Fig. 5:Studs connected with steel sheet

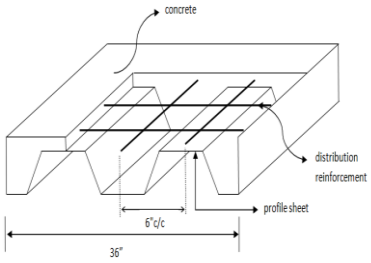

Fig. 6: Distribution of rebars

Fig. 7: Concrete placement

4. EXPERIMENTAL TEST SETUP

The tensile stability and compressive stability of the components is tested using a universal device referred to as Universal Testing Machine. The "universal" portion of the title shows that many conventional tensile and pressure experiments can be carried out. In this study, Universal Testing Machine capacity of 3000 KN is used for measuring the load carrying capacity of the specimens. The arrangement for the simply supported composite slab configuration with an effective length (L) of 36" subjected to one point located.

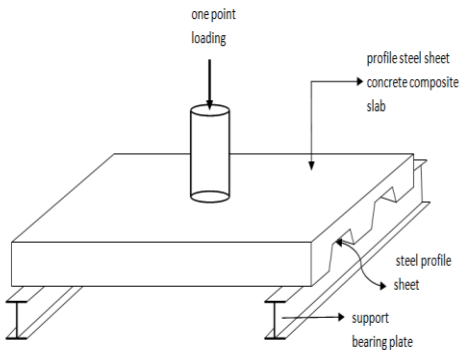

Fig. 8: Schematic view of experimental test setup

Fig. 9: Details view of experimental test setup in universal testing machine

The schematic view of one-point loading is shown in Fig. 8 and Fig. 9 shows the complete experimental setup in the laboratory. Each composite deck-reinforced slab was tested on simple span supports and subjected to a symmetrical mode of loading, consisting of either a single concentrated point load as shown in Fig. 9. In this experiment, load was applied by universal testing machine and deflection was measured by the strain gauge at the point of load application. Uniform load is applied by inflating a 0.5inch thick 24inch length cylinder, which is confined by the top surface of the test slab. A steel plate with 2inch thick by 4inch diameter is placed over the pad.

5. RESULTS AND DISCUSSIONS

5.1 Experimental results

The failure load, failure mode and types of failure have been observed for the specimens during testing. The failure mode of the slabs after peak load is observed. The crack propagation starts from the point of loading. Gradually the cracks increased with the increase

of load. Different types of crack propagation are generated those are presented in Fig. 10 and Fig 11. Concrete cover is separated after reaching ultimate capacity of the slab and end plate also detached during applying load (see Fig. 12-13).

Fig.10: Failure modes of slab under loading

Fig.11: Crack propagation of slab under loading

Fig.12: Concrete cover separation

Fig.13: Plate end interfacial deboning

During test the failue modes are criritcally examine to understand the behaviour of the decking system. Ultimate capacity of the deking system is measured carefully. After reaching peak load shear bond and flexure failure modes were noticed. Shear bond leads the diagonal cracks and brittle failure has been occured. Due to brittle failure end-slip has been occured for separation of concrtete from steel sheet. Bending failures started after yielding of steel and crushing of concrete. Most of the major cracks are occured for the bending or flexural failures and the sudden failure at peak capacity. End-slip and debonding of steel sheet and concrete is not noticed for the bending failure. Bending failure are because of under reinforced steel decking system and sudden collapse is not experienced in the total composite system. Tearing of steel deck is the result of yielding of steel sheet and ductile behaviour of the sheet has shown in the entire section of the system. In case of over reinforced decking system, flexural crushing has been started and concrete crushing at ultimate load and sudden collapse of the entire system has experienced.

The test results for different composite slabs are presented in Table 1-3. Load-deformation curve is shown in Fig. 14 and the ultimate capacity of the Type-I slabs are much more than the other composite slabs.

Table 1: Variation of load with respect to deformation for Type-I slab (including studs)

Serial No.	Load (KN)	Deflection (mm)	Serial No.	Load (KN)	Deflection (mm)
1	0	0	6	50	2.10
2	10	0.40	7	60	2.40
3	20	0.75	8	70	2.65
4	30	1.25	9	80	2.90
5	40	1.65	10	90	3.05

Table 2: Variation of load with respect to deformation for Type-II slab (including reinforcement)

Serial No.	Load (KN)	Deflection (mm)	Serial No.	Load (KN)	Deflection (mm)
1	0	0	5	40	1.45
2	10	0.35	6	50	1.65
3	20	0.75	7	60	1.90
4	30	1.15	8	70	2.05

Table 3: Variation of load with respect to deformation for Type-III slab (no reinforcement)

Serial No.	Load (KN)	Deflection (mm)	Serial No.	Load (KN)	Deflection (mm)
1	0	0	3	20	1.10
2	10	0.45	4	30	1.40

The graphical presentation of the experimental test results is shown in Fig. 14. Typical load-deformation curve generated by the load gauge and deflection gauge. The failure of the specimen has occurred basically for the separation of concrete from the steel sheet. Regular failure modes are not noticed in reinforced steel decking system. Irregular cracks or failure starts and continues until exceeded bond strength and local bond failure due to flexural and bond stress. Collapse initiates from the end of the concrete slab and moves forward that initiates larger cracks. This failure has been occurred for debonding of concrete and steel sheet. Composite actions are not properly worked if shear studs are not used. Shear studs are acted as anchorage between steel sheet and concrete and composite actions effectively provided. Shear studs transfer the loads from concrete to the steel deck. From the load-deformation curves, it is found that the ultimate capacity of the system is 90 kN for type-III slab and failure occurs at 3.05 mm deflection.

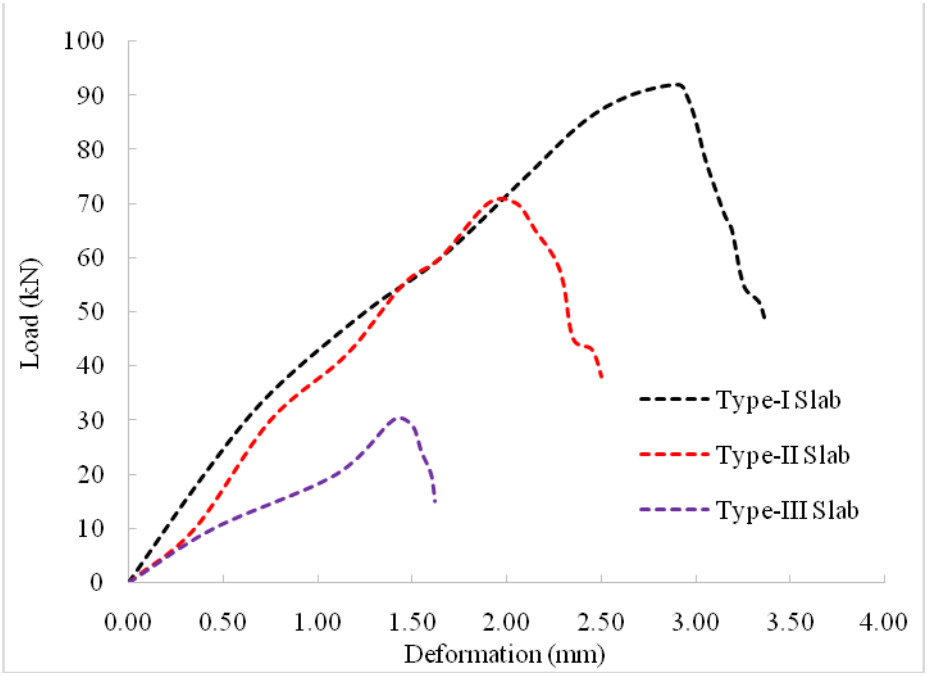

Fig. 14: Comparison of load-deflection curve of composite slab for different condition

To increase the shear bond capacity of the composite slabs without end anchorage shear studs are widely used. The composite actions are easily created by providing sufficient number of shear studs. The capacity of the composite slabs with end anchorage are compared with the one span composite slabs. Initially the capacity is almost same for both system before end slip initiation. With further increase of applied load shear bond slip has been started and the concrete is de-bonded for cracking.
The load-deflection curves were more linear for concrete composite slab including studs than including reinforcement before the shear-bond failure. After the load increase, the de-bonding

cracking at the sheet-concrete interface and the load-deflection curves then became non-linear for composite slabs. The load carrying capacity of steel profile deck concrete composite slab increases with the increase of thickness of the steel profile sheet.

In this research three different types of steel profile concrete composite slabs were established including studs, minimum reinforcement and without reinforcement. Based on the experimental investigation, the following conclusion is arrived. The load carrying capacity of composite slab using reinforcement and studs was increased two times and three times than reference test of no reinforcement slab. The ultimate capacity of three composite systems are 22kN, 65kN and 90kN respectively and the comparison is shown in Fig. 15.

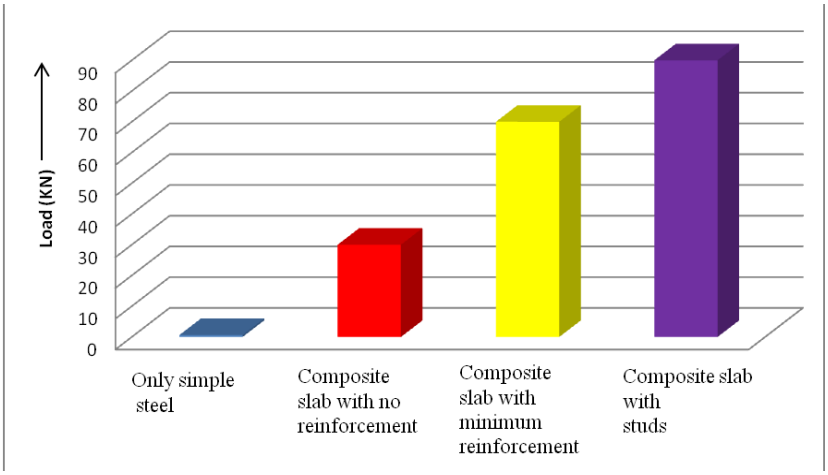

Fig. 15: Comparison of load carrying capacity of steel profile concrete composite slab

5.2 Experimental results validation

Analytical model is used for validation of experimental test results. For the analytical model load and deformation is calculated by the proposed equation. Deflection of the slab is obtained by the sum of deflections of the profiled sheets during the construction phase and deflection of the concrete slab. Traphezoidal cross section of the slab is shown in Fig 16. The slab spans work independently from each other, therefore for calculations,

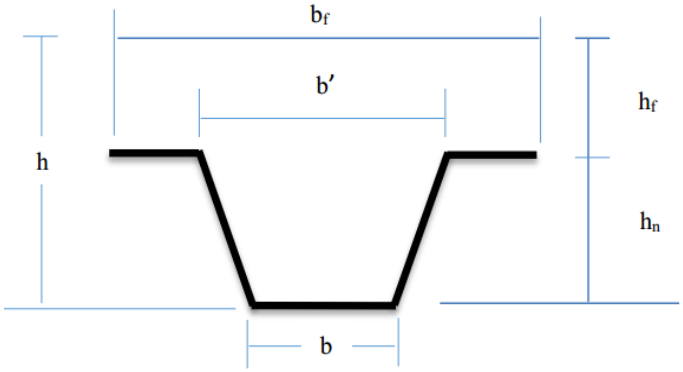

Fig. 16: Traphezoidal cross section of the slab

$P_u = s * l^2 * \left(\frac{1}{r}\right)_{max}$ where, $s = \frac{5}{48}$ = coefficient depending on the stress diagram and the type of a load. l = length of the span and $\left(\frac{1}{r}\right)_{max}$ = maximum curvature in the section with the maximum bending moment from the load. The load-deformation curve is developed for the analytical model results. The validation is performed for experimental test results and it shows very good agreement with experiemtal test results for all composite slabs (see Fig. 17).

$$J_{red} = \frac{b_f h_f^3}{12} + \frac{bh_n^3}{12} + b_f h_f (y_0 - \frac{h_f}{2})^2 + bh_n (\frac{h_n}{2} + h_f - y_0)^2 \dots\dots\dots\dots\dots\dots\dots\dots (1)$$

$$y_0 = \frac{b_f h_f^2 + bh_n(2h_f + h_n)}{2(b_f h_f + bh_n)} \dots\dots\dots\dots\dots\dots\dots\dots\dots\dots\dots\dots\dots\dots\dots\dots\dots\dots\dots\dots\dots\dots (2)$$

J_{red} = momentof inertia of the effective cross-section relatively its center of gravity.

$(\frac{1}{r_1}) = (\frac{M}{Eb1 * jred})$

Where, E_{b1} -deformation modulus of compressed concrete depending on duration of the load. The slab spans work independently from each other, therefore on-span beam is used as the stress diagram for calculations;

For short term loads

$E_{b1} = 0.85\ E_b = 0.85 * 10000000 = 8500000\ KN/m^2$

For long term loads;

$E_{b1} = (\frac{Eb}{1+\phi b,cr}) = (\frac{10000000}{1+3.65})$, where, $\phi_{b,cr}$ = 3,65-creep coefficient for concrete

From the figure no (16),

Here, b_f = 0.3429m, b = 0.1397m

h_f = 0.0254m, h_n = 0.0254m

from equation no (1), $J_{red} = 5.06*10^{-5} m^2$

from equation no (2), y_0 = 0.041m

The load-deformation of different slabs is calculated by the analytical formula. Three different slabs carried different capacity at corresponding deformation presneted in table 4.

Table 4: Variation of load with respect to deformation for different types of slabs

Type-I Slab		Type-II Slab		Type-III Slab	
Deformation (mm)	**Load (kN)**	**Deformation (mm)**	**Load (kN)**	**Deformation (mm)**	**Load (kN)**
0	0	0	0	0	0
0.4	20	0.35	10	0.45	10
0.75	35	0.75	30	1.10	20
1.25	50	1.15	42	1.40	30
1.65	60	1.45	55	1.50	29
2.10	75	1.65	60	1.55	24
2.40	85	1.90	70	1.60	20
2.65	90	2.05	70	1.62	15
2.90	92	2.15	65	--	--
2.95	90	2.25	60	--	--
3.00	85	2.30	55	--	--
3.05	78	2.35	45	--	--
3.15	68	2.45	43	--	--
3.19	65	2.50	38	--	--
3.25	55	--	--	--	--
3.33	52	--	--	--	--
3.36	49	--	--	--	--

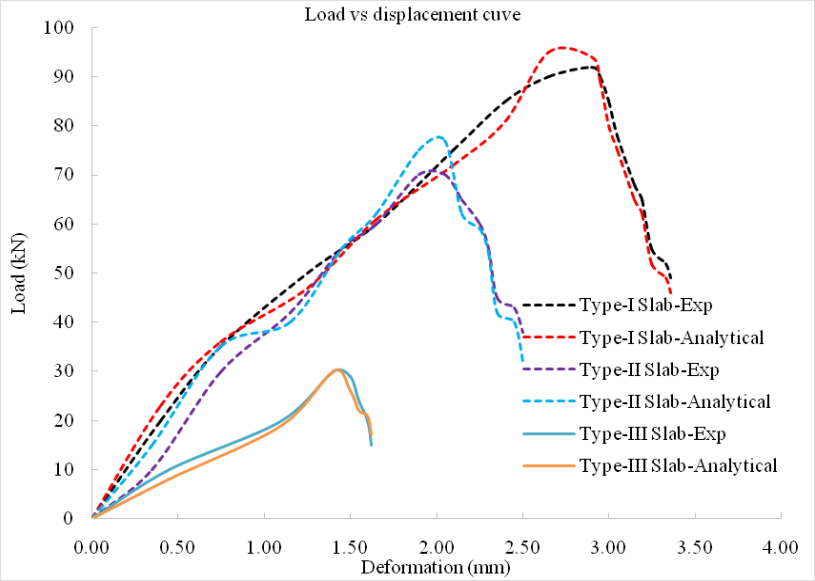

Fig. 17: Validation of experimental test data by analytical model for different condition

6. CONCLUSIONS

In this research three different types of steel profile concrete composite slabs are introduced including studs, minimum reinforcement and without reinforcement. Based on the experimental investigation, the following conclusion is drawn. The ultimate capacity of composite slab using reinforcement and studs is increased two times and three times than reference test of no reinforcement slab. The load-deflection curves are more linear for concrete composite slab including studs than including reinforcement before the shear-bond failure. After the load increase, the de-bonding, cracking at the sheet-concrete interface and the load-deflection curves then became non-linear for composite slabs. Comparisons of the experimental and analytical results agrees well with the test results, and is capable of predicting the behavior and the load carrying capacity of composite slabs.

ACKNOWLEDGEMENTS

The authors are grateful to Abul Khair Steel Mills, Dhaka, Bangladesh for supplying the test specimens.

REFERENCES

Andrade, V. (2004). Standardized composite slab systems for building constructions. Journal of Constructional Steel Research, 60(03-05), 493-524.

Calixto, J. & Lavall, A. (1998). Behavior and strength of composite slabs with ribbed decking. Journal of Constructional Steel Research, 46(1-3), 211-212.

Chen, S. (2003). Load carrying capacity of composite slabs with various end constraints, Journal of Construction Steel Research, 59(03), 385-387.

Crisinel, M. & Marimon, F. (2004). A new simplified method for the design of composite slabs. Journal of Constructional Steel Research, 60(03-05), 481-491.

Eurocode 4 (2001). Design of composite steel and concrete structures-part 1.1: General rule and rules for building, EN 1994-1-1: 2001, Draft No. 3, European committee for standardization, Brussels.

Leon, R. T. & Rassati, G. A. (2013). Ultimate Strength of Continuous Composite Concrete Slab. In: 7th International conference on composite construction, Palm Cove, North Queensland, Australia.

Makelainen, P., Sun, Y. (1999). The longitudinal behavior of a newsteel sheeting profile for composite floor slabs, Journal of Constructional Steel Research, 49(02), 117-128.

Marimuthu, V., Seetharaman, S., Arul, S., Chellappan, A., Bandyopadhyay, T. & Dutta, D (2006). Experimental studies on composite deck slabsto determine the shear-bond characteristic (m-k) values of the embossed profiled sheet. Journal of construction steel research, 63 (06), 791-803.

Porter, M., Ekberg, C. (1971). Investigation of cold-formed steel-deck-reinforced concrete floor slabs. In: Yu W-W, editor. First specialty conference on cold-formed steel structures. Rolla: University of Missouri-Rolla.

Rackham, J. W., Couchaman, G. H., Hicks, S. J. (2009). Composite slabs and beams using steel decking: Best practice for design and construction. MCRMA technical paper, No. 13, CI publication.

Stanislava N. A. (2015). Design of the composite flooring slab with profiled sheets t-153 (ruukki) for a residential building, Bachelor's thesis.

Veljkovic, M. (1998). Influence of load arrangement on composite slab behaviour and recommendations for design. Journal of Constructional Steel Research, 45(2), 149-178.

Wright, H., Evans, H. & Harding, P. (1987). The use of profiled steel sheeting in floor construction. Journal of Constructional Steel Research, 7(04), 279-295.

Proceedings of the 5th International Conference on Civil Engineering for Sustainable Development (ICCESD 2020), 7~9 February 2020, KUET, Khulna, Bangladesh (ISBN-978-984-34-8764-3)

RHEOLOGICAL AND MECHANICAL PROPERTIES OF RECYCLED WASTE GLASS CONCRETE AS PARTIAL REPLACEMENT OF FINE AGGREGATE

Md. Saeid Ebna Maleque*[1], Md. Mizanur Rahaman[2] and Md. Habibur Rahman Sobuz[3]

[1]Graduate Student, Department of Building Engineering and Construction Management, Khulna University of Engineering & Technology, Bangladesh, e-mail: ennamaleque.mdsaeid@gmail.com
[2]Graduate Student, Department of Building Engineering and Construction Management, Khulna University of Engineering & Technology, Bangladesh, e-mail: mrahaman495@gmail.com
[3]Assistant Professor, Department of Building Engineering and Construction Management, Khulna University of Engineering & Technology, Bangladesh, e-mail: habib@becm.kuet.ac.bd

***Corresponding Author**

ABSTRACT

The amount of used waste glass has been increased significantly in the last few decades. This high amount of unused waste glass could be a major problem for public health and the environment. This pullulating issue of waste glass can be solved by adopting a disposal system rather than simply dumping on landfills. To solve this problem, researchers in building construction technology conducted analytical studies highlighting the reuse of waste glass. As the waste glass is less expansive than other materials in concrete, especially fine aggregate, uses of crushed glass in concrete could be economical for construction, as well as, it would reduce the amount fo disposable wastes. Thus, the fundamental aim of this study is to investigate rheological properties and mechanical strengths of concrete replacing fine aggregate with 5%, 10%, 15%, and 20% of waste glass. In this study, the fine aggregate was replaced by locally available consumer by-product waste glass in different percentile and examined for 7 and 28 days curing period with a 0.45 water-cement ratio. As this paper is based on managing waste glass in the concrete industry to minimizing the cost, no extra chemical or admixture was used in this experiment. A series of standard tests such as slump test, compressive strength test, flexural strength test, splitting tensile strength test was conducted. The test results showed that slump value is decreased with increasing of waste glass percentage. Consequently, mechanical properties such as compressive, tensile and flexure strength were decreased with the increasing percentage of waste glass. For 5% replacement of waste glass, compressing strength decrease 8.06% and 6.57% respectively while for 20% compressing strength decreases up to 36.36% and 27.14% at 7 days and 28-day curing period while this decreasing rate increased with adding weight of waste glass. Tensile strength and flexure strength also show the same tendency of strength for 5% replacement where the strength decreases 9.6% and 31.79% respectively for 7 days curing periods and at a maximum 20% replacement in the fine aggregate the strength decreases 40.16% and 21.69% for 28 days curing period while compared with normal concrete. This decline in the strength could be caused by the adhesive strength between glass aggregate and cement paste as well as FM values of materials and compacting factors. Finally, from the results, it was concluded that there was a slight reduction on the mechanical strength as well as rheological properties of the concrete mix. This optimum percent of waste glass replacement in concrete not only help to reduce the environmental impact and landfill area but also produce sustainable and economic concrete.

Keywords: *Recycled waste glass, Glass aggregate, Compressive strength, Cement mortar, Waste management.*

1. INTRODUCTION

Humans are using glass for centuries. For its exceptional properties such as transparency, strength, durability, transmittance, people use it almost everywhere. In the building construction industry, different types of glass are used including, float glass, shatterproof glass, chromatic glass, tinted glass and each has a different application. Unfortunately, those glass has a limited life span and, in most cases, after using those glasses are dumped into the landfills. In the Republic of Korea, people use approximately 4.2 million tons of glass every year, which are typically used in building windows, bottles, etc. (Park, Lee, & Kim, 2004). Theoretically, glass is a 100% recyclable material; it can be indefinitely recycled without any loss of quality. Many developing countries are already recycling and reusing waste glass. The United States recycled about 2.99 million of tons' of common household glasses in 2014 (Gorospe, Booya, Ghaednia, & Das, 2019b). Moreover, reusing and recycling of waste glass in the construction industry could save our environment, saving landfill spaces and our precious natural resources (Rakshvir & Barai, 2006).

Different researchers performed various experiments to find out the reaction of waste glass in concrete mortar. Meyer, Egosi, and Andela (2001) depicted various methods and steps for collection, separation, grading to apply as aggregate in the concrete industry. Some findings showed that the type of glass and color of glass can impact the physical and mechanical properties of concrete when the waste glass is used as an aggregate (Gorospe, Booya, Ghaednia, & Das, 2019a; Topçu, Boğa, & Bilir, 2008). One of the problems of glass using in concrete is that it expands due to Alkali-Silica Reaction (ASR). To mitigate this problem, studies are conducted using natural and chemical admixtures such as fly ash, Li_2CO_3 (Topçu et al., 2008). There are few experiments are conducted to replace aggregate with waste glass. Topcu and Canbaz (2004) totally replaced traditional coarse aggregate with waste glass, whereas, Ismail and Al-Hashmi (2009) and Park et al. (2004) partially replaced fine aggregate with different colors of glasses. Additionally, other researchers used waste glass to replace aggregate on lightweight concrete, self-compacting concrete, masonry blocks etc. (Kou & Poon, 2009; Kralj, 2009; Palmquist, 2004).

In Bangladesh, most of the glass materials are thrown away after its first use in buildings and other packaging purposes. The idea of replacing fine aggregate i.e. sand with glass powder in the concrete mix will not only save landfill space but also mitigate the high demands of natural aggregate. By this means, it is possible to preserve our natural resources and cost, labor associated with shipping those raw materials. It will essentially reduce time and budget in a construction project.

2. METHODOLOGY

2.1 Materials

Type I Portland cement King Brand Cement (BDS EN 197-1:2003, CEM-I, 52.5 N. ASTM C-150, Type–I) was used in this investigation. For Coarse Aggregate, Brick chips (khoa) were used to prepare cylindrical specimens and short beam for flexure. The fineness modulus and average size of course aggregate is 7.61 and 9.5 mm to 12.5mm respectively. The maximum size of course aggregate is 25.4 mm. Local Sylhet sand was used as fine aggregate for all test specimens. The fineness modulus and average size of fine aggregate are 2.93 and 0.30 mm to 1.15 mm respectively. The maximum size of the fine aggregate is 4.75 mm. The fineness modulus of glass aggregate is 3.76.

Table 1: Approximate compositions and uses common forms of glass (Siam, 2011)

Type of Glass	Type of Glass	Usages
Soda-Lime-Silica	73% Silica-14% Soda-9% Lime-3.7% Magnesia-0.3% Alumina	Glass Widows, Bottles, Jars
Boro-Silicate	81% Silica-12% Boron Oxide-4% Soda – 3% Alumina	Pyrex Cookware, Laboratory Glassware
Lead (Crystal)	57% Silica-31% Lead Oxide-12% Potassium Oxide	Lead Crystal Tableware
Alumino-Silicate	64.5% Silica-24.5% Alumina-10.5% Magnesia-0.5% Soda	Fiberglass Insulation – Halogen Bulbs

2.2 Mix Design

The waste glass was replaced as fine aggregate as 0%, 5%, 10%, 15% and 20% in the concrete specimens. The ratio of cement, sand and brick chips was 1:2:3. And Cement water ratio was 0.45. Waste glass was crushed manually by using hammer and steel rods. First, coarse aggregate, fine aggregate, and cement with waste glasses were preliminary mixed and then sufficient water was used to the final mix. No admixture was used for this experiment. A hand mixture process was used to mixing the concrete. Different types of hand mixing tools were used, such as trowels, spades, tapping rods, buckets.

2.3 Sample Preparation

Cylinder moulds (100 x 200) mm were used to cast the specimens for compression and tensile test. For the flexure test, prism specimens (100 x 100 x 500 mm) were used. The proportions of materials were determined including cement, sand, aggregate, and water. All the materials were weighted by machine. The materials were mixed by handing batches with size of 25 percent greater than moulding test specimens. Then slump of each concrete batch was measured after blending according to standard code ASTM-C143/C143M-12. Figure 1 shows the materials of concrete for each batch. The moulds were placed horizontal surface and lubricated inside the surface with proper lubricant material. The green concrete was placed into the mould in three equal layers. Then, each layer was compacted uniformly, applying 25 stokes on each layer with a tamping rod that had a diameter of 16 mm. After finishing the top layer of the mould, a trowel was used to finish off the surface level with the top of the mould and stored in a room for hardening about 24 hours. After 24 hours the moulds were removed carefully so that no damage occurs of the specimens during unmoulding. The specimens were cured for 7 and 28 days. Plastic curing tanks were used to cure the specimens.

Figure 1: Sample preparation for concrete

2.4 Curing Period

The mixed loose concrete was moulded in the mould and given each specimen an identification number. Then the mould was kept for 24 hours for hardening at room temperature and 65% humidity environment. After this period of time, the concrete samples were demoulded and kept in water for curing. To conduct flexural, splitting tensile and compressive tests, half of each type specimens were cured for 7 days and other half of specimens were cured for 28 days. A rectangular tank with tap water was used for the curing of specimens. Before the test about 24 hours earlier the specimens were kept to dry for the test.

2.5 Test Methodology

2.5.1 Slump Test

The slump test was accomplished with a steel slump cone according to the ASTM-C143/C143M-12 test method. The slump cone was 30 cm in height, 10 cm in top diameter, and 20 cm in bottom diameter. The slump was measured for without mixing glass and with each percent of glass replacing fine aggregate with standard procedure.

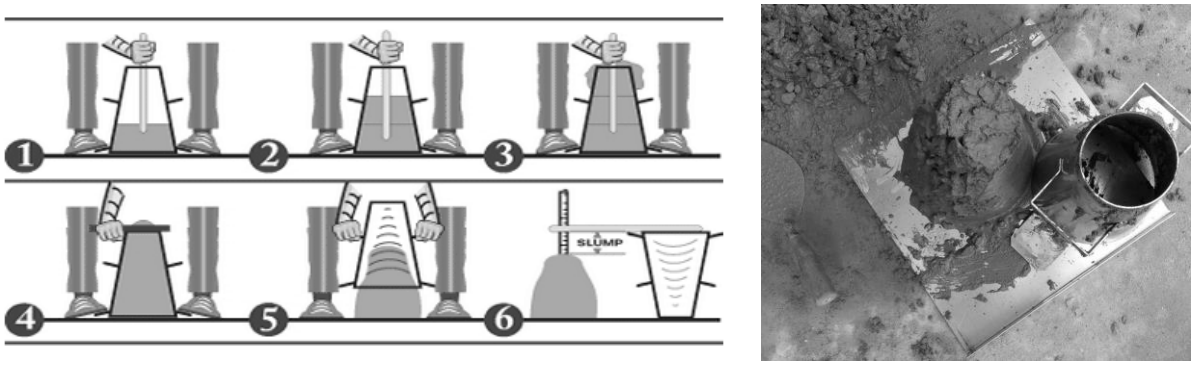

Figure 2: Concrete slump test procedure

2.5.2 Compressive Test

All cylinder specimens for compression tests were conducted according to the standard ASTMC39/C39M-12. All specimens were 100x200 mm in size cylinder to determine the compressive strength of waste glass concrete. The compressive strength of concrete specimens was investigated using a 3000kN digital compression testing machine which is shown in figure 3 and the load application rate was maintained 0.3 MPa/sec for all of the specimens tasted with the machine and applied until the concrete specimen fails.

Figure 3: Digital Compression Testing Machine

2.5.3 Split Tensile Test

Standard ASTM C496/C 496M–04 test procedure adopted for testing splitting tensile strength. For splitting tensile tests, all the specimens were investigated with the same digital compressive the load rate was same as the compressive test.

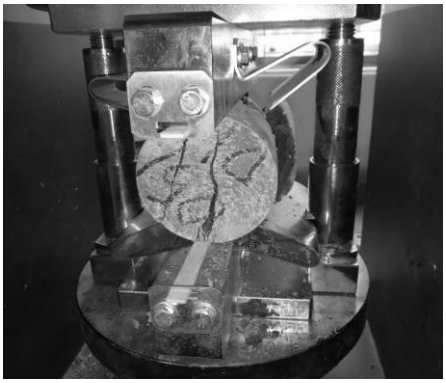

Figure 4: Splitting Tensile Testing Device with concrete mortar

2.5.4 Flexure Test

The flexural test was done according to ASTM-C78-02 which is known as the four-point loading method. A digital flexural testing machine of 200 KN was used to determine the flexural strength of specimens. The load application rate was maintained 0.3 MPa/sec for all of the specimens tasted with the machine. For 7 and 28 days cured simple beam specimens measuring 100x100x500 mm were used. Figure 5 shows the four-point loading method for testing flexural strength.

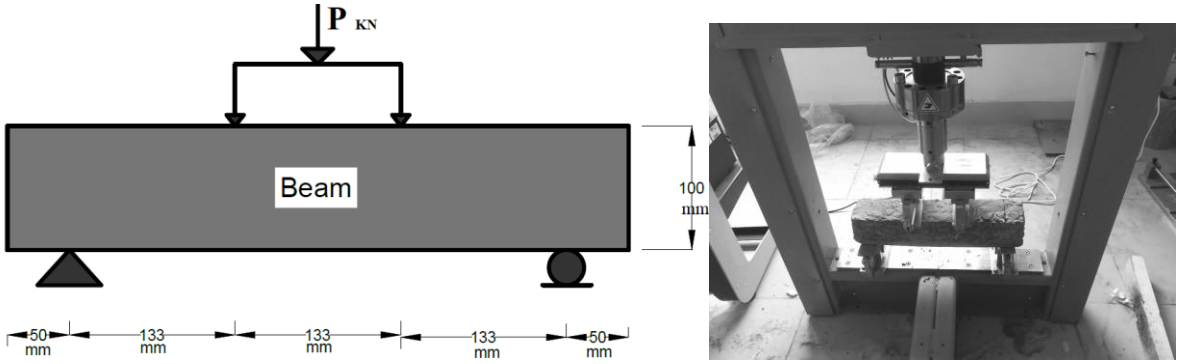

Figure 5: Digital flexure testing machine (four-point loading method)

3. RESULTS AND DISCUSSIONS

3.1 Effect of Glass Aggregate on Slump Value

The results showed that the slump value has a tendency to decrease with the increment of waste glass on the concrete mortar. This general tendency of the slump value is due to less fluidity of fresh concrete as glass aggregate had sharper and angular grain shapes and higher fineness modules than used sand. Additionally, with the increment of glass aggregate, more cement pastes got to attach on the outer layer of the glass, which caused less accessibility of cement paste for the fluidity of fresh concrete. It is noted that the slump values of 15% and 20% of waste glass mortar are same.

Table 1: Approximate compositions and uses common forms of glass

% of waste glass	0	5	10	15	20
Slump value (mm)	75.0	65.0	55.0	50.0	50.0

Figure 6 illustrates the decreasing ratio of glass aggregate on fresh concrete. For 5% waste glass it initially decreases by 13.33%. At 10% replacement decreasing rate it about 26.67%. For 15% and 20% replacement, decreasing rate is slightly low and it is 33.33%.

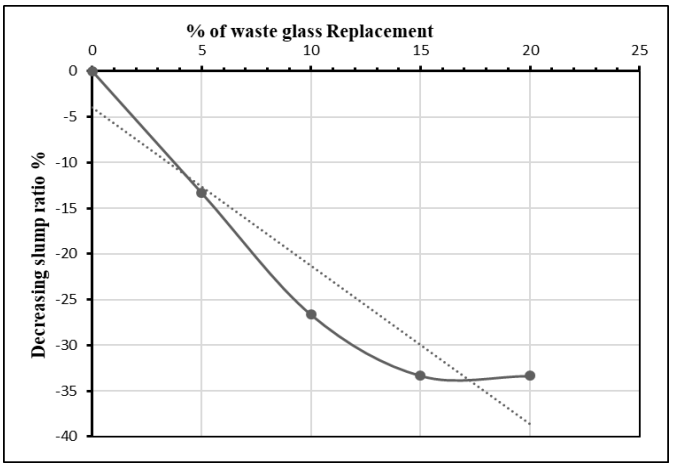

Figure 6: Decreasing ration of the slump.

3.2 Effect of Glass Aggregate on Compressive Strength

The result showed that the compressive strength of the concrete decreased when the percentage of waste glass increased. At 7 days of curing, decreasing rate of compressive strength is 8.06%, 16.99%, 24.19% and 36.36% for 5%, 10%, 15% and 20% of waste glass replacement from zero percent replacement concrete strength. It has the same impact on 28 days of curing. At 28 days this rate is 6.57%, 12.02%, 23.85% and 27.14% for 5%, 10%, 15% and 20% of waste glass replacement. This inclination is due to the decrease in adhesive strength between the surface of the waste glass aggregates and the cement paste as well as the increase in FM of the fine aggregates and the decrease in workability in accordance with the increase in the mixing ratio of the waste glasses, which is also observed in splitting tensile strength and flexural strength. Figure 7 (a) shows that the compressing strength with respect to the increasing percentage of waste glass on concrete for 7- and 28-days curing period.

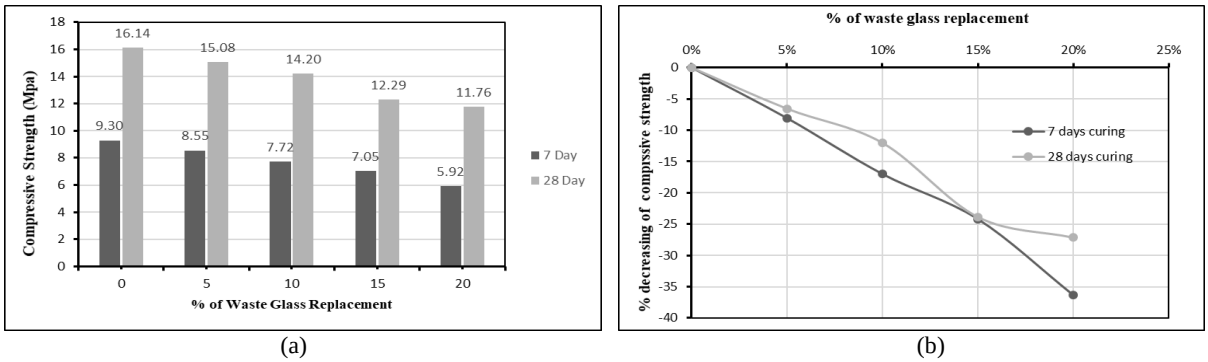

(a) (b)

Figure 7: (a) Test results of compressive strength; (b) Decreasing rate of compressive strength

3.3 Effect of Glass Aggregate on Splitting Tensile Strength

Test results in Figure 8 (a) indicate that the tensile strength of the concrete increased when percentage of waste glass decreased gradually. Figure 8 (b) represents that after increasing the percentage of waste glass content tensile strength of concrete decrease and this decrease rate for 7 days of curing are 9.6%, 19.77%, 27.12%, 36.16% for replacement of 5%, 10%, 15%, 20% of waste glass. Also, 28 days curing concretes show the same tendency of decreasing tensile strength which is slightly similar to one-week curing concrete. Decreasing rate for 28 days are 6.74%, 14.24%, 23.83%, 40.16% for replacement of 5%, 10%, 15%, and 20% of waste glass.

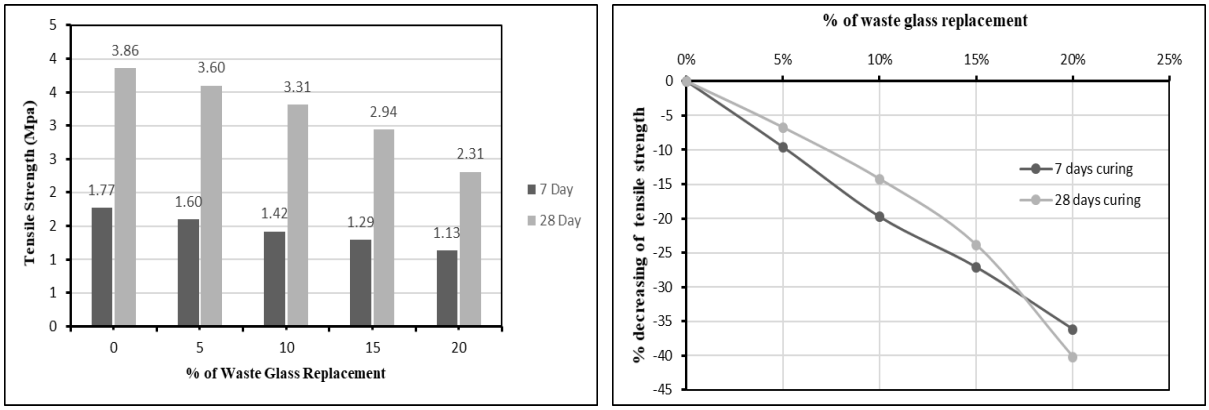

(a) (b)

Figure 8: (a) Test results of tensile strength; (b) Decreasing rate of tensile strength

3.4 Effect of Glass Aggregate on Flexural Strength

The curing period has a significant effect on concrete tensile strength. Figure 9 (a) illustrate the comparison between 7 days curing and 28 days curing for 0%, 5%, 10%, 15% and 20%. The decreasing rate of the tensile strength decreases uniformly for 5% and 10% replacement of waste glass on 7 days and 28 days curing period while for 15% and 20% replacement of waste glass shows lower decreasing rate in 28 days curing period compared to 7 days curing period shown in Figure 9 (b).

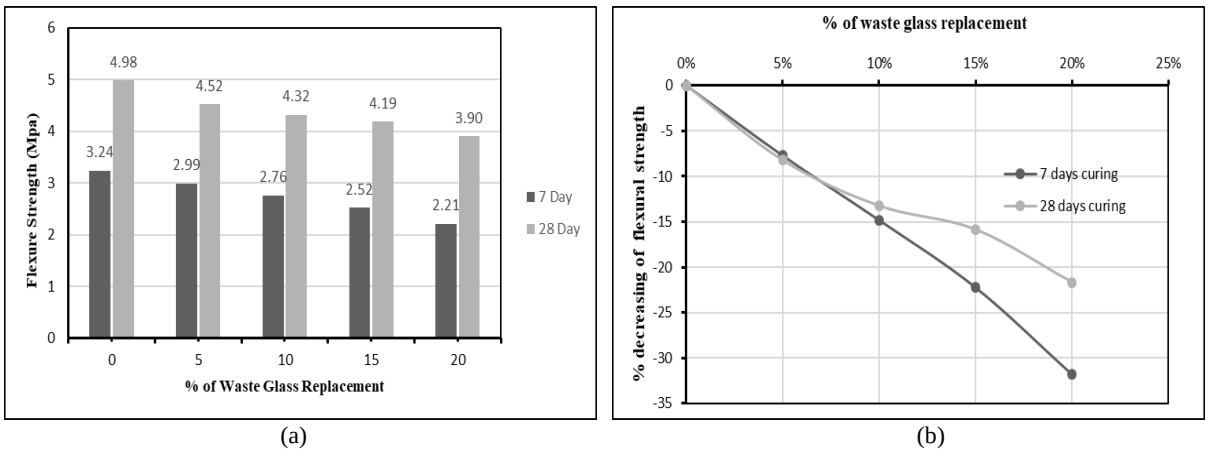

(a) (b)

Figure 9: (a) Test results of flexural strength; (b) Decreasing rate of flexural strength

4. CONCLUSIONS

The goal of this study is to investigate the properties of concrete containing glass as fine aggregate to reuse and recycle waste glass. The result showed that the slump value of concretes decreases with the increment of waste glass in concrete. The shape, size and angle of glass aggregate, attachment of cement paste on glass surface caused less fluidity for fresh concrete. Additionally, mechanical strength such as compressive strength, splitting tensile strength, flexural strength also decreases

gradually with the percentile increment on the waste glass on concrete. FM value of aggregates, the adhesive bond between glass particles on fine aggregate and cement paste, compacting factor plays a vital role in decreasing mechanical strengths. Decreasing of strength from plain concrete for 5% replacement is lower than others. It was also observed that the decreasing rate for splitting tensile strength higher than compressive strength and flexural strength. The results show that waste glass could be used in concrete as well as in the construction industry. However, more studies should be conducted to gain optimum results using chemical properties and admixtures.

ACKNOWLEDGEMENTS

This paper is made possible through financial aid and laboratory support from the Department of Building Engineering and Construction Management at Khulna University of Engineering & Technology, Khulna-9203, Bangladesh.

REFERENCES

Gorospe, K., Booya, E., Ghaednia, H., & Das, S. (2019a). Effect of various glass aggregates on the shrinkage and expansion of cement mortar. *Construction and Building Materials, 210*, 301-311.

Gorospe, K., Booya, E., Ghaednia, H., & Das, S. (2019b). Strength, durability, and thermal properties of glass aggregate mortars. *Journal of Materials in Civil Engineering, 31*(10), 04019231.

Ismail, Z. Z., & Al-Hashmi, E. A. (2009). Recycling of waste glass as a partial replacement for fine aggregate in concrete. *Waste Management, 29*(2), 655-659.

Kou, S., & Poon, C. (2009). Properties of self-compacting concrete prepared with recycled glass aggregate. *Cement and Concrete Composites, 31*(2), 107-113.

Kralj, D. (2009). Experimental study of recycling lightweight concrete with aggregates containing expanded glass. *Process Safety and Environmental Protection, 87*(4), 267-273.

Meyer, C., Egosi, N., & Andela, C. (2001). *Concrete with waste glass as aggregate.* Paper presented at the Proceedings of the international symposium concrete technology unit of ASCE and University of Dundee, Dundee.

Palmquist, S. M. (2004). Compressive behavior of concrete with recycled aggregates.

Park, S. B., Lee, B. C., & Kim, J. H. (2004). Studies on mechanical properties of concrete containing waste glass aggregate. *Cement and Concrete Research, 34*(12), 2181-2189.

Rakshvir, M., & Barai, S. V. (2006). Studies on recycled aggregates-based concrete. *Waste Management & Research, 24*(3), 225-233.

Siam, A. A. D. (2011). Properties of concrete mixes with waste glass. *Properties of Concrete Mixes with Waste Glass*.

Topçu, İ. B., Boğa, A. R., & Bilir, T. (2008). Alkali–silica reactions of mortars produced by using waste glass as fine aggregate and admixtures such as fly ash and li2co3. *Waste Management, 28*(5), 878-884.

Topcu, I. B., & Canbaz, M. (2004). Properties of concrete containing waste glass. *Cement and Concrete Research, 34*(2), 267-274.

Proceedings of the 5th International Conference on Civil Engineering for Sustainable Development (ICCESD 2020), 7~9 February 2020, KUET, Khulna, Bangladesh (ISBN-978-984-34-8764-3)

LATERAL LIVE-LOAD DISTRIBUTION FACTORS OF A CURVED COMPOSITE BRIDGE

M. Hossain*[1], M. B. Zisan[2] and P. K. Das[2]

[1]Department of Civil Engineering, CUET, Bangladesh, email: mhossain.cuet@gmail.com
[2]Department of Civil Engineering, CUET, Bangladesh, email: basirzisan@gmail.com
[3]Department of Civil Engineering, CUET, Bangladesh

***Corresponding Author**

ABSTRACT

The live-load distribution factor is the key parameter in the design and construction of Highway Bridges. Numerous studies, as well as AASHTO and AASHTO-LRFD specification on live-load distribution, covered the conventional bridge only whereas the curved bridges yet remain hidden. The complexities in construction procedure and curvature provide in the curved bridge itself a unique feature. The objectives of the current study are investigating the effect of curvature, slab stiffness, girder stiffness and diaphragm spacing on live-load distribution. The numerical study consists of modeling and verification of an existing curved bridge model using ANSYS program. The analysis was performed using AASHTO HS20-44 design truck. This study shows that the live -load distribution factor of outer girder is increased about 38% for outer girder loading and 62% for inner girder loading with a decreasing radius of curvature. On the other hand, the distribution factor of inner girder is decreased about 78% and 36.5% for outer and inner girder loading respectively. The numerical analysis explored the live-load distribution for shear.

Keywords: *Live-Load Distribution Factor, Curved Composite Bridge, Curvature, ANSYS, AASHTO HS20-44 Truck*

1. INTRODUCTION

The use of horizontally curved bridges is increasing in complex and important highway interchanges and river crossing in urban and suburban regions to meet increasing traffic capacity demands. Usually, modernized curved bridges such as curve twin I-girder bridges (CTIGB), are becoming familiar for short and medium span highway bridges (Kim, Kawatani, & Hwang, 2004). The rationalize structures have advantages like simplicities for fabrication, design, and construction. Also, this type of construction gives a very economical performance, due to the less number of girders and secondary members (Awall, Hayashikawa, Matsumoto, & He, 2012). The American Association of State Highway and Transportation Officials (AASHTO) for highway bridges did not account the effect of curvature for curve bridges in live-load distribution factor (AASHTO (1994a), 1994). AASHTO gave Standard specification for straight bridges. Later in 1994, AASHTO LRFD gave a correction factor for skew bridge (AASHTO (1994b), 1994). But it did not mention any correction factor or specification considering the curvature effect. The distribution of load in a curve bridge is different than that of a normal straight bridge because of out-plane bending and excessive torsional effects (Brockenbrough, 1986). When the vehicular load is applied on the outer girder (with respect to origin of bridge curvature) of a twin I-girder curve bridge, uplift force will be induced in the inner girder support *(Zisan, Hayashikawa, Matsumoto, & He, 2015)*. But this is normally not happened in a straight bridge case. Hence, it is required to check the lateral live-load distribution in curved composite bridge

1.1 Live-Load Distribution Factors

The live-load distribution factor is the amount of the vehicular load carried by each girder. The live-load distribution factors for conventional bridges are given by the AASHTO Standard Specifications for Highway Bridges since 1931. The earlier approaches were based on the work done by Westergaard (1930) and Newmark (1938), but the factors were modified as new research results became available (Barr, Eberhard, & Stanton, 2001). If a concrete bridge deck is constructed on prestressed concrete girders and carrying more than one lanes of traffic, the distribution factor (AASHTO 1996) is S/5.5, where S is the girder spacing in feet (AASHTO, 1996; Zokaie, 2000). The design moment will be the multiplication of this factor with the moment on a single girder, generated by one lane of wheel load. The changes in the code over the years have also created inconsistencies *(Zhang, Huang, & Wang, 2005)*. The objective of this study is to find out the live-load distribution factor of a composite bridge by finite element modeling and following the code specification for different bridge parameters. After that, the disparity between the live-load distributions factor obtained from the finite element analysis to the present practiced code is determined.

2. FINITE ELEMENT MODELING

2.1 Model Description

This study adopted a simply supported horizontal curved twin I-girder bridge of having a span length of 50 m. For model verification and validation an existing bridge model was chosen for this study from *Awall et al. (2012)*. The bridge model is consisting of two lanes for the vehicle along with two pedestrian lanes for cycling and walking. It has two main I-girders of 3 m deep and spaced transversely by 6 m. In this study, the radii of curvatures defined as the distance between the origin to the centerline of the circular arc. Thus, the length of the two main girders varies according to the bridge curvature, while the total mass of the bridge remains the same. The deck slab (10.5 m wide and 0.3m thick) is assumed to act compositely with steel girders. The two main girders are laterally interconnected by intermediate and end diaphragms at a uniform spacing of 5 m. The cross-sectional layout and geometric properties of the bridge are presented in Figure 2.1, and Table 1, respectively.

2.2 Bridge Model

In this study, the concrete and steel members were modeled by using SOLID45 and SHELL63 elements respectively. The SOLID 45 is a hexagonal 8-node element that has a large deflection and strain capability with three degrees of freedom at each node. Whereas the SHELL63 element is a quadrilateral

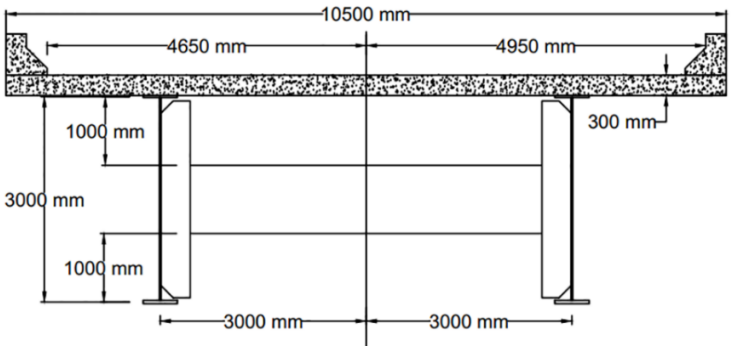

Figure 2.1: Cross-section of the bridge

Table 1: Geometric properties of the bridge (Awall et al., 2012)

Span length (m)	50
Deck thickness × width (m)	0.3 × 10.5
Dimensions of main girders (mm)	Upper FLG500×30, Lower FLG 500×50
Dimensions of intermediate cross-beams (mm)	WEB 1000×16, FLG 300×25
Dimensions of end cross-beams (mm)	WEB 3000×16, FLG 300×25

Table 2: Bridge boundary condition (Awall et al., 2012)

Type	U_1	U_2	U_3	θ_1	θ_2	θ_3
Hinged	Fix	Fix	Fix	Free	Free	Free
Movable	Fix	Free	Fix	Free	Free	Free

4-node element that has stress stiffening, bending, membrane, and large deflection capabilities with six degrees of freedom at each node. The main girders are supported by two types of support such as hinged support and roller support in the tangential direction as described in Table 2. The 3-D model of the curved bridge was created by taking advantage of the cylindrical coordinate system of ANSYS. Here, all the boundary conditions and elements are defined based on this system. For the material properties, the concrete has a modulus of elasticity, Poisson's ratio, and mass density of 28.57 GPa, 0.20, and 2,500 kg/m^3 respectively. A modulus of elasticity of 200 GPa, a mass density of 7,850 kg/m^3 and a Poisson's ratio of 0.30 was used for steel.

2.3 Model Verification

The verification of the bridge model was done by comparing the natural frequencies and mode shapes of this bridge with the existing bridge model. The existing bridge model was taken from *Awall et al. (2012)*, where the natural frequencies of a numerical model of a two-span twin I-girder bridge are given. The cross-section, span number, boundary conditions, and other properties are same as the bridge adopted in this study. Therefore, the bridge is modeled with the same process using ANSYS, and natural-vibration analysis is performed to measure and compare it with existing data. Figure 2.2 shows Frequencies obtained from this analysis are similar to those obtained by Awall et al. (2012). Figure 2.3 shows the numerical natural vibration frequencies and mode shapes. Therefore, it can be concluded that the FE modeling technique for the bridge is appropriate.

2.4 Vehicle Parameters

The vehicle used in this study is an HS20-44 design truck, which is a major design vehicle for highway bridge design specified by AASHTO consisting of six wheels and three-axle tractor-trailer system. The front axle and rare axle load are 43KN and 145KN respectively. The distance between the axles is 4.3m and the width of the vehicle is 1.8m. In this study, vehicle transverse position used as only vehicle parameter. It is found that the vehicle transverse position has a significant effect on the live-load distribution factor

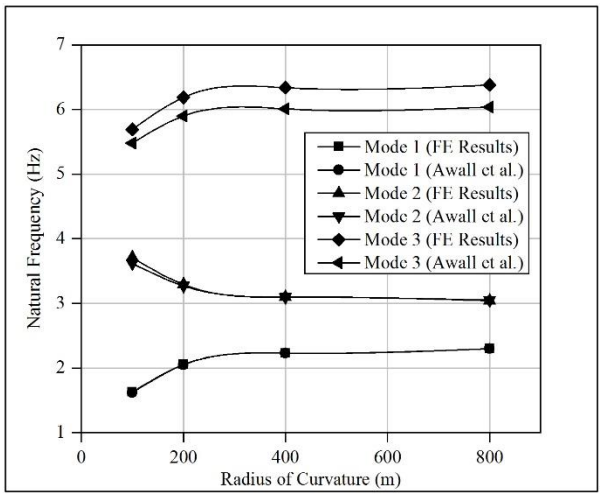

Figure 2.2: Comparison of Natural frequencies of the bridge with the existing model

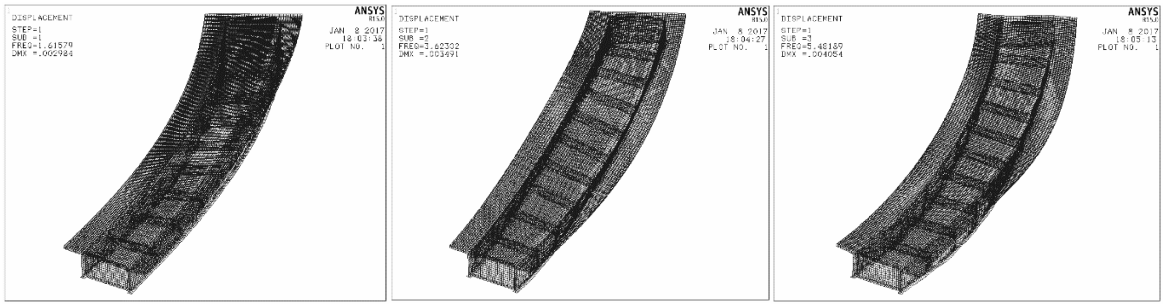

1st Mode (1st bending) FE Analysis: 1.62 Hz | 2nd Mode (1st torsion) FE Analysis: 3.62 Hz | 3rd Mode (2nd bending and torsion) FE Analysis: 5.48 Hz

Figure 2.3: Different mode shapes and natural vibration frequencies

3. LIVE-LOAD DISTRIBUTION FACTOR

3.1 Effect of Curvature on Distribution Factor

Curvature has a significant effect on the live load distribution factor in a curve bridge. The ratio of distribution factor for curve bridge to straight bridge is used to describe the effect of curvature. A bridge with a small radius of curvature shows negative shear at inner girder support. In Figure 3.1, two locations were selected to apply vehicle load (HS20-44 truck) on the bridge named as Pi and Po. The girders are designated by Gi and Go for inner and outer girders respectively. Here, when the load applied at location Pi and measured distribution factor in girder Gi (Inner) than it is denoted by GiPi and similarly others.

Figure 3.2 shows the effect of the bridge radius on the LLDFs. For both girders, the distribution factors are changed up to 500 m radius of the curve than they remain straight. The AASHTO guide 1993 gives a highly conservative distribution factor. Whereas, lever rule gives a slightly conservative distribution factor.

Figure. 3.3 shows the variation of distribution factor with L/R ratio, where L and R named as span length and radius of curvature respectively. When the truckload applied on the outer girder (Po), the distribution factor of inner girder (GiPo) is decreasing with the decrease of radius of curvature and the distribution factor of outer girder (GoPo) is uniformly increased with the decrease of radius of curvature. The distribution factor of outer girder (GoPo) is 0.68 and 0.32 for inner girder (GiPo) when the bridge

is nearly straight (radius of curvature is above 1000m). Though the distribution factor of outer girder (GoPo) is increased to 0.94 with a decreasing radius of curvature (radius of curvature is 100m), whereas it rapidly decreased to 0.07 for inner girder (GiPo).

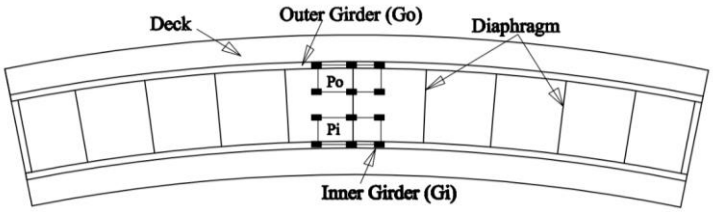

Figure 3.1: Plan view of the curved bridge

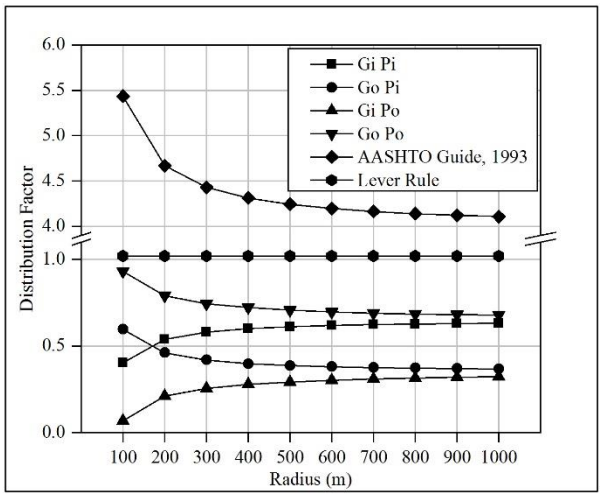

Figure 3.2: Effect of bridge radius on distribution factor

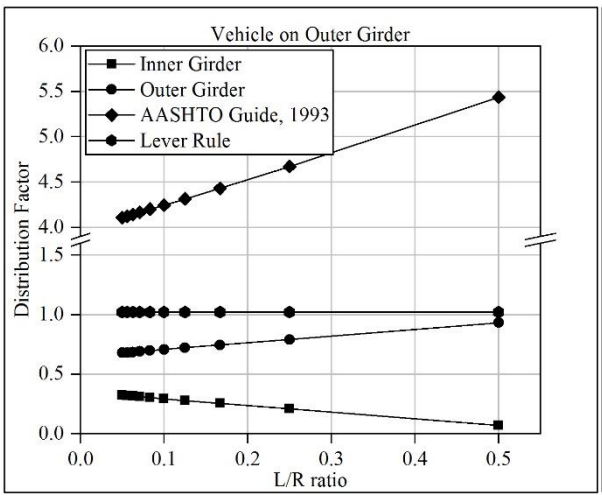

Figure 3.3: Effect of bridge curvature on distribution factor [Vehicle on outer girder (P_o)]

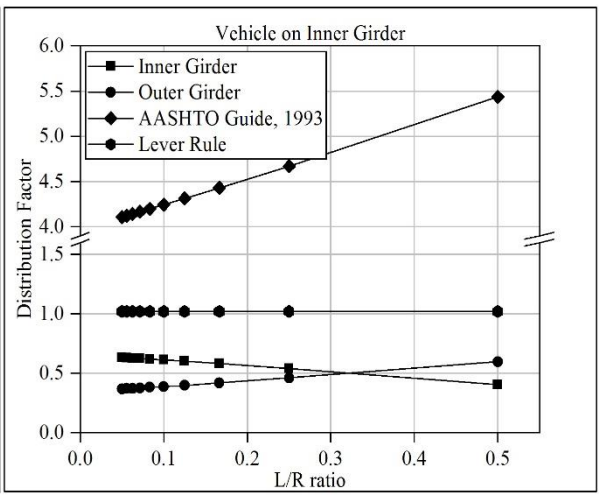

Figure 3.4: Effect of bridge curvature on distribution factor [Vehicle on inner girder (P_i)]

Figure 3.4 shows that when the load applied to the inner girder the distribution factor is increasing for outer girder (G_oP_i) and decreasing for inner girder (G_iP_i) with decreasing radius of curvature. When the bridge is nearly straight, the maximum load will be carried by the inner girder and the distribution factor is 0.63 whereas 0.37 for outer girder. As the bridge getting curved (small radius of curvature), the distribution factor is increased to 0.60 for outer girder and decreased to 0.40 for inner girder. The

distribution factor for outer and inner girder is intersecting when the radius of curvature is approximately 150m.

3.2 Effect of Slab Thickness on Distribution Factor

Figures 3.5 & 3.6 shows that slab thickness has little effect on the live-load distribution factor. Here, the slab thickness varies from 0.25 to 1 m. When the vehicle on the outer-girder, live-load distribution factor of the outer girder is increasing with an increasing slab stiffness. Whereas, the distribution factor for inner girder is decreasing. This variation in distribution factor occurs due to increasing slab stiffness. On the other hand, when the vehicle position on inner-girder, the distribution factor is nearly similar for both inner and outer girders. But this time the loaded girder distribution factor is not increased like outer girder vehicle position. From the figure, it can be noted that the AASHTO standard specification gave a highly conservative distribution factor for both inner and outer girders. But the lever rule gives a close distribution factor for outer girder loading and a slightly conservative for inner girder loading.

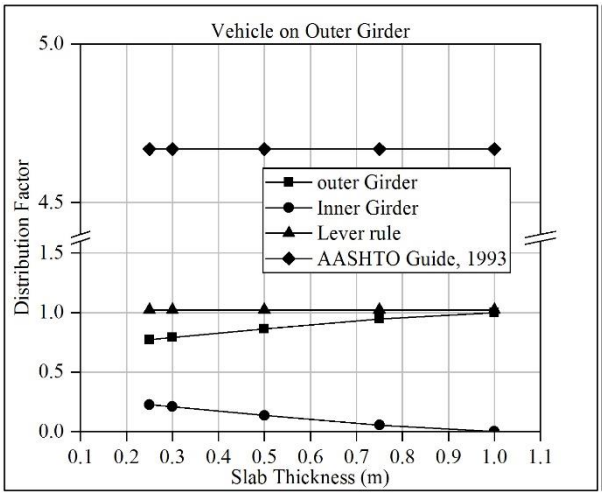

Figure 3.5: Effect of slab thickness on distribution factor [Vehicle on outer girder (P_o)]

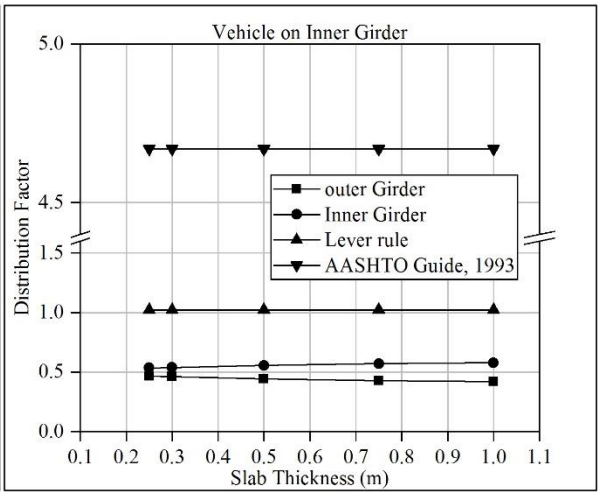

Figure 3.6: Effect of slab thickness on distribution factor [Vehicle on inner girder (P_i)]

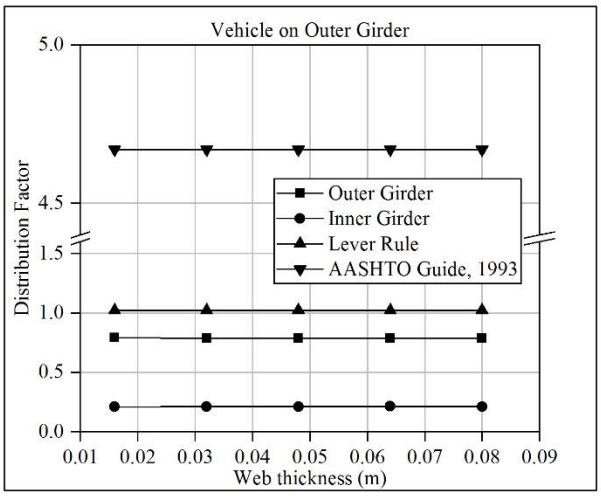

Figure 3.7: Effect of web thickness on distribution factor [Vehicle on outer girder (P_o)]

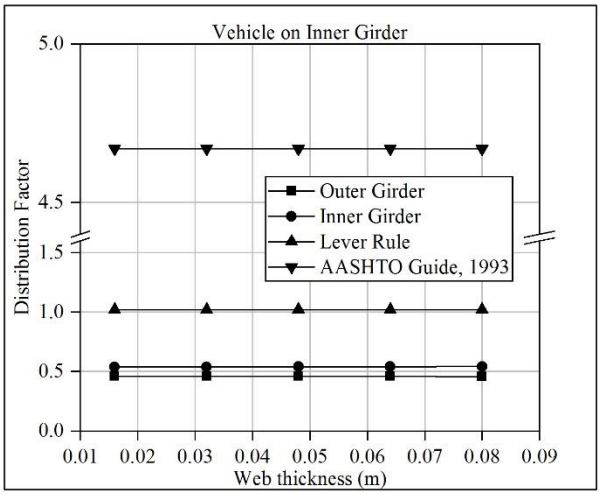

Figure 3.8: Effect of web thickness on distribution factor [Vehicle on inner girder (P_i)]

3.3 Effect of Girder Stiffness on Distribution Factor

In this study, the effect of girder stiffness on the distribution factor has been evaluated. Figures 3.7 & 3.8 show that the girder stiffness doesn't have any effect on the distribution factor in curve bridge.

3.4 Effect of Diaphragm spacing on Distribution Factor

Figures 3.9 & 3.10 show that the diaphragm spacing has no influence on the live-load distribution factor at all. Here, the distribution factor for different diaphragm spacing has been evaluated. The diaphragm spacing ranges from 5 to 25 m. The FE results show no effect on the distribution factor. It can be observed that AASHTO standard specification gives a highly conservative distribution factor whereas lever rule provides slightly conservative results.

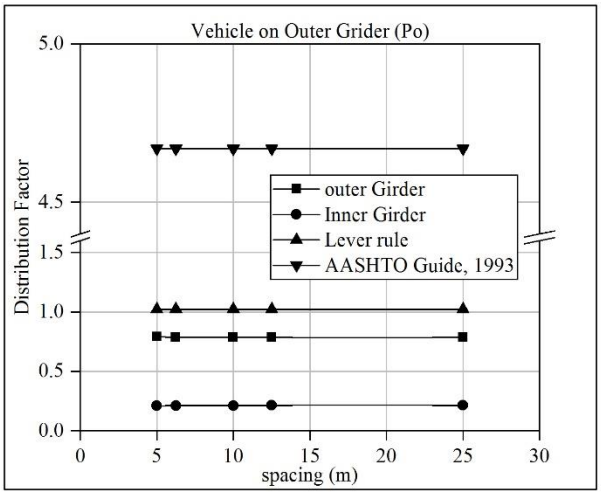

Figure 3.9: Effect of diaphragm spacing on distribution factor [Vehicle on outer girder (P_o)]

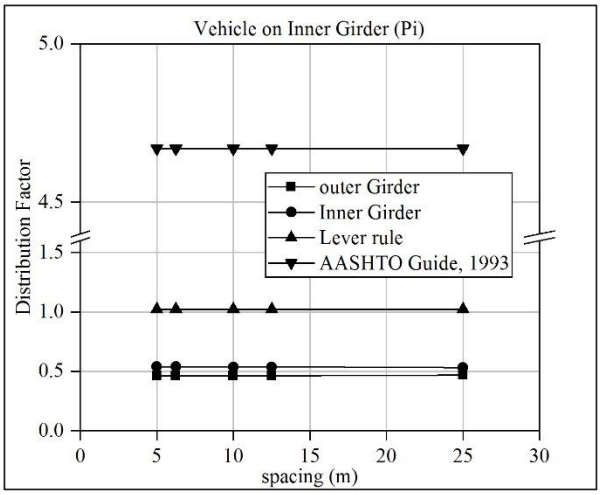

Figure 3.10: Effect of diaphragm spacing on distribution factor [Vehicle on inner girder (P_i)]

4. CONCLUSIONS

The accurate estimations of distribution factors for live-load is very important to bridge design. If the distribution factors are underestimated, the bridge members may be under-designed and will experience serviceability problems. On the contrary, if distribution factors are overestimated, the bridge members will be over-designed and the cost of the bridge construction will increase unnecessarily. Based on the FE study and result of the curve bridge, the following conclusions are made: (1) curvature has a significant effect on live-load distribution in a Curved twin I-girder bridge; (2) the distribution factor of inner girder is decreased for both loading condition with decreasing radius of curvature. It is decreased 78% and 36.5% for outer and inner girder loading respectively; (3) the distribution factor of outer girder is increased for both loading conditions with decreasing radius of curvature. It is increased 38% for outer girder loading and 62% for inner girder loading; (4) AASHTO Guide, 1993 gives a highly conservative distribution factor. However, lever rule method gives a fairly conservative distribution factor; and (5) the finite element results also show that the slab stiffness has considerable effect. Whereas, the girder stiffness and diaphragm spacing have no effect on the distribution factor. Considering this curvature effect some correction factor needs to be added to the standard specification.

REFERENCES

AASHTO. (1996). *Standard specifications for highway bridges* (16th Ed.). Washington, DC.

AASHTO (1994a). (1994). *LRFD Bridge Design Specifications* (1st Ed.). Washington, DC.

AASHTO (1994b). (1994). *LRFD Bridge Design Specifications* (2nd Ed.). Washington, DC.

Awall, R., Hayashikawa, T., Matsumoto, T., & He, X. (2012). Effects of bottom bracings on torsional dynamic characteristics of horizontally curved twin I-girder bridges with different curvatures. *Journal of Earthquake Engineering and Engineering Vibration*, *11*(2), 149–162. https://doi.org/10.1007/s11803-012-0106-4

Barr, P. J., Eberhard, M. O., & Stanton, J. F. (2001). LIVE-LOAD DISTRIBUTION FACTORS IN PRESTRESSED CONCRETE GIRDER BRIDGES. *Journal of Bridge Engineering*, *6*(5), 298–306.

Brockenbrough, R. L. (1986). Distribution factors for curved I-girder bridges. *Journal of Structural Engineering (United States)*, *112*(10), 2200–2215. https://doi.org/10.1061/(ASCE)0733-9445(1986)112:10(2200)

Kim, C. W., Kawatani, M., & Hwang, W. S. (2004). Reduction of traffic-induced vibration of two-girder steel bridge seated on elastomeric bearings. *Engineering Structures*, *26*(14), 2185–2195.

Zhang, H., Huang, D., & Wang, T.-L. (2005). Lateral Load Distribution in Curved Steel I-Girder Bridges. *Journal of Bionic Engineering*, *10*(3), 281–290. https://doi.org/10.1061/(ASCE)1084-0702(2005)10:3(281)

Zisan, B., Hayashikawa, T., Matsumoto, T., & He, X. (2015). Dynamic response and distortion-stress in curved multi-girder bridges subjected to high-speed moving vehicles. *Journal of Structural Engineering*, *61A*.

Zokaie, B. T. (2000). AASHTO-LRFD LIVE LOAD DISTRIBUTION SPECIFICATIONS. *Journal of Bridge Engineering*, *5*(2), 131–138.

Proceedings of the 5th International Conference on Civil Engineering for Sustainable Development (ICCESD 2020), 7~9 February 2020, KUET, Khulna, Bangladesh (ISBN-978-984-34-8764-3)

EXPERIMENTAL INVESTIGATION ON MECHANICAL PROPERTIES OF NATURALLY CORRODED STEEL BARS

Matiur Rahman Raju*[1], Amel Cato[2] and Ignasi Fernendez[3]

[1]Senior Lecturer, City University, Bangladesh, e-mail: raju06civil@yahoo.com
[2]Construction Engineer, Sweco, Sweden, e-mail: amel.cato@hotmail.com
[3]Senior Lecturer, Chalmers University of Technology, Sweden, e-mail: ignasi.fernandez@chalmers.se

***Corresponding Author**

ABSTRACT

Corrosion affects reinforced concrete structures in many ways, however, the impact of corrosion in the mechanical properties of the bar itself presents still many uncertainties. The impact of natural corrosion effect and corrosion type in the measured mechanical properties by experimental investigation would be the main objective of this study. The corrosion levels were measured by using different methods such as gravimetric (weight loss) and 3D scanning techniques. Therefore, to perform monotonic tests on steel bars measured by Digital Image Correlation (DIC) techniques were conducted by using different bar diameters and lengths for uncorroded and corroded specimens, with the underlying purpose to investigate the impact of corrosion on the mechanical properties of the steel reinforcement. Further, the post-processing of the results was carried out with the software GOM Correlate Professional. Based on the performed analysis, the 25mm length extensometer was used in combination with the measured force to obtain all the relevant results: strains, displacements, and other important values needed to further acquire engineering stress-strain curves. The obtained results indicate that the mechanical properties of the reinforcing steel bars are strongly affected by corrosion due to loss of cross-sectional area in global and local cases for naturally corroded specimens. Those factors cause degradation of the mechanical properties by increasing corrosion levels.

Keywords: *Steel reinforcement, Digital Image Correlation (DIC), Tensile test, Engineering stress-strain, Critical cross-section.*

1. INTRODUCTION

Despite the used technology at the leading edge and substantial innovations in construction practice and design, corrosion of steel bars in reinforced concrete structures is still considered to be one of the main reasons of deterioration which causes high costs due to repairing and replacing critical corroded elements in reinforced concrete structures (Fernandez, Bairán and Marí, 2016; Tahershamsi et al., 2017). This has directed to rising demand and needs for a better understanding of the structural effects of corrosion. Corrosion of reinforcing steel can be divided into two subcategories: Pitting corrosion and generalized corrosion. Pitting corrosion is characterized by the formation of localized pits along the steel bar when generalized corrosion can be seen as several local pits distributed along the bar. The common outcome for the two subcategories is increased in volume of corrosion products and by so causing the surrounding concrete cover to expand and crack. Furthermore, when a reinforcing steel bar is affected by pitting corrosion and subjected to tension, local effects at the cross-section due to stress concentration and local bending are unveiled. In addition, multi-axial stress behavior is also observed due to the presence of those pits. Hence, due to those mentioned effects, the apparent mechanical properties that state the overall steel bar behavior are affected, producing a performance reduction (Fernandez, Bairán and Marí, 2015, 2016). This leads to a major concern to the structural behavior in serviceability and ultimate limit states, which is investigated in this study.

Many researchers such as U, 2001; Du, Clark and Chan, 2005; Apostolopoulos, 2007; Zhang et al., 2012; Apostolopoulos, Demis and Papadakis, 2013; François, Khan and Dang, 2013; Balestra et al., 2016; Tahershamsi et al., 2017; Zhu et al., 2017; Fernandez, Bairán and Marí, 2016; Fernandez, Bairán and Marí, 2015 have already studied the effects for different corrosion types of steel reinforcement and its influence on the mechanical properties. An experimental study of both natural and artificial corroded specimens for tensile test results showed a significant degradation in ultimate strength. Further studies show that naturally corroded rebars have more affecting mechanical results than artificial corroded rebars (Zhang et al., 2012). Due to the generalized and pitting corrosion of steel reinforcement, the cross-section geometry is changing by the loss of the real cross-section diameter of the specimens (Fernandez, Bairán and Marí, 2016). Many experimental studies were done for artificially corroded rebars than naturally corroded to investigate the impact of corrosion on the mechanical properties of the steel reinforcement. The effects of corrosion on the mechanical properties of reinforcement are critical to understanding the real behavior of naturally corroded reinforced concrete structures is needed. A smaller amount of studies has been conducted to evaluate the mechanical properties of naturally corroded and uncorroded steel bars.

In this current experimental work, the monotonic tests on steel bars measured by Digital Image Correlation (DIC) techniques were conducted to investigate the impact of corrosion degree on the mechanical properties of the steel reinforcement have been identified and discussed.

2. RESEARCH METHODOLOGY

2.1 Test Specimens

In this experimental study, a total of 49 reinforcement test specimens divided into two different sets, organized by the source and characteristics of the bars were tested, see Figure 1. Each group was at the same time divided into two groups to differentiate between corroded and uncorroded specimens. The subtypes are:

- Type A1: 16mm naturally corroded, skewed, reinforcing bars.
- Type A2: 16mm uncorroded, skewed reinforcing bars.
- Type B1: 16mm naturally corroded, straight reinforcing bars.
- Type B2: 16mm uncorroded, straight reinforcing bars.

(a) (b) (c)

Figure 1: Images of some specimens from different sources where figures (a) shows the type A1 and B1 naturally corroded 16mm rebars, (b) shows type A2 uncorroded 16mm rebars, (c) shows type B2 uncorroded 16mm rebars.

2.2 Preparation of Test Specimen

For the experiment purpose, rebars were cut by a horizontal band saw machine with ranging lengths of 300 and 400mm. According to Fernandez et al. (Fernandez, Lundgren and Zandi, 2018), the most common methods to clean the corrosion products of the rebars are metallic brushing, acid immersion and sandblasting. The comparison results of 3D scanning and gravimetric measurements for different cleaning methods shown that the sandblasting cleaning method has the best agreement irrespective of the actual corrosion level. Consequently, after cutting the rebars in specific lengths, the sandblasting cleaning method was used with silica particles to remove all corrosion products from the reinforcing steel in a closed-loop system. After the removal of corrosion products from the corroded specimens, the diameter of the rebars was measured by using the Vernier caliper.

2.3 Corrosion Level Measurements

To be able to draw parallels between the corrosion level and how it is impacting the mechanical properties of the reinforcement steel it is crucial to use accurate and reliable corrosion level measurements. In this study, gravimetric measurements and 3D scanning measurements were used to determine the corrosion level.

2.3.1 Gravimetric Measurements

Gravimetric measurement is a method where the calculations are based on weighted corroded and non-corroded steel reinforcement, i.e. weight loss. This procedure was used because the initial weight of each bar before corrosion was unknown.
When the reference weight of the non-corroded steel reinforcement is established, then the calculation can be performed to check the average corrosion degree by using equation 1. See Table 1 for the calculated corrosion levels for the tested bars.

$$avg.cor.lev = \frac{(n.C. - C.)}{n.C.} \quad (1)$$

where:

n.C is the average weight of the non-corroded reference specimen.

C is the actual corroded specimen weight.

2.3.2 3D Scanning Measurements

The 3D scanning technique method that relies on optical measurements. The 3D-scanned results used in this study are research work conducted at Chalmers University of Technology (Das, unpublished; Berrocal, 2017). For those research works the scanning was performed by using a pair of industrial scaled cameras of five megapixels each, set to film in the stereo setting. A maximum accuracy of 2.0 μm was possible to obtain due to the used cameras, which is sufficient in conditions where the corrosion imperfections on the surface of the reinforcing steel need to be measured. The consequence of the scanning resulted in a fine mesh of surface polygons with triangular shape connected by nodes. For every scanning a number of 2,000,000 to 4,000,000 triangular elements was obtained, creating a high-resolution 3D picture of the scanned specimen detailed enough to gain important information such as: pit distribution, pit depth, pit length and loss of cross-sectional area along the reinforcing steel bar see Figure 2 (Tahershamsi et al., 2017).

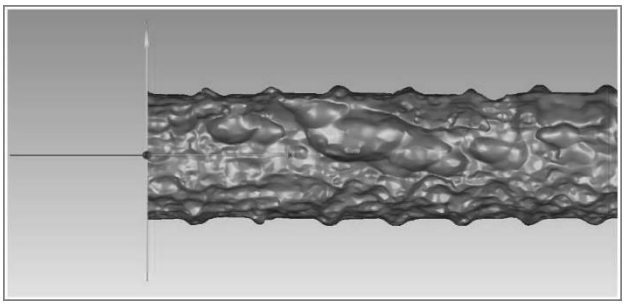

Figure 2: 3D scanned surface of the bar (Tahershamsi et al., 2017)

Based on these two methods the cross-sectional area of the rebar was reduced in two ways: the average (idealized) corroded area along with the rebar, founded on the actual, uncorroded radius and critical cross-section (CCS) reduced area from the 3D scan. The actual (uncorroded), average corroded and CCS areas are respectively displayed in Figure 3. The detailed description of all the acquired parameters is summarized in Table 1.

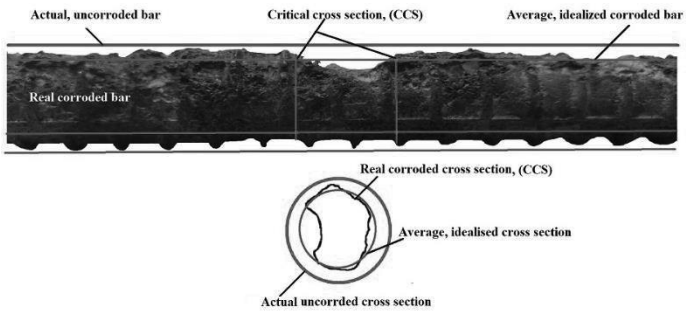

Figure 3: Different type of steel reinforcement areas used in this study

Table 1: Measured specifications of test samples

Type of specimen	Specimen number	Actual diameter [mm]	Average corrosion level (wt. loss) [%]	Average corrosion level (3D scan) [%]	Corrosion at critical cross-section (3D scan) [%]	Actual area [mm^2]	Average (Idealized) area (wt. loss) [mm^2]	Average (Idealized) area (3D scan) [mm^2]	Critical cross-sectional (CCS) area [mm^2]
Type A1	1	16,59	7,5	4,5	13,4	216,05	200	206	187
	3	16,59	8,2	11,4	25,5	216,05	198	191	161
	5	16,59	8,7	7,4	12,3	216,05	197	200	189
	6	16,59	7,2	7,8	21,4	216,05	200	199	170
	8	16,59	7,0	4,0	14,6	216,05	201	207	184
	9	16,59	7,7	8,2	19,3	216,05	199	198	174
	10	16,59	10,1	8,5	12,9	216,05	194	198	188
	11	16,59	8,2	5,9	9,7	216,05	198	203	195
	16	16,59	8,6	7,7	16,7	216,05	197	199	180
	17	-	-		-	-	-	-	-
	18	16,59	7,8	11,5	20,0	216,05	199	191	173
Type A2	U49	16,59	-	-	-	216,05	-	-	-
	U51	16,59	-	-	-	216,05	-	-	-
	U53	16,59	-	-	-	216,05	-	-	-
	U54	16,59	-	-	-	216,05	-	-	-
	U55	16,59	-	-	-	216,05	-	-	-
Type B1	2	16,41	8,0	5,9	11,2	211,60	195	199	188
	4	16,41	9,5	13,5	30,6	211,39	191	183	147
	7	16,41	14,0	10,6	17,8	211,39	182	189	174
	12	16,41	8,7	13,3	26,9	211,39	193	183	155
	13	16,41	5,3	4,3	10,1	211,39	200	202	190
	14	16,41	10,9	12,6	20,0	211,39	188	185	169
	15	16,41	8,9	11,4	16,3	211,39	193	187	177
	19	16,41	8,2	12,5	24,3	211,39	194	185	160
	20	16,41	14,5	16,0	27,1	211,39	181	178	154
	21	16,41	14,2	15,4	19,7	211,39	181	179	170
	22	16,41	5,8	3,4	7,7	211,39	199	204	195
	23	16,41	8,3	8,7	16,7	211,39	194	193	176
	24	16,41	6,1	5,5	17,7	211,39	198	200	174
	25	16,41	7,6	8,2	14,6	211,39	195	194	181
	26	16,41	14,3	15,6	25,0	211,39	181	178	158
	27	16,41	12,8	14,4	18,4	211,39	184	181	173
	28	16,41	7,9	6,6	13,0	211,39	195	197	184
	29	16,41	11,6	10,4	19,1	211,39	187	189	171
	30	16,41	5,8	6,0	13,1	211,39	199	199	184
	31	16,41	4,9	1,7	6,5	211,39	201	208	198
	32	16,41	11,2	9,7	21,8	211,39	188	191	165
	33	16,41	17,8	18,2	30,4	211,39	174	173	147
	34	16,41	5,4	7,6	14,2	211,39	200	195	181
	35	16,41	4,4	3,7	10,3	211,39	202	204	190
	36	16,41	15,4	15,6	20,9	211,39	179	178	167
	37	16,41	15,4	15,4	28,5	211,39	179	179	151
	38	16,41	18,7	25,5	39,0	211,39	172	158	129
	39	16,41	12,3	12,3	20,6	211,39	185	185	168

Type of specimen	Specimen number	Actual diameter [mm]	Average corrosion level (wt. loss) [%]	Average corrosion level (3D scan) [%]	Corrosion at critical cross-section (3D scan) [%]	Actual area [mm^2]	Average (Idealized) area (wt. loss) [mm^2]	Average (Idealized) area (3D scan) [mm^2]	Critical cross-sectional (CCS) area [mm^2]
Type B1	36	16,41	15,4	15,6	20,9	211,39	179	178	167
	37	16,41	15,4	15,4	28,5	211,39	179	179	151
	38	16,41	18,7	25,5	39,0	211,39	172	158	129
	39	16,41	12,3	12,3	20,6	211,39	185	185	168
Type B2	U48	16,41	-	-	-	211,39	-	-	-
	U50	16,41	-	-	-	211,39	-	-	-
	U52	16,41	-	-	-	211,39	-	-	-
	U58	16,41	-	-	-	211,39	-	-	-
	U59	16,41	-	-	-	211,39	-	-	-

2.4 Assessment of Mechanical Properties

After assessing the specifications of the bars, the tensile test to failure was performed on a UTM machine of 250kN capacity with a loading increment of 0.5kN/s. Between the two clamps, the specimen's length was chosen 200mm and the remaining length placed in each clamp for uniform stress distribution. The Digital Image Correlation (DIC) optical non-contact 3D measuring system techniques were used to recorded applied load and elongation with a high-speed camera until the specimen failure. The equipment is, at the same time, connected to a computer responsible for recording the acquired images. The system allows the acquisition of other external data, by connecting it to the optical channels available. In this project, the calibration was set up for measuring areas of 100mm x 20mm following the manufacturer`s guidelines and standards (Wanat, 2016). To use the DIC system a stochastic pattern needs to be applied to the specimen. The post-processing of such measurements allows the obtention of many other relevant parameters. The setup of the DIC system is shown in Figure 4.

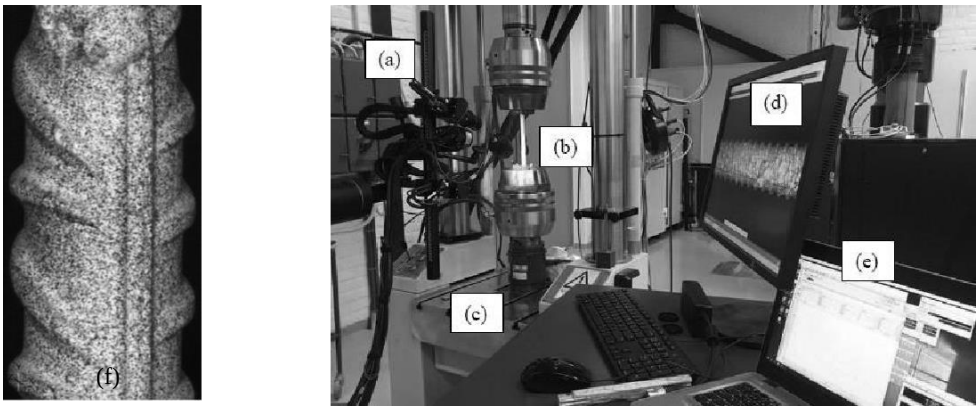

Figure 4: Setup of the Digital Image Correlation (DIC) testing system. (a) double cameras and LED lights, (b) tested specimen, (c) tensile test machine, (d) DIC software, (e) controls for a tensile test machine (f) displays the painted reinforcement bar in a zoomed-in setting displaying the stochastic pattern.

2.5 Post-Processing Analysis Method

In cases of Digital Image Correlation (DIC) method, a tool in the software named "Extensometer" was used to obtain the requested data. GOM tool works in the same manner when compared to physical extensometers. After establishing the function for the GOM extensometer, an analysis of the strain distributions along the measured length was done. For this analysis extensometers length, 25mm was used between the ribs of the reinforcing steel bar. The interference with ribs generates a lot of so-called noise, due to discontinuities in the measurements of the DIC system.

3. RESULTS AND DISCUSSIONS

The experimental results are analyzed and discussed with respect to the influence of corrosion are presented in this section. The main types of graph engineering stress-strain were used extracted and collected different mechanical parameters for the tested rebars.

3.1 Engineering Stress-Strain Correlation

Figure 5 and Figure 6 displays the engineering stress-strain curves for the different type of naturally corroded rebars at various corrosion levels for average and critical cross-section with respect to the uncorroded steel bar. Also considered the increasing corrosion level at a critical cross-section, the stress value is much higher than for average corroded cross-section with increasing corrosion level. The effects of different corrosion levels for different types of bars are analyzed to obtain a correlation between the strengths and corrosion levels. Finally, the behavior of modulus of elasticity with increased corrosion levels is also discussed.

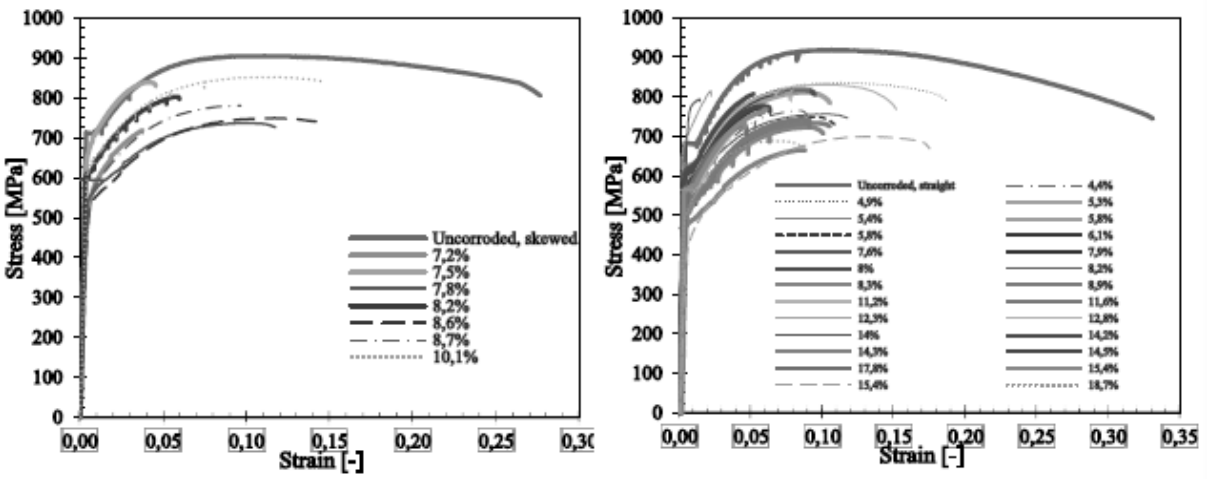

(a) A1 and A2, 16mm skewed bars (b) B1 and B2, 16mm straight bars

Figure 5: Engineering stress-strain curves for a different type of naturally corroded rebars of various corrosion levels at the average cross-section.

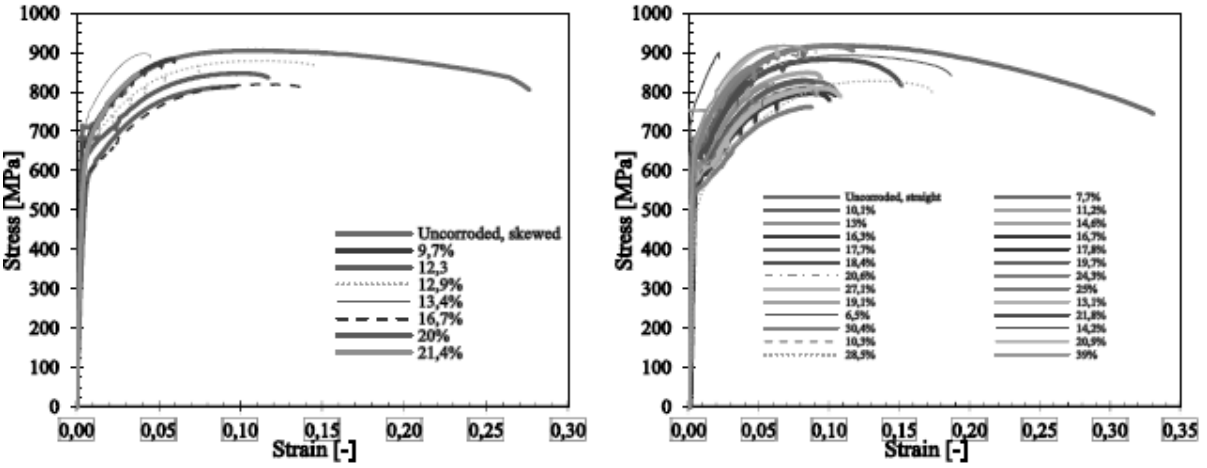

(a) A1 and A2, 16mm skewed bars (b) B1 and B2, 16mm straight bars

Figure 6: Engineering stress-strain curves for a different type of naturally corroded rebars of various corrosion levels at the critical cross-section.

3.1.1 Yield and Ultimate strength

The change of yielding and ultimate strengths depended on increasing corrosion levels which are presented in Figure 7 and Figure 8. The yielding and ultimate strengths produced a reduced trend for considered corrosion levels at the average corrosion level and constant trend for the critical cross-section. For both corrosion levels in Figure 7 and Figure 8, the polynomic fit was used for type (B1, B2) to obtain a high coefficient of correlation, where the linear function was used for type (A1, A2). With this limitation, most of the curves showed that strengths are reducing with increased average corrosion levels. On the other hand, several researchers (Apostolopoulos, 2007; Zhang *et al.*, 2012; Fernandez, Bairán and Marí, 2015) also observed the similar decreasing behavior of yielding and ultimate strengths with increased corrosion levels.

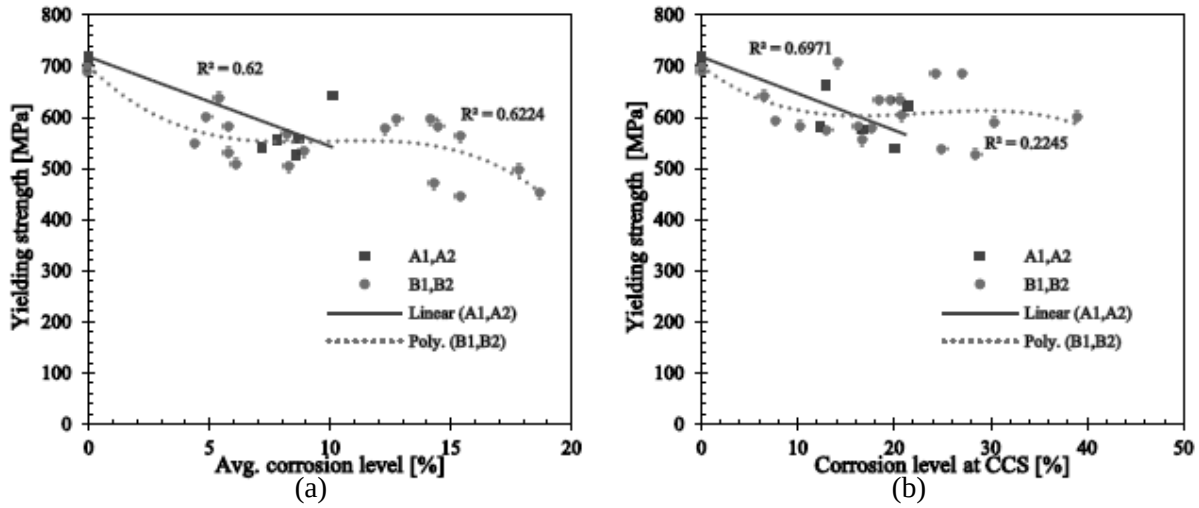

(a) (b)

Figure 7: The yielding strength effect on corrosion levels for a different type of naturally corroded rebars.

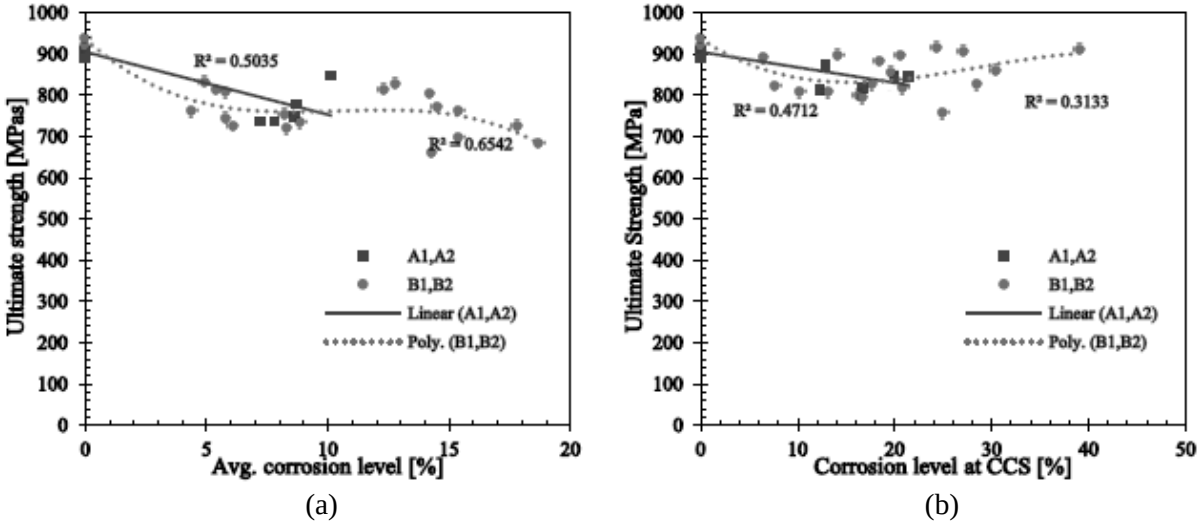

(a) (b)

Figure 8: The ultimate strength effect on corrosion levels for a different type of naturally corroded rebars.

In Figure 7(a) and Figure 8(a) the reducing yield and ultimate strength when considering the average corrosion level. The reduction of the load is higher than the reduction of an area with the increase of corrosion. Due to this difference in reduction, the strength ratio will always be slightly reduced. This reducing behavior was also observed by Llano Trueba, 2015. Further for the CCS section, a reduction

was not noticed as for the average corrosion level, instead, the strength value stayed constant. This can be explained by the CCS method of measuring corrosion level is more realistic and more accurate than average corrosion level, creating a force reduction close to the expected one. The ratio between the force and the area is more or less of the same magnitude and by so resulting in a constant strength value as observed in Figure 7(b) and Figure 8(b).

3.1.2 Modulus of Elasticity

The effect of different corrosion levels on the modulus of elasticity is presented in Figure 9. The modulus of elasticity displayed the highly scatter data disregard of used corrosion type. Because of that, a trustworthy correlation could not be established.

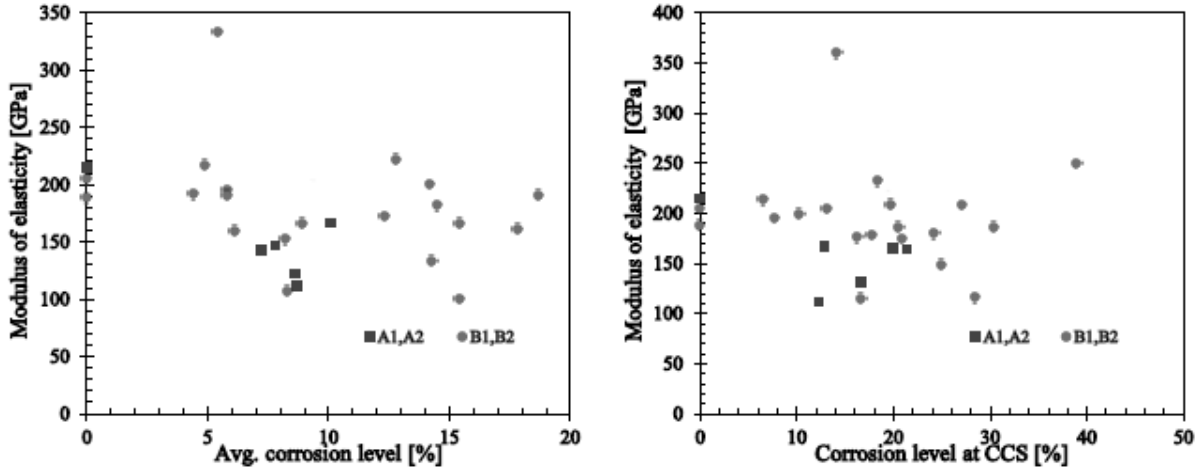

Figure 9: The modulus of elasticity effect on corrosion levels for different type of naturally corroded rebars.

4. CONCLUSIONS

In this study, the average and critical cross-section (CCS) corrosion levels ranged from 0-20% and from 0-40% respectively. However, the observations made for the different parameters were not proportional to the measured corrosion level. The findings presented in this study showed that both the corrosion method i.e. average corrosion and critical corrosion affected the considerate mechanical properties. It can be summarized that method of measuring corrosion in the critical cross was more realistic in its way of describing the behavior. This information will lead to better understanding of the behavior for the reinforced concrete structures and how much they are affected by corrosion.

ACKNOWLEDGMENTS

This research study was undertaken at the Chalmers University of Technology, Division of Structural Engineering and Building Technology, Sweden. We would like to express the sincerest gratitude and appreciation to Ignasi Fernendez, Senior Lecturer, Chalmers University of Technology and his research-team for the support, specifically through hours of meetings, useful advice, expert knowledge, and guideline throughout this study. The authors of the manuscript would like to acknowledge Sebastian Almfeld, a research engineer at the Chalmers University of Technology, for his valuable contribution to the experimental work.

REFERENCES

Apostolopoulos, C. A. (2007) 'Mechanical behavior of corroded reinforcing steel bars S500s tempcore under low cycle fatigue', *Construction and Building Materials*, 21(7), pp. 1447–1456. doi: 10.1016/j.conbuildmat.2006.07.008.

Apostolopoulos, C. A., Demis, S. and Papadakis, V. G. (2013) 'Chloride induced corrosion of steel reinforcement - Mechanical performance andpit depth analysis', *Constr uction and Building Materials*. Elsevier Ltd, 38, pp. 139–146. doi: 10.1016/j.conbuildmat.2012.07.087.

Balestra, C. E. T. *et al.* (2016) 'Corrosion Degree Effect on Nominal and Effective Strengths of Naturally Corroded Reinforcement', *Journal of Materials in Civil Engineering*, 28(10), p. 4016103. doi: 10.1061/(ASCE)MT.1943-5533.0001599.

Berrocal, Carlos G. (2017). 'Corrosion of Steel Bars in Fibre Reinforced Concrete: Corrosion mechanisms and structural performance'. 10.13140/RG.2.2.18233.88166.

Du, Y. G., Clark, L. A. and Chan, A. H. C. (2005) 'Residual capacity of corroded reinforcing bars', *Magazine of Concrete Research*, 57(3), pp. 135–147. doi: 10.1680/macr.2005.57.3.135.

Das, P. (Unpublished) '3D Scanning of naturally corroded steel bars. An assessment of corrosion behavior and correlations to critical cross-sections', Unpublished.

Fernandez, I., Bairán, J. M. and Marí, A. R. (2015) 'Corrosion effects on the mechanical properties of reinforcing steel bars. Fatigue and σ-ε behavior', *Construction and Building Materials*. Elsevier Ltd, 101, pp. 772–783. doi: 10.1016/j.conbuildmat.2015.10.139.

Fernandez, I., Lundgren, K. & Zandi, K. Mater Struct (2018) 51: 78. https://doi.org/10.1617/s11527-018-1206-z

Fernandez, I., Bairán, J. M. and Marí, A. R. (2016) 'Mechanical model to evaluate steel reinforcement corrosion effects on σ-ε and fatigue curves. Experimental calibration and validation', *Engineering Structures*. Elsevier Ltd, 118, pp. 320–333. doi: 10.1016/j.engstruct.2016.03.055.

François, R., Khan, I. and Dang, V. H. (2013) 'Impact of corrosion on mechanical properties of steel embedded in 27-year-old corroded reinforced concrete beams', *Materials and Structures/Materiaux et Constructions*, 46(6), pp. 899–910. doi: 10.1617/s11527-012-9941-z.

Llano Trueba, L. (2015) 'Patterns of corroded rebar surfaces and their impact on tensile mechanical properties.', (August). Available at: http://epubs.surrey.ac.uk/808602/.

Gom.com (2018). *Gom.com*. Retrieved 2018-04-01 from https://www.gom.com/3d-software/gom-system-software/aramis professional.html.

Tahershamsi, M. *et al.* (2017) 'Investigating correlations between crack width, corrosion level and anchorage capacity', *Structure and Infrastructure Engineering*.

U, A. A. A. (2001) 'Effect of degree of corrosion on the properties of reinforcing steel bars', pp. 361–368.

Wanat, S. F. (2016) 'Acquisition : Basic Issues', 25(2), pp. 142–147.

Zhang, W. *et al.* (2012) 'Tensile and fatigue behavior of corroded rebars', *Construction and Building Materials*. Elsevier Ltd, 34, pp. 409–417. doi: 10.1016/j.conbuildmat.2012.02.071.

Zhu, W. *et al.* (2017) 'Influences of corrosion degree and corrosion morphology on the ductility of steel reinforcement', *Construction and Building Materials*. Elsevier Ltd, 148, pp. 297–306. doi: 10.1016/j.conbuildmat.2017.05.079.

Proceedings of the 5th International Conference on Civil Engineering for Sustainable Development (ICCESD2020), 7~9 February 2020, KUET, Khulna, Bangladesh (ISBN-978-984-34-8764-3)

EXPERIMENTAL STUDY OF FIBER REINFORCED CONCRETE USING METALLIC AND NON-METALLIC FIBERS

Shah Newaz Aftab[1], Chaiti Karmakar[2], Hasan Mohammod Zakaria[3] and Sristi Das Gupta*[4]

[1,]Department of Civil Engineering, Ahsanullah University of Science and Technology, Bangladesh,e-mail:chayonshah15091@gmail.com
[2]Department of Civil Engineering, Ahsanullah University of Science and Technology, Bangladesh, e-mail:chaitykarmakar15094@gmail.com
[3]Department of Civil Engineering, Ahsanullah University of Science and Technology, Bangladesh, e-mail: zakariaorko@gmail.com
[4]Faculty of Civil Engineering, Ahsanullah University of Science and Technology, Bangladesh, e-mail: payelcuet@gmail.com

***Corresponding Author**

ABSTRACT

Concrete is a brittle material with strong compressive strength but with little tensile strength (approximately 10% of its compressive strength) having little resistance to cracking.The fragile characteristic of concretecan be overcome by blending the concrete with fibrous material, which is termed as fiber reinforced concrete. Fiber-reinforced concrete (FRC) has become a sustainable material used in various constructions such as building pavements, large industrial floors, and runways. With the modern technology, fibers are two types, such as: artificial fibers and natural fibers. This paper deals with the concept of using metallic (and non-metallic fibers in concrete. In this research, GI (Galvanized Iron) and Jute chopped fibers were used to develop an FRC material to study the possible improvement in the 28-days strength. Clumping of fibers at high fiber amounts caused mixing and casting problems. These problems become even more severe when long fibers are used at the high fiber dosage amount. In this study, different composition of Jute (0.1%, 0.2%, 0.3%) and GI fibers (1%, 1.5% and 2%) with different lengths are added in concrete. A significant increment of compressive and tensile strength between plane concrete and fiber reinforced concretes were found. The aim of this paper is to study the strength characteristics of metallic fiber and non-metallic fiber in concrete and make a comparison with normal plain concrete specimens.

Keywords: *Metallic fiber, Non-metallic fiber, Jute, G.I fiber, Strength.*

1. INTRODUCTION

Concrete is a composite material obtained by permitting a carefully proportioned mixture of cement, sand and gravel or other aggregate and water to harden in forms of the shape and dimensions of the desired structure. The materials are mixed together until a cement paste is developed, filling most of the voids in the aggregates and producing a uniform dense concrete.Concrete is relatively brittle and its tensile strength is relatively low in contrast with thecompressive strength (Sivakumer*et al*., 2007).For the sustainable development with higher strength is the growing demand in construction industry. Concrete reinforcement by natural fibers are more promising to insure the concrete strength improvement with nonhazardous impact on environment as well as the effective use of available natural assets. To achieve this goal, numerous researchers have used the fiber as well as yarn very effectively as a concrete reinforcing material ((Nemati, 2013).

For many applications, it is becoming increasingly popular to reinforce the concrete with small amount of randomly distributed fibers. The concept of using fibers as reinforcement is not new. Research into new fiber-reinforced concretes continues today. Fibers include steel fibers, glass fibers, synthetic fibers and natural fibers - each of which lend varying properties to the concrete. From the light of the structural steel reinforcement contribution to the tensile strength of concrete, steel fibre usage in concrete industry has also been developed recently. Steel fibre reinforced concrete has superior tensile performance with respect to plain concrete depending on the type and amount of steel fibers. In contrast to metallic fiberusing natural fiber in concrete can be a cost effectivesolution for making FRC.

Fiber reinforced concrete (FRC) may be defined as a composite materials made with Portland cement, aggregate, and incorporating discrete discontinuous fibers (Gupta S D *et al.*,2016).Fibers are usually used in concrete to control cracking due to plastic shrinkage and to drying shrinkage. Some types of fibers produce greater impact, abrasion, and shatter resistance in concrete. Their main purpose is to increase the toughness of the materials and also increase the tensile and flexural strengths of concrete, and thus reduce steel reinforcement requirements and control the crack widths tightly.

Among two different types of fibers (natural fibers and artificial polymer-based fibers) natural fibers are promising to use as reinforcement to overcome the inherent deficiencies in FRC reinforced with polymer-based fiber (Parveen*et al*, 2013). The main deficiencies associated with the use of artificial fibers are relatively high cost, health and environmental hazards. On the contrary, natural fibers which are biodegradable, inexpensive, environmentally friendly, and easily available as are produced from naturally available resources, for instance, coconut tree, banana tree, cotton, and jute. Researchers have conducted numerous studies on the effect of natural fibers on the mechanical and physical behavior of concrete to investigate the extent of improvement. In recent years, unrelenting efforts have been observed for using natural fibers in FRC for improving the energy efficiency, economy, and eco-friendliness flavour.

Jute fibers, which come from annual plants, are available in plenty in Bangladesh.These fibres are extracted from the ribbon of the stem. It is a long, soft and shiny vegetable fiber having off-white to brown color. High tensile strength and low extensibility are some key properties of jute fiber. Recent studies have shown that jute fibre delays the hardening of concrete and improves the resistance of concrete against cracking.Nowadays, metallic fibers(galvanized steel) are also used as the fiber reinforcement to boost up the strength of concrete. Galvanized steel wire is made of carbon steel zinc plated. The diameter of the wire generally varies 0.30 mm to 1.2 mm. Specific gravity of the G.I. wires are also ranges between 6000-7500 Kg/m3.

Basically the Conventional concrete is brittle and has poor resistance to crack opening. Numerous liturratures showed that use of Jute fibers and GI fibers in lower strength concretes increase the compressive strength significantly when it is compared to plain un-reinforced matrices and is directly related to volume fraction of fiber used. This study provides in-depth look into the metallic and non-metallic fiber reinforced concrete properties like tensile strength and compressive strength.The effects of two types of fiber (Jute and Steel) reinforcement on concrete is reported in this paper.

2. MATERIALS AND METHODS

2.1 Materials

In this experiment, Ordinary Portland cement (OPC) was used. The percentage of clinker and gypsum in the cement was 95 - 100% and 0-5% respectively. Coarse sand was used as fine aggregate while crushed stone chips was used as coarse aggregate..In this research, jute fiber of 15 mm was used with the proportion of cement, coarse aggregate and sand with the fixed water cement ratio of 0.38. The specimens were prepared for different volumetriccontent of jute fibers, 25mm (0.1%, 0.2%, 0.3%) and curing was done for 28 days. Furthermore for G.I. fiber, 40 mm of length was used with the proportion of (1%, 1.5%, 2%).

Mix design was conducted as per American Concrete Institute (ACI, 2009). The goal was to obtain target strength of 35 MPa at 28 days considering a slump value of 75–100 mm. Before the test all aggregates were taken to SSD condition. Cements and aggregates content kept same for all mixes while water was varied to obtain target slump value.The detailed concrete mix proportions of constituent materials, metallic and non-metallic fiber used for the study are given below in Table 1.

Table 1: Mix proportions of the concretes used in experimental work

Mix	Water (Kg/m3)	Cement (Kg/m3)	Coarse aggregate (Kg/m3) [SSD (OD)]	Fine aggregate (Kg/m3) [SSD(OD)]	Fiber (Kg/m3)
Pc (0%)	205	539.5	999 (992)	601 (594)	0.0
J1(0.1%, 25mm)	206	539.5	999 (992)	601 (594)	0.2345
J1(0.2%, 25mm)	208	539.5	999 (992)	601 (594)	0.4690
J1(0.3%, 25mm)	212	539.5	999 (992)	601 (594)	0.7035
G1(1%, 40mm)	211	539.5	999 (992)	601 (594)	2.345
G2(1.5%, 40mm)	214	539.5	999 (992)	601 (594)	3.5175
G3(2%, 40mm)	217	539.5	999 (992)	601 (594)	4.690

2.2 Concrete Mixing

Concrete was mixed using a machine mixer. Appropriate quantity of coarse aggregate, fine aggregates (SSD) and cement, were first dry mixed for a period of 2 minutes. The mixing water was then added to the mixer. Fibers were dispersed by hand in the mixture to achieve a uniform distribution throughout the concrete, which was mixed for a total of 4 min. After mixing, the workability of concrete was determined using slump cone. The concrete was placed in the fabricated mould and tamping is done using a tamping rod. A smooth steel trowel was used to finish the fresh concrete.

2.3 Strength Testing

The strength of concrete was determined by casting 6-inchcube specimen. The specimens were tested by universal testing machine after 28 days curing. Load was applied gradually at the rate of 2mm/min till the specimens fails.

3. RESULTS & CONCLUSIONS

3.1 Compressive and Tensile Strength

The paper reported experimental results on using Metallic (GI) and Non-metallic (Jute) fibre in concrete with respect to the plain concrete.Concrete compressive and tensile strength data are given in Table

2.Relationship between the Jute fiber and GI fiber content with concrete compressive strength are shown in Figure 1.

Table 2: Strength characteristics of fiber reinforced concretes

Type of concrete	Compressive strength (MPa)	Tensile Strength (MPa)
Pc	36.5	2.13
J1	38.87	2.99
J2	39.62	3.20
J3	41.03	3.37
G1	39.92	3.62
G2	40.86	3.93
G3	42.35	4.03

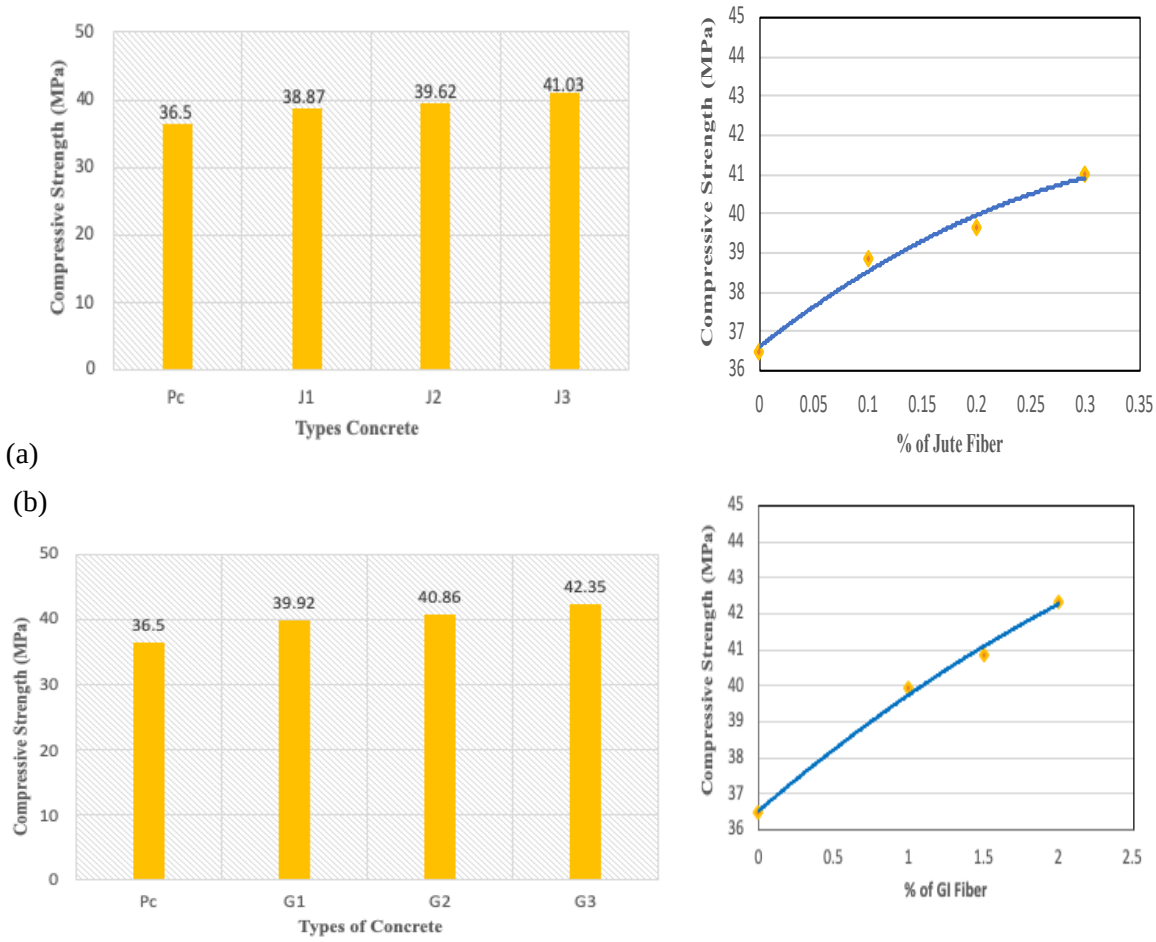

Figure1: Relationship between fiber content and compressive strength of (a) non-metallic fiber reinforced concrete; and(b) metallic fiber reinforced concrete

It is observed from the Figure 1 that with the increasing of fiber contents compressive strength of concrete also aincreased for both cases. This is because interlocking effect of concrete matrix increased and better bond achieved between fibers and concrete.With the addition of 0.1%,0.2% and 0.3% jute fiber (non-metallic fiber) the compressive strength of concrete was increased respectively 6.5%,8.0% and 12.5% in contrast to GI fiber while the compressive strength of concrete increased 9.4%,12% and 16% by adding 1%,1.5% and 2% Galvanized steel (Metallic fiber) respectively. A maximum of 12.5% increment in compressive strength (with respect to the control concrete) was noted with addition of

0.3% volume of jute fibers (J3) in the concrete (Fig.1a).on the other hand, addition of 2% GI fibers (G3) maximum compressive strength of 16% was found (Fig.1b). Relationship between the Jute fiber and GI fiber content with concretesplit tensile strength are shown in Figure 2.

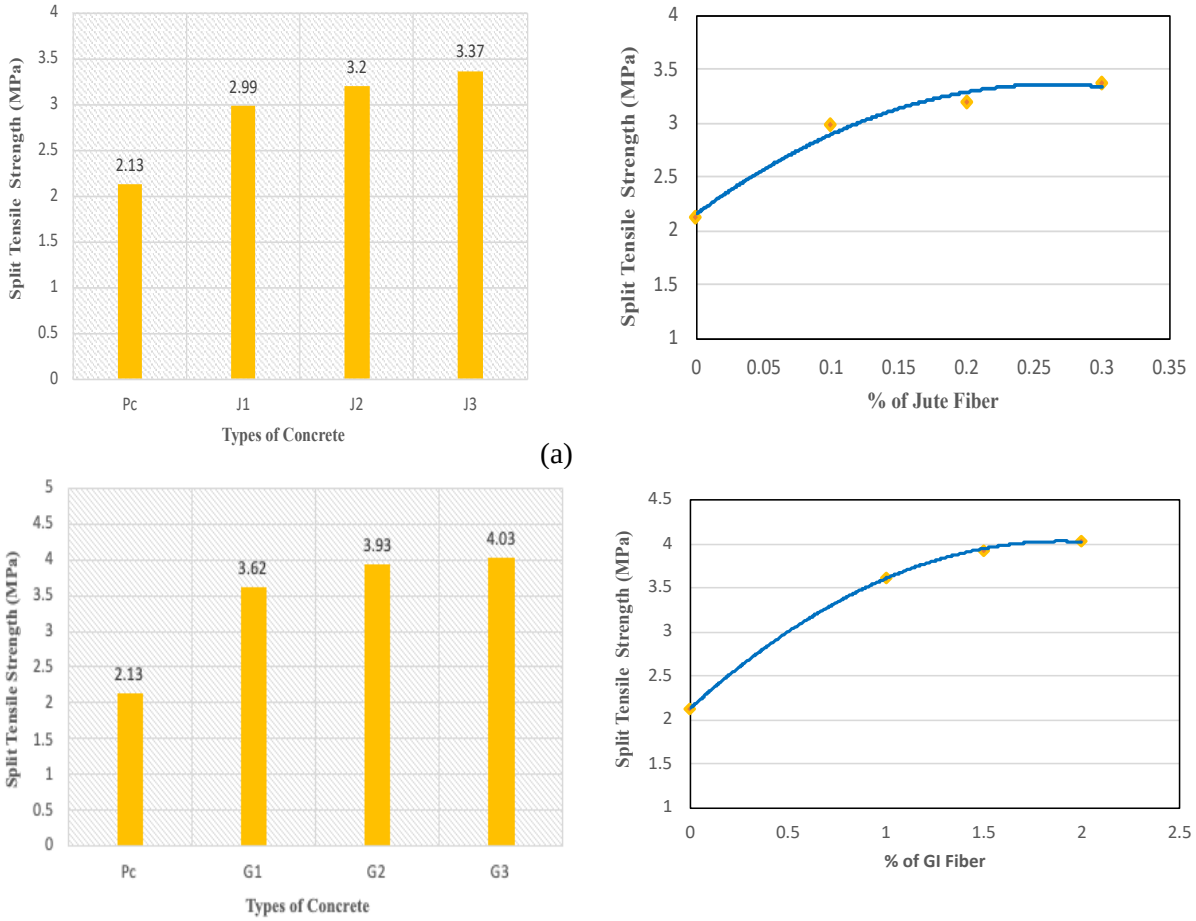

Figure2: Relationship between fiber content and split tensile strength of (a) non-metallic fiber reinforced concrete; and(b) metallic fiber reinforced concrete

From Figure 2, it is stated that the tensile strength was improved with addition of small quantity of fibers.The tensile strength increased respectively 40.4%,50.2% and 58.2% with the addition of jute fibers by volume fraction compared to the plain concrete while the increment of tensile strength was observed 70%,84.5% and 89.2% by adding GI fibers in concrete compared to plain concrete. The role of crack bridging ability of fibers and interfacial adhesion mainly prevented the concrete from splitting. Best result achieved for 2% GI fiber addition and approximately 89% increase in the split tensile strength was noted, while this was approximately 58% for 0.3% Jute fiber addition. The crack-bridging capacity of the fibres mainly prevented from the splitting of concrete.

4. CONCLUSIONS

The paper reported experimental results on using metallic (GI) and non-metallic (Jute) fibre in concrete with respect to the plain concrete. The following conclusions can be drawn from the above experimental results:

- With the addition of jute fiber (non-metallic fiber) the compressive strength increases from 6.5% - 12.5% with respect to plain concrete.

- The compressive strength of metallic fiber (GI fiber) reinforced concrete increased from 9.4% -16% with respect to plain concrete.
- The fiber content of mamimum compressive strength was found in case of 2% addition of GI fiber in concrete.
- The tensile strength increases by 40.4% - 58.2% compared to the plain concrete with the addition of jute fiber in concrete.
- By adding GI fiber in concrete significant increment of tensile strength 70% - 89.2% was found compared to the plain concrete.
- The highest enhancement of tensile strength was found in case of 2% addition of GI fiber in concrete.

REFERENCES

ACI 211.1-91. Mix design of concrete, American Concrete Institute.

ACI 211.1-91 (Reapproved 2009). Standard Practice for Selecting Proportions for Normal, Heavyweight and Mass Concrete, American Concrete Institute, Farmington Hills, MI, 48331-3439 USA.

Gupta, S.D., Islam, G.M.S., (2014). Evaluating plastic shrinkage of fiber reinforced concrete. In: Proceedings of 2nd International Conference on Advances in Civil Engineering (2nd ICACE), December 26–28. Chittagong University of Engineering & Technology (CUET), Chittagong - 4349, Bangladesh.

Islam S.M.G, Gupta S D (2016).Evaluating plastic shrinkage and permeability ofpolypropylenefiber reinforced concrete.*International journal of sustainable built environment*, Vol-5, pp.345–354.

Nemati K. M. (2013). Fiber Reinforced Concrete(FRC), CM-425, concrete technology, University of Washington.

Nilson H.A, Darwin D, Dolan W.C, (2016). Design of concrete structures, ISBN-007-339794-6, Mc-Graw-hill, America.

Parveen, Sharma, A., (2013). Structural behaviour of fibrous concrete using polypropylene fibres. *Int. J. Mod. Eng. Res.* 3 (3), 1279–1282.

Sivakumar A, Santhanam M, (2007). A quantitative study on the plastic shrinkage cracking in high strength hybrid fibre reinforced concrete, ‘*’Cement & Concrete Composites*,’’ Vol- 29, pp.575–581.

Proceedings of the 5th International Conference on Civil Engineering for Sustainable Development (ICCESD 2020), 7~9 February 2020, KUET, Khulna, Bangladesh (ISBN-978-984-34-8764-3)

A STUDY ON IMPACTS, CONSTRUCTION CHALLENGES AND OVERCOMES OF PADMA MULTIPURPOSE BRIDGE, BANGLADESH

Md. Munirul Islam*[1], A. S. M. Fahad Hossain[2], S. M. Abbas[3], Sadia Silvy[4] and Md. Sayeed Hasan[5]

[1]Assistant Professor, Ahsanullah University of Science and Technology, e-mail: saeedce@yahoo.com
[2]Assistant Professor, Ahsanullah University of Science and Technology, e-mail: fahadrubel@gmail.com
[3]Graduate Student, Ahsanullah University of Science and Technology, e-mail: onukabbo30@gmail.com
[4]Graduate Student, Ahsanullah University of Science and Technology, e-mail: sadiapunni0987@gmail.com
[5]Graduate Student, Ahsanullah University of Science and Technology, e-mail: sayeedswapnil18@gmail.com

***Corresponding Author**

ABSTRACT

Bangladesh is the riverine country located in South Asia with a coastline of 580 km on the northern littoral of the Bay of Bengal. There are 213 rivers in our country where 20 major bridges were constructed in our country. Five more bridges are now under construction among them Padma Multipurpose Bridge is the largest and most challenging. It will be the first fixed river crossing for road traffic and it will connect Louhajong, Munshiganj to Shariatpur and Madaripur, linking the south-west of the country, to northern and eastern regions. With 150 m span, 6150 m total length and 18.10 m width it is going to be the largest bridge in the Padma-Brahmaputra-Meghna river basins of country in terms of both span and the total length. The study discusses about both positive and negative impacts of the project on different aspects of Bangladesh. The study also discusses about the challenges faced during construction of the main bridge and viaducts by field survey. From the study, it is revealed that the construction of the Padma Bridge would significantly help improve various sectors of the economy nationally and regionally. Capital inflow will increase promoting industrial and commercial activity and increasing economic and employment opportunities for the local population. Construction the bridge is very challenging as Padma become a fast flowing river during monsoon and the bridge is sited in active seismic area. Advanced computational analysis and engineering solution have been employed to meet the challenges.

Keywords: *Impacts, Constructional challenges, Overcomes.*

1. INTRODUCTION

Bangladesh is riverine country. According to Bangladesh Water development board (BWDB) about 230 rivers currently flow in Bangladesh. The river network of Bangladesh as the most important transport artery in the country's communication sector plays a vital role in national life. Almost all big cities, towns and commercial centers of the country grew up on the banks of its rivers. Bangladesh, to the east of India on the Bay of Bengal, is a South Asian country marked by lush greenery and many waterways. Its Padma (Ganges), Meghna and Jamuna rivers create fertile plains, and travel by boat is common. Main bridges in Bangladesh are – Jamuna Bridge, Hardinge Bridge, Lalon Shah Bridge, Meghna Bridge, Padma Bridge, Shah Amanat Bridge, Khan Jahan Ali Bridge & Kean Bridge. Each bridge has different purposes and importance. The Padma Multipurpose Bridge and associated facilities are of great importance for the development of Bangladesh. This project has remarkable impacts on whole country and contributes to the socio-economic development on Southwest region. In addition, industrial development will be accelerated.

2. LITERATURE REIEW

The Padma Multipurpose Bridge is a multi purpose road-rail bridge across the Padma River under construction in Bangladesh. It will connect Louhajong, Munshiganj to Shariatpur and Madaripur, linking the southwest of the country to the northern and eastern regions. Padma Bridge is the most challenging construction project in the history of Bangladesh. The two-level steel truss bridge will carry a four-lane highway on the upper level and a single track railway on a lower level. With 150 m spans, 6150 m total length and 18.10 m width, it is going to be the largest bridge in the Padma-Brahmaputra-Meghna river basins of the country in terms of both span and the total length. Figure 1 shows a probable view of the dream bridge Padma Multi-purpose Bridge.

Figure 1: The Padma Multipurpose Bridge (www.padmabridge.gov.bd)

3. IMPACTS OF PADMA BRIDGE IN BANGLADESH

The proposed Padma Multipurpose Bridge will be a multipurpose road-rail bridge across the Padma River and it will be the largest bridge in Bangladesh and the first fixed river-crossing for road traffic. The Padma Multipurpose Bridge will transform the lives of nearly 30 million people living in the country's southwest region, promoting industrial and commercial activities and increasing economic and employment opportunities, according to various studies and reviews on the major economic impact of the bridge project. At least 30 million people, almost one-fifth of the country’s total population, will directly benefit from the bridge, according to a study by the World Bank

3.1 Positive Impacts

Padma Multipurpose Bridge would significantly help improve various sectors of the economy nationally and regionally. With the bridge, capital inflow will increase, promoting industrial and commercial activity, increasing economic, and employment opportunities for the local population.

3.1.1 Communication

The construction of Padma Multipurpose Bridge will solve the communication problem of the southwestern part of Bangladesh, which comprises 25% of the total land mass. Introduction of both the road and the rail will help to transport raw materials from the port of Chittagong at a cheaper rate. By constructing the bridge, economic development of the southwest will promote industrial and commercial activity and improve economic and employment opportunities for local people.

3.1.2 Quicker Travel Time and Reduction of Distance

The proposed bridge will provide direct links between two major seaports of the country. The distance from Dhaka to nearly all major destinations in the southwest region will be reduced by 100 kilometers (km) or more and hauling time of vehicles will reduce by over 3 hours each trip that will bring considerable savings in passenger and commodity movement time and costs.

3.1.3 Safety of Public Lives

There is an urgent need to replace unsafe ferry and launch operations between Dhaka and the southwest region by safer and more reliable surface transport. Overloaded vessels frequently sink in this waterway when passing through the turbulent confluence of the Padma and Meghna Rivers. Construction of Padma Multipurpose Bridge is a remedy to this misery.

3.1.4 Electricity, Telecommunication and Gas Supply

Construction of Padma Multipurpose Bridge will connect the southwestern part of the country with national power grid. An electric circuit will join the two halves. Therefore, this immense power supply will generate both present economy and rapid industrialization.

3.1.5 Agriculture

The economy of the southwestern region was dependent on irrigation system. Non-availability of power forced the local farmers to use fuel based irrigational pumps. With its limited capacity and fuel consumption, very often made its use uneconomical. With the availability of electricity, the production cost of agro-products are bound to come down, with a considerable increase on production.

3.1.6 Industrialization

The major setback, which the southwestern region faced due to the absence of a bridge, is the industrialization of the region. No industry except those based on local resources could be established because of the transportation and consequence-marketing problem of both raw material and finished good. Now that the Padma Multipurpose Bridge will bring the power necessary for industrialization at the doorstep of common people, industries of various scale and dimension will flourish on the region ultimately boosting the national economy.

3.1.7 Improvement of living Standard

For construction, residences nearby the sites had to be evacuated and a large number of local people had to be relocated to resettlement sites. These local people moving to resettlement sites will greatly improve the living environment since many civic amenities and social infrastructure would be made available.

3.1.8 Cultural Integration

In Bangladesh, diversity in language, food habit and culture is seen in different regions. People from one region sometimes find it difficult to understand the language of another. The Bridge, which will play the

role of a development catalyst for the nation's culture. The cumulative socializing effects of all this will bring people closer in thought, outlook, interaction and action, which are likely to be more uniform than what it is now.

3.2 Negative impacts

Because of the sudden economic development in the southwestern region, the livelihood and lifestyle of many will change. With this change, many other social and political factors will arise which may pose threat to the success of Padma Bridge in the future.

3.2.1 Loss of Households

The project will need to acquire 755 hectares (ha) of land for the construction of the bridge and its associated infrastructure, including the development of five resettlement sites. In addition, about 163 ha of land will be temporarily required for construction sites for a period of about 6 years. About 5500 households comprising of 26,500 persons would be affected. Total population affected (directly and indirectly) may run into Mawa - 70,000-80,000 and Paturia - 40,000-45,000.

3.2.2 Loss of Agricultural Land

A total of about 507 thousand acres of land will be affected Munshiganj, Shariatpur and Madaripur districts because of the component. Of the total land affected, the majority of land affected is located on the Janjira side amounting to 83% of the total acquired land, whereas the remaining affected land lies on the Mawa side. About 30,000 people in 10,000 households will lose their income and livelihoods due to the loss of agricultural land.

3.2.3 Income Loss

25,000 people will suffer income loss from affected fisheries, services, trading and transportation, and wage employment. Some of these people will be affected indirectly upon the opening of the bridge to traffic.

3.2.4 Environmental Affect

The salient findings from the initial environmental assessment study were reported as part of the feasibility study but have not yet been included in the proposed mitigation measures and proper management plan. The salient findings include the following:

- The impact of the bridge on regional hydrology and flooding patterns, as the high-water level of the Padma River rises due to the bridge construction, is not expected to be significant, but detailed assessment will be required.
- Adequate openings on the planned right bank, approach road are required for drainage.
- Limited erosion and siltation is expected, but detailed assessment will be required.
- About 295,072 trees loss (Excluding 485,074 bamboo and banana trees).
- About 58 ponds covering 4.18 ha and 74 ditches covering 2.66 ha will be affected by the Project. Total loss of fish breeding area about 767 ha.
- The Padma River is an important migratory route for hilsa fish. Fish production losses of about 11 tons per year may be compensated by fish culture in new ponds in borrow pits.
- About 50 million cubic meter dredge material will be generated from the river.
- Traffic congestion, safety hazards, noise pollution, sanitation, health and hygiene, waste generation etc.

4. CONSTRUCTION CHALLENGES AND OVERCOMES OF PADMA MULTIPURPOSE BRIDGE

At 6.15 km in length the Padma Multipurpose Bridge will be a landmark structure in Bangladesh and one of the great river crossings of the world. The design of the bridge has been a major challenge with

the river changing in nature dramatically during the monsoon season, when the flow rate and major fluctuations in river bed level threatening to undermine any bridge piers. . The bridge site is also in an area of considerable seismic activity. To design the bridge, advanced computational analysis and engineering solutions have been employed, in order that the bridge will be able to meet the challenges of nature during its long life. Figure 2 illustrates the installation of Padma Multipurpose Bridge.

Figure 2: Intallation of Span (www.padmabridge.gov.bd)

4.1 Construction Challenges

The constructional challenges of Padma Multi-purpose Bridge are discussed below.

4.1.1 Insufficient Pile Capacity

According to design, each pile should have the capacity of 8200 ton. But where clay layer is encountered, Pile capacity has reduced to about 6250 ton.

4.1.2 Increased Scouring at Banks

The length of pile varies from pier to pier. The average length of pile is taken as 115-120m. But due to increased scouring at the bank (Janjira) Pile length has to be increased (123.75m) under some piers (P-37, P-38, P-39, P-40, P-41).

4.1.3 Limitations in Increasing Pile Length

Bearing capacity of piles can be increased by increasing skin friction which requires an increase in pile length. But it is found that there is presence of stiff clay layers at the depth of 130-160 m which will cause accountable settlement. So increase in pile lengths cannot be taken as a solution.

4.1.4 Limitations in increasing Pile Number

Capacity to support the piers can also be increased by simply increasing the number of piles under each. But increasing the number of piles (more than 7) will make the design complex and also will require further space. So not more than 7 piles can be provided under each pier (excluding viaducts).

4.1.5 Skin Grouting

The procedure of skin grouting is another challenge in this project. Recently this process is being tested on the piles of viaducts.

4.1.6 Rising of Bed

The piling depth of Padma Multipurpose Bridge is a world record (115-120m). For this huge pile a deep hole had to be dug up. When the work started, the dredged soil was deposited in river bed. As a result, there rose a bed creating problems for river vehicle.

4.1.7 Sedimentation

Sedimentation in Padma also creates problems for the floating crane by reducing water depth which requires dredging.

4.1.8 Pile Driving Hammer

For pile driving purpose 3 MENCK hammers are used with the capacity of 3500kj, 2400kj, and 1800kj respectively. Such massive hammers are being used in our country for the first time and their operation and maintenance can be considered as a challenge. The pile driving hammer is shown oin figure 3.

Figure 3: Pile Driving Hammer (youtube.com)

4.1.9 Lowered Water Surface

The largest floating crane is introduced to carry the spans of the bridge. But the problem is it needs sufficient depth of water to float. But in December 2017, due to dry season the surface water level had lowered at a huge depth. For this it was not possible to carry the spans through the cranes. So the work had to be stopped for a while.

4.2 Overcomes of Challenges of Padma bridge

4.2.1 Inclined Piles

To deal with the massive river current the designers decided to provide inclined piles. The piles were designed in 1H:6V ratio. Because of this it can resist more lateral force which also helps to resist earthquake as well. A pile arrangement is shown in figure 4.

Figure 4: View of pile Layout (UNB)

4.2.2 Provision of one Extra Pile

According to initial design, each pier supposed to have 6 steel tabular driven piles beneath. But due to insufficient bearing capacity and inability to increase pile length, 22 of the piers are later decided to be provided with7 piers to support them. These piers are P-6,P-7,P-8,P-9,P-10,P-11,P-12,P-15,P-19,P-24,P-25,P-26,P-27,P-28,P-29,P-30,P-31,P-32,P-33,P-34,P-35 and P-36.

4.2.3 Base Grouting

Base Grouting is another effective process to increase the capacity of piles. Micro-Fine cement grout is used for this process (P14-4). Grout Mix Design-Water: Micro-Fine Cement (Prefine-80): Admixture (Basf master Rheobuild 1000) = 0.8 : 1 : 0.01

4.2.4 Artificial River

To place the 5th span on no. 41 and 42 piers, an artificial river was created by dredging. It provided sufficient depth for the floating crane to move.

5. CONCLUSIONS

The Padma Multipurpose Bridge will stand as a landmark structure in Bangladesh, not only providing a vital communications link, but also signaling another milestone engineering solution in a region of extreme environmental hazards. The Padma Multipurpose Bridge will provide a vital missing link in the transport network of Bangladesh. The bridge will provide significant travel time savings, particularly between the Dhaka Division to the south-east of Bangladesh and possibly onto India. The bridge will be a safe and easy fixed river crossing replacing the often unsafe and unreliable ferries. Nevertheless, the possible prospective impacts discussed before has proven the worth of having this bridge in place. All the people of Bangladesh can hope now is a successful completion of the construction of this Multipurpose Bridge.

REFERENCES

De Silva, S., Wightman, N.R. & Kamruzzaman, Md. 2010. “Geotechnical ground investigation for Padma Main Bridge”. Proc. IABSE – JSCE Conference, Dhaka, 10-12 August 2010.

Islam, M.R. 2010. “General and design features of Padma Multipurpose Bridge”. IABSE – JSCE Conference, Dhaka, 8-10 August 2010.

McLean, D., Neill, C. & Oberhagemann, K. 2010. “Design of River Training Works for Padma Multipurpose Bridge”, Bangladesh. Proc. IABSE – JSCE Conference, Dhaka, 10-12 August 2010.

Sham, S.H.R. & Tapley, M.J. 2010. "The design of Padma Multipurpose Bridge – challenges and solutions in design of the river spans". Proc. IABSE-JSCE Conference, Dhaka, 10-12 August 2010.

Sham, S.H.R., Yu & De Silva, S. 2010. "Foundation Design Methodology for Padma Main Bridge". Proc. IABSE – JSCE Conference, Dhaka, 10-12 August 2010

Tapley, M.J., Sham, S.H.R. & Holmberg, R.A. 2010. "Developing the Operations and Maintenance Strategy for the Padma Multipurpose Bridge". Proc. IABSE-JSCE Conference, Dhaka, 10-12 August2010.

Wheeler, W.K., Aves R.J., Tolley, C.J., Zaman Md., Islam, M.R. 2010. "Detailed design of Padma Multipurpose Bridge- Bangladesh, An overview". . IABSE – JSCE Conference, Dhaka, 8-10 August 2010.

Proceedings of the 5th International Conference on Civil Engineering for Sustainable Development (ICCESD 2020), 7~9 February 2020, KUET, Khulna, Bangladesh (ISBN-978-984-34-8764-3)

INFLUENCE OF TIRE CHIPS SIZE ON THE DURABILITY BEHAVIOR OF RUBBERIZED CONCRETE

Afroja Sultana*[1], Md. Roknuzzaman[2], Md. Belal Hossain[3] and Abdullah Al Shourov [4]

[1]Graduate Student, Hajee Mohammad Danesh Science and Technology University, Bangladesh, e-mail: afrojamimi.ce.hstu15@gmail.com
[2]Assistant Professor, Hajee Mohammad Danesh Science and Technology University, Bangladesh, e-mail: mrz.civil@hstu.ac.bd
[3]Assistant Professor, Hajee Mohammad Danesh Science and Technology University, Bangladesh, e-mail: belal_ce_05@yahoo.com
[4]Graduate Student, Hajee Mohammad Danesh Science and Technology University, Bangladesh, e-mail: shourovmon@gmail.com

***Corresponding Author**

ABSTRACT

This study describes the effect of the tire chips size on durability properties of rubberized concrete. Recently a large no of researcher's point of interest is to work with rubberized concrete. They are hardly trying to utilize waste, discarded tires in environmentally safe ways. The rubberized concrete is one of those techniques. It is benificial to use scrap tire in concrete but durability of resulting concrete is one of the major concerns. Concrete structures may occasionally exposed to adverse weather, chemical attack, abrasion, electrolytic action etc. Although there are a different ways of testing durability of concrete like absorption test, rapid chloride permeability test etc. in this work, durability test by acid curing is adopted. The rubberized concrete is prepared with partially 7.5% aggregate replacement with tire chips. Same amount of coarse aggregate was replaced with different size tire chips as like 5mm×5mm, 10mm×10mm, 15mm×15mm and 20mm×20mm. After 28 days normal water curing the concrete specimens are kept in 5% H_2SO_4 acid curing for another 28 days. After that the compressive strength test is performed as the principal test criteria. The weight loss test is also carried out as reference. From durability point of view it is clear that tire chips size has strong relations with the durability behavior of rubberized concrete. Tire chips with smaller fragments are found to produce more durable concrete than larger fragments from compressive strength point of view. 5mm×5mm rubber performs best with a minimal strength reduction of 10.60% as compared to the same specimen in case of normal water curing. Recommendation is therefore made to use 5mm×5mm rubber chip replacement to get best result and the resulting concrete can be conveniently used for plain concrete slabs, embankment protection blocks, cement concrete pavements for low to moderately loaded roads etc.

Keywords: *Durability, Rubberized concrete, Scrap tire, Acid curing, Compression strength.*

1. INTRODUCTION

The durability of cement concrete can be defined as its ability to resist weathering action, chemical attack, abrasion and any other phenomenon of deterioration. Durable concrete will retain its original form, quality and serviceability when revealed to its environment. For a long time, concrete was considered to be very durable material requiring a little or no maintenance. The assumption is largely true except when it is subjected to highly aggressive environments. We build concrete structures in highly polluted urban areas and industrial areas, aggressive marine environments, harmful sub-soil water in coastal area and many other hostile conditions where other materials of construction are found to be non-durable and unsuitable. Since the use of concrete in recent years, have spread to highly harsh and hostile conditions, the earlier impression that concrete is a very durable material is being threatened, particularly on account of premature failures of number of structures in the recent past. In the past days, only strength of concrete was considered in the concrete mix design procedure assuming strength of concrete is an all-pervading factor for all other desirable properties of concrete including durability. Although compressive strength is a measure of durability to a great extent but it is not entirely true that the strong concrete is always a durable concrete. For instance, while it is structurally possible to build a jetty pier in marine conditions with 20 MPa concrete, environmental condition can lead this structure to a disastrous consequence. In addition to strength of concrete another factor, environmental condition or what is generally call exposure condition has become an important consideration for durability now-a-days. Concrete having a low permeability to water and dissolved chemicals will generally be durable in most exposure conditions. Permeability of concrete is impacted by water to cementitious materials ratio (w/cm), and type and proportions of cementitious materials used in the mixture. The w/cm is the ratio of the weight of mixing water to the weight of all cementitious materials. (Shetty, 2005).

A study on the experimental investigation of durability test on concrete cubes was held which is the characteristic strength for M30 grade of concrete and for micro concrete is checked. The cubes after 28 days of curing in water is immersed in 5% H_2SO_4 and 5% HCL of the total volume of water separately for 28 and 56 days to evaluate the decrement in the strength as compared to normal condition and showed that the compressive strength is reduced and the reduction slightly more at immersing in H_2SO_4 as compared to HCL (Patel et al., 2017). ACI 318 defines Exposure Classes (EC) within each Exposure Category based on the severity of exposure. Increasing severity is represented by higher numerical value in the EC designation. The numeral number "0" is used when the condition does not apply. The designer is required to assign the durability EC for each member type in a structure. This sets the basis and lends clarity to the requirements for concrete. Following Table 1 shows durability requirements for different exposure classes as described below in accordance with American Concrete Institute (ACI) standards.

Table 1: Minimum specified strength $f_c^{'}$ and max w/cm for ACI 318 durability exposure classes

Exposure Class	Max w/cm	Min $f_c^{'}$ (psi)
F0, S0, W0, C0, C1	None	2500
F1	0.55	3500
S1, W1	0.50	4000
S2, S3, F2, F3 (plain)	0.45	4500
C2, F3 (reinforced)	0.40	5000

The exposure classes are explained as:

Freezing and thawing exposure (Category F)

F0 for no exposure

F1 for a lower level of saturation when exposed to freezing

F2 for higher level of saturation and
F3 for higher level of saturation and the potential for application of deicing chemicals

Sulfate Exposure (Category S)

ECs (Exposure Classes) are defined based on concentration of water-soluble sulfates (SO_4^{2-}) in soil (% by mass) or water (ppm) in contact with the member.

S0	<0.10%	<150ppm
S1	0.10-0.20%	150-1500 ppm and seawater
S2	0.20-2.00%	<1500-10000 ppm
S3	>2.00%	>10000 ppm

Corrosion protection of reinforcement (Category C)

C0 for members dry in service
C1 for moist in service
C2 for moist and exposed to an external source of chlorides

Concrete in contact with water (Category W)

W0 for dry in service or in contact with water where low permeability is not required
W1 for concrete in contact with water requiring low permeability

2. METERIALS AND METHODS

2.1 Materials

In this study the materials used to produce the concrete mixtures were sand as fine aggregate, stone chips as coarse aggregate, cement as binder, water and tire chips (Figure 1) as partial replacement of coarse aggregate. Sulphuric acid was used for acid curing to observe durability characteristics (Patel et. al., 2017). All these materials were collected from convenient local sources in Dinajpur, Bangladesh. Maximum size of coarse aggregate was 19 mm. Potable water was used for concrete preparation conditioned to the room temperature. The waste tires were collected from local machinery workshop. The tire fibers without any metal wire had been selected and cut in different sizes as per requirement. The collected tire was cut into 5mm×5mm, 10mm×10mm, 15mm×15mm and 20mm×20mm sizes. American Society for Testing and Materials (ASTM) standard procedures were adopted to determine several properties of materials. Properties of materials are presented in Table 2.

Coarse aggregate Fine aggregate

Tire chips

Figure 1: Materials; coarse aggregate, fine aggregate and tire chips

Table 2: Material Properties

Coarse Aggregate (Stone Chips)	Specific Gravity:2.73 Water Absorption: 1.12% Fineness Modulus: 6.87
Fine Aggregates (Sand)	Specific Gravity: 2.67 Water Absorption: 1.35% Fineness Modulus: 2.71
Tire Chips	Specific Gravity: 1.26 Water Absorption: 0.03% Thickness: 5 mm Colour: Ashy
Binding Materials (Ordinary Portland Cement)	Normal Consistency: 24% Initial setting time: 120 min Final setting time: 300 min 3-days compressive strength (50 mm cube): 22.9 MPa 7-days compressive strength (50 mm cube): 34.8 MPa 28-days compressive strength (50 mm cube): 41.4 MPa
Water	Potable water
Acid	5% Sulphuric acid

2.2 Identification of Mix Arrays

Tire chip or rubber content was kept fixed as 7.5% of coarse aggregate volume and water cement ratio was also kept constant as 0.45. A typical 1:1.5:3 proportioned (volumetric) concrete mixes was taken

into account. Keeping all other factors identical, only variation was made in size of tire chips. Each of the mixes with different rubber sizes are designated with a letter as presented in Table 3.

Table 3: Designations of mix arrays

Mix Designation	Size of added tire chips (mm×mm)
A	-
B	5×5
C	10×10
D	15×15
E	20×20

2.3 Preparation of Specimen

Coarse aggregates are sieved and a well graded aggregate is prepared for the specimens. Collected tire is cut into required sizes manually. Concrete mix was prepared (Figure 2) and filled in the mold of size 100mm × 200mm. Mold is filled in 3 equal layers, layers are being compacted by a compaction rod with 25 strokes as per ASTM standard. Total 12 specimens for each mix designation were prepared among which 6 are for compressive strength test and the other 6 are for durability test.

Figure 2: Preparation of specimen

2.4 Laboratory Tests

The test specimens were subjected to compressive strength tests and durability tests. Compressive strength tests were conducted after 28 days curing of the cylindrical specimens following standard procedure as described in ASTM C39/C39M-12. To observe the behavior of rubberized concrete durability test by acid curing was adopted. The specimens were cured in water for 28 days. After 28 days curing in ordinary water, the specimens were allowed to cure for further 28 days in 5% sulphuric acid solution. At the end of acid curing, the specimens were subjected to compressive strength test.

3. RESULTS AND DISCUSSIONS

The durability of concrete can be defined as its ability to withstand weathering action, chemical attack, abrasion or any other process of deterioration. Durable concrete will retain its original form, quality and serviceability when exposed to its environment. In addition to strength of concrete another factor, environmental condition or what is generally called exposure condition has become an important consideration for durability. The test specimens for durability test were primarily cured in potable water. At its 28 days curing, cylinder surfaces were cleaned and weighed. The identified specimens were then immersed in 5% sulfuric acid solution for another 28 days. Compressive strength test results after acid curing of the specimens are given in Table 4.

Table 4: Compressive strength after water curing and acid curing

Mix type	Added rubber chips size	Strength after water-curing (MPa)	Strength after acid-curing (MPa)	Reduction of Strength (%)
A	-	29.51	26.2	11.22
B	5mm×5mm	26.31	23.52	10.60
C	10mm×10mm	20.11	16.94	15.76
D	15mm×15mm	17.64	14.55	17.52
E	20mm×20mm	15.93	12.52	21.41

The Table 4 shows the strength loss due to acid curing which gives an indication of its durability. The changes are presented graphically in Figure 3.

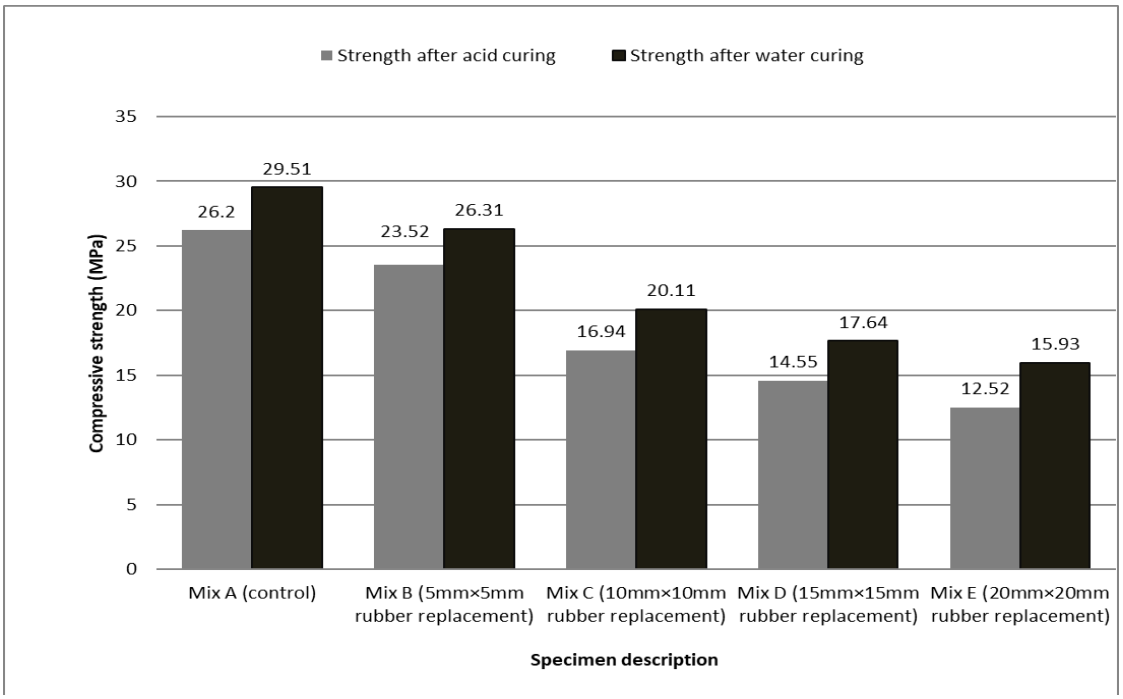

Figure 3: Compressive strength before and after durability test

According to ACI 318 Exposure Classes (EC), control specimen is durable for F1, F0, S0, W0, C0 and C1exposure conditions whereas mix B is applicable in F0, S0, W0, C0, C1 conditions. Due to rubber addition, the mix B fails to satisfy the requirement for exposure F1 condition. The other mixes C, D and E are not applicable in any of the exposure conditions defined by ACI 318 from durability point of view. A comparative picture of strength loss due to acid curing is shown in Figure 4.

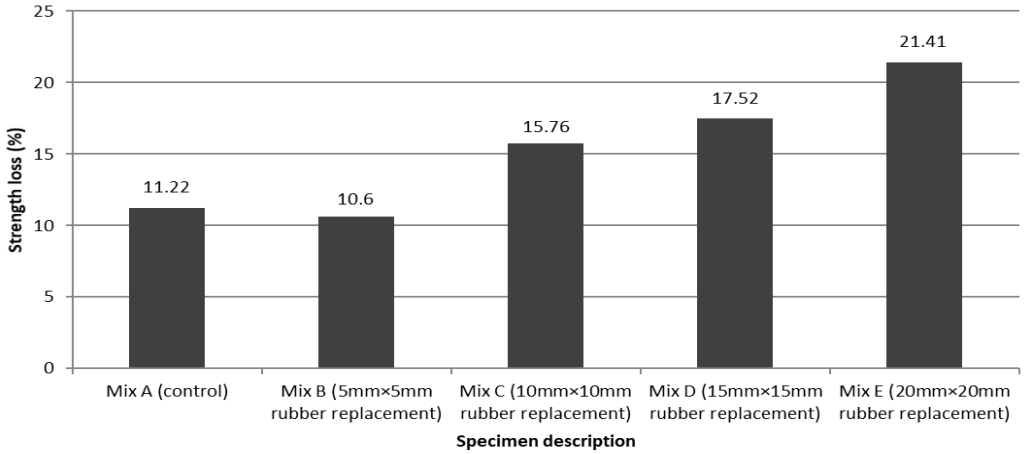

Figure 4: Strength losses due to acid curing

Weight loss measured after end of acid curing are tabulated at Table 5. The graphical representation of that is presented immediately below the table.

Table 5: Weight loss (%) due to 28 days acid curing

Specimen No	Added rubber chips size	Weight loss (%)
A	-	3.9
B	5mm×5mm	2.4
C	10mm×10mm	1.77
D	15mm×15mm	0.99
E	20mm×20mm	0.97

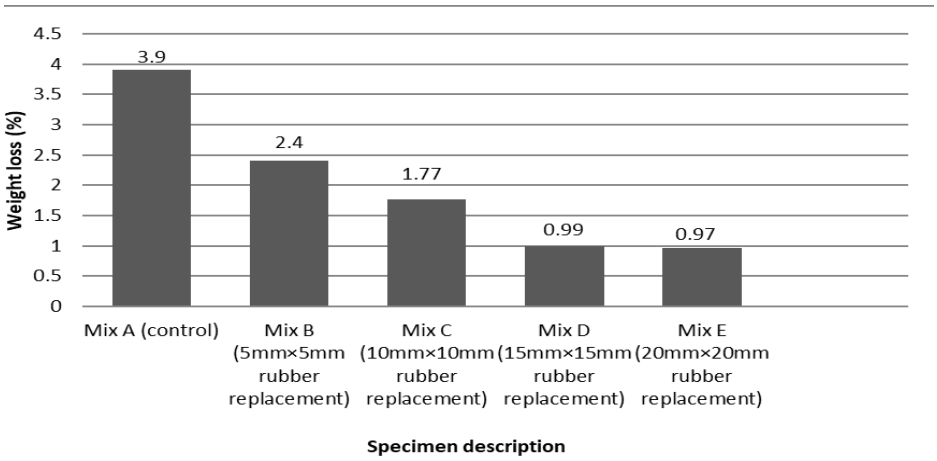

Figure 5: Weight loss due to acid curing

In case of rubberized concrete specimens, there was reduction in weight loss with the size of rubber chips increment. The reason behind this matter of fact may be the reaction between sulfuric acid and the cement constituent of concrete which causes the conversion of calcium hydroxide to calcium

sulfate which, in turn, may be converted to calcium sulfoaluminate. The formation of calcium sulfate leads to softening of the concrete (Attiogbe et. al., 1988).

4. CONCLUSIONS

In this research work 7.5% rubber derived from waste tire was used to replace the coarse aggregates. Different size fractions were used as 5mm×5mm, 10mm×10mm, 15mm×15mm and 20mm×20mm. It is clear that tire chips size has strong relations with the durability behavior of rubberized concrete. Tire chips with smaller fragments are found to produce more durable concrete than larger fragments from compressive strength point of view. By durability concern the rubber chips of size 15mm×15mm and 20mm×20mm are totally rejected, 10mm×10mm may be accepted with cautions and 5mm×5mm can be accepted conveniently for various exposure conditions.

ACKNOWLEDGEMENTS

The authors praise Almighty ALLAH, the merciful and passionate, for the support and blessings throughout this journey . The authors leave heartfelt thanks to Md. Roknuzzaman and Md. Belal Hossain for humble guidance. The authors acknowledge the sacrifice of their parents and others of the families that has enabled them to attain this level.

REFERENCES

ACI Committee, and International Organization for Standardization, Building code requirements for structural concrete (ACI 318-08) and commentary, American Concrete Institute, 2008.

ASTM, C. (2012). Standard test method for compressive strength of cylindrical concrete specimens. *ASTM C39/C39M-12*.

Attiogbe, E. K., & Rizkalla, S. H. (1988). Response of concrete to sulfuric acid attack. *ACI materials journal*, *85*(6), 481-488.

Patel, H., Jain, P., Engineer, K. & Kajalwala, M., V., M. (2017). The Experimental Investigation of Durability Test on Concrete Cubes. *International Journal of Advance Engineering and Research Development*, 4(5), 855-861.

Shetty, M. S. (2005). Concrete Technology Theory and Practice, Chand S. and Company LTD.

Proceedings of the 5th International Conference on Civil Engineering for Sustainable Development (ICCESD 2020), 7~9 February 2020, KUET, Khulna, Bangladesh (ISBN-978-984-34-8764-3)

ANALYTICAL MODELING FOR CONSTITUTIVE RELATIONSHIP OF ULTRA-HIGH-PERFORMANCE FIBER REINFORCED CONCRETE WITH VARYING SIZES

Arafat Alam*[1] and Md. Habibur Rahman Sobuz[2]

[1]Undergraduate Student, Department of Building Engineering and Construction Management, Khulna University of Engineering and Technology, Bangladesh, e-mail: arafat.alam1892@gmail.com
[2]Assistant Professor, Department of Building Engineering and Construction Management, Khulna University of Engineering and Technology, Bangladesh, e-mail: habib@becm.kuet.ac.bd

***Corresponding Author**

ABSTRACT

In modern construction, ultra-high-performance fiber-reinforced (UHPFRC) concrete plays a pivotal role by significantly increasing strength and ductility. Application of UHPFRC ranges vast, from bridges to high-rise structures. In this research, the primary focus is on the size-dependent analytical constitutive relationship of UHPFRC of varying heights. The model was then verified with the prior experimental data. The experimental part involves the testing of cylinders with three different volume of fiber contents of 1 %, 2%, and 3%. The heights of the cylindrical specimen were also varied by 200mm, 300mm and 400mm heights and having a fixed diameter of 100 mm. The analytical constitutive relationship was numerically approximated based on empirical equations proposed by Popovics. A regression analysis was carried out which resulted into equations for peak strain of different fiber-volume and these equations are then incorporated into the model to predict stress-strain relationships from one size to any other sizes. Finally, the model, was validated with the experimental data. It is observed that the model can predicts the stress-strain relationship in a rather conservative way. Thus, it is concluded that there exists a correlation between the stress-strain of UHPFRC concrete and the varying sizes of the specimen.

Keywords: *UHPFRC; Size-dependent behavior; Stress-strain response; Fiber content; Ductility.*

1. INTRODUCTION

Ultra-high-performance concrete (UHPC) is a relatively new class of concrete that transcends typical compressive, tensile and durability behavior of normal weight concrete (B. A. Graybeal, 2007). UHPC is a new-generation high mechanical performant cementitious matrix material (Pierre Richard, 1995). UHPC mainly overcomes the weakness of concrete strength and brittleness and shows high strength and post-cracking tensile strength (Shafieifar, Farzad, & Azizinamini, 2017; Sobuz et al., 2016). But to achieve UHPC, unorthodox mix design by mixing Portland cement, fine sand, silica fume, ground quartz, superplasticizers, steel or organic fibers and water with low w/c ratio of typically less than 0.25 is applied (B.A. Graybeal, 2003). Coarse aggregate is reduced in this type of concrete, which in turn reduces the size of microcracks and thus using reactive powder, the concrete may have compressive strength ranging from 200MPa to 800MPa (Pierre Richard, 1995). Even without complex mixing, research has shown that compressive strength in the range of 130-160 MPa is achievable using only conventional materials (Sobuz et al., 2016). Applications of UHPC can be architectural and structural but it is most favorable for bridge construction and precast construction for its life-cycle cost (B.A. Graybeal, 2003). The inclusion of steel fibers in UHPC opens up the door for Ultra-high-Performance Fiber-Reinforced Concrete(UHPFRC), which shows improved elastic modulus, tensile strength, elastic post-cracking bending strength and ductility*(*Toledo Filho, Koenders, Formagini, & Fairbairn, 2012*)*.Graybeal has maintained that UHPC shows enhanced durability due to the discontinuous pore structure (B.A. Graybeal, 2003). Normal weight concrete exhibits lower post-peak strength and shorter strain time and fails in sudden explosive behavior but UHPFRC exhibit higher post-peak strength, longer strain time and due to the integrated fiber and matrix bonding, even in the failure the surface remains intact (Shafieifar et al., 2017). Different fibers with a good elastic property are seen to enhance the durability of UHPFRC. Ductility is the phenomenon of undergoing large deformation before failure, and it is important as it provides a warning prior to structural failure. Yoo et al conducted biaxial flexural performance of UHPFRC with three different fiber lengths and two placement methods of which, the result was higher load-carrying and deflection capacity with longer fiber length (Yoo & Yoon, 2016). Considering the type of steel fiber, previous research shows that twisted steel fibers improve both post-peak tensile strength and ductility capacities (Kim, 2011; Wille K, 2014). Lubell et al conducted in his experiment, as the fiber volume fraction increased, peak strengths and post-peak ductility in compression, flexure, and direct shear also increased. This phenomenon is explained as steel fibers partially restraining the lateral expansion and enabling larger axial deformation. Lubell et al also showed in his research that the ascending branch has a linear slope which is independent of fiber content (Kazemi & Lubell, 2012).

Size-dependency is another factor that controls the stress-strain properties of concrete in addition to material mixing. The same materials with different shapes and sizes produce different stress-strain behavior (Chen, Visintin, Oehlers, & Alengaram, 2014). Research has shown that size and shapes directly control the compressive strength of concrete specimens *(*Frettlöhr, H. Reineck, & W. Reinhardt, 2012*;* Lubell*;* Pierre-Claude Aitcin, 1994*;* YI, 2002*)*. With the increase in size, length or depth, compressive strength, and ductility reduce significantly (Mindessb). These research shows that other material properties such as axial tension, flexure, combined bending and axial forces, Elastic limits, Tensile stresses also show anomaly with different specimen sizes. Cube specimens have slightly higher compressive strength than the same mixing cylinders, but in stages of higher compressive strength, the strength difference declines. For the softening branch, cube shows a milder slope while cylinder shows a steeper slope (del Viso, Carmona, & Ruiz, 2008). There has been no accurate relationship established between the peak compressive strength of cylinder and cube samples of different sizes for various volume fractions (Davis, 2008). Implementation of the UHPC has not produced the expected impact due to a lack of material and production knowledge and high costs. (Maher KT, 2016). Analytical methods for stress-strain determination can mitigate these problems. Popovic, Carreira and Chu, Neville, Wee et al are some of those researchers who have proposed empirically-based numerical approximations for stress-strain behavior of particular concretes (Ayub, 2014; Popovics, 1973). But, as of now, there is not any equation pertaining to the prediction of the stress-strain behavior of UHPFRC (B. A. Graybeal, 2007). A numerical model predicting stress-strain behavior of UHPFRC which also accounts for size-dependency characteristics will accelerate knowledge gaining on UHPFRC. Chen et

al, in his paper, focused on the importance of wedge sliding from the shear-friction mechanism which varies with shape and to measure the global strain of a specimen, wedge sliding is necessary to quantify. Then he proposed a stress-strain relationship for normal-weight concrete (NWC) which is shape and size-dependent and can be used to derive various stress-strain models from one fixed-sized stress-strain data.

This study predicts and compares the size-dependency characteristics of UHPFRC with experimental data. The experimental tests are done to create UHPFRC with different fiber volume content and specimen sizes. The varying height incorporates the size-dependency characteristics of UHPFRC, and varying percentages of fiber are done to evaluate the fiber-effect on the compressive strength of UHPFRC with varying height. Popovics's stress-strain model is then corrected with size-dependency formulation as suggested by Chen et al. Using the model, different heights (size) and volume-fraction fiber content specimens are modeled numerically to compare with the experimental data to study the effect of size and fiber-content in both experimental and numerical model.

2. METHODOLOGY

2.1.1 Analytical Investigation

Nonlinear analysis is the primary method for analyzing compression failure of structural members and for nonlinear analysis, the complete stress-strain curve of the unconfined concrete is necessary (Zhao-Hui Lu and Yan-Gang Zhao). To predict the stress-strain curve of particular concrete, an enormous amount of experimental and theoretical research has been conducted and many researchers have proposed empirically-based numerical approximations for this matter (Lu & Zhao, 2010; Mansur, Chin, & Wee, 1999; Popovics, 1973). However, due to concrete being a mixture of different materials and without a uniform mix design, there is no universal consensus equation available (B. A. Graybeal, 2007). Moreover, there is not any equation available which can generally predict the stress-strain curve of UHPFRC (B. A. Graybeal, 2007).

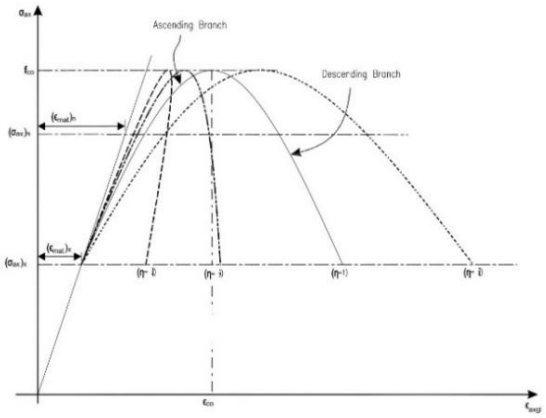

Figure 1: Size-Dependent σ_{ax}- ε_{axgl} from Chen. et. al (2014)

The size-dependency of concrete specimens is important as different sized specimen produce different results (Kazemi & Lubell, 2012). From global strain (ε_{axgl}) it is possible to understand the size-effect on stress-strain relationship of a specimen. Chen et al. (Chen et al., 2014) suggested an equation for global stress-strain,

$$(\varepsilon_{axgl-2})_n = [(\varepsilon_{axgl-1})_n - (\varepsilon_{mat})_n]\frac{L_{pr-1}}{L_{pr-2}} + (\varepsilon_{mat})_n \quad (1)$$

In equation (1), ε_{axgl-1} is the global strain of a standard cylinder of 200 mm and L_{pr-1} is the specific length of that, ε_{mat} is the material strain and L_{pr-2} is the specific length of the required specimen. The subscript η is the size factor equivalent to L_{pr-1}/L_{pr-2}. Fig 1 illustrates the diagram of the equation for the stress level $(\sigma_{ax})_n$. It can be seen that up to $(\sigma_{ax})_x$, every specimen has same material strain and the ascending

branch has a similar linear slope for every specimen. Test stress-strain relationship for η =1 is used as a base to plot other stress-strain relationships for different lengths L_{pr-2}. Figure 1 illustrates that as the η reduces, reduction in ductility in the descending branch is apparent and contrary, as the η increases, an increase in ductility in the descending branch is seen. Moreover, fig 1 also illustrates the ductile behavior of UHPC – it shows considerable residual stress even in higher strain after reaching peak strain.

To make the existing peak strain-based stress-strain relationships size-dependent, Chen et al proposed an adjusted value of $\boldsymbol{\varepsilon_{co}}$ for size-dependency characteristics (Chen et al., 2014). This adjusted $\boldsymbol{\varepsilon_{co}}$ strain makes the stress-strain size-dependent and stress-strain relationship for any size can be derived from one standard size. While using this equation, the slenderness factor **μ** has to be equal to or more than 2. Here, **μ** is the ratio of length to diameter for cylinder specimen. Graybeal et al conducted in his paper that the increase in the size of fiber-reinforced concrete significantly reduces the compressive strength (B. A. Graybeal, 2007). But there is not any existing consensus equation that can predict size-dependent stress-strain behavior of UHPFRC. Previous researches have shown that fiber significantly improves post-peak behavior and enhances strain characteristics of concrete in both compression and tension (Dwarakanath & Nagaraj, 1991; Nataraja, Dhang, & Gupta, 1999).

2.1.2 Popovics's Model (1973)

The model proposed by Popovics can estimate the complete stress-strain diagram of concrete. This model predicts both the ascending and descending branches of the stress-strain curve.

$$f = f_0 \frac{\varepsilon}{\varepsilon_0} \frac{n}{n-1+\left(\varepsilon/\varepsilon_0\right)^2} \tag{2}$$

This model predicts good stress-strain behavior for up to 69 MPa concrete. For incorporating size-depending behavior, Chen et al have modified the Popovics's equation by replacing peak strain (ε_o) with an adjusted peak strain (ε_{co}) and n with r , which is a factor that controls the ductility of the concrete, and $r = \frac{E_c}{[E_c-(f_{co}/\varepsilon_{co})]}$. Chen et al used regression analysis on test results of normal weight concrete for the value of ε_o.

Thus, the modified Popovics's formula for the size-dependent stress-strain diagram is,

$$f = f_{co} \frac{\left[\frac{(\varepsilon ax)pop}{\varepsilon co}\right] r}{r-1+\left[\frac{(\varepsilon ax)pop}{\varepsilon co}\right]^r} \tag{3}$$

This yields the size-dependent stress-strain relationship for Popovics's equation. The authors in this study have conducted regression analysis for deriving Chen's moderated factors (ε_{co}**)** for three different fiber-volume content of UHPFRC and incorporated the factors in previously proposed Popovics's analytical model equation (2) to propose a size-dependent stress-strain model of UHPFRC.

2.1.3 Extracting Regression

Global strain at peak stress (f_{co}) for a specimen of length 200 mm, $\boldsymbol{\varepsilon_{co\text{-}200}}$, can be utilized to formulate size-dependent characteristics for the predictive model. Peak strain can be converted into global strain for a specimen of length 200 mm by using Chen's equation-(Chen et al., 2014),

$$\varepsilon_{co-200} = \left(\varepsilon_{co-test} - \frac{f_{co}}{Ec}\right) \frac{L_{pr-test}}{200} + \frac{f_{co}}{Ec} \tag{4}$$

Where,

f_{co} = Peak stress

$\boldsymbol{\varepsilon_{co\text{-}test}}$ = Peak strain from test result

$L_{pr\text{-}test}$ = Length of test specimen

$L_{pr\text{-}200}$ = Test specimen length converted to 200 mm

The authors have performed linear regression on 121 published test results pertaining to the relevant topic (Al-Azzawi & Sarsam, 2010; Bencardino, Rizzuti, & Spadea, 2007; Bencardino, Rizzuti, Spadea, & Swamy, 2008; Bhargava, Sharma, & Kaushik, 2006; Earle, Bowden, & Guy; Graybeal, 2005; B. Graybeal, 2007; Jiao, Sun, Huan, & Jiang, 2009; Jo, Shon, & Kim, 2001; Lavanya, Dattatreya, M.Neelamegam, & Seshagiri Rao, 2010; Lavanya, J K, & Neelamegam, 2014; Lee; Mansur et al., 1999; Suksawang, Wtaife, & Alsabbagh, 2018) to determine relationships between $\boldsymbol{\varepsilon_{co\text{-}200}}$ and $f_{co.}$. Later, the authors have divided the test results by 3 different volume percentages of steel fibers – 1%, 2%, and 3% and performed linear regression for the aforementioned percentages with test results of a similar percentage of steel fiber. For 1% fiber-volume content, the linear regression gave the following equation relationships between $\varepsilon_{co\text{-}200}$ and $f_{co,}$

$$\varepsilon_{co-200} = 6.42 \times 10^{-6} f_{co} + 2.88 \times 10^{-3} \quad (5)$$

For 2%, the linear regression gave the following equation relationships between $\boldsymbol{\varepsilon_{co\text{-}200}}$ and $f_{co,}$

$$\varepsilon_{co-200} = -1.78 \times 10^{-6} f_{co} + 3.88 \times 10^{-3} \quad (6)$$

For 3%, the linear regression gave the following equation relationships between $\boldsymbol{\varepsilon_{co\text{-}200}}$ and $f_{co,}$

$$\varepsilon_{co-200} = 1.08 \times 10^{-6} f_{co} + 3.44 \times 10^{-3} \quad (7)$$

The model will incorporate equations (4-7) to produce an estimate for size-dependent stress-strain curves for UHPFRC.

2.2 Experimental Test Specification

The experimental test was initiated to investigate the size-dependent compressive strength and stress-strain behavior of UHPFRC. Two major influencing factors in preparing test specimens are – Varying fiber volume-content and size of the specimen. For each fiber content from 1% to 3%, size-wise three types of cylinder, with a fixed diameter of 100 mm and varying height 200 mm, 300 mm and 400 mm were cast. To get a more accurate result, for each type of cylinders, 3 cylinders were cast and the mean value was used in the paper.

The mix composition was adopted from the previous work (Sobuz et al., 2016). One commercially available fiber – Dramix 4D was used and are available from Bekaet Ltd in South Australia. All of the steel fibers were hooked end wired type. The compression strength tests were carried out according to the standard (ASTM-C39/C39M-12, 2012). An Amsler Compressive Testing Machine with a maximum capacity of 5000 kN was used to determine stress-strain behavior. Load control was the controlling measure up to the peak strength and after that, the specimens were under deflection control. The loads were applied on the top surface of 100 mm diameter cylinders. The load application rate was maintained at 50 kN/min in the ascending branch. After the peak load, for the descending branch, the displacement was at 0.1 mm/min. At day 56, 4 LVDTs were equipped to measure the total platen to platen axial deformation and 3 LVDTs equally spaced laterally at mid-height were equipped to measure the total lateral dilation. For measuring axial strain due to concentric load, two axial gauges were used and for lateral strain, three lateral strain gauges were used.

3. EXPERIMENTAL TEST RESULTS

Axial stress-strain results involving peak strength, peak strain, failure strength and failure strain of different fiber content are presented in Table 1. Predominantly, it can be seen from Table 1 that, the strength ranges from 137 MPa to 160 MPa with corresponding peak strain .004156 to .004515 for test series 1, strength ranges from 124 MPa to 142 MPa with corresponding peak strain 0.003544 to 0.003708 for test series 2 and strength ranges from 140 MPa to 143 MPa with corresponding peak strain 0.004027 to 0.004389 for test series 3.

Table 1: UHPFRC experimental test result

Specimen Designation	Test Series	Fiber %	Peak Strength (MPa)	Peak Strain	Failure Strength (MPa)	Failure Strain
S-100x200-1	1	1	137	0.004156	6.683	0.101
S-100x200-2	1	2	155	0.004437	4.394	0.148
S-100x200-3	1	3	160	0.004515	7.234	0.187
S-100x300-1	2	1	124	0.003544	0.6288	0.0923
S-100x300-2	2	2	142	0.003664	2.476	0.1098
S-100x300-3	2	3	142	0.003708	1.469	0.1322
S-100x400-1	3	1	140	0.004027	0.981	0.0660
S-100x400-2	3	2	142	0.003963	1.948	0.0797
S-100x400-3	3	3	143	0.004389	2.819	0.0918

It is noted that the highest peak strength observed was 160 MPa for S-100x200-3 specimen and the highest peak strain was 0.004515 for S-100x200-3 specimen. It satisfies that with the introduction of higher fiber content, the peak strain and failure strain increases significantly for each size.

From table 1, it can be seen that failure strain for UHPFRC is significantly higher than normal-weight concrete at higher strain. For NWC, the failure strain is in the vicinity of 0.005 whereas, for UHPFRC, the lowest failure strain observed in the experiment is 0.0660 (Lim & Ozbakkaloglu, 2014). This phenomenon indicates that serviceability for UHPFRC is significantly higher than NWC and exhibits more ductile behavior

4. ANALYTICAL RESULTS

It is possible to predict stress-strain behavior for other lengths of specimen after testing one standard specimen length. After selecting a standard length of specimen, equation (4) can be applied to convert other specimen lengths to the standard one. This way the global strain for standard $\boldsymbol{\varepsilon_{co\text{-}standard}}$ can be converted into global strain for other length $\boldsymbol{\varepsilon_{co\text{-}others}}$**.** For instance, global strain for $\mathbf{L_{pr\text{-}200}}$ is $\boldsymbol{\varepsilon_{co\text{-}200}}$**,** which can be converted into $\boldsymbol{\varepsilon_{co\text{-}300}}$ for specimen length of 300 mm and likewise.

For this study, the authors have used three base specimen sizes for three different fiber-volume percentages to predict stress-strain behavior of other sizes in a similar fiber-volume percentage. For the similar fiber-volume percentage, predicted derived numerical stress-strain behaviors for other specimen sizes are then compared with previous experimental results.

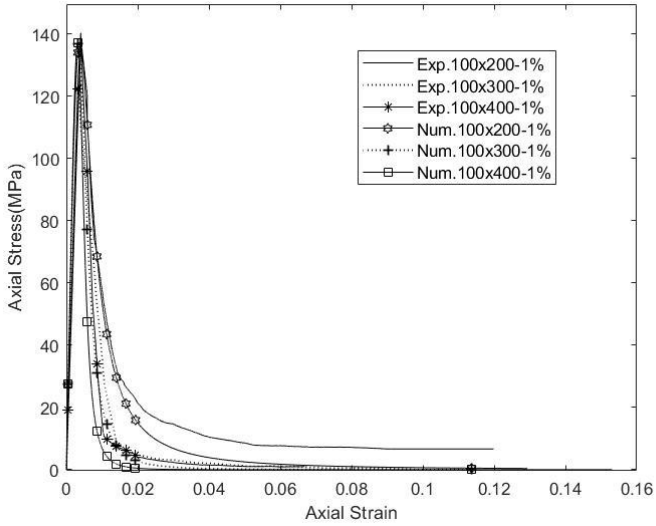

Figure 2: Experimental data vs numerical data for 1% fiber-volume content

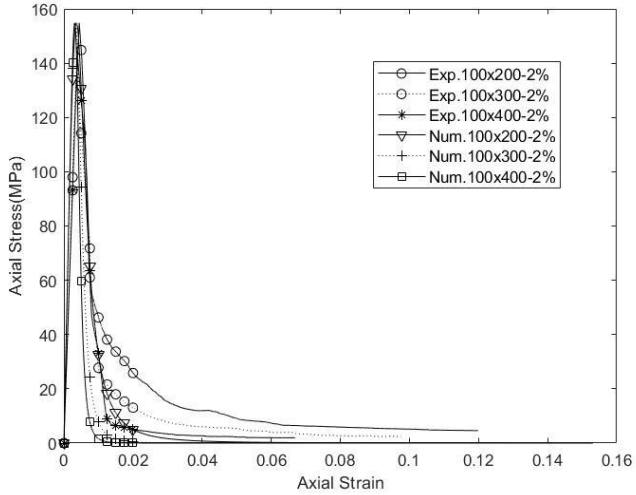

Figure 3: Experimental data vs numerical data for 2% fiber-volume content

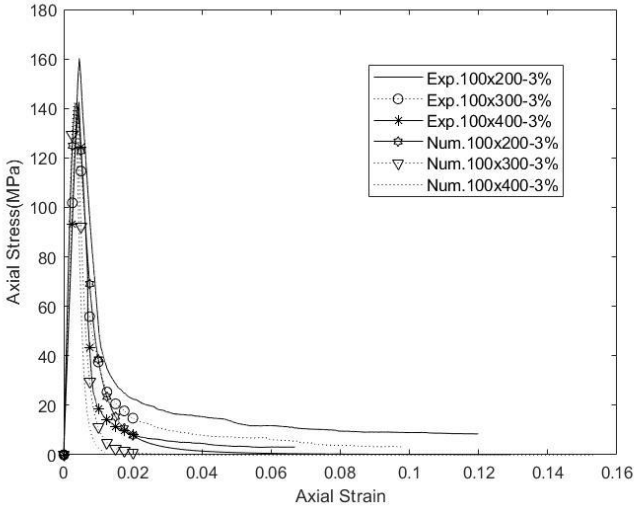

Figure 4: Experimental data vs numerical data for 3% fiber-volume content

For 1%, 100x200 mm is taken as the base size specimen. Numerical behavior of for 100x200 mm, 100x300 mm and 100x400 mm with 1% fiber-volume is derived using equations (4) and (5) which is exhibited in figure 2. Both experimental and numerical stress-strain graph shows linearity till the peak stress. The model accurately predicts linear behavior equivalent to the experimental. The model also predicts compressive peak stress with accuracy. For UHPC, a steep post-peak is observed in both works of literature (Mansur et al., 1999) and in this experimental result. The model closely predicts steep post-peak behavior relative to the experimental post-peak behavior. The specimen exhibits relatively higher residual stress even in higher strain – 100x200 mm exhibits around 36 MPa for a strain of 0.016 and the model is able to predict closely similar residual stress in a similar strain. This indicates the ductility characteristics of UHPFRC; hence, the model is also able to predict the ductility property of UHPFRC.

For 2%, 100x200 mm is taken as a base specimen. Numerical behavior of 100x200 mm, 100x300 mm, and 100x400 mm with 2% fiber-volume is derived using equations (4) and (6) which is shown in figure 3. Figure 3 and figure 4 shows that similar characteristics to 1% can be observed for 2%. With the increase of fiber-volume, compressive strength tends to be higher (Kazemi & Lubell, 2012). In this study, 2% fiber-volume increased compressive strength to 155 MPa for 100x200 mm specimen. The model predicts closely to the increased compressive strength for 2%. Moreover, it is noted that with increased specimen size, lower compressive strength is obtained (Kazemi & Lubell; Lubell). In this study, 100x300 mm and 100x400 mm exhibited lower compressive strength than 100x200 mm and the model is able to predict the drop in compressive strength with increased size. For 3%, a similar procedure was followed and similar results were obtained using equations (4) and (7), which is shown in figure 4. Figure 4 predicts similar correlation – linear behavior, peak stress, steeper post-peak behavior, analogous stress-strain behavior with the influence of specimen-size and ductility property. Thus, the model predicts a conservative estimate with the experimental results.

5. CONCLUSIONS

The study was undertaken to construct a model for estimating size-dependent stress-strain curves for UHPFRC. For establishing the model, using Popovic et al's (Popovics, 1973) equation and Chen et al's (Chen et al., 2014) global strain equation, regression analysis was conducted on 121 published test results to generate size-dependent stress-strain equations for UHPFRC. Three equations were generated for three different fiber-volume contents – 1 %, 2 %, and 3 %. A comparison of the prediction from this model and experimental test data manifests good consistency. The model accurately predicts up to material strain and provides a conservative estimate for the softening branch with the experimental data. Commensurate estimate for softening branch allows future research pertaining to high cyclic load, fatigue, earthquake by utilizing this model. It is possible to estimate any specimen sized stress-strain behaviors using this model just by experimenting with one standard size. As a result, a significant reduction of cost, time and material can be achieved while conducting future research in UHPFRC.

ACKNOWLEDGEMENTS

The authors wish to acknowledge the financial support of the Australian Government Department of Defense's ''Defense Science and Technology Organization". The experimental study was conducted in the Chapman structural laboratory of the School of Civil, Environment and Mining Engineering, The University of Adelaide, South Australia. The numerical modeling part of the research was carried out in the high-speed computers in BIM laboratory in the Department of Building Engineering and Construction Management, Khulna University of Engineering and Technology, Khulna-9203, Bangladesh.

REFERENCES

Al-Azzawi, Z., & Sarsam, K. (2010). Mechanical Properties of High-Strength Fiber Reinforced Concrete. *Engineering and Technology Journal, 28*, 2442.

Ayub, T. (2014). *Stress-Strain Response of High Strength Concrete and Application of the Existing Models* (Vol. 8).

B.A. Graybeal, P. E., J.L. Hartmann, P.E. (2003). *ULTRA-HIGH PERFORMANCE CONCRETE MATERIAL PROPERTIES*. Paper presented at the Transportation Research Board Conference.

Bencardino, F., Rizzuti, L., & Spadea, G. (2007). Experimental tests vs. theoretical modeling for FRC in compression. *Proceedings of the 6th International Conference on Fracture Mechanics of Concrete and Concrete Structures, 3*, 1473-1480.

Bencardino, F., Rizzuti, L., Spadea, G., & Swamy, R. (2008). Stress-Strain Behavior of Steel Fiber-Reinforced Concrete in Compression. *Journal of Materials in Civil Engineering - J MATER CIVIL ENG, 20*. doi:10.1061/(ASCE)0899-1561(2008)20:3(255)

Bhargava, P., Sharma, U. K., & Kaushik, S. (2006). Compressive Stress-Strain Behavior of Small Scale Steel Fibre Reinforced High Strength Concrete Cylinders. *Journal of Advanced Concrete Technology - J ADV CONCR TECHNOL, 4*, 109-121. doi:10.3151/jact.4.109

Chen, Y., Visintin, P., Oehlers, D. J., & Alengaram, U. J. (2014). Size-Dependent Stress-Strain Model for Unconfined Concrete. *Journal of Structural Engineering, 140*(4). doi:10.1061/(asce)st.1943-541x.0000869

Davis, B. G. a. M. (2008). Cylinder or Cube: Strength Testing of 80 to 200 MPa (11.6 to 29 ksi) Ultra-High-Performance Fiber-Reinforced Concrete. *ACI MATERIALS JOURNAL, 105*(6).

del Viso, J. R., Carmona, J. R., & Ruiz, G. (2008). Shape and size effects on the compressive strength of high-strength concrete. *Cement and Concrete Research, 38*(3), 386-395. doi:10.1016/j.cemconres.2007.09.020

Dwarakanath, H. V., & Nagaraj, T. S. (1991). *Comparative study of predictions of flexural strength of steel fiber concrete* (Vol. 88).

Earle, P., Bowden, D., & Guy, M. (2012). Twitter earthquake detection: Earthquake monitoring in a social world. *Annals of geophysics = Annali di geofisica, 54*. doi:10.4401/ag-5364

Frettlöhr, B., H. Reineck, K., & W. Reinhardt, H. (2012). Size and Shape Effect of UHPFRC Prisms Tested under Axial Tension and Bending. In (Vol. 2, pp. 365-372).

Graybeal, B. (2005). Characterization of the behavior of ultra-high performance concrete.

Graybeal, B. (2007). Compressive Behavior of Ultra-High-Performance Fiber-Reinforced Concrete. *ACI MATERIALS JOURNAL, 104*, 146-152.

Graybeal, B. A. (2007). Compressive Behavior of Ultra-High-Performance Fiber-Reinforced Concrete. *ACI MATERIALS JOURNAL, 104*(2).

Jiao, C., Sun, W., Huan, S., & Jiang, G. (2009). Behavior of steel fiber - Reinforced high-strength concrete at medium strain rate. *Frontiers of Architecture and Civil Engineering in China, 3*, 131-136. doi:10.1007/s11709-009-0027-0

Jo, B.-W., Shon, Y.-H., & Kim, Y.-J. (2001). The Evalution Of Elastic Modulus for Steel Fiber Reinforced Concrete. *Russian Journal of Nondestructive Testing, 37*(2), 152-161. doi:10.1023/A:1016780124443

Kazemi, S., & Lubell, A. (2012). Influence of Specimen Size and Fiber Content on Mechanical Properties of Ultra-High-Performance Fiber-Reinforced Concrete. *ACI MATERIALS JOURNAL, 109*, 675-684. doi:10.14359/51684165

Kim, D. J., Park, S.H., Ryu, G.S., & Koh, K.T. . (2011). Comparative flexural behavior of Hybrid Ultra High Performance Fiber Reinforced Concrete with different macro fibers. *Construction and Building Materials, 25*(11), 4144-4155.

Lavanya, S., Dattatreya, J., M.Neelamegam, & Seshagiri Rao, M. (2010). STUDY ON STRESS-STRAIN PROPERTIES OF REACTIVE POWDER CONCRETE UNDER UNIAXIAL COMPRESSION. *International Journal of Engineering Science and Technology, 2*.

Lavanya, S., J K, D., & Neelamegam, M. (2014). STRESS STRAIN BEHAVIOUR OF ULTRA HIGH PERFORMANCE CONCRETE UNDER UNIAXIAL COMPRESSION. *International Journal of Civil Engineering and Technology (IJCIET) 0976-6316, 5*, 187-194.

Lee, I. Complete Stress-Strain Characteristics of High Performance Concrete.

Lim, J. C., & Ozbakkaloglu, T. (2014). Stress-Strain Model for Normal- and Light-Weight Concretes under Uniaxial and Triaxial Compression. *Construction and Building Materials, 71*. doi:10.1016/j.conbuildmat.2014.08.050

Lu, Z.-H., & Zhao, Y.-G. (2010). Empirical Stress-Strain Model for Unconfined High-Strength Concrete under Uniaxial Compression. *Journal of Materials in Civil Engineering - J MATER CIVIL ENG, 22*. doi:10.1061/(ASCE)MT.1943-5533.0000095

Lubell, S. K. a. A. S. Influence of Specimen Size and Fiber Content on Mechanical Properties of Ultra-High-Performance Fiber-Reinforced Concrete. *ACI MATERIALS JOURNAL, 109*(6).

Maher KT, V. Y. (2016). Taking Ultra-High Performance Concrete to New Height – The Malaysian Experience. *Aspire the Concrete Bridge Magazine, Summer 2016*, 36-38.

Mansur, M. A., Chin, M., & Wee, T. (1999). Stress-Strain Relationship of High-Strength Fiber Concrete in Compression. *Journal of Materials in Civil Engineering - J MATER CIVIL ENG, 11*. doi:10.1061/(ASCE)0899-1561(1999)11:1(21)

Mindessb, G. C. a. S. (2000). Size Effect in Compression of High Strength Fibre Reinforced Concrete Cylinders Subjected To Concentric And Eccentric Loads. *Materials for Buildings and Structures*.

Nataraja, M., Dhang, N., & Gupta, A. P. (1999). *Stress–strain curves for steel-fiber reinforced concrete under compression* (Vol. 21).

Pierre-Claude Aitcin, B. M., Willliam D. Cook, and Denis Mitchell. (1994). Effects of Size and Curing on Cylinder Compressive Strength of Normal and High-Strength Concretes. *ACI MATERIALS JOURNAL, 91*(4), Title no. 91-M34.

Pierre Richard, M. C. (1995). COMPOSITION OF REACTIVE POWDER CONCREXES *Cement and Concrete Research, Vol. 25*.(7), 1501-1511.

Popovics, S. (1973). A NUMERICAL APPROACH TO THE COMPLETE STRESS-STRAIN CURVE OF CONCRETE. *Cement and Concrete Research, 3*, 583-599.

Shafieifar, M., Farzad, M., & Azizinamini, A. (2017). Experimental and numerical study on mechanical properties of Ultra High Performance Concrete (UHPC). *Construction and Building Materials, 156*, 402-411. doi:10.1016/j.conbuildmat.2017.08.170

Sobuz, H. R., Visintin, P., Mohamed Ali, M. S., Singh, M., Griffith, M. C., & Sheikh, A. H. (2016). Manufacturing ultra-high performance concrete utilising conventional materials and production methods. *Construction and Building Materials, 111*, 251-261. doi:10.1016/j.conbuildmat.2016.02.102

Suksawang, N., Wtaife, S., & Alsabbagh, A. (2018). Evaluation of Elastic Modulus of Fiber-Reinforced Concrete. *ACI MATERIALS JOURNAL, 115*. doi:10.14359/51701920

Toledo Filho, R. D., Koenders, E. A. B., Formagini, S., & Fairbairn, E. M. R. (2012). Performance assessment of Ultra High Performance Fiber Reinforced Cementitious Composites in view of sustainability. *Materials & Design (1980-2015), 36*, 880-888. doi:10.1016/j.matdes.2011.09.022

Wille K, T. N., Parra-Montesinos GJ. (2014). Fiber distribution and orientation in UHP-FRC beams and their effect on backward analysis. *Materials and Structures, 47(11)*, 1825–1838.

YI, J.-K. K. a. S.-T. (2002). Application of size effect to compressive strength of concrete members. *S¯adhan¯a, 27*, 467-484.

Yoo, D.-Y., & Yoon, Y.-S. (2016). A Review on Structural Behavior, Design, and Application of Ultra-High-Performance Fiber-Reinforced Concrete. *International Journal of Concrete Structures and Materials, 10*(2), 125-142. doi:10.1007/s40069-016-0143-x

Zhao-Hui Lu and Yan-Gang Zhao, M. A. (2010). Empirical Stress-Strain Model for Unconfined High-Strength Concrete under Uniaxial Compression. *JOURNAL OF MATERIALS IN CIVIL ENGINEERING © ASCE, 22(11)*, 1181-1186. doi:10.1061/ASCEMT.1943-5533.0000095

Proceedings of the 5th International Conference on Civil Engineering for Sustainable Development (ICCESD 2020), 7~9 February 2020, KUET, Khulna, Bangladesh (ISBN-978-984-34-8764-3)

A STUDY ON SEISMIC VULNERABILITY ASSESSMENT OF BUILDINGS OF A SELECTED AREA IN DHAKA SOUTH CITY CORPORATION BY RVS METHOD

Md. Hisamuzzaman[1], Fazle Azim Saif [2], Muhaiminul Ahmed Faisal[3], Pialy Biswas[4] and Md. Saiful Islam[5]

[1,2]Lecturer, Department of Civil Engineering, World University of Bangladesh, Bangladesh, e-mail: azimsaif104@gmail.com
[3,4,5] Department of Civil Engineering,World University of Bangladesh, Bangladesh, e-mail: pialybiswas883@gmail.com

***Corresponding Author**

ABSTRACT

The structures which are vulnerable or prone to collapse in an earthquake can cause loss of life and property. To increase earthquake resilience, it is important to know the condition of the existing structures. This study is focused on identifying the seismic vulnerability of buildings. The paper represents a scenario of the structural vulnerability of the buildings which are situated in ward No 35 in Dhaka South City Corporation, Bangladesh. The approach is based on the rapid visual screening (RVS) procedure which is described in FEMA 154. In the RVS procedure an analyzed building is entitled to a score (S) based on some parameters. Major parameters that have effects on the building score are primary structural lateral-load-resisting system, construction material, and other seismic related characteristics such as soil type and building irregularities. Building with higher S scores corresponding to a better seismic performance. The result of this study will show the percentage of buildings that are vulnerable to seismic risk in the selected area as well as in need of further detail assessment.

Keywords: *Earthquake, RVS, FEMA 154, Seismic vulnerability*.

1. INTRODUCTION

Bangladesh is one of the calamities prone country. It's prevailing among the most at risk countries in the world with its high population density and rapid urbanization. Dhaka South City Corporation lies in an active earthquake prone area of Bangladesh. In Great Indian Earthquake of 12 June 1897, this city was damaged severely due to a surface wave magnitude of 8.1 (Sarker et al., 2010). According to World Risk Report (2016), Bangladesh is the fifth most vulnerable country to disasters (UN, 2016). Earthquake causes comprehensive destruction of life and property. For providing seismic safety in building structures, it is needed to ensure their conformance to the current seismic design codes which is valid approach for new buildings. Often, rapid assessment of seismic vulnerability in an area is done through visual inspection of the buildings and by providing a performance score using predefined forms based on adequate seismic resistance features usable in the building. This process is known as rapid visual screening (RVS), as one can cover large number of buildings within a short period of time. FEMA (Federal Emergency Management Agency) 154 provides the detailed procedure for carrying out RVS of buildings. Rapid Visual Screening (RVS) is a qualitative seismic vulnerability assessment method (Yadollahi, Adnan & Zin, 2012). RVS method is popular in US and other countries as a tool for ranking the buildings regarding seismic vulnerability consideration. The RVS method was applied as a preliminary evaluation to determine the level of performance suitability of the Emergency Care Installation Buildings of Dr. Sardajito Hospitals for the effects of earthquake (Aritonang, Satyarno & Supriyadi, 2011). Another study was also carried out which include screening of 1,057 public buildings in Western Oregon in US (Wallace & Miller ,2008), they implemented RVS to identify potential seismic hazards for Oregon's public facilities including hospital, school, police station, fire station, community college and emergency response center. Further, RVS was used to identify, inventory and rank all high-risk buildings in a specified region in Greek to form a strategy of priority-based interventions to buildings. (Kapetana & Dritsos ,2007). This research is focused on identifying and ranking of buildings in particular area of Dhaka South City Corporation to assess seismic vulnerable buildings through RVS method and will prescribe further detail assessment requirement against earthquake force. These types of assessments were previously conducted by many researchers (Wahid et al., 2005). However, the study area was different.

1.1 Study Area

The initial step is to select a community or group of Buildings. The study area is chosen as old Dhaka under the Dhaka south city corporation since it is the most seismic vulnerable portion of Dhaka city. The study area consists of ancient buildings which are located very close to each other. The assessment is carried out only considering the buildings situated both sides of the selected roads. The survey was started from Bangshal Road to end of the Abul Hasnat Road. It turned right to Aga Sadek Road, and ended up with Sikkatuli Lane and Abdul Hadi Lane of 35 no. ward in the Dhaka South City Corporation. Figure 1 shows the map of the study area and representative buildings.

Figure 1: Map and representative buildings on the study Area (ward no.35 under DSCC)

2. METHODOLOGY

Rapid Visual Screening (RVS) method was originally developed by the Applied Technology council (ATC) in the late 1980 and published in 1988 in the FEMA 154. It is a side walk survey approach that enabled users to classify surveyed buildings into categories: a. Buildings those are risk to life and property; b. Those seismically hazardous buildings that should be investigate extensively by a design professional experienced in seismic design. Total one hundred and two buildings were screened for the building vulnerability assessment. The screening process was conducted by filling up a data collection form includes building identification, information comprising its use and size, a photograph of the building, sketches, and documentation of pertinent data.

3. RESULTS AND DISCUSSION

The survey was mainly concentrated on earthquake issues such as identifying building type, plot size and shape, clear distances from surrounding structures, road width and basic information of the building, year of construction, no. of story, no. of inhabitants etc. Digital photographs of each building from at least two directions were taken. A database was compiled in MS Excel among the 102 structures in the aforementioned study area. From the surveyed buildings around 78 buildings are R.C.C structures, 12 of them are soft storied and the rest 24 buildings are un-reinforced masonry (URM). The findings of the survey are tabulated in Table 1 and Table 2. Table 1 shows the percentages of different parameters considered for the seismic vulnerability assessment of buildings and table 2 shows the total number and percentages of buildings used for different purpose.

Table 1: Percentages of Different Parameters

	Total Number	**Percent**
Total Number of Building	102	
Number of Pre-Code Building	22	21.57 %
Number of Post-Benchmark Building	80	78.43 %
Number of Pounding Type Building	80	78.43 %
Falling Hazards from taller adjacent building	1	0.98 %
Number of C1 Type Building	64	62.75%
Number of C2 Type Building	14	13.73%
Number of URM Type Building	24	23.53 %
Number of Additions Type Building	16	15.69 %
Number of Soft Story Type Building	12	11.76 %
Number of Plan irregularity Type Building	23	22.55 %
Number of Vertical irregularity Type Building	51	50 %
Number of 2nd Story Building	6	5.88 %
Number of 3rd Story Building	22	21.57 %
Number of 4th Story Building	11	10.78 %
Number of 5th Story Building	26	25.49 %
Number of 6th Story Building	24	23.53 %
Number of 7th Story Building	11	10.78 %
Number of 8th Story Building	1	0.98 %
Number of 10th Story Building	1	0.98 %
Final level 1 score (0.3)	3	2.94%
Final level 1 score (0.6)	1	0.98%
Final level 1 score (0.9)	3	2.94%
Final level 1 score (1.0)	11	10.78%
Final level 1 score (1.1)	2	1.96%
Final level 1 score (1.6)	6	5.88%
Final level 1 score (1.7)	2	1.96%
Final level 1 score (1.8)	1	0.98%
Final level 1 score (2.6)	6	5.88%

Final level 1 score (2.8)	1	0.98%
Final level 1 score (3.3)	4	3.92%
Final level 1 score (3.4)	23	22.55%
Final level 1 score (4.1)	31	30.39%
Final level 1 score (4.8)	8	7.84%
Number of One-unit building	52	50.98 %
Number of Two-unit building	49	48.04%
Number of Four-unit building	1	0.98 %

Table 2: Usage of buildings

Usage of Buildings	**Total number of Buildings**	**Percent**
Residential	26	25.49%
Commercial and Residential	66	64.71%
Industrial and Residential	4	3.92%
Office and Residential	1	0.98%
Commercial, School, Office and Residential	1	0.98%
Office, Industrial and Residential	2	1.96%
Industrial, Commercial and Residential	1	0.98%
School	1	0.98%

From Table 1 the parameters can be illustrated as follows. The illustration can be started with the Pre code and Post benchmark parameters. Figure 2 shows the first parameter mentioned as the comparison between pre code and post benchmark parameters. From figure 2 it is found that 21.57 % Buildings are pre-code building which means 21.57 % of total buildings are constructed before the code was gazetted where 78.43% buildings were built after the BNBC code was published.

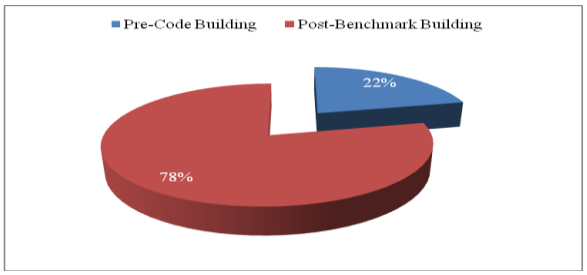

Figure 2: Comparison of Pre-Code & Post Benchmark Buildings.

The second parameter is pounding which represents the minimum separation gap between two consecutive buildings. Figure 3 shows the percentages of pounding and without pounding buildings.

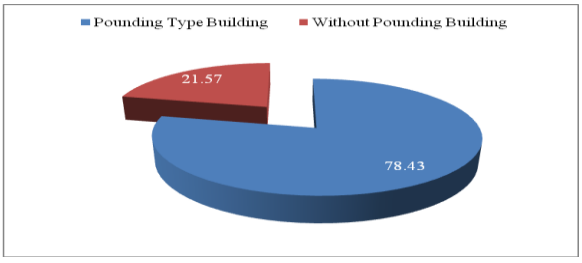

Figure 3: Comparison between pounding type buildings.

From the figure 3 it is found that 78.43 % buildings are pounding type building which means 78.43 % of total buildings do not obey the minimum separation gaps between adjacent buildings which is mentioned in the code.

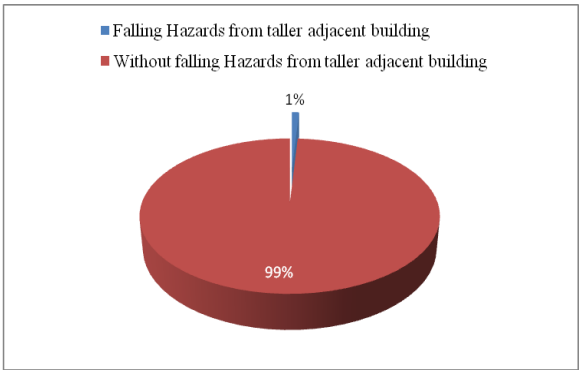

Figure 4: Comparison of falling hazards from taller adjacent buildings.

Again, the third parameter is possibly falling hazardous vulnerability from adjacent buildings. From the Figure 4, it is found that approximate 1% building has falling hazardous vulnerability from the adjacent building.

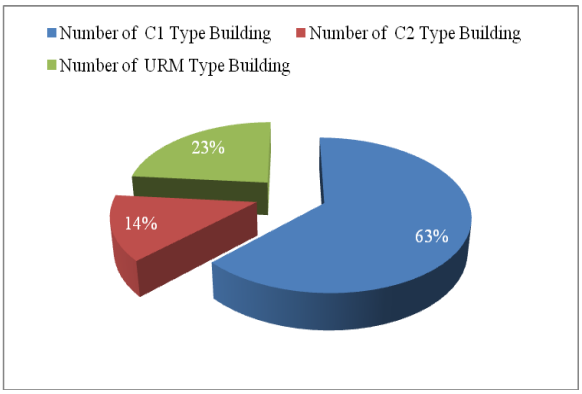

Figure 5: Comparison of C1, C2 & URM Type Buildings.

The fourth parameter is the comparison of C1, C2 & URM type Buildings. Figure 5 shows that, 62.75 % building are C1 type buildings (concrete moment-resisting frame buildings), 13.73 % building are C2 type buildings (concrete shear-wall buildings) and 23.53% are unreinforced masonry buildings (URM).

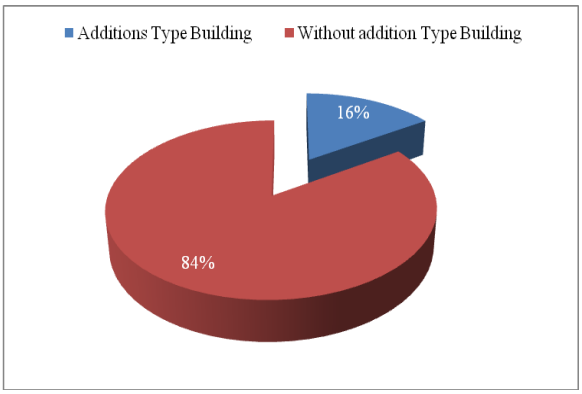

Figure 6: Comparison of Additions of buildings.

The fifth parameter is considered as further addition (buildings are modified with vertical or horizontal additions after the original construction). From the figure 6 it is found that, 15.69 % buildings are additional type buildings.

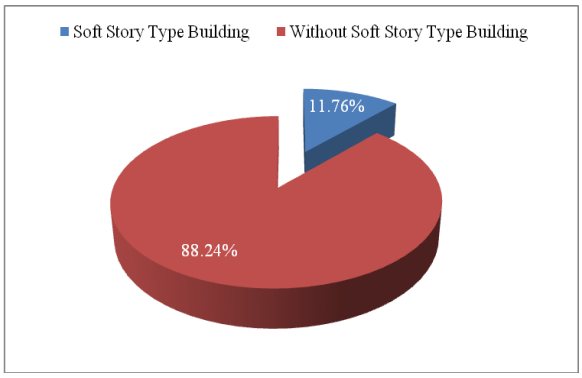

Figure 7: Comparison of Soft story buildings.

The sixth parameter is taken to be the buildings consisting of soft story. Figure 7 shows that, 11.76 % buildings comprise soft story. Soft story can be defined as the buildings which has a ground story or one of other story is built without any interior partition wall used for car parking or market or industry or office.

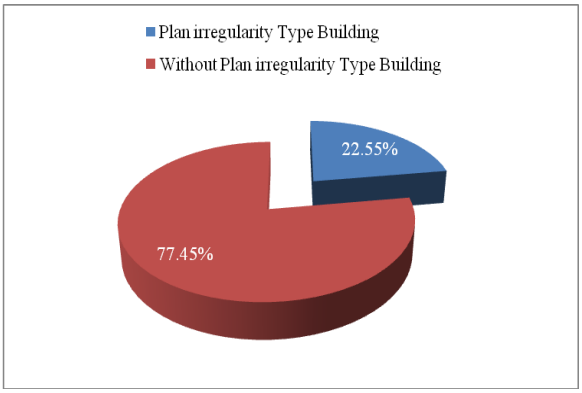

Figure 8: Comparison of plane irregularity of buildings.

The seventh parameter is established according to plan irregularities. From the figure 8 it is found that, 22.55% buildings have plan irregularity.

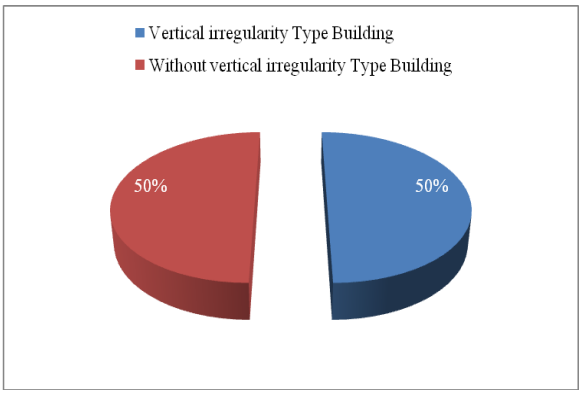

Figure 9: Comparison of vertical irregularity of buildings.

The eighth parameter is considered as vertical irregularities. Figure 9 shows that 50% buildings have vertical irregularity.

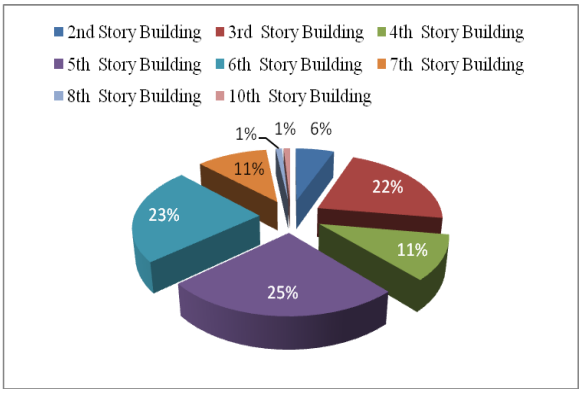

Figure 10: Comparison of story of buildings.

The ninth parameter is based on the story of the buildings. From the Figure 10 it is found that, among the seismic vulnerability assessed buildings, 5.88% buildings has two story, 21.57% buildings contains three story, 10.78% buildings comprises of four story, 25.49% buildings has five story, 23.53% buildings are six storied, 10.78% buildings consists of seven story, 0.98% buildings has eight story and 0.98% building are two storied buildings.

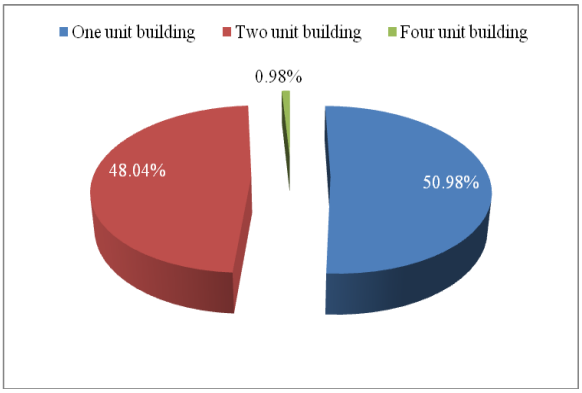

Figure 11: Units of buildings.

The tenth parameter is based on units of buildings. Figure 11 displays that, 50.98 % building has one unit, 48.08% building comprises two unit and 0.98% building consists of four unit.

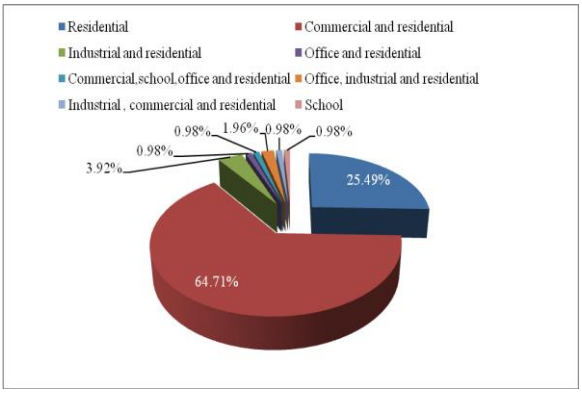

Figure 12: Usage of buildings.

The eleventh parameter is based on the usage of buildings. Figure 12 shows that, around 64.71% buildings are used as commercial cum residential, 25.49% buildings are built for the purpose of residential use, 3.92% buildings are used both as industrial and residential, 1.96% buildings consists three types of usage such as office, industrial and residential, 0.98% building comprises of four types of usage i.e. commercial, school, office, residential, 0.98% building consists of three types of usage resembling as industrial, commercial, residential, 0.98% building have two types of usage such as office and residential and 0.98% buildings are school buildings.

Based on the above parameters all the buildings are entitled to a score. The process of scoring is precisely described in FEMA 154. According to the FEMA 154 manual, if the building has a score less than 2 it will be considered as a seismic vulnerable building.

Figure 13 shows that, 28.43% buildings have final score below 2, on the other hand 71.56% buildings has a final score higher than 2. Moreover, On the basis of building score, the buildings are considered as the most seismic vulnerable which have a score below 1 and need further detail assessment. Further, seismic vulnerable buildings can be enlisted as the buildings which comprises a score below 2. Furthermore, which buildings have the score above 2 can be considered as safe during small magnitude of earthquake.

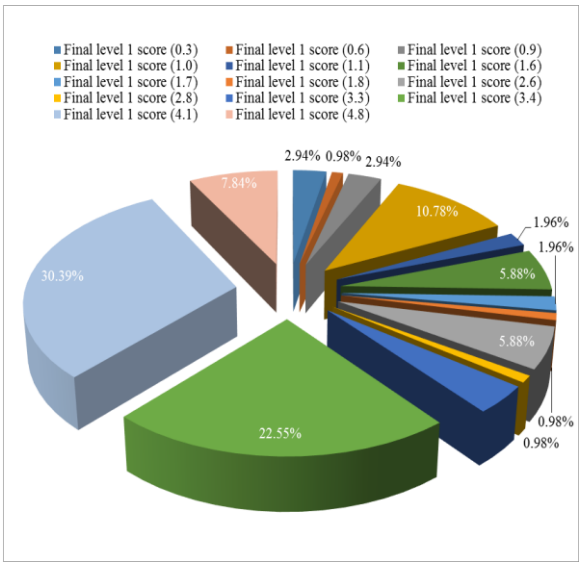

Figure 13: Scoring of buildings.

Figure 14 shows that, 19.61% buildings are the most vulnerable against earthquake, 8.82% buildings are vulnerable and 71.57% buildings are stable during small magnitude of earthquake.

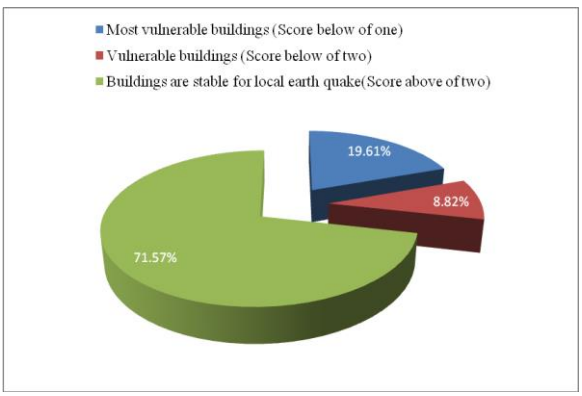

Figure 14: Vulnerability of buildings against earthquake.

4. CONCLUSIONS

This study focused on the structural vulnerability of buildings of the study area. Based on the results obtained from the study, following conclusions and recommendations can be drawn.

1. According to the building vulnerability survey, around 28.43% buildings are in vulnerable condition. To avoid casualties and fatalities in an earthquake, appropriate steps need to be taken for to strengthen of those buildings.

2. Detailed Engineering Assessment (DEA) can be done for those buildings possessing a RVS score below score 2 by an expert in seismic design.

The present study was conducted at a very small area. Further study can be carried out in a large area. From this research approximately 28.43% buildings are found seismic vulnerable. Therefore, details analysis can be carried out for the seismic vulnerable buildings.

REFERENCES

Aritonang, T. S. ., Satyarno, I., & Supriyadi, B. (2011). Performance Evaluation of The IRD RSUP DR. Sardjito Building to The Influence of Earthquake. Civil Engineering Forum, XX(September), 1183–1188.

Federal Emergency Management Agency (FEMA) 154 (2002). *Rapid Visual Screening of Building for Potential Seismic Hazard*, A Handbook. Washington DC: Applied Technology Council.

Kapetana, P., & Dritsos, S. (2007). *Seismic assessment of buildings by rapid visual screening procedures*. Earthquake Resistant Engineering Structures VI, I, 409– 418. doi:10.2495/ERES070391.

Sarker JK, Ansary MA, Rahman MS, Safullah AMM (2010) "Seismic hazard assessment for Mymensingh, Bangladesh", Environmental Earth Science, 60:643.

UN. (2016). World Risk Report 2016, United Nations. Accessed October 08, 2018 from https://collections.unu.edu/eserv/UNU:5763/WorldRiskReport2016_small_meta.pdf

Wallace, N., & Miller, T. (2008). Seismic *Screening of Public Facilities in Oregon's Western Countries*. Practice Periodical on Structural Design and Construction, 13(4), 189–197. doi:10.1061/(ASCE)10840680(2008)13:4(189).

Yadollahi, M., Adnan, A., & Zin, R. (2012). Seismic vulnerability functional method for rapid visual screening of existing buildings. Archives of Civil Engineering, LVIII(3). doi:10.2478/v.10169-012-0020-1.

A COMPARATIVE STUDY ON LATERAL LOAD ANALYSIS BY USING ETABS CONSIDERING TWO DIFFERENT VERSIONS OF BNBC

Md. Imran Islam Rabbi*[1], Simoom Sadik[1]

[1] *Student, Department of Civil Engineering, Rajshahi University of Engineering & Technology, Bangladesh, e-mail: imran140105@gmail.com*

Corresponding Author

ABSTRACT

Remarkable changes have been introduced in BNBC 2017 with regard to analysis of lateral loads. Modifications regarding design parameters and analysis methodology were proposed which primarily pivoted around analysis of seismic loads. In case of wind load, changes were introduced by modifying method of analysis and load projection, basic wind speed, gust response factor, external and internal pressure co-efficient, topographic effect, exposure and enclosure classification. For seismic analysis, design spectral acceleration had been reformulated. To identify the changes in design and analysis of various structures a comparative study is necessary between existing code and the previous one. This study aims at the comparison of provisions of earthquake and wind load analysis only given in BNBC 1993 and BNBC 2017. The lateral drift, torsional effect, wind and seismic base shear are obtained by BNBC 2017 vary significantly from the obtained value by BNBC 1993. Then the analysis and design of a typical 8 story residential building situated in Dhaka city with same number of stories using two codes are presented. The basic differences in both seismic base shear and story drift is also made using two versions of BNBC code. Design of reinforced concrete buildings for seismic load in BNBC-2017 is relatively economic than BNBC-1993 since amount of reinforcement required is less in BNBC-2017.

Keywords*: BNBC-1993, BNBC-2017, Applied wind & earthquake load, Inter story drift, Maximum lateral displacement, Base shear, Overturning moment.*

1. INTRODUCTION

Bangladesh National Building Code 2017 has been developed for the further advancement of more rational design of structures to ensure improved serviceability and safety. The primary differences between BNBC 1993 and 2017 are based on the analysis of seismic and wind loads which are relatively more complicated than static gravity load. In terms of analysis, significant changes have been introduced to wind and seismic loads. The sole purpose of this study is to investigate these changes from structural and economic point of view. So, a typical structural analysis of 8 story residential building has been conducted in accordance with both versions of code. For seismic base shear, maximum lateral displacement and inter story drift is higher in BNBC 2017 than BNBC 1993. Design of reinforced concrete buildings for lateral load in BNBC-2017 is relatively economic than BNBC-1993 as the amount of reinforcement requirement is less in BNBC-2017. The main objectives of this study are: Determination of the base shear, base moment, story shear and inter story drift according to BNBC 1993 and BNBC 2017. Comparison of base shear, story shear, base moment and inter story drifts by preparing an identical model to understand the comparison between the two codes. Analysis and design of a corner column and an interior column for both BNBC 1993 and BNBC 2017. Comparing the column axial forces, column dimensions and reinforcement requirement. The proposed changes to BNBC 1993 was first brought up by the research team [5]. They conducted a thorough study on Peak ground acceleration (PGA), spectral acceleration, soil classification system, site-dependent response spectrum and worked extensively in defining seismic design category. They showed that BNBC 1993 needs a major update in term of provision for design and structural analysis. Atique and Wadud (2001) presented Comparison of BNBC-93 with other building codes with respect to Earthquake and Wind analysis. Research conducted by Bari M.S., Das T (2014) had been one of the most compressive studies where a detailed parametric comparison was put forth based on BNBC-2017, BNBC-1993, and code of India 2005 (NBC-India 2005).

2. METHODOLOGY OF THE PRESENT STUDY

A typical 8 storied residential building (22.5m X 22.5m) situated in Dhaka city is selected for the comparison of BNBC 2017 and BNBC 1993.The buildings are assumed to be fixed at the base and the floors act as rigid diaphragms with a 3m height for each story, regular in plan is modeled. Finally, the buildings have been modeled by using ETABS software version-2017.

3. ANALYSIS RESULTS AND FINDINGS FROM BNBC 1993 AND BNBC 2017

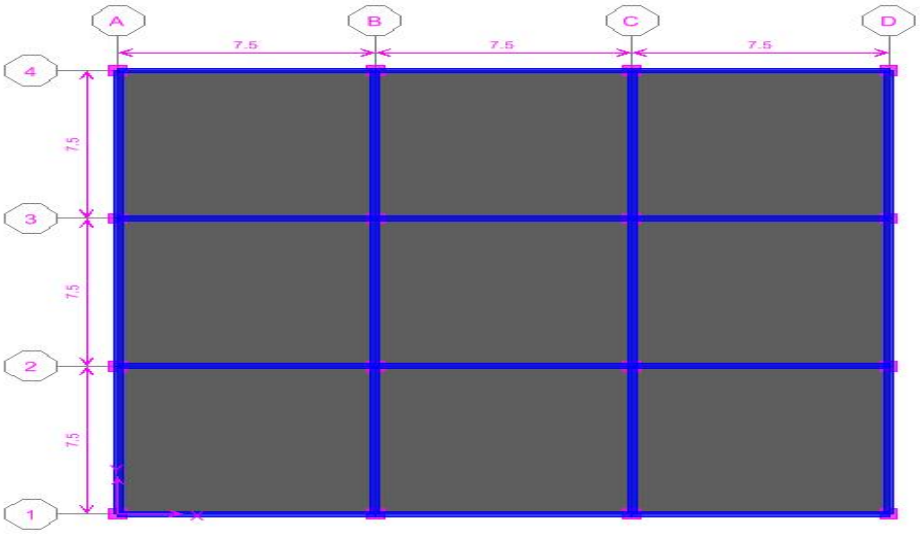

Figure 1: Plan of a typical storey

Table 1: Analysis parameter - seismic load analysis

Parameter	**BNBC 1993**	**BNBC 2017**
Seismic Zone Coefficient – Z	0.15	0.28
Site Classification	S3	SD
Site Coefficient – S	1.5	1.35
Importance Factor – I	1	1
Time Period – *T*	$T=C_t h_n^m$, $C_t=0.035$	$T=C_t h_n^m$
Reduction Factor – R	R=8	R=6
ETABS Analysis Algorithm	UBC 94	User Coefficient

Table 2: Analysis parameter – wind load analysis

Parameter	**BNBC 1993**	**BNBC 2017**
Analysis Method	Surface Area Method	Analytical Procedure
Basic Wind Speed – VS	Fastest mile speed: 210 km/hr	3 sec Gust wind: 232km/hr
Exposure Category	A (Urban area)	A (Urban area)
Standard Occupancy Structure IF	1	1
Max Deflection Limit	h/500 for 100% wind effect	h/500 for 70% wind effect
Other factors	Combined height and exposure coefficient Cz	Topographical Factor Kzt -1.00 Directionality Factor Kd - 0.85 Velocity exposure coefficient Kz
ETABS Analysis Algorithm	UBC 94	ASCE 7-05

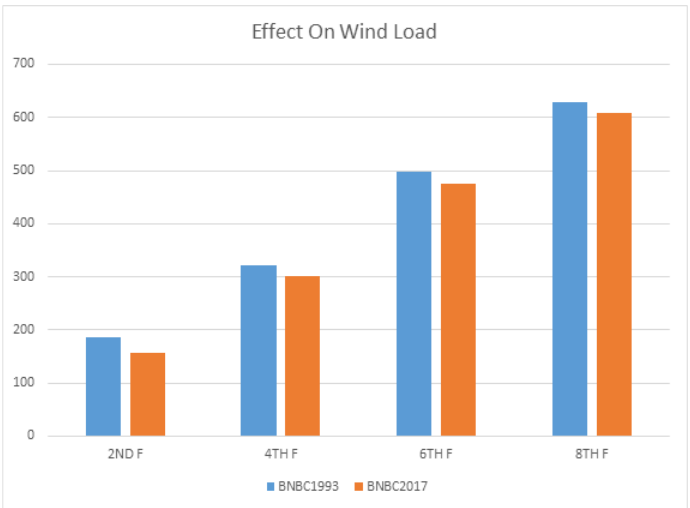

Figure 2: Wind load vs. No. of Story

To ease to understand how much storey shears are varying for two different codes the shear forces are represented together as diagrams below:

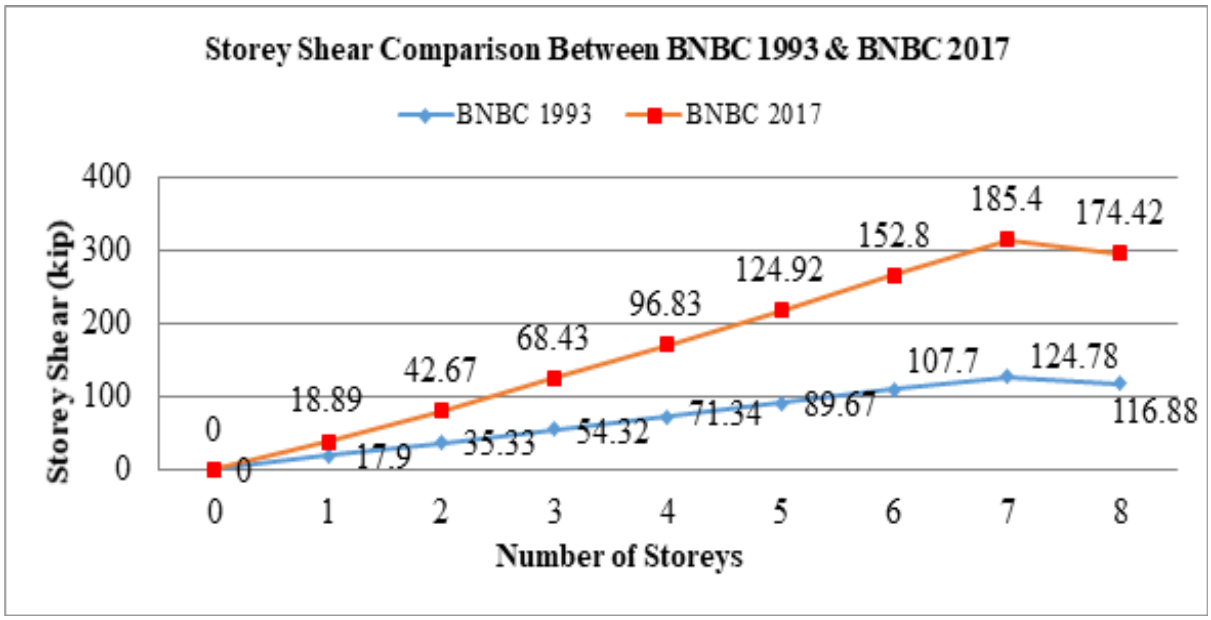

Figure 3: Storey shears comparison between BNBC 1993 and BNBC 2017

To understand how much base shears are varying for two different codes the base shears are represented together as bar charts below:

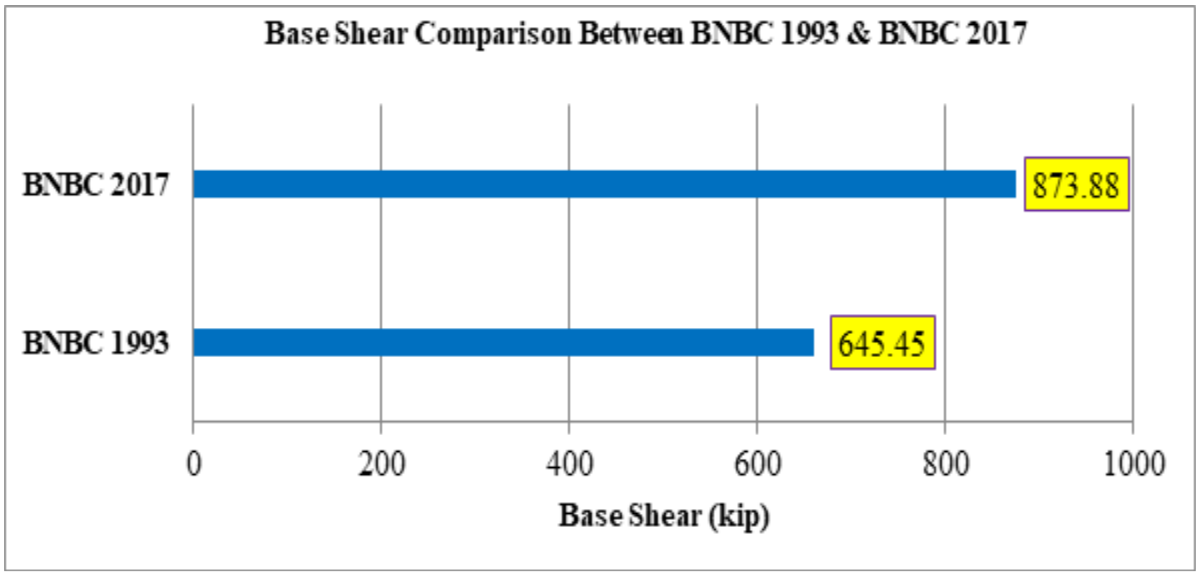

Figure 4: Base shears comparison between BNBC 1993 and BNBC 2017

3.1 Storey Displacement and Drift Analysis

The drift analysis is done for every floor to see the gradual displacement of the floors. To make it easier to understand how much inter storey drifts and storey displacements are varying for both codes some figures are given below:

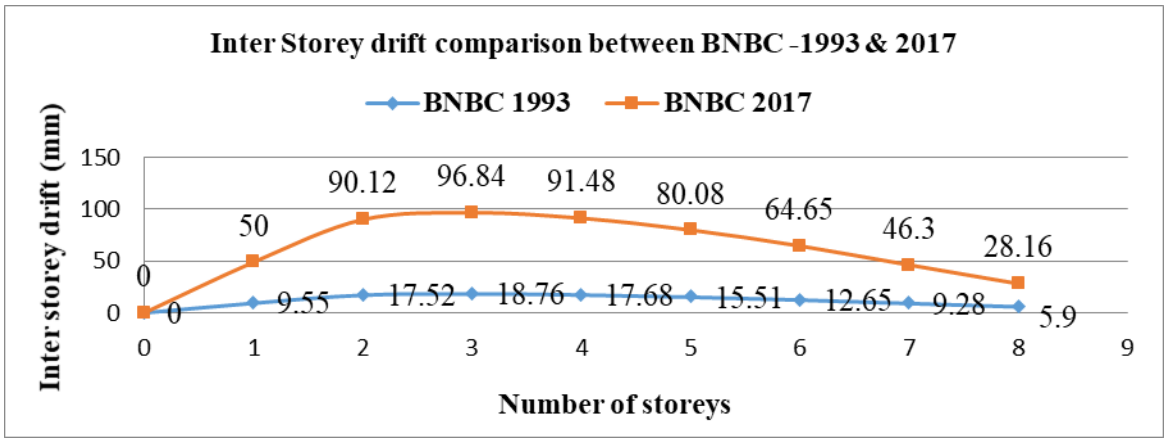

Figure 5: Comparison of inter storey drifts (mm) according to BNBC-1993 and BNBC-2017

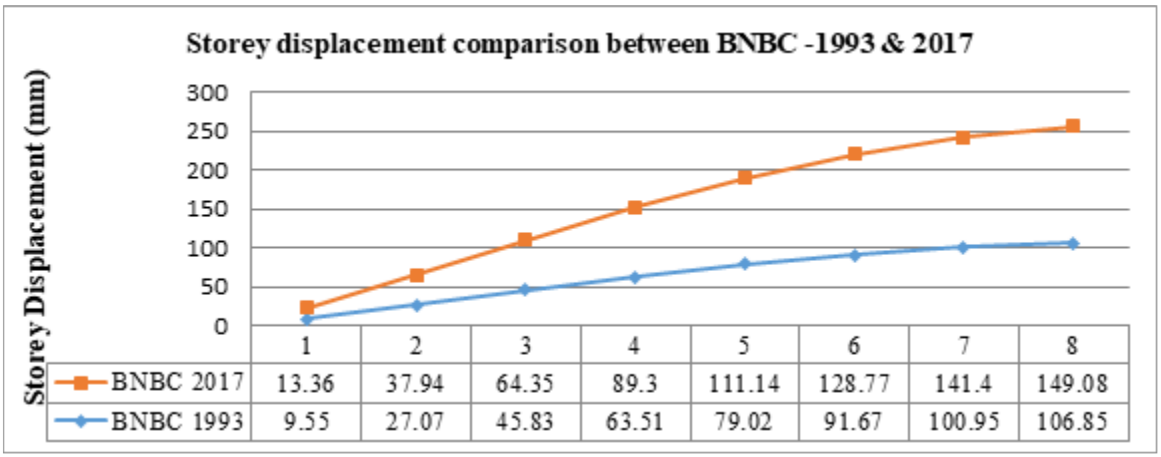

Figure 6: Comparison of storey displacement (mm) according to BNBC-1993 and BNBC-2017

3.2 Corner and an Interior Column Analysis and Design

For analysing and design purpose a corner column and an interior column have been selected for both BNBC-1993 and 2017 so that we can make a clear comparison of column dimensions and number of bar requirements as well as bar diameters. Here are the tables showing differences of findings of columns forces and steel area (in^2).

Table 3: Column forces in kip according to BNBC-1993 and BNBC-2017

BNBC-1993		**BNBC-2017**	
Corner column force (kip)	**Interior column force (kip)**	**Corner column force (kip)**	**Interior column force (kip)**
554.45	1639	380.33	1317.45

Table 4: Column dimensions (in x in) according to BNBC-1993 and BNBC-2017

BNBC-1993		**BNBC-2017**	
Corner column size (in x in)	**Interior column size (in x in)**	**Corner column size (in x in)**	**Interior column size (in x in)**
18x18	30x30	15x15	30x24
		Steel area required (in^2)	
3.27	9.3	2.19	7.18

Table 5: Required bar diameter (mm) for columns according to BNBC-1993 and BNBC-2017

BNBC-1993		**BNBC-2017**	
Corner column	**Interior column**	**Corner column**	**Interior column**
8-20mmΦ	16-22mmΦ	6-20mmΦ	12-22mmΦ

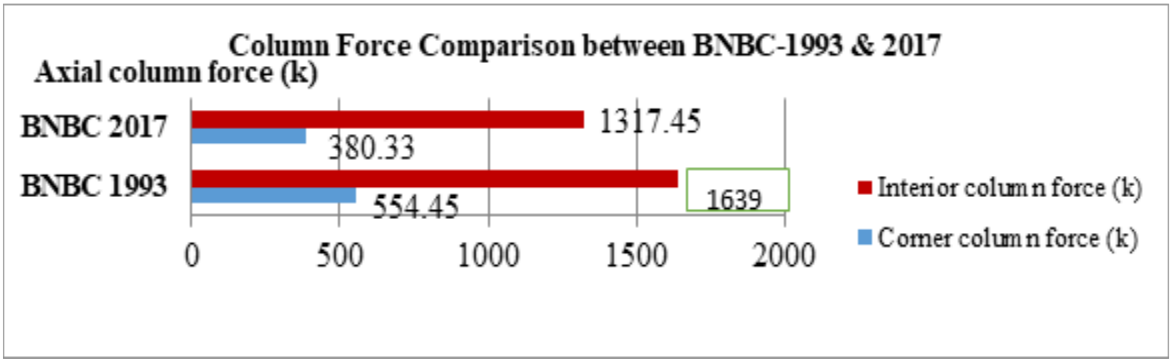

Figure 7: Comparison of column forces (kip) according to BNBC-1993 and BNBC-2017

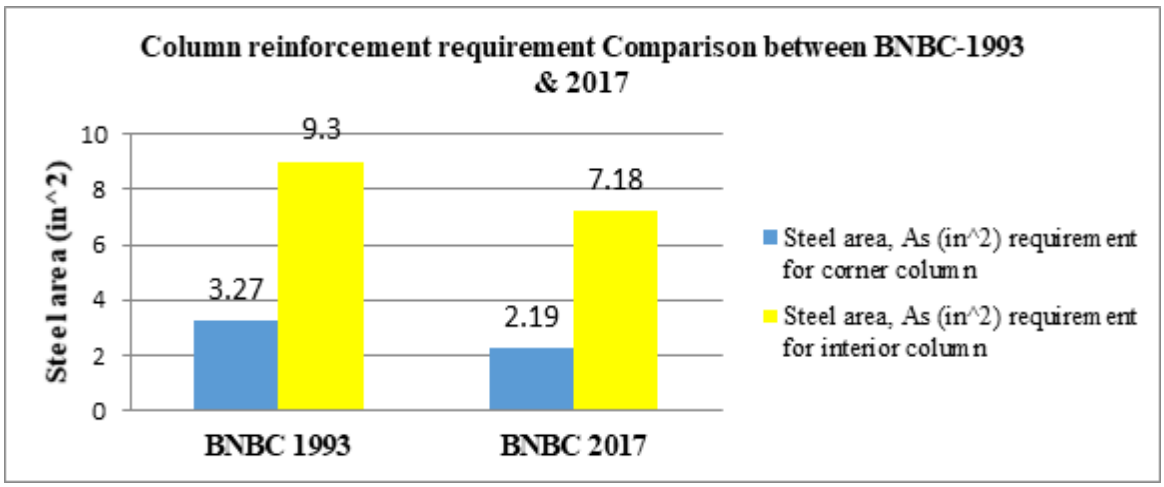

Figure 8: Comparison of steel area (in^2) requirement for a corner and an interior column according to BNBC-1993 and BNBC-2017

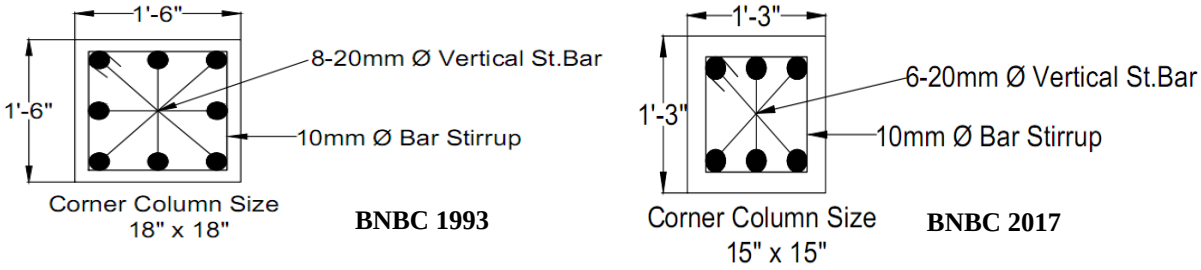

Figure 9: Comparison of column area (in^2) and bar diameter (mm) for corner columns according to BNBC-1993 and BNBC-2017

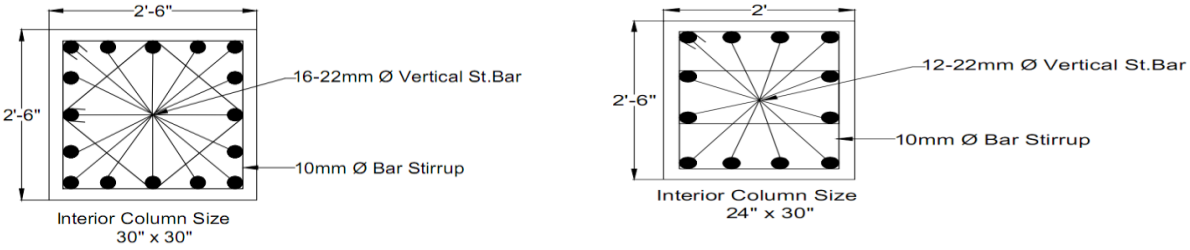

Figure 10: Comparison of column area (in^2) and bar diameter (mm) for interior columns according to BNBC-1993 (Left) and BNBC-2017 (Right)

4. CONCLUSION

Base shear is increased in BNBC-2017 than BNBC-1993 due to increase in zone coefficient (z), structural system factor(R) and self-weight (W). The design basis earthquake is not properly defined in BNBC-1993. The design basis earthquake is 0.67 times of the maximum earthquake in BNBC-2017. In BNBC-1993 load factor 1.4(0.75*1.7*1.1) is used with earthquake load. It means the earthquake load is increased 40% because of the uncertainty of load. This factor is not quite needed because the maximum earthquake is taken for design. It is seen that base shear and storey shear are much higher for BNBC-2017 than BNBC-1993 from base shear versus no. of storey graph and storey shear versus no. of storey graph. Maximum lateral drift is also found to be higher for BNBC-2017 than BNBC-1993. Design of reinforced concrete buildings for seismic and wind load in BNBC-2017 is economic than BNBC-1993. As the quantity of reinforcement required is less in BNBC-2017 which is applicable for Dhaka city only.

5. RECOMMENDATIONS

The following recommendations can be made for future research work:

- The case study performed in this research is for Dhaka city only. For different parts of Bangladesh, the seismic zone coefficient varies.
- In BNBC-1993 load factor 1.4(0.75*1.7*1.1) is used with earthquake load. It means the earthquake load is increased 40% due to the uncertainty of load and that's why the column forces are more in BNBC 1993 compared to BNBC 2017. However, this factor is not needed since the maximum credible earthquake is considered for design in BNBC-2017.
- In this study only column axial forces were taken during analysis. So it is recommended to consider column moments too for future research study.s
- For other types of buildings such as steel frames, ordinary moment resisting frames and masonry structures etc. located in different places with different site condition, similar study can be performed.

REFERENCES

BNBC 1993 & 2017, ―Bangladesh National Building Code (BNBC), Bangladesh House Building Research Institute, Dhaka.

Manual for Seismic Design of Reinforced Concrete Building- PWD, Bangladesh.

Eqball, M. S., 2011, ―A comparison of Proposed BNBC-2012 with Other Building Codes Regarding Seismic Provisions", B. Sc. Engr. Thesis, Dept. of Civil Engr. BUET, Dhaka.

Hasan, M. R. and Hoque, M. T., 2007, ― Comparative Studies of Different Building Codes In Context of Bangladesh National Building Code.

Al-hussaini, T.M., Hossain T.R., Al-Noman MN (2012). Proposed changes to the geotechnical earthquake engineering provisions of the Bangladesh National Building Code, Geotechnical Engineering Journal of the SEAGS & AGSSEA, Vol.43, No.2.

Proceedings of the 5th International Conference on Civil Engineering for Sustainable Development (ICCESD 2020), 7~9 February 2020, KUET, Khulna, Bangladesh (ISBN-978-984-34-8764-3)

EFFECTS OF RICE HUSK IN CLAY BLOCKS

Shegufta Zahan*[1], Sanzida Akter[2] and Raquib Ahsan[3]

[1]Postgraduate student, Department of Civil Engineering, Bangladesh University of Engineering and Technology, Dhaka, Bangladesh, e-mail: shegufta174@gmail.com
[2]Postgraduate Student, Department of Civil Engineering, Bangladesh University of Engineering and Technology, Dhaka, Bangladesh, e-mail: asanzida25@gmail.com
[3]Professor, Department of Civil Engineering, Bangladesh University of Engineering and Technology, Dhaka, Bangladesh, e-mail: raquibahsan@gmail.com

***Corresponding Author**

ABSTRACT

Rice Husk Ash (RHA) is one of the agricultural waste byproducts available widely in the world and contains large amount of silica. This study aims to produce light weight block aggregate with sufficient strength utilizing RHA at low cost. In Bangladesh, stones cannot be used as coarse aggregate in infrastructure work as stones are not available here. They are imported from abroad. For this reason, brick aggregates are cheaper and more widely used in Bangladesh than stone aggregates. Clay is the raw material for producing brick aggregate. Rice husk ash can be utilized to produce better quality block aggregates with lower cost replacing clay content in the bricks. In this study six different types of RHA from different mills are characterized through XRD & SEM. The result of XRD confirmed the amorphous state of rice husk ash. Fineness test of RHA is also conducted and the result shows that the highest fineness of 2720 cm^2 /gm was obtained for "RHA 3" sample which was uniformly burnt. At the same time characterization of clay was also conducted. The results of the tests conducted for determination of clay property assured the clay sample as "silty clay" with specific gravity of 2.59 and 14% optimum moisture content. The unconfined compressive strength was found to be 28MPa. Blocks were produced with six different types of rice husk ash with different composition by volume with clay. Then the mixture was manually compacted in mould and then subjected to dry in oven at 120°C for 7 days. After that dried blocks were placed in furnace at 1200°C to produce ultimate blocks. Loss on ignition test, apparent density, crushing strength test, efflorescence test and absorption test were conducted.

With addition of RHA in blocks cold crushing strength first decrease with increasing percentage of RHA and then increase in 40% RHA then again decrease. The sample having 40% rice husk ash from "RHA 3" shows maximum crushing strength of 60 MPa while the highest strength was obtained for 100% clay was 48.1 MPa. Moreover, absorption and firing shrinkage of blocks are also minimum at 40% RHA combination. RHA can be used to reduce volume and weight of clay in blocks up to 40% as found for the samples tested in the present study.

Keywords: *Rice husk ash, Pozzolanic material, Cementitious, Furnace, Finest particles.*

1. INTRODUCTION

Various researches are trying to replace clay from bricks as its use is decreasing the top soil from the earth. Rice milling industry generates a lot of rice husk during milling of paddy which comes from the fields. This rice husk is mostly used as a fuel in the boilers for processing of paddy. RHA is a carbon neutral green product. Lots of ways are being thought of for disposing them by making commercial use of this RHA. RHA is a good super-pozzolan. This super-pozzolan can be used in a big way to make brick aggregates. Pozzolan increases the mechanical strength of the aggregates. That is why in this study we tried to mix RHA with pure clay to see the difference.

Most of the husk from the rice milling industry is either burnt or dumped as waste in open fields and a small amount is used as fuel for boilers, electricity generation, etc. (RHA market study, 2003). Paddy on an average consists of 72% of rice, 5 - 8% of bran, and 20 - 22% of husk, on weight basis (Ou et al., 2007; Basha et al., 2005; Bouzoubaa and Fournier, 2001; Prasad et al., 2000). This husk contains about 75 - 80 % organic volatile matter and the balance 20 - 25 % of the weight of this husk is converted into ash during the firing process, is known as rice husk ash (RHA). This husk is used as fuel in the rice mills to generate steam for the parboiling process. This RHA usually contains around 85% - 97% amorphous silica with small amount of alkalis and other trace elements (Ou et al., 2007; Basha et al., 2005; Bui et al., 2005; Asavapisit and Ruengrit, 2005; Adylov et al., 2003; Bouzoubaa and Fournier, 2001; Saha et al., 2001; Prasad et al., 2000; Natio, 1999). This silica is highly porous and light weight, with exceedingly external surface area. Rice husk ash (RHA) is a term describing all types of ash produce from burning rice husks which vary considerably according to burning techniques. The silica in the ash undergoes structural transformations depends on conditions (time and temperature) of combustion.

Bangladesh is the fourth highest paddy rice producing country all over the world and rice husk is abundantly produced. Recently RHA has attracted more attention to the researchers as an additive of cement. During growth, rice plants absorb silica from the soil and accumulate it into their structures. The accumulated silica concentrated by burning at high temperatures in RHA, which makes the ash valuable. The chemical composition of rice husk is found to vary from sample to sample due to the differences in the type of paddy, crop year, climate and geographical conditions (Chandrasekhar et al., 2003).

Rice husk is the outer covering of paddy and accounts for 20% – 25% of its weight. It is removed during rice milling and is used mainly as fuel for heating in homes and rice milling industries in Bangladesh. Its heating value of 13 – 15 MJ/kg (Natarajan et al., 1998; Jenkins, 1989) is lower than most woody biomass fuels. However, it is extensively used in rural Bangladesh because of its widespread availability and relatively low cost. In the major rice-producing countries, much of the husk produced from the processing of rice is either burnt or dumped as waste (Chindaprasirt et al., 2009; Mathur, 2006; Chindaprasirt and Rukzon, 2006). The RHA is usually producing through controlled and uncontrolled combustion process. Uncontrolled combustion process is used in most of the cases in Bangladesh. The characteristic of RHA depends on the combustion process and variation of temperature. The fine particulate matter which is carried away from the combustion zone by the flue gas produces fly ash. The ash produced with stoker and suspension fired boilers is closed to 100% amorphous.

The proportion of bottom ash to fly ash depends upon the boiler type and operating conditions. Critical economic and environmental situations of the current days encourage companies and researchers to develop and improve technologies intended to reduce or minimize industrial wastes. As a consequence, much effort has been expended in different areas, including the agricultural production. In recent years, studies have been carried out by different researchers using wastes generated from the agricultural and industrial activities as concrete-making materials. Wastes such as rice husk, sawdust, cork granules and coconut pitch have been used as filler or aggregate for concrete

(Ramaswamy et al., 1983; RCTT, 1979; Paramasivam and Loke, 1978; Cook et al., 1977; Mehta, 1977).

2. METHODOLOGY

Processing of raw materials included selecting the suitable types of raw materials to be used for preparing the specimens, primary processing of these materials to make them suitable for next operation and determining chemical compositions. The raw materials used in this experiment were: normal clay, rice husk ash and water.

2.1 Material Preparation

The clay used here was normal clay, collected from Azimpur where excavation was done for construction of foundation. The lumps of the clay were crushed to make fine particles and then normally dried for several days to remove the inherent moisture so that it cannot vary the moisture amount used for making specimen. The clay particles were sieved to avoid any unwanted foreign particles like stones, large aggregates or other substances and to get homogeneous fine clay. On the other hand, Rice Husk Ash was collected from 6 different mills and then blended for 5 minutes in a blender; then passed through no.100 sieve.

2.2 Clay and RHA Characteristics Determination

Moisture absorption test, Fineness Test, XRD and SEM test were done to characterize the rice husks from different mills.

Field identification, Specific gravity test, Atterberg limit test, Optimum moisture content test, Unconfined Compression test were done to characterize the clay.

2.3 Specimen Preparation

Clay and ash were taken by volume percentage shown in Table 3.1 of total brick volume

Table 1: Different proportion of clay and RHA

Clay content (volume%)	Rice husk ash (volume%)
80	20
70	30
60	40
50	50
40	60

For the mixing process, clay and RHA were taken in a bowl. With 20% moisture of total volume, proper hand mixing was done. For different percentages of RHA, repeatedly the process was done. Water was added to provide sufficient bonding so that they can hold together during molding. A total of 93 cube specimens were prepared using mould size of 2in x 2in x 2in. Thus, 90 cube specimens were prepared for volume fraction of RHA and the other 3 was clay specimen. Then the specimens were dried in oven for 7 days to remove excess moisture and then it was fired in an oven at 1200°C for 6 hours.

2.4 Test Program

The test program of cube specimens involved compressive strength test, loss on ignition test, apparent density test, water absorption test and efflorescence test of the blocks incorporating RHA with clay for different percentages.

3. RESULTS AND DISCUSSION

The comparison of RHA samples produced from different mills are discussed and a viable method has been suggested to manufacture good quality Rice Husk Ash in controlled conditions in rural areas of Bangladesh.

3.1 Characteristics of RHA

Result of moisture absorption test of 6 types of RHA is shown below in Figure 4.1 where we can see that RHA 4; which is a mixing of RHA and nutshell absorbs more moisture from the atmosphere than all other RHA types.

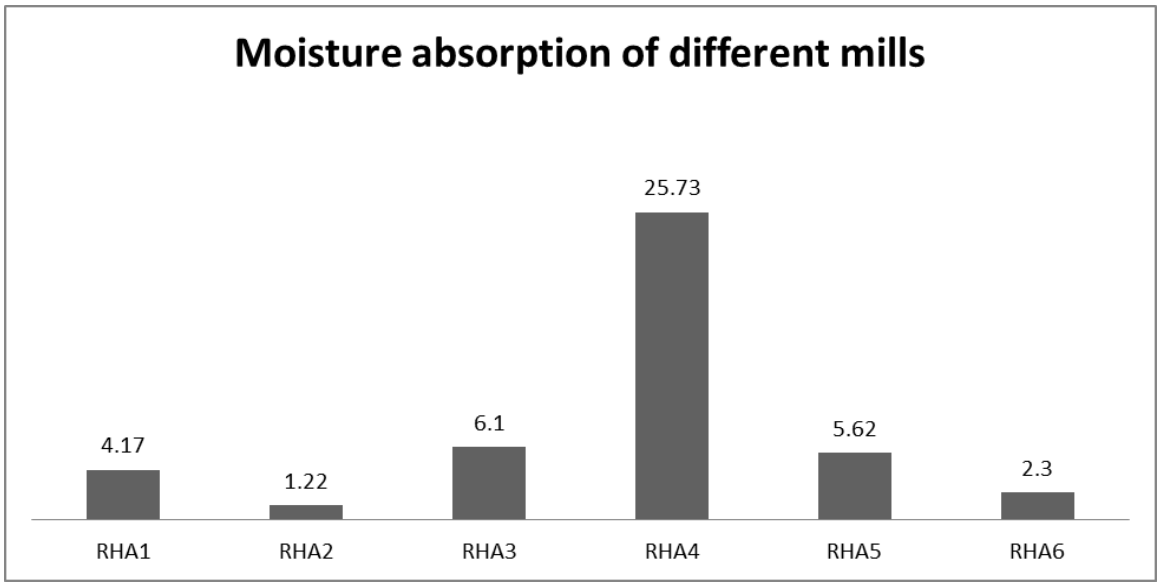

Figure 1: Moisture absorption of different mills

The result of fineness is given below in Table 4.1 where RHA 3 shows better fineness than others. The more the fineness of the RHA, the more contact area of the particles will contribute to the strength of the blocks.

Table 2: Fineness of RHA from different mills

Sl. No.	Types of RHA	Blaine fineness (cm^2/gm)
1	RHA 1	1150
2	RHA 2	1685
3	RHA 3	2720
4	RHA 4	1755
5	RHA 5	1673
6	RHA 6	1937

From the XRD and SEM tests, it was observed that the RHA were on amorphous states. Figure 2 shows the XRD results for RHA 3 that is the finest among others. In case of all samples of rice husk ash, no sharp peak was observed in XRD analysis indicates that the ash is non-crystalline form. A rather broad peak spanning 2θ angle range of 18-30° which is characteristic of amorphous structures is observed.

On the other hand, the particle size and texture of RHA were analyzed with SEM (Scanning Electron Microscope) and the observation is shown in Figure 3 that represents the result for RHA 3. It is clear from 300- and 3000-times magnification that the shape of the ash particle is angular in texture. The porosity and the formation of the binder can be seen by using SEM analysis. The formation of the pore and binder can be analysed corresponding to the various applications of the manufactured aggregate.

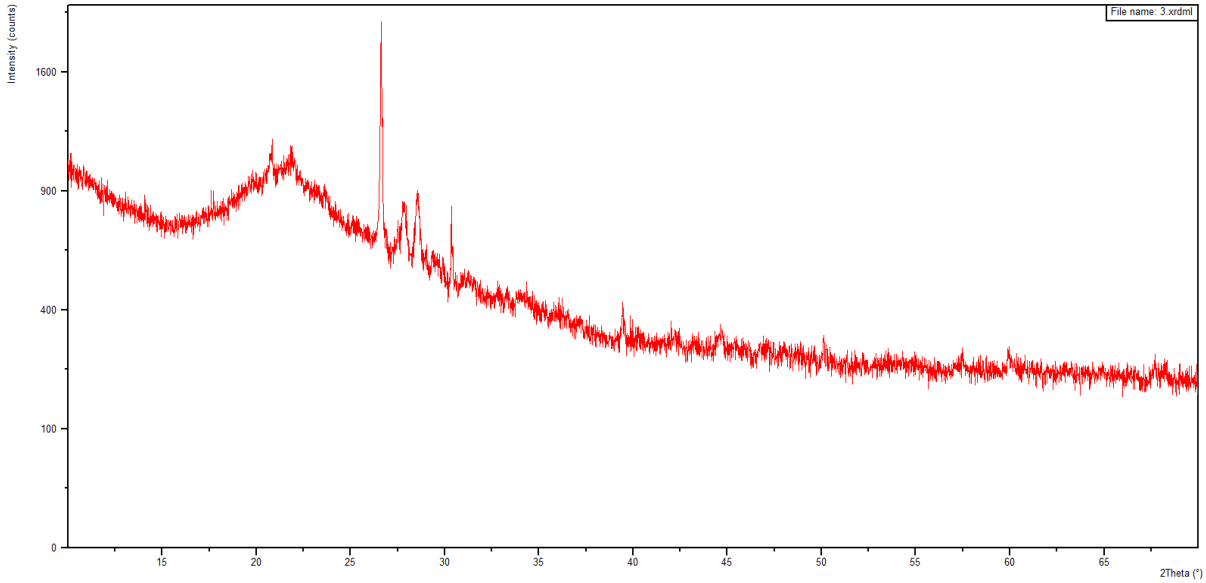

Figure 2: XRD result of RHA 3

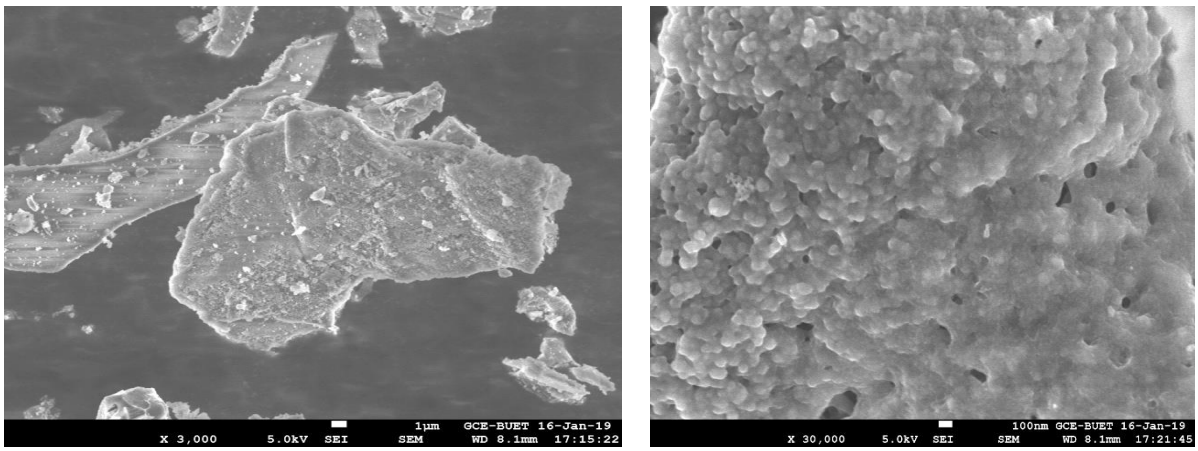

Figure 3: SEM image of RHA 3

3.2 Characterization of Clay

From the field identification test it was observed that the clay sample type was ‘silty clay’. And specific gravity was 2.59, also maximum relative density was 2gm/cm3 at 14% moisture content. At 15% strain compressive strength of the soil sample is 28 MPa.

3.3 Effects of RHA on blocks

The result of loss on ignition test in given below in Figure 4, where the straight line represents the loss on ignition of 100% clay blocks. It is observed that at 40% RHA, the loss is less for most of the RHA types except RHA 4.

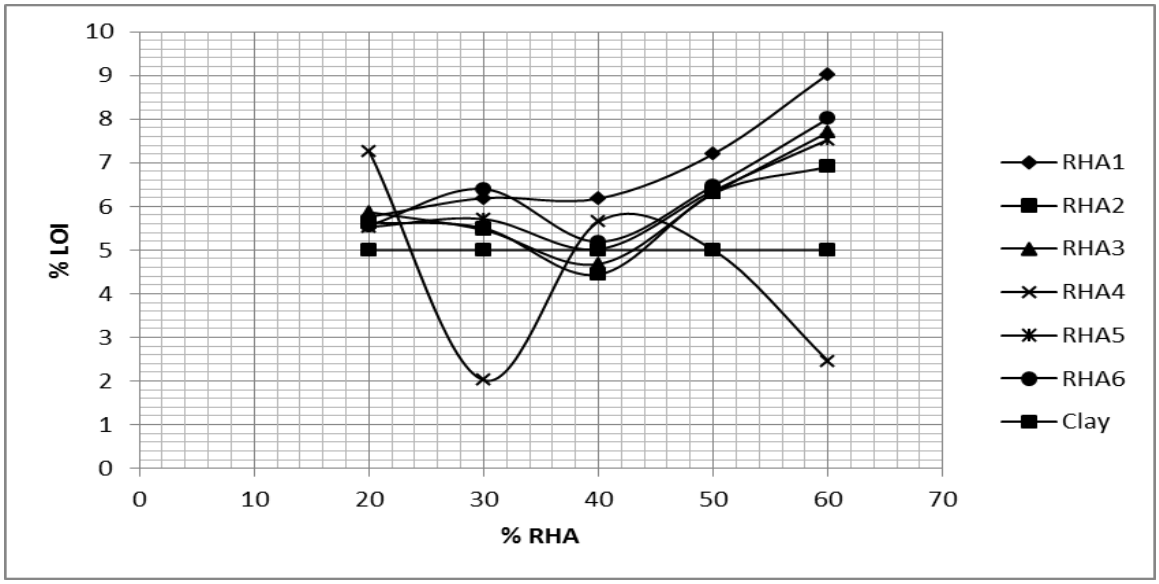

Figure 4: Loss on ignition for different percentages of RHA for RHA from different mills

The apparent density for different percentages of RHA is given below for RHA 3 as it is the finest in Figure 5 which again indicates lowest density at 40% of RHA.

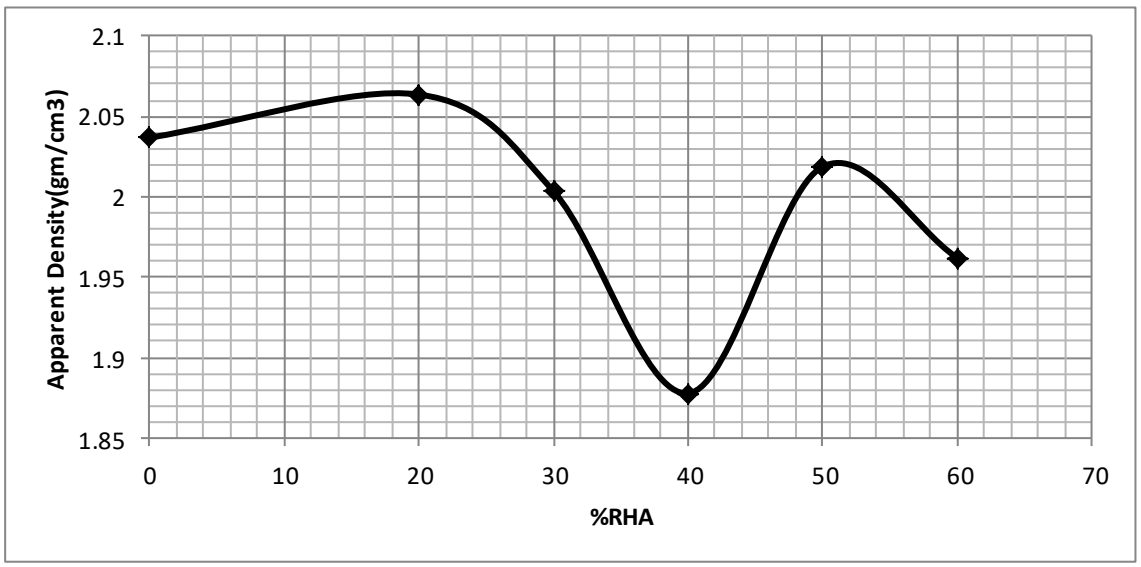

Figure 5: Apparent density of RHA3 for different percentages of RHA

The result of absorption test is given below in Figure 6. This figure denotes that absorption is less for 40-50% for most of the RHA. It was also seen from previous figure that the density is less for 40%. That means at 40% RHA, the blocks not only become light weighted but also become more compacted.

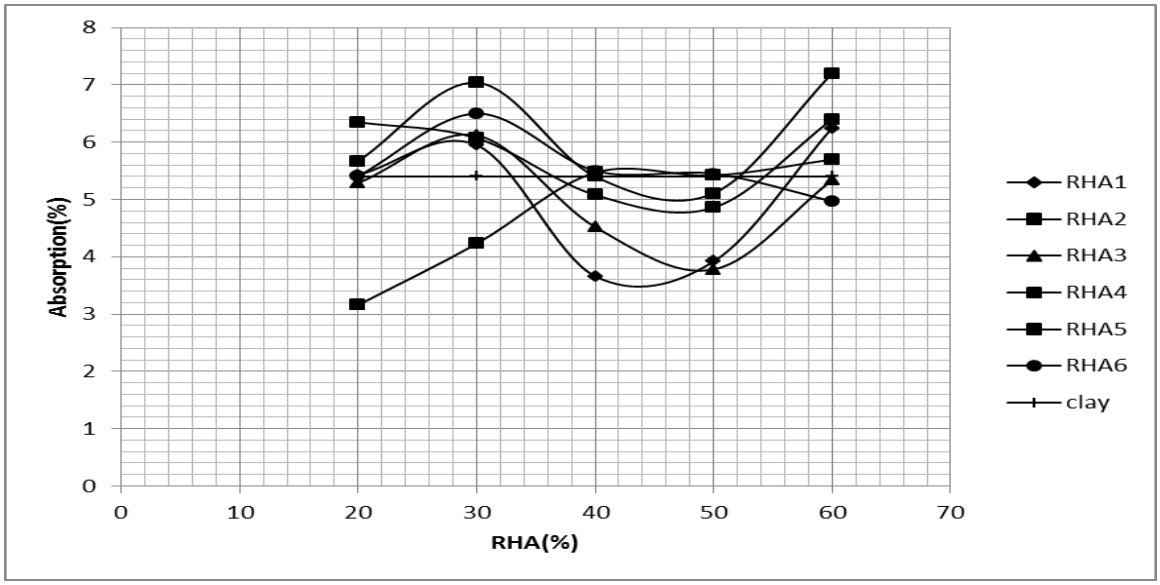

Figure 6: Absorption of blocks incorporating different percentages of RHA from different mills

The result of compressive strength test is given below in Figure 7. This figure also indicates that for 40% of RHA the compressive strength of the blocks incorporating finer RHA is higher than the blocks containing 100% clay.

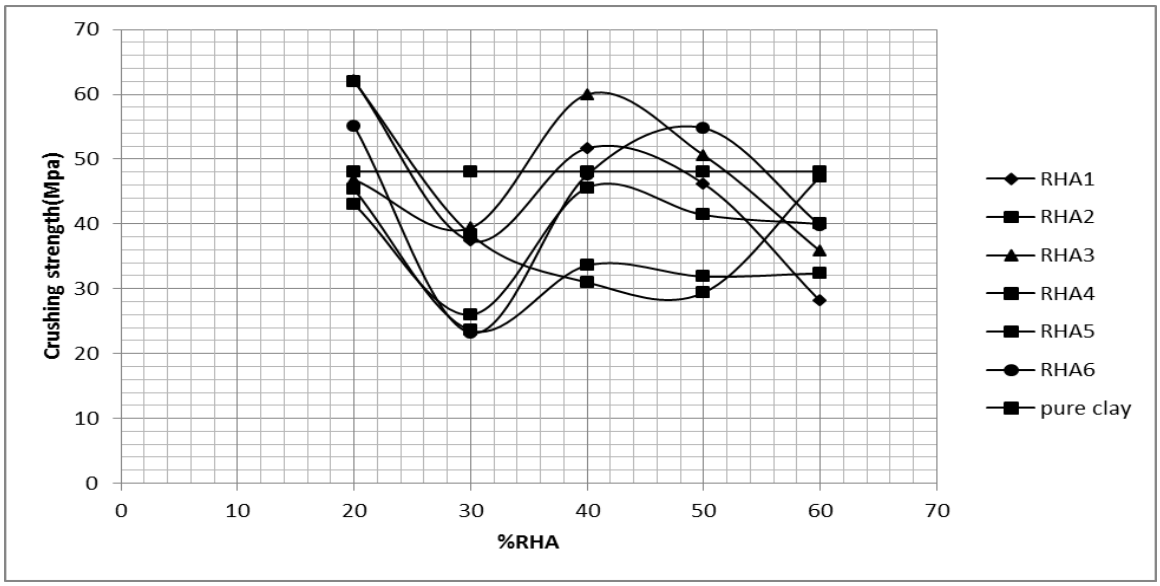

Figure 7: Compressive strength of blocks incorporating different percentages of RHA from different mills

Efflorescence test of the blocks were done by putting the blocks in a bowl of water for 7 days and the results were observed. The efflorescence effects on the blocks incorporating RHA was negligible.

4. CONCLUSIONS

The experiments were conducted for the development of blocks incorporating rice husk ash in this study. To fulfill the requirement of the objectives the experiments were conducted and subsequent results are presented. On the basis of the extensive experimental observations and discussions the following conclusions are drawn.

i) RHA performance increases if it is uniformly burnt from the mill and if the fineness is greater than 2500 cm^2/gm; in this experiment RHA 3 showed these properties properly.

ii) Crushing strength is first lowered with increasing percentage of RHA and then suddenly increases in 40% RHA, then again decreases.

iii) The crushing strength is higher than clay up to 40 % RHA combination for the finer RHA. So 40% volume of clay brick can be replaced by RHA.

iv) The absorption rate for 40% RHA is lower than other combinations; even pure clay.

v) Efflorescence effect is not excessively observable.

vi) L.O.I is also lowest for 40% RHA except RHA 4.

vii) The combination of RHA and clay only performs better than the combination of RHA, nutshell and clay.

viii) Apparent density decreases at 40 % that indicates light weight of the brick aggregates.

ACKNOWLEDGEMENT

The authors express and acknowledge a deep gratitude to Dr. Raquib Ahsan, Professor, Department of Civil Engineering, BUET for his continuous support to carry out the thesis. The authors are grateful to the Department of Civil Engineering, BUET, Department of Glass and Ceramic Engineering, BUET and the Department of Materials and Metallurgical Engineering, BUET for providing the facilities that were invaluable.

REFERENCES

Adylov G, Faiziev SH, Paizullakuhanon M, Mukhsimov S and Nodirmatov E, (2003). Silicon Carbide materials obtained from rice husk. Tech. Phys. Lett. 29(3): 221- 223

Asavapisit S and Ruengrit N, (2005). The role of RHA blended cement in stabilizing metal containing wastes. Cem Concr Compos 27: 782-787.

Basha EA, Hashim R, Mahmud HB and Muntohar AS, (2005). Stabilization of residual soil with RHA & cement. Constr. Build. Mater. 19: 448-453.

Bouzoubaa N and Fournier B, (2001). Concrete incorporating rice husk ash: Compressive strength and chloride ion penetrability. Mat Tech Lab, Report MTL 2001-5(TR), CANMET, Department of Natural resources, Canada: 1-16.

Bui DD, Hu J and Stroeven P, (2005). Particle size effect on the strength of rice husk ash blended gap-graded Portland cement concrete. Cement & Concrete Composites 27: 357-366.

Chandrasekhar S, Pramada SKG and Raghavan PN, (2003). Review Processing, properties And Applications of Reactive Silica from Rice Husk-An Overview. Journal of Materials Science, 38: 3159-3168

Chindaprasirt P and Rukzon S, (2006). Strength, Porosity and Corrosion Resistance of Ternary Blend Portland Cement, Rice Husk Ash and Fly Ash Mortar. Constr. Build. Mater., 22: 1601-1606.

Chindaprasirt P, Jaturapitakkul C and Rattanasak U, (2009). Influence of Fineness of Rice Husk Ash and Additives on the Properties of Lightweight Aggregate. Fuel, 88: 158-162.

Cook DJ, Pama PP and Paul RK, (1977). Rice husk ash-lime cement mixes for use in masonry unit. Building and Environment, 12: 282-288.

Mathur VK, (2006). Composite Materials from Local Resources. Constr. Build. Mater., 20; 470-477.

Mehta PK and Pitt N, (1977). A new process of rice husk utilization. International conference on the utilization of rice by-products, Valencia: IATA: 45-58.

Naito N, (1999). Low-cost technology for controlling soybean insect pests in Indonesia. Association for International Cooperation of Agriculture and Forestry, Japan.

Natarajan E, Nordin A and Rao AN, (1998). Overview of combustion and gasification of rice husk in fluidized bed reactors. Biomass Bioenergy, 14: 533

Ou E, Xi Y and Corotis R, (2007). The Effect of Rice Husk Ash on Mechanical Properties of Concrete Under High Temperatures, 18th Engineering Mechanics Division Conference (EMD2007).

Paramasivam P and Loke YO, (1978). Study of Sawdust Concrete. Proc. Int. Conf. on Materials of Constr.for Developing Countries, Bangkok, Thailand, 169-179.

Prasad CS, Maiti KN, Venugopal R,(2000). Effect of RHA in white ware composition. Ceram Int 27: 629-635.

Ramaswamy SD, Murthy CK and Nagaraj TS, (1983). Use of waste materials and industrial by-products in concrete construction. In: R.N. Swamy (Ed.), Concrete Technology and Design, Vol. 1: New Concrete Materials. Surrey University Press, London, UK, 137-172.

Regional Centre for Technology Transfer (RCTT) (1979). Rice husk ash cement. United Nations Industrial Development Organization /ESCAP/RCTT, India.

Rice Husk Ash Market Study (2003). Confidential Report, 1.29 http://www.dti.gov.UK/renewables/Publication/pdfs/ exp129.pdf

Saha JC, Diksit K and Bandyopadhyay M, (2001). Comparative studies for selection of technologies for arsenic removal from drinking water. In: BUET-UNU international workshop on technologies for arsenic removal from drinking water, Bangladesh.

Proceedings of the 5th International Conference on Civil Engineering for Sustainable Development (ICCESD 2020), 7~9 February 2020, KUET, Khulna, Bangladesh (ISBN-978-984-34-8764-3)

MECHANICAL BEHAVIOR OF CONCRETE INCORPORATING RECYCLED PLASTIC BOTTLE FIBERS

MD. Rashedul Haque*[1], MD. Shakil Mostafa[2] and Sujit Kumar Sah[3]

[1]Assistant Professor, Department of Civil Engineering, Hajee Mohammad Danesh Science and Technology University , Bangladesh, e-mail: rashed.civil@hstu.ac.bd
[2]Undergraduate Student, Department of Civil Engineering, Hajee Mohammad Danesh Science and Technology University, Bangladesh, e-mail: shakilmimo@gmail.com
[3]Undergraduate Student, Department of Civil Engineering, Hajee Mohammad Danesh Science and Technology University, Bangladesh, e-mail: sahsujit.ss64@gmail.com

***Corresponding Author**

ABSTRACT

Concrete is a common and most widely used construction material in the world. Due to the rapid growth of concrete construction by excessive usage of natural aggregates resulted in the search for alternative source of concrete aggregate. The environmental pollution from non-biodegradable products is causing a serious problem to human lives and plastc type product is one of them. The objective of the study is to investigate the influence of two different types of recycled plastic bottle fibers on compressive strength of concrete. And mechanical properties such as ductility, toughness, cracking are also observed in this study. It is well konwon that Polyethylene Terephthalate (PET) is usually used for carbonated beverage and water bottles and fibers from these recycled bottles are used in this investigation. In this study, two types of fiber are used: straight and zigzag fiber. Fibers with lengths of 40 mm, aspect ratio of 40 and volume fractions of 0 and 0.75%, replacing the volume of coarse aggregate are used in straight fiber made concrete and zigzag fiber made concrete respectively. Design mixing ratio 1:2:3 for M20 concrete and water-cement ratio 0.58 are used in this study. Curing is done in field condition and weathering action is allowed in curing time. The experimental results show that crushing strength of plain concrete, straight and zigzag fiber made concrete are 19.84 MPa, 19.54 and 18.49 MPa respectively in case of destructive test at 28 days. The compressive strength of plain concrete, straight and zigzag fiber made concrete are 13.58 MPa, 10.36 and 8.21 MPa respectively in case of non-destructive test at 28 days. Use of fibers changes failure mode of concrete and splitting portion from straight fiber made concrete is more than zigzag fiber made concrete in failure mode. Addition of fibers decreases workability of concrete and shows toughness, cracking, ductility properties. Use of zigzag pattern fibers shows interlocking property just like deformed rebars which are used for reinforcing the concrete.

Keywords: *Recycled plastic bottle fiber, Straight plastic fiber, Zigzag plastic fiber, PET fiber, Failure mode.*

1. INTRODUCTION

Due to rapid growth of industrialization & urbanization around the world, lots of infrastructure developments are taking place and environmental pollution is occurring due to use of non-biodegradable products. Polyethylene Terephthalate, known commonly as PET or PETE is best known as the clear plastic used for water, soda bottle containers and for domestic purpose etc. As a raw material, PET is globally recognized as a safe, non-toxic, strong, lightweight, flexible material that is 100% recyclable. Plastic is a non-biodegradable product which is harmful for our environment. Plastic does not decompose in over 500 years. Bangladesh imports plastic raw materials worth Tk 2,000 crore and every day Bangladesh generates around 1,700 tonnes of plastic waste but only half of the plastic waste is recycled and annually around 3 lakh tonnes of plastic waste is dumped in the open areas (Ayan, 2018). So, plastics should be disposed properly to save our environment. Ismail & Al-Hashmi (2008) insured that reusing waste plastic as a sand-substitution aggregate in concrete gives a good approach to reduce the cost of materials and solve some of the solid waste problems posed by plastics.

It is well known that concrete is strong in compression and has high brittle property. But concrete is weak ductility and toughness. With addition of fibers and allowing little variation in compressive strength from plain concrete, these disadvantages can be overcome. It is also known that deformed rebar is used for reinforcing the concrete because deformed rebar gives interlocking property and gives a good bonding between rebar and concrete. In this study, straight fibers where no deformed shape is given and deformed shape zigzag pattern type fibers are used with concrete to study the mechanical properties of concrete reinforcing with recycled plastic fibers.

2. METHODOLOGY

Extensive laboratory testing has been carried out to evaluate the properties of coarse aggregate, fine aggregate, cement and plastic. There are 3 cases have been considered in the present study to understand the effect of plastic fiber on the compressive strength of concrete. Plain concrete (control case) which is 0% fiber by volume of coarse aggregate and concrete made with straight and zigzag plastic fiber respectively by 0.75% volume of coarse aggregate, are the total 3 cases are being considered to understand the effect of recycled plastic bottle fiber replacement on the compressive strength of concrete. Other mechanical behavior: toughness, cracking resistance and ductility are also observed. Volume of recycled plastic fibers is multiplied by its density to get the weight of fibers in grams and then it was replaced with the amount of coarse aggregate. According to ACI 211.1-91, design mix 1:2:3 of M20 concrete is determined. Water cement ratio (w/c) = 0.58 is used. All cases of specimen have been tested at the age of 28 days curing under weathering action to understand the effect of the compressive strength of both plain and recycled plastic fiber made concrete.

2.1 Materials

Portland composite cement (PCC), locally available fine sand and crushed stones were used for casting concrete specimens. Recycled plastic bottles were collected for making plastic fibers.

2.1.1 Coarse Aggregate

Crushed stones were used as coarse aggregate. Maximum size of aggregate was 20mm and gradation of coarse aggregate was done confirming to ASTM C33. Specific gravity, unit weight and absorption capacity were found 2.584, 1539.362kg/m^3 and 0.838% respectively.

2.1.2 Fine Aggregate

Locally available sand was used as fine aggregate. Specific gravity, unit weight, absorption capacity and fineness modulus were 2.136, 1602.373kg/m^3, 6.383% and 2.756 respectively. Gradation of fine aggregate was done confirming to ASTM C33.

2.1.3 Binder

The binding material was Portland composite cement (PCC) which contains 65%-79% clinker, 0-5% gypsum, slag, fly ash, limestone 21%-35%. Specific gravity, initial setting time, final setting time and normal consistency were found 3.15, 125min, 210min and 28.5% respectively.

2.1.4 Recycled Plastic Fibers

Fibers having length 40mm, width 4mm, thickness 0.2mm and equivalent diameter 1mm were used both for straight and zigzag fibers. Aspect ratio (L/D) was 40. Unit weight of fiber was 1370kg/m^3. Plastic bottle cutter and zigzag pattern making device were used to give the fibers proper shape. Equivalent diameter of plastic fiber was determined by equation (1).

$$T \times B = (\pi/4) \times D^2 \quad (1)$$

Where, L = Length of fiber
T = Thickness of fiber
B = Width of fiber
D = Equivalent diameter of fiber
And figure 1 shows two types of fiber.

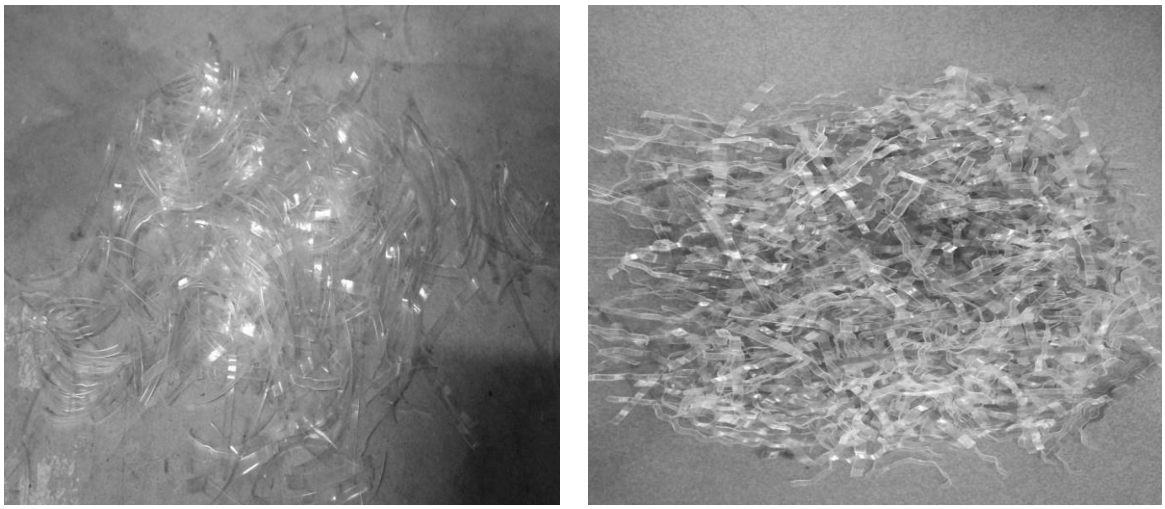

(a) (b)

Figure 1: (a) Straight plastic fibers (b) Zigzag plastic fibers

2.2 Concrete Mix Design

The mix was designed as per ACI 211.1-91 for M20 grade concrete with 0.58 water-cement ratio. Concrete mixes were prepared by 0% and 0.75% volume replacement of coarse aggregate with straight and zigzag fibers respectively. The percentage of volume of coarse aggregate was taken and it was multiplied with unit weight of fiber and thus weight of fibers was taken. Then weight of coarse aggregate was replaced by weight of fibers. Table 1 shows mixing proportion of concrete.

Table 1: Mix proportion for each m^3 of concrete

S.N.	% of CA replacement	Cement(kg)	Sand(kg)	Stone(kg)	Water(kg)	Fiber(kg)
1	0% PF	360	801.19	1154.52	145	-
2	0.75% ST PF	360	801.19	1146.81	145	7.71
3	0.75% ZZ PF	360	801.19	1146.81	145	7.71

PF = Plastic fiber, ST = Straight and ZZ = Zigzag, CA= Coarse Aggregate

2.3 Test Specimens and Test Procedures

For compressive strength test, cylindrical specimens of 4in diameter and 8in height were used. Total six sets of specimens were casted, three sets for destructive test and other three sets for non-destructive test. Three specimens were used for each set and average value of compressive strength was used. Compressive strength for each specimen was determined by destructive and non-destructive Rebound Hammer test according to ASTM C39 and ASTM C805 respectively. Workability measurement was done according to ASTM C143.

3. RESULTS & DISCUSSIONS

3.1 Results of Fresh Concrete Properties

There are many properties of fresh concrete. In this study, only workability measurement is done. From table 2, it can be seen that the addition of fibers decreases workability. Reduction of workability of concrete made with zigzag fibers is a little bit more than concrete made with straight fibers.

Table 2: Slump test

% of CA replacement	Slump value in inch		
	Plain concrete	Concrete with straight fiber	Concrete with zigzag fiber
0	5	-	-
0.75	-	4.6	3.8

3.2 Results of Hardened Concrete Properties

In this study, compressive strength test (DT) and Rebound Hammer test (NDT) are performed. From table 3 & 4, it can be said that addition of fibers decreases compressive strength of concrete because of poor bonding between plastic fibers and cement-sand paste. Compressive strength of concrete obtained by non-destructive Rebound Hammer test shows lower values than that of destructive test. Due to exposure of curing to environment, weathering actions such as rain, sunlight variation, change in temperature, growth of organic content affect hydration process of concrete and strength gaining process of concrete.

Table 3: Destructive compression test

% of CA replacement	Crushing Strength in MPa		
	Plain concrete	Concrete with straight fiber	Concrete with zigzag fiber
0	19.84	-	-
0.75	-	19.54	18.49

It is well known that a concrete with low strength and low stiffness will absorb more energy to yield in a lower rebound value. Results from table 4 obtained by Rebound Hammer test, it can be said that addition of fibers helps concrte to absorp energy that means concrete will show toughness property. So, allowing a little variation in crushing strength of concrete from plain concrete, both straight and zigzag plastic fibers can be used.

Table 4: Rebound Hammer test

% of CA replacement	Crushing Strength in MPa		
	Plain concrete	Concrete with straight fiber	Concrete with zigzag fiber
0	13.58	-	-
0.75	-	10.36	8.21

3.3 Failure Surface of Concrete

The presence of fibers changes the mode of failure. Shear fracture occurs in plain concrete. Axial split occurs in concrete made with straight and zigzag fibers respectively. From figure 2, it can be said that concrete with fibers shows some ductility property but plan concrete shows brittle property. Splitting portion from concrete made with straight fibers is more than concrete made with zigzag fibers. Zigzag fibers in concrete hold some concrete portion during concrete failure and thus it provides interlocking property with concrete.

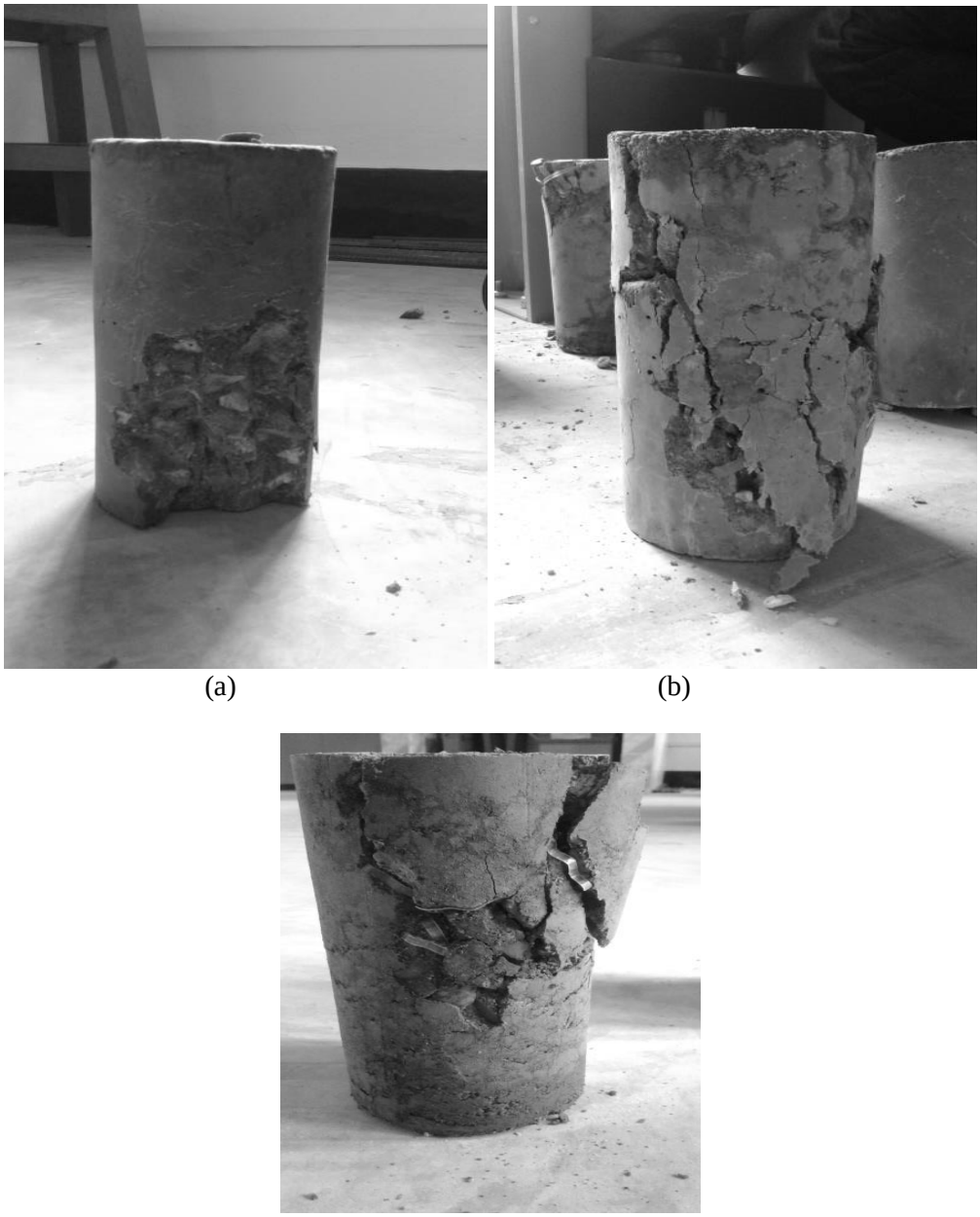

(a) (b)

(c)

Figure 2: (a) Plain concrete (b) Concrete with straight fibers (c) Concrete with zigzag fibers

4. CONCLUSIONS

Based on the results and discussions, following conclusions are drawn

i. Overflow of water, variation of sunlight, growth of organic content is found, as curing is exposed to environment and these factors affect hydration process and strength gaining process of concrete.

ii. The workability of concrete decreases by using plastic fibers.
iii. The presence of plastic fibers changes the mode of failure.
iv. Addition of fibers decreases brittle property of concrete but increases ductility and toughness of concrete.
v. Low amount of plastic fibers should be used in concrete so that variation in compressive strength becomes negligible.
vi. Deformation of fibers in zigzag pattern provides interlocking property with concrete.
vii. Compressive strengths of concrete made with straight and zigzag fibers at 0% and 0.75% replacement with coarse aggregate by volume are 19.84MPa, 19.54MPa, 18.49MPa in case of destructive test and 13.58MPa, 10.36MPa, 8.21Mpa in case of non-destructive test.

ACKNOWLEDGEMENTS

The authors would like to express their deepest gratitude to all concerned persons of the Department of Civil Engineering, Hajee Mohammad Danesh Science and Technology University for their valuable information and constructive suggestions. Acknowledgements are very due for Dr. Ismail Saifullah, Associate Professor, Department of Civil Engineering, Khulna University of Engineering & Technology, for his coordination and valuable suggestions about this research.

REFERENCES

ASTM, C. (2018). Standard Test Method for Compressive Strength of Cylindrical Concrete Specimens. *ASTM C39/C39M-18*.

ASTM, C. (2018). Standard Test Method for Rebound Number of Hardened Concrete. *ASTM C805/C805M-18*.

ASTM, C. (2015). Standard Test Method for Slump of Hydraulic-Cement Concrete. *ASTM C143/C143M-15a*.

ASTM C33, A. (2004). Standard Specification for Concrete Aggregates. *American Society for Testing and Material*, 1-11.

Ayan, A. (2018, July 20). Turning plastic wastes to resources. *The Daily Star*. Retrieved from https://www.thedailystar.net/environment/turning-plastic-wastes-resources-curbing-pollution-profitably-1608376

Committe, A. C. I. 211.1-91., Reapproved 2002. *Standard Practice for Selecting Proportions for Normal, Heavyweight, and Mass Concrete*, 1-24.

Ismail, Z. Z., & Al-Hashmi, E. A. (2008). Use of waste plastic in concrete mixture as aggregate replacement. *Waste management*, *28*(11), 2041-2047.

Proceedings of the 5th International Conference on Civil Engineering for Sustainable Development (ICCESD 2020), 7~9 February 2020, KUET, Khulna, Bangladesh (ISBN-978-984-34-8764-3)

BEHAVIOR OF MORTAR INCORPORATE WITH FLY ASH AND STONE DUST CURING IN SALINE WATER

Iffat Haq *[1] and Nur- E - Jannat Pollen[2]

[1]Graduate student, Khulna University of Engineering & Technology, Bangladesh, e-mail: iffat.haq.kuet@gmail.com
[2]Graduate student, Khulna University of Engineering & Technology, Bangladesh, e-mail: pollen.kuet@gmail.com

***Corresponding Author**

ABSTRACT

Construction activities are increasing day by day in different regions and utilities are causing scarcity of natural resources which is being forced due to its over exploitation. Depletion of natural resources boosting up the threat to the environment. Since construction activities cannot be stopped, conservation of natural resources has become one of the greatest challenges for engineers. Finding alternative materials which can be fully or partially replaced by naturally available materials in construction can be effective approach in this regard. Mortar is a mixture of sand, water and cement which is used widely in construction industry due to good performance in plastering and bedding work.In one hand, stone dust is such an alternative material which can be effectively being used in construction as partial replacement of natural sand. On the other hand, use of fly ash and stone dust will decrease the land fill of waste disposal. However, a portion of the world's carbon dioxide emission is attributed to cement industry, which is the vital constituent of mortar so replacement of cement will also be beneficial for environment. Construction officials in coastal areas have long been facing the challenge of building and maintaining durable structures in a salty environment. Gradual penetration of sea salts and the subsequent formation of expansive and leachable compounds lead to disintegration of structure. The successful performance of a coastal structure depends to a great extend on its durability against the aggressive coastal environment. Disintegration of structures in saline environments is mostly caused by chemical deterioration such as sulfate attack, chloride attack and leaching. Physical deterioration from crystallization of soluble hydrated salts in pores of the surface erosion and abrasion promotes further disintegration. The overall results of these attacks on stuctures are softening, cracking and partial removal of cover mortar. This in turn exposes a fresh surface for further attack. Also in order to save fresh drinking water, saline was used for curing to obseve the applicability of salty water of coastal areas. Experimental investigation was performed in this study to describe the change in compressive strength and water absorption of mortar cubes in salty exposures. Mortar cubes were casted varying the quantity of fly ash and stone dust for the replacement of cement and sand. From this experiment optimum use of fly ash and stone dust can be suggested where fly ash is 10-20% of cement with 100% stone dust in mortar paste for saline environment. More than 30% replacement of cement with fly ash is not recommended for drastic reduction of compressive strength.

Keywords: *Fly ash, Stone dust, Saline environment, Land fill, Carbon dioxide.*

1. INTRODUCTION

Mortar can be considered as workable paste which is used to build up bonding among the bricks, stones and gaps sometimes. For creating mortar, a mixture of cement and sand has to be made and mixed thoroughly in dry condition. Shovels can be used to mix the water. Then with the hydration cement will gain the strength gradually. Until the hydration has taken place, it is necessary to see that mortar is wet. After laying mortar, the process of ensuring sufficient moisture content for hydration is known as curing. Water is sprayed for curing. Curing is normally done within 6–24 hours after mortar is used. It may be noted that initial period for water requirement is more for hydration and gradually it reduces. Hydration of cement begins with the addition of water and it binds sand particles and also the surrounding surfaces of masonry and concrete. Well-proportioned is called when mortar provides impervious surface. As leaner mix is not capable of closing the voids in sand, the plastered surface is porous. The strength of mortar is affected by the proportion of cement and sand. In construction field we use mortar in various purposes. Mortar has been using for thousand years as a means of adhering bricks or concrete blocks with one another. Again, cement mortar continues to be used in various types of constructions as to plaster slab and walls which make them impervious, to provide neat finishing to walls and concrete works, masonry joints pointing, for making building blocks, as a filler material in ferro cement works, for filling joints and cracks in walls also, as a filler material in stone masonry. In thermal power plant fly ash is the produced. For the low heat hydration and higher workability, it is used in mortar or concrete. Surprisingly, there is only 14 percent of total production of fly ash was utilized each year, other than that was disposed in landfills (Kuan & Saleh, 2016). Use of fly ash should be increased for reducing landfill. Normally, sand is used as common fine aggregate in construction work. On the other hand, Stone powder from stone crushing zones appears as a problem for effective disposal (Mahzuz, Ahmed, & Yusuf, 2011). If sand can be replaced with stone dust it can be a part of solution of this problem. Again, only 2.5% of the world's water bodies are said to be of fresh water and the remaining constitute of contaminated water with salt or other substances. According to the report of the World Meteorological Organization, more than half of the world's population would not have enough drinking water by 2025 (Pravallika & Lakshmi, 2014). The total amount of salinity affected land in Bangladesh was 83.3 million hectares in 1973, which had been increased up to 102 million hectares in 2000 and the amount has risen to 105.6 million hectares in 2009 and continuing to increase, according to the country's Soil Resources Development Institute (SRDI). Salinity increased around 26 percent in the last 35 years, in this country, spreading into non-coastal areas as well (Haider, 2019). In coastal areas, saline water can be used for construction instead of fresh water and to do so an optimum percentage of fly ash with stone dust should be determined.

2. BACKGROUND OF THE STUDY

Mainly, there can be two sources of producing carbon dioxide emissions one is natural and other is human. In natural sources, decomposition, ocean release and respiration may be included. Where as in Human sources can be comprised from activities like cement production at industry and in application, deforestation as well as the burning of fossil fuels like coal, oil and natural gas (Main sources of carbon dioxide emissions, 2017). From the data of World Resources Institute (WRI), it is shown that in the last 200 years, humans have added 2.3 trillion tones of CO2 to the atmosphere. Out of this 2.3trillion tone of CO2 around half of this amount was added in the last 30 years alone. The most heat-trapping gases are present in the environment; there can be some other gases which include methane (CH4), nitrous dioxide (NO2), and several artificial gases (Hydro fluorocarbons (HFCs), Per fluorocarbons (PFCs); and Sulphur hexafluoride (SF6). These are the main 6 groups which are considered for under the Kyoto Protocol. In Construction and demolition also, debris constitutes a considerable portion of solid waste. Thus, reducing the carbon dioxide emission is gaining the instantaneous importance and there by Sustainable Construction has high priority in the recent construction era. Out of several cementing materials, fly ash is the most commonly used material worldwide. According to the American Concrete Institute (ACI) Committee, fly ash is defined as "the

finely divided residue that results from the combustion of ground or powdered coal and that is transported by flue gasses from the combustion zone to the particle removal system." Worldwide, the estimated annual production of coal ash in 1998 was more than 390 million tons (Rai, Kumar, & Satish, 2014). The main contributors of the coal ash were China and India. By the year 2010, about 780 million tons of fly ash produced worldwide annually. If fly ash is not utilized, may present environmental concerns, and its storage/disposal will be costly (Yerramala & Desai, 2012). The majority of fly ash is low calcium fly ash which is produced in India. The use of fly ash as admixture in cement mortar/concrete not only extends technical advantages to the properties of cement mortar/concrete but also contributes to the environmental pollution control (Rai, Kumar, & Satish, 2014). The storage of engineering materials (sand, stone) are limited so, day by day the dependency on them must be minimized. Hence, some other materials should be introduced for replacing sand. Stone dust is one of such alternatives of sand that can be used satisfactorily for the demand of fine aggregate. In Bangladesh, Jaflong is a tourist spot in the division of Sylhet. Stone collections and the location of the Khasi tribe make this place renowned which lies sixty kilometers to the northeast of sylhet. In the economy of a developing country like Bangladesh this tourism spot that can play a very significant role. Due to unplanned activities, the beauty of Jaflong is can be reduced day by day. Extraction of stone from river can affect the present condition of physical, chemical and biological process. In Jaflong there are a number of stone crushers, as a result of these huge labour oriented economic activities, a large number of low-income workers live in Jaflong and around (Haque & Ray, 2012). During the crushing of stones, a large amount of dust is created. They have been considered as a waste in the local areas. They are not given any importance and thrown here and there. While landfills are commonly used for disposal of stone dust in Bangladesh, rapid urbanization has made it increasingly difficult to find suitable landfill sites. Several attempts are seen in different researchers' activity to find out proper utilization and disposal of waste (Mahzuz, Ahmed, & Yusuf, 2011). When structure is exposed to the coastal area, the carbondioxide present in the salt water and surrounding atmosphere permeates into the structure carbonates it and reduce the alkainity (KV, SS, & J, 2010). Salinization is a highly complex process of intrusion into surface and ground water, seepage through thin geological structures into shallow pockets of freshwater coming towards abstraction wells in Bangladesh because of the surging motion of a lava lamp and salt water intrusion after floods caused by storm. While extraction of groundwater increases, salt from the groundwater can be sucked up from depth. In the coastal zone, absorption of saline water from tidal marshes and unprotected canals can increase the problem. Local conditions may have an effect on flushing out salt, it may take several years for fresh water to 'flush' salt out of groundwater reservoirs. Sometimes, the monsoons accelerate this flushing process so long as more saline surface water does not infiltrate Incorporation of fly ash as cement replacement improve the resistance of carbonation (McIntyre, 2014). Therefore, this study was to reduce the use of fresh water in curing and analyze the property of mortar with the fly ash and stone dust replacement in the coastal area.

3. OBJECTIVES

- To determine the effects of saline water for curing on mortar.
- To determine the best resistive percentage of fly ash against saline environment.
- To determine the effect of stone dust on mortar.

4. METHODOLOGY

In this study 5 types of specimens were casted varying the percentage of fly ash with alternation of sand and stone dust as Table 4.1 & cured with saline water for 7, 14 & 28 days. Variation in compressive strength, water absorption, & density was recorded.

Table4.1: Trial mix detailing

Trial Mix	(Cement +Fly Ash)	Sand/Stone Dust
M1	100% Cement	100% Sand
M2	90%C+10%Fly Ash	100% Stone Dust
M3	80%C+20% Fly Ash	100% Stone Dust
M4	70%C+30% Fly Ash	100% Stone Dust
M5	60%C+40% Fly Ash	100% Stone Dust

5. MATERIALS

5.1 Cement: Ordinary Portland cement was used for this test. To have a generalized idea about the Weight ratio of the Constituents of the ordinary Portland cement a pie chart is created according to the information from a website (Ordinary Portland Cement -Constituents, Properties, Types and Uses).

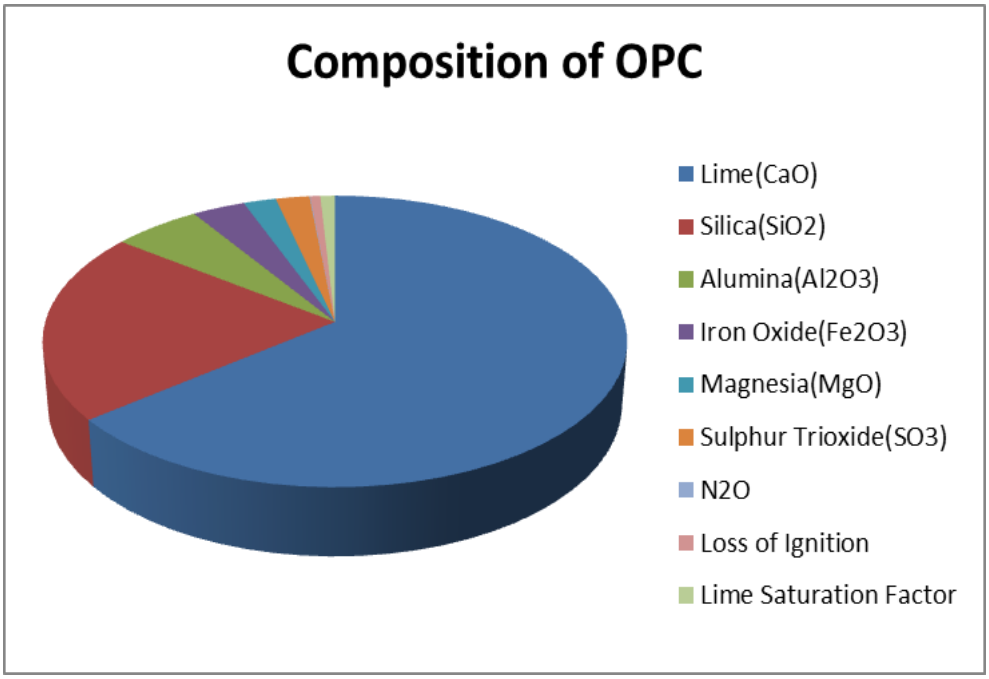

Fig. 5.1.1: Composition of OPC

5.2 Stone Dust: Stone dust was collected from Noapara, Jashore. Dust passing by No. 16 seive and retained by No.100 seive was used for casting for ensuring more uniformity among the particle and keeping the FM value (2.61) similar with the sand. Chemical composition of lime stone powder (Shuhua, Peiyu, & Jianwen) is shown below in the table5.2.1

Table 5.2.1: Chemical compositions of limestone powder/%

SiO_2	Al_2O_3	Fe_2O_3	CaO	MgO	TiO_2	SO_3	K_2O	Na_2O	L.I
2.50	0.60	0.36	54.03	0.54	0.05	0.01	0.10	0.08	41.59

5.3 Fly Ash: **Fly ash was collected from Noapara, Jashore.**

5.4 Saline: Sea water has about 35 grams of salt per litre of water, which is almost 60 times more than the 0.6 grams of salt per litre standard for the water in coastal areas of Bangladesh (McIntyre, 2014). In this study, concentration of salt in water was 13gm/L which means 1.3% where the concentration of chloride was 12,500mmg/L

Fig. 5.2.1: Stone Dust

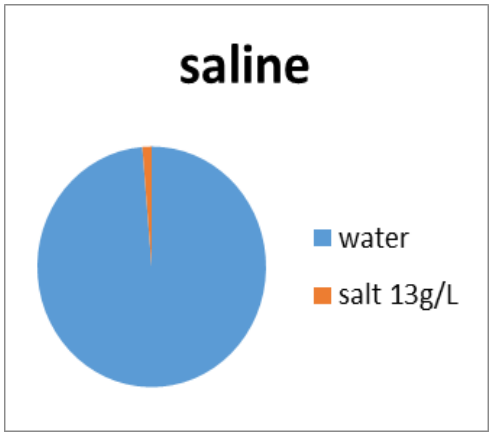

Fig. 5.4.1: Concentration of Salt

6. PROCEDURE

Compressive strength of mortar was determined by using 2 inch or 50.8mm cubes as per ASTM C109 / C109M – Standard Test Method for Compressive Strength of Hydraulic Cement Mortars. 5.08cm cubes moulds (25.8cm^2 face area), apparatus for gauging and mixing mortar, vibrator, compression testing machine etc. were used.

- Cement and sand were mixed in dry condition with a trowel for 1 minute.
- Then water was added and mixed with the sand and cement until the mixture is of uniform colour also took the weight of the empty mould (W3).
- Immediately after mixing the mortar, mortar was placed in the cube mould and prod with the help of the rod.
- The mortar was prodded 20 times in about 8 sec to ensure elimination of entrained air and took the weight of mould full of mortar (W4).
- After 24 hours cubes were removed from the mould and their weight were measured (W1) and kept for 72 hours in oven at 105^0 C then immediately submerged in a bowl full of saline water of given concentration till testing.
- When curing age reached, specimens were taken out, cleaned with absorbent paper and again took the measurement of weight (W2) and stored in oven with 100°C for 24 hours in order to dry it for crushing.
- The whole procedure was repeated for other specimens only the sand and cement were replaced according to mix detail table.
- For determining water absorption this theory:(W2-W1)*100/W1 was used.

- For determining density, the theory used was: (W4-W3) *100/Volume of mould.

7. RESULTS AND DISCUSSIONS

Compressive strength in different time periods are shown graphically also graphical comparison of water absorption and densities of all the trial mixes are given below consequently.

Fig-7.1 shows that compressive strength decreases with the increasing percentage of fly ash. This might be for slow hydration process since fly ash is slow reactive pozzolans which slow down the process (Kuan & Saleh, 2016). In one hand, addition of stone dust ameliorates this condition by showing the optimum reaction with optimum filler capacity (Rai, Kumar, & Satish, 2014). On the other hand, curing with saline water accelerate the hydration process (Khan, Izhar, Mumtaz, & Ahad, 2016) tough it makes the compressive strength a litle bit lower by forming leachable white compounds on the surface of the mortar. For M1 compressive strength of 7, 14 & 28 days were consequently 26.30, 28.30 & 32.40 N/mm^2. For M2 these were 14.50, 20.60 & 28.80 N/mm^2, for M3 the strength was 13.60, 18.26 & 28 N/mm^2, for M4 compressive strength were 9.10, 10.10 & 11.45 N/mm^2 and finally for M5 the compressive strength was 6.30,8.00 & 8.00 N/mm^2. From the result M2 and M3 gives quiet good strength after 30 days curing as according to ASTM C109M-13 & IS 2250 21.6 N/mm^2 is considered for strong mortar. On the other hand, compressive strength of M4 is too low comparing with M2 and M3 because of the increase in fly ash percentage. For the low compressive strength M4 will not be good for structural use especially in coastal areas & M5 is too weak (as according to ASTMC109M-13 6.9 N/mm^2 for mortar is considered as weak mortar) in compressive strength to use.

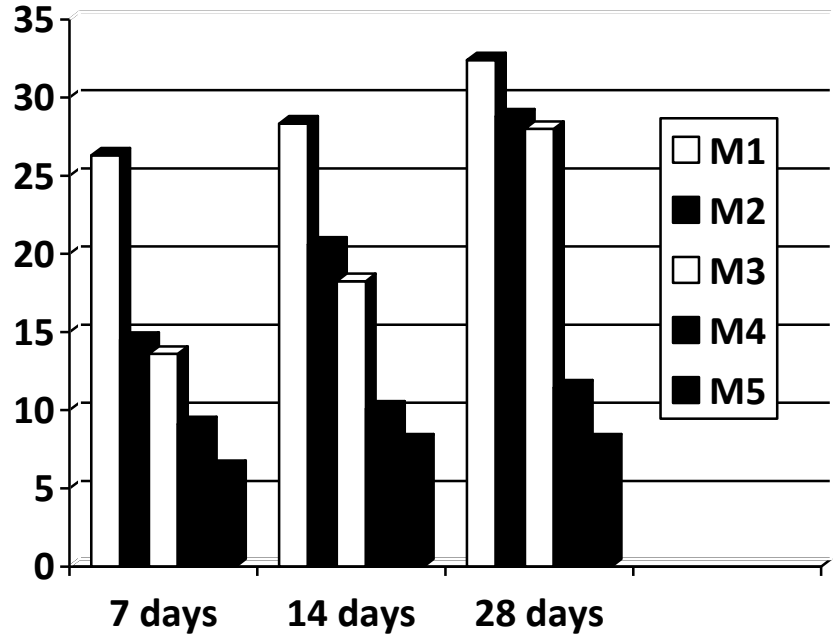

Fig. 7.1: Compressive strength in N/mm^2 over the time period.

Water absorption decreases with the increasing rate of fly ash showed in fig-7.2. Which means durability of mortar increases with the percentage of fly ash replacement.M1 has the highest water absorption rate where M5 shows the lowest. It can be explained as fly ash react with calcium hydroxide in cement to form calcium silicate hydrate (C-S-H). With increase of C-S-H, the interconnected pore structures of mortar are filled of it. Fly ash reduces the permeability (Kuan & Saleh, 2016).

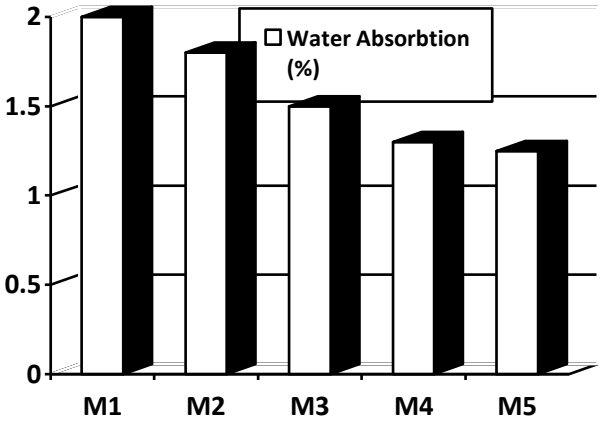

Fig. 7.2: Water absorption rate of trial mixes.

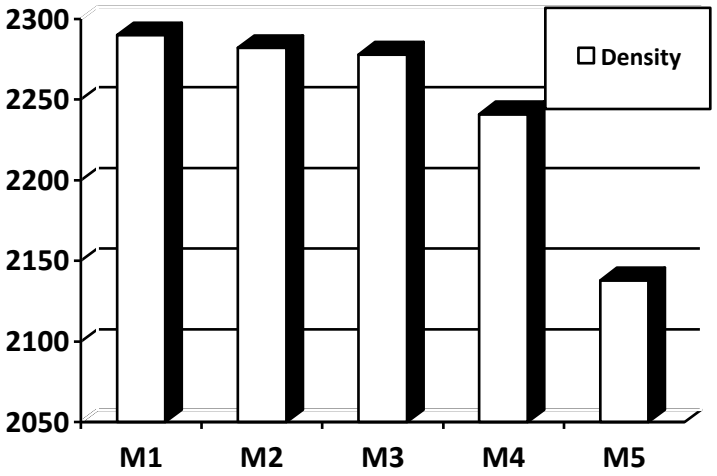

Fig. 7.3: variation densities of trial mixes.

As shown in fig-7.3 density is decreasing with the addition of fly ash which is very little for M1, M2 & M3 but M5 shows the lowest density. This may occur when the stone dust used is not pure or mixed with other substances and causes less cohesion among the particles sometimes can entrap air which create gap.

CONCLUSIONS

Effect of saline water on the specimens was noticeable. The grey colour was turning whitish grey because of salt composition on the surface of the specimen. This study indicates that among the all replaced specimens M2 shows the best performance with the compressive strength of 28.80 N/mm^2 and M5 shows the lowest compressive strength which is 8.00 N/mm^2 also M5 gives the lowest density. That means more than 30% of replacement of cement with fly ash will not be suitable to use. On the other hand, use of stone dust shows excellent performance by ameliorating the drastic reduction of compressive strength for fly ash. For coastal areas 10-20% replacement by fly ash is recommended with the use of stone dust.

ACKNOWLEDGMENTS

Special thanks to our honourable supervisor Dr. Kazi ABM Mohiuddin. Without his help and support this study was hard to do.

REFERENCES

Haider, R. (2019). *Climate Change-Induced Salinity Affecting Soil Across Coastal Bangladesh.* United News of Bangladesh.

Haque, M., & Ray, S. (2012). Use of Stone Powder with Sand in Concrete and Mortar: A. *ARPN Journal of Science and Technology*.

Kuan, F. K., & Saleh, S. (2016). EFFECT OF MORTAR INCORPORATE FLY ASH CURING WITH SEAWATER. *Journal of Innovative Research and Development*.

KV, B., SS, G., & J, T. (2010). Deterioration of concrete structures in coastal environment due to carbonation. *J Environ Sci Eng*.

Mahzuz, H., Ahmed, A., & Yusuf, M. (2011). Use of stone powder in concrete and mortar as an. *African Journal of Environmental Science and Technology Vol. 5(5), pp. 381-388,*.

McIntyre, P. (2014). *Water security.* IRC.

Pravallika, S., & Lakshmi, V. (2014). A STUDY ON FLY ASH CONCRETE IN MARINE ENVIRONMENT. *International Journal of Innovative Research in Science, Engineering and Technolog*.

Rai, B., Kumar, S., & Satish, K. (2014). Effect of Fly Ash on Mortar Mixes with Quarry Dust asFine Aggr. *Advances in Materials Science and Engineering*.

Shuhua, L., Peiyu, Y., & Jianwen, F. (n.d.). Effect of Limestone Powder and Fly Ash on Magnesium. *Journal of Wuhan University of Technology-Mater. Sci. Ed. Aug.2010,* 701.

Yerramala, A., & Desai, B. (2012). INFLUENCE OF FLY ASH REPLACEMENT ON STRENGTH PROPERTIES OF CEMENT MORTAR. *International Journal of Engineering Science and Technology*.

Main sources of carbon dioxide emissions. (2017, December 13). Retrieved from https://www.che-project.eu/news/main-sources-carbon-dioxide-emissions

Ordinary Portland Cement -Constituents, Properties, Types and Uses. (n.d.). Retrieved from The Constructor: https://theconstructor.org/concrete/ordinary-portland-cement/23181/

Proceedings of the 5th International Conference on Civil Engineering for Sustainable Development (ICCESD 2020), 7~9 February 2020, KUET, Khulna, Bangladesh (ISBN-978-984-34-8764-3)

THERMAL DEGRADATION OF ENAMEL PAINT COATING ON CEMENT PLASTER

Samiul Kaiser*[1] and M. S. Kaiser[2]

[1]Department of Civil Engineering, Bangladesh University of Engineering and Technology, Dhaka-1000, Bangladesh
[2]Directorate of Advisory, Extension and Research Services, Bangladesh University of Engineering and Technology, Dhaka-1000, Bangladesh

***Corresponding author**

ABSTRACT

The effect of temperature on the stability and visual color of enamel paint on cement plaster is evaluated through light intensity ratio of three primary colors (RGB). The painted cement plaster is isochronally heated in an electric resistance furnace at different temperatures for one hour. Up to 100°C the original color of the plaster samples remains more or less unchanged which are observed through optical image analysis. Again, thermal degradation of the samples becomes evident in color when they are heated beyond 200°C and at 350°C the color becomes already burned. The microstructural images of the samples at room temperature show fine and uniform grains. But at higher heating condition the microstructure of the sample is characterized by coarsening grain. The color of the heated samples are then studied through tristimulus color 'L*', 'a*' and 'b*' values which were analyzed and evaluated in MATLAB software. The results show that after 200°C the hunter 'L*' value starts to decrease greatly up to 250°C. The hunter 'a*' value shows an increasing trend up to 100°C and then begins to decrease until 200°C. After 200°C the same increasing character is showed till 300°C. The change of hunter 'b*' value remains insignificant up to 100°C and shows decreasing trend between 100°C-250°C range and an increase after 250°C up to 300°C. It is graphically shown that the proportion of all three colors decreases with the increasing temparature. The overall change of color occurs with increasing heating temperature due to moisture releasing, chemical changes and thermal degradation simulteneously.

Keywords: *Color, cement plaster, thermal degradation, tristimulus values, microstructure.*

1. INTRODUCTION

Enamel paint is a type of paint that air-dries to a hard, usually sheeny finish, used for coating surfaces that are outdoors or otherwise subject to hard wear or variations in temperature [1, 2]. For its availability, easy application, high durability and wide range of color variations enamel paint is frequently used on plasters, concrete, woods, metals etc. There are different types of enamel paint available to serve different purposes but generally 'Floor Enamel' paint is used in case of plaster, concrete, stairs, basements, porches, patios etc. Generally, dehydrated castor oil, titanium dioxide, colophony resin ester, anti-oxidants, zinc oxide, proprietary complex driers etc. are the main components of enamel paint [3, 4]. Usually enamel paints are applied with oil or water on the surface. A basic advantage of enamel paint is that it can dry quickly in exposed environment. The final output provides a lot smoother finish with little glossiness which depends on the oil content of paint. Though oil-based enamel paint takes a longer time to dry, it provides a long-lasting finish. Thus, enamel paint coating can last for many years. It is mildew-resistant and can be frequently washed if it gets stained. Moreover, the paint coating can resist the effect of high temperature on the material surface up to a certain temperature. At higher temperature certain physical changes on the coating can be noticed more specifically the change in colors of the material. The gradual changes of color can be identified using several parameters. The 'CIELAB' color space is one of them. It expresses color as three values. Those are '*L*',' a** 'and '*b** '. *L** indicates the lightness from black (0) to white (100). Similarly, *a** indicates changes from green (−) to red (+), and *b** indicates from blue (−) to yellow (+). CIELAB was designed so that the same amount of numerical change in these values corresponds to roughly the same amount of visually perceived change [5, 6].

In the present paper, the thermal degradation of enamel paint coating over cement plaster is examined using simple optical images and microstructures of the samples. The thermal degradation is analysed by detecting the change of color of the composite samples subjected to isochronal heating at temperatures ranging from 25°C (room temperature) to 350°C for a period of one hour. The potential of the method is then verified through the visual color change as well as microstructures of the samples.

2. METHODOLOGY

Cement and sand are mixed into 1:3 ratios to produce the plaster samples. The dimension of plaster sample is 50 mm x 50 mm x 50 mm and six samples of same dimension are taken. All the samples are painted with white enamel paint on one particular surface. The samples are kept one day for drying. After drying the plaster samples are heated isochronally. An electric furnace is used for thermal treatment of the plaster samples. Heating is applied on different samples at room temperature (25°C) to 350°C range for one hour. Samples are tested for various physical and optical properties after coming into natural temperature.

The images of the heated samples are taken with DSLR camera for examine the visual changes. The optical micrographs of the samples are also taken with USB digital microscope for grain size analysis. The images of the samples are analysed through MATLAB software for determining the tristimulus color parameter L*, a* and b* values. The changes of these values with respect to temperature changes are shown graphically. The changes in proportion of the basic color red, green and blue with respect to temperature changes are also shown graphically. Figure 1 gives an idea about the setup of the experiment carried out for this study.

Figure 1: Experimental setup, a) plaster samples, b) enamel painting, c) electrical furnace and d) heated samples

3. RESULTS AND DISCUSSIONS

For analysing the thermal degradation of the plaster samples, all six specimens were isochronally heated at different temperatures for one hour and the corresponding optical images were recorded, which are shown in Figure 2. The images show that, the samples are thermally affected when they are heated with increasing temperature. But up to 100°C no significant change is found. After 100°C the color change is noticeable and it is because of the evaporation of water molecules from the paint. After 200°C the color has changed drastically because of the chemical change of paint ingredients [7]. Finally, at 350°C the sample got burned and the paint layer came out from the plaster.

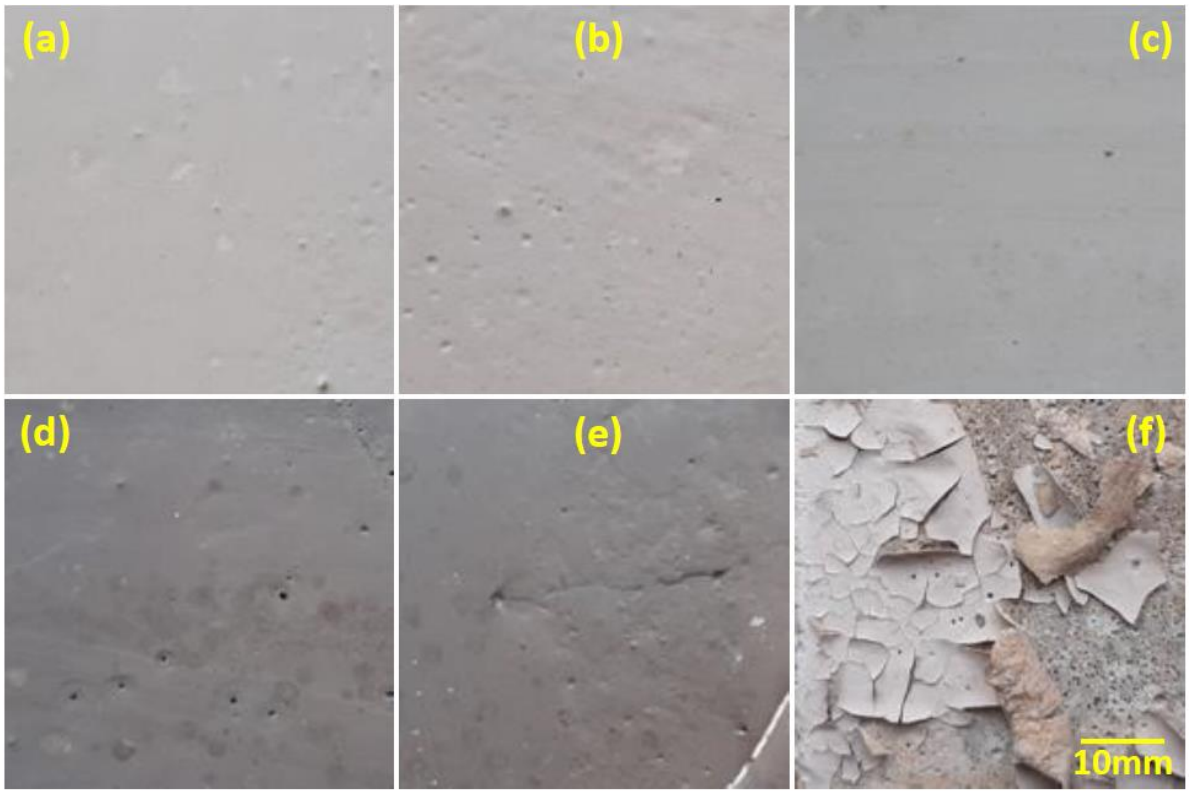

Figure 2: Change of color of different plaster samples after heating at different temperatures for 1 hour, a) 25°C b) 100°C, c) 200°C, d) 250°C, e) 300° and f) 350°C

The microstructures of the samples are taken for grain analysis which is shown in Figure 3. The change in grain sizes also remains insignificant up to 100°C. Because of the evaporation of water molecules, the grain size becomes thicker after 100°C and changes drastically after 200°C due to the chemical change of carbonaceous materials of paint [8]. At 350°C the microstructure defines total burning structure of the coating layer.

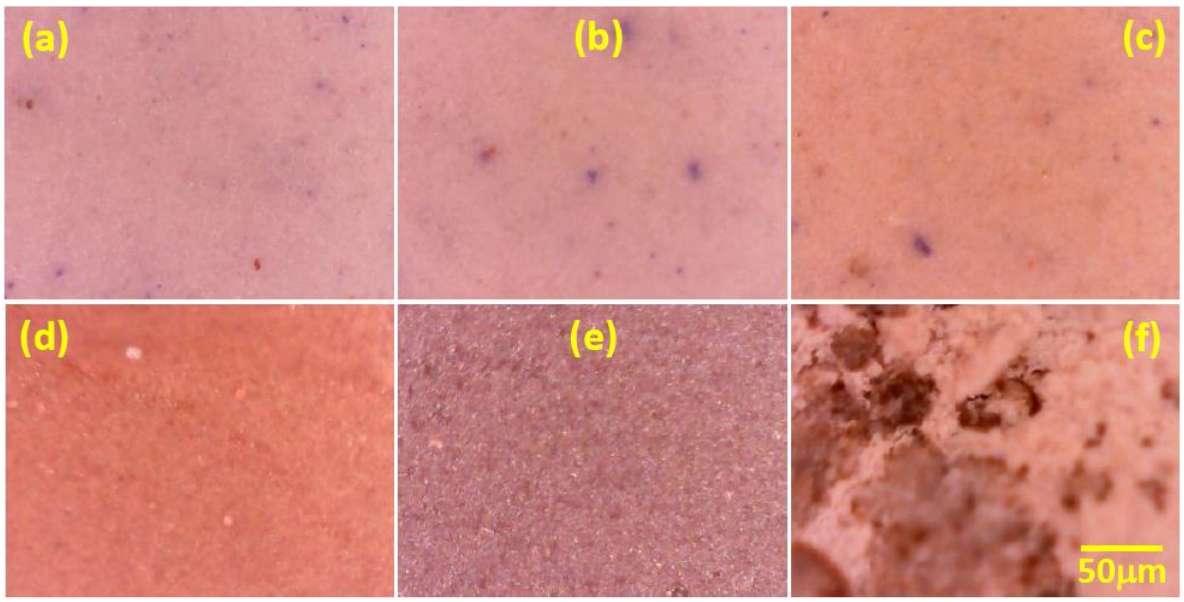

Figure 3: Optical micrograph of color of different plaster samples heated at a) 25°C , b) 100°C, c) 200°C, d) 250°C, e) 300°C and f) 350°C for one hour.

The color change of the samples are examined by tristimulus colour parameter 'L*', 'a*' and 'b*' values. The graphical representations of change of these values are shown in Figure 4. The 'L*' value vs heating temperature graph shows that up to 200°C there is a small decrease in 'L*' value. After 200°C the value starts to decrease greatly up to 250°C and then shows a slight increase from 250°C to 300°C. The 'a*' value vs heating temperature graph indicates the increase of 'a*' value up to 100°C and then a significant decrease up to 200°C and then again shows an increase with a large slope till 250°C and finally with a smaller slope till 300°C. The change of 'b*' value remains insignificant until 100°C and then shows a decreasing behaviour up to 250°C and finally increases from 250°C to 300°C range before the samples got burned. It seems to be increase in darkness by the heating effect. Because of the heating effect the color of the samples begins to get darker and so the portion of relatively darker colors like black, red and blue increases. Especially in 200°C to 250°C range the change in color becomes evident and thus the changes in 'L*', 'a*' and 'b*' values have occurred with a larger slope. Here, decrease in 'L*' value indicates increase of black portion. Similarly, the increase of 'a*' value and decrease of 'b*' value indicates the increase of red and blue portion respectively.

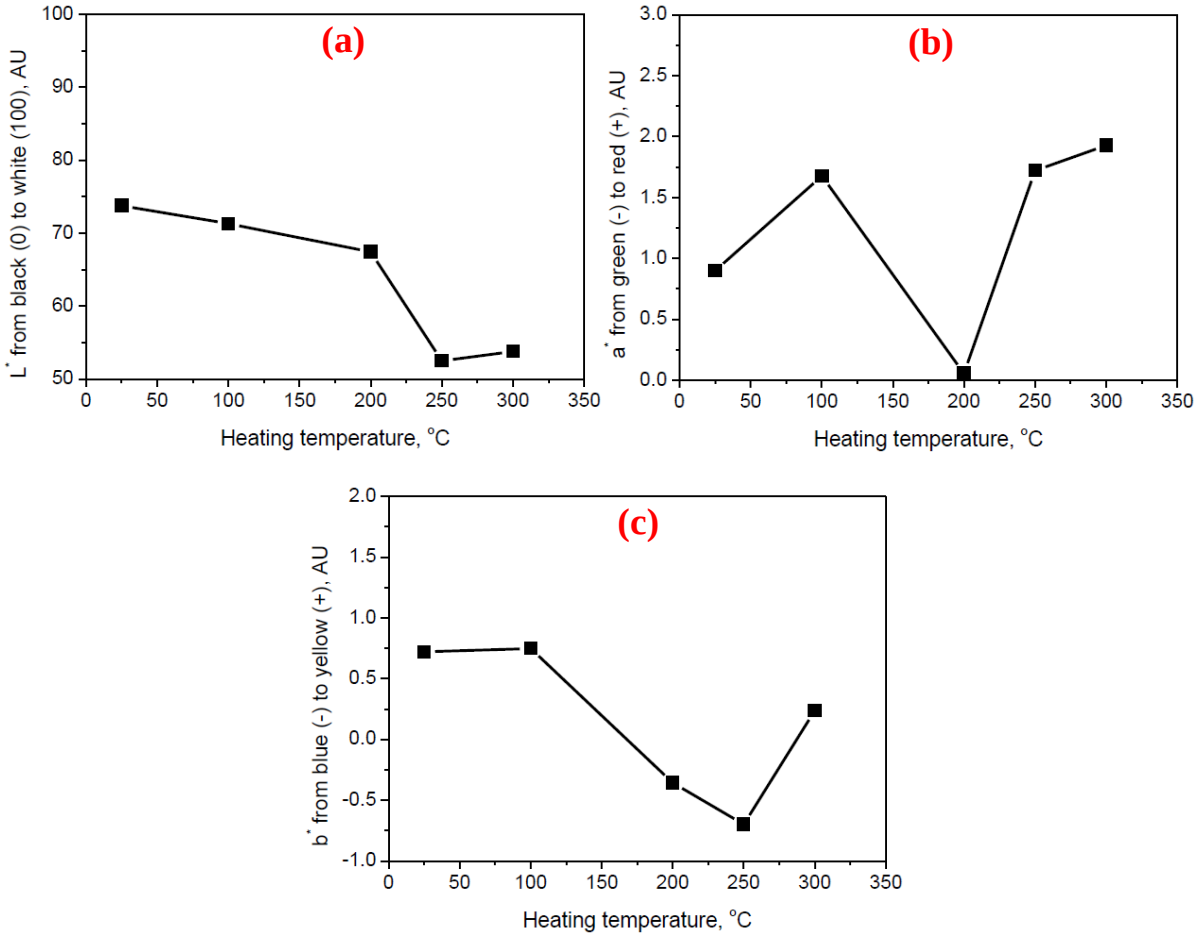

Figure 4: Change of color of plaster samples after heating at different temperatures for one hours, a) L* , b) a* and c) b*

The proportion of three basic colors (Red, Green and Blue) with respect to temperature changes are shown graphically in Figure 5. The red color proportion shows a decreasing trend with a smaller slope up to 200°C and then decreases drastically till 250°C. Finally, it shows a slight increasing trend from 250°C to 300°C before getting burned. Similarly, the Blue and Green color proportion also show almost the same pattern. It happens because when the samples are heated the proportion of black color (black color indicates the absence of other colors) increases as the samples tend to be burned. Thus, the proportions of all three colors begin to decrease [9].

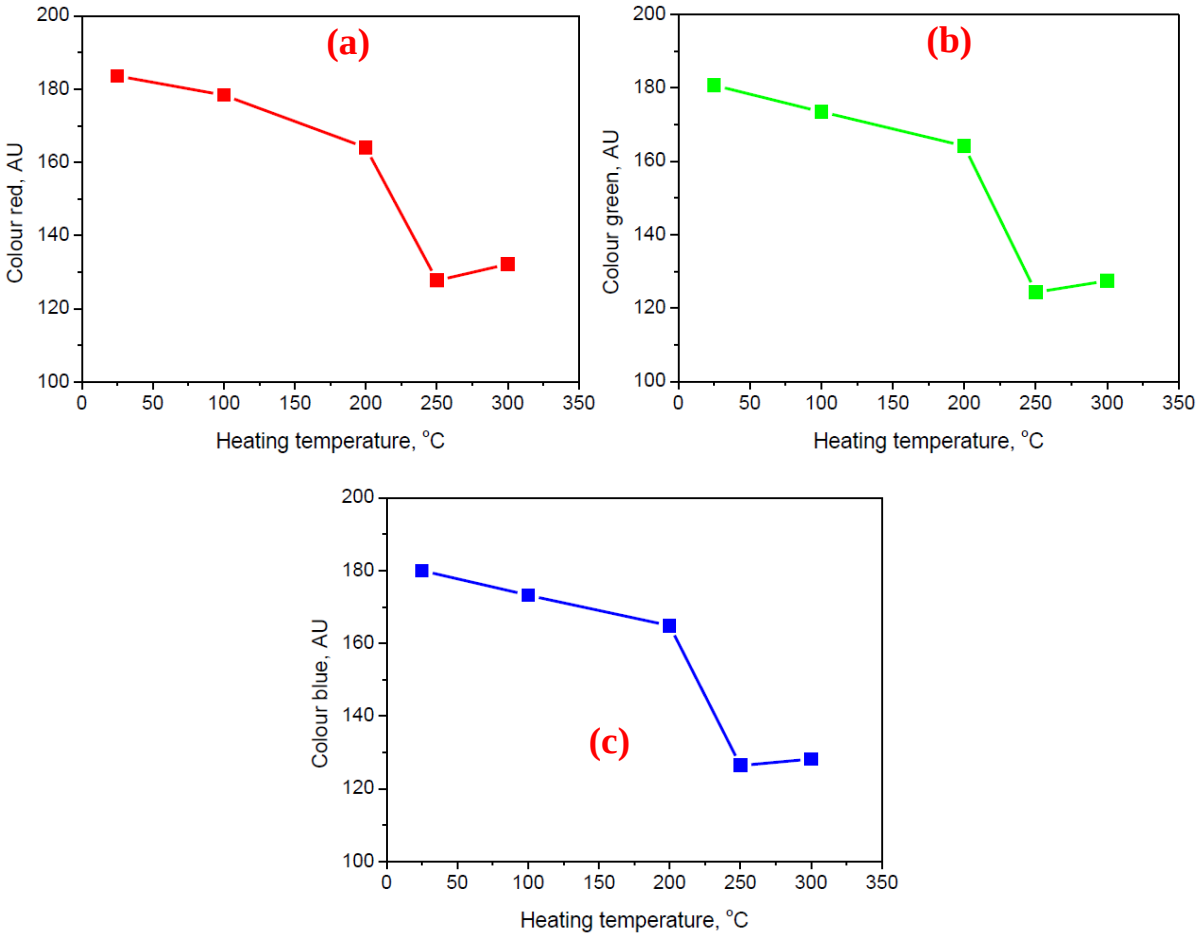

Figure 5: Change of color of plaster samples after heating at different temperatures for one hours, a) Red , b) Green and c) Blue

4. CONCLUSIONS

To achieve an approximate idea of safe temperature of enamel paint coated cement plaster in terms of heating as well as thermal degradation is the main contribution of the study. A simple visual inspection method is applied to analyse the thermal degradation of the plaster samples. Particularly, the degradation is analysed based on the change in color of the optical images of the samples taken after every thermal treatment performed at a certain interval of temperature. No significant change in color of the images is observed up to the heating performed at 100°C. It is because only after 100°C the water molecules from the painted surface begin to evaporate. After 200°C the changes become more noticeable as the carbonaceous materials of paint start to be changed chemically. When the samples are heated at 350°C the enamel coating on plaster is burned completely as reflected in corresponding colour of the sample images. The microstructure analysis also shows the coarsening of grains with increasing temperatures. Finally, the variation of tristimulus colour parameters indicates the effect of significant increase of darkness after heating beyond 200°C. The proportion of combination of three basic colors (RGB) also decreases with increasing temperatures and thus it is very much correlational with the visual examinations.

ACKNOWLEDGEMENTS

Thanks to DAERS office Bangladesh University of Engineering and Technology, Dhaka-1000, for assisting with adequate laboratory facilities.

REFERENCES

Lambourne, R and Strivens, T.A, (1999), Paint and surface coatings: Theory and practice, second edition, published by Woodhead Publishing Ltd, Abington Hall, Abington, Cambridge CB1 6AH, England.

Piper, R. (1965), The hazards of painting and varnishing, British Journal of Industrial Medicine, 22, 247-260

Madankar, C.S., Karadbhajne, V.Y., Waykar, N.G. and Walhekar, A.G, (2011). Synthesis of Enamel Paint based on Novel Rosinated Maleinized Castor Oil using Zinc Oxide as a Natural Drier, International Journal of ChemTech Research, 3(1), 391-397.

Kumar, S.S, (2015) Development of Industrial Automotive Paint with Natural Raw Material Castor Oil as a Substitute of Polymeric Plasticizer, International Journal of Engineering and Applied Sciences (IJEAS) ISSN: 2394-3661, Volume-2, Issue-12.

Popov-Raljić, J.V., Lakić, N.S., Laličić-Petronijević, J.G., Barać, M.B., and Sikimić, V.M, (2008). Color Changes of UHT Milk During Storage, .Sensors (Basel) ; 8(9): 5961–5974.

Wojciech Mokrzycki, Maciej Tatol, (2011). Color difference Delta E - A survey, Machine Graphics and Vision 20(4):383-411.

Berg, Jorrit & Van den Berg, Klaas Jan & Boon, Jaap. (1999). Chemical changes in curing and ageing oil paints. 12th Triennial Meeting. 248-253.

Erhardt, D., Tumosa, C. and Mecklenburg, M. (2005). Long-Term Chemical and Physical Processes in Oil Paint Films. Studies in Conservation, 50(2), 143-150.

Bentley, J. and Turner, G. P. A. (1997). Introduction to paint chemistry and principles of paint technology. CRC Press.

Proceedings of the 5th International Conference on Civil Engineering for Sustainable Development (ICCESD 2020), 7~9 February 2020, KUET, Khulna, Bangladesh (ISBN-978-984-34-8764-3)

EXPERIMENTAL INVESTIGATION ON THERMAL PERFORMANCE OF CEMENT PLASTER INCORPORATING INSULATING MATERIALS

Al-Ishmam*[1] and Md. Mahfuzur Rahman[2]

[1]Graduate Student, Department of Civil Engineering, Khulna University of Engineering & Technology, Bangladesh, e-mail: ishmam1726@gmail.com
[2]Associate Professor, Department of Civil Engineering, Khulna University of Engineering & Technology, Bangladesh, e-mail: mahfuz11@ce.kuet.ac.bd

***Corresponding Author**

ABSTRACT

Thermal insulation is a major contributor and obvious practical and logical first step towards achieving energy efficiency, especially the buildings located in sites with harsh climatic conditions. The aim of this project was to evaluate the performance of different thermal insulation materials in cement plaster. In this context, five cement mortar slab samples were prepared; one was considered as control sample, two samples incorporating jute fibre and two samples incorporating Super Absorption Polymer (SAP). At first, alkali treatment was performed for jute fibres and the properties of fibre were investigated. Jute fibre was used in mortar with 1% of cement by mass dosage. For SAP, absorption capacity was determined and used in mortar with a percentage of 0.1% of cement by mass. 90 gm/gm extra water was added during the preparation of mortar in case of sample with SAP. Three companion 2 inch mortar cubes were cast for each slab sample to determine the compressive strength of the corresponding batch of mortar. Finally the thermal performance of five samples were investigated in a small-scaled rectangular shape box which was divided into two compartments by the sample. Six temperature sensors were used during the tests to measure the temperature of two compartments of the box: heat source compartment and opposite compartment, and one sensor was used to measure the temperature of the atmosphere. All the sensors were connected with an open-source electronics platform Arduino to record the temperature over time. The temperature of the heat source compartment was kept constant at 60 ºC (±2 ºC) and the consequent temperature of the opposite compartment was measured during the tests. 60 ºC temperature was remained constant in the side of heat source. For control sample the temperature was recorded as 46 ºC, for jute fibre it was 44 ºC and 39 ºC for SAP sample at 7 days. For 28 days, the temperatures were varied 45 ºC, 45 ºC and 43 ºC for control sample, jute sample and SAP sample respectively. Thermal performances of mortar containing SAP were found out to be better than that of other two types of samples.

***Keywords**: Arduino, Jute fibre, Mortar, Super Absorbent Polymer, Thermal performance.*

1. INTRODUCTION

Construction industry is now-a-days moving towards more sustainable and energy efficient solution. However, global warming has been triggering more usage of air conditioning system in residential as well as office area (Mallik, 1996). Therefore, energy consumption has been grown largely over the years. In this context, an economical solution is necessary to maintain the temperature of habitational area comfortable. Many natural and artificial materials have been used as thermal insulator over the years (Al-homoud, 2005, Jelle et. al., 2012, Papadopoulos, 2005). Jute fibre and Super Absorbent Polymer can be regarded as natural and artificial material, respectively, having thermal insulation properties (Jin et. al., 2000). The main objectives of this study was to establish an experimental setup for measuring thermal performance of cement plaster and to determine the performance of cement plaster incorporating natural fibre (jute fibre) and Super Absorption Polymer (SAP). In this context, five cement mortar slab samples were prepared; one was considered as control sample, two samples incorporating jute fibre and two samples incorporating Super Absorption Polymer (SAP) to determine the thermal performance of mortar plaster.

2. METHODOLOGY

2.1 Insulating materials

2.1.1 Super Absorbent Polymer (SAP)

Super Absorbent Polymers are usually composed of ionic monomers and can absorb high amount of moisture using a low cross-linked density. They can absorb moisture up to several hundred times of its own weight under pressure (Mechtcherine, 2016). Considering the workability and strength of mortar, SAP dosage of 0.1% of the cementitious material was found to provide better result within the range of 0.1%~0.3% SAP of cementitious material used in mortar (Dang & Zhao, 2018). In this context, the dosage of SAP was adopted as 0.1% of binder material in this experiment.

2.1.2 Alkali treatment of jute fibres

Jute fibre was also utilized as the insulating material in this research work. However, hydrophilic properties of Jute fibre was the main challenge to use it in the mortar. To overcome this issue, the jute fibres were treated in alkali solution. A 5% NaOH solution with a liquor ratio of 15:1 was used and the temperature was kept constant at 30 ^{0}C (Figure 1). The jute fibre length was approximately 12 mm. Alkali treatment of Jute fibre was applied because of the increase in tensile strength of Jute fibre compare to that of untreated Jute fibre (Ray et al., 2002). After the alkali treatment process continued for 4 hours, Jute fibres were thoroughly washed by distilled water to remove the NaOH from the Jute fibre surface. Finally the Jute fibre were oven dried for 6 ^{0}C for 6 hours to remove any moisture content from the fibre.

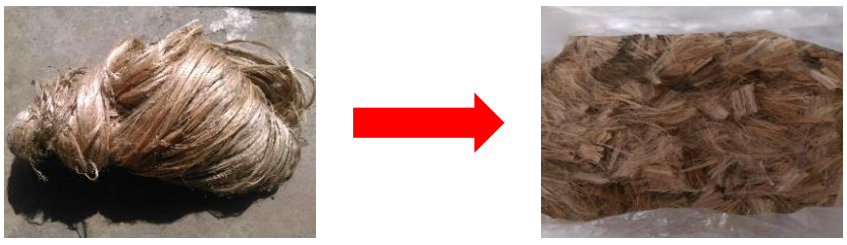

(a) Jute fibres cut into small pieces (Approx.12 mm in length)

(b) Jute fibres soaked with 5% NaOH solution for 4h.

(c) Jute fibres after treatment

Figure 1: Alkali treatment of jute fibres

2.2 Specimen Preparation

Slab samples, made of cement mortar were used in this research work. Two insulating materials - SAP and jute fibres were used in this experimental work. Therefore, total five samples; two for each categories of insulating materials and one as control sample were used in this experimental work. All samples were identical in shape having dimension of 1000 mm × 1000 mm × 25 mm as shown in Figure 2. The thickness of sample was considered to be the representation of wall plaster. Three mortar cube samples were also prepared with each slab sample for determining their corresponding compressive strength.

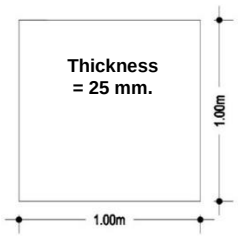

Figure 2: Specimen with dimension

2.3 Mix proportions

For samples with SAP, 0.1% of cement and 90 gm of extra water per gram of polymer was used for this experimental work. For samples with natural fibres, 1% of cement by mass was used which is summarized in Table 1. For control sample, the mortar ratio was 1:4 according to ASTM C926 and the water-cement ratio was 0.485 according to ASTM C109.

Table 1: Specimen with different proportion of insulating materials

Specimen type	Insulating materials	No. of specimen
CS (Control Sample)	Controlled Sample	01
SS (SAP Sample)	SAP (0.1% of cement)	02
JS (Jute Sample)	Jute Fibre (1% of cement)	02

2.4 Preparation of the small-scaled box

A small-scaled box was prepared with wooden pieces of 1 inch thickness having dimensions of 2 m × 1 m × 2 m (*L*×*H*×*W)* as shown in Figure 5. Inside the box, there were two pairs of wooden bits to hold the specimen remaining upright vertically, which divided the box into two compartments and act as a thermal barrier between two compartments of the box. One part of the compartment was accommodated with heat source while the other was represented as an interior of a room. GLS (General Lamp Shape)

bulbs of 800 watt were used as the source of heat to perform the entire test. Holes were made for the passage of wires from heat source, temperature controllers and sensors to outsides of the small-scaled box.

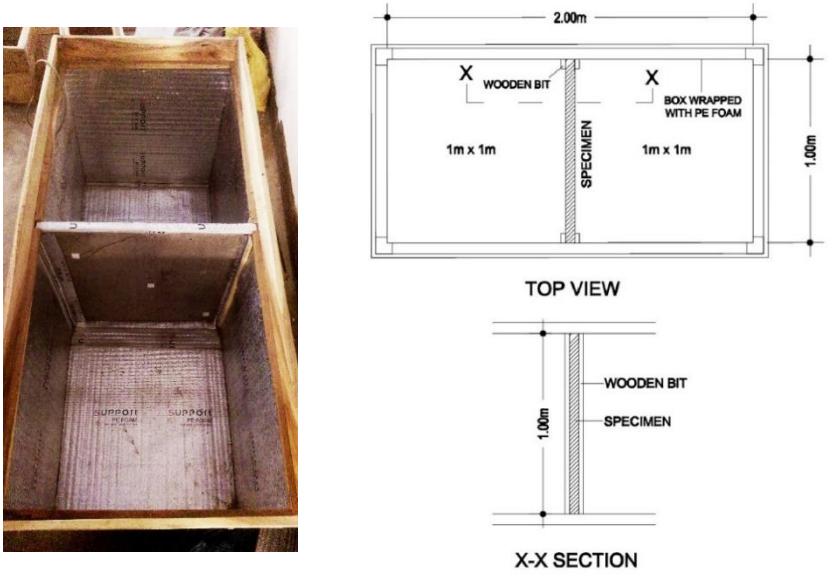

Figure 5: Small-scaled rectangular shape box with different views

The inner portion of the box was covered with PE foam with uniform addition of proper adhesives and the inner side of lid of the box was also covered with the foam to store heat inside the box as shown in Figure 6. The edges of the specimen with wooden bit were also being insulated properly ensuring heat will pass from heat source compartment to other compartment only through the mortar slab sample. All holes were filled with foams and tapes preventing escape of heat from inside to outside of the box.

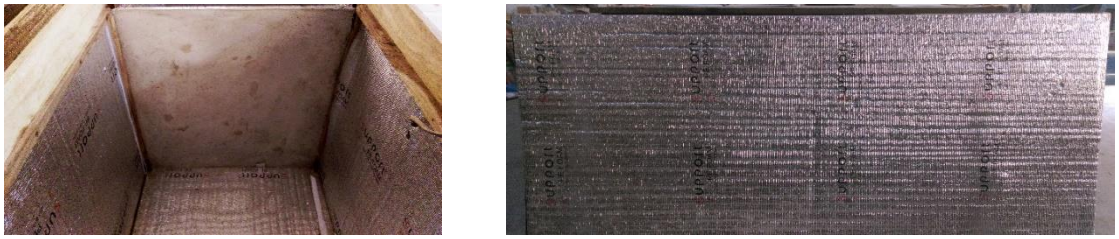

Figure 6: Insulation of box with PE foam

2.5 Data collection process

Six DHT22 temperature and relative humidity sensors were attached on the slab sample to perform the test covering both the side of the heat source compartment and the opposite side as shown in figure 7 and one sensor was used to record the ambient relative humidity and temperature.

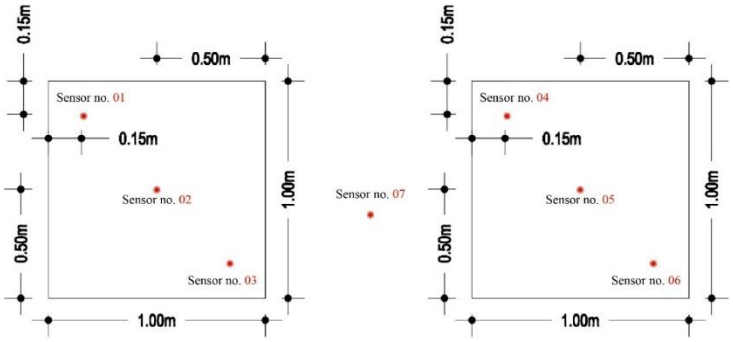

(a) Heat source side (b) Opposite side

Figure 7: Position of sensors over specimen

Each sensors were attached with serial numbers to identify readings they recorded. All data were collected and recorded from sensors with Arduino connected with a laptop as shown in Figure 8.

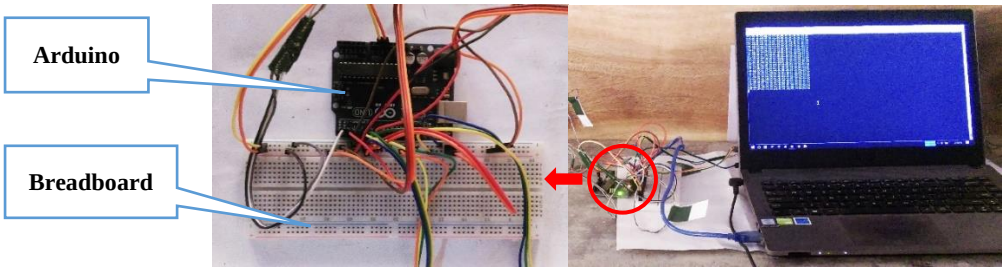

Figure 8: Data collection process from sensors

3. RESULTS AND DISCUSSION

The properties of fine aggregate, Jute fibre were determined according the corresponding standard tests and the obtained results are summarized in Table 2 and 3, respectively.

Table 2: Physical properties of fine aggregate

Test name	Results	Test method
Specific Gravity	2.4	ASTM C128
Fineness Modulus (FM)	2.67	ASTM C136
Moisture content (%)	3.5	ASTM C 70
Absorption (%)	4.6	ASTM C128
Unit weight (Kg/m^3)	1498	ASTM C 29

Table 3: Tensile Test results of Jute Fiber Composite

Tensile Parameters	Results
Maximum Deformation (mm)	0.98
Ultimate Strength (MPa)	88
Modulus of Elasticity (MPa)	4295

The cube samples were divided into several groups with according to the usage of insulating materials in mortar. Each set had different insulating materials. Compressive strengths were tested at 7 days and

28 days after casting. Water curing was carried out for all specimens with their companion cubes except the sample with SAP. SAP samples were air cured for 7 and 28 days after casting.
Cubic samples were tested with mortar ratio of 1:2.75 and water-cement ratio of 0.485 by following test method ASTM C109. The compressive strength of mortar containing the insulating materials along with the controlled samples are presented in Table 4 and 5.

Table 4: Mortar Compressive Strength of different samples at 7 days

Sample type	Mortar age (Days)	Curing medium	Avg. Compressive Strength (MPa)
Controlled Sample	7	water	17.50
Jute Sample -01			23.9
Jute Sample-02			22.3
SAP Sample-01		air	21.3
SAP Sample-02			21.5

Table 5: Mortar Compressive Strength of different samples at 28 days

Sample type	Mortar age (Days)	Curing medium	Avg. Compressive Strength (MPa)
Controlled Sample	28	water	47.6
Jute Sample -01			27.1
Jute Sample-02			27.2
SAP Sample-01		air	26.8
SAP Sample-02			27.1

3.1 Temperature variation at 7 days

Figure 9 shows the temperature variation graph for control sample. Temperature of two compartments of the box separated by the slab specimen were recorded over time during the test and presented in Figure 9 to Figure 13. Figure 14 also shows the comparison of temperature variation among Jute, SAP and control samples at 7 days.

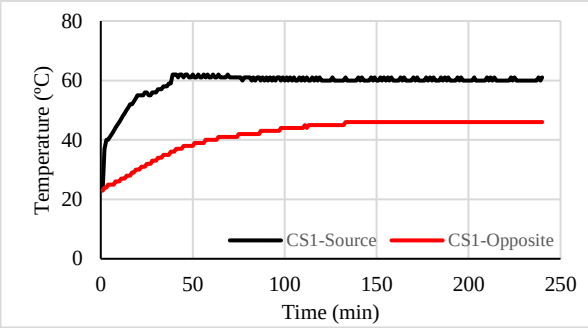

Figure 9: Temperature Variation for Control Sample at 7 days

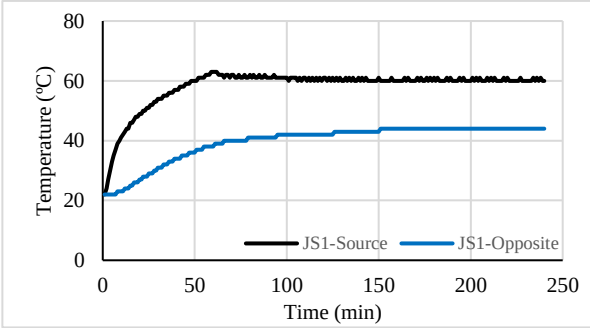

Figure 10: Temperature Variation for Jute Sample-1 at 7 days

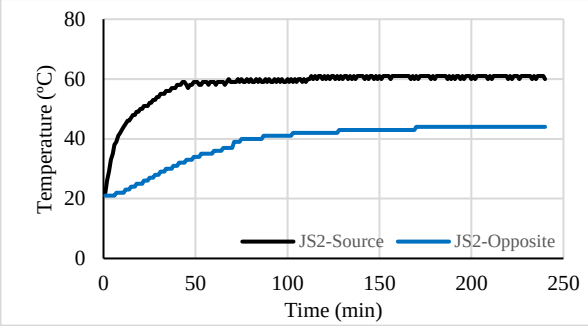

Figure 11: Temperature Variation for Jute Sample-2 at 7 days

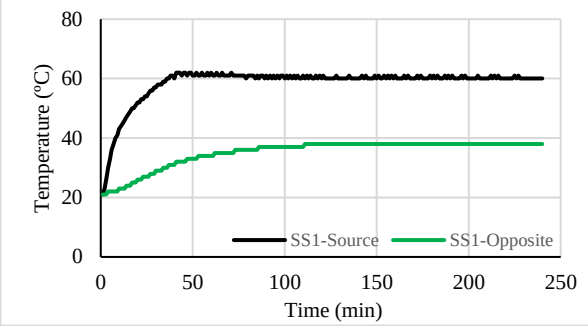

Figure 12: Temperature Variation for SAP Sample-1 at 7 days

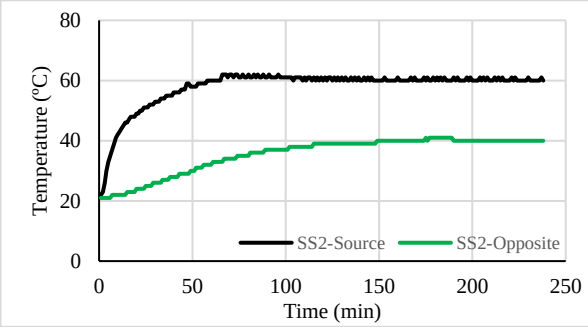

Figure 13: Temperature Variation for SAP Sample-2 at 7 days

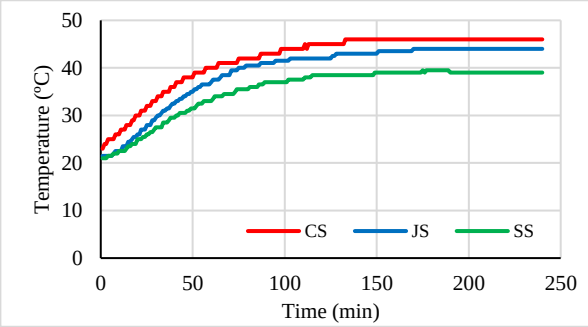

Figure 14: Temperature variation among different types of insulation at 7 days

3.2 Temperature variation at 28 days

Figure 15 reflects the temperature variation for control sample. Furthermore, Fig. 16 and Fig. 17 show the thermal variation of jute sample and SAP sample respectively after 28 days.

Figure 18 shows that the obtained temperatures are 45 ºC, 45 ºC and 43 ºC for control sample, Jute sample and SAP sample respectively. SAP sample shows 2 ºC temperature less than that of other samples. Therefore, it is clearly demonstrated that the thermal performance with SAP sample was better than that of jute sample and control sample after 28 days.

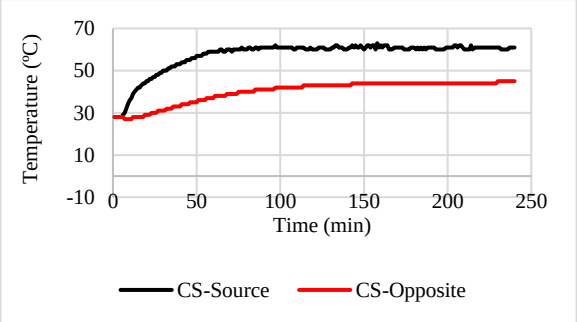

Figure 15: Temperature Variation for Control Sample at 28 days

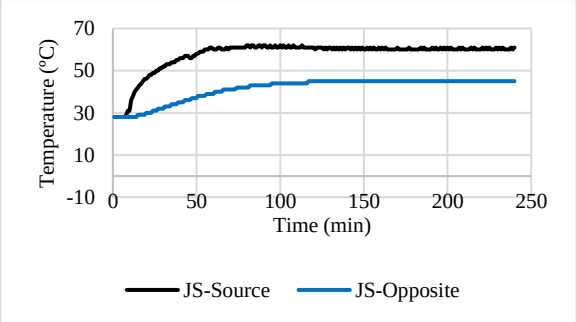

Figure 16: Temperature Variation for Jute Sample at 28 days

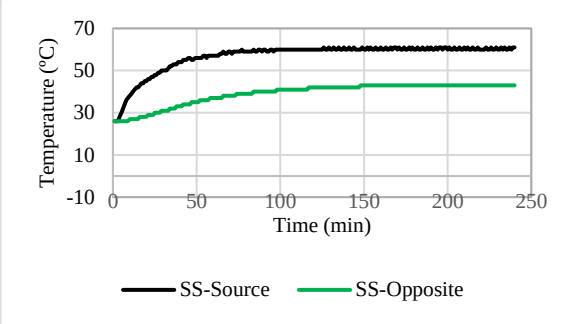

Figure 17: Temperature Variation for SAP Sample at 28 days

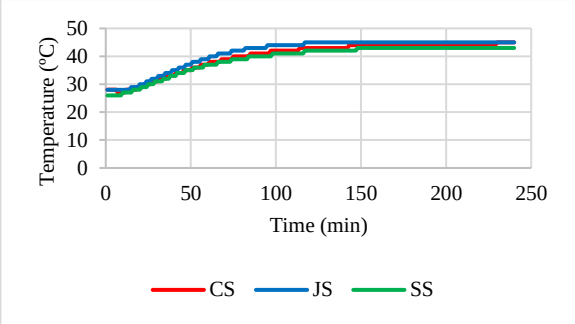

Figure 18: Temperature variation among different types of insulation at 28 days

4. CONCLUSIONS

The following conclusions were drawn from the experiments conducted and the results obtained –

- It was observed that the compressive strength of mortar with jute fibre was higher than the rests.
- It was also found that thermal performances of mortar containing SAP and sample incorporating jute fibres were better than that of control sample.
- The compressive strength of the samples with SAP was almost close to the conventionally cured sample for 7 days test.
- In terms of thermal insulation and mechanical properties, sample made with super absorbent polymer appears to be the best.

REFERENCES

Al-Homoud, M. S. (2005). Performance characteristics and practical applications of common building thermal insulation materials. *Building and environment*, *40*(3), 353-366.

Dang, J., Zhao, J., & Du, Z. (2017). Effect of superabsorbent polymer on the properties of concrete. *Polymers*, *9*(12), 672.

Jelle, B. P., Gustavsen, A., & Baetens, R. (2012, April). Innovative high performance thermal building insulation materials-todays state-of-the-art and beyond tomorrow. In *Proceedings of the 3rd Building Enclosure Science & Technology (BEST 3-2012) Conference*.

Jin, Z. F., Asako, Y., Yamaguchi, Y., & Yoshida, H. (2000). Thermal and water storage characteristics of super-absorbent polymer gel which absorbed aqueous solution of calcium chloride. *International journal of heat and mass transfer*, *43*(18), 3407-3415.

Mallick, F. H. (1996). Thermal comfort and building design in the tropical climates. *Energy and buildings*, *23*(3), 161-167.

Mechtcherine, V. (2016). Use of superabsorbent polymers (SAP) as concrete additive. *RILEM Technical Letters*, *1*, 81-87.

Papadopoulos, A. M. (2005). State of the art in thermal insulation materials and aims for future developments. *Energy and buildings*, *37*(1), 77-86.

Proceedings of the 5th International Conference on Civil Engineering for Sustainable Development (ICCESD 2020), 7~9 February 2020, KUET, Khulna, Bangladesh (ISBN-978-984-34-8764-3)

PERFORMANCE-BASED DESIGN AND SEISMIC RESPONSE OF MASS IRREGULAR REINFORCED CONCRETE SPECIAL MOMENT FRAME (RC-SMF)

A F M Salman Akhter[1] and Yoyong Arfiadi*[2]

[1]Research Scholar, Department of Civil Engineering, Universitas Atma Jaya Yogyakarta, Indonesia. e-mail: engr.salmanakhter@gmail.com
[2]Professor, Department of Civil Engineering, Universitas Atma Jaya Yogyakarta, Indonesia. email: yoyong.ar@uajy.ac.id

***Corresponding Author**

ABSTRACT

This research work concentrates on the investigation of the seismic response of mass irregularities in Reinforced Concrete Special Moment Frame (RC-SMF) which were designed by performance-based plastic design method. This design method uses the modified energy-work balance concept for calculating the design base shear and beam-column design moment, as well as the inelastic state-based formula to distribute the lateral forces. Three 8-story RC-SMF structures with mass irregularity at 1st, 4th and 8th floor, respectively, and one 8-story RC-SMF structure without mass irregularity were considered in this study. These 4 RC-SMF buildings were subjected to 20 ground motions with 2% target drift and a seismic hazard level of 1% probability of exceedance in 50 years. The seismic response of these buildings was observed by Incremental Dynamic Analysis (IDA) with an intensity measure ranging from 0.1 to 3.5g using OpenSees software. It is found that the response curves ideally show the behavior of four RC-SMF structure under strong ground motions.

Keywords: *Mass irregular structure, Performance-based plastic design, IDA.*

1. INTRODUCTION

The perfect regular structure is an idealized concept to analyze the structure. However, real-life buildings are almost always irregular. Due to the usage of buildings, the common irregularities found in the structures are mass, geometry and stiffness irregularities. Hence, it is important to evaluate the seismic performance of irregular type structures that will provide the behavior of the structural member under strong ground shaking. A number of researches have been performed to investigate the irregularities effects in buildings during big earthquakes (Chopra and Goel 2004) on the limit capacity of buildings. Moreover, the damage occurs in code-compliant irregular type RC structure due to inelastic behavior shows the need for more research on designing procedure and seismic response evaluation of structures that have irregularities.

The current design code generally considers the elastic deformation although the structure undergoes large inelastic deformation under strong earthquakes. Additionally, the elastic analysis accounts the equivalent static design force to calculate the required strengths of elements. However, strength and deformation demand require proper inelastic behavior of elements to prevent undesired failure or collapse. Hence, the Performance-Based Plastic Design (PBPD) has been developed with a series of research works by several researchers. The important concept of this method is the target drift and yield mechanism used to achieve the target building performance and demonstrate the inelastic response of elements during a strong earthquake (Leelataviwat et al. 1999; Lee and Goel 2001). The modified work-energy concept is then used to calculate the design base shear and beam-column moment (Lee and Goel 2001). A lateral force distribution method that considers the inelastic response of the structure is used in this PBPD method for getting the more accurate seismic response (Chao et al. 2007). A number of comprehensive researches using PBPD method have been performed on the different type of structure like eccentrically braced frame, special moment truss, high-rise buckling-restrained braced frames, tall hybrid coupled walls, reinforced concrete special moment frame etc. (Chao and Goel 2005; Chao and Goel 2006; Chao and Goel 2008; Liao and Goel 2014; Chan-anan et al. 2016). From those studies, the seismic response of the structures which were designed by PBPD method have evenly distributed story drift over height while the structures designed with seismic code-based method have undesired story drift or soft story failure over height. However, research works have only been performed on Reinforced Concrete Special Moment Frame (RC-SMF). Therefore, further research is needed using this methodology for another type of RC structure like RC-SMF with irregularity (mass, geometry and stiffness), RC moment frame with shear wall, Reinforced Concrete Ordinary Moment Frame (RC-OMF), Reinforced Concrete Intermediate Moment Frame (RC-IMF) etc. In this study, the RC-SMF with mass irregularity is taken for designing and analyzing using the proposed seismic design method.

The main objective of this research was to apply the PBPD method to the mass irregular RC-SMF structures to analyze the seismic response of the structures through the IDA curve. Four 8 story RC-SMF structures were selected to design it's all elements using PBPD design method which has mass irregularity at 1st, 4th and 8th floor and one without mass irregularity, respectively. All four RC-SMF structures were assumed as multipurpose buildings, located in Padang Indonesia on soil type E (soft soil). The advantage of this method is to set hazard level and performance limit depends on the necessity of the structures and later evaluate the response of structures by performing the nonlinear time history analysis. Similarly, these structures were designed for 2% target drift with a seismic hazard level of 1% probability of exceedance in 50 years. The nonlinear model was implemented on OpenSees 2.5.0, a PEER's open-source structural analysis and simulation software. Moreover, the analysis results used to present as seismic responses of structures through incremental dynamic analysis (Vamvatsikos and Cornell 2002).

2. PERFORMANCE-BASED PLASTIC DESIGN METHOD

The Performance-Based Plastic Design (PBPD) method uses elastic-plastic single-degree-of-freedom-system to represent the work-energy balance concept which is more rational design concept than the code-based method which is developed by Leelataviwat et al. (1999) and modified by Lee and Goel (2001). The work-energy equation is made by external work equal to the internal work of an elastic-

plastic single-degree-of-freedom-system. The external work is calculated by pushing the structure up to target drift monotonically which is equal to the energy need of an equivalent elastic-plastic single-degree-of-freedom (EP-SDOF) system as shown in Fig. 1. The work-energy balance equation is given by (Liao and Goel, 2014):

$$\left(E_e + E_p\right) = \gamma.\left(\frac{1}{2}M.S_v^2\right) = \frac{1}{2}\gamma.M\left(\frac{T}{2\pi}S_a.g\right)^2 \tag{1}$$

where E_e and Ep are elastic and plastic components of total energy needed, respectively, to push the structure up to the target drift. The γ is energy modification factor, T is natural period and M is total mass of the structure. The S_v and Sa are the design pseudo-spectral velocity and pseudo-spectral acceleration, respectively. The energy modification factor γ is obtained from the inelastic spectra (Lee and Goel 2001) as shown by Eq. 2.

$$\gamma = \frac{2\mu_s - 1}{R_\mu^2} \tag{2}$$

where Rμ is ductility reduction factor and μs is structural ductility factor.

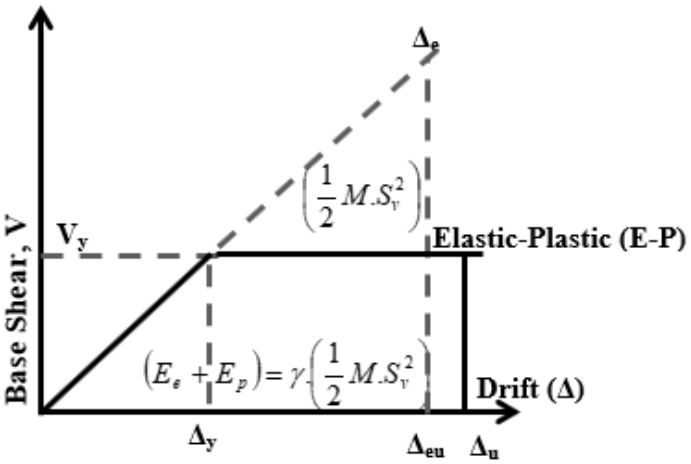

Fig. 1 Required energy by elastic-plastic-single degree-of-freedom system (work-energy balance concept)

Following Liao and Goel (2014), the design base shear formula of PBPD method is obtained from the work-energy balance equation (Eq. 1) and the simplified form of the equation is shown in Eq. 3.

$$\frac{V_y}{W} = \frac{-\alpha + \sqrt{\alpha^2 + 4.\gamma.S_a^2}}{2} \tag{3}$$

where V_y/W is design base shear coefficient, V_y is the design base shear, W is the total seismic weight of the structure, and α is a dimensionless parameter given by:

$$\alpha = \left(\sum_{j=1}^{n}(\beta_i - \beta_{i+1}).h_i\right).\left(\frac{w_n h_n}{\sum_{j=1}^{n} w_j h_j}\right)^{0.75T^{-0.2}} \left(\frac{\theta_p 8\pi^2}{T^2 g}\right) \tag{4}$$

where β is the shear distribution factor, θ_p is plastic component of target drift, w_n and w_j is top floor seismic weight and j^{th} floor seismic weight respectively, and h_n and h_j is the structure height at top floor and j^{th} floor respectively. T is calculated according to ASCE/SEI 7-16 (2017).

The lateral design force distribution is based on inelastic dynamic response and higher mode effects (Chao et. al. 2007) as follow:

$$F_i = (\beta_i - \beta_{i+1}).V_n \tag{5}$$

where Fi is lateral force at level i, and V_n is static story shear at top-level. The static story shear and lateral force at top-level are same, hence the formula is given in Eq. 6.

$$V_n = F_n = \left(\frac{w_n h_n}{\sum_{j=1}^{n} w_j h_j} \right)^{0.75T^{--0.2}} .V_y \tag{6}$$

The story shear distribution factor is the ratio between static story shear and static story shear at top-level as shown in Eq. 7.

$$\frac{V_i}{V_n} = \beta_i = \left(\frac{\sum_{j=1}^{n} w_j h_j}{w_n h_n} \right)^{0.75T^{--0.2}} \tag{7}$$

The main target of PBPD method is to provide sufficient strength to beam to get desired performance level. The plastic hinge is formed at the both end of beam and only at column base. The structural strength follows the story shear distribution along the building height to prevent the yielding from concentrating at upper story level (Chao et. al 2007). The moment capacity of beam at each level is determined by plastic design which is external work equal to internal as follow:

$$\sum_{i=1}^{n} F_i h_i \theta_p = 2.M_{pc}\theta_p + \sum_{i=1}^{n} 2\beta_i \left(M_{pb-positive} + M_{pb-negetive} \right).\gamma_i \tag{8}$$

where θ_p is kinematic rotation angle and M_{pc} is the plastic moment at column base for the yield mechanism, M_{pb} is beam positive and negative moment strength.

According to PBPD, the column strength is determined by taking factored gravity load and maximum beam strength. The joint condition is based on strong-column weak-beam concepts, which is the sum of nominal flexural strength of column to the sum of nominal flexural strength of beam is more than 1.2 according to ACI 318-14, and 1.3 according to FEMA P695. The shear force in interior and exterior columns can be obtained by using (Moehle and Mahin, 1991):

$$V_i = \frac{\left|M_{pr(+)}\right|_i + \left|M_{pr(-)}\right|_i}{L'} + \frac{w_{i-tributary}.L'}{2} \tag{9}$$

$$V_i' = \frac{\left|M_{pr(+)}\right|_i + \left|M_{pr(-)}\right|_i}{L'} - \frac{w_{i-tributary}.L'}{2} \tag{10}$$

where M_{pr} is the maximum beam strength which is multiplied by an over strength factor (Moehle and Mahin 1991), L' is the beam length between to hinge, and w_i is the unit seismic weight. The lateral forces in exterior and interior columns can be obtained by using:

$$\alpha_i F_{L-ext} = \frac{\sum_{i=1}^{n} (M_{pr-})_i + \sum_{i=1}^{n} V_i \left(\frac{L - L'}{2} \right)_i + M_{pc}}{\sum_{i=1}^{n} \alpha_i h_i} \tag{11}$$

$$\alpha_i F_{L-\text{int}} = \frac{\sum_{i=1}^{n}(\left|M_{pr-}\right|_i + \left|M_{pr+}\right|_i) + \sum_{i=1}^{n}[V_i + V_i^{'}].\left(\frac{L-L^{'}}{2}\right)_i + 2M_{pc}}{\sum_{i=1}^{n}\alpha_i h_i} \quad (12)$$

3. MODELING AND ANALYSIS APPROACH

In this study, eight story SMF irregular concrete structures were considered. Three structures were chosen to represent mass irregularity at 8th, 4th, and 1st story, and denoted as MI-8, MI-4, and MI-1, respectively. One structure named as MI-S to represent the structure without mass irregularity. The number of bays is the same for all structures as shown in Fig. 2. The frame of grid line no. 3 was taken from all four structures to design by PBPD and perform nonlinear time history analysis to get the seismic responses of these frames (Fig. 3). The seismic weight in each floor was 1300 KN, except for 1st, 4th and 8th floor of MI-1, MI-4, and MI-8, respectively. The seismic weight of these floor was 2100 KN, which means the mass irregularity exists on that floor according to ASCE/SEI 7-16 (2017).

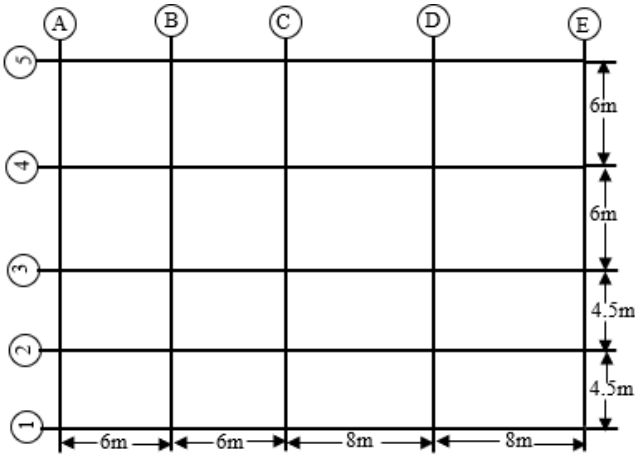

Fig. 2 Floor plan of MI-8, MI-4, MI-1, and MI-S

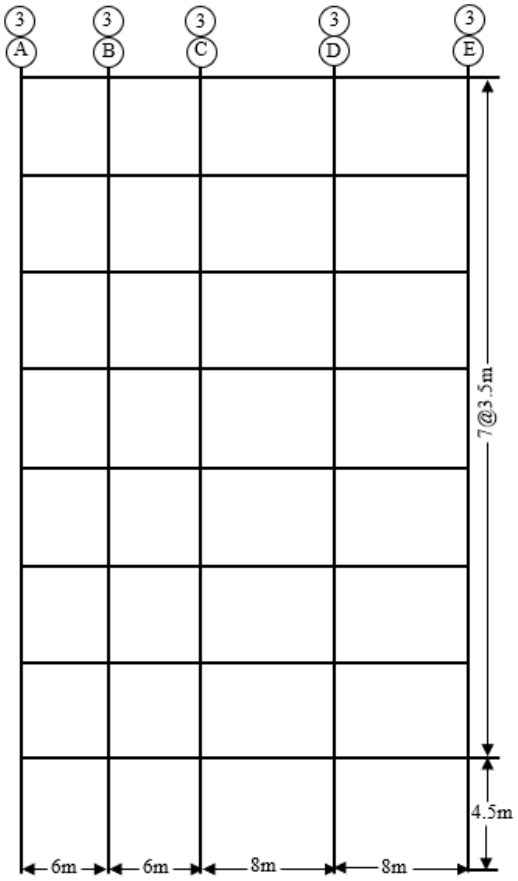

Fig. 3 Frame of grid line 3

The structures were considered as a multi-purpose building which located in Padang, Indonesia on soil type E. The design response spectrum (Sa) was taken from the Indonesia national earthquake database for soil type E as shown in fig. 4 (PUSKIM 2018).

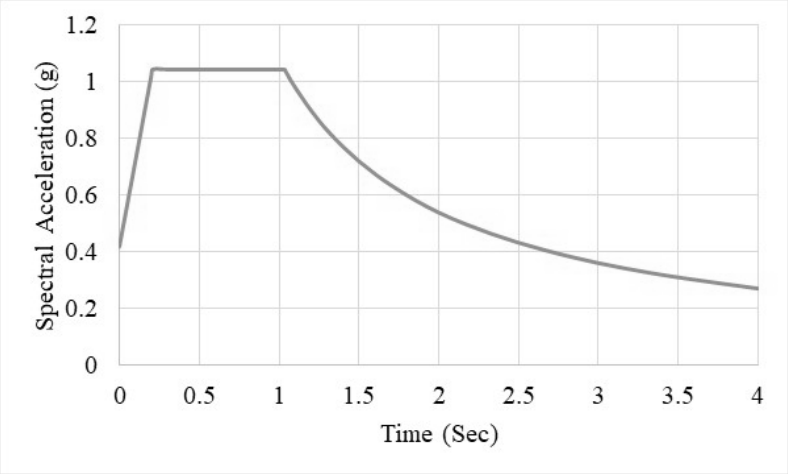

Fig. 4 Design response spectrum for soil type E in Padang, Indonesia

All structure's natural period was assumed the same as 1.35 sec following ASCE approximation formula. The total seismic weight and other parameters are given in Table 1. The design base shear varies from 2010 kN to 2170 kN, which was distributed as lateral force over structure height using Eqs. 5 -7.

Table 1 Design parameters of four structures

Structure, RC-SMF	**MI-8**	**MI-4**	**MI-1**	**MI-S**
Floor height, h (m)	29	29	29	29
Period, T (sec)	1.35	1.35	1.35	1.35
Total seismic weight, W (kN)	11342.4	11342.4	11342.4	10675.2
Dimensionless parameter, α	1.43	1.36	1.37	1.38
Spectral acceleration, S_a	0.797	0.797	0.797	0.797
Design Base Shear, V_y (kN)	2100	2170	2150	2010

In this research, the distributed plasticity approached was used to model the beam-column element in OpenSees. The main advantage of distributed plasticity is it has several integration points over element length as shown in Fig. 5. As a result, the integration points show yielding conditions over the length of the element. The Gauss-Lobatto integration approach places integration point at the both end of element; hence it is the most common way to evaluate the force-based element responses for distributed plasticity (Neuenhofer and Filippou, 1997; Scott and Fenves, 2006). In this study, fiber section with suitable number of patches and layers was used to define the beam-column sections and force-beam-column element. Five Gauss-Lobatto integration points along the element length was used to define a beam-column element. The uniaxial hysteretic constitutive material model namely ConcreteCM (Mander et. al 1988; Chang and Mander 1994) and Giuffre-Menegotto-Pinto steel material (Filippou et. al. 1983) was used to model the core and cover concrete, and steel rebars.

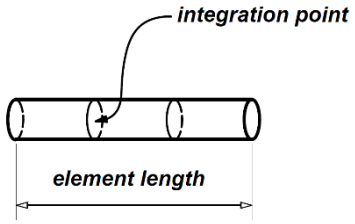

Fig. 5 Element with Gauss-Lobatto integration point

The nonlinear modelling needs earthquakes data to get seismic responses of structure. PEER ground motion database contains wide ranges of ground motions (PEER 2018). In this study, 20 ground motions with magnitude ranges M 6.0 to M 7.7 were selected to show the responses of the structures through IDA curves. To obtain IDA curve, the nonlinear analysis using OpenSees was performed, where the intensity measures started from 0.1g until structure collapse. The ground motions were scaled in different IM (Intensity Measure) level with 5% damping ratio. This step was done by using SeismoSingnal2018.

4. RESULTS AND DISCUSSION

The PBPD method considers the nonlinear behavior and target performance level into the design process from the start. The design output of the column and beam are shown in Figs. 6 to 9.

Firstly, the design base shear and lateral force distribution of MI-1, MI-4, and MI-8 are almost the same although the mass irregularity exists on different floors in these structures. As a result, the design outcome shows that the beam-column properties of these structures nearly similar. On the other hand, the MI-S contains 800 kN less seismic weight than the other three structures, therefore the design base shear and lateral force distribution is less. However, there are few dissimilarities in the beam-column size among these four structures. Finally, the nonlinear analysis performed in OpenSees shows the satisfactory performance of these structures under severe ground motions.

Secondly, the positive and negative beam reinforcement ratio of MI-1, MI-4, and MI-8 at 8th floor is the same. Although, the MI-8 has an extra 800 kN more load at 8th floor. The rebar ratio of the beam at 4th floor of MI-1 and MI-4 is same, but mass irregularity exists at 4th floor in MI-4. Moreover, the rebar ratio of beam at 1st floor of MI-1 and MI-4 is same, however, the 1st floor of MI-1 has extra load. The positive and negative moment of beam is calculated by eq. (8) which is not only based on seismic weight of structure but also based on the shear distribution factor and plastic component of target drift.

Thirdly, the column rebar properties are determined by eq. (9 to 12) which is based on maximum beam strength factor, shear force in column and distance between beam hinge. The column size of these structures is almost the same. The new design approach considers the strong column weak beam mechanism which is justified in nonlinear analysis by achieving the performance of structure. The uniform distribution of interstory drift showed that all columns dissipate earthquake energy properly and minimize the excessive inelastic deformation. The IDA curve (figs. 10 to 13)

The time history analyses of were performed to create incremental dynamic analysis (IDA) curve for each structure. The response of the structure plotted in IDA curve was the maximum interstory drift, and intensity measure (IM). The IM was spectral acceleration, S_a at T_1 with 5% damping ratio of the scaled ground motion. The S_a value range was 0.1g to 3.3g with an increment of 0.1g, but it depended on the structure collapse. The analysis results as IDA curve is shown in Figs.10 to 13. The IDA curve shows that maximum story drift lies within the target drift of all four structures. The drift of four structures increased linearly up to yield drift, and the structure collapsed after the target drift. The uniform distribution of story drift implies that the PBPD considers no soft story failure and it is justified in this study.

The mass irregularity at 4th floor has less probability of collapse than other structure. In comparison between mass irregularity effect at 1st and 4th floor, the section size and rebar properties of these two structures are very similar. However, the collapse probability of the 1st floor mass irregularity is higher than the 4th floor mass irregularity. In addition, the interstory drift and probability of collapse due to mass irregularity at 8th floor was also higher than regular structure. Moreover, the seismic responses of these structures also showed that the maximum drift values are under yield drift in S_a value 1g.

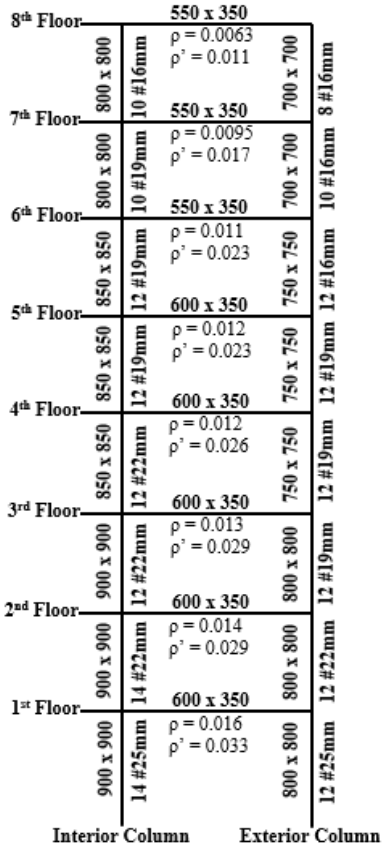

Fig. 6 Colum-beam properties of MI-1

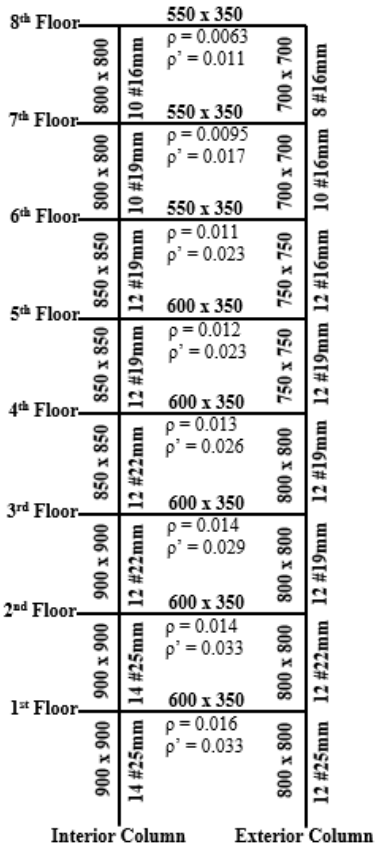

Fig. 7 Colum-beam properties of MI-4

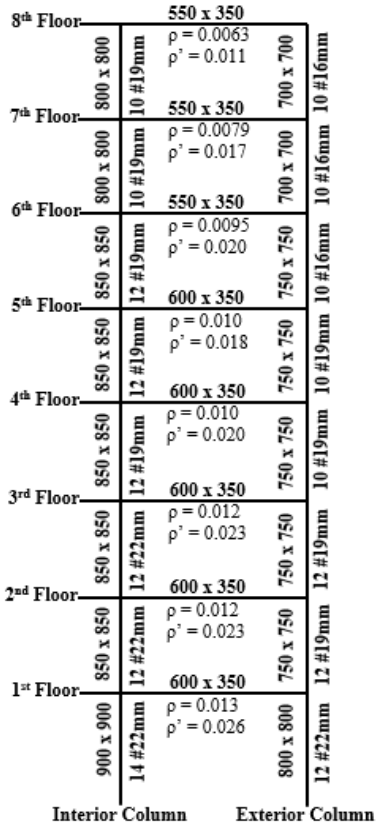

Fig. 8 Colum-beam properties of MI-8

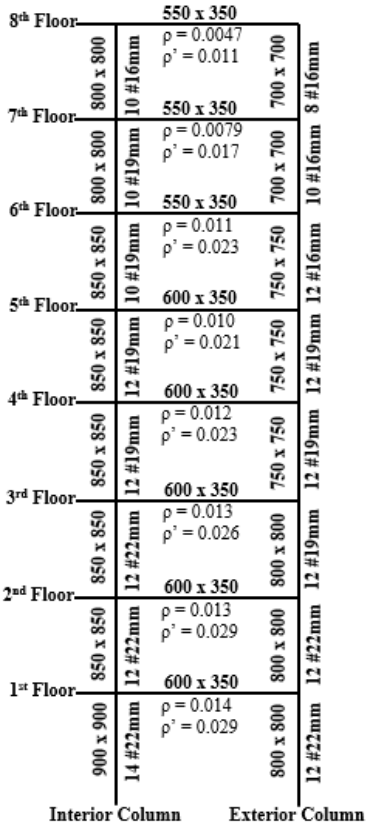

Fig. 9 Colum-beam properties of MI-S

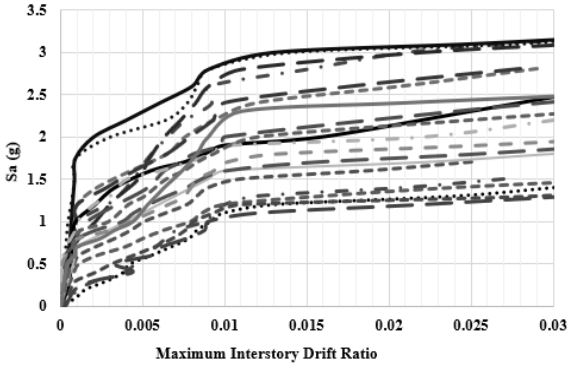

Fig. 10 IDA curve of MI-1(T_1=1.35sec)

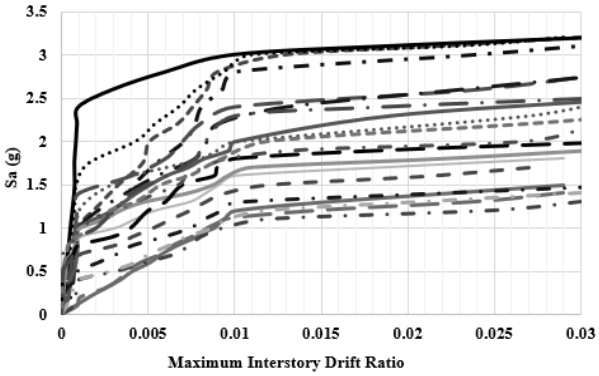

Fig. 11 IDA curve of MI-4 (T_1=1.35sec)

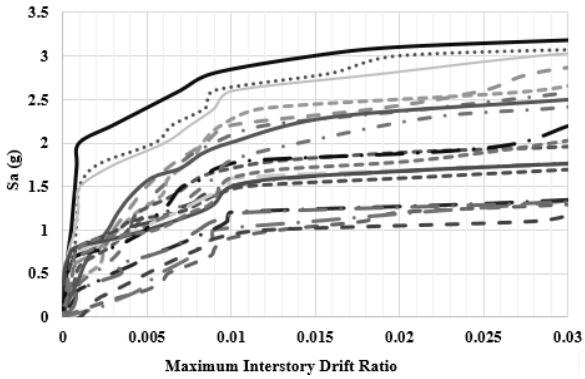

Fig. 12 IDA curve of MI-8 (T_1=1.35sec)

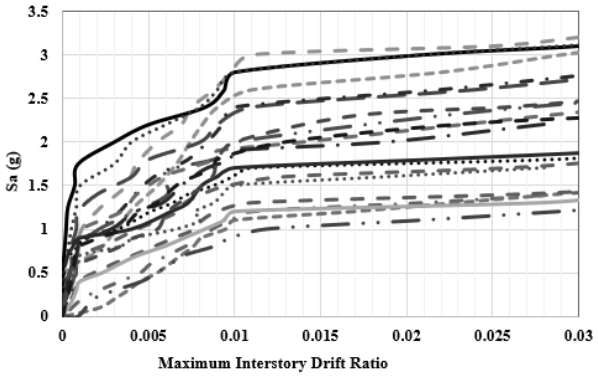

Fig. 13 IDA curve of MI-S (T_1=1.35sec)

5. CONCLUSIONS

The main objective of this study is to predict seismic performance of mass irregular and regular RC-SMF designed by PBPD method. The seismic responses from time history analysis are shown through IDA curves. The seismic performance of all four structure achieved the target performance hence it validated the PBPD method. The study needs to be extended for more cases and needs comparison with code based designed structure in order to get most suitable method for practice. The mass irregularity effects up to mid-floor has less chance of collapse than top floor. The interstory drift and collapse probability at spectral acceleration 1.5g is very low, but as spectral acceleration increased the collapse probability elevates highly.

REFERENCES

ACI 318-14 (2014). Building Code Requirements for Structural Concrete. American Concrete Institute, Michigan. doi:10.14359/51688187

ASCE/SEI 7-16 (2017). Minimum Design Loads and Associated Criteria for Buildings and Other Structures. American Society of Civil Engineers, Reston. doi:10.1061/9780784414248

Chan-Anan W, Leelataviwat S, Goel SC (2016) Performance-based plastic design method for tall hybrid coupled walls. Struct Design Tall Spec Build 25(14):681–699. doi:10.1002/tal.1278

Chang GA, Mander JB (1994) Seismic Energy Based Fatigue Damage Analysis of Bridge Columns: Part I– Evaluation of Seismic Capacity. Technical Report NCEER-94-0006, State University of New York, Buffalo.

Chao SH, Goel SC, Lee SS (2007) A Seismic Design Lateral Force Distribution Based on Inelastic State of Structures. Earth Spect 23(3):547–569. doi:10.1193/1.2753549

Chao SH, Goel SC (2005) Performance-Based Seismic Design of EBF Using Target Drift and Yield Mechanism as Performance Criteria. Technical Report UMCEE 05- 05, Department of Civil and Environmental Engineering, University of Michigan, Michigan.

Chao SH, Goel SC (2006) Performance-Based Plastic Design of Seismic Resistant Special Truss Moment Frames (STMF). Technical Report (UMCEE 06-03). Department of Civil and Environmental Engineering, University of Michigan, Michigan.

Chao SH, Goel SC (2008) Performance-Based Plastic Design of Special Truss Moment Frames. AISC Eng J 45(2):127-150.

Chopra AK, Goel GK (2004) A modal push over analysis procedure to estimate seismic demands for unsymmetric-plan buildings. Earth Eng Struct Dyn 33:903-927.

FEMA/P695 (2009) Quantification of Building Seismic Performance Factors. Federal Emergency Management Agency, Washington DC.

Filippou FC, Popov EP, Bertero VV (1983) Effects of Bond Deterioration on Hysteretic Behavior of Reinforced Concrete Joints. Technical Report EERC 83-19, Earthquake Engineering Research Center, University of California, California.

Lee SS, Goel SC (2001) Performance-Based Design of Steel Moment Frames Using Target Drift and Yield Mechanism. Technical Report UMCEE 01-17, Department of Civil and Environmental Engineering, University of Michigan, Michigan.

Leelataviwat S, Goel SC, Stojadinovic B (1999) Toward Performance-Based Seismic Design of Structures. Earth Spect, 15(3):435-461.

Liao WC, Goel SC (2014) Performance-Based Seismic Design of RC SMF Using Target Drift and Yield Mechanism as Performance Criteria. Adv Struct Eng 17(4):529-542.

Mander JB, Priestley MJN, Park R (1988) Theoretical Stress-Strain Model for Confined Concrete. J Struct Eng ASCE 114(8):1804-1826. Moehle JP, Mahin SA (1991) Observations on the Behavior of Reinoforced Concrete Buildings during Earthquakes. American Concrete Institute SP-127:67-90.

Neuenhofer A, Filippou FC (1997) Evaluation of Nonlinear Frame Finite-Element Models. J Struct Eng ASCE 123(7):958–966. doi:10.1061/(asce)0733-9445(1997)123:7(958)

OpenSees version 2.5.0 (2019) Pacific Earthquake Engineering Research Center, California. (**Software)** PEER (2018) Earthquake Data. Pacific Earthquake Engineering Research Center, California. https://ngawest2.berkeley.edu/ (**Data**)

PUSKIM (2018) Response spectrum of different type of soil in Indonesia. http://puskim.pu.go.id/Aplikasi/desain_spektra_indonesia_2011/ (**Data**)

Scott MH, Fenves GL (2006) Plastic Hinge Integration Methods for Force-Based Beam–Column Elements. J Struct Eng 132(2):244–252. doi:10.1061/(asce)0733-9445(2006)132:2(244)

SEAOC Blue Book (1999) Recommended lateral force requirements and commentary. Structural Engineers Association of California, California

SEAOC Vision 2000 (1995) Performance Based Seismic Engineering of Buildings. Structural Engineers Association of California, California.

Seismosignal version 2018 (2018) Seismosoft Ltd. Italy. (**Software**)

Stefano MD, Pintucchi B (2008) A review of research on seismic behaviour of irregular building structures since 2002. Bull Earth Eng 6:285–308.

Vamvatsikos D, Cornell CA (2002) Incremental dynamic analysis. Earth Eng Struct Dyn 31(3):491–514. doi:10.1002/eqe.141

Proceedings of the 5th International Conference on Civil Engineering for Sustainable Development (ICCESD 2020), 7~9 February 2020, KUET, Khulna, Bangladesh (ISBN-978-984-34-8764-3)

EFFECTS OF SUGARCANE BAGASSE ASH ON PROPERTIES OF STRUCTURAL MORTAR

Rashidul Hasan[1], Nazmus Sakib[2], Rakib Hasan[3], Md. Saiful Islam[4] and Tanver Hasan[5]

[1]Department of Civil Engineering, Bangladesh Army University of Engineering & Technology, Bangladesh, e-mail: mrhasanraj@gmail.com
[2]Department of Civil Engineering, Bangladesh Army University of Engineering & Technology, Bangladesh, e-mail: sakib.khs@gmail.com
[3]Department of Civil Engineering, Bangladesh Army University of Engineering & Technology, Bangladesh, e-mail: rhsaj94@gmail.com
[4]Department of Chemistry, Bangladesh Army University of Engineering & Technology, Bangladesh, e-mail: msaifuli2007@gmail.com
[5]Department of Civil Engineering, Bangladesh Army University of Engineering & Technology, Bangladesh, e-mail: tanvertuhin87466t@gmail.com

***Corresponding Author**

ABSTRACT

This paper depicts the possibility of utilizing Sugarcane Bagasse Ash as supplementary cementations material in mortar. The use of supplementary cementing materials has become an integral part of preparing high strength and high-performance structural mortar. Sugarcane bagasse ash (BA) is a by-product of sugar factories that found after burning sugarcane bagasse. It is found after the extraction of all economical sugar from sugarcane. Bagasse ash, comprising a high percentage of silica (SiO_2), is considered as a sensible pozzolanic material with non-reactive behavior and has the potential to be used in replacement of cement in the production of concrete and mortar. Bagasse ash (BA) with high fineness is a good pozzolanic material and its reactivity depends on the degree of crystallinity of silica, the presence of impurities, particle size, and fineness. In this study, bagasse ash (BA) is used as partial replacement of cementitious material in preparation of cement mortars. Substitution of cement with pozzolanic materials (BA) (up to 30%) in structural mortar is used in this research and the setting time, chemical properties of bagasse ash, Strength Activity Index (SAI), Compressive strength of mortar, the durability of mortar (sorptivity, Chloride penetration test) are determined. The outcomes of these tests demonstrate that, this Bagasse Ash can be used as a pozzolanic material to replace a part of cement in concrete or structural mortar and also facilitates to cope with environmental concerns through reduction of sugar industry waste material.

Keywords: *Bagasse ash, Structural mortar, Pozzolanic material, Sugarcane bagasse, crystallinity.*

1. INTRODUCTION

All over the world are focusing on ways of utilizing either industrial or agricultural wastes as a source of raw materials for the construction industry. These wastes utilization would not only be economical, but may also help to create a sustainable and pollution free environment. The utilization of waste materials in concrete manufacture provides a satisfactory solution to some of the environmental concerns and problems associated with waste management (Biricik, Akoz , Berktay, Tulgar 1999). Ordinary Portland cement is recognized as a major construction material throughout the world. Portland cement is the conventional building material that is responsible for about 5% - 8% of global CO_2 emissions. This environmental problem will most likely be increased due to the exponential demand of Portland cement. Researchers all over the world today are focusing on ways of utilizing either industrial or agricultural waste, as a source of raw materials for industry. Currently, there has been an attempt to utilize a large amount of bagasse ash, the residue from an in-line sugar industry and the bagasse-biomass fuel in the electric generation industry. When this waste is burned under controlled conditions, it also gives ash having amorphous silica, which has pozzolanic properties (Cook JD. 1986). A few studies have been carried out on the ashes obtained directly from the industries to study pozzolanic activity and their suitability as binders, partially replacing cement. Therefore, it might possible to use sugarcane bagasse ash (SCBA) as cement replacement material to improve quality and reduce the cost of construction materials such as mortar, concrete pavers, concrete roof tiles, and soil cement interlocking block, etc. This waste utilization would not only be economical but may also result in foreign exchange earnings and environmental pollution control.
Meanwhile, Bagasse ash is useful for its light weight, high strength, durability and workability of concrete, it contains a high amount of silica (87%) and is a valuable pozzolanic material for making ceramic products (Dyna 2010). Though its cost is almost equal to fly ash but bagasse ash reduces negative environmental effect and landfill volume. Countries like Bangladesh, India grow a lot of sugarcane to produce sugar. Bagasse Ash is a by-product of the sugar production industry. Excess amount of bagasse ash is nowadays damping into landfill sites, which is a major threat to the environment (Mehta PK 1992; Tayyeb Akram, Shazim Ali Memon, Humayun Obaid 2009). Therefore, an alternative to disposeing of this ash needs to be investigated. As, this ash posses pozzolanic property, it can be used to replace a part of cement in the production of mortar and concrete. Optimum replacement of cement by locally produced bagasse ash in mortar and concrete has not been studied previously. Durability properties of mortar have also not been studied. Therefore, a study is necessary to fulfill this gap in scientific knowledge (James J, Subba Rao M. 1986).

The main objective of this investigation is to evaluate the possibility of utilizing Sugarcane Bagasse Ash as supplementary cementation material in mortar.

2. METHODOLOGY

For determining the expected results some procedures are followed. Materials preparation and laboratory experiments were performed sincerely for evaluating the expected result. The standard river sand was used as fine aggregate for the preparation of mortar. Here is a methodological structure for this thesis work.

I. The experiment work was divided into three steps:
II. First Step
    Grinding of BA (using Los Angles Ball mill)
    Preparation of mortar (BA is mixed with cement)
III. Second Step
    Mix Design (The mixes were produced by replacing OPC with 5%, 10%, 15%, 20%, 25% and 30% of BA by weight of cement, using Hobart mixture machine for mixing). Preparation and curing of specimens.
IV. Third Step

➢ **Experimental Investigations**

Strength activity index, initial and final setting time, SSD and Dry density, Sorptivity, durability test. For all mixes, 50mm length, 50mm width and 50 mm height of square specimens were casted for compressive strength testing. They were tested at the ages of 7, 14, 28 and 56 days. The reported results are the average of three samples. The compressive strength of the mortar cube (50 mm x 50 mm x 50mm) was determined according to the BSEN196-1testing standard by using a Universal testing machine (UTM).For the durability test same specimens (50 mm x 50 mm x 50mm) were prepared and kept those specimens for curing in 20% NaCl water to find out the mass and strength loss.

Figure 1: Methodological Structure

3. RESULT AND DISCUSSION

3.1 The Microstructure of Baggage Ash

The Scanning Electron Microscope (SEM) analysis was done according to the 30KV VP-SEM method in Bangladesh Council of Scientific and Industrial Research (BCSIR). Normally ash's SEM pic looks like a sponge. But due to uncontrolled burning, it doesn't look like a sponge (Porous body). That also confirms that the ash is crystalline in nature. So, no chemical reaction is expected. But pozzolanic action will be governed by filler action in this case.

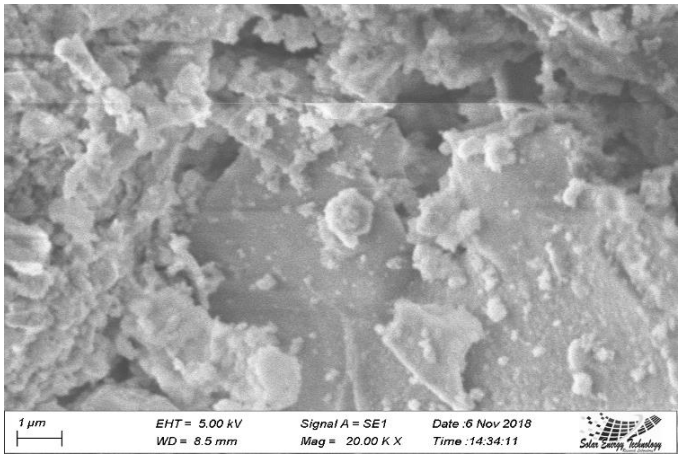

Figure 2: SEM image for baggage ash

3.2 Compressive Strength:

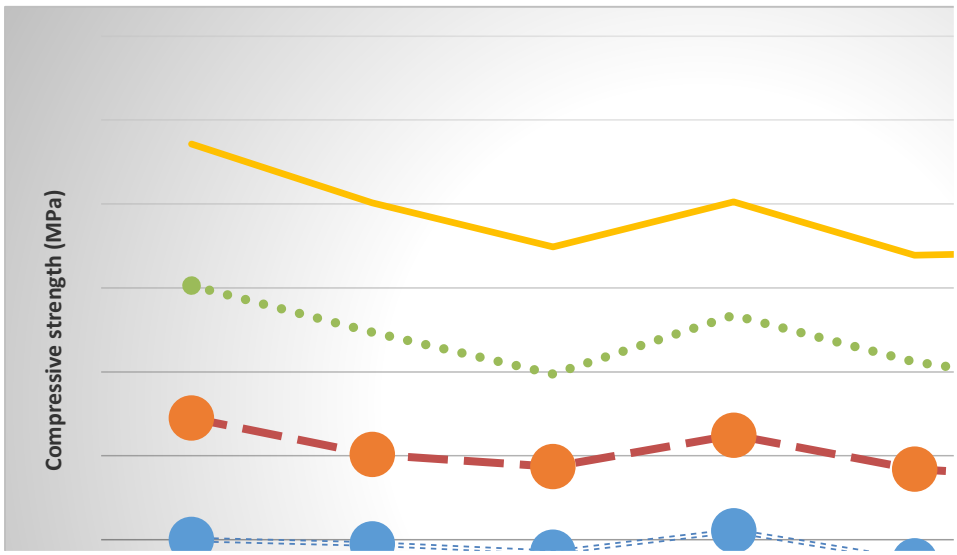

Figure 3: Compressive strength of mortar

According to the values of compressive strength it can be said that 25 and 30 % gives higher strength at 56 days that are comparable to the control mix. Therefore, in terms of strength up to 30 % replacement can be done. Point to be noted that, moreover sometimes the value of replacement of bagasse ash is above from the control mixing which proves that bagasse can be used as alternative cementations or filler material.

3.3 Setting Time:

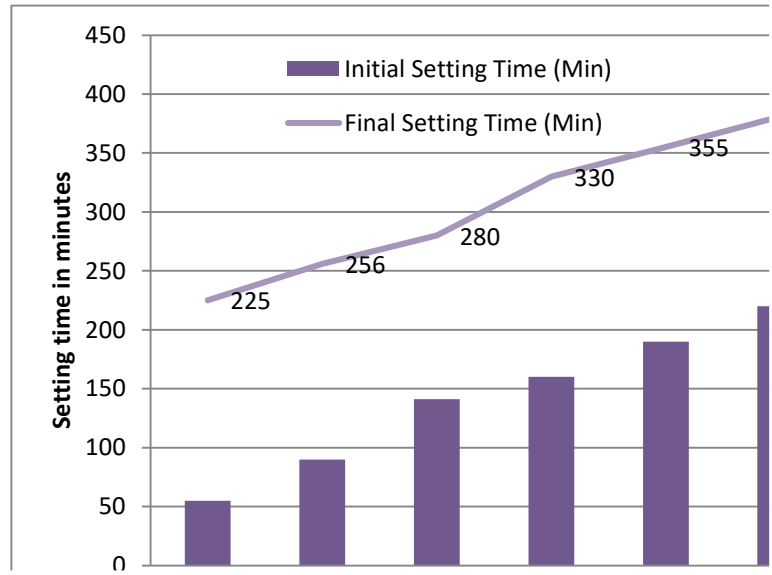

Figure 4: Initial and final setting times of BA blended cement paste

In the study of setting time, it is clear that, when the amount of bagasse ash is increased in the replacement of cement, the initial and final setting time increases gradually. Most of the pozzolanic materials cause a delay in the hydration process, thus increase the setting time. To improve this condition, controlled burning of ash is required.

3.4 Compressive Strength of Chloride Environment Specimens (28 Days):

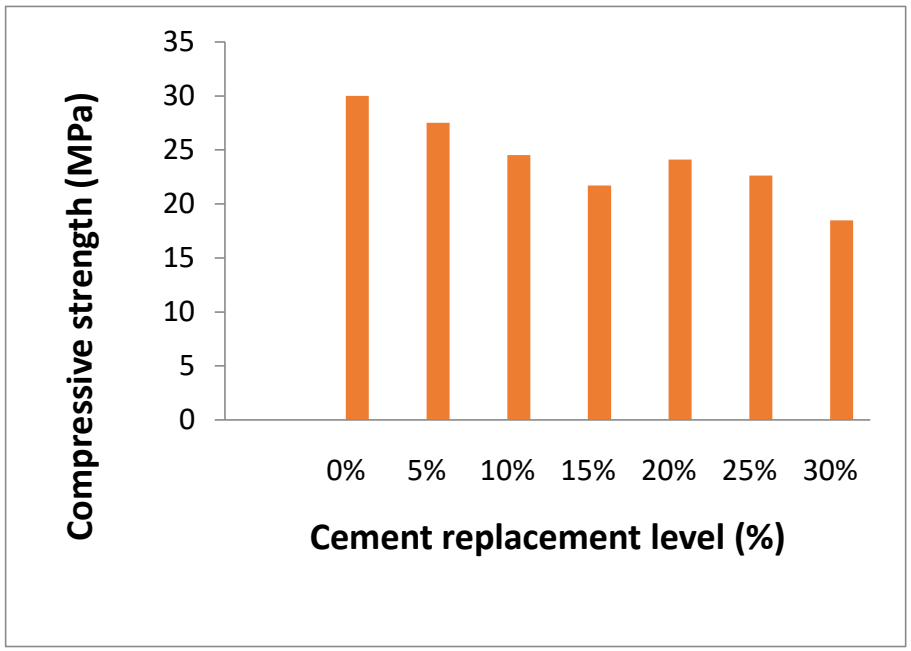

Figure 5: Compressive Strength in Chloride Environment

The graph of the compression test in a chloride environment shows that the strength in the specimen reduces. The 28 days tests result in decreases from the other compressive strength test. Also, mass loss was observed.

4. CONCLUSIONS

From this study, the following conclusions can be made:

i. In the study of setting time, it is clear that, when the amount of bagasse ash is increased in the replacement of cement, the initial and final setting time increases gradually. Most of the pozzolanic materials cause a delay in the hydration process, thus increase the setting time. To improve this condition, controlled burning of ash is required. It seems that after an increase of bagasse ash about 15% the workability is not okay because that increase the standard setting time which is not viable for concrete and mortar work.

ii. Normally, compressive strength decreases with the increase in cement replacement percentage. However, 15% cement replacement with baggage ash showed up to 90% strength compared to the control specimens. This might be due to the pozzolanic effect of baggage ash governed by the filler effect. This effect is pronounced at a later age of 56 days, where the mortar specimen with even 30% replacement of cement achieved up to 96% strength as compared to the control mortar. At 7, 14, 28 and 56 days, the relative increase in strength decreases therefore, in terms of strength up to 30 % replacement can be done.

iii. Density should decrease with the increase in replacement percentage. Because the unit weight of baggage ash is likely to be less than the unit weight of cement. From the density (Table-4) determined in the result it is clear that, when the amount of bagasse ash increase in the cement replacement then the density reduces.

iv. For the durability test by comparing to the mass loss of control specimens to other replacement specimens it is seen that the control specimen losses the most amount of its weight. The weight loss of two specimens of control mixture varies from 6 to 7gm where as other replacement ratios losses 4 to 5gm of its weight. Therefore, it can be said that, the mass loss of control specimens is the most.

v. The addition of bagasse ash in mortar and concrete is an acceptable way to utilize BA ash as alternative cementitious material instead of sending it to landfill. With the addition of bagasse ash, mortar properties changed to a positive way and some of the stages increased the strength of mortar. So, it is good to use in construction work rather than sending it to landfills.

From the present investigation, finally the following conclusion can be drawn, up to 20% of ordinary Portland cement can be optimally replaced with well-burnt bagasse ash without any adverse effect on the desirable properties of mortar.

ACKNOWLEDGMENTS

The authors would also like to express their sincere appreciation and deepest gratitude to Dr. A. B. M. Amrul Kaish, Lecturer (Structural Engineering and Construction Materials), of the Department of Civil Engineering, Infrastructure University Kuala Lumpur (IUKL). Without his continuous guidance, this thesis work would have not been finished.

REFERENCES

Biricik H, Akoz F, Berktay I, Tulgar AN (1999). “Study of pozzolanic properties of wheat straw ash.” CemConcr Res; 29:637–43.

Cook JD. (1986) Rice husk ash. In: Swamy RN, editor. Concrete technology and design. Cement replacement material, 3. London: Surrey Uni-versity Press; p. 171–95.

Dyna, (2010) Sugarcane bagasse ash as a partial-portland-cement replacement material, Universidad Nacional de Colombia,Colombia. vol. 77(163), 47-54

Mehta PK (1992). Rice husk ash – A unique supplementary cementing material. In: Malhotra VM, editor. Proceeding of the international symposium on advances in concrete tech, Athens, Greece; P.407–30.

Tayyeb Akram, Shazim Ali Memon, Humayun Obaid, (2009). Production of low-cost self-compacting concrete using bagasse ash, Construction and Building Materials 23, 703–712, www.elsevier.com/locate/conbuildmat

James J, Subba Rao M. (1986) Silica from rice husk through thermal decomposition, Thermochim Acta, vol. 97. Amsterdam: Elsevier Science; p. 329–36.

Proceedings of the 5th International Conference on Civil Engineering for Sustainable Development (ICCESD 2020), 7~9 February 2020, KUET, Khulna, Bangladesh (ISBN-978-984-34-8764-3)

COMPARATIVE STUDY BETWEEN RECTANGULAR AND SPECIALLY SHAPED R.C. COLUMN ON SEISMIC RESPONSE FOR MULTISTORIED BUILDING

Md. Rashedur Rahman*[1], Tohur Ahmed [2] and Afia Anjum Ulka Mony[3]

[1]Department of Civil Engineering, Rajshahi University of Engineering & Technology, Bangladesh e-mail: rashedurrahman114@gmail.com
[2]Professor, Department of Civil Engineering, Rajshahi University of Engineering & Technology, Bangladesh, e-mail: tohurruet@gmail.com
[3]Department of Civil Engineering, Rajshahi University of Engineering & Technology, Bangladesh, email: monyulka@gmail.com

***Corresponding Author**

ABSTRACT

In a RC building, columns are structural elements that are predominantly subjected to axial load,and moments, and transfers them from the super structure to the substructure. Various shapes of the columns are used. Some common shapes are square, rectangular, circular columns and some special shapes of columns are L-shaped, T- shaped and plus (+) shaped columns, which are not commonly used but gives more indoor space than commonly used shapes of column. Specially shaped columns avoid obstructions in a room which increases usable floor area. The objective of this study is to assess the comparative seismic and wind performance of buildings with Rectangular columns and buildings with specially shaped columns of a multistoried building. The proposed building is analyzed using equivalent static analysis for zone II in Dhaka city. The parameters are considered moment of inertia of column, maximum story drift, lateral displacement etc. The Bangladesh National Building Code (BNBC), 2006 has been considered in the computer aided analysis performed by ETABS 2016. Seismic analysis was performed by equivalent static force method. Based on the results, calculations are drawn showing the effectiveness of different shapes of the column under the effect of seismic loads.

Keywords: *Rectangular column, Special shape column, Seismic analysis, lateral displacement, Drifts.*

1. INTRODUCTION

It is the prime duty of a civil engineer to ensure safety to the life of occupants of a building by replacing conventional construction practices by modified techniques so that huge population can be accommodated in given area and large commercial space can be created in a confined area for upgrading the living environment. So, it is important to replace conventional construction practices with modified one. Buildings, which are generally designed for office, institutional or commercial use, are among the most distinguished space definitions in the architectural history of urbanization in the twentieth century. They are primarily a reaction to the rapid growth of urban population and the demand by business activities to be as close to each other as possible. Many researches and studies have been done in order to mitigate excitations and improve the performance of buildings against lateral load. Columns play very important role in buildings because total load is transferred through columns. (Gumble, 2015) Various shapes of columns are used in the construction such as rectangular columns, Square columns, circular columns, T-shaped columns, L-shaped columns, Cross (+) shape columns, where Rectangular, Square and Circular columns are called as Regular columns and T-shape columns, L-shape columns, Cross (+) shape columns are called as specially shaped columns. (Yang, 2008)

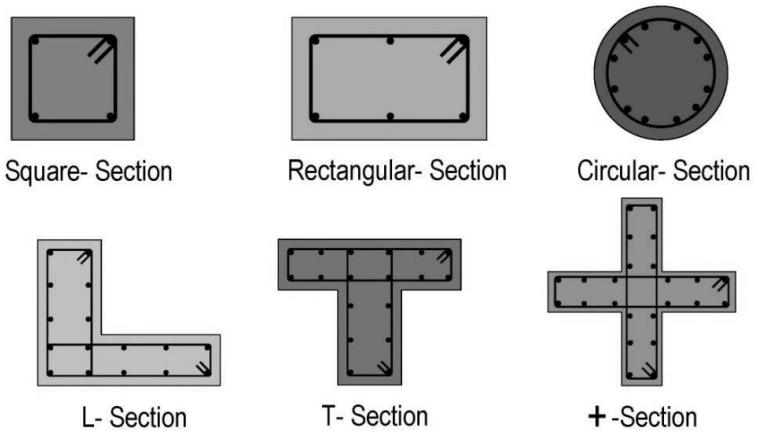

Figure 1: Section of column with lateral and longitudinal reinforcement

This project involves the numerical analysis of effect of column shape on the response to wind and earthquake load and makes a comparison of rectangular column shaped building & special column shaped building by using ETABS software and also checks out the specification detailed in BNBC 2006.

2. METHODOLOGY

A 20 storied arbitrary building with plan area of 4144 sq. ft is considered for this study. The models are of same plan area and same height. The material properties of the models are also same.Total analysis has been performed by ETABS, the leading structural design and analysis-based software. Here total loading is applied as distributed loading. Modeling is performed with great care. All model maintains same area and heights. Before analyze the models, the models are re-checked once again.

2.1 SPECIFICATION OF MODEL COMPONENTS

Table 1 has information about column sizes and Table 2 is about the material properties used at the building.

Table 1: Specifications of model components

Model component	**Specification**
Square column	Total depth-24in, Total width-24in
L shaped column	Total depth-40in Total width—40in Horizontal and Vertical leg thickness-8in
T shaped column	Total depth-40in Total width-40in Flange and Web thickness-8in
Cross (+) shaped column	Total depth-40in Total width-40in Flange and Web thickness-8in

Table 2: Material properties

Concrete	Grade of concrete	3 ksi
Steel	Grade of steel	60 ksi

Figure 2 has the plan and 3D view of the model building that was used for the analysis. The Plan was done using AutoCAD software.

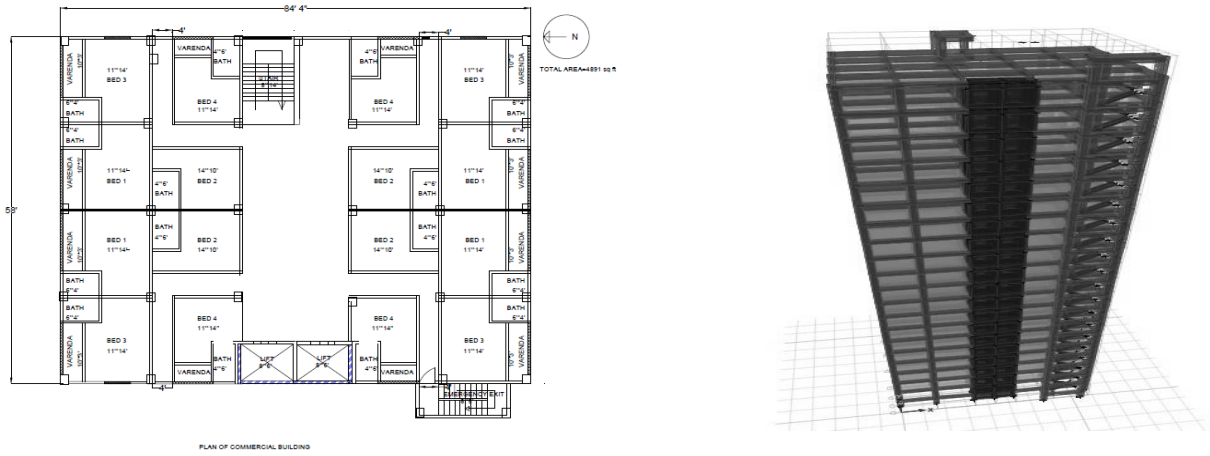

Figure 2: Plan view and 3D model of the building

2.2 ANALYSIS AND RESULT

2.2.1 CASE 1

In this case usual building is considered as specified in above. Column size considered 24" x 24". Plan of the building is show

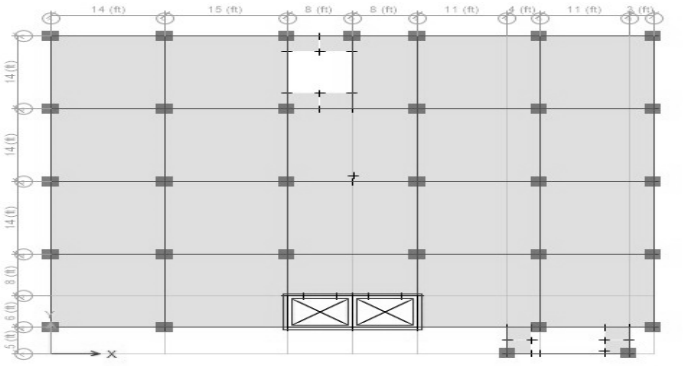

Figure 3: Plan view of rectangle shaped column

2.2.2 CASE 2

In this case square column is changed into specially shaped column. Plan of the building is shown in figure 4.

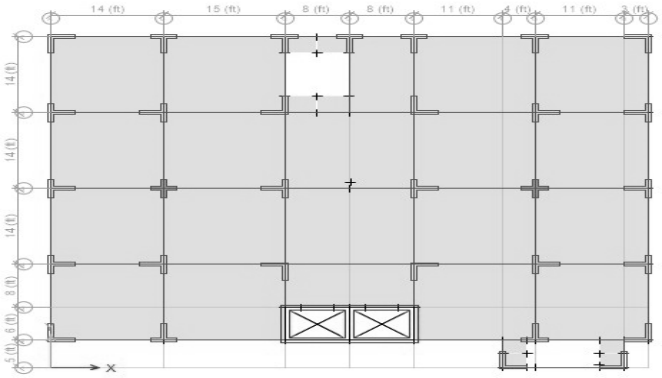

2.3 SIESMIC LOAD

For seismic analysis, the equivalent static force method is used in this paper.In BNBC Bangladesh has been divided into three seismic zones based on the possibility of severe intensity of seismic ground motion. These are: Zone I, Zone II& Zone III (Fig.1). Zone III is the most severe zone among these zones. (BNBC,2006)

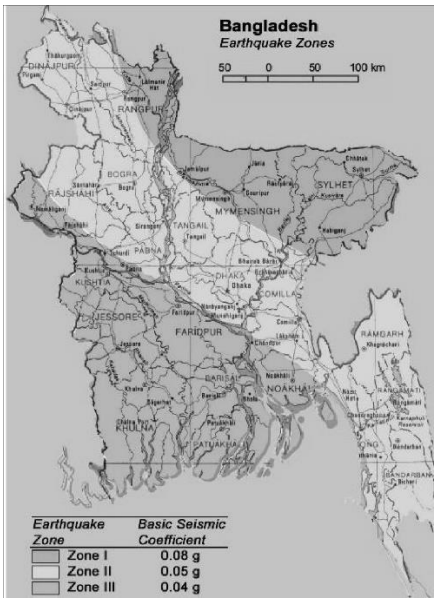

Figure 5: Earthquake zone in Bangladesh

Dead load includes the self-weight of the building components. Live loads are taken from BNBC. The selected city is Dhaka. According to seismic zoning map of Bangladesh, Dhaka is under zone II. The total load calculations have been done as per BNBC 2006. The corresponding equations are as follows:

$$V = \frac{ZIC}{R} W \quad (1)$$

Where, V=Base Shear,
Z= Seismic zone coefficient,
I= Structure importance coefficient,
R= Response modification coefficient,
W= Total dead load +some specified live load
C= Numerical coefficient

$$C = \frac{1.25S}{T^{2/3}} \quad (2)$$

S= Site coefficient for soil characteristics
T= Time period
And $T = (h_n)^{3/4}$ (3)
h_n = height of the building

2.4 LOADING

The created model is subjected to uniformly distributed load which are provided to its intensity. Loading parameters are:

•Dead load
•Live load
•Self-weight

•Seismic load

Table 3: Vertical load

Dead load	**Self-weight**	**Program calculated automatically**
	Floor finish	25psf
	Wall load	.5 k/ft
	Parapet wall load	.15k/ft
	Partition wall	30psf
Live load	On floor	60psf
	On stair	100psf

2.5 ANALYSIS

After creating the model, the structure is ready to be analyzed. Before the analysis all the systems, properties and loading conditions are rechecked once again. Reaction, moment, displacements and story drift are obtained from this analysis

3 RESULT AND DISCIUSSION

Analysis for all the building models are carried out. After the analysis performed corresponding results have been obtained. The results are shown in tabular, bar-chart and graphical form. From those table and chart, we can easily find out the variations between different models.

3.1 COMPARISON OF MOMENT OF INERTIA

Table 4: Moment of inertia comparison

Column shape	**Cross section area (in^2)**	I_X **(in^4)**	I_Y **(in^4)**
Square column	576	27648	27648
L shaped column	576	80440.89	80440.89
T shaped column	576	80440.89	44032
Cross(+) shaped column	576	44032	44032

From table 4, it is shown that the moment of inertia of L shaped column is highest. Then T shaped and cross shaped has higher value. Square column has the least moment of inertia. Moment of inertia does not affect the strength of section directly but it affects another property of section, radius of gyration. Which ultimately defines the strength of section.

3.2 MAXIMUM DISPLACEMENT DUE TO EARTHQUAKE LOAD

Load combination used for analysis $1.05DL+ 1.275LL+ 1.4E_{qx}$In X direction and for Y direction Load Combination used was $1.05DL+ 1.275LL+ 1.4E_{qy}$ (BNBC,2006)

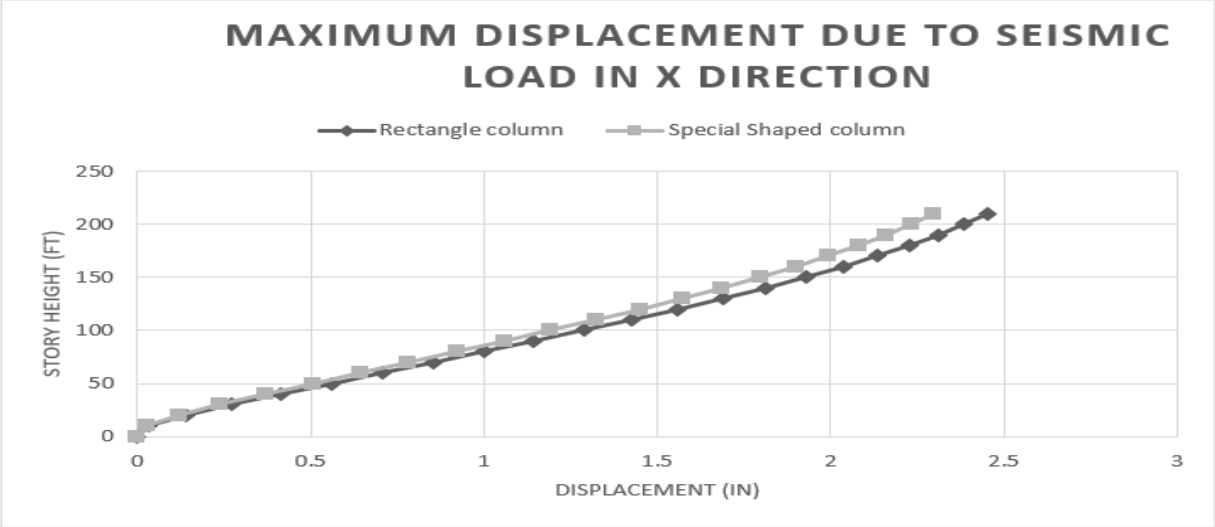

Figure 6: Variation of displacement of 20 story building along X

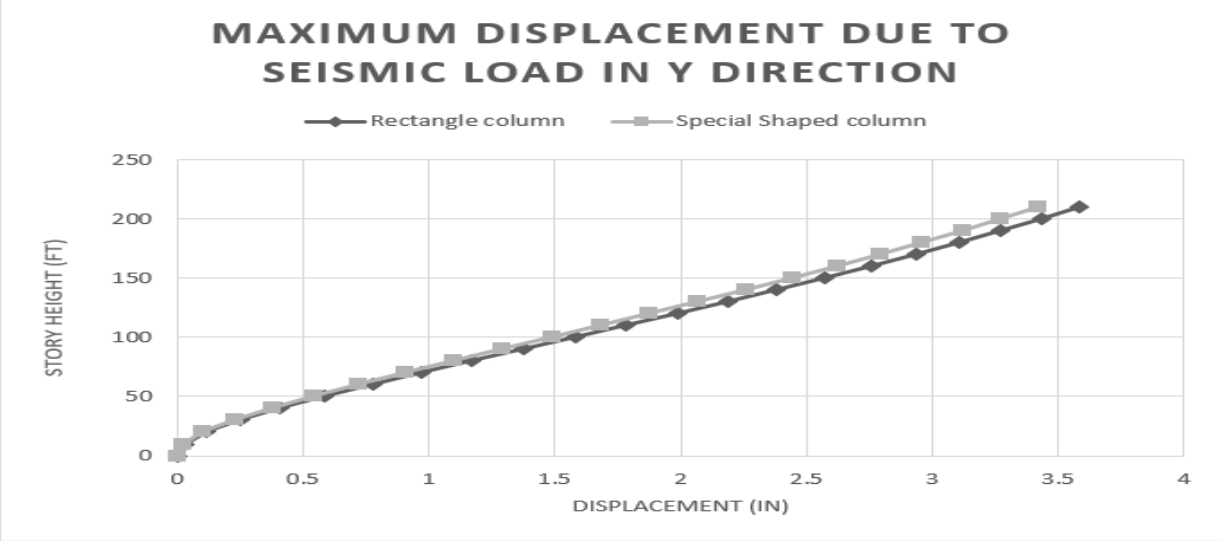

Figure 7: Variation of displacement of 20 story building along X

The figure 7 & 8 shows that with the increment of story height, the displacement due to seismic load in X direction and Y Direction increases non-linearly. It is clearly seen that the displacement is lower for the special shaped column than the rectangular shaped column

3.3 STORY DRIFT DUE TO EARTHQUAKE LOAD

Story drift is the difference of displacement between two consecutive stories divided by the height of that story. Mathematically, story drift at 20th floor= (displacement at 20th floor – displacement at 19th floor) / floor clear height

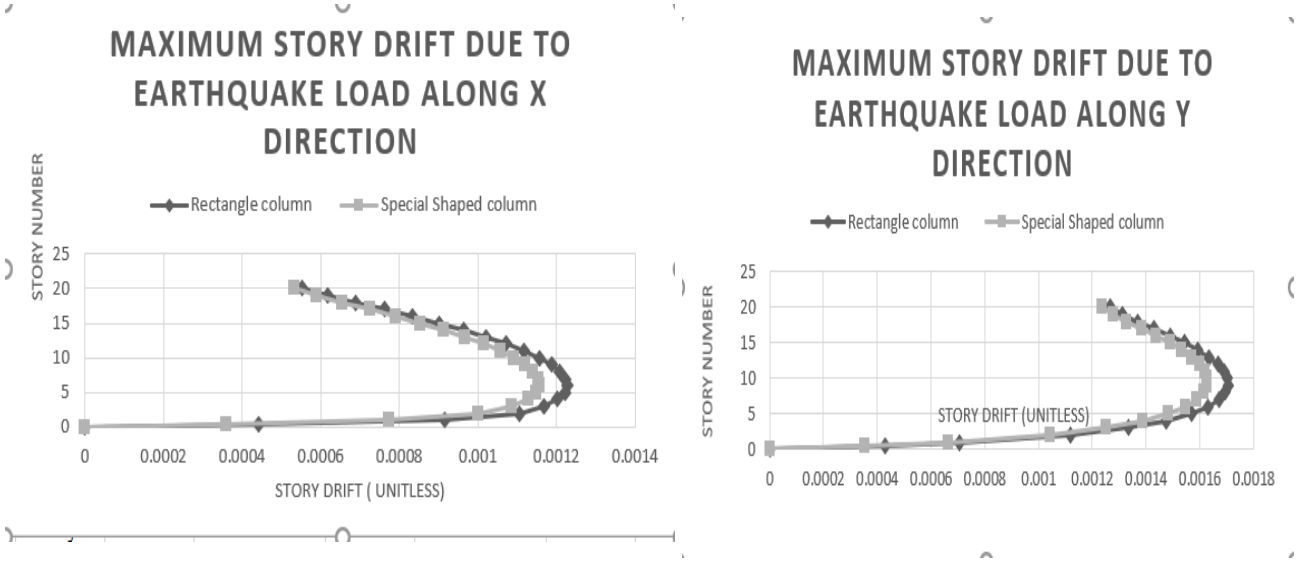

Figure 8: Variation of maximum story drift due to seismic load in X& Y direction

Since the mass is in Z direction, the cumulative mass increases from top to bottom story, story drift due to seismic load in X direction increases from top to bottom story. But due to fixed support at the bottom of the structure it becomes zero at base. The figure 9 shows that story drift is lower for special shaped column structure.

4. CONCLUSIONS

The buildings were analyzed by using"equivalent static force method" according to BNBC code. A numerical investigation is carried out to evaluate the effect of building shape on drift and displacement due to seismic load. From theresults, the following broad conclusions can be made in this respect:

1) Displacement depends on the relative stiffness of frame. In this study, displacement in rectangle column building is the highest due to seismic load. It is due to the fact that, Square column has the least moment of inertia. Moment of inertiaaffects another property of section, radius of gyration. Which ultimately defines the strength of section.
2) The special shaped column building is safer and considering all conditions the special shaped column
3) Story drift is in special shaped column structure is less then rectangular column structure
4) Specially shaped columns give more usable floor area at the corner of room as compared to rectangular column in R.C. structure. And no obstruction will be created by the offset of column in case of special shaped column

AKNOWLEDGEMENT

Special thanks to Professor Dr. Tohur Ahmed sir for guiding and helping throughout the process.

REFERENCE

Gumble, A. N., & Pajgade, P. S. (2015). Comparison Between Specially Shaped Columns And Rectangular Columns In RC Structure. *Development*, *2*(5).

Bangladesh National Building Code (BNBC) (2006)

Yang, P., Liu, H., & Huang, Z. (2008). A COMPARISON OF SEISMIC BEHAVIOR BETWEEN SPECIALLY SHAPED COLUMN FRAME STRUCTURE AND RECTANGULAR COLUMN FRAME STRUCTURES. *Beijing, China, October*, 12-17.

Chandurkar, P. P., & Pajgade, D. P. (2013). Seismic analysis of RCC building with and without shear wall. *International journal of modern engineering research*, *3*(3), 1805-1810.

Proceedings of the 5th International Conference on Civil Engineering for Sustainable Development (ICCESD 2020), 7~9 February 2020, KUET, Khulna, Bangladesh (ISBN-978-984-34-8764-3)

ANALYSIS AND DESIGN OF SPIRAL STAIR OF A HIGH RISE BUILDING SUPPORTED ON A CENTRAL COLUMN

Tanzima Fahmid*[1] and Tohur Ahmed[2]

[1]*Student, Rajshahi University of Engineering & Technology, Bangladesh, e-mail: raty280@gmail.com*
[2]*professor, Rajshahi University of Engineering & Technology, Bangladesh, e-mail: tohurruet@gmail.com*

***Corresponding Author**

ABSTRACT

Increased population densities due to migration of people from the countryside to the cities, combined with the rising price of developable land provide the urban planners with no better solution than to build higher. In recent decades, dwellers of Rajshahi city are constructing high rise buildings to support the current demand. Due to this increased population the demand of the number and capacities of egress routes are increased. Because of their attractive appearances and less space requirements spiral stairs become popular now-a-days. This paper involves analysis and design of a spiral stair which is supported on a central column subjected to gravity and lateral load on a 10 storied rectangular building of 93ft × 75ft size. The stair is modelled as a cantilever structure. Using the analysis results, comparative graphs are plotted among the maximum story displacements along axes (X axis and Y axis) and the permissible displacements according to BNBC 2006. It is found that the displacements are within the allowable limit. The stair is then designed and their reinforcement details are shown. It is needed to note that the central column diameter is not uniform. The diameter of spiral column is 26 inch up to story 2 and it is reduced to 20 inch in story 3 and further reduced to 16 inch in story 6 to make the design economic.

Keywords: *Spiral stair, Story displacements, Spiral column, Cantilever stairs.*

1. INTRODUCTION

The number of people especially in the cities is growing rapidly. With the increasing number of people, number of high rise building also increases simultaneously. As a result, population density in these buildings also increases. These highly populated buildings need maximum amount of exit points in the form of corridors, doors, stairways etc. In case of simple one storied building, it is very easy to evacuate the building but in case of high rise building which have floors above or below the ground, it is a very complicated case because of the vertical movement factor. Stair is the most essential element among all the exiting points in case of high rise or low rise buildings. In case of earthquake, fire accident, peak hours in a commercial building, market, office and business center, stair gives us an easy solution and makes things convenient for us. Stair can make a building more beautiful, attractive and most importantly it can make any building assembled.

Now-a-days spiral stairs are gaining popularity because of their attractive appearances and they require small amount of space. Because of their attractive appearances, they are found in many important commercial buildings besides residential buildings. Spiral column along with landing connected to main building frame provide sufficient rigidity to carry load. Therefore, extra supports are not required.

Two papers dealing with the subject has come to the attention of the author. In one paper (OVE ARUP and PARTNERS, 1959), it is confined to the particular case of simply supported column with stairs in the form of one complete turn of the spiral, and biaxial bending is not considered. In another paper, a method is proposed for the analysis of a central column supporting uniformly loaded cantilever stairs. Maximum resultant span moments obtained by means of the Newton-Raphson method are also given in tabular form (Rutenberg A., 1975). Here the purpose of this study is to analyze the stair subjected to gravity and lateral load and to design the spiral column, stair beams and stair. Comparison between the maximum story displacements along axes (X axis and Y axis) and the permissible displacements according to BNBC 2006 is also carried out.

2. METHODOLOGY

A 10 storied reinforced concrete building along with a spiral stair in its center was analyzed using ETABS 2016 software. After application of selected load patterns and load combinations according to BNBC 2006, the building was analyzed. With the analysis results, the maximum story displacements along X axis and Y axis were compared with the permissible displacements according to BNBC 2006 and the displacements were found within the allowable limit. The design of the stair was then carried out and their reinforcement details were shown. Table 1 represents the details of the building.

Table 1: Details of the building

Description	Parameter
Plan	93 ft × 75 ft
Story height	10 ft
Building type	Residential
Seismic zone	1
Basic wind speed	155 km/hr (Rajshahi)
Building column size	14 in × 14 in
Stair column diameter	i) Up to story 2 = 26 in ii) Up to story 5 = 20 in iii) Up to story 10 = 16 in
Beam size	i) Floor beam = 12 in × 18 in ii) Grade beam = 15 in × 21 in
Thickness of slab	5 in
Stair slab thickness	8 in
Compressive strength of concrete at 28 days	4000 lb/in^2
Maximum yield strength of rebar material	60000 lb/in^2
Minimum tensile strength of rebar material	90000 lb/in^2
Specification	BNBC 2006
Concrete Design Code	ACI 318-08

2.1 Modelling

A rectangular grid of 93ft with 7 bays along X-direction and 75ft with 5 bays along Y-direction has considered with height of about 10 stories. The stair is located at the middle of the plan. The stair is connected with the building by its landing only and there is no structural connection between the steps of the stair and the building. The stair has modelled as a cantilever structure where the central column supports the stair. The rotation angle of each flight of stair is 270°. Each flight consists of 20 steps having a turning angle of each step is 13.5°. The beams are located at the landing slab at the starting and ending of each flight. The columns of the building are rectangular while the central column of the spiral stair is circular.

Figures 1(a) and 1(b) represents the plan view and three dimensional view of 10 story building with spiral stair and Figure 1(c) represents the three dimensional view of 10 story spiral stair.

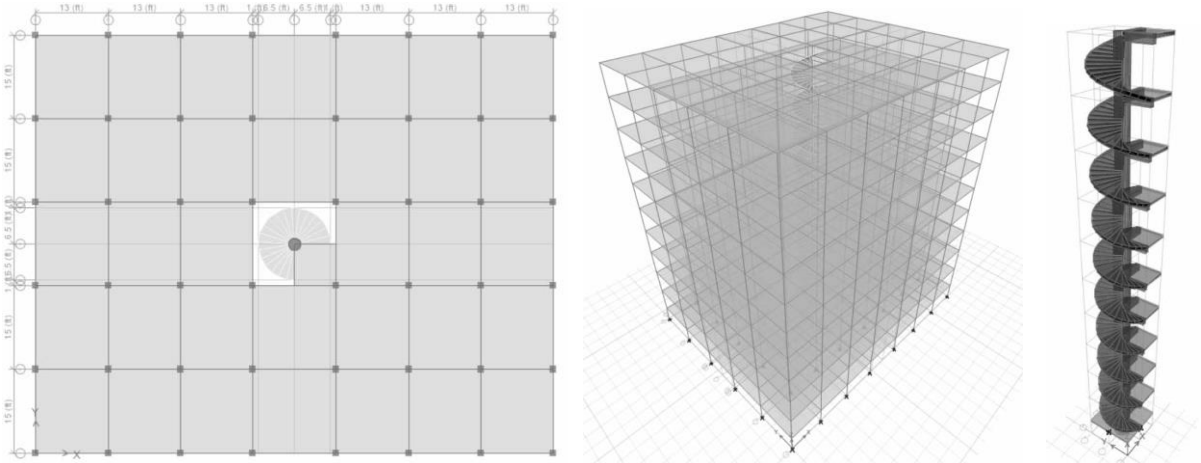

(a) (b) (c)

Figure 1: (a) Plan view of 10 story building with spiral stair, (b) Three-dimensional view of 10 story building with spiral stair, (c) Three-dimensional view of 10 story spiral stair

2.2 Load Patterns

The loads to be applied on the building are shown in Table 2.

Table 2: Selected load patterns

Load	Type	Applied load
Dead Load	Dead	Self-weight of stair
Building Live Load	Live	50 psf (BNBC 2006)
Stair Distributed Load	Live	100 psf (BNBC 2006)
Stair Concentrated Load	Live	1.05 k (BNBC 2006)
Handrail Load	Superimposed Dead	0.03 k (BNBC 2006)
Floor Finish	Superimposed Dead	30 psf (BNBC 2006)
Partition Wall Load	Superimposed Dead	30 psf (BNBC 2006)
Earthquake X	Seismic	According to BNBC 2006
Earthquake Y	Seismic	According to BNBC 2006
Wind Load X	Wind	According to BNBC 2006
Wind Load Y	Wind	According to BNBC 2006

2.3 Spiral Column Dimension

From the design, it has found that the spiral column diameter of 26 inch is adequate from GF to story 2 and 20 inch is adequate from story 3 to story 5. Again, the spiral column diameter of 16 inch is adequate from story 6 to story 10. So, the diameter of the spiral column is reduced to 20 inch in story 3 and further reduced to 16 inch in story 6 to make the design economic. As the total dimension of the staircase is uniform and the column diameter is not same throughout the total height of the building, so the width of the trade is not uniform, it varies with the distance from column face to the free end. The following are some of the modelling information of stair provided in Table 3.

Table 3**:** Modelling information of stair

Story	Column diameter in	Width of stair	Width of trade at column face in	Width of trade at free end in
Story 10	16	5'-10"	1.90	18.34
Story 9	16	5'-10"	1.90	18.34
Story 8	16	5'-10"	1.90	18.34
Story 7	16	5'-10"	1.90	18.34
Story 6	16	5'-10"	1.90	18.34
Story 5	20	5'-8"	2.40	18.34
Story 4	20	5'-8"	2.40	18.34
Story 3	20	5'-8"	2.40	18.34
Story 2	26	5'-5"	3.10	18.34
Story 1	26	5'-5"	3.10	18.34

3. ANALYSIS AND DESIGN

3.1 Analysis Results and Comparison

From the analytical analysis of the model the result of various parameters like lateral story displacement, story drift etc. are observed and the comparative study of maximum story displacement with respect to permissible story displacement according to BNBC 2006 has done. Story wise maximum displacements are shown in Table 4.

Table 4: Story wise maximum displacements

Story	Maximum story displacement according to BNBC 2006 in	Story displacement along X axis in	Story displacement along Y axis in
Story 10	4.80	1.156985	1.289929
Story 9	4.32	1.117233	1.270331
Story 8	3.84	1.055994	1.228851
Story 7	3.36	0.975456	1.163728
Story 6	2.88	0.878018	1.075609
Story 5	2.40	0.766038	0.964894
Story 4	1.92	0.642355	0.834220
Story 3	1.44	0.509508	0.682412
Story 2	0.96	0.369939	0.510522
Story 1	0.48	0.228098	0.324074

The maximum story displacement along X axis and Y axis occurred in the model are compared with the permissible maximum story displacement according to BNBC 2006 in Figures 2 and 3 respectively.

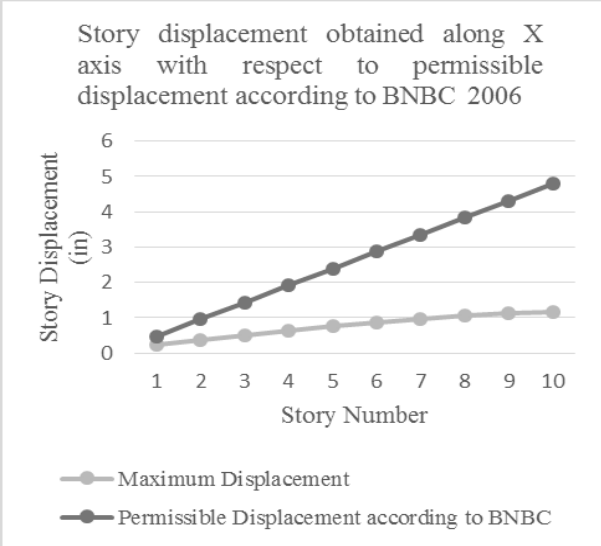

Figure 2: Story displacement along X axis

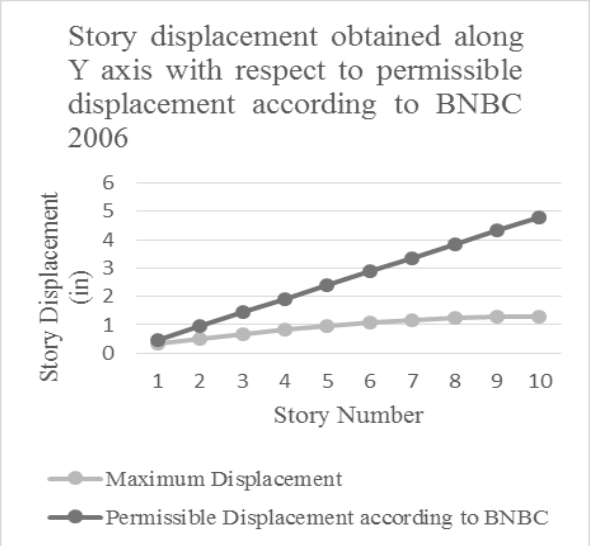

Figure 3: Story displacement along Y axis

From Figures 2 and 3, it is observed that the maximum story displacement along X axis and Y axis are less than the permissible value obtained from BNBC 2006. Also, story displacement along X axis and Y axis increases almost linearly with the increase of story height up to 10th story.

3.2 Design Considerations and Reinforcement Details

The design of spiral stair along with the beams and central column and their reinforcement details are as follows.

3.2.1 Design of Beam

The identification of beam is represented by the following Figure 4:

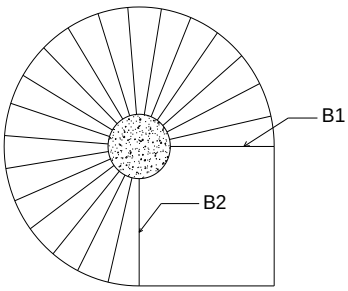

Figure 4: Identification of beam

The beam schedule is shown in Table 5 and typical reinforcement details of beams are shown in Figures 5 and 6.

Table 5: Concrete beam schedule

Beam ID	Story	Span length H	Section size			Longitudinal bars		Stirrup	Typical section
			Width in	Depth in	Effective depth in	Top bars A	Bottom bars B		
B1	Story 10	6'-10"	12	18	15.5	3#5	3#5	#3@6" c/c	1S
B2	Story 10	6'-10"	12	18	15.5	3#5	4#5	#3@6" c/c	2S
B1	Story 9	6'-10"	12	18	15.5	3#5	4#5	#3@6" c/c	2S
B2	Story 9	6'-10"	12	18	15.5	3#5	4#5	#3@6" c/c	2S
B1	Story 8	6'-10"	12	18	15.5	3#5	4#5	#3@6" c/c	2S
B2	Story 8	6'-10"	12	18	15.5	3#5	4#5	#3@6" c/c	2S
B1	Story 7	6'-10"	12	18	15.5	3#5	4#5	#3@6" c/c	2S
B2	Story 7	6'-10"	12	18	15.5	3#5	3#5	#3@6" c/c	1S
B1	Story 6	6'-10"	12	18	15.5	3#5	4#5	#3@6" c/c	2S
B2	Story 6	6'-10"	12	18	15.5	3#5	3#5	#3@6" c/c	1S
B1	Story 5	6'-8"	12	18	15.5	3#5	4#5	#3@6" c/c	2S
B2	Story 5	6'-8"	12	18	15.5	3#5	3#5	#3@6" c/c	1S
B1	Story 4	6'-8"	12	18	15.5	3#5	3#5	#3@6" c/c	1S
B2	Story 4	6'-8"	12	18	15.5	3#5	3#5	#3@6" c/c	1S
B1	Story 3	6'-8"	12	18	15.5	3#5	3#5	#3@6" c/c	1S
B2	Story 3	6'-8"	12	18	15.5	3#5	3#5	#3@6" c/c	1S
B1	Story 2	6'-5"	12	18	15.5	3#5	3#5	#3@6" c/c	1S
B2	Story 2	6'-5"	12	18	15.5	3#5	3#5	#3@6" c/c	1S
B1	Story 1	6'-5"	12	18	15.5	3#5	3#5	#3@6" c/c	1S
B2	Story 1	6'-5"	12	18	15.5	3#5	3#5	#3@6" c/c	1S
B1	GF	6'-5"	15	21	18.5	4#5	4#5	#3@4" c/c	3S
B2	GF	6'-5"	15	21	18.5	4#5	4#5	#3@4" c/c	3S

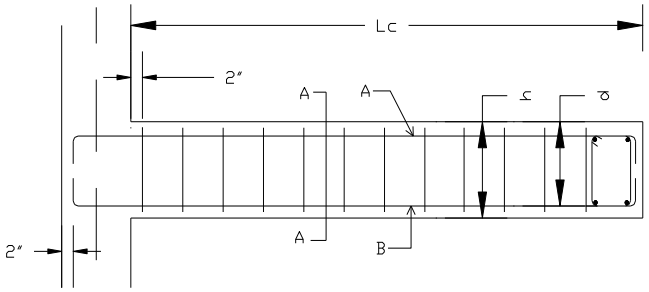

Figure 5: Typical concrete beam elevation

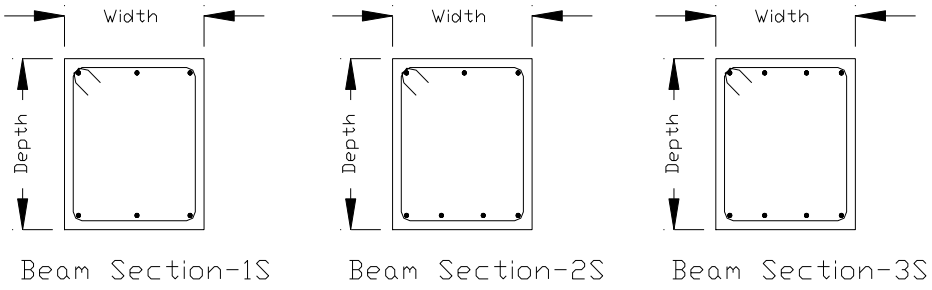

Figure 6: Typical concrete beam sections

3.2.2 Design of Spiral Column

The central column supports the stair and the beams. The column in each story is divided into three ties zone. Table 6 represents the column schedule and typical reinforcement details of column are shown in Figures 7(a) and 8(a). Reinforcement details of column and stair is shown in Figure 7(b). Figure 8(b) represents magnified view of lapping of column reinforcement.

Table 6: Concrete column schedule

Story	Length of ties zone A ft	Length of ties zone B ft	Length of ties zone C ft	Section	Reinforce-ment	Ties zone A	Ties zone B	Ties zone C
Story 10 Story 9 Story 8 Story 7 Story 6	1'-8"	6'-8"	1'-8"	C-C	12#5 bar	#3@4" c/c	#3@6" c/c	#3@4" c/c
Story 5 Story 4 Story 3	1'-8"	6'-8"	1'-8"	B-B	12#5 bar			
Story 2 Story 1 GF	2'-2"	5'-8"	2'-2"	A-A	12#6 bar			

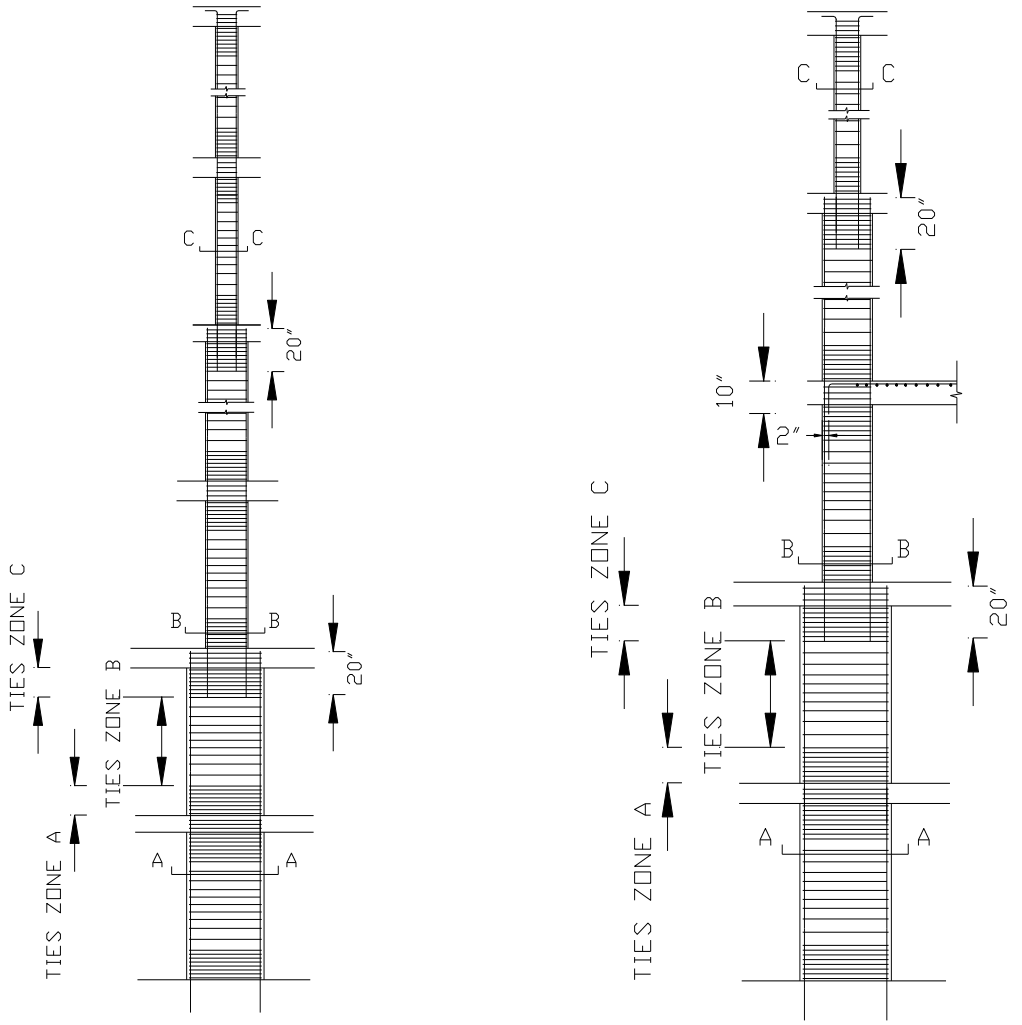

(a) (b)

Figure 7: (a) Reinforcement details of central column, (b) Reinforcement details of column with stair connection

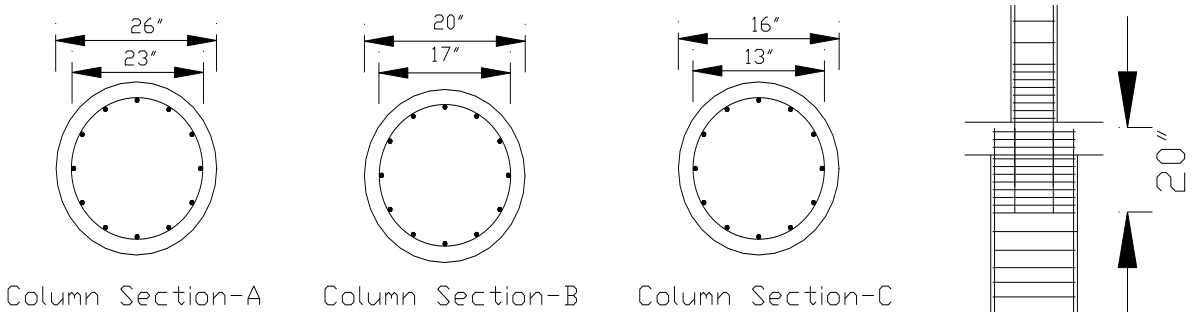

(a) (b)

Figure 8: (a) Reinforcement details of column sections, (b) Magnified view of lapping of column reinforcement

3.2.3 Design of Stair

In the design of stair, #4 bar is used as main reinforcement. The spacing of main reinforcement at various sections of stair are shown in Table 7 as follows.

Table 7: Spacing of main reinforcement (#4 bar)

Story		Location	Spacing in
From	**To**		
Story 6	Story 10	Column face	3
		Mid span	14.625
		Outer face	29.25
Story 3	Story 5	Column face	3.75
		Mid span	18.25
		Outer face	29.25
Story 1	Story 2	Column face	4.875
		Mid span	23.75
		Outer face	29.25
Note: 1. Outer face is located 2" from the edge of free end of stair.			

But according to ACI code, spacing should not be more than 18". Therefore alternative #3 bars are placed in between #4 bars. #3 bar is located in between #4 bar from free end to a distance of 2' towards the center of column.

#3 bar is used as distribution reinforcement @ 7.5" c/c. These reinforcements are continuous at the edge of landing slab. The details of stair reinforcement at section C-C is shown in Figure 9(a) and Figure 9(b) represents the magnified view of reinforcement details of column and stair connection. Figures 10 and 11 represent reinforcement details of stair at outer face and column face respectively.

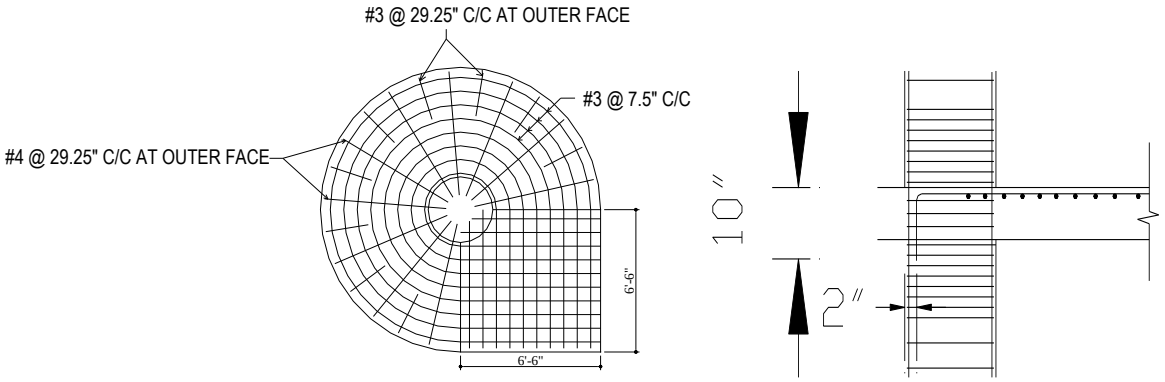

(a) (b)

Figure 9: (a) Reinforcement details of stair at section C-C, (b) Magnified view of reinforcement details of column and stair.

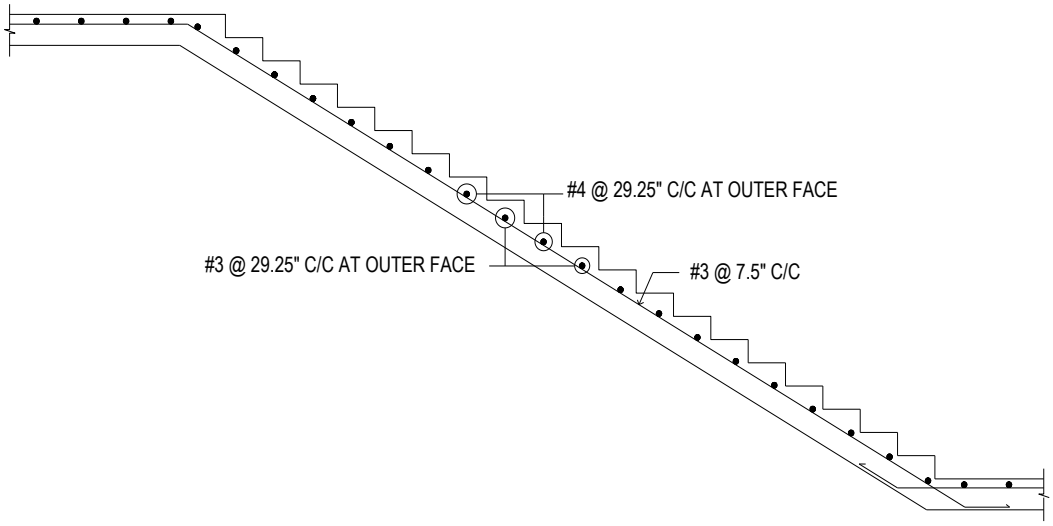

Figure 10: Reinforcement details of stair at outer face

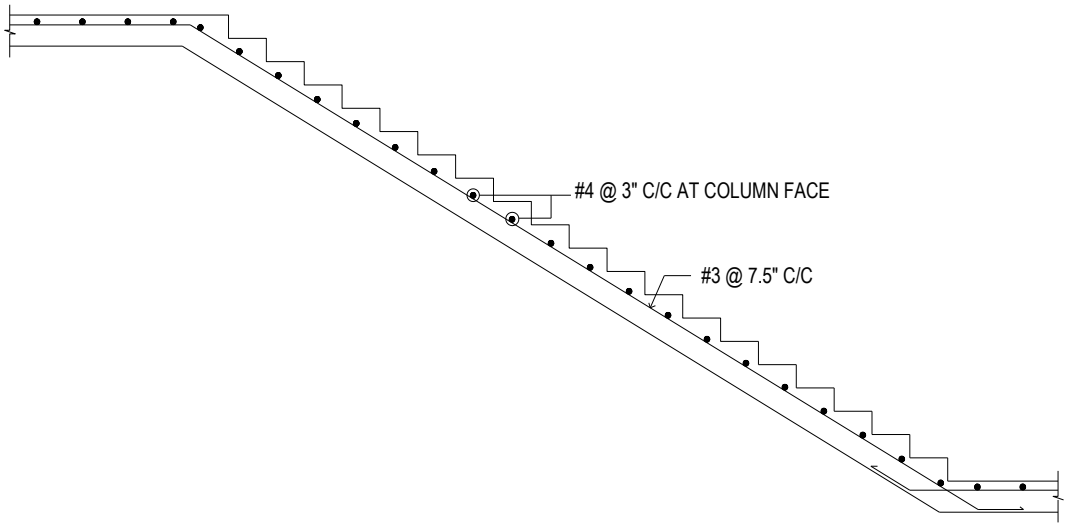

Figure 11: Reinforcement details of stair at column face

4. CONCLUSIONS

a. The maximum story displacement along X axis and Y axis occurred in the spiral stair model are compared with the permissible maximum story displacement according to BNBC 2006. The maximum story displacement along X axis and Y axis are less than the permissible value obtained from BNBC 2006.

b. Story displacement along X axis and Y axis increases almost linearly.

c. In economic point of view, the diameter of the spiral column is not uniform. The column diameter of 26 inch is adequate for all the story. But the diameter of 26 inch is not required above story 2 and diameter of 20 inch is required above story 2. However, diameter of 20 inch is not required above story 5. So, the diameter of the spiral column is reduced to 20 inch in story 3 and further reduced to 16 inch in story 6 to make the design economic.

REFERENCES

Bangladesh National Building Code (BNBC) (2006).

OVE ARUP and PARTNERS (1959). "A Method of Design of Spiral Stairs." *Technical Note No. 9*, London (1959).

Rutenberg A. (1975). "Analysis of Spiral Stairs Supported on a Central Column." *Build Sci.* Vol. 10, pp. 37-42. Pergamon Press 1975. Printed in Great Britain.

Proceedings of the 5th International Conference on Civil Engineering for Sustainable Development (ICCESD 2020), 7~9 February 2020, KUET, Khulna, Bangladesh (ISBN-978-984-34-8764-3)

NON-FIRED BUILDING BLOCK USING INDUSTRIAL WASTES

Sudipta Sarker[1], G. M. Sadiqul Islam[*2], Monower Sadique[3] and Ali Abdulhussein Shubbar[4]

[1]Research Associate, GCRF Project, Department of Civil Engineering, Chittagong University of Engineering and Technology (CUET),Chittagong 4349, Bangladesh, e-mail:s.sarkerce@gmail.com [2]Professor, Department of Civil Engineering, Chittagong University of Engineering and Technology (CUET),Chittagong 4349, Bangladesh, e-mail: gmsislam@cuet.ac.bd
[3]Reader, Department of Civil Engineering, Liverpool John Moores University, Liverpool L3 3AF, UK, e-mail: M.M.Sadique@ljmu.ac.uk
[4]PhD Candidate, Department of Civil Engineering, Liverpool John Moores University, Liverpool L3 2ET, UK, e-mail: A.A.Shubbar@2014.ljmu.ac.uk

***Corresponding Author**

ABSTRACT

Demand for bricks is rising following the growth of the construction industry aimd infrastructure boom in Bangladesh. Bricks produced from traditional technique and agricultural clay contribute considerably to some of the worst air pollutions in the world. There is an urgent need to start using an environment-friendly alternative material/approach instead of conventional bricks to save the fertile topsoil and conserve a clean environment. This research, therefore, is aimed to explore different options to produce non-fired bricks. The study incorporated different types of industrial waste including Fly ash and Ladle Furnace Slag (LFS) as a partial replacement of CEM I and lime. Induction Furnace Slag (IFS) is used as a partial or full replacement of virgin fine aggregate (local sand) in non-fired building block manufacturing process at laboratory scale. The use of abundant solid waste from steel and power plants in brick production could be a potential solution for the management of these hazardous residues. The prepared building blocks without using any agricultural clay conforms to the minimum compressive strength requirement of 10.3 MPa as per ASTM C62 and BDS 208 while the maximum compressive strength was found to be 40.6 MPa. This highly promising performance pronounced the use of industrial waste materials in non-fired brick production to achieve a cleaner, environment friendly sustainable society as well as a potential waste management approach for hazardous industrial waste.

Keywords: *Industrial waste, Ladle Furnace Slag (LFS), Induction Furnace Slag (IFS), Waste management, Building block, Sustainability.*

1. INTRODUCTION

People have been using as an essential building construction material for thousands of years or its manifold superiorities over other earthen construction materials. The first clay brick was produced traced back to 10,000 BCE, found in Egypt which were hand-moulded and then sun-dried. The historic city Ur (modern Iraq) adopted clay bricks as the main construction materials around 4000 BCE. Archaeological evidence has been found of 5000 BCE on using fire to produce clay-based bricks for better performance. Since then, the brick industry has been developing using modern machinery, such as powerful excavation equipment, motors, tunnel kilns. 1500 billion units fired brick production was estimated in 2015 globally (CCAC, 2015). Despite the workability of conventional brick production, fired clay brick production consumes a considerable amount of virgin resource and energy. In the production of 1 tonne brick an estimated 706 kWh energy is required and 0.15 tonne carbon dioxide (CO_2) is being emitted (Carbon Trust, 2011). This considerable energy consumption and carbon footprint is barrier to achieve sustainable development.

Apart from that, the construction contributes to a loss of 1% of agricultural land annually Bangladesh. Approximately 80% of this loss is due to unplanned rural housing also over 17% to brick kilns. Excavation of per hectare of fertile topsoil could cause up to Tk. 3.1 million economic loss. The brick industries in this country are producing approximately 25 billion units every year by eliminating 100 million tonnes of topsoil considerably affecting agricultural production and achieving sustainable development. As a result, around 50 million people would face food shortage by 2050 when the country's population would reach 245 million (The Daily Star, 2018). An annual 80 million tonnes of CO_2 emission are estimated for this country of which ¼ is accounted from only 7,900 registered (constructed following proper design and environmental rules) conventional brick kilns. The number of unregistered conventional brick kilns is even higher than the registered ones. These kilns also consume 5 million tonnes of coal and 3 million tonnes of wood annually (Hossain, 2017). In Dhaka, 58% of air pollution is accounted for conventional brick kilns.

A survey by the Department of Environment (DoE) of Bangladesh during 2013-18 found brick kilns are the top air polluter in seven major cities of the country of which Narayangonj has the most polluted air followed by Dhaka. During production (dry) season November-April the air quality of these metropolises becomes extremely unhealthy by emitting lot of particles in the air. Another study in association with Norwegian Institute for Air Research (NILU), DoE conducted during 2013-16 in Dhaka and Chattogram city found 58% of the main air pollutants (Particulate Matter 2.5) originate from the conventional brick kilns. The country, therefore, is in urgent need of immediately start using an environment-friendly alternative instead of conventional bricks to save its fertile topsoil and conserve the environment. Turning to alternatives like compressed or thermal blocks incorporating waste residues is crucial in ensuring food security and thereby sustainable development.

Considering both environmental and economic issues, studies have been conducted to produce sustainable bricks as a way to minimize the large carbon footprint from this conventional clay brick producing industry. An alternative of conventional bricks could be cement based building blocks from Ordinary Portland Cement (OPC). However, the production of cement clinker is highly energy intensive; 1 kg clinker requires 1.5 kWh energy and releases about 1 kg of CO_2 to the atmosphere. In addition, the aggregates are obtained from quarrying and thus have the same issues as clay-based brick. Current global waste generation volumes are approximately 1.3 billion Metric tonnes per year and are expected to increase to 2.2 billion Metric tonnes by 2025. To reduce environmental pollution, decrease the amount of generated wastes and preserve virgin materials, thereby contributing to sustainability; researchers have made remarkable efforts to develop different bricks from various types of waste materials.

In near future, coal burning power plant will be the major source of power generation in Bangladesh. The current power generation of Barapukuria coal power plant is 525 MW and approximately

1,09,200 Metric tonnes fly ash is being generated every year (Tamim, Dhar & Hossain, 2013). The situation will be worsened once 3 others under construction coal burning power plant will come into full generation of 3840 MW. Considering a linear interpolation, the annual production of fly ash will rise to 865,000 MT per annum from 2024 onwards. For a densely populated country like Bangladesh; this volume of fly ash is an enormous amount to dispose of. Considering the chemical composition of Fly ash, incorporating it in non-fired eco-friendly brick can be a two-way solution for this problem.

Bangladesh has over 400 steel mills of different categories and sizes with annual production of over 4 million tons. Most of the Bangladesh steel industries use induction furnaces which produce approximately 3.2 million tons of steel every year along with along with 250 thousand tons of Induction Furnace Slag (IFS) (Rezaul et al., 2017). Approximately 60–80 kg of Ladle Furnace Slag (LFS) is recovered for each ton of steel to be refined. Some of this amount reintroduced in the production process, however, a considerable amount of LFS is dumped as landfill. Chemical composition of the powder like material indicates its potential as a supplementary cementitious material.

The supply chain e.g., waste-to-resources has been seriously considered in many industrial parks around the globe (Rashad, 2019). Conventional steel waste management by dumping or landfilling has a negative impact on the surrounding environment leading to pollution in addition to the cost needed to dispose of these. The incorporation of steel mills waste materials in brick production could be a potential solution for the management of these hazardous residues. Thus, strategically industries can take advantage of market opportunities and neutralize threats arising from environmental issues. The aim of this research is to explore different options to produce non-fired brick/building blocks from several industrial solid wastes including fly ash, LFS by full or partial replacement of cementitious media such as Portland based cement and lime powder. In addition, IFS is used to replace sand in the media.

2. MATERIALS AND METHODOLOGY

Characterization of the raw materials is described and then the performance of material composition in the pressurized building block preparation system was evaluated in terms of compressive strength. Industrial wastes- LFS and fly ash is used as supplementary binder in the production of building block. Another steel industry waste material IF is used as filler/fine aggregate. CEM I, building lime and local sands are other associated materials used in this research.

CEM I of strength class 52.5N with fineness 99.3% (#200 sieve) and building lime (passing through 1mm sieve) obtained from local sources. Fly ash is obtained from Barapukuria coal burning power plant in Bangladesh. A maximum of 73% fly ash (of total binder content) is used for building block preparation. LFS and IFS are collected from BSRM Steel Mills Ltd., Chittagong, Bangladesh. The LFS passing through 2mm sieve is used as binder. Induction furnace slag (IFS) of two different sizes (0-4 mm; F.M 2.33 and 4-8 mm; F.M 3.54) was collected from BSRM steel mills Ltd. It was used as a full or partial replacement of sand. A maximum of 60% IFS (both size same proportion) of total dry mix was used in the building block preparation. The local sand used for the study was prepared according to graded sand requirements ASTM C778-17.

2.1 Material Characterization

2.1.1 Particle size distribution (PSD)

Particle size distribution of binders' viz. CEM I, fly ash, LFS and building lime are obtained using a LASER particle size analyser. Approximately 1g of sample (fly ash/LFS) is dispersed in water using an ultrasonic attachment in the sample vessel of the equipment. In the case of CEM I and lime, these are dispersed in propanol (to prevent reaction). Commercial software is used to create particle size distributions from the degree of scattering of a collimated, monochromatic, dual laser beam (red and blue) passing through the mixture of sample and solvent. At least three measurements are carried out

for each sample. Although repeated distributions are found to be similar for a given material, an average distribution result of these, created by the computer software, is reported. Figure 1 shows combined PSD of CEM I, fly ash, LFS, lime and IFS after 1-hour grinding. The mean size of CEM I (22.77 μm) and fly ash (20.1 μm) was found similar. However, the other two binders, building lime (49.37 μm) and LFS (59.2 μm) gave much higher mean particle size.

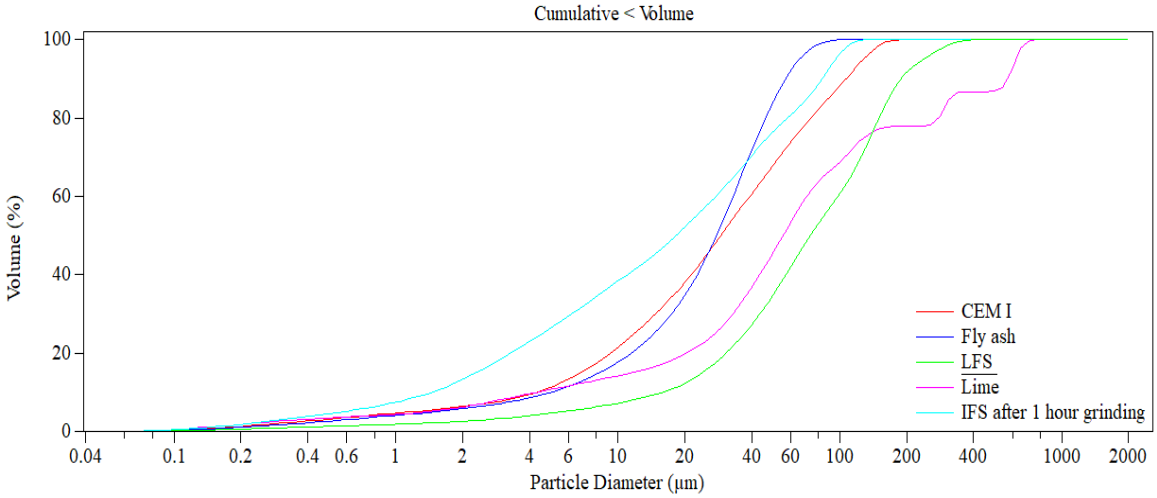

Figure 1: Particle Size Distribution of CEM I, Fly ash, LFS, Lime and IFS

2.1.2 Chemical compositions of materials used

The chemical compositions of fly ash, steel slags (IFS and LFS) and other binders are determined using X-ray Florescence (XRF) technique. All these works are conducted at Department of Pharmacy, Liverpool John Moore University, England. The chemical composition of fly ash satisfies the criteria of being Low calcium fly ash (Class F) according to ASTM C618. The chemical composition of LFS shown in Table 3.1 conforms to that found in literature elsewhere.

Table 2: Chemical composition of materials used in this study

Materials	**CaO %**	**SiO_2%**	**Al_2O_3 %**	**Fe_2O_3 %**	**MgO %**	**Na_2O %**	**K_2O %**	**TiO_2 %**	**MnO %**
IFS	4.92	46.80	6.58	16.35	3.22	1.50	0.33	1.05	7.52
FA	0.71	52.92	17.12	2.58	0.43	0.32	0.77	2.78	0.01
Lime	93.26	1.085	0.56	0.66	0.75	1.93	0.09	0.11	1.01
LFS	47.44	29.35	5.57	0.74	2.27	1.57	0.09	0.89	1.61
Cement	64.38	22.36	4.59	2.81	2.08	1.52	0.72	0.63	0.04

2.1.3 Morphology analysis by SEM

Figure 2 shows high magnification ESEM micrographs of the materials used in this study. SEM mode with an accelerating voltage of 15 kV in combination with a Links System Si(Li) X-ray detector is used. Selected samples are also analysed using the Energy-dispersive X-ray spectroscopy (EDX) mode at 20 kV voltage to identify the nature of crystalline deposits on their surfaces. Double sided adhesive carbon tape is secured to a 10mm diameter aluminium stub and the sample is sprinkled on it. Specimens are coated by Pd-Au alloy vapour to prevent charging during the test.

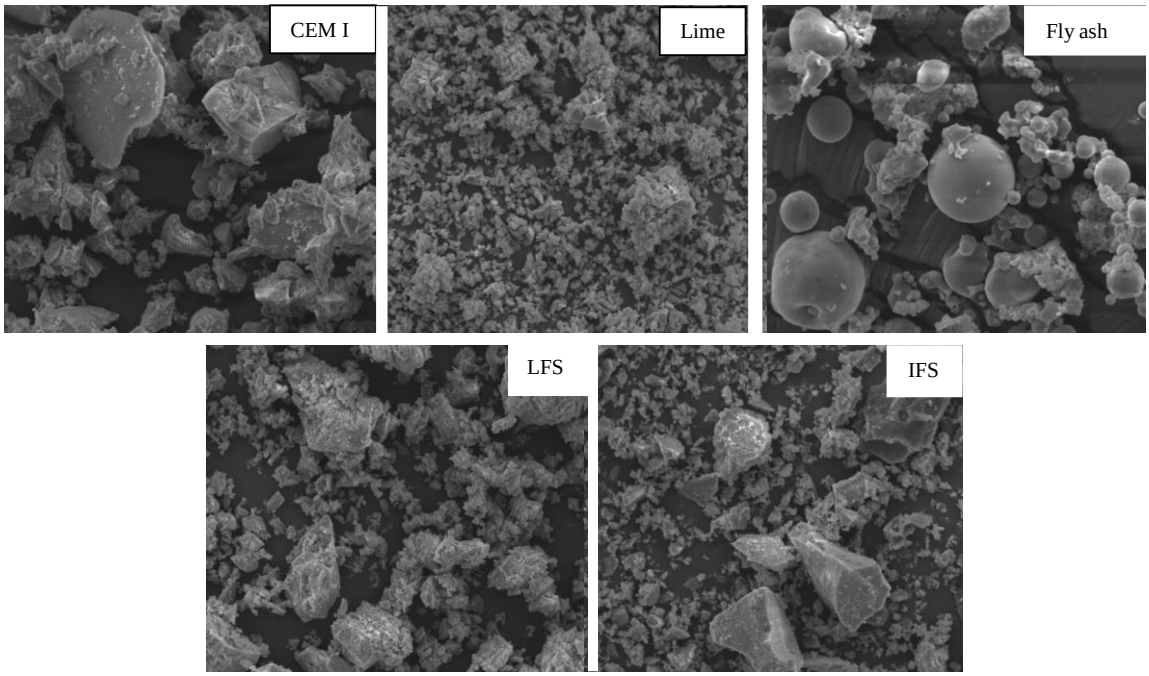

Figure 2: SEM images of materials used

2.2 Mix Details and Preparation of Building Blocks

2.2.1 Mixing Process

Mix details of the fly ash based and high-pressure building block are given in Tables 3 and 4 respectively. The required materials for building block preparation are first taken in an automatic pan mixer of 50 kg capacity. The mixer is kept rotating at a constant speed by a 1.5 kW motor. All the materials except water were mixed for 30 minutes. After that, water is added in such a way that no water comes out after squeezing by hand from the mix but moisture can be palpable in the hand. As pressure is applied to compact the building blocks lowest possible amount of water (maximum amount of water used is 15.7% of total dry mix) is added in the mixing stage. Excess amount of water could bleed out while applying pressure. After adding water, the mixing process is continued for another 30 minutes.

Table 3: Mix details of fly ash building blocks (kg/m^3)

Batch ID	Water	Binder			Fine Aggregate	
		Fly ash	Cement	Lime	Local sand	IFS
IF100C7.5LP7.5	248.0	651.0	122.1	122.1	---	732.4
IF67C7.5LP7.5	254.7	648.3	121.6	121.6	240.7	488.7
IF33C7.5LP7.5	254.7	648.3	121.6	121.6	488.7	240.7
IF00C7.5LP7.5	248.0	651.0	122.1	122.1	732.4	---
IF100C5LP10	234.4	656.4	82.1	164.1	---	738.5
IF100C10LP5	234.4	656.4	164.1	82.1	---	738.5

(IF100C7.5LP7.5 contains 100% IFS as fine aggregate; 7.5% cement and lime each and 40% fly ash of total dry mix was used as binder)

Table 4: Mix details of high-pressure building blocks (kg/m^3)

Batch ID	Water used	Binder		Fine Aggregate	
		LFS	Cement	Local sand	IFS
C10L05S25	159.6	111.4	222.7	556.9	1336.4

Batch ID	Water used	Binder		Fine Aggregate	
		LFS	Cement	Local sand	IFS
C10L10S20	163.1	222.4	222.4	444.8	1334.4
C10L15S15	163.1	333.6	222.4	333.6	1334.4
C7.5L7.5S25	149.2	167.8	167.8	559.5	1342.7

(C10L05S25 contains 10%, 5% and 25% of total dry mix are CEM I, lime powder and local sand respectively. Other 60% of total dry mix was IFS)

2.2.2 Casting and curing of the building block

A mould of surface dimension 9″×4″ (230mm×102mm) is used for building block casting. The finished height is around 75mm. Around 3.3 kg freshly mixed materials is required for each fly ash building block preparation. For high pressure building block approximately 4.2 kg mix was required. Fly ash blocks are greyish while high pressure block without Fly ash are brownish in colour. Figure 3 and 4 gives compaction machine with its application for building block preparation.

A constant bar pressure is applied by hydraulic jack 3 times, summing a total of 11 second (5s+3s+3s). In total 70 and 200 bar pressure are applied for fly ash and high-pressure building blocks. After casting, the blocks are taken from the mould instantly and kept at ambient temperature for 12 hours. Then those are kept under water for 7 days. At day 8 the samples are taken out of water and kept at room temperature for next 14 days. During this period, the blocks are immersed in water for 1 minute, at an interval of 8 hours. Then simple air curing was continued for the last 7 days prior to testing at total age of 28 days. Figure 5 shows the curing process of the building block samples.

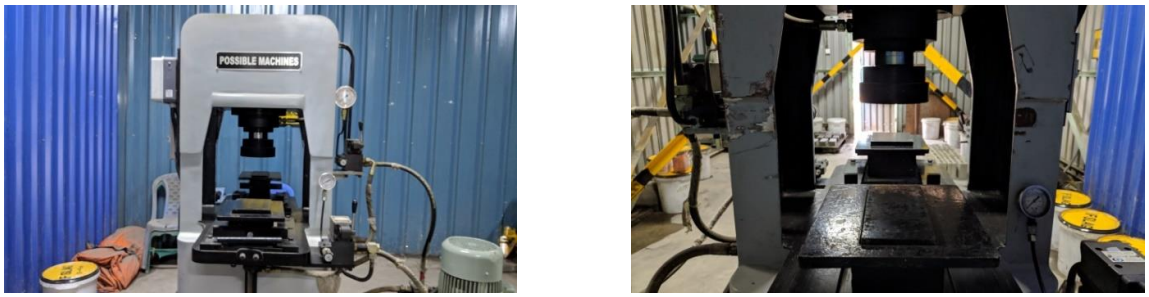

Figure 3: Building block casting machine

Figure 4: Pressure applying and casting

(a) Building blocks kept at ambient temperature

(b)Water curing of Building blocks

(c) Blocks after immersion in water for 1 minute

Figure 5: Curing process of building blocks

2.2.3 Water Absorption and Compressive Strength Test

The water absorption is calculated as the difference in weight after 7 days water curing from its weight prior to water curing and expressed in percentage. The compressive strength of a material is the uni-axial compressive stress reached when the material fails completely. For building blocks set of three blocks were tasted in each case and the average value of these three was reported as per ASTM C39-18.

(a) Compression test set up

(b) Fly ash block

(c) High pressure block

Figure 6: Compressive strength test and failure planes of building blocks

3. RESULTS AND DISCUSSIONS

3.1 fly ash-based building blocks

Fly ash incorporated building blocks are prepared using ternary combination of CEM I, fly ash and lime as binder with IFS and local sand as fine aggregate. Table 4.4 gives details of binder and fine aggregate combination and their corresponding compressive strength. IF00C7.5LP7.5 gives the maximum compressive strength of 18.5 MPa and 40.6 MPa at 7 and 28 days. The sample incorporated 100% IFS (45% of total mix content) as fine aggregate. The rest 55% of the mix includes 40% fly ash and 7.5% CEM I and lime each. With a gradual increase in CEM I content, 28 days compressive strengths are increased. For a fixed content of binder (fly ash, lime and cement) highest strength is obtained with local sand as fine aggregate.

Table 5: Compressive strength of fly ash-based blocks

SAMPLE	Materials, % of total dry mix						Compressive Strength (MPa)	
	Binder			Fine Aggregate		water		
	Cement	Fly Ash	Lime	IFS	Local sand		7 Days	28 Days
IF100C7.5LP7.5	7.5	40	7.5	45	---	15.2	11.8	19.1
IF67C7.5LP7.5	7.5	40	7.5	30	15	15.7	11.3	23.7
IF33C7.5LP7.5	7.5	40	7.5	15	30	15.7	14.1	26.6
IF00C7.5LP7.5	7.5	40	7.5	---	45	15.2	18.5	40.6
IF100C5LP10	5.0	40	10.0	100	0	14.3	9.2	14.4
IF100C10LP5	10.0	40	5.0	100	0	14.3	9.6	20.3

3.1.1 Effect of IFS and Lime in Fly ash Blocks

Figure 7 shows the variation of strength for 0%, 33%, 67% and 100% replacement of local sand by IFS. Approximately 40-50% strength is increased at 28 days from that obtained at 7 days. With the gradual increase in IFS content compressive strength decreased. For 28 days strength the decrease of strength (14 MPa) is high between 0 to 33% replacements of sand by IFS. After that, the strength decreases at a slower rate and with 100% IFS (as aggregate) give 47% strength of blocks with 100% sand (as aggregate). At 7 days the strength variation is relatively less. The lowest strength is obtained for building blocks with 67% IFS + 33% local sand as aggregate. Building blocks used 100% IFS gives strength of 11.8 MPa which still satisfies the minimum strength requirement by ASTM C62-17 (standard specification for building bricks). Therefore, even the compressive strength is found lower compared to the local sand, 100% IFS could be used as fine aggregate to produce building block to apply in the non-exposed weather condition such as interior partition walls.

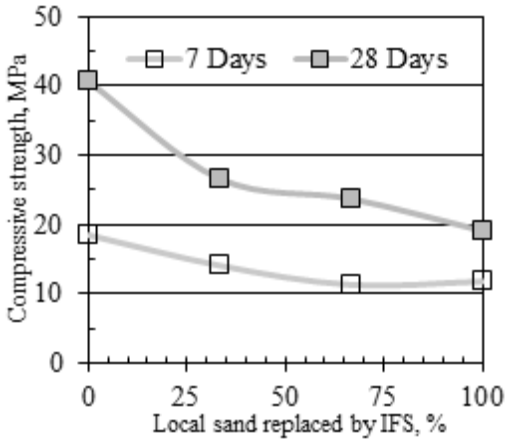

Figure 7: Compressive strength vs sand replaced by IFS (40% fly ash)

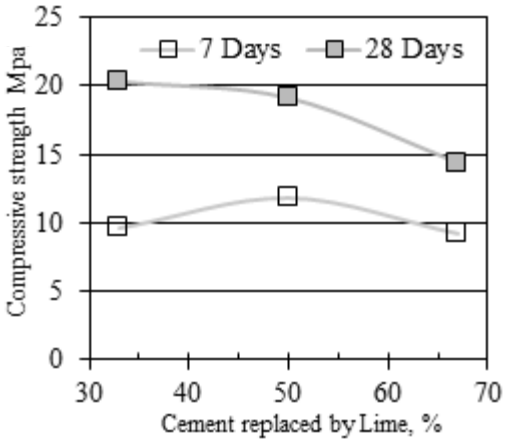

Figure 8: Compressive strength vs % cement replaced by lime (40% fly ash)

Considering 28 days compressive strength from Figure 8, it is evident that with the increase in CEM I replacement by lime compressive strength decreased. 28 days compressive strength reduces to 14.4 MPa from 20.3 MPa while cement replacement level increase from 33% to 67%. However, the reduction for 50% cement replacement is minor and therefore, it could be concluded that lime and fly ash combination could work similar to that of cement and fly ash.

3.2 High pressure Building Blocks

High pressure (200 bar) building blocks is prepared using 60% IFS with limited amount local sand (15-25%) and instead of lime and fly ash, LFS was used in a limited scale (5-15%). Table 6 shows mix combination and their compressive strength at 7 and 28 days. Sample C10L10S20 gives the

highest 7- and 28-days strength than all other batches. 10% LFS is found optimum considering same number of IFS (60%) and Cement (10%) are used. C10L05S25 shows the lowest 28 days strength of 29.4 MPa. Nonetheless, the average strength of high-pressure building block is higher than the average strength of fly ash incorporated blocks indicating significant contribution of high pressure in obtaining compressive strength.

Table 6: Mix combination and compressive strength of high-pressure building block

SAMPLE	Mix combination, % dry mix				water content, %	water absorption %	Compressive Strength (MPa)	
	IFS	Cement	LFS	Local sand			7 Days	28 Days
C10LRF05S25	60.0	10.0	5.0	25.0	7.2	2.6	25.2	29.4
C10LRF10S20	60.0	10.0	10.0	20.0	7.3	3.2	27.2	38.0
C10LRF15S15	60.0	10.0	15.0	15.0	7.3	3.2	25.6	34.1
C7.5LRF7.5S25	60.0	7.5	7.5	25.0	6.7	3.0	23.1	31.1

3.2.1 Effect of LFS content on high pressure building block

As shown in Figure 9, 10% LFS content gives better compressive strength performance both in 7 and 28 days. 5% LFS content give lowest compressive strength in both for 7 and 28 days. The strength increment rate for 10% LFS content is the highest among all the samples. For this, the 28 days compressive strength is 10.8 MPa greater than that of 7 days compressive strength.

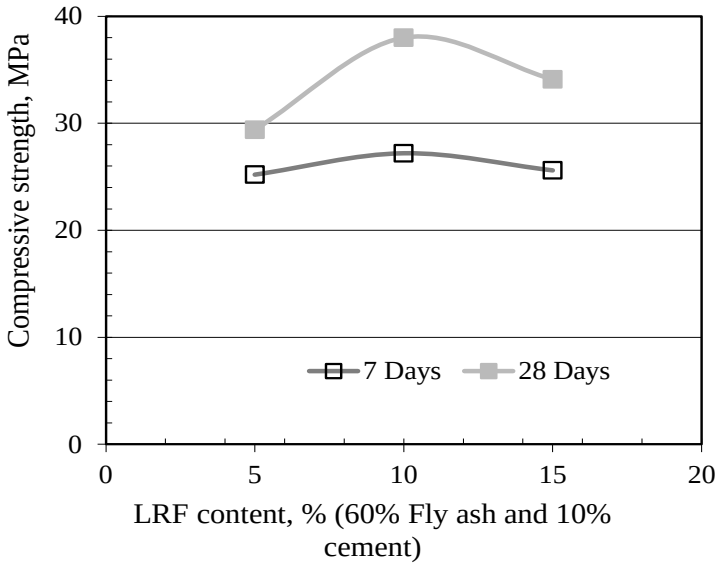

Figure 9: Compressive strength VS % LFS content

3.3 Excess water absorption and compressive strength of high-Pressure building block

The original total weight of the ingredients required to produce one building block is noted. After 7 days underwater curing the samples were surface dried and weighted. Figure 10 and 11 shows the water absorption rate (%) and compressive strength of fly ash incorporated building blocks and high-pressure building blocks. For fly ash blocks, the highest 7 days compressive strength (18.5 MPa) is obtained for IF00C7.5L7.5 batch which give lower water absorption (2.8%). Generally higher water absorption (above 3%) is obtained for the samples having low compressive strength (below 10MPa).

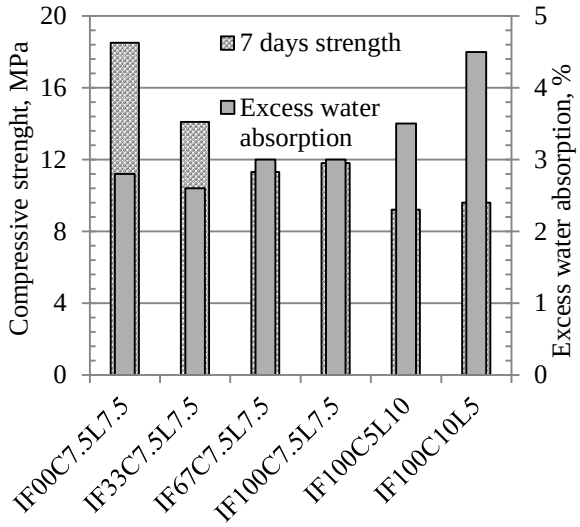

Figure 10: Water absorption (%) and compressive strength of fly ash based building block.

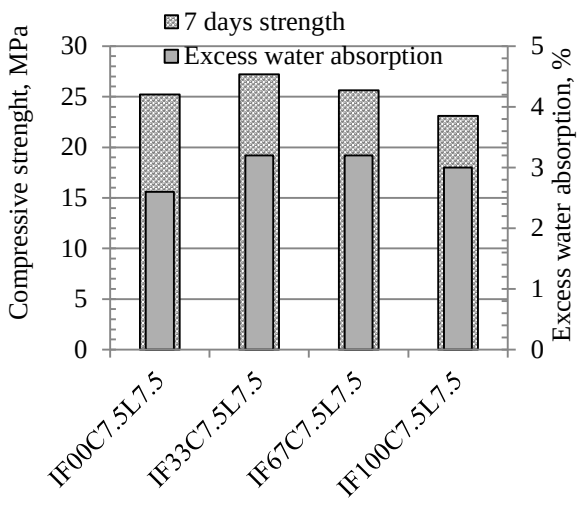

Figure 11: Water absorption (%) and compressive strength of high pressure building block.

The water absorption is small (≤3%) for highly pressurized building blocks however, no definite correlation was found between the 7 days excess water absorption and compressive strength. The highest compressive strength at 7 days was found to be 27.2 MPa for which excess water absorption is 3.2%. C10L05S25 sample give the lowest water absorption (2.6%) for which the strength is 25.2 MPa. Though it is not the lowest 7 days strength, its 28 days strength (29.4 MPa) is lowest of all. The water absorption rate for every sample of high-pressure system always gives lower value than that of fly ash-based building block. This is due to around 2000 psi higher pressure is applied to the high-pressure building block. In the mix, fly ash requires a higher level of water to make it workable.

4. CONCLUSIONS & RECOMMENDATIONS

The research aimed to assess the feasibility of non-fired brick/building block production using waste materials. In this regard, the compressive strength of fly ash-based blocks (70 bar pressure) increases with the replacement of IFS by local sand and maximum strength of 40.6 MPa was achieved. By applying a higher pressure (200 bar), the compaction level was improved and this increased the compressive strength of the building blocks. Overall the study with potential waste materials gave promising indication that with further modification, these materials could be used as an alternate of clay brick production. Researchers have a huge scope for further development to improve the quality of bricks. Durability tests such as chloride penetration/carbonation, water and gas permeability, dimensional performance/efflorescence, leaching of any heave metal/harmful constituents from the building blocks are required to carry out for its efficient use. For pressurized building blocks the effect of variable compaction pressures could be evaluated. Strength performance with other waste materials such as Rice Husk Ash, Ceramic waste could also be evaluated.

ACKNOWLEDGEMENTS

The financial support to carry out the project was received from Research England. The laboratory support provided by Chittagong University of Engineering & Technology (CUET), Bangladesh and Liverpool John Moors University, England are gratefully acknowledged. Materials supports received from BSRM Steel Mills Ltd., Royal Cement Ltd. and Barapukuria Coal Power Plant.

REFERENCES

The Daily Star (2019). "Brick kilns top polluter". Retrieved from www.thedailystar.net/frontpage/news/brick-kilns-top-polluter-170187

Carbon Trust (2011). "Industrial Energy Efficiency Accelerator –Guide to the metalforming sector". Retrieved from www.carbontrust.com/media/206500/ctg062-metalforming-industrial-energy-efficiency.pdf

CCAC (2015). "Mitigating black carbon and other pollutants from brick production", Climate and Clean Air Coalition, United Nations Environment Programme, Paris, France.

Hossain, M. (2017). To cut brick kiln pollution, Bangladesh constructs new building materials. *Reuters.* Retrieved from www.reuters.com/article/us-bangladesh-construction-climatechange/to-cut-brick-kiln-pollution-bangladesh-constructs-new-building-materials-idUSKBN1D81IA

Rashad, A.M. (2019). "A synopsis manual about recycling steel slag as a cementitious material". *Journal of Materials Research and Technology*, 8(5), 4940-55.

Rezaul, R.M., Atahar, R., Tasnim, T.B., Kurny, A., Momtaz, R. & Gulshan, F. (2017). "Reuse of Induction Furnace Steel Slag as a Replacement of Coarse aggregate in Construction." Proceedings of the International Conference on Mechanical Engineering and Renewable Energy 2017 (ICMERE2017) 18 –20 December, 2017, CUET, Chittagong, Bangladesh

The Daily Star (2018). "Shun burnt bricks to save topsoil-Use of environment-friendly hollow blocks is the answer, experts tell a roundtable". (September 20, 2018). Retrieved from www.thedailystar.net/backpage/news/manufacturing-burnt-bricks-100m-tonnes-top-soil-ruined-year-1636384

Tamim, M.M., Dhar, A. and Hossain, M.S. (2013). "Fly ash in Bangladesh- an Overview". *International Journal of Scientific & Engineering Research*, 4(4).

.

Proceedings of the 5th International Conference on Civil Engineering for Sustainable Development (ICCESD 2020), 7~9 February 2020, KUET, Khulna, Bangladesh (ISBN-978-984-34-8764-3)

PROPERTIES OF LIGHT WEIGHT FOAMED CONCRETE MADE WITH VERY FINE LOCAL SAND

Md. Nahid Hossain[*1], Abu Zakir Morshed[2], Mostafizur Rahman[3] and Md. Sakib Ul Hafiz[4]

[1]Graduate Student, Department of Civil Engineering, Khulna University of Engineering & Technology, Khulna-9203, Bangladesh, email: hossainmdnahid64@gmail.com
[2]Professor, Department of Civil Engineering, Khulna University of Engineering & Technology, Khulna-9203, Bangladesh, email: azmorshed@ce.kuet.ac.bd
[3]Sr. Manager, RCC LAB LTD., Dhaka, Bangladesh, email: raju.kuet@gmail.com
[4]Graduate Student, Department of Civil Engineering, Khulna University of Engineering & Technology, Khulna-9203, Bangladesh, email: sakibhafiz16@gmail.com

***Corresponding Author**

ABSTRACT

Foamed concrete has become a very well-known material that has excellent thermal insulation properties. Foamed concrete offers benefits such as decreasing the dead weight of a structure and it decreases high temperature related problems. The scope of this project was to compare the concrete physical, mechanical and thermal properties between normal weight concrete and foamed concrete by using different percentages of pea-gravel, local sand, foam and admixture. Four batches of concrete cylinders were made for determination of density, water permeability, rapid chloride permeability and compressive strength. Densities of foamed concrete varied from 1404 kg/m^3 to 1459 kg/m^3 with different percentages of pea-gravel where density of normal weight concrete was found 2330 kg/m^3. Compressive strength was found 17.7 and 22 MPa at 7 and 28 days respectively for normal weight concrete. The compressive strength of foamed concrete was varying from 4.3 to 6 MPa and 6 to 8 MPa at 7 and 28 days, which is lower than normal weight concrete by 66-74% and 63-72% respectively. The compressive strength of foamed concrete was gradually decreasing with increasing pea-gravel content. Water permeability and rapid chloride permeability of foamed concrete with different percentages of pea-gravel were gradually decreasing with increasing pea-gravel content, which is higher than normal weight concrete. Two slab specimens were made from each batch for testing of thermal insulation performance under specified range (35^{0}C to 50^{0}C) of temperature. The bottom surface temperature was varying from 35^{0}C to 50^{0}C where the top surface temperature of normal weight concrete, 0%, 10% and 20% pea-gravel foamed concrete were varying from 26.2^{0}C to 40.8^{0}C, 26^{0}C to 37.8^{0}C, 27.5^{0}C to 36.8^{0}C and 26^{0}C to 35.8^{0}C respectively. The foamed concrete with 20% pea-gravel shows the better insulation performance than the other types of slab.

Keywords: *Foamed concrete, Thermal properties, Density, Permeability, Compressive strength.*

1. INTRODUCTION

Bangladesh is a tropical country with average monthly temperature of 30°C to 40°C in summer season. Thermal movements occur due to high temperature changes, which could destroy building formations and contents. Keeping buildings with low temperature variation helps in maintain the integrity of building formations and contents. This can be obtained through the proper use of thermal insulation, which also increase the lifetime of building structures. The term thermal insulation is defined as a material or combination of materials that when properly applied, obstruct the rate of heat flow by conduction (heat flow through a material by molecular contact), radiation (heat transfer by the movement of particles with an alteration in their heat content) and convection (heat transfer by electromagnetic waves with the help of a gas or vacuum (Zahari et al., 2009). Due to high thermal movements many problems occur on the top floor of the building. These problems are summertime high energy demand, air conditioning costs, air pollution and greenhouse gas emissions, heat-related illness and mortality and uncomfortable for the users. So the main concern of this study is to reduce the high temperature of the top floor of the building. There are many insulating materials and techniques available for the purpose of reducing high temperature on the top floor of the building. From the last decades, foamed concrete has become a popular material for thermal insulation in buildings (Zahari et al., 2009). Foamed concrete primarily consists of a cement based mortar mixed with at least 20% of volume of air. Foamed concrete offers benefits such as decreasing the dead weight of a structure which economies the design of supporting structures including the walls and foundation of lower floors (Amarnath & Ramachandrudu, 2017). It was used in trench reinstatement, bridge abutment, void filling, roof insulation, road sub base, wall construction, tunneling etc. In this study, the thermal insulating properties of foamed concrete made with locally available very fine sand was investigated. Besides, the physical and mechanical propeties were also investigated. The physical properties were assessed in terms of it density, water permeability and rapid chloride permeability. Mechancial property was assesed in terms of its compressive strength at 28 days and thermal insulating property was evaluated by uni-directional heat flow by creating an artificial environment.

2. METHODOLOGY

2.1 Materials

Portland cement was used as binder. Local sand having FM of 0.72 was used at fine aggregate. Pea-gravel passing 3/8 in. and retained on No.8 ASTM standard sieve was used as coarse aggregate for light weight concrete while stone chips (12.5 mm nominal maximum size) was used as coarse aggregate in normal weight concrete. Foaming agent (conplast f297)was used to produce foam which was required to produce Light weight concrete (LWC) and polyethylene foam (PE foam) was used to insulate the box which was used for thermal insulation test. Water reducing and plasticizing admixture (Sika) was used to produced flowable concrete.

2.2 Determination of Material Properties

ASTM standard test methods were followed to determine the unit weight, voids content, specific gravity, absorption, moisture content, gradation and fineness modulus of aggregates.

2.3 Preparation of Normal Weight Concrete

Normal weight concrete (NWC) was made to serve as a reference batch to compare its characteristic parameters to that of the foamed concrete. A mix design for C22 grade NWC was prepared following ACI mix design procedure. The ratio of Cement : Fine Aggregate : Coarse Aggregate (by mass) was 1: 1.42 : 2.95 and the water-to-cement ratio (w/c) was kept as 0.54 by mass. The mix proportion is shown in Table 1.

2.4 Preparation of Foamed Concrete

The main constituents of foamed concrete are foam, water, admixture, cement and fine aggregate. The

fine aggregate was replaced by 10% and 20% pea-gravel to produce more light weight concrete. For foam generation, the foaming agent and admixture was mixed with water in a bucket. Then the whole solution was stirred by using a drill machine to produce foam. Finally, the cement and sand were added in the bucket and rotated the mixture to produce light weight foamed concrete. The mixing was continued until a homogeneous concrete mass was produced. The mixing procedure of foamed concrete is shown in Figure 1. The dry-weight proportions of concrete mix designs for NWC and foamed concrete (FC) with different percentage of pea-gravel are shown in Table 1.

Figure 1: Mixing procedure of foamed concrete

Table 1: Mix Proportions for Normal Weight Concrete (NWC) and Foamed Concrete (FC) **(Kg/m^3)**

Batch ID	Water	Cement	CA	FA	Pea-Gravel	Foaming Agent	Admixture
NWC	216	400	1180	569	_	_	_
FC-0-PG	200	400	_	200	_	1.714	0.400
FC-10-PG	200	400	_	179.93	22.15	1.714	0.400
FC-20-PG	200	400	_	159.84	44.30	1.714	0.400

2.5 Specimen Preparation

Figure 2: Cylindrical and slab specimens

Four batches of concrete were made; among which one batch was for reference NWC and three batches for foamed concrete, where the fine aggregate was replaced by 0%, 10% and 20% pea-gravel and named as FC-0-PG, FC-10-PG and FC-20-PG, respectively. Concrte cylinders of 100 mm dia. and 200 mm height were made from each batch and were used to determine density, compressive strength and permeability of concrete. In addition, 2 slab specimens were made from each batch for testing of thermal insulation performance. The cylindrical and slab specimens are shown in Figure 2.

2.6 Determination of Density

The density of concrete is a measurement of concrete's solidity. A higher or lower density of concrete end product is dependent on the mix proportion of the constituent materials. After demolding the cylindrical mold, the mass, diameter and height of the specimen was taken both for normal weight concrete and foamed concrete. Then, the density was calculated by dividing the mass by the volume of the specimen.

2.7 Determination of Compressive Strength

Compressive Strength of concrete is one of the most important and significant properties. The compressive strength of concrete cylinders was measured by applying continuous compressive load by using universal testing machine over the cylinder until failure occurs. Test method ASTM C39 was followed to determine the compressive strength of cylindrical concrete specimens.

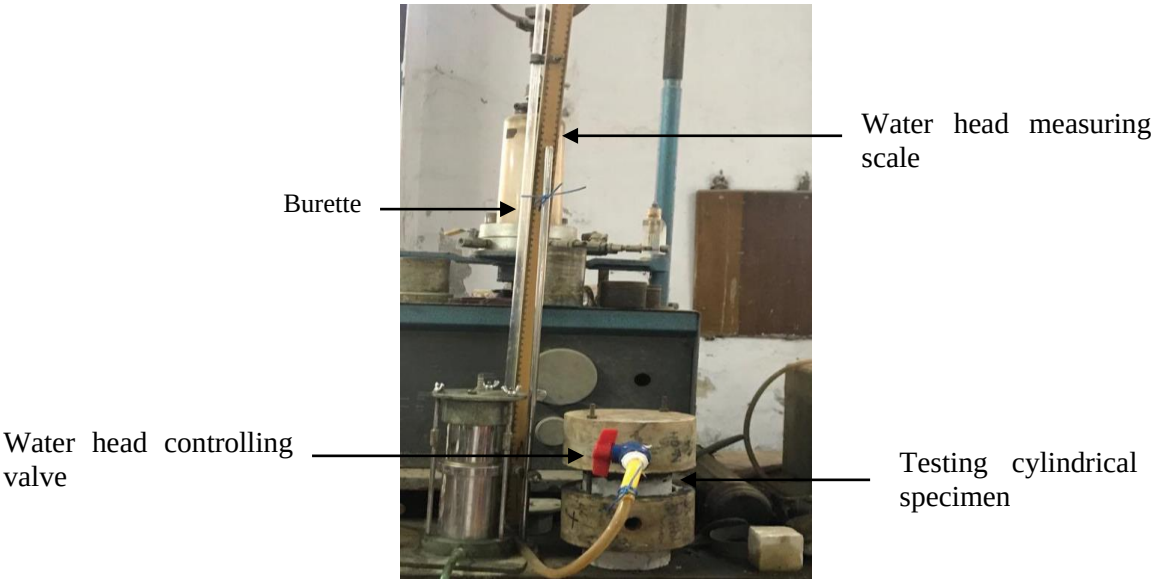

Figure 3: Experimental setup for permeability test

2.8 Determination of Water Permeability

Permeability is defined as the property that regulate the rate of flow of a fluid into a porous solid. Cylindrical specimens from each batch were sliced to a thickenss of 5 cm by a concrete saw so that the test specimens ended up with a disk of 5 cm height and 10 cm diameter. The specimens were made saturated surface dry before placing in the test column, which was connected with a standpipe or burette. A 100 cm height scale was also attached with the standpipe. The standpipe was filled with water in such a manner that all the air bubbles were removed from the standpipe. Then the test started by allowing water to a desired level to flow through the sample. The time required for change in water level in the standpipe from an upper limit to a designated lower limit was recorded. The test was performed at the age of 7 and 28 days curing and it was continued for 10 hours. Figure 3 shows the experimental setup for permeability test.

2.9 Rapid Chloride Permeability Test (RCPT)

The capability of concrete to prevent the intrusion of invasive elements like chloride ions is key to the durability of reinforcing steel in concrete. To determine the resistance of concrete against chloride penetration, this test was done according to ASTM C1202. Two specimens at the age of 7 and 28 days were taken from each batch and a 50mm thick slice was made from the center of the specimen by a concrete saw. Subsequently, the specimens were setup into two Plexiglas half cells and sealed using M-seal. To perform this test filter paper with 100 No. sieve and two stainless steel bars were placed at two ends of the test specimen. Those two bars acted as an anode and cathode, respectively. Each half-cell contained a reservoir filled with a solution of 0.3N NaOH at positive side and 3.0% NaCl at

negative side. Both cells were subjected to a 60-volt DC voltage through the specimen's 50 mm longitudinal section for a duration of 6 h. Changes in voltage and current were measured by using a multimeter at every 30 min. The recorded values were adjusted by converting the charge passed through the diameter of the test specimens (100 mm) to the equivalent charge passed through a standardized diameter (95 mm). The schematic diagram of RCPT test is shown in Figure 4.

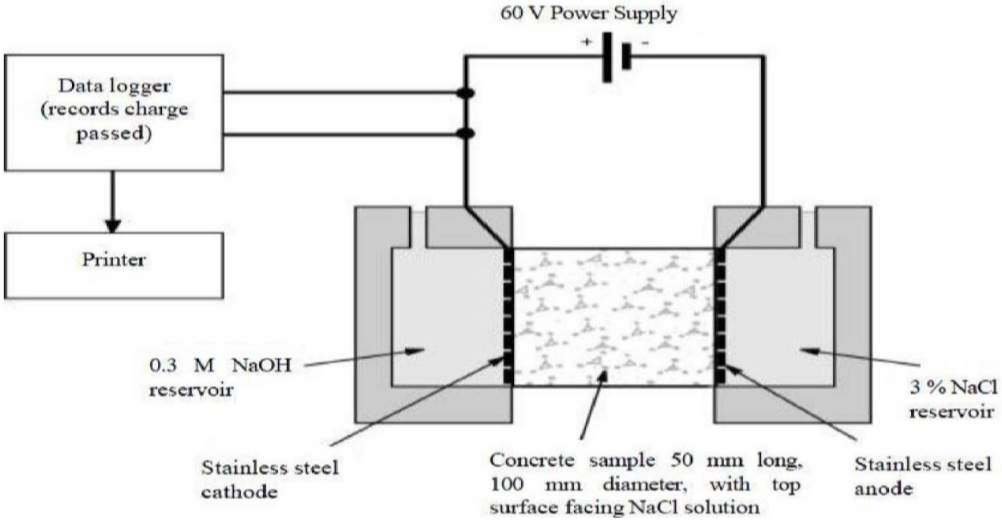

Figure 4: Schematic diagram for RCPT test

2.10 Experimental Setup for Testing of Thermal Insulation Performance of Slab

Two small scaled boxes were prepared with wooden pieces of 1 in. thickness having dimensions of 16 in. × 16 in. × 15.5 in. (L × W × H). Inner side the box was insulated by using polyethylene foam so that it acts as an airtight box. Inside the box, 2 in. width wooden bits were used to hold up the slab specimen. Two19 mm dia. holes in two boxes were made for the passage of wires of heater and sensors. A heater was placed inside of the box to produce heat. A sensor was attached with the bottom of the slab which is connected with the heater on/off switch, which helped to maintain the definite temperature (35 to 50^{0}C) inside the box automatically. For each temperature, this test procedure was run for 4.5 hours in order to stabilize the input temperature. Three DHT22 temperature sensors were attached on the other face of the slab and another box was placed over it to insulate the output side. The sensors were connected with a computer by the help of an Arduino and breadboard to measure the temperature of the top surface of the slab automatically. Average value from the three sensors were counted. This test was performed after 28 days curing of slab specimen. The experimental setup for thermal insulation test as shown in Figure 5.

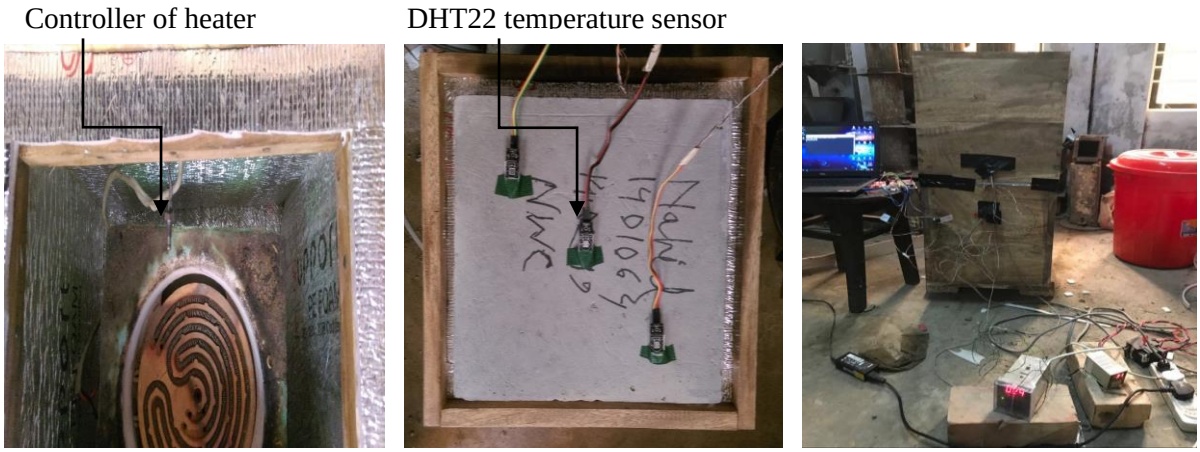

Figure 5: Experimental setup for thermal insulation

3. RESULTS AND DISCUSSIONS

3.1 Test Results for Materials Properties

The material properties for coarse aggregates (CA), fine aggregates (FA) and pea-gravel were determined according to ASTM standard procedures and those are shown in Table 2. The gradation curve for both CA and Pea-Gravel is shown in Figure 6.

Table 2: Physical Properties of Aggregates

Types of materials	FA	CA	Pea-Gravel
Bulk density (kg/m^3)	1412	1530	1542
Bulk specific gravity, G_{sb}	2.40	2.66	2.65
Water absorption (% by weight)	3.60	2.20	2.67
Moisture Content (% by weight)	3.00	1.50	0.70
Voids (% by volume)	41	43	41
Fineness Modulus (FM)	0.72	-	-

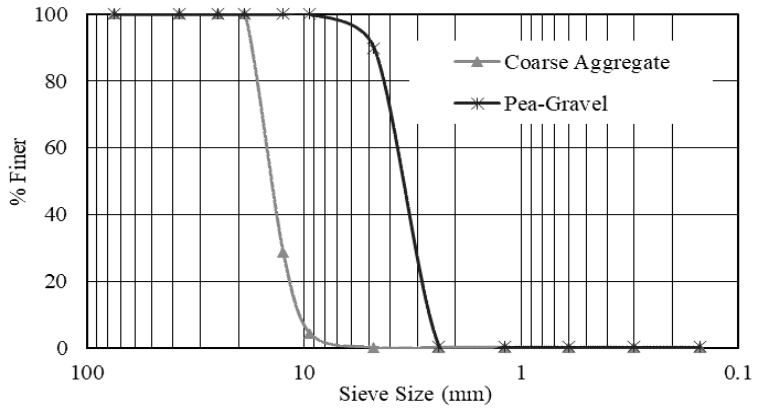

Figure 6: Gradation Curve for Coarse Aggregate and Pea-Gravel

3.2 Physical Properties of Concrete

3.2.1 Density

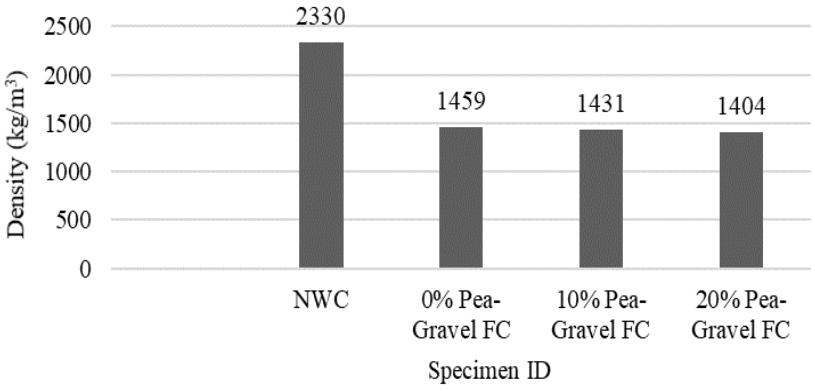

Figure 7: Comparison of Density of NWC and Foamed Concrete

Figure 7 shows the variation of the density of normal weight concrete (NWC) and foamed concrete (FC) with the different percentage of pea-gravel. It is seen that the density of foamed concrete with different percentage of pea-gravel varies from 1404 to 1459 kg/m^3 and the density of normal weight concrete is 2330 kg/m^3. The density ranges of light weight foamed concrete belongs to 400 to 1600

kg/m^3 (Ramamurthy et all., 2009). The obtained results reside inside the range of light weight foamed concrete. The density of normal weight concrete is greater than foamed concrete. It also shows that the density of foamed concrete reduced gradually with the increase in pea-gravel content. The main function of fine aggregates is to fill up the voids between the coarse aggregates. The density of foamed concrete decreases as voids in concrete increase with the increase in pea-gravel content.

3.2.2 Water Permeability

Figure 8 shows the variation of the coefficient of water permeability of normal weight concrete (NWC) and foamed concrete (FC) with different percentage of pea-gravel. The permeability range for foamed concrete lies between 10^{-8} to 10^{-10} cm/s (Sulaiman, 2011). The obtained values are not within the acceptable ranges for foamed concrete. Figure shows that the permeability of foamed concrete is higher than normal weight concrete and it gradually increases with the increase in pea-gravel content due to decrease in density of concrete. It also shows that the permeability of concrete decreases with the increase in the age of concrete.

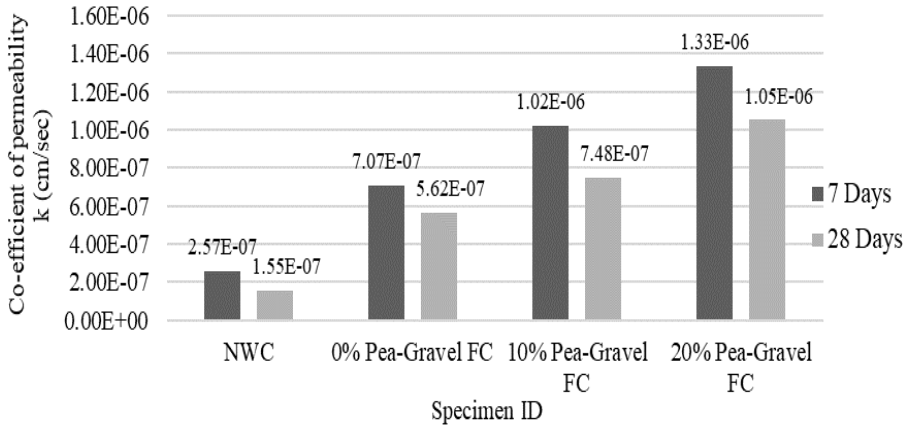

Figure 8: Comparison of Water Permeability of NWC and Foamed Concrete

3.2.3 Rapid Chloride Permeability

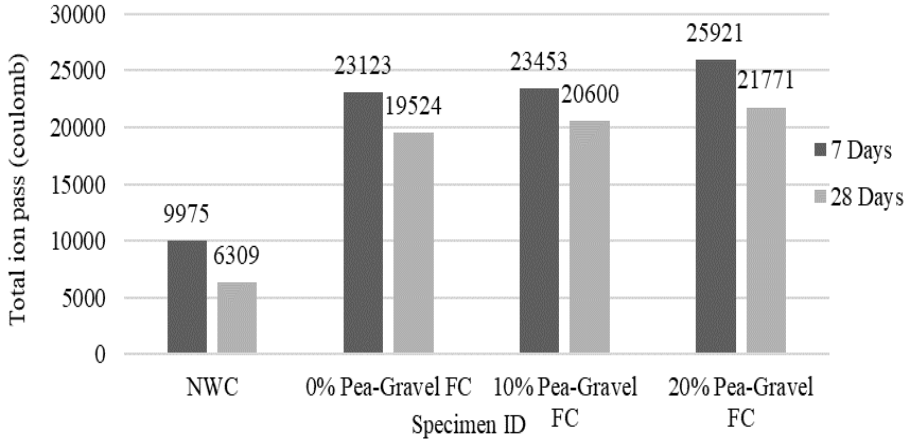

Figure 9: Comparison of Rapid Chloride Permeability of NWC and Foamed Concrete

Figure 9 shows the variation of Rapid Chloride Permeability of normal weight concrete (NWC) and foamed concrete (FC) with different percentage of pea-gravel. It is seen that the total charge passed varied from 23123 to 25921 coulomb and 19524 to 21771 coulombs at 7 and 28 days respectively for foamed concrete with different percentage of pea-gravel. On the other hand, the total charge passed for normal weight concrete ranged between 9975 and 6309 coulombs at 7 and 28 days respectively.

The results show that the total ion passed through foamed concrete was much higher than that of the normal weight concrete and it gradually increased with the increase in pea-gravel content due to increase in percentage of voids in concrete. It is obvious from Figure 9 that due to progressive hydration of cement chloride ion permeability decreased with the age of concrete for both NWC and LWC.

3.3 Mechanical Properties of Concrete

3.3.1 Compressive Strength

The results of compressive strength for normal weight concrete and foamed concrete with different percentage of pea-gravel are shown in Figure 10. It shows that the compressive strength of foamed concrete is less than normal weight concrete and it gradually decreases with increase in pea-gravel content. The target compressive strength of normal weight concrete was 22 MPa at 28 days. The obtained compressive strength of normal weight concrete is 17.7 and 22.0 MPa at 7 and 28 days respectively. Figure shows that the compressive strength of foamed concrete with different percentage of pea-gravel varied from 4.7 to 6 and 6.3 to 8 MPa at 7 and 28 days, which is lower than normal weight concrete by 66-74% and 63-72% respectively. The compressive strength range of foamed concrete lies between 0.5 to 10 MPa (Sulaiman, 2011). These obtained values are within the acceptable ranges for foamed concrete. The test results indicate that this type of concrete is suitable for non-structural purposes such as thermal insulation of roof, void filling etc.

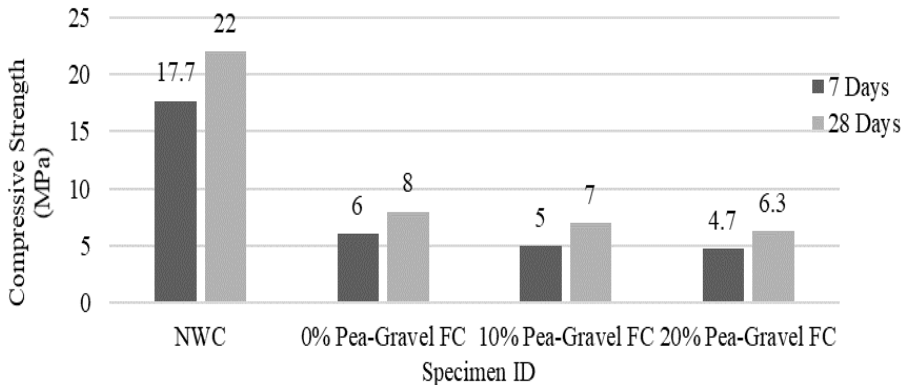

Figure 10: Comparison of Compressive Strength of NWC and Foamed Concrete

3.4 Thermal Insulation Performance of Slab

For thermal insulation test of slab specimen, the temperature at bottom of the enclosed area was created artificially from 35^0C to 50^0C at an interval of 5^0C. Then the top surface temperature of the slab was measured at an interval of 10 min. The variation of top surface temperature with respect to time for bottom temperature 35^0C, 40^0C, 45^0C and 50^0C is shown in Figure 11, Figure 12, Figure 13 and Figure 14 respectively. It shows that the thermal insulation behavior of foamed concrete slab with different percentage of pea-gravel is better than normal weight concrete slab. For foamed concrete the thermal insulation behavior gradually increased with increasing pea-gravel content due to lower density. If the density of a specimen is lowered, then better thermal insulation performance of this specimen can be achieved (Zahari et al., 2009). The results show that the top surface temperature of normal weight concrete slab varies from 26.2^0C to $32.8\ ^0$C, 26.5^0C to 35.8^0C, 28.3^0C to 37.7^0C and 28.8^0C to 40.8^0C respectively, when the bottom surface temperature is varies from 35^0C to 50^0C. The results also show that the top surface temperature of foamed concrete slab with different percentage of pea-gravel varies from 26^0C to 37.8^0C, 27.5^0C to 36.8^0C and 26^0C to 35.8^0c respectively for different bottom surface temperature. The starting temperature of different slab specimens varies due to the variation of the room temperature. During testing, the room temperature varies from 26^0C to 29^0C, so that the starting temperature is not same for all slab specimens. From this figure it is seen that the 20% pea-gravel foamed concrete shows better result in thermal insulation test than other foamed and normal weight concrete.

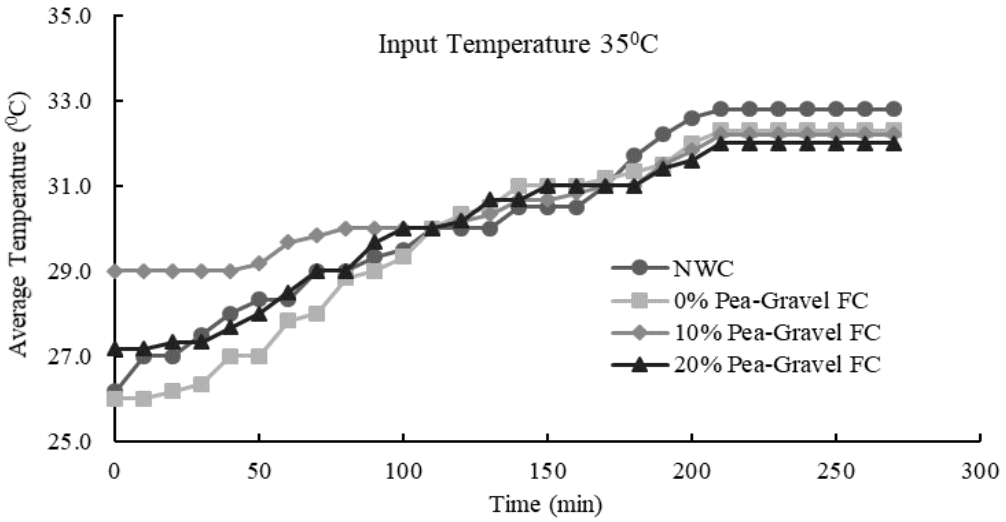

Figure 11: Comparison of Temperature Variation with Time of NWC and Foamed Concrete

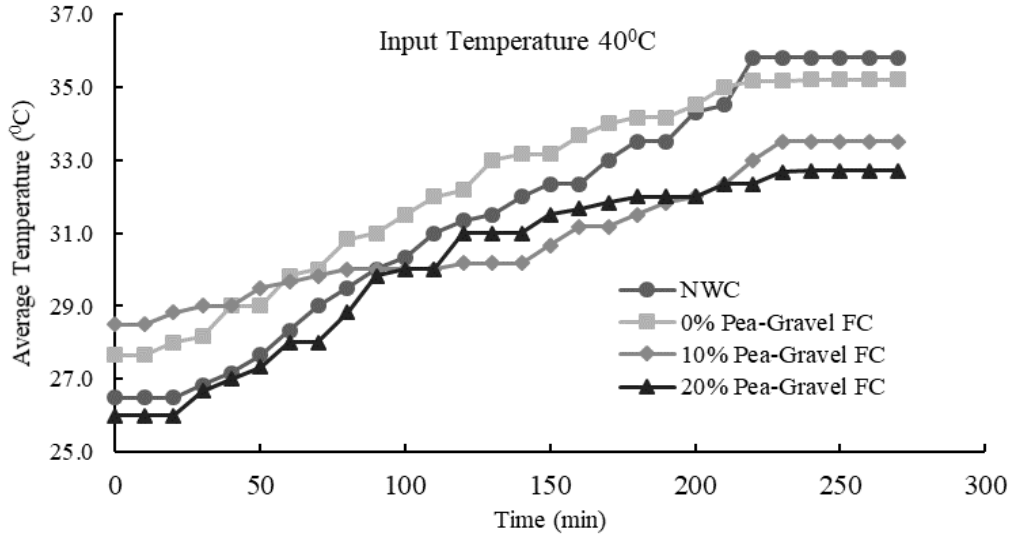

Figure 12: Comparison of Temperature Variation with Time of NWC and Foamed Concrete

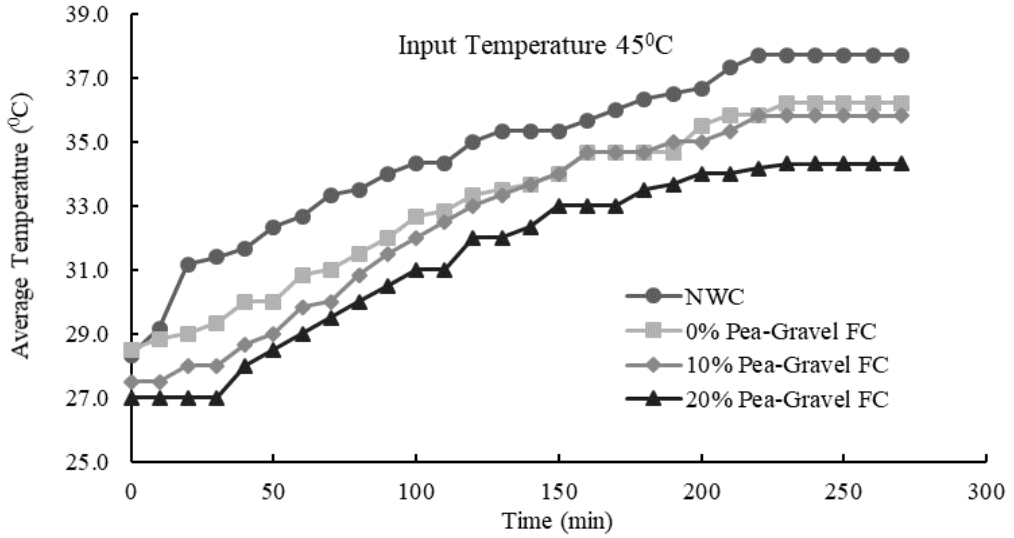

Figure 13: Comparison of Temperature Variation with Time of NWC and Foamed Concrete

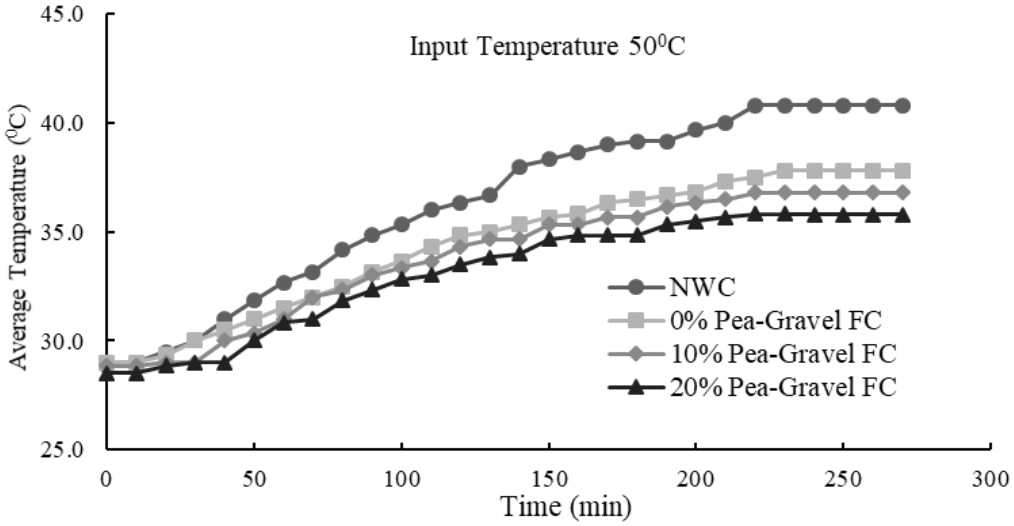

Figure 14: Comparison of Temperature Variation with Time of NWC and Foamed Concrete

4. CONCLUSIONS

The important findings based on the experimental results are summarized below:

- The density of normal weight concrete is higher than foamed concrete with different percentage of pea-gravel. The density of foamed concrete with different percentage of pea-gravel are gradually decreases with increasing pea-gravel content.
- The water permeability and rapid chloride permeability of foamed concrete with different percentage of pea-gravel is higher than normal weight concrete and it is gradually increased with increasing pea-gravel content.
- The compressive strength of normal weight concrete is close to target strength (24 MPa). But the compressive strength of foamed concrete with different percentage of pea-gravel is lower than the normal weight concrete and it is gradually decreased with increasing pea-gravel content.
- During insulation test, temperature of top surface of slab for normal weight concrete was found 26.2^0C to 40.8^0C, when the bottom surface temperature varies from 35^0C to 50^0C.
- For 0%, 10% and 20% pea-gravel foamed concrete, the temperature variation of top surface was found 26^0C to 37.8^0C, 27.5^0C to 36.8^0C and 26^0C to 35.8^0C respectively.
- The thermal insulation property of foamed concrete was gradually increased with increasing pea-gravel content due to decrease in density.

REFERENCES

ACI Standard 211.1, “Recommended Practice for Selecting Proportions for Concrete”.

ASTM C 39, “Standard Test Method for Compressive Strength of Cylindrical Concrete Specimens”.

ASTM C 1202, “Standard Test Method for Electrical Indication of Concrete’s Ability to Resist Chloride Ion Penetration”.

Amarnath, Y., & Ramachandrudu, C. (2017). Production and properties of foamed concrete , (April), P-15–25.

Zahari, N. M., Rahman, I. A., & A Mujahid A Zaidi. (2009). Foamed Concrete: Potential Application in Thermal Insulation. Muceet, 47–52. Retrieved from http://eprints.uthm.edu.my/1759/1/Muceet_2009.pdf.

Ramamurthy, K., Nambiar, E. K., & Ranjani, G. I. S. (2009). A classification of studies on properties of foam concrete. Cement and concrete composites, 31(6), 388-396.

Sulaiman, S. (2011). Water permeability and carbonation on foamed concrete (Doctoral dissertation, Universiti Tun Hussein Onn Malaysia).

Proceedings of the 5th International Conference on Civil Engineering for Sustainable Development (ICCESD 2020), 7~9 February 2020, KUET, Khulna, Bangladesh (ISBN-978-984-34-8764-3)

STRENGTHENING OF REINFORCED CONCRETE BEAMS BY USING EXTERNAL STEEL ANGLE

Md. Omar Ali Mondal*[1] and Abu Zakir Morshed[2]

[1]Doctoral Student, Department of Civil Engineering, Khulna University of Engineering & Technology, Bangladesh, e-mail: moamondal@gmail.com
[2]Professor, Department of Civil Engineering, Khulna University of Engineering & Technology, Bangladesh, e-mail: azmorshed@ce.kuet.ac.bd

***Corresponding Author**

ABSTRACT

Strengthening of existing Reinforced Concrete (RC) structures may be required due to inadequate design, overloading, aging of building, environmental impact, corrosion of reinforcement, unfavorable condition such as earthquake, blasts, etc., the changes in the use of the structure and inadequate maintenance of the structure. The aim of this study was to investigate the flexural capacity of reinforced concrete beams after strengthening using external steel angles. Four reinforced concrete beams having cross-sectional dimensions of 150mm × 250mm and a length of 2700mm were prepared in this manner. 2-ø10mm bars were used as flexural reinforcement and 2-ø10mm bars were used on the top of the beam's web for holding the stirrups. The beams were designed strong enough against shear with ø6mm stirrups at a center to center distance of 100mm. Among the four beams, two beams were used ascontrol specimens. To find the ultimate capacity of the beams the control beams were tested after 28 days curing by using 3rd point loading. The average ultimate capacity of the control beams was 49.1kN. To simulate service load condition other two beams were preloaded up to75% of the ultimate capacity of the control beams. Some initial cracks formed due to the preloading. After the observation of initial cracks, the load was released. For the attachment of external steel angles (25mm×25mm×4mm)to the bottom corner by welding the lower and side (50mm) concrete cover of the beams was removed. After the attachment of external steel angles on the corner of the bottom stirrups by welding,the bottom part of the beams was cleaned. To cover the external steel angles the bottom part of the beams was cast again with new concrete. After 28 days curing the strengthened beams were tested in the same wayto find the ultimate capacity of strengthened beams. The ultimate capacity of the control beams was 124.4kN & 116.8kN which was 153% and 138% higher than the control beams. The experimental result shows the potentiality of using external steel angles as a strengthening technique to be followed with convenience.

Keywords: *Flexural strengthening, Strengthening techniques, Preloading, External steel reinforcement, External steel angles.*

1. INTRODUCTION

Civil infrastructure is a constituent of an uppermost portion of the national wealth. Nowadays, buildings are found to be out of service. The most widely used building materials in civil engineering applications is concrete (Zhang, Han, Ng, & Wang, 2018). Deterioration of RC structures is one of the major problems in the civil infrastructures, as a large number of buildings are constructed according to older design standards(Sundarraja&Rajamohan, 2009). Strengthening of reinforced concrete (RC) structures is usually required due to overloading, corrosion of the steel reinforcement, mechanical damage and inadequate maintenance, exposure to unfavorable conditions like earthquakes and blasts, the changes in the use of the structure and design and construction faults (Iskhakov, Ribakov, Holschemacher, & Mueller, 2013; Gul, Alam, Khan, Badrashi, &Shahzada, 2015). If a heavy earthquake with a 7.0 or greater magnitude arises in this country, it will lead to an extensive human wreck due to the faulty structural design of many buildings and proper awareness. According to the Geological Survey of Bangladesh, the country had experienced at least 465 earthquakes of several magnitudes between 1971 and 2006(Paul & Bhuiyan, n.d.).

Bangladesh is suffering from disasters such as Cyclones, Floods, Storm Surges and Tornados including Earthquakes regularly. Out of 5,000 public buildings in Bangladesh, around 3,000 were constructed before 1993 when the Bangladesh National Building Code (BNBC 1993) was enacted (Bangladesh, PWD, MHPW, 2015). These buildings have low resistant ability against earthquakes. According to the report of PWD, if an earthquake of M7.5 on Madhupur Fault in the Dhaka suburb occurs, the damage estimation for the Dhaka city became VIII of MMI seismic intensity scale, and out of the total 326,000 buildings, 72,000 buildings will damage beyond repair. About 50% of them would be reinforced concrete and about 30 percent would be brick masonry buildings. Also, moderately damaged buildings are estimated to be 49%. Further, if the earthquake occurs at 2:00 am, about 90 thousand people will die.

Also, most of the buildings in Bangladesh are low-rise buildings. With the rapid development of construction, the land becomes more and more scarce and the construction of the new structure is quite expensive (Islam, Islam, Talukder, & Hossain, 2013). Under such situations, maintenance of the building's construction quality and improvement of the safety of the buildings are necessary for Bangladesh. To overcome this upcoming hazard, the structures are required modification or strengthening to satisfy current building code requirements.

Strengthening by steel is popular in the world due to its cheapness, easy to work, available, meet the required strength, good at the ductile property and high fatigue strength. Steel is a universal, cheap, and effective construction material. The addition of steel reinforcement significantly increases the strength of concrete but to produce concrete with homogeneous tensile properties, the micro-cracks develop inconcrete should be suppressed(Raut, & Kulkarni,2014).

Gul, A., et.al (2015) investigate the flexural strengthening of reinforced concrete beams by using external steel. External steel bar & steel angle was used by removing bottom concrete cover and welding with the stirrups for the strengthening of different reinforced concrete beams. The flexural capacity of reinforced concrete beams strengthened with external steel reinforcement was greatly enhanced and showed a uniform distribution of flexure cracks. The failure of the strengthened beam resulted in a very favorable mode as compared to the control reinforced concrete beam. Beams strengthened with steel angles enhanced the load-carrying capacity more than the beams strengthened with external steel bars, indicating high flexural resistance. Better ductility was showed by the RC beam, strengthened with external steel angles than the RC beams strengthened with external steel bars.

2. METHODOLOGY

For this study, eight half-scaled reinforced concrete beam specimens were constructed. The cross-sectional area of the beams was 150mm × 250mm and the length of the beams was 2700mm. The

compressive strength of the concrete at 28 days was 33.3MPa. 500w deform bars used as main reinforcement. Table 1 shows the design summary of all specimens.

Table 1: Design summary of all beams

Specimen ID	Types of Beams	Cross-section b × h (mm × mm)	Main Reinforcement	External Reinforcement	Fastening Mechanism
B1-1	Control Beams	150 × 250	2- ø10 mm	-	-
B1-2		150 × 250	2- ø10 mm	-	-
B5-1	Strengthened Beams	150 × 250	2- ø10 mm	2- 25mm × 25mm × 4mm steel angle	Welding with stirrups
B5-2		150 × 250	2- ø10 mm		

2.1 Design of Control Beams

The moment capacity of the control beams $M_{n(c)}$was determined by using basic concepts for the rectangular reinforced concrete beams as given in the ACI code ACI-318-08 section 10.5. For the comparison of results, the beams were designed with minimum steel ratio

$$A_{s(min)} = 3\frac{\sqrt{f_c'}}{f_y}bd \geq \frac{200}{f_y}bd \quad (1)$$

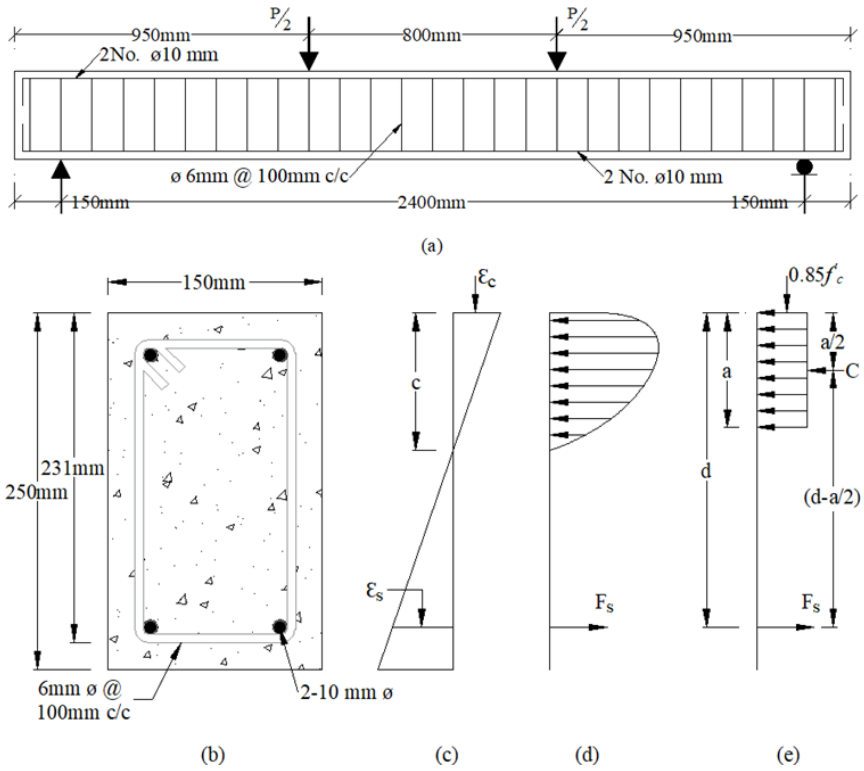

Figure 1: Schematic diagram of control beams (a) long section (b) x-section (c) strain diagram (d) nonlinear stress diagram (e) rectangular stress block

As a requirement of minimum steel two ø10 mm bars were used as flexural reinforcement. To hold the stirrups two ø10 mm bars were placed on top of the beam's web. The beams were designed strong enough against shear. The maximum shear force was found on the basis of $A_{s(max)}$calculated after the design of strengthened beams.

$$A_{s(max)} = \rho_{max} b d_{ave} \quad (2)$$

$$M_{n(c)} = A_s f_y \left(d - \frac{a}{2}\right) \quad (3)$$

$$a = \frac{A_s f_y}{0.85 f_c'} \quad (4)$$

$$M_{n(max)} = A_{s(max)} f_y \left(d_{ave} - \frac{a}{2}\right) \quad (5)$$

$$V = \frac{3M_{n(max)}}{L} \quad (6)$$

Where

$V = maximum\ shear\ force$

$M_{n(c)} = moment\ capacity\ of\ control\ beams$

$M_{n(max)} = maximum\ moment\ capacity\ of\ strengthened\ beams$

For the above maximum shear force, beams were designed and provided with ø6 mm 500w steel bars placed at 100mm on center throughout the length of the beams. Figure 1 shows the reinforcement detailing, strain diagram, nonlinear stress diagram and rectangular stress block of control beams.

2.2 Design of Strengthened Beams

The same flexural design procedure was used for the external strengthening of reinforced concrete beams as the regular rectangular beams. To find the external steel area the strain compatibility and rectangular stress block were used by Gul et al. (2015) in the case of Strengthening with external steel angles. This procedure was also the same as the ACI method for RC flexural members.

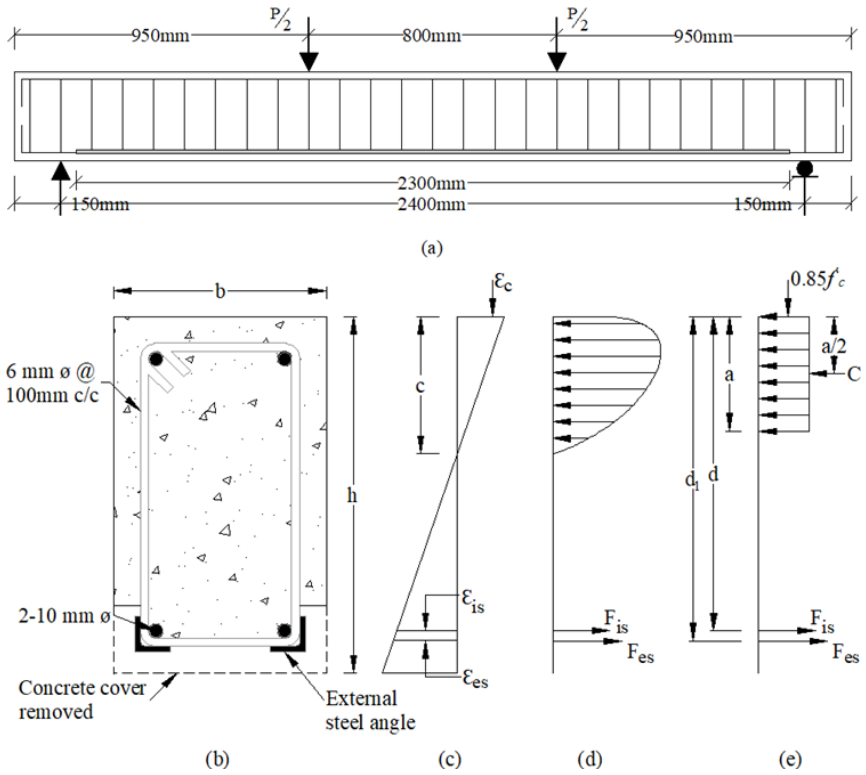

Figure 2: Schematic diagram of beams strengthened with external steel angles (a) long section (b) x-section (c) strain diagram (d) nonlinear stress diagram (e) rectangular stress block

The regular formulas for the design of RC beams were used to calculate the steel area for external reinforced concrete beams. The external steel area worked as the second flexural force acting member at the center of the external steel. Figure 2 shows the reinforcement detailing, equivalent strain, nonlinear stress and rectangular stress diagram of beams strengthened with steel angles. The design

procedure for externally strengthening of RC beams was based on maximum reinforcement ratio as given by ACI 318-08 Section 10.2 $\rho_{max} = \rho_{balance}$. The calculate steel area divided into two parts. Internal steel area $A_{s(c)}$ and external steel area $A_{s(ext)}$.

$$A_{s(ext)} = A_{s(max)} - A_{s(c)} \quad (7)$$

Where:

$A_{s(c)} = steel\ area\ of\ control\ beams$

$A_{s(ext)}$ = *external steel area provided for strengthening purpose*

The moment capacity of strengthened beams calculated as

$$M_{n(total)} = A_{s(c)} f_{y(c)} \left(d - \frac{a}{2}\right) + A_{s(ext)} f_{y(ext)} \left(d_1 - \frac{a}{2}\right) \quad (8)$$

Where:

$M_{n(total)} = momentcapacityofstrengthenedbeam$s

$f_{y(c)} = yieldstrengthofsteelusedincontrolbeams$

$f_{y(ext)} = yieldstrengthofexternalsteel$

2.3 Capacity of Beams

The ultimate capacity of different beams (control beams and Strengthened beams) was calculated according to ACI 318-08. A beam can fail in two basic modes. Failure in compression and failure in tension. The ultimate capacity of beams in compression was found by equation 9 and the capacity in tension was found by equation 3or equation 8.

$$M_{u(c)} = \rho_{max} f_y b d^2 \left(1 - 0.59 \rho_{max} \frac{f_y}{f_c'}\right) \quad (9)$$

$$\rho_{max} = 0.85 \beta_1 \frac{f_c'}{f_y} \frac{\varepsilon_u}{\varepsilon_u + 0.004} \quad (10)$$

The maximum moment capacity M_n was found from the minimum value of equation 3, equation 8 or equation 9 and using this value the maximum load was calculated.

3. EXPERIMENTAL PROGRAM

3.1 Sample Preparation

Four reinforced concrete beams were prepared for the experimental investigation. The cross-sectional area of the beams was 150mm × 250mm and the length of the beams was 2700mm. 2-ø10mm deform bars were used as main reinforcement. To hold the stirrups, 2-ø10mm deform bars were used on top of the beam's web. ø6mm deform bars used as shear reinforcement at @100mm c/c. Table 2 shows the tensile properties of reinforcing steel. Wooden formworks were made for the casting of beams according to ACI 318-08 section 6.1. Polyethylene was used on the formwork to get a smooth surface and preventing water absorption by the wooden formwork.

Table 2: Tensile properties of steel bar, steel angle & steel plate

Description	Yield Strength (MPa)	Ultimate Strength (MPa)
Ø6 mm bar	565	668
Ø10 mm bar	552	643
Steel Angle	426	530

3.2 Test of Control Beam

To find the flexural capacity of control beams two beams (B1-1 & B1-2) were tested up to the failure loadby using 3rd point loading according to ASTM C78. The beams were simply supported at a clear span of 2400mm and loaded symmetrically in four-point bending. A 300kN hydraulic jack was used for the application of load arranged vertically and divided into two equal point loads at a distance of 400mm on each side of the centerline of the beam through a transfer beam. The rate of loading maintained at 4.5kN/min according to ASTM C78. A 500kN load cell and 5 LVDTs (Linear variable differential transformer) were used to collect data directly by TML TDS-303 data logger. The 1stLVDT was placed at the center of the beam, 2ndand 3rdLVDTs were placed under the beam to the point load. 4thand 5thLVDTs were placed in the midpoint of support and the point load. Figure 3 shows the schematic diagram of the test setup.

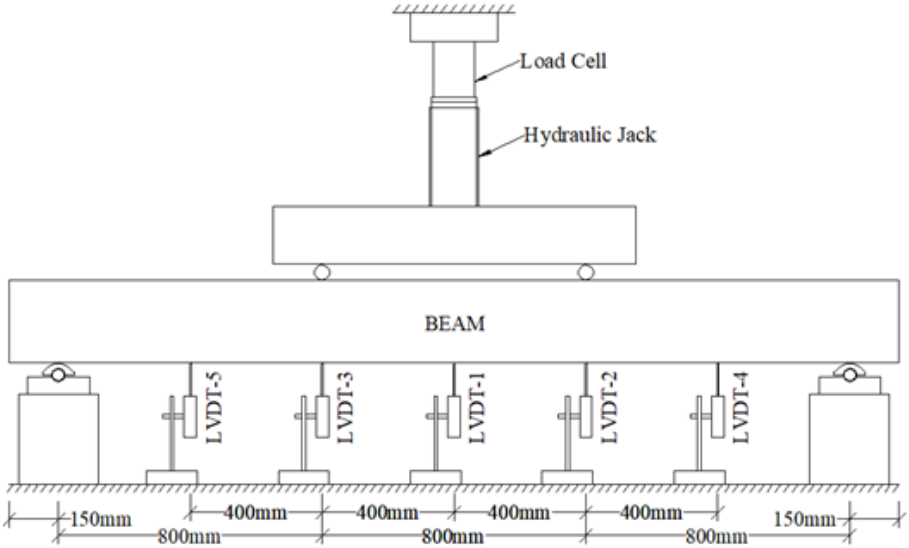

Figure 3: Schematic diagram of the experimental setup

3.3 Preloading

The other two beams (B5-1& B5-2) were preloaded up to 75% of the ultimate load of control beam by the standard test methods ASTM C78 to simulate the service load condition. The arrangement of LVDTs and loading patterns werethe same as the control beams. Some initial cracks formed due to preloading. After the observation of the initial cracks, the load was released.

3.4 Strengthening of Beams

After the release of the preload, the beams were ready for strengthening. The bottom concrete cover and the side concrete cover (up to 50mm) were removed to add steel angles with the bottom corners of the stirrups. The bottom face was cleaned. Twosteel angles were added in two sides of the beams with bottom stirrups by welding. After attaching the steel angles, the beams were cleaned and the exposed part was covered with new concrete.

3.5 Test of Strengthened Beams

After 28 days of curing of the new concrete, the beams were tested to find the ultimate capacity of the strengthened beams. 3rd point bending test was used to test the strengthened beams according to ASTM C78. According to ASTM C78, the loading rate was maintained 4.5kN/min. The loading data was recorded and new cracks were marked with a red marker.

4. RESULTS

4.1 Control Beams

The reinforced concrete beams (B1-1) & (B1-2) shown the same elastic behavior up to a load of 16.5kN and 14.5kN respectively and the corresponding mid-span deflection at the elastic load was 1.38mm and 1.30mm respectively. The destruction of stiffness started after the elastic load and the relation was again linear up to a load of 44.5kN and 45.8kN for the control beams and the mid-span deflection was 10.55mm and 9.82mm at that stage. Figure 4 shows the load-deflection relationship of control beams. The first flexure crack formed at the bottom of the beam surface at a load of 23.9kN and 24.8kN respectively and propagated rapidly towards the upper part of the beams.

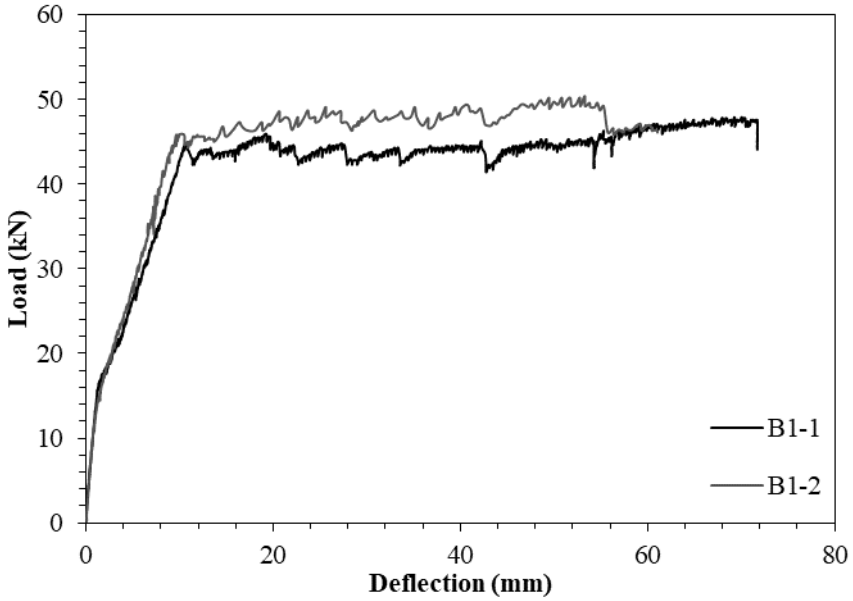

Figure 4: Load-deflection relationship of control beams

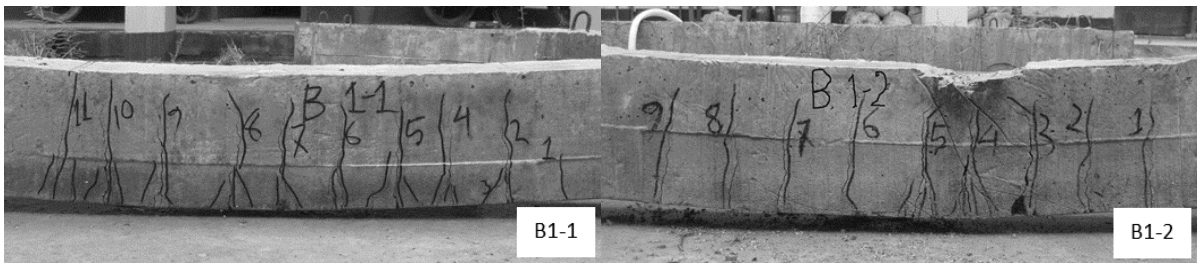

Figure 5: Failure mode and crack pattern of control beams

Most of these cracks were in the region of the maximum bending moment. The ultimate load of control beams was 47.9kN & 50.4kN. The calculated load-carrying capacity of the control beams was 43.1kN while the experimental ultimate load-carrying capacity was found to be 11% & 17% higher than the calculated load-carrying capacity. The average ultimate load of control beams was 49.1kN. The beams failed by flexure after the yielding of steel reinforcement and showed a pure bending behavior. Figure 5 shows the cracks pattern and failure mode of the control beams. The yield and ultimate load and ductility index of two beams were very close. The ultimate load for B1-1 was 47.9kN which was 50.4kN for B1-2. Those values were 11% and 17% higher than the calculated capacity of control beams.

4.2 Preloading

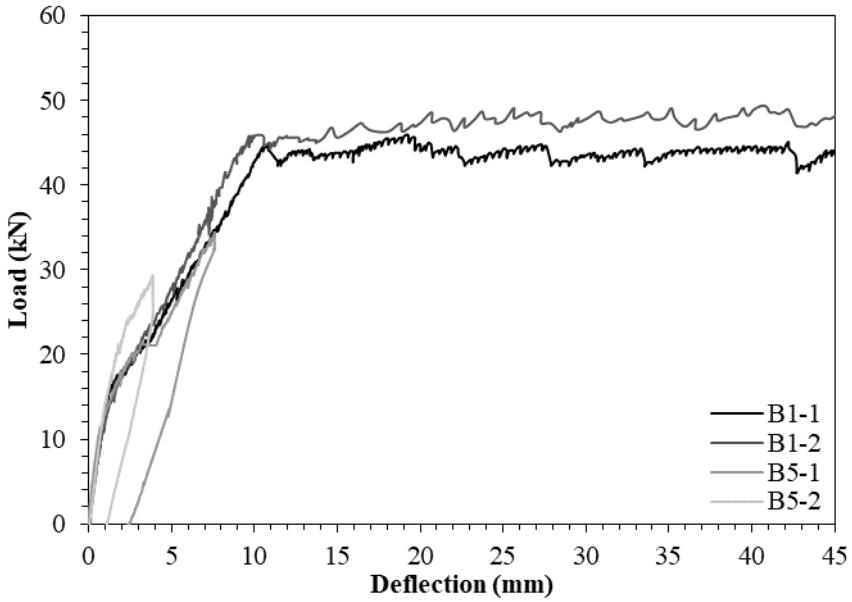

Figure 6: load-deflection relationship of beams due to preloading

Figure 6 shows the load-deflection relationship of beams (except control beams) preloaded with (65-75) % of the ultimate capacity of the control beams. All the beams showed similar behavior for preloading and had some permanent deflection after unloading. Table 3 shows the maximum applied load for preloading, maximum deflection with the corresponding load, permanent deflection after unloading and the number of cracks form due to preloading. Figure 7 shows the crack pattern due to preloading.

Table 3: Summary of preloading

Specimen ID	Applied Load (kN)	Maximum Deflection (mm)	Permanent Deflection (mm)	No of cracks
B5-1	34.5	7.58	2.36	15
B5-2	29.3	3.88	1.04	8

Figure 7: Crack pattern due to preloading

4.3 Strengthening

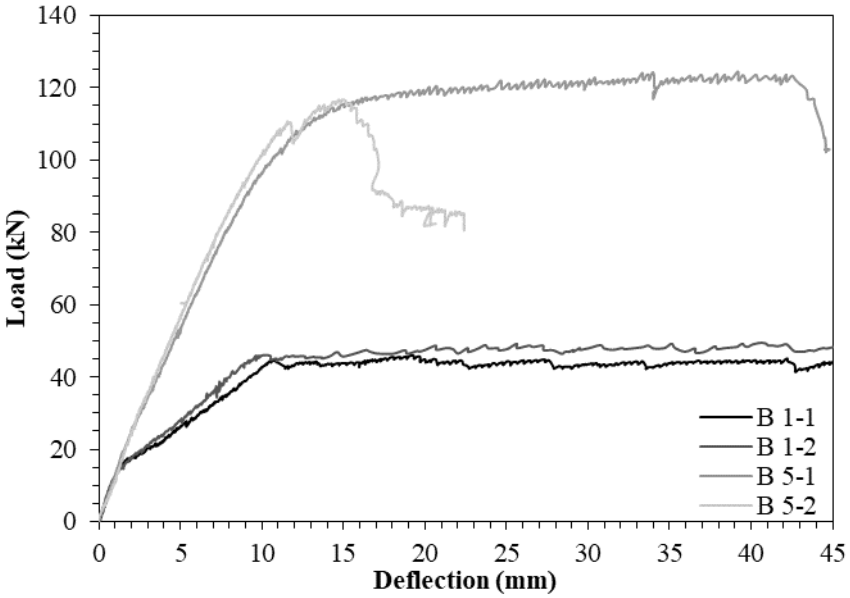

Figure 8: load-deflection relationship of strengthened beams

Figure 8 shows the load-deflection relationship of beams strengthened with external steel angles (B5-1 & B5-2) attached with bottom stirrups by welding. The elastic limit of B5-1 was 18.8kN at mid-span deflection of 1.11mm. The relationship was again linear up to a load of 79.2kN while the mid-span deflection was 6.94mm. The ultimate load was 124.4kN at mid-span deflection of 39.20mm. The experimental ultimate load-carrying capacity was 105% of the calculated load carrying capacity for that beam which was 118.2kN. The beam was failed by crushing of compressive concrete after the yielding of steel bars and external steel angles. Ten new cracks (red) formed some of them were in the shear region and some in the flexural region. The length and width of the new flexural cracks are smaller than the preloaded cracks. B5-2 showed similar behavior like B5-1 in flexure up to a load of 110.4kN and mid-span deflection of 11.26mm. The ultimate load was 116.8kN at mid-span deflection of 14.76mm. The experimental ultimate load-carrying capacity was 99% of the calculated load-carrying capacity. B5-1 showed better ductile behavior than B5-2. The ductility index for B5-2 was 1.27 which was 2.76 for B5-1. The reduction of ductility may be due to more welding failure in the case of B5-2. Total of seven new cracks (red) formed in the shear region. The bottom part which was cast after the attachment of steel angles tended to separate from original concrete which may be due to the failure of welding. The failure mode tended to switch from flexural to shear failure. Figure 9 shows the failure mode and crack pattern of the beams strengthened with external steel angles.

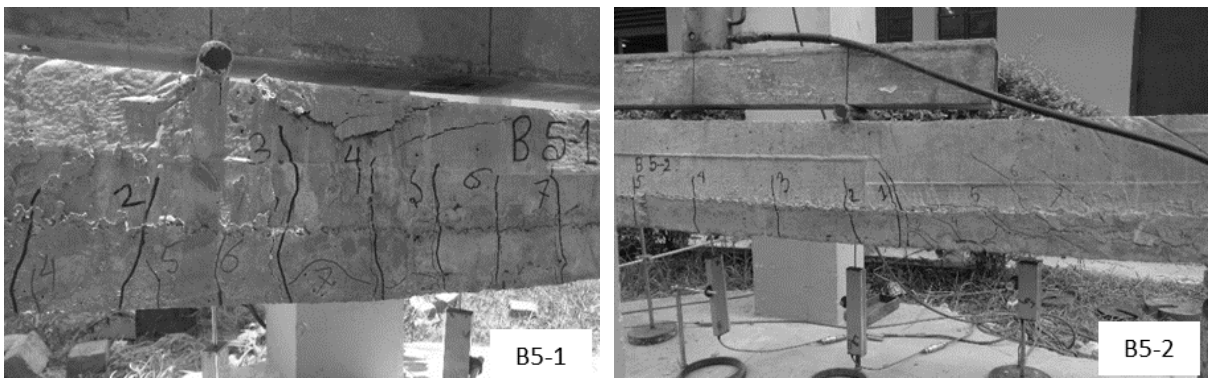

Figure 9: Failure mode of beam strengthened with steel angles

4.4 Comparison of results

Table 2: Summary of test results

Types of Beams	Specimen ID	$P_{u(c)}$ (KN)	$P_{u(e)}$ (KN)	Δ_u (mm)	I_u (%)	$\frac{P_{u(c)}}{P_{u(e)}}$
Control	B1-1	43.2	47.9	69.22	N/A	1.11
	B1-2	43.2	50.4	53.32	N/A	1.17
Strengthened	B5-1	118.2	124.4	39.20	153	1.05
	B5-2	118.2	116.8	14.76	138	0.99

$P_{u(c)}$= calculated ultimate capacity; $P_{u(e)}$= ultimate experimental load-bearing capacity; Δ_u= deflection at ultimate load; I_u Increase in ultimate load-bearing capacity.

Attaching external steel angles, the flexural strength of RC beams increased significantly. The ultimate capacity of the strengthened beams was 124.4kN and 116.8kN which was 153% and 138% higher than the ultimate capacity of control beams. The ultimate capacity was 105% and 99% of the calculated value for the strengthened beams. The beams failed by the yielding of main steel bars and external steel angles. Although ductility decreased due to strengthening the capacity increased at a significant rate.

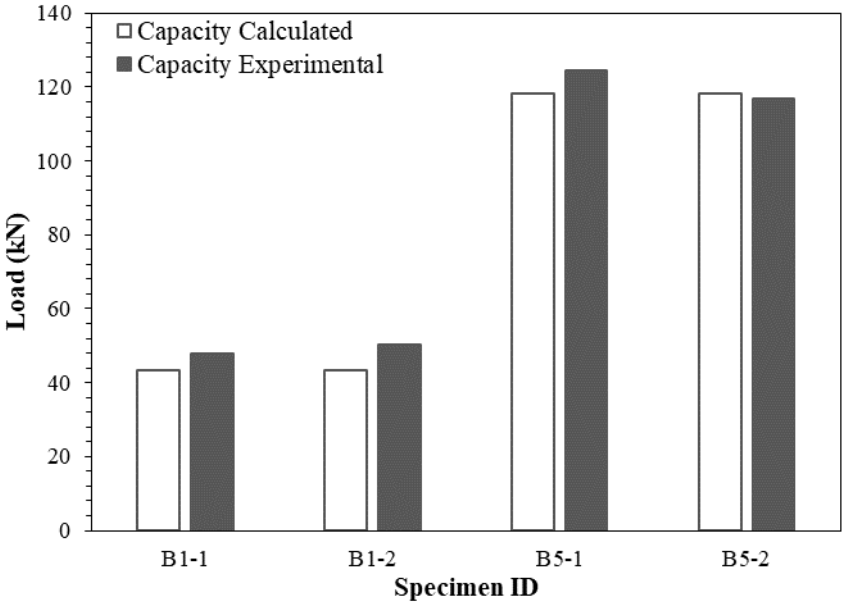

Figure 10: Relationship between calculated and experimental capacity

5. CONCLUSIONS

RC beams strengthened with external steel angles have shown that this is a very effective strengthening technique. The average flexural capacity of the simply supported control beams was 49.1kN. After strengthening the ultimate capacity increased to 124.4kN and 116.8kN which was 153% and 138% higher than control beams. In the case of external steel angles, the ultimate load was 105% and 99% of the calculated capacity.

ACKNOWLEDGEMENTS

Authorswould like to express profound respect and deepest gratitude and the hardest thanks to everybody who involved directly or indirectly in this study. This accomplishment would not have been possible without them.

REFERENCES

ACI Committee, & International Organization for Standardization. (2008). Building code requirements for structural concrete (ACI 318-08) and commentary. American Concrete Institute.

ASTM, C. (2010). Standard test method for flexural strength of concrete (using simple beam with third-point loading). In *American society for testing and materials* (Vol. 100, pp. 19428-2959).

Bangladesh, Public Works Department, Ministry of Housing 6677 and Public Works. (2015). *Project for Capacity Development on Natural Disaster-Resistant Techniques of Construction and Retrofitting for Public Buildings in The People's Republic of Bangladesh*. Retrieved from http://open_jicareport.jica.go.jp/pdf/12252391_01.pdf

Gul, A., Alam, B., Khan, F. A., Badrashi, Y. I., &Shahzada, K. (2015). Strengthening and Evaluation of Reinforced Concrete Beams for Flexure by Using External Steel Reinforcements. *International Journal of Scientific Engineering and Technology*, *4*(4), 260-263.

Iskhakov, I., Ribakov, Y., Holschemacher, K., & Mueller, T. (2013). High performance repairing of reinforced concrete structures. *Materials & Design*, *44*, 216-222. https://doi.org/10.1016/j.matdes.2012.07.041

Islam, S., Islam, M. R., Talukder, M. A. Q., & Hossain, S. R. (2013). Strengthening Technique of Reinforce Concrete Structure: Bangladesh Perspective. *American Academic & Scholarly Research Journal*, *5*(6), 17.

Paul, B. K., & Bhuiyan, R. H. (n.d.). Urban earthquake hazard: Perceived seismic risk and preparedness in Dhaka City, Bangladesh. *Disasters*, *34*(2), 337-359.

Raut, L. L., & Kulkarni, D. B. (2014). Torsional strengthening of under reinforced concrete beams using crimped steel fiber. *International Journal of Research in Engineering and Technology*, *3*(6), 466-471.

Sundarraja, M. C., &Rajamohan, S. (2009). Strengthening of RC beams in shear using GFRP inclined strips - An experimental study. *Construction and Building Materials*, *23*(2), 856-864. https://doi.org/10.1016/j.conbuildmat.2008.04.008

Zhang, P., Han, S., Ng, S., & Wang, X.-H. (2018). Fiber-Reinforced Concrete with Application in Civil Engineering [Research article]. https://doi.org/10.1155/2018/1698905

Proceedings of the 5th International Conference on Civil Engineering for Sustainable Development (ICCESD 2020), 7~9 February 2020, KUET, Khulna, Bangladesh (ISBN-978-984-34-8764-3)

PERFORMANCE OF CONCRETE UNDER ELEVATED TEMPERATURE

Md. Arifuzzaman*[1], Md. Maruf Molla[2] and Muhammad Harunur Rashid[3]

[1] Bridge Engineer, Spectra Engineers Ltd., e-mail: arifjsr.apon@gmail.com
[2] Lecturer, Department of Civil Engineering, Khulna University of Engineering & Technology, Bangladesh, e-mail: marufmolla@ce.kuet.ac.bd
[3] Professor, Department of Civil Engineering, Khulna University of Engineering & Technology, Bangladesh, e-mail: mhrashid@ce.kuet.ac.bd

***Corresponding Author**

ABSTRACT

In this study, the variation of different mechanical properties of high strength concrete at elevated temperatures was investigated. The mechanical properties such as compressive strength and splitting tensile strength under different temperatures (200°C, 400°C and 600°C) were determined following three various cooling conditions (immediately after heating i.e. no cooling, 24 hours cooling and water cooling). Concrete cylindrical specimens (100 mm dia. and 200 mm height) were prepared by maintaining a mix ratio of 1:1.8:1.95 among binder, Fine Aggregate, Coarse Aggregate and with water to cement ratio of 0.4. After completing 28 days of curing period, the compressive and tensile strength of 6 nos. of specimens were tested at room temperature (32°C) and rest of them were heated in a laboratory furnace for 1 hour at 200°C, 400°C, 600°C temperature, following 3 hours of preheating at 105±5°C temperature. After that, the strength tests of the heated specimens were completed at the three different cooling conditions. Compressive and tensile strengths were found as 44.7 MPa and 4.04 MPa respectively at room temperature. From the results of this study, it was observed that no remarkable changes in compressive and tensile strengths of concrete were observed between 200°C and 400°C heating temperature. Whereas, gradual decrease in the mechanical properties were found at 200°C and rapid reduction was observed after 400°C due to explosive spalling. Maximum reduction in compressive and tensile strengths were observed as 55.5% and 63.6% respectively at 600°C for testing after water cooling condition when compared to the controlled specimens. Moreover, the tensile strength of concrete decreased more promptly than compressive strength after 400°C temperature.

Keywords: High strength concrete, Compressive strength, Tensile strength, Elevated temperature.

1. INTRODUCTION

Concrete is the most widely used construction material in the world. The main functional elements of concrete are cementing medium, fine aggregate, and coarse aggregate. Based on the strength requirements, there are mainly two types of concrete, such as, normal strength concrete (NSC) and high strength concrete (HSC). According to American Concrete Institute (ACI 363R, 1997), concrete having 28 days compressive strength above 41 MPa, can be considered as HSC. The demand of high strength concrete is increasing day by day as the performance (in terms of strength and durability) of high strength concrete is superior than NSC (Neville & Brooks, 2010). Fire accident in concrete structures has become one of the most unavoidable hazards in the world. Though it is thought that high strength concrete has a good fire resistance, its exposure to fire affects badly the mechanical properties (Malhotra, 1956; Neville, 2012). In the past, extensive investigations have been conducted to examine the behavior of NSC exposed to fire (Lea, 1920; Kim, Han, & Song, 2002; Shoukry, William, Downie, & Riad, 2011); however, very limited studies are found regarding brick aggregate based HSC.

Earlier at 20th century, Lea (1922) outlined in a review report that concrete prepared with ground brick and cement, gain strength up to 650°C heating temperature. Chan, Peng, & Chan (1996) carry out an extensive research regarding compressive and tensile strength of HSC in comparison with NSC. Fire exposure for the samples were varied from 400°C to 1200°C. Finally, it was found that the strength reduction of HSC occurred with a higher rate than NSC. Similar trend regarding calcareous aggregate based HSC and NSC was observed from the experiment conducted by Noumowe, Clastres, Debicki, & Costaz (1996). Again, the effect of high temperatures and cooling regimes on regarding high performance concrete (HPC) and NSC, was investigated (Chan, Luo, & Sun 2000). In that case, rapid cooling caused more strength loss than gradual cooling.

Husem (2006) had examined the variation of flexural and compressive strength of high-performance micro-concrete (HPMC) and ordinary micro-concrete (OMC) at elevated temperatures following different cooling regimes. The results showed that rapid reduction in flexural and compressive strength was observed at 200°C when compared to the reference specimens. After 600°C heating temperature, both the strengths decreased, showing a little increasing trend between 200° and 400°C. Moreover, Bastami, Chaboki-Khiabani, Baghbadrani, & Kordi (2011), examined the performance of HSC, prepared with varying water to cement ratio, fine aggregate ratio and silica fume ratio under elevated temperature exposure. Most of the researches were regarding limestone aggregate based concrete.

In the recent years, several fire incidents, are frequently occurring in Bangladesh due to various reasons. Most of them broke out in industries, factories, shopping complexes, residential buildings, etc., which not only caused significant loss of valuable lives, livelihoods, and equipment but also seriously affected the structures. Moreover, burning was not the only reason behind the life loss as well as injury. In fact, the structural failure of the building was also responsible for the life loss (Wadud, Huda, & Ahmed, 2014). On the other hand, the structure is required to be rebuilt or repaired to allow the structure functional again after a fire incident has happened. In that case, it is required to investigate the residual capacity of the structure after being exposed to fire hazard. Being a major construction material of reinforced concrete structures, the residual capacity of concrete at high temperatures, can give a very important indication about the structural strength. So, it is required to investigate the residual capacity of the structure. Besides, brick aggregate is one of the most commonly used coarse aggregate for concrete in Bangladesh. Furthermore, a few research works are available on HSC with brick aggregate as coarse aggregate. Thus, the objectives of this study are to determine the mechanical properties (compressive strength and tensile strength) of HSC after being heated to high temperatures (200°C, 400°C and 600°C) and to compare the effect of different cooling regimes on the residual strength of HSC with respect to the strength at room temperature.

2. EXPERIMENTAL PROGRAM

2.1 Materials and Mix Proportions

Portland Cement Composite (PCC) confirming to ASTM C595/C595M as a binder material, coarse sand as fine aggregate (FA), 19 mm downgrade 1st class brick aggregate as coarse aggregate (CA) were used to prepare the concrete mix. The material properties of the binder and aggregates are tested in the laboratory according to ASTM standard procedure and tabulated in Table 1 below. The mix ratio among binder, FA and CA was 1 : 1.8 : 1.95, maintained to prepare the test specimens.

Table 1: Material Properties of binder and aggregate

Materials	Properties	Unit	Value	Test Standards
Binder (PCC)	Initial Setting Time	min	170	ASTM C191
	Final Setting Time	min	295	ASTM C191
Fine Aggregate (Coarse Sand)	Specific Gravity (SSD)	-	2.44	ASTM C128
	Absorption	%	2.4	ASTM C127
	Fineness Modulus	-	2.91	ASTM C136
	Unit Weight	Kg/m³	1605	ASTM C29
Coarse Aggregate (Brick Aggregate)	Absorption	%	13.7	ASTM C127
	Unit Weight	Kg/m³	1130	ASTM C29

2.2 Preparation of Concrete Specimens and Curing

70 nos. of cylindrical specimens (100 mm diameter and 200 mm height) were cast using the mix ratio. For each batch of mixing, slump test was performed and the value was recorded 80 ~ 90 mm. The top surface of the specimens was finished with 1 (cement): 1 (fine sand) rich mortar mix by using a straight edge before reaching to initial set. Then the samples were placed at a moist place to avoid the unexpected surface moisture loss. After 24 hours, the samples were demolded and placed in a curing chamber to promote the hydration process. The samples were cured for 28 days.

2.3 Heating

After completion of the curing period the samples were removed from the chamber and kept in air to drying up the surface water. A preliminary drying process was carried out for 3 hours at a temperature of 105±5°C in an electric oven as shown in figure 1 below. Preheating was necessary to reduce the internal water content of the specimens.

(a) (b) (c)

Figure 1: (a) Specimens placed in the oven for preheating, (b) Electric oven for preheating, (c) Specimen after preheating in oven at

After that the samples were placed in a laboratory furnace for heating the samples at 200°C, 400°C and 600°C temperature following the ASTM E 119 standard time-temperature curve. The maximum heating capacity of the furnace was 1200°C temperature. The samples were heated for 1 hour after being reached to the desired temperature.

(a) (b)

Figure 2: (a) Placement of the specimens in the furnace, (b) Furnace during heating process

2.4 Test Methods

The Compressive and splitting tensile strength tests were carried out according to ASTM C 39 and ASTM C496 respectively. Both of the tests were performed in a Compression Testing Machine with a capacity of 1000 kN. After completing the heating of the specimens, compressive and splitting tensile strength tests were performed for three different cooling conditions. The cooling conditions were: (i) No cooling (i.e., test immediately after heating), (ii) water cooling and (iii) cooling for 24 hours after heating. The compressive and tensile strength of the controlled specimens were also determined at room temperature. Three samples were tested to get the average experimental results.

Figure 3: (a) Compressive strength test, (b) Tensile strength test

3. RESULTS & DISCUSSION

3.1 Compressive strength at different elevated temperature

The test results of compressive strength of concrete specimens at room temperature and several exposed temperatures (200°C, 400°C and 600°C), based on three separate cooling conditions, are presented in figure 4. At ambient temperature the average compressive strength of concrete specimens was found to be 44.7 MPa. The compressive strength decreased rapidly with increasing temperature up to 200°C. No remarkable change was observed between 200°C and 400°C temperature for the specimens tested after 24 hours of heating and immediately after heating. This slow decreasing rate attributed to the removal of crystalline water from the samples (Lie, 1992). After 400°C rapid reduction in the concrete compressive strength occurred for all the cooling conditions. The minimum compressive strength was found to be 24.47, 23.05 and 19.08 MPa for the test after 24 hours of heating, immediately after heating and water cooling respectively. However, spalling, especially explosive spalling is the major reason behind the strength reduction of high strength concrete. Spalling of concrete from surface of the cylindrical specimens were noticed at 600°C heating temperature. In high strength concrete, less amount of pore spaces exists inside due to high density. So, there is less scope for vapor pressure to escape from concrete when subjected to high temperatures, causing explosive spalling of concrete and accordingly the compressive strength of concrete may also decrease (Chan et al., 2000).

The test results show that compressive strength reduction rate is affected by the cooling conditions considered in this study. The maximum reduction was found for the specimens tested after water cooling as the water spray on heated specimens caused cracking and crumbling of concrete due to conversion of calcium oxide to calcium hydroxide (Arioz, 2007). However, there is a slight reduction of concrete compressive strength for the test immediately after heating than that of for the test after 24 hours of heating, which may occur due to the partial recovery of concrete strength.

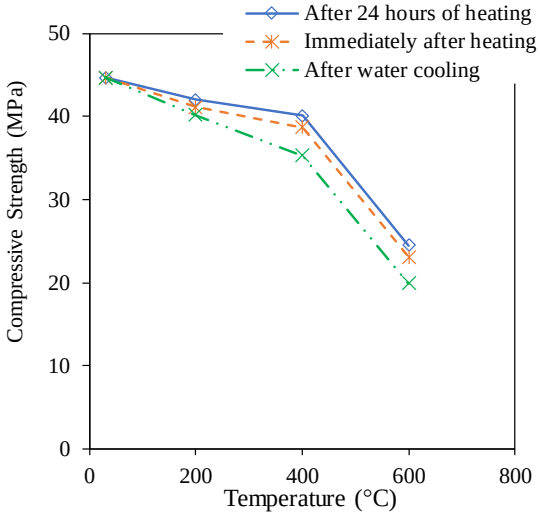

Figure 4: Compressive strength at different elevated temperatures

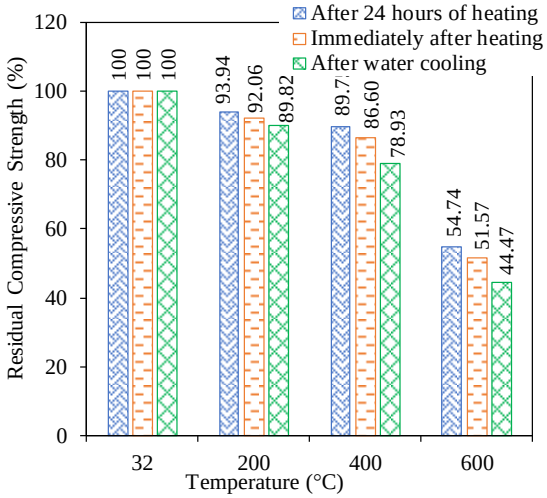

Figure 5: Residual compressive strength at different elevated temperatures

In figure 5 the relative residual compressive strengths as a percentage of average strength obtained by testing control specimens, were presented against various high temperatures, for different cooling conditions. About 7~10% of compressive strength reduction was observed at 200°C. Subsequently, showing a little decrease at 400°C temperature, the compressive strength rapidly decreased when the samples were heated at 600°C. At 600°C temperature, maximum of 45.26%, 48.43% and 55.53% strength reduction were observed with respect to the control specimen for the test after 24 hours of heating, immediately after heating and after water cooling respectively. Similar trend with little different reduction in compressive strength were obtain from Chan, Peng, & Anson (1999), Husem (2006).

3.2 Splitting Tensile Strength at Different Elevated Temperature

The splitting tensile strength test was performed for all of the test conditions and the average results of the specimens are presented in figure 6 below. From the figure, it can be shown that the slope of the tensile strength vs temperature curve showed distinct nature with increasing temperature which behaves similar to the trend followed by compressive strength. A significant decrease in the tensile strength observed when the specimens were exposed to temperature between 400°C and 600°C. The maximum tensile strength was found to be 4.04 MPa at ambient temperature and the minimum tensile strength was found to be 1.47 MPa for the test after water cooling and 1.65 MPa for the test immediately after heating. Moreover, due to regain of strength after 24 hours of cooling phase the tensile strength was found to be 1.88 MPa. All the minimum values of tensile strength were observed at the maximum temperature 600°C.

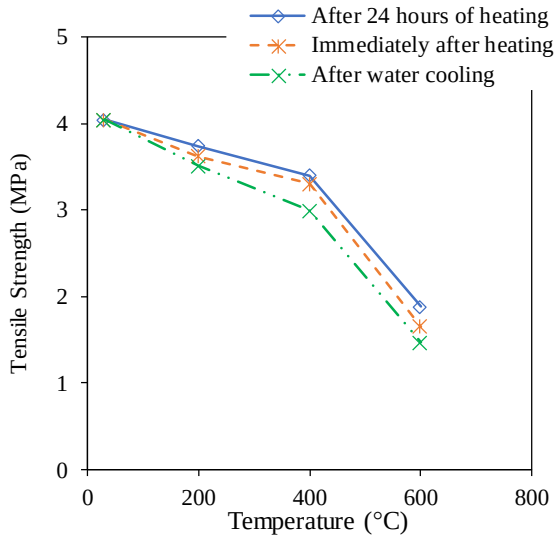

Figure 6: Tensile strength at different elevated temperatures

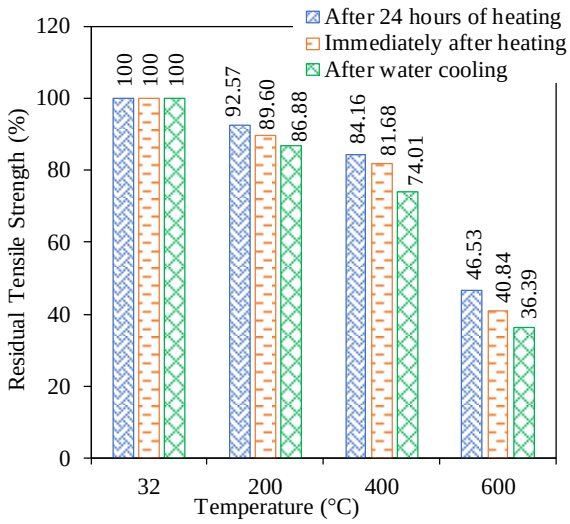

Figure 7: Residual tensile strength at different elevated temperatures

The relative residual tensile strength of concrete was calculated as the percentage strength of unheated specimens and presented in figure 7. The residual tensile strengths of concrete with respect to the control specimens were obtained as 46.53%, 40.84% and 36.39% for the specimens tested after 24 hours of heating, immediately after heating and after water cooling respectively at 600°C temperature. Among these three cooling conditions, maximum tensile strength reduction of 63.61% was occurred due to water cooling of the samples.

The splitting tensile strength to compressive strength ratio at different elevated temperatures are shown in Figure 8. The tensile strength to compressive strength ratio of concrete remained almost identical up to 400°C heating temperature. But in case of heating the samples at 600°C temperature, the ratio was 15.0%, 20.8% and 18.3% lower than that of control specimens for three different cooling conditions respectively. The observations showed that the tensile strength decreased more promptly than compressive strength. Hence, the concrete strength depends on the load resisting area of concrete which decreased with increasing crack in concrete. Besides, the cracks approaching closer when subjected to compressive load and contrarily, they become more prominent under tensile load. Therefore, the effect of crack coalescence in concrete is more pernicious to tensile strength (Behnood and Ghandehari 2009; Peng *et al.* 2006; Chen 2007).

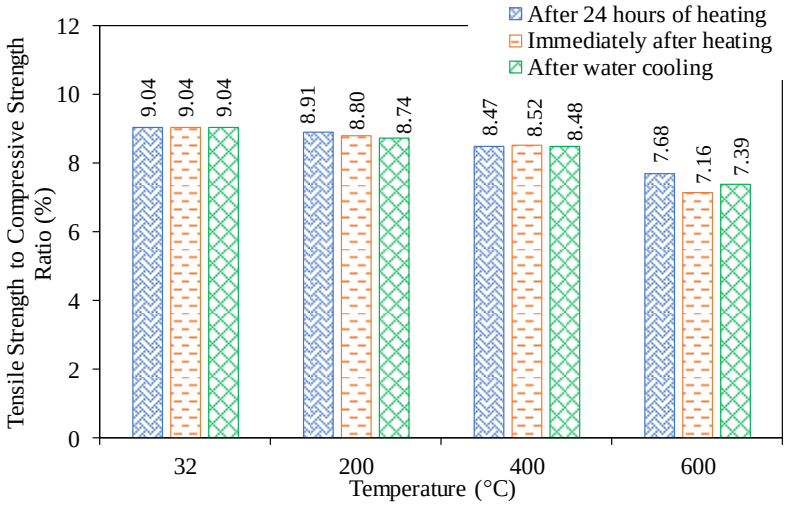

Figure 8: Ratio of splitting tensile strength to compressive strength of concretes at different temperatures

4. CONCLUSION

In this study the different mechanical properties of high strength concrete at high temperatures (200°C, 400°C, 600°C) were determined and the following conclusions may be outlined from the experimental results:

- The average compressive and tensile strength of HSC were found to be decreased with increasing temperature. The decreasing rate was not significant between 200°C and 400°C temperature.
- A severe strength reduction as well as explosive spalling of the concrete specimens were observed at 600°C exposure temperature.
- Relative strength reduction at different elevated temperatures are affected by the cooling conditions. When the samples were subjected to the peak temperature of 600°C, the residual compressive strength of HSC relative to the control specimen dropped to approximately 54.74%, 51.57% and 44.47% for after 24 hours cooling process, immediately after heating and after water cooling respectively.
- Moreover, the residual tensile strength of HSC relative to the control specimen dropped to approximately 46.53%, 40.84% and 36.39% for the three different cooling conditions respectively.
- Therefore, the rate of decrease in both the mechanical properties of HSC is maximum for the specimens tested after rapid water cooling following the high temperature exposure.
- Tensile strength is more sensitive to high temperature than compressive strength. Thus, the rate of decrease of compressive strength is higher than that of tensile strength at high temperature.

REFERENCES

ACI 363R. (1997). State-of-the-Art Report on High-Strength Concrete. *American Concrete Institute*, *92*(Reapproved).

Arioz, O. (2007). Effects of elevated temperatures on properties of concrete. *Fire Safety Journal*, *42*(8), 516–522. https://doi.org/10.1016/j.firesaf.2007.01.003.

ASTM C 39. (2015). Compressive Strength of Cylindrical Concrete Specimens. *ASTM Standards*, 1–7. https://doi.org/10.1520/C0039.

ASTM C127. (2015). Standard Test Method for Relative Density (Specific Gravity) and Absorption of Coarse Aggregate. *ASTM International*, *I*, 5. https://doi.org/10.1520/C0127-15.2.

ASTM C128. (2015). American Society for Testing and Materials. ASTM C128: Standard Test Method for Relative Density (Specific Gravity) and Absorption of Fine Aggregate. *ASTM International*, *i*, 6. https://doi.org/10.1520/C0128-15.2.

ASTM C136. (2014). *Standard Test Method for Sieve Analysis of Fine and Coarse Aggregates*. 3–7. https://doi.org/10.1520/C0136.

ASTM C191. (2013). Standard Test Method for Time of Setting of Hydraulic Cement by Vicat Needle. *ASTM International*, *i*(May), 1–8. https://doi.org/10.1520/C0191-13.2.

ASTM C29/C29M. (2009). Standard Test Method for Bulk Density ("Unit Weight") and Voids in Aggregate. *ASTM International*, *i*(c), 1–5. https://doi.org/10.1520/C0029.

ASTM C496. (2014). Standard Test Method for Splitting Tensile Strength. *Annual Book of ASTM Standards*, *i*, 1–5. https://doi.org/10.1520/C0496.

ASTM C595/C595M. (2018). Standard Specification for Blended Hydraulic Cements. In *Annual Book of ASTM Standards*. https://doi.org/10.1520/C0595.

ASTM E119. (2000). Standard Test Methods for Fire Tests of Building Construction and Materials. *Analysis*, 1–25. https://doi.org/10.1520/E0119-10B.1.2.

Bastami, M., Chaboki-Khiabani, A., Baghbadrani, M., & Kordi, M. (2011). Performance of high strength concretes at elevated temperatures. *Scientia Iranica*, *18*(5), 1028–1036. https://doi.org/10.1016/j.scient.2011.09.001.

Behnood, A., & Ghandehari, M. (2009). Comparison of compressive and splitting tensile strength of high-strength concrete with and without polypropylene fibers heated to high temperatures. *Fire Safety Journal*, *44*(8), 1015–1022. https://doi.org/10.1016/j.firesaf.2009.07.001.

Chan, S. Y. N., Luo, X., & Sun, W. (2000). Effect of high temperature and cooling regimes on the compressive strength and pore properties of high performance concrete. *Construction and Building Materials*, *14*(5), 261–266. https://doi.org/10.1016/S0950-0618(00)00031-3.

Chan, S. Y. N., Peng, G. F., & Chan, J. K. W. (1996). Comparison between high strength concrete and normal strength concrete subjected to high temperature. *Materials and Structures/Materiaux et Constructions*, pp. 616–619. https://doi.org/10.1007/bf02485969.

Chan, Y. N., Peng, G. F., & Anson, M. (1999). Residual strength and pore structure of high-strength concrete and normal strength concrete after exposure to high temperatures. *Cement and Concrete Composites*, *21*(1), 23–27. https://doi.org/10.1016/S0958-9465(98)00034-1.

Chen, W. F. (2007). Plasticity in reinforced concrete. J. Ross Publishing.

Husem, M. (2006). The effects of high temperature on compressive and flexural strengths of ordinary and high-performance concrete. *Fire Safety Journal*, *41*(2), 155–163. https://doi.org/10.1016/j.firesaf.2005.12.002.

Kim, J., Han, S. H., & Song, Y. C. (2002). Effect of Temperature and Aging on the Mechanical Properties of Concrete Part I . Experimental Results. *Cement and Concrete Research*, *32*, 1087–1094.

Lea, F. C. (1920). The effect of temperature on some of the properties of materials. Engineering, 110(3), 293-298.

Lea, F. C. (1922). The resistance to fire of concrete and reinforced concrete. *Journal of the Society of Chemical Industry*, *41*(18), 395R-396R. https://doi.org/10.1002/jctb.5000411814.

Lie, T. T. (Ed.). (1992, January). Structural fire protection. American Society of Civil Engineers.

Malhotra, H. L. (1956). The effect of temperature on the compressive strength of concrete. *Magazine of Concrete Research*, *8*(1), 85–94. https://doi.org/doi:10.1680/macr.1956.8.23.85.

Neville, A. M. (2012). Properties of concrete. In *Proceedings of the 5th IASTED International Conference on Signal Processing, Pattern Recognition, and Applications, SPPRA 2008* (5th ed.). Prentice Hall.

Neville, A. M., & Brooks, J. J. (2010). *Concrete Technology* (2nd ed.). Pearson Education Limited.

Noumowe, A. N., Clastres, P., Debicki, G., & Costaz, J. L. (1996). Transient heating effect on high strength concrete. *Nuclear Engineering and Design*, *166*(1), 99–108. https://doi.org/10.1016/0029-5493(96)01235-6.

Peng, G. F., Chan, S. Y. N., Song, Q. M., & Yi, Q. X. (2006). Effect of high temperature on concrete: A review. *Key Engineering Materials*, *302–303*(50108001), 138–149. https://doi.org/10.4028/www.scientific.net/kem.302-303.138.

Shoukry, S. N., William, G. W., Downie, B., & Riad, M. Y. (2011). Effect of moisture and temperature on the mechanical properties of concrete. *Construction and Building Materials*, *25*(2), 688–696. https://doi.org/10.1016/j.conbuildmat.2010.07.020.

Wadud, Z., Huda, F. Y., & Ahmed, N. U. (2014). Assessment of Fire Risk in the Readymade Garment Industry in Dhaka, Bangladesh. *Fire Technology*, *50*(5), 1127–1145. https://doi.org/10.1007/s10694-013-0349-2.

Proceedings of the 5th International Conference on Civil Engineering for Sustainable Development (ICCESD 2020), 7~9 February 2020, KUET, Khulna, Bangladesh (ISBN-978-984-34-8764-3)

PERFORMANCE OF MORTAR INCORPORATING CERAMIC WASTE POWDER AS PARTIAL REPLACEMENT OF CEMENT

S.M. Shaik-ul-Karim*[1], Shafkat Ahmed[1] and Ismail Saifullah[2]

[1]Undergraduate Student, Department of Civil Engineering, Khulna University of Engineering & Technology (KUET), Bangladesh, e-mail: rishad.ce1501012@gmail.com
[1]Undergraduate Student, Department of Civil Engineering, Khulna University of Engineering & Technology (KUET), Bangladesh, e-mail: ahmed1501024@stud.kuet.ac.bd
[2]Associate Professor, Department of Civil Engineering, Khulna University of Engineering & Technology (KUET), Bangladesh, e-mail: saifullah@ce.kuet.ac.bd

***Corresponding Author**

ABSTRACT

As construction industry is growing larger at an extreme rate, the generation of construction waste has increased largely. Ceramic tile is one of the major solid wastes generated from construction activities. The solid wastes generated from construction causes undesirable problem so the reusability of these wastes to enhance environmental safety has drawn attention of many researchers. In this study, ceramic waste powder (CWP) from residual ceramic tile was used as a partial replacement of cement in mortars to understand the effect of CWP on the mechanical properties (compressive and tensile strength) of mortar at different curing period. Cement was replaced by CWP at percentages of 10%, 15%, 20%, 25% and 30% in relevant standard cubes and briquette molds to observe their respective strengths at 3 days, 7 days and 28 days curing. Based on the test results, it has been observed that the compressive strength and tensile strength of mortar decreases gradually with the increases percentage of ceramic waste powder (CWP). However, there is no significant reduction of strength observed up to 20% replacement of cement using CWP. The outcomes of this study suggested that up to 20% cement replacement by ceramic waste powder is feasible in mortar which consequences the reduction of cement consumption in construction.

Keywords: *Construction waste, Ceramic tile, CWP, Compressive strength, Tensile strength.*

1 INTRODUCTION

In the modern world, fast growing population has led to a large consuming requirement. To meet the consumers' need, tremendous amount production is being carried out. Large amount of production results in large amount of waste generation. A major solid waste generated from construction work is ceramic tile. Approximately 12 million m^2 ceramic tile are manufactured worldwide (Mohammadhosseini, et al., 2019). Torkittiku & Chaipanich (2010) reported that approximately 30% of ceramic production is reported to be wasted. In Bangladesh, the wasted ceramic tiles from construction work are generally dumped at roadside or around the construction area. The idea of green construction has attracted researchers to recycle and reuse the ceramic wastes in various engineering field.

In some of the solid wastes, cementitious properties were found and are being used as supplementary materials with cement (LI, Zhuo, Zhu, Chen, & Kwan, 2019). Firing clay, Feldspar and quartz are the basic ingredient of ceramic tile. The main chemical elements of ceramic tile are Silicon dioxide (SiO_2) and Aluminium Oxide (Al_2O_3). Besides, Oxides of Iron (Fe_2O_3), Calcium (CaO), Potassium (K_2O), Sodium (Na_2O) and Zirconium (ZrO_2) are also found (Asiwaju-Bello, Olalusi, & Olutoge, 2017). Ceramic waste can be grinded to form Ceramic waste powder (CWP) to use it as a partial replacement of construction material. Researches have been made to test the ability of CWP to replace binders or aggregates in concrete or mortar. In mortar CWP can be used to substitute cement, cement paste or sand as shown in Figure 1.

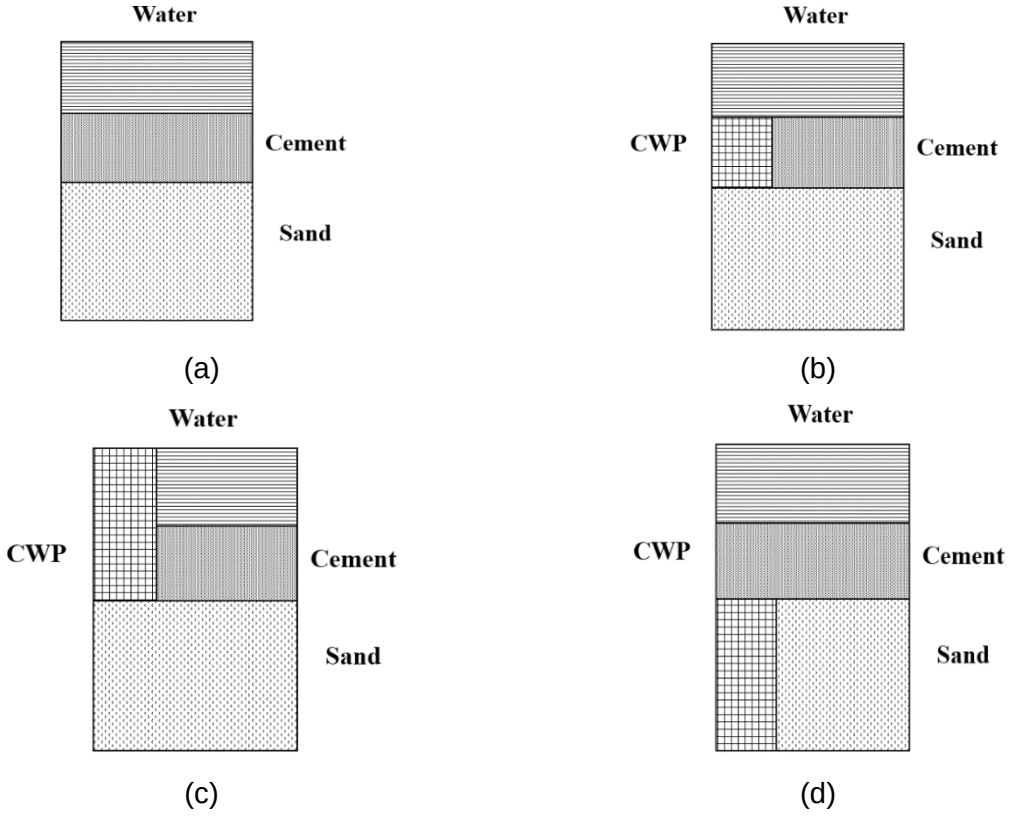

Figure 1: (a) Normal Mortar, (b) CWP replacing cement in mortar, (c) CWP paste is replacing water and cement, and (d) CWP is replacing fine aggregate.

Using CWP as replacement of cement can reduce the amount of cement used. Generally, 1 ton of Portland cement production generates almost equal amount of Carbon dioxide (CO_2) (Najim, Al-Jumaily, & Atea, 2019). It is reported that 5% to 8% of greenhouse gas emission is caused by cement manufacturing (El Dieb & Kanaan, 2018). El Dieb and Kanaan (2018) informed that ceramic waste

has potential to be used as concrete ingredient but further research is required. CWP have pozzolanic activity that can contribute to concrete (Rahhul, Irassar, Castellano, Pavslik, & Cerny, 2014). According to Irassar et al. (2014) using CWP as pozzolanic material simulates hydration due to more effective water cement ratio. They also observed good pozzolanic activity after 28 days. The utilization of CWP as cement replacement can decrease thermal property but increase thermal insulation (Pokornŷ, Fort, Pavlikova, Studnika, & Pavlic, 2014). Wang and Tian (2019) showed that incorporating CWP in mortar reduced the heat of hydration and increased shrinkage. Concrete permeability can be reduced through the replacement of cement by CWP (Cheng, Huang, Liu, Hou, & Li, 2016). According to Reiterman et al. (2014), replacement of 10% cement by using CWP can reduce mechanical property of concrete by 3%. When CWP is used as replacement of fine aggregate, there is a great effect on workability due to greater water absorption properties (Matias, Faria, & Torres, 2014). Incorporation of CWP in concrete can also reduce permeability and increase durability (Bignozzi & Bondua, 2011).

In this study, an effort was made to use the CWP as binding material to replace cement. Grinded ceramic tile was used as CWP to replace different percentages of weight of cement in mortar. The main focus of the study was the effect of CWP on the mechanical properties (compressive and tensile strength) of mortar at different curing period. This research mainly accomplished to find scopes to recycle and reuse waste ceramic tiles to develop sustainable and eco-friendly construction.

2 MATERIALS AND METHODS

2.1 Ceramic waste powder

Ceramic powder was made from waste tiles. At first tiles were broken at small size. These broken tiles were put on aggregate crushing machine for hydraulic pressure (near 200kN). Then the crushed ceramics were put on “Los Angels Abrasion Machine” for 15 min. The grinded ceramics were sieved by #200 sieve as shown in Figure 2.

Fig 2: Preparation of ceramic waste powder through #200 passing

2.2 Cement

Cement is used in mortar and concrete as a binding material at huge amount. The binding of mortar depends on the binding property of cement. Ordinary Portland Cement is used in this study. The initial and final setting time of cement were measured in accordance with ASTM C191 and found 160 minutes and 285 minutes respectively, which satisfies the standard requirement (ASTM C595) for both Ordinary Portland Cement (OPC) and Portland Composite Cement (PCC).

2.3 Sand

According to ASTM C1329 blended sand needs to be used for the preparation of cement mortar. In this research, Ottawa sand was used to prepare cement mortars. The gradation of blended sand was performed in accordance with ASTM C778.

2.4 Preparation of specimen

Cube specimens (2in x 2in x 2in) with cement sand ratio of 1:2.75 were prepared for compressive strength test. Cement was replaced by ceramic waste powder (CWP) at different percentage such as 10%, 15%, 20%, 25%, and 30%. Water cement ratio was kept constant at 0.485. Total 54 cubes were prepared for compression testing. Some prepared samples for compressive strength test of mortar are shown in Figure 3(a). Nine (09) cubes from each percentage were made for 3 days, 7 days and 28 days curing. Table 1 presents the estimated amounts of materials required for three (03) 2in x 2in x 2in cubes of corresponding percentage.

Table 1: Material quantity for preparation of three (03) 2in x 2in x 2in cubes

ID	Ceramic (gm)	Cement (gm)	Sand (gm)	Water (gm)
0%	0	250	687.5	121.25
10%	25	225	687.5	121.25
15%	37.5	212.5	687.5	121.25
20%	50	200	687.5	121.25
25%	62.5	187.5	687.5	121.25
30%	75	175	687.5	121.25

For tensile strength test, 1:3 mortar was used to prepare the briquette. Here also cement was replaced by CWP at different percentage (10%, 15%, 20%, 25%, and 30%). Water cement ratio was taken 0.485. Total 54 briquettes were prepared among which nine (09) specimens from each percentage were made for 3 days, 7 days and 28 days curing. The estimated amounts of materials required for three (03) briquettes of corresponding percentage is presented in Table 2. Some prepared samples for tensile strength test of mortar are shown in Figure 3(b).

Table 2: Material quantity for preparation of three (03) briquettes

ID	Ceramic (gm)	Cement (gm)	Sand (gm)	Water (gm)
0%	0	125	375	60.625
10%	12.5	112.5	375	60.625
15%	18.75	106.25	375	60.625
20%	25	100	375	60.625
25%	31.25	93.75	375	60.625
30%	37.5	87.5	375	60.625

(a) Cube specimens (b) Briquette specimens

Figure 3: Prepared cube and briquette specimens

2.5 Experimental Set-up

2.5.1 Compressive Strength Test

Compressive strength test was performed according to ASTM C109. 2in x 2in x 2in cube mortar was used. Control specimens were made designated as 0%. Cement was replaced by ceramic waste powder at different percentage. 10%, 15%, 20%, 25%, and 30% of ceramic powder was used in mortar. Compressive test was done after 3days, 7days and 28 days curing. The load was applied until failure of the specimen. Figure 4(a) illustrates the compressive strength test set-up for cube specimen.

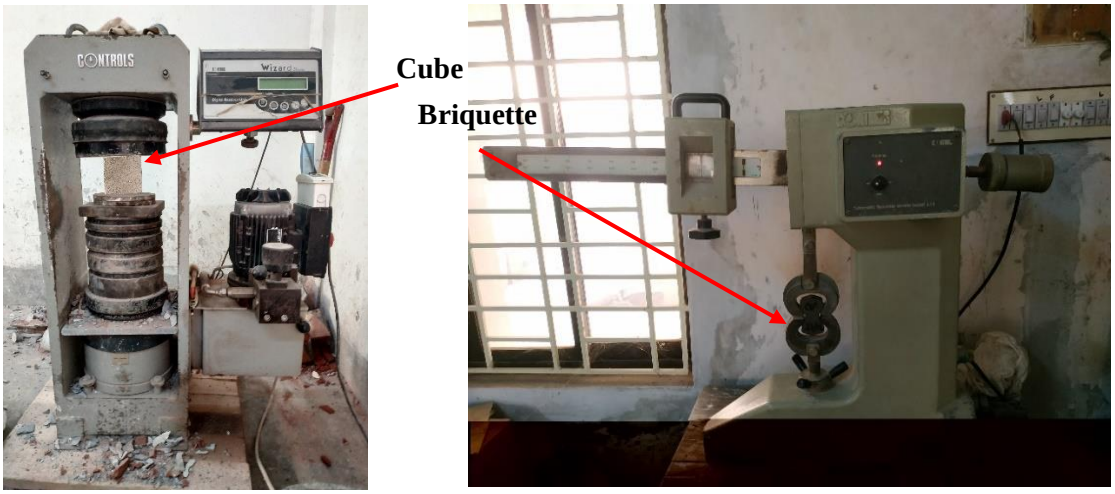

(a) Compressive strength test set up (b) Tensile strength test set up

Figure 4: Experimental Set-up

2.5.2 Tensile Strength Test

Tensile strength test was carried out in accordance with ASTM 1860. Briquette specimen was used in this test. The briquette was 3" long, 1.75" wide, 1" wide in contracted mid-section and 1" deep as per ASTM standard. Specimen without CWP is designated as control specimens. Here also, 0%, 15%, 20%, 25%, and 30% of cement was replaced by the CWP to prepare mortar. Samples were cured for 3 days, 7 days and 28 days. The tensile strength test set-up for briquette specimen is presented in Figure 4(b). The load was applied until failure of the specimen.

3 RESULTS AND DISCUSSIONS

3.1 Compressive Strength of Mortar

Curing time enhances the compressive strength of mortar as shown in Figure 5. Curing of mortar increase the binding property among the materials. Figure 5 is providing a clear evidence that compressive strength is decreasing gradually with the increasing amount of ceramic waste powder (CWP). The compressive strength for control specimen (0%) was found 17.57 MPa, 27.47 MPa and 40.24 MPa for the curing period of 3days, 7days and 28 days respectively. However, 31.23 MPa and 30.70 MPa compressive strength was gained for 25% CWP and 30% CWP respectively after 28 days curing. In the Figure 5, 25% CWP and 30% CWP specimens had gained 19.98 MPa and 19.17 MPa after 7 days curing which is very marginal according to standard. ASTM C150 reported that the minimum compressive strength for OPC cement at 3days, 7days and 28 days is 12MPa, 19MPa and 28MPa respectively. However, according to ASTM C595, the minimum compressive strength for PCC cement at 3days, 7days and 28 days is 13MPa, 20MPa and 25MPa respectively.

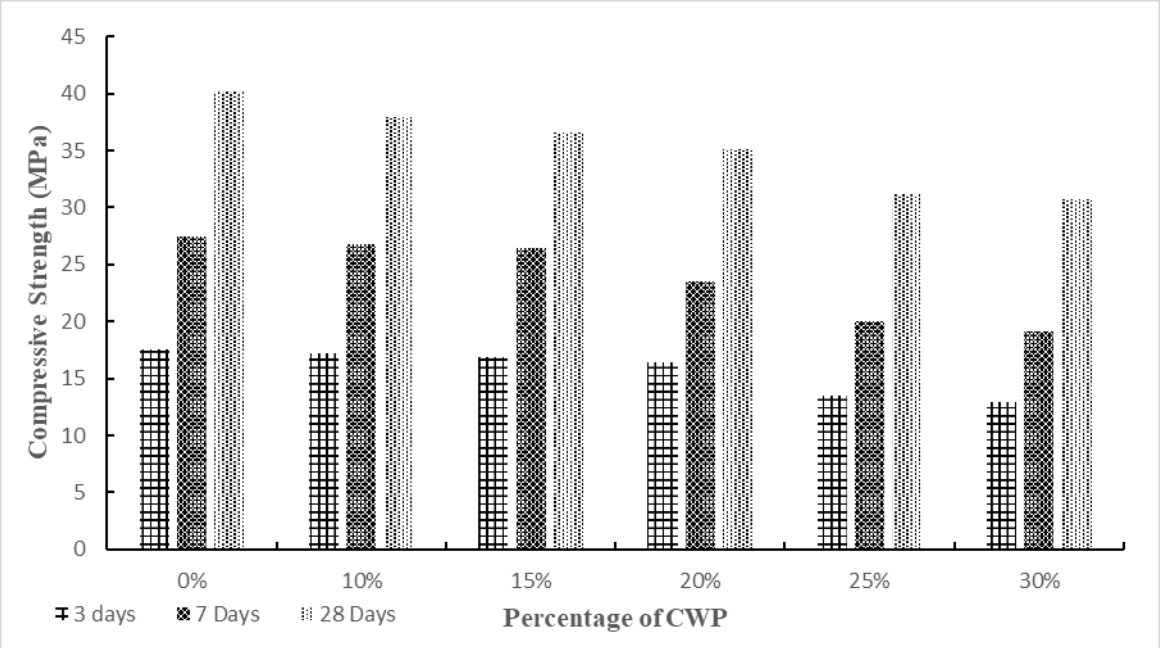

Fig 5: Variation of strength of mortar with curing time

Table 3 represents the reduction in compressive strength with respect to control specimen. Using 25% CWP in mortar results 23.24%, 27.27% and 22.38% strength reduction at 3 days, 7 days and 28 days curing respectively. The strength also decreases by 26.7%, 30.23%, and 23.7% at 3 days, 7 days, and 28 days curing correspondingly due to 30% replacement of cement by CWP. However, the reduction of compressive strength is not observed to be significant up to 20% cement replacement by CWP as illustrated in Table 3. Strength reduction may occur due to reduced proportion of binding material. The CWP induced disturbance in the binding property of cement up to a certain proportion. Compressive strength for 20% CWP containing specimen is 16.42 MPa, 23.55 MPa and 35.07 MPa for 3 days, 7 days and 28 days respectively which are fulfilling the standard requirements for both OPC and PCC cement used in construction.

Table 3: Compressive strength reduction with respect to reference specimen

Curing (days)	Strength (MPa)	Strength reduction with respect to reference specimen (%)				
	0%	10%	15%	20%	25%	30%
3	17.57	2.06	3.68	6.55	23.24	26.7
7	27.47	2.31	3.91	14.29	27.27	30.23
28	40.24	5.84	9.09	12.85	22.38	23.7

3.2 Tensile Strength of Mortar

The tensile strength of mortar increases with the increase of the curing period as shown in Figure 6. Figure 6 also illustrates that the reduction of strength is gradual with respect to increasing percentage of CWP. Tensile strength of control specimen was found 2.48 MPa, 2.76 MPa and 3.1 MPa for the curing period of 3days, 7days and 28 days respectively. At 28 days, the tensile strength of 25% CWP and 30% CWP containing mortar is 2.41 MPa and 2.34 MPa respectively. Table 4 represents the reduction in tensile strength with respect to control specimen. Replacement of 25% and 30% of cement by CWP cause 22.22% and 24.44% reduction of tensile strength of mortar at 28 days. It has been observed that the tensile strength reduction is not significant up to 20% replacement of cement by ceramic waste powder as presented in Table 4. Strength reduction due to using 20% CWP in mortar is 16.61%, 17.5% and 15.56% after 3 days, 7 days and 28 days of curing respectively. While 20% CWP was used in specimen, tensile strength was gained 2.07 MPa, 2.28 MPa and 2.62 MPa at 3 days, 7 days and 28 days curing respectively which can be fulfilled requirements for both OPC and PCC cement used in construction.

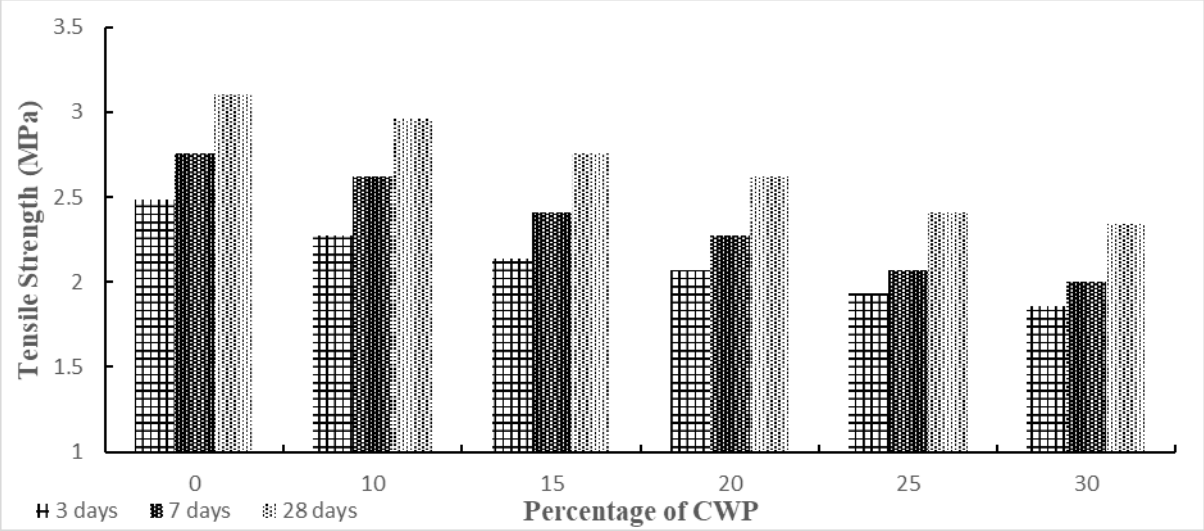

Figure 6: Variation of Tensile of Mortar with Curing Time

Table 4: Tensile Strength reduction with respect to reference specimen.

Curing (days)	Strength (MPa)	Strength reduction with respect to reference specimen (%)				
	0%	10%	15%	20%	25%	30%
3	2.48	8.33	13.89	16.67	22.22	25.0
7	2.76	5.0	12.5	17.5	25.0	27.5
28	3.10	4.44	11.11	15.56	22.22	24.44

4 SUMMARY AND CONCLUSIONS

Construction waste management is one of the major concern for sustainable construction. Ceramic is widely used in construction. This study emphases on reusing of broken ceramic tiles in the form of ceramic waste powder as binding material to replace cement. Grinded ceramic tile was used as CWP to replace different percentages of weight of cement in mortar. The main focus of the study was to investigate the effect of CWP on the mechanical properties (compressive and tensile strength) of mortar at different curing period. Based on the compressive and tensile strength of mortar, it can be concluded that there is no significant reduction of strength up to 20% replacement of cement using CWP. Moreover, when desirable strength can be gained in mortar or concrete by effective replacement of cement using CWP, then it would be economically beneficial as well as environmentally friendly. Therefore, it is recommended that up to 20% cement replacement by ceramic waste powder is feasible in mortar which consequences the reduction of cement consumption in construction. In excess of the study, micro-structural characterization can provide better understanding of the binding property of CWP.

References

Asiwaju-Bello, I., Olalusi, O., & Olutoge, F. (2017). Effect of Salt Water on the Compressive Strength of Ceramic Powder Concrete. *American Journal of Engineering Research, 6*(4), 158-163. Retrieved 2019

Bignozzi, M., & Bondua, S. (2011). Alternative blended cement with ceramic residues: Corrosion resistance investigation on reinforced mortar. Cement and Concrete Research, 41, 647-654.

ASTM C109 (2005). Standard Test Method for Compressive Strength of Hydraulic Cement Mortars. American Society for Testing and Materials, 4.01. Retrieved from www.astm.org

ASTM C1329 (2005). Standard Specification for Mortar Cement. American Society for Testing and Materials, 4.01.

ASTM C150 (2005). Standard Specification for Portland Cement. American Society for Testing and Materials, 4.01.

ASTM C1860 (2019). Standard Test Methods for Measurement of Tensile Strength or Bond Strength of Portland Cement-Based Plaster by Direct Tension. American Society for Testing and Materials, 4.01.

ASTM C191 (2005). Standard Test Method for Time of Setting of Hydraulic Cement. American Society for Testing and Materials, 4.01.

ASTM C595 (2005). Standard Specification for Blended Hydraulic Cements. American Society for Testing and Materials, 4.01.

ASTM C778 (2005). Standard Specification for Standard Sand. American Society for Testing and Materials, 4.01.

Cheng, Y., Huang, F., Liu, R., Hou, J.-L., & Li, G.-L. (2016). Test research on effects of waste ceramic polishing powder on the permeability resistance of concrete. Materials and Structures, 49(3), 729-738.

El Dieb, A. S., & Kanaan, D. M. (2018). Ceramic waste powder an alternative cement replacement - Characterization and evaluation. Sustainable Materials and Technologies, 17.

Irassar, E., Rahhal, V., Tironi, A., Trazza, M., Pavlik, Z., Pavlikova, M., . . . Cerny, R. (2014). Utilization of ceramic wastes as pozzolanic materials. NSTI-Nanotech 2014, 3, 230-233.

Kanaan, D. M., Abubakr, S. H., EL-Dieb, A. S., & Taha, M. M. (2017). High performance concrete incorporating ceramic waste powder as large partial replacement of Portland cement. Construction and Building Materials, 35-41.

LI, L., Zhuo, Z., Zhu, J., Chen, J., & Kwan, A. (2019). Reutilizing ceramic polishing waste as powder filler in mortar to reduce cement content by 33% and increase strength by 85%. Powder Technology, 355, 119-126.

Matias, G., Faria, P., & Torres, I. (2014). Lime mortars with ceramic wastes: characterization of components and their influence on the mechanical behavior. Construction and Building Materials, 73, 523-534.

Mohammadhosseini, H., Lim, N. A., Tahir, M. M., Alyousef, R., Alabduljabbar, H., & Samadi, M. (2019). Enhanced performance of green mortar comprising high volume of ceramic waste in aggressive environments. Construction and Building Materials, 212, 607-617.

Najim, K., Al-Jumaily, I., & Atea, A. (2019). Characterization of sustainable high performance/self-compactiong concrete produced using CKD as a cement replacement material. Construction and Building Materials, 103, 123-129.

Pokornŷ, J., Fort, J., Pavlikova, M., Studnika, J., & Pavlic, Z. (2014). Application of mixed ceramic powder in cement based composites. 177-181.

Rahhul, V., Irassar, E., Castellano, C., Pavslik, Z., & Cerny, R. (2014). Utilization of ceramic waste as replacement of portland cements. International Conference on Constructions and Materials Structures, (pp. 208-213).

Reiterman, P., Holpcapek, O., Cachova, M., Vogel, F., Jogl, M., & Konvalinka, P. (2014). Basic and hygric properties of concrete containing fine ceramic powder. Advanced Materials Research, 897, 188-191.

Torkittiku, P., & Chaipanich, A. (2010, July). Utilization of ceramic waste as fine aggregate within portland cement and fly ash concretes. Cement & Concrete Composites, 32(6), 440-449.

Wang, G., & Tian, B. (2019). Effect of waste ceramic polishing powder on the properties of cement mortars. International Conference on Energy and Environment Technology, 1, pp. 101-104.

Proceedings of the 5th International Conference on Civil Engineering for Sustainable Development (ICCESD 2020), 7~9 February 2020, KUET, Khulna, Bangladesh (ISBN-978-984-34-8764-3)

INFLUENCE OF MIXING WATER TEMPERATURE ON COMPRESSIVE STRENGTH OF CEMENT GROUT

Md. Maruf Molla*[1], Major Md Anisur Rahman[2], Md. Akhtar Hossain [3], Muhammad Harunur Rashid[4], Nazifa Zia[5] and Firoz Mahmud[6]

[1]Lecturer, Department of Civil Engineering, Khulna University of Engineering & Technology, Khulna-9203, Bangladesh, e-mail: marufmolla@ce.kuet.ac.bd

[2]Deputy Project Director, Dhaka-Khulna (N-8) Project, Bangladesh, e-mail: anis7388@yahoo.com

[3]Assistant Professor, Department of Civil Engineering, Khulna University of Engineering & Technology, Khulna-9203, Bangladesh, e-mail: akhtar@ce.kuet.ac.bd

[4]Professor, Department of Civil Engineering, Khulna University of Engineering & Technology, Khulna-9203, Bangladesh, e-mail: mhrashid@ce.kuet.ac.bd

[5]PG Student, Department of Civil Engineering, Khulna University of Engineering & Technology, Khulna-9203, Bangladesh, e-mail: nazifa29106@gmail.com

[6]PG Student, Department of Civil Engineering, Khulna University of Engineering & Technology, Khulna-9203, Bangladesh, e-mail: 2k13firoz@gmail.com

***Corresponding Author**

ABSTRACT

Grouting plays a very crucial role to develop the bonding among the tendons and surrounding concrete in the pre-stressed members. The performance of grout greatly depends on the mixing temperature of grout. This study mainly focuses on the compressive strength of grout with two type of cement (Ordinary Portland Cement-OPC and Portland Cement Composite-PCC), casting under varing mixing temperature. Seven different mixing temperature (i.e 10°C, 15°C, 20°C, 25°C, 30°C, 40°C and, 50°C) were used to prepare the cement grout. Using the cement grout, 126 nos. of 50 mm × 50mm cube specimens were prepared to find out the mixing temperature effect on the compressive strength of the cement grout. The cubes were tested at three different curing ages (3 days, 7 days and 28 days) of the cement grout. It was found that the compressive strength for OPC grout samples varies from 74% to 110% with respect to 25°C mixing samples. Whereas, for PCC grout samples, the compressive strength ranges from 62% to 122% with respect to 25°C mixing samples. This indicates that PCC grout samples are more susceptible with the mixing temperature than OPC grout samples. Moreover, it can be also observed that the gap between the compressive strength of OPC and PCC is getting closer with respect to the curing of the grout cube specimens.

Keywords: *Post-tensioning, Cement grout, Mixing temperature, Compressive strength*

1 INTRODUCTION

Pre-stressing technology is considered as one of the most significant invention in the field of construction technologies in the recent years. The post-tensioning (PT) technology of the pre-stressed system began widely used for the construction of many bridges, spanning large distances in the United States of America and the Europe in the 1950s. In the last few decades, PT technology has played a significant role in the infrastructure development projects, such as, the construction of warehouses, bridges, dams, nuclear and blast-containment structures, foundations, pavements, stadiums, marine structures, water retaining structures, silos, etc. in the world (Clark, 2013; Corven & Moreton, 2013).

Amin & Okui (2015) outlined in their paper that the pre-stressed concrete technology was first introduced in Bangladesh between 1969 and 1974, through the construction of Tora, Aminbazar and Noyarhat bridges in Dhaka. In recent few years, a huge number of structures including bridges, flyovers, have constructed using pre-stressed technology in Bangladesh. The notable post-tensioned bridges on major rivers in Bangladesh includes Meghna Bridge (1991) in Dhaka, Bangabandhu Bridge (1998) on Jamuna river in Sirajganj, Bhairab Bridge (2002) in Kishoreganj, Gabkhan Bridge (2003) in Jhalakathi, Lalon Shah Bridge (2004) in Bheramara, Khan Jahan Ali Bridge (2005) in Khulna, Muktarpur Bridge (2008) in Munsiganj, Sultana Kamal Bridge (2010) in Dhaka, Shah Amanat Bridge (2010) in Chattogram, Dapdapia Bridge (2011) in Barisal, Kanchpur Bridge (2019) in Dhaka and Gumti Bridge (2019) in Cumilla (Uddin and Mizunoya, 2019).

Moreover, a number of ongoing projects including Mass Rapid Transit (MRT) mega project are employing post-tensioning technology at different locations in the country. However, Kamalakannan et al. (2018) reported that the most commonly used grout materials for post-tensioning system in developing countries do not comply the requirements of the international standards. Therefore, there is a huge scope of research on grouting practices in Bangladesh. The high tensile strand or tendons are used in Post-tensioning to transfer the pre-stressing force and grouts act as the duct filler, to fill the interstitial spaces between the ducts and strands. Main constituents of cementitious grouting material are Portland cement, mineral additives, admixtures, aggregates, and water.

Ordinary Portland Cement (OPC) and Portland Cement Composite (PCC) are used as a cementitious material in the grout mixture. The OPC and PCC are used in accordance with ASTM C 150 and ASTM C595/C595M respectively (Chen & Duan, 2014). Grouting materials primarily provide protection against corrosion in bonded tendons and also form a good bonding with surrounding concrete. Pillai (2018) studied the effect of water/binder (w/b) ratio on various properties of cementitious grout mixes considering varying proportion of OPC, a locally available fly ash and a commercially available Poly Carboxylate Ether based super plasticizer. In the studies, the w/b ratios were varied between 0.30 and 0.44. The flow properties (as per BS EN 445), bleeding resistances (according to ASTM C 940-10a), and retention of flow properties over time of the each grout mixes were determined and compared. The paper reported that the reduction of the w/b ratio improves the flow properties (i.e., low yield stress, low plastic viscosity) of the grout mixes and the use of 25% fly ash produced almost no bleed water of the fresh mixes. He also compared the properties of optimized grout (with 25% fly ash) with a commercially available grout with plasticized expansive grout admixture and a Pre-Packaged Grout (PPG) available in USA.

Moreover, Kamalakkannan et al., (2018) focuses on present state of art on the grouting practices during post-tensioning in India and concluded that optimum mixing speed and ambient temperature significantly influence the performance of PPG and Plasticized Expansive Admixture (PEA) grout. Mirza et al., 2013 performed several laboratory tests of different fresh and hardened state properties of OPC, Type-III Portland Cements and seven others commercially available microfine cementitious grouts. Two different variables such as water-cement ratio (varying between 0.5 and 1.2) and three different temperatures (4°C, 10°C and 20°C) were employed during the laboratory tests.

Several physical properties (i.e. grain size distribution), fresh state properties (i.e. viscosity, bleeding and setting time), and hardened state properties (i.e. Young's modulus, Poisson's ratio, compressive strength, bond strength and change in volume) of the grout were studied in this research. It was concluded that all the rheological and mechanical properties are substantially affected by water-cement ratio and at 10°C temperature compressive strength and Young's modulus were found to be maximum. Several studies reported that the performance of grout is affected by several factors like, mixing time, setting time, viscosity, fineness, ambient temperature (mixing environment, mixing and curing water) and compressive strength of the grout (Bras, Gião, Lúcio, & Chastre, 2013; BS EN 445, 2007; Kamalakannan, Thirunavukkarasu, Pillai, & Santhanam, 2018; Mirza et al., 2013). Bras et al., (2013) concluded that rapid reduction in viscosity of grout mixtures occurs at high temperature. Moreover, Mirza et al., (2013) found that setting time of grout decreases with increasing the temperature of the grout mixtures. This phenomenon occurs as the hydration of cementitious material accelerated at high temperature.

There is very limited research available in the literature on the performance of grouting materials under low temperature. Furthermore, very limited studies are reported the performance of different properties of grout at higher temperatures considering monsoon climatic conditions (Erol and François, 2014). Due to the geographical location of Bangladesh, a warm and monsoon season lasts at most of the time in a year. As a result of the climate change effect, the temperature patterns (i.e. durations, starting time, end time, magnitude of temperature etc.) have been modified globally and fluctuate rapidly within a week. Nasher *et al.* (2013) reported that the lowest temperature was recorded as 3.4°C during winter and highest of 45.1°C temperature was recorded during monsoon over the study period between 1964 and 2012. Thus, it is quite difficult to maintain a constant temperature condition during the mixing of grout materials. This paper will address the most significant mechanical property (compressive strength) of the cement grout material at different mixing temperatures considering OPC and PCC as a cementitious material.

2 EXPERIMENTAL PROGRAM

2.1 Materials

In Bangladesh, OPC and PCC are widely used in preparing cement grout. Therefore, the effect of cement type should also be investigated. In this study, the test specimen were prepared using OPC conforming to ASTM C 150, PCC conforming ASTM C595/C595M and grouting agent (kind of admixture which is commonly used for cement grouting). The chemical characteristics with its composition (% by mass) of OPC, PCC and grouting agent are presented in Table 1. Particle size distribution along with fineness of the cements and the grouting agent can be found in Table 2.

Table 1 Chemical characteristics of materials

Composition (% by mass)	Type-I (OPC)	Type-II (PCC)	Grouting Agent
Silica	19.09	17.6	9.5
Alumina (Al_2O_3)	6.14	3.89	3.47
Ferric Oxide (Fe_2O_3)	3.51	3.42	1.95
Calcium Oxide (CaO)	61.70	52.62	28.05
Magnesium Oxide (MgO)	1.79	2.76	1.92
Sulfur trioxide (SO_3)	2.54	2.40	34.64
Chloride (Cl)	0.03	0.04	0.11
Sodium oxide (Na_2O)	0.13	0.12	0.04
Potassium oxide (K_2O)	0.47	0.65	0.75
Total Alkalis (Na_2O+0.658 K_2O)	0.440	0.554	0.540
Insoluble Residue (IR)	1.60	11.40	12.00
Loss on Ignition (LOI)	2.56	4.55	7.50

Table 2 Physical properties of materials

Parameters	Unit	Type-I (OPC)	Type-II (PCC)	Grouting Agent
Fineness (Blaine method)	cm^2/gm	3074	3455	4758
Particle size (Sieve analysis)	Above 90 µm (%)	0.25	0.37	2.96
	45 µm ~ 90 µm (%)	3.23	3.49	6.84
	Below 45 µm (%)	96.52	96.14	90.20
Moisture Content	(%)	0.75	0.74	1.46

2.2 Mixing Ratio

Test specimens were prepared by mixing OPC/PCC, grouting agent and water. The ratio among cement, grouting agent and water was maintained as 1 : 0.1 : 0.4 which was determined in accordance with ASTM C 938. The properties of the cement grout are provided in Table 3.

Table 3 Properties of the cement grout

Parameters	Unit	OPC Grout Mix	PCC grout Mix	Reference
Initial setting time	mins	570	620	ASTM C953
Final setting time	mins	720	770	ASTM C953

2.3 Preparation of Test Specimens

Four different mixing temperatures (20°C, 30°C, 40°C and 50°C) were chosen to determine the mixing temperature effect of the grout. During, preparation of the test specimens these mixing temperatures were maintained by controlling the mixing water temperature. The schedule of grout mixes is given in Table 4.

Table 4: Schedule of Grout Mix

Sample designation	Mixing Temperature (°C)	Cement Type	Sample designation	Mixing Temperature (°C)	Cement Type
10-OPC	10	OPC	10-PCC	10	PCC
15-OPC	15		15- PCC	15	
20-OPC	20		20- PCC	20	
25-OPC	25		25- PCC	25	
30-OPC	30		30- PCC	30	
40-OPC	40		40- PCC	40	
50-OPC	50		50- PCC	50	

To prepare 50mm × 50mm cube specimen for compressive strength test, three gang mold were made ready as shown in figure 1(a), following ASTM C 109. In the beginning, the materials used for the preparation of grout mixes were stored under ambient temperature (20°C) temperature for 24 h prior to mixing. Then, cement and grouting agent were taken in a mixing bowl and hand mixed with a trowel. After that proper amount of mixing water was added with the cement-grout composite. Figure 1(b) illustrates the mechanical mixing machine of the cement grout. Finally, the composition was mixed properly for about 3 minutes with the mixer following the standard mixing method described in ASTM C 938-10. After completion of each mixing step, the temperature of the mixture was measured by means of a thermometer with 0.1°C accuracy. Then the samples were poured in the previously prepared cube mold for finalizing the sampling procedure as shown in Figure 2.

Forty-two batches samples, as mentioned in Table 4, were prepared with different cement types as well as different mixing temperatures. For each batch, three numbers of cube samples were prepared for testing. The desired mixing temperature at every mix was maintained by controlling the mixing water temperature. The temperature was maintained within ±1°C.

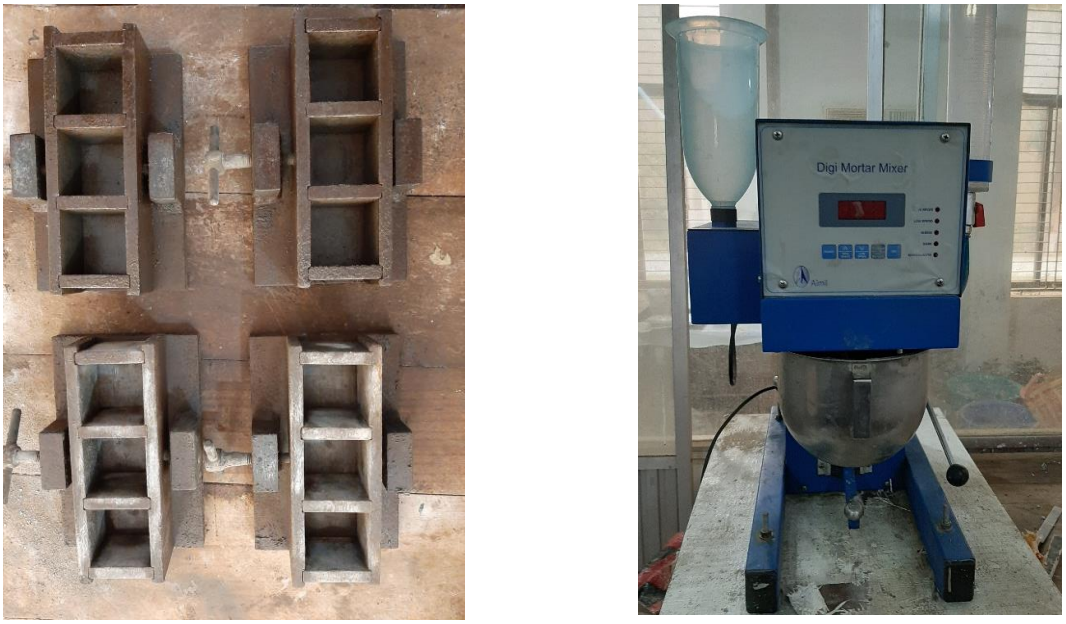

(a) (b)

Figure 1: (a) Gang Mold, (b) Mechanical mixing machine

Figure 2: Casting of grout samples

After completion of the molding, the test specimens were placed in a moist room exposed to moist air for minimum of 24 hours. After being finally set the specimens were demolded and each of the samples were given a unique identification mark for further analysis. Then all of the specimens were preserved in a curing chamber as described in ASTM C 109, to obtain desired strength.

2.4 Compressive Strength Test

After completion of desired curing period, compressive strength test of the cube specimens was performed by using a compression testing machine (maximum capacity of 1000 kN) as shown in Figure 3. Compressive strength of the specimens was determined for 3, 7 and 28 days of curing period. The compressive strength tests were conducted as described in ASTM C 109.

Figure 3: Placement of the cube in the testing machine

3 RESULTS AND DISCUSSION

The compressive strength of the tested samples was presented in Table 5. It can be seen from the table that the optimum compressive strength among the tested samples was found for 30°C for both types of cement as well as three different curing ages of samples. Specimens, prepared with OPC based grout, showed higher strength than that of prepared with PCC based grout. For OPC based grout, the maximum compressive strength of 67.1 MPa, was found corresponding to 30°C mixing temperature and that of minimum of 35.9 MPa was found at 50°C mixing temperature. Whereas, for PCC based grouts, the maximum (57.3 MPa) was found at 30°C mixing temperature and minimum (19.6 MPa) at 10°C mixing temperature.

Table 5 Compressive strength of the tested batches of cement grout

Sample ID	Compressive Strength (MPa)			Sample ID	Compressive Strength (MPa)		
	3 days	7 days	28 days		3 days	7 days	28 days
10-OPC	37.58	49.85	60.15	10-PCC	19.6	34.97	46.98
15-OPC	38	50.43	60.04	15- PCC	19.95	36.25	49.25
20-OPC	40	53.09	63.2	20- PCC	21	38.16	50.6
25-OPC	41.2	54.32	63.85	25- PCC	24.26	41.07	55.58
30-OPC	42.9	56.35	67.1	30- PCC	26.1	45.65	57.3
40-OPC	36.8	52.13	58.8	40- PCC	24.2	41.34	52.5
50-OPC	35.9	50.78	57.3	50- PCC	23.3	40.88	51.6

Comparison between compressive strength between OPC and PCC based cementitious grout specimens are represented in Figure 4. It was observed that the specimens made with PCC based grout showed higher strength at early ages than that of in OPC based grout. The compressive strength ratios between PCC based grout and OPC based grout specimens were between 52~66 % for 3 days of samples, between 70~81% for 7 days of samples, and increased up to 78~90% at 28 days curing age. With increasing in curing age, the ratio between the PCC and OPC based grout increases for all mixing temperatures in this study.

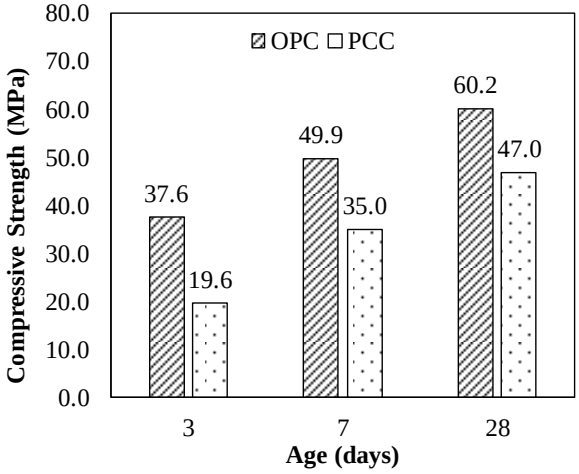

(a) 10°C mixing temperature

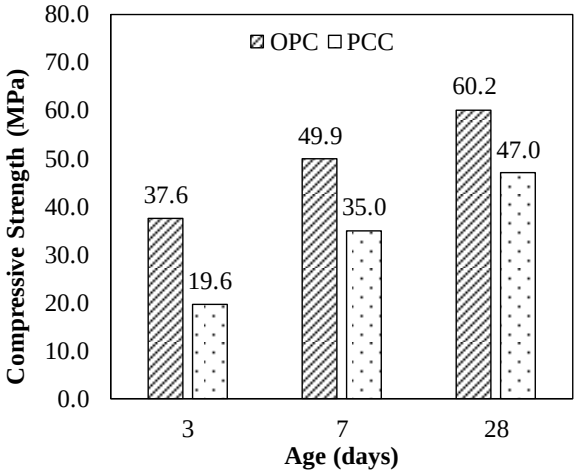

(b) 20°C mixing temperature

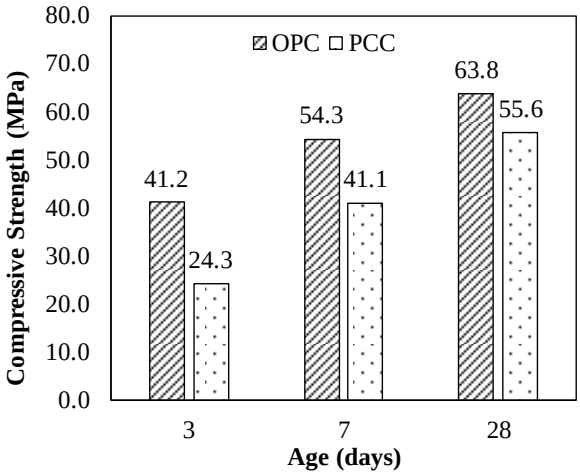

(c) 25°C mixing temperature

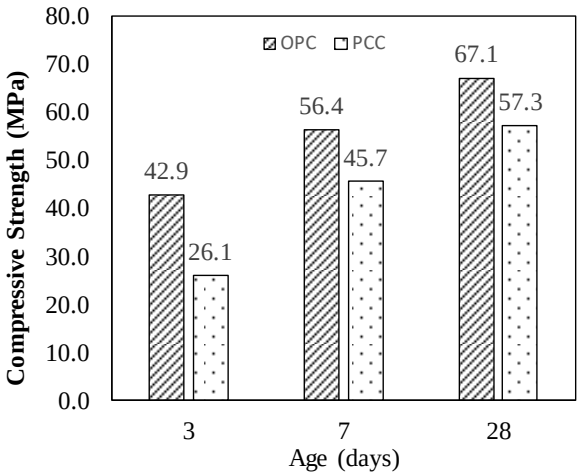

(d) 30°C mixing temperature

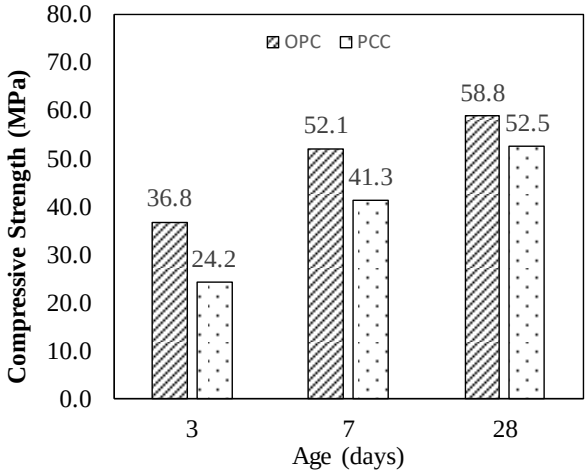

(e) 40°C mixing temperature

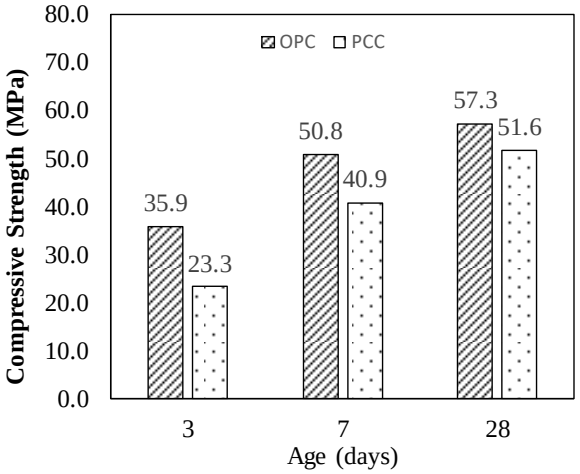

(f) 10°C mixing temperature

Figure 4: Comparison between compressive strength of OPC and PCC based grout sample at different age

Figure 5 shows the variation of compressive strength of grout (OPC and PCC) with different curing ages at various mixing temperature. The tested results show that the gap between compressive strength between OPC grout and PCC grout for 3 days samples are more than 28 Days samples. This indicate that OPC grout achieve compressive strength faster than PCC grout.

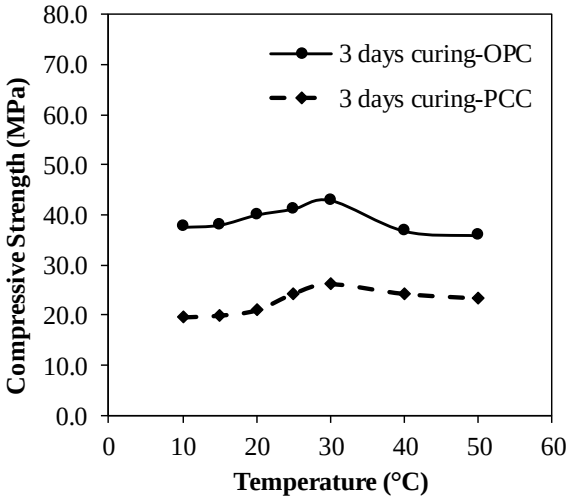

(a) at 3 days curing period

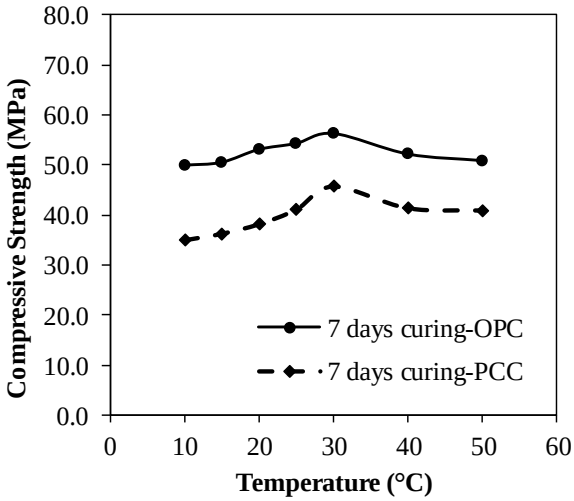

(b) at 7 days curing period

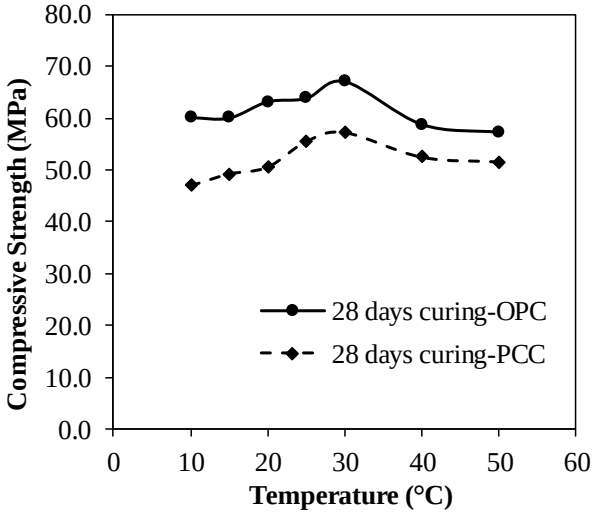

(b) at 28 days curing period

Figure 5: Variation of compressive strength with different mixing temperature

The percentage variation of the tested samples compared with 25°C mixing temperature for both OPC and PCC grout are presented in Table 6. The samples were compared with 25°C mixing temperature as 25°C represents the standard ambient temperature (Wardhono et al, 2015). It has been found that the compressive strength of the OPC grouting sample varies from 74% to 110% relative to the 25°C mixed sample. For PCC grouting samples, the compressive strength ranged from 62% to 122% relative to the mixed sample at 25°C.

Table 6: Percentage variation of the different batches with respect to 25°C samples

	% variation for OPC			% Variation for PCC		
Temperature (°C)	**3 days**	**7 days**	**28 days**	**3 days**	**7 days**	**28 days**
10	82%	84%	88%	62%	70%	69%
15	84%	86%	88%	64%	77%	77%
20	94%	95%	98%	73%	86%	82%
25	100%	100%	100%	100%	100%	100%
30	108%	107%	110%	115%	122%	106%
40	79%	92%	84%	100%	101%	89%
50	74%	87%	79%	92%	99%	86%

4 CONCLUSION

Based on the experimental results, the following conclusions are made:

a) Variation in mixing temperature influences the compressive strength of cementitious grout. The compressive strength of the cement grout decreases with increasing mixing water temperature above 30°C. So, this reduction in the compressive strength of cement grout should be considered while doing the mix design for grout as seasonal variation of temperature is a continuous process in Bangladesh.

b) Cement grout prepared with OPC cement provides higher early strength than that of PCC. When the construction period is very short or it is necessary to complete the pre-stressing work within short period, then OPC based grout might be preferable.

REFERENCES

ASTM C 109. (2010). Standard Test Method for Compressive Strength of Hydraulic Cement Mortars (Using 2-in. or 50-mm Cube Specimens). https://doi.org/10.1520/C0109.

ASTM C 150. (2007). Standard Specification for Portland Cement. *Annual Book of ASTM Standards*, *I*(April), 1–8. https://doi.org/10.1520/C0150.

ASTM C 938-10. (2010). Standard Practice for Proportioning Grout Mixtures for Preplaced-Aggregate Concrete. *ASTM International*, *i*(c), 55–57. https://doi.org/10.1520/C0938-10.2.

ASTM C 940-10a. (2010). Standard Test Method for Expansion and Bleeding of Freshly Mixed Grouts for Preplaced-Aggregate Concrete in the Laboratory. https://doi.org/10.1520/C0940-10a.2.

ASTM C595/C595M. (2015). Standard Specification for Blended Hydraulic CementS. In *Annual Book of ASTM Standards*. https://doi.org/10.1520/C0595.

ASTM C953. (2010). Standard Test Method for Time of Setting of Grouts for Preplaced-Aggregate Concrete in the Laboratory. *ASTM International*, *87*(c). https://doi.org/10.1520/C0953-10.2.

Bras, A., Gião, R., Lúcio, V., & Chastre, C. (2013). Development of an injectable grout for concrete repair and strengthening. *Cement and Concrete Composites*, *37*(1), 185–195. https://doi.org/10.1016/j.cemconcomp.2012.10.006

BS EN 445. (2007). *Grout for prestressing tedons - Test methods*. *3*.

Chen, W. F., & Duan, L. (2014). Segmental Concrete Bridges. In *Bridge Engineering Handbook, Second Edition*. https://doi.org/10.1201/b16523-4.

Clark, G. M. (2013). Post-tensioned structures - improved standards. *Proceedings of the Institution of Civil Engineers: Forensic Engineering*, *166*(4), 171–179. https://doi.org/10.1680/feng.13.00010.

Corven, J., & Moreton, A. (2013). *Post-Tensioning Tendon Installation and Grouting Manual, Federal Highway Administration (FHWA), US Department of Transportation*. Retrieved from Federal Highway Administration (FHWA), US Department of Transportation website: http://www.fhwa.dot.gov/bridge/construction/pubs/hif13026.pdf.

Erol, S., & François, B. (2014). Efficiency of various grouting materials for borehole heat exchangers. *Applied thermal engineering*, *70*(1), 788-799.

Kamalakannan, S., Thirunavukkarasu, R., Pillai, R. G., & Santhanam, M. (2018). Factors affecting the performance characteristics of cementitious grouts for post-tensioning applications. *Construction and Building Materials*, *180*, 681–691. https://doi.org/10.1016/j.conbuildmat.2018.05.236.

Kamalakkannan, S., Thirunavukkarasu, R., Pillai, R., & Santhanam, M. (2018). *Assessment of Grouts for Post-Tensioning Applications*. (April).

Mirza, J., Saleh, K., Langevin, M. A., Mirza, S., Bhutta, M. A. R., & Tahir, M. M. (2013). Properties of microfine cement grouts at 4 C, 10 C and 20 C. *Construction and Building Materials*, *47*, 1145–1153. https://doi.org/10.1016/j.conbuildmat.2013.05.026

Nasher, N. R., & Uddin, M. N. (2013). Maximum and minimum temperature trends variation over northern and southern part of Bangladesh. *Journal of Environmental Science and Natural Resources*, *6*(2), 83-88.

Pillai, R. (2018). *Cementitious Grout for Post-Tensioned , Segmental Concrete Cementitious Grout for Post-Tensioned , Segmental*. (April).

Uddin, M. Z., & Mizunoya, T. (2019). An economic analysis of the proposed Dhaka–Chittagong Expressway in Bangladesh with the viewpoint of GHG emission reduction. *Asia-Pacific Journal of Regional Science*, 1-30.

Wardhono, A., Law, D. W., & Strano, A. (2015). The strength of alkali-activated slag/fly ash mortar blends at ambient temperature. *Procedia Engineering*, 125, 650-656.

Proceedings of the 5th International Conference on Civil Engineering for Sustainable Development (ICCESD 2020), 7~9 February 2020, KUET, Khulna, Bangladesh (ISBN-978-984-34-8764-3)

PERFORMANCE OF WASTE GLASS POWDER CONCRETE SUBJECTED TO FIRE

Md. Khaliqul Bari*[1], Ismail Saifullah[2], Abdullah-Al-Taharat[3] and Md. Abir Hossan[4]

[1]Undergraduate Student, Department of Civil Engineering, Khulna University of Engineering & Technology (KUET), Bangladesh, e-mail: bari.ce.kuet084@gmail.com
[2]Associate Professor, Department of Civil Engineering, Khulna University of Engineering & Technology (KUET), Bangladesh, e-mail: saifullah@ce.kuet.ac.bd
[3]Undergraduate Student, Department of Civil Engineering, Khulna University of Engineering & Technology (KUET), Bangladesh, e-mail: aongontaharat@gmail.com
[4]Undergraduate Student, Department of Civil Engineering, Khulna University of Engineering & Technology (KUET), Bangladesh, e-mail: abirhossan6686@gmail.com

***Corresponding Author**

ABSTRACT

The implementation of recycling materials in concrete is increasing progressively because of the development of sustainable construction. A significant amount of waste glasses are generating all over the world. However, most of the waste glasses have been intentionally dumped into landfills. These waste glasses are not environmental friendly as glasses are not biodegradable, and, tremendous cost to individual corporations and municipalities to manage these waste. The increasing consciousness of glass recycling speeds up assessments on the utilization of waste glass powder in the concrete construction sector. This study mainly investigates the mechanical properties of concrete incorporating waste glass powder with partial substitution of binding material (cement) under when subjected to fire at elevated temperatures. This study also explores the influence of cooling approach on the glass powder concrete after burning in fire. Moreover, the density of the concrete both before and after burning in fire is also investigated. Total 108 cylindrical specimens were prepared with selected mixing ratio of 1:1.5:3 at a constant water cement ratio. Cement was substituted to some extent by waste glass powder at 10%, 15%, 20%, 25% and 30% by weight. After burning the specimens at elevated temperature, two seperate systems were followed for cooling the specimens (nature cooling in air and forced cooling in water) for the duration of 24 hours. The results show that 20% substitution of cement in concrete by using waste glass powder is found the feasible compressive and tensile strength compared to concrete containing without glass powder. It is also remarked that when concrete is subjected to fire, natural cooling approach provides better performance compared to forced cooling approach. However, there is no considerable reduction of concrete density observed due to substitution of cement by waste glass powder.

Keywords: *Waste glass powder, Fire, Compressive strength, Natural cooling, Forced cooling.*

1. INTRODUCTION

The generation of waste is increasing enormously because of the rapid growth of population and industry worldwide. Therefore, recycling of waste materials is becoming an acute concern all over the world (Taha & Nounu, 2009). Since the waste glass does not putrefy in the atmosphere, it becomes an unsustainable when it is disposed as landfills (Islam, Rahman, & Kazi, 2016). Shayan & Xu (2004) reported that the major industrial emissions of carbon dioxide (CO2) is because of the manufacture of cement which consequences to around 5% of worldwide man-made emissions. The implementation of recycling materials in concrete is increasing steadily because of the key goals of sustainable construction. Glasses are one kind of inert materials that could be recycled and used several cycles devoid of varying its chemical properties (Shayan & Xu, 2004). Jangid & Saoji (2014) reported that glass is a nebulous material containing high silica resulting to potential pozzolanic when particle magnitude is not as much of 75 μm.

The utilization of recycled glass in construction assist to save of energy. The increasing consciousness of glass recycling speeds up assessments on the utilization of waste glass with several patterns in numerous research fields. The amount of waste glass is gradually increased over the modern years by reason of an ever-growing usage of glass products. Nevertheless, most of the waste glasses have been get rid of into landfill spots which is disagreeable as glasses are not biodegradable, consequently less environmental friendly as well as tremendous cost to individual corporations and municipalities. There is an enormous prospective for utilizing waste glass in the sector of concrete construction. When waste glasses are recycled in manufacture of concrete members, the manufacture cost of concrete will be reduced (Topçu and Canbaz 2004; Srivastava et al. 2014).

Fire safety is crucial for the reinforced concrete structures. With the development of technology, constructions have been imparting additional competent facility and wellbeing for civilization in the former era (Durgun & Sevinç, 2019). During fire, the temperature can extent up to 1100˚C in building structures and steady up to 1350˚C in tunnel structures. When the temperature of the concrete conceeded 500˚C, the compressive strength of concrete typically declines 50% to 60%, and the concrete is measured as entirely damaged (Hager, 2013). Pozzolanic materials enhance the fire endurance of the concrete (Yüksel, Siddique, & Özkan, 2011).

Based on the mechanical properties of concrete as well as its alkali-silica reactivity, several researchers (such as Bažant et al. 2000; Shayan and Xu 2006; Schwarz and Neithalath 2008; Kataria 2010; De Castro and de Brito 2013) explored the suitability of waste glass powder as substitution of cement in concrete. Finely ground glass powders encompass substantial amount of silica (SiO_2) and exhibited very high pozzolanic activity (Shi et al. 2005; Carsana, Frassoni, & Bertolini, 2014; Kong et al. 2016; Omran et al. 2017; Khmiri et al. 2013). The finer the glass powder, the higher its pozzolanic reactivity. Pan, Tao, Murphy, & Wuhrer (2017) revealed that the exploitation of glass powder reduced the Ca(OH)2 amount along with the thermal conductivity. Besides, glass powder usage reduced the deficiency and spalling of the high-strength concrete under high temperatures (Ali, Dinkha, & Haido, 2017). Du and Tan (2015) investigated the mechanical and durability behavior of concrete integrating recycled glass powder and concluded that because of the pozzolanic reaction of glass powder, it can be utilized in concrete as substitution of cement to some extent and resulting to the reduction of carbon footprint. The exchange of Portland cement with ground glass powder also decreases the expansion because of the alkali-aggregate reactions (ASTM C1260). The integration of glass powder in mortars could considerably decrease the drying shrinkage of the glass mortars irrespective of its fineness (Lu et al. 2017). Therefore cement can be substituted by waste glass powder to some extent in concrete and participate to develop strength of concrete.

This study mainly focuses to the investigation of the mechanical properties of concrete incorporating waste glass powder with partial substitution of binding material (cement) under when subjected to fire at elevated temperatures. This study also explores the influence of cooling approach on the glass powder concrete after burning in fire. Moreover, the density of the concrete both before and after burning in fire is also highlighted.

2. METHODOLOGY

2.1 Materials and Methods

In this study Ordinary Portland cement, black stone chips, and Sylhet sand were used as raw materials. The physical properties of these construction materials were determined in accordance with relevant ASTM Standards as presented in Table 1. The disposed waste glasses were collected from locally available sources. Glass powder were prepared by grinding followed by several sequences till the passing of #200 sieve. Figure 1 depicts the entire procedures of preparation of glass powder.

Table 1: Physical properties of materials

Materials	Material Properties	Unit	Value
Coarse Aggregate	Specific Gravity	-	2.75
	Absorption	%	1.80
	Unit Weight	Kg/m^3	1517
Fine Aggregate	Specific Gravity	-	2.65
	Absorption	%	4.33
	Fineness Modulus	-	2.64
	Unit Weight	Kg/m^3	1600

a. Collection of waste glasses

b. Crushed glasses

c. Preparation of glass powder

Figure 1: Several strategies of making glass powder

2.2 Preparation of Specimens

The specimens was prepared with selected mixing ratio of 1:1.5:3. The water cement ratio for each specimen was 0.48. In this study cement was to some extent substituted with waste glass powder at different percentages such as 10%, 15%, 20%, 25% and 30% by weight. Total 108 cylindrical samples of 100 mm diameter and 200 mm height were cast. Among these specimens, 54 specimens were prepared for compressive strength test and 54 samples were prepared for splitting tensile strength test. Among 108 specimens, 36 specimens were prepared for each conditions like as control specimens, natural cooling and forced cooling. The samples were stored at water for the curing ages of 28 days. The workability of concrete for each batch mixing was also determined through slump test. The entire steps of preparation of cylindrical samples are presented in Figure 2.

a. Mixing Materials b. Workability Test c. Preparation of Specimens

Figure 2: Several steps for preparation of specimens

2.3 Testing of Specimens

2.3.1 Burning of Specimens

A fire chamber size of 550 x 450 x 400mm was prepared with electric coil heater for testing of concrete subjected to fire. Eight electric coil plates were used in the chamber surrounding walls. Each coil contains 2000 watt. The samples were stored in the chamber for one hour under fire conditions. The typical burning process of specimens is shown in Figure 3. The temperature was measured using thermocouple placed inside the chamber and found temperature ranging from 27^0C to 600^0C for the duration of one hour. The variation of temperature with regard to duration of burning of specimens is illustrated in Figure 4. After burning the specimens were cooled in two processes. One of them naturally cooled in air, other one forcedly cooled by water.

Figure 3: Burning of the specimens

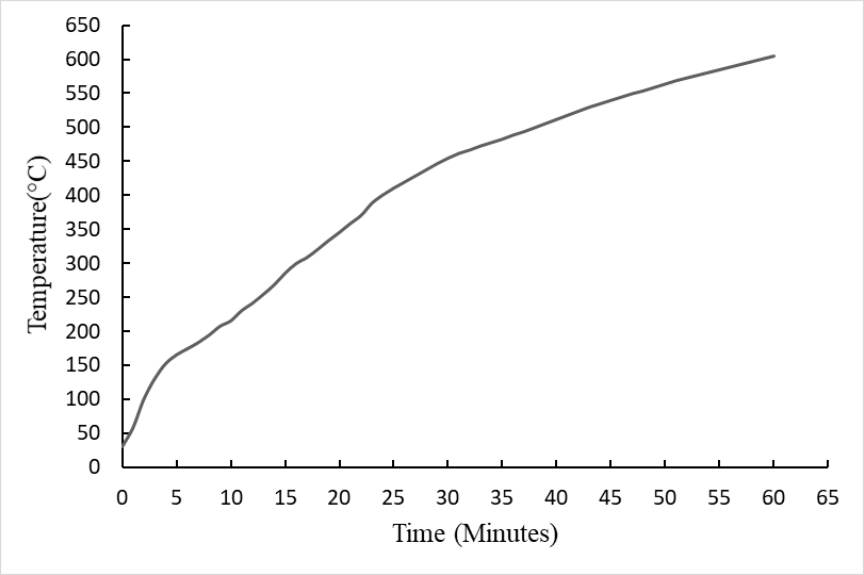

Figure 4: Variation of temperature with respect to Burning Period

2.3.2 Compressive Strength Test

The crushing strength of waste glass powder concrete at normal condition as well as after completion of the cooling process was conducted in accordance with ASTM C39 by using compression testing machine in the Engineering Materials Laboratory of KUET. The specimens were vertically setup in the machine. Figure 5 shows a typical test set-up for the determination of crushing strength of concrete. The load was executed gradually as per ASTM C39 standard while waiting for failure of the cylindrical samples. The compressive strength of concrete was obtained by divided the crushing load by cross sectional area of the specimens.

Figure 5: Typical test set-up for determination of crushing strength of concrete

2.3.3 Splitting Tensile Strength Test

The splitting tensile strength of waste glass powder concrete at both normal condition and after completion of the cooling process was carried out according to ASTM C496 by using compression testing machine. The samples were placed horizontally with the provision of bar along the long axis of the cylindrical specimen (shown in Figure 6). A typical test set-up for determination of splitting tensile strength of concrete is depicted in Figure 6.

Figure 6: Typical setup for spliting tensile strength determination

The load was applied gradually as per ASTM C496 standard till failure of the cylindrical samples. The splitting tensile strength of concrete was computed by using the Equation (1).

$$\sigma = \frac{2P}{\pi dl} \quad (1)$$

Where,
σ = splitting tensile strength, MPa
P = Largest applied load specified in the testing machine, kN
d = diameter of the sample, mm
l = length of the sample, mm

3. RESULTS AND DISCUSSIONS

3.1 Workability of Concrete

Workability means that the concrete easily flows and compacted without any segregation. Workability are remarkably influenced by aggregate property, water content and hydration of cement. The test results of workability at relevant percentage of cement replacement with glass powder is presented in Table 2. It has been found that waste glass powder increases the water demand that's why workability of the concrete containing waste glass powder gradually decrease with increase the percentage substitution of cement by waste glass powder in conjunction with a steady water cement ratio of 0.48.

Table 2: Determination of workability of glass powder concrete

Sample ID	Workability (mm)
0% GP	87
10% GP	81
15% GP	75
20% GP	72
25% GP	68
30% GP	65

3.2 Compressive strength of concrete

The compressive strength of concrete with the partial replacement of cement by waste glass powder have been investigated. At 28 days, the compressive strength generally decreases with glass powder

containing around 15% as illustrated in Figure 7. However, no significant reduction of strength was detected for concrete incorporating 20% glass powder in comparison to concrete without glass powder (shown in Table 3). It can be occurred because of the pozzolanic reaction among cement hydration and glass powder products. This insignificant strength reduction was not detected for concrete where higher than 20% cement is substituted by glass powder. The pozzolanic reaction necessitates the hydration products, CH, whose extent is controlled through the cement content (Carsana, Frassoni, & Bertolini, 2014). Hence, there is a maximum boundary for the level of cement substitution, further than no additional pozzolanic reaction of glass powder can take place. In this condition, glass powder mainly behave as inert filler without being initiated. The results in this investigation point toward that glass powder exhibits noticeable pozzolanic reaction when the substitution amount of cement is approximately 20%. Du and Tan (2014) reported that the pozzolanic reaction enhances the pore structure in the bulk cement paste in addition to the interfacial transition zone among cement paste and coarse aggregates. This interfacial transition zone dominates the mechanical properties of concrete because of its more porousness in comparison with the bulk paste. Du and Tan (2014) also stated that CH content is also comparatively greater at interfacial transition zone which facilitates the pozzolanic reaction of waste glass powder. The improved microstructure at interfacial transition zone has participated to the compressive strength of concrete with approximately 20% glass powder content.

From Table 3 it can be observed that concrete compressive strength decreases significantly when subjected to fire at elevated temperature. After burning the specimens in fire, cooling process was carried out for the duration of 24 hours in both natural cooling and forced cooling approach. It is observed that the compressive strength of concrete at natural cooling approach provides better performnce compared to forced cooling approach as depicted in Figure 7 and Table 3.

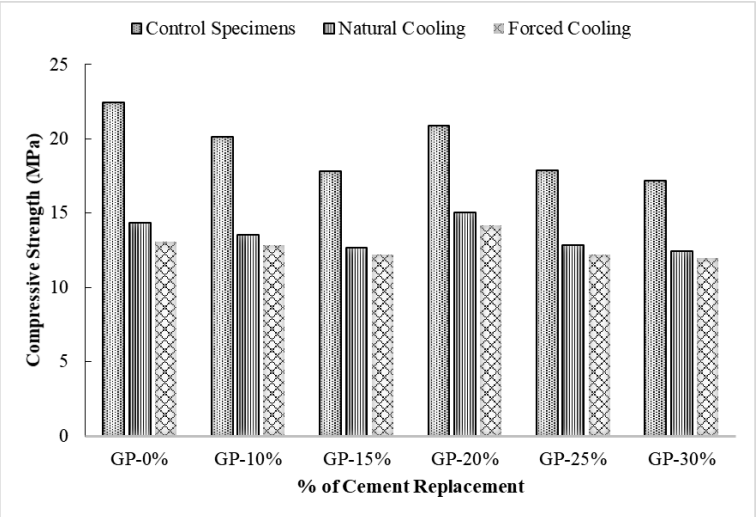

Figure 7: Assessment of compressive strength of glass powder concrete at different conditions.

Table 3: Compressive strength of concrete at 28 days

Sample ID	Control specimens (MPa)	Strength reduction in regard to control samples (%)	Natural cooling (MPa)	Strength reduction in regard to control samples (%)	Forced cooling (MPa)	Strength reduction in regard to control samples (%)
0% GP	22.43	--	14.32	36.16	13.05	41.82
10% GP	20.15	10.16	13.53	32.85	12.82	36.38
15% GP	17.82	20.55	12.66	28.96	12.22	31.43
20% GP	20.90	6.82	15.05	28.02	14.16	32.25
25% GP	17.85	20.42	12.87	27.90	12.21	31.60
30% GP	17.18	23.41	12.44	27.60	11.98	30.27

3.3 Tensile strength of concrete

In this study the tensile strength of concrete containing waste glass powder as partial substitution of cement have also been investigated. From Figure 8 it can be stated that the splitting tensile strength reduces with the increase of the incorporating glass powder of approximately 15%. However, there is no significant reduction of tensile strength witnessed for concrete encompassing 20% glass powder compared to control specimens as presented in Table 4. It can be occurred because of the pozzolanic reaction among cement hydration and glass powder products. Nevertheless, the reduction of tensile strength of concrete increases when more than 20% cement is replaced by waste glass powder. Hence, there is an upper limit boundary for the level of cement substitution, further than no additional pozzolanic reaction of glass powder can take place. The illustrations of the reason are already mentioned in section 3.2. Therefore, the results of this study specify that glass powder exhibits noticeable pozzolanic reaction when the replacement level of cement is approximately 20%.

From Table 4 it can be specified that the splitting tensile strength of concrete declines considerably under fire at elevated temperature. After burning the specimens in fire, similar cooling process suhc as natural cooling and forced cooling was performed for the duration of 24 hours. It has also been remarked that the spliiting tensile strength of concrete at natural cooling approach provides better performnce in comparison to forced cooling approach as depicted in Figure 8 and Table 4.

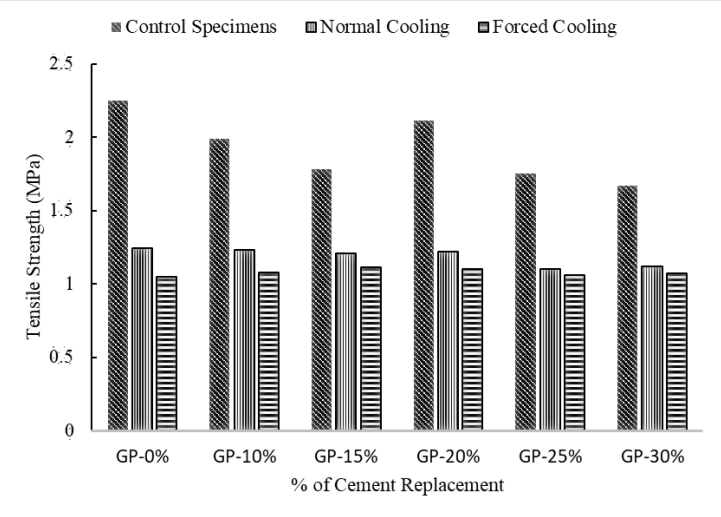

Figure 8: Assessment of spliting tensile strength of glass powder concrete at different conditions.

Table 4: Spliting Tensile strength of concrete at 28 days

Sample ID	Control specimens (MPa)	Strength reduction in regard to control samples (%)	Natural Cooling (MPa)	Strength reduction in regard to control samples (%)	Forced Cooling (MPa)	Strength reduction in regard to control samples (%)
0% GP	2.25	--	1.24	44.89	1.05	53.33
10% GP	1.99	11.56	1.23	38.19	1.08	45.73
15% GP	1.78	20.89	1.21	32.02	1.11	37.64
20% GP	2.11	6.22	1.22	42.18	1.10	47.87
25% GP	1.75	22.22	1.10	37.14	1.06	39.43
30% GP	1.67	25.78	1.12	32.93	1.07	35.91

3.4 Density

The density of concrete at non burnt condtions was measured at the ages of 28 days. It has been remarked that there is no significant reduction of concrete density due to replacement of cement by waste glass powder as exhibited in Table 5. The density of glass powder concrete slightly decreases with the increases of the percentage replacement of cement by waste glass powder. At non burnt condition, when the concrete incorporating no glass powder it possesses the density of 2559 kg/m^3 whereas the density becomes 2514 kg/m^3 for 30% substitution of cement by waste glass powder. After burning in fire, the specimens were cooled by naturally in air and forcedly by water, and measured the density of concrete at both conditions. It was found that at fire conditions there is no significant variation of concrete density compared to concrete at non burnt condtion. However, the density of concrete at natural cooling approach shows slightly lower density than forced cooling approach.

Table 5: Density of concrete at 28 days

Sample ID	Density(Kg/m^3)		
	Control Specimens	Natural Cooling	Forced Cooling
0% GP	2559	2370	2537
10% GP	2543	2349	2528
15% GP	2530	2316	2513
20% GP	2527	2337	2506
25% GP	2523	2332	2499
30% GP	2514	2335	2492

4. SUMMARY AND CONCLUSIONS

This study mainly investigates the mechanical properties of concrete incorporating waste glass powder with partial substitution of binding material (cement) under when subjected to fire at elevated temperatures. This study also explores the influence of cooling approach on the glass powder concrete after burning in fire. Based on the experimental studies, the comprehending conclusions have been achieved:

- The workability of the waste glass powder concrete gradually decreases with the increase of the partial substitution of cement by waste glass powder at a steady water cement ratio.
- There is no substantial reduction of both compressive and tensile strength observed for concrete incorporating 20% glass powder as substitution of cement in comparison to concrete without glass powder. This study designate that glass powder exhibits recognizable pozzolanic reaction when the replacement level of cement is approximately 20%. Therefore, it is suggested that approximately 20% cement can be substituted by using waste glass powder to make viable structural concrete resulting to the lower amount of cement consumption in

construction, and hence proving environmentally friendly as well as economically beneficially construction.

- Based on the compressive and splitting tensile strength of concrete after burning in fire, it can be stated that natural cooling approach provides better performnce compared to forced cooling approach.
- The density of glass powder concrete slightly declines with the increases of the percentage replacement of cement by waste glass powder. However, there is no considerable reduction of concrete density observed due to partial substitution of cement by waste glass powder.

ACKNOWLEDGEMENTS

We want to express our acknowledgements to all of the Laboratory employees of Engineering Materials, Department of Civil Engineering, Khulna University of Engineering & Technology for their valuable cooperation during the course of the research period.

REFERENCES

Ali, M. H., Dinkha, Y. Z., & Haido, J. H. (2017). Mechanical properties and spalling at elevated temperature of high performance concrete made with reactive and waste inert powders. Engineering Science and Technology, an International Journal, 20(2), 536-541.

ASTM C39. 2018. Standard Test Method for Compressive Strength of Cylindrical Concrete Specimens. Annual Book of ASTM Standards, Volume 04.02.

ASTM C496. 2017. Standard Test Method for Splitting Tensile Strength of Cylindrical Concrete Specimens. Annual Book of ASTM Standards, Volume 04.02.

ASTM C1260. 2014. "Standard Test Method for Potential Alkali Reactivity of Aggregates (Mortar-Bar Method)." Annual Book of ASTM Standards, Volume 04.02.

Bažant, Z. P., Zi, G., & Meyer, C. (2000). Fracture mechanics of ASR in concretes with waste glass particles of different sizes. Journal of engineering mechanics, 126(3), 226-232.

Carsana, M., Frassoni, M., & Bertolini, L. (2014). Comparison of ground waste glass with other supplementary cementitious materials. Cement and Concrete Composites, 45, 39-45.

De Castro, S., & de Brito, J. (2013). Evaluation of the durability of concrete made with crushed glass aggregates. Journal of Cleaner Production, 41, 7-14.

Du, H., & Tan, K. H. (2015). Durability performance of concrete with glass powder as supplementary cementitious material. XIII International Conference on Durability of Building Materials and Components - XIII DBMC, Sao Paulo, Brazil, 928-935.

Du, H., & Tan, K. H. (2014). Waste glass powder as cement replacement in concrete. Journal of Advanced Concrete Technology, 12(11), 468-477.

Durgun, M. Y., & Sevinç, A. H. (2019). High temperature resistance of concretes with GGBFS, waste glass powder, and colemanite ore wastes after different cooling conditions. Construction and Building Materials, 196, 66-81.

Hager, I. (2013). Behaviour of cement concrete at high temperature. Bulletin of the Polish Academy of Sciences: Technical Sciences, 61(1), 145-154.

Kataria, A., Kumar, M. G., & Goyal, S. G. (2010). Studies on Mechanical Properties of Concrete Containing Waste Glass Powder and Post Consumer Waste Plastic (Doctoral dissertation). Thapar Univers, Patiala.

Khmiri, A., Chaabouni, M., & Samet, B. (2013). Chemical behaviour of ground waste glass when used as partial cement replacement in mortars. Construction and building materials, 44, 74-80.

Kong, Y., Wang, P., Liu, S., Zhao, G., & Peng, Y. (2016). SEM analysis of the interfacial transition zone between cement-glass powder paste and aggregate of mortar under microwave curing. Materials, 9(9), 733.

Islam, G. S., Rahman, M. H., & Kazi, N. (2017). Waste glass powder as partial replacement of cement for sustainable concrete practice. International Journal of Sustainable Built Environment, 6(1), 37-44.

Jangid, J. B., & Saoji, A. C. (2014). Experimental investigation of waste glass powder as the partial replacement of cement in concrete production. In International Conference on Advances in Engineering & Technology (pp. 55-60).

Lu, J. X., Zhan, B. J., Duan, Z. H., & Poon, C. S. (2017). Using glass powder to improve the durability of architectural mortar prepared with glass aggregates. Materials & Design, 135, 102-111.

Omran, A. F., Etienne, D., Harbec, D., & Tagnit-Hamou, A. (2017). Long-term performance of glass-powder concrete in large-scale field applications. Construction and Building Materials, 135, 43-58.

Pan, Z., Tao, Z., Murphy, T., & Wuhrer, R. (2017). High temperature performance of mortars containing fine glass powders. Journal of Cleaner Production, 162, 16-26.

Schwarz, N., & Neithalath, N. (2008). Influence of a fine glass powder on cement hydration: Comparison to fly ash and modeling the degree of hydration. Cement and Concrete Research, 38(4), 429-436.

Shayan, A., & Xu, A. (2006). Performance of glass powder as a pozzolanic material in concrete: A field trial on concrete slabs. Cement and concrete research, 36(3), 457-468.

Shayan, A., & Xu, A. (2004). Value-added utilisation of waste glass in concrete. Cement and concrete research, 34(1), 81-89.

Shi, C., Wu, Y., Riefler, C., & Wang, H. (2005). Characteristics and pozzolanic reactivity of glass powders. Cement and Concrete Research, 35(5), 987-993.

Srivastava, V., Gautam, S. P., Agarwal, V. C., & Mehta, P. K. (2014). Glass waste as coarse aggregate in concrete. Journal of Environmental Nanotechnology, 3(1), 67-71.

Taha, B., & Nounu, G. (2009). Utilizing waste recycled glass as sand/cement replacement in concrete. Journal of materials in civil engineering, 21(12), 709-721.

Topcu, I. B., & Canbaz, M. (2004). Properties of concrete containing waste glass. Cement and concrete research, 34(2), 267-274.

Yüksel, İ., Siddique, R., & Özkan, Ö. (2011). Influence of high temperature on the properties of concretes made with industrial by-products as fine aggregate replacement. Construction and building materials, 25(2), 967-972.

Proceedings of the 5th International Conference on Civil Engineering for Sustainable Development (ICCESD 2020), 7~9 February 2020, KUET, Khulna, Bangladesh (ISBN-978-984-34-8764-3)

FLEXURAL PERFORMANCE OF STEEL-POLYPROPYLENE HYBRID FIBER REINFORCED CONCRETE BEAM: EXPERIMENTAL INVESTIGATIONS

Khandokar Bakhtiar Rahman*[1], Ismail Saifullah[2], S.M. Shaik-ul-Karim[3] and Shafkat Ahmed [4]

[1]Undergraduate Student, Department of Civil Engineering, Khulna University of Engineering and Technology (KUET), Bangladesh, e-mail: khdipro4040@gmail.com
[2]Associate Professor, Department of Civil Engineering, Khulna University of Engineering and Technology (KUET), Bangladesh, e-mail: saifullah@ce.kuet.ac.bd
[3]Undergraduate Student, Department of Civil Engineering, Khulna University of Engineering and Technology (KUET), Bangladesh, e-mail: rishad.ce1501012@gmail.com
[4]Undergraduate Student, Department of Civil Engineering, Khulna University of Engineering and Technology (KUET), Bangladesh, e-mail: ahmed1501024@stud.kuet.ac.bd

***Corresponding Author**

ABSTRACT

This study mainly investigates the flexural performance of reinforced concrete beam (RCC) using polypropylene and steel fibers separately as well as combination of both fibers. Prior to specimen preparation, the physical and mechanical properties of polypropylene and steel fibers were determined. Moreover, the physical properties of binding material, coarse aggregates and fine aggregates were determined. In this research, four categories of beam specimens (4´ x 6´´ x 6´´size and selected suitable mixing ratio of 1:2:4) were constructed encompassing normal RCC beam (control); addition of 1.5% steel fiber; 2% polypropylene fiber; and combination of 0.5% steel fiber and 1.5% polypropylene fiber in volume of concrete. Experimental results showed that there is considerable increase of flexural strength due to addition of 1.5% steel fiber and 2% polypropylene fiber in concrete. However, the addition of both fibers (hybrid fiber) in combined not only increase the flexural performance but also the ductility of reinforced concrete beam members resulting to the cost effective. Hybrid fiber shows synergic effect on flexural behavior of concrete.

Keywords: *Polypropylene fiber, Steel fiber, Hybrid fiber, RCC beam, Flexural strength.*

1 INTRODUCTION

As concrete offers numerous well-known benefits such as low cost, wide obtainability and applicability, it is the most widely used construction material. Since concrete is brittle in nature, therefore, numerous materials have been utilized now-a-days to enhance this essential characteristics of concrete. Fibers are being used extensively in construction arenas because fiber reinforcement in concrete can decrease brittleness of concrete and make improvement of the properties of concrete especially in tensile strength and toughness (Wang, Huang, Jiang & Wu, 2012). Wang et al. (2012) also reported that different types of fibers are used to get different desired properties such as wire steel fiber are used to enhance the toughness properties of concrete once cracking, the use of mill cut steel fibers can increase initial cracking strength of concrete with its superior bond on concrete and polypropylene fibers can make improvement of impact strength of concrete. Therefore, the interest in the utilization of hybrid fiber in concrete has persistently growing now-a-days in prospect of obtaining concrete with enhanced properties.

Concrete with the inclusion of polypropylene fibers have appreciated an extensive rise in its application, comprising ground slab, concrete pipe, bridge deck, tunnel, pavement construction, canal, and repair and rehabilitation works (Al-Hadidy & Yi-Qiu, 2009; Behfarnia & Behravan, 2014; Kassimi, El-Sayed & Khayat, 2014; Khan & Ali, 2016). The surface roughness of the concrete matrix increases due to the integration of steel fibers (Armandei & de Souza Sanchez Filho, 2017). Based on the experimental study, Usman, Farooq, Umair & Hanif (2020) established that the utilization of steel fibers in high strength concrete has small effect on the compressive strength, although it expressively enhanced the ductility and post peak performance of concrete. Rapoport, Aldea, Shah, Ankenman & Karr (2002) conducted experimental study to examine the permeability of concrete containing steel fibers, and specified that the permeability of concrete decreases with the increase of steel fibers substance. However, macro polypropylene fibers demonstrate the benefits of light weight in addition to no corrosion (Ding, Li, Zhang & Azevedo, 2017).

Mohseni et al. (2017) made an effort to use steel or polypropylene fibers in concrete and investigated that there is considerable enhancement of splitting tensile strength as well as permeability attributable to increase of fiber contents. The tensile strength and toughness of concrete increases with the addition of steel fibers (Ahmadi, Farzin, Hassani & Motamedi, 2017; Gao, Zhang & Nokken, 2017; Gao & Zhang, 2018). The fracture energy as well as toughness of concrete after exposure to elevated temperatures can be significantly enhanced due to inclusion of steel fibers (Chen, Yang, Lin, Chen, He & Zhang, 2016). Zollo (1984) revealed that concrete incorporating polypropylene fibres (19mm long) and acrylic material (10mm long) exhibit lower shrinkage and crack width. The splitting tensile and flexural strengths of concrete increases with the incorporation of 0.5 % polypropylene fibers (Fathima & Varghese, 2014). Hanumesh et al. (2018) performed experimental study to observe the performance of recycle aggregate concrete containing polypropylene fibers and found that the compressive, split and shear strengths of concrete increases because of integration of polypropylene fibers. Zhao (1999) investigated that the incorporation of steel fibers with volume fraction larger than 2% may consequence in intense reduction of concrete flowability. Conversely, the effect of steel fibers with volume fraction lesser than 0.5% in concrete is unremarkable. Several researches disclosed that the integration of steel fibers with other kinds of fibers (for instance, polypropylene fibers, carbon fibers, glass fibers) into the plain concrete can evidently enhance the bond strength (Aslani & Nejadi, 2012; Hameed, Turatsinze, Duprat & Sellier, 2013; Ganesan, Indira & Sabeena, 2014). Amalgamation of fiber of different length enhances not only the toughness but also the impermeability of concrete (Lawler et al. 2002). Huang, Xu, Chi, Deng & Zhang (2019) investigated the performance of bond strength of embedded deformed bar in steel-polypropylene hybrid fiber reinforced concrete matrix, and revealed that the execution of steel-polypropylene hybrid fiber have noticeable optimistic effects on the bond strength, because of the substantial influences in preventing the spread of cracks at multi-scale as well as multi-phases.This study mainly investigates the flexural performance of reinforced concrete beam (RCC) using polypropylene and steel fibers separately as well as combination of both fibers. Prior to specimen preparation, the physical and mechanical properties of polypropylene and steel fibers were determined.

2 EXPERIMENTAL WORKS

2.1 Materials

In this study, Ordinary Portland cement (OPC), fine aggregate, coarse aggregate, polypropylene fibers, steel fibers and deformed bars were utilized to make concrete. The laboratory testing program for these materials comprised of the sieve analysis of both fine and coarse aggregates, unit weight of fine aggregate, coarse aggregates, steel fiber and polypropylene fiber, tensile strength test of steel fiber, polypropylene fiber and deformed bars.

2.1.1 Cement

Portland cement is commonly used around the world as a fundamental constituent of concrete. Ordinary Portland Cement (OPC) of type CEM I encompassing a strength of 52.5 MPa was used in this study. The specific gravity, initial setting time and final setting time of this type of cement were determined and obtained 3.15, 155 minutes and 270 minutes correspondingly, following standard specification (ASTM C150) for Portland cement.

2.1.2 Aggregates

Coarse (Sylhet) sand were used as fine aggregate to produce concrete. Sieve analysis for both fine aggregates and coarse aggregates was carried out in accordance with ASTM C136 to obtain fineness modulus and gradation curves as exhibited in Table 1 and Figure 1 respectively. The specific gravity, fineness modulus, bulk density, moisture content and water absorption of sand were determined and found 2.60, 2.56, 1560 kg/m^3, 1.7% and 2.3% respectively. Stone chips were used in concrete as coarse aggregate. The utilized nominal size of stone chips was 19 mm. The specific gravity, fineness modulus, bulk density, moisture content and water absorption of used stone chips were found 2.69, 7.74, 1490 kg/m^3, 1.1% and 0.3% respectively.

Table 1: Determination of fineness modulus of fine aggregates through sieve analysis

Sieve#	Wt Retained (gm)	Cum wt. retained (gm)	Cum wt. retained (%)	% Finer	FM
#4	5.6	5.6	1.1	98.9	2.56
#8	13.0	18.6	3.7	96.3	
#16	51.9	70.5	14.1	85.9	
#30	177.7	248.2	49.6	50.4	
#50	192.4	440.6	88.1	11.9	
#100	56.2	496.8	99.4	0.6	
Sum of Cumulative Weight Retained (%) =			256.0		

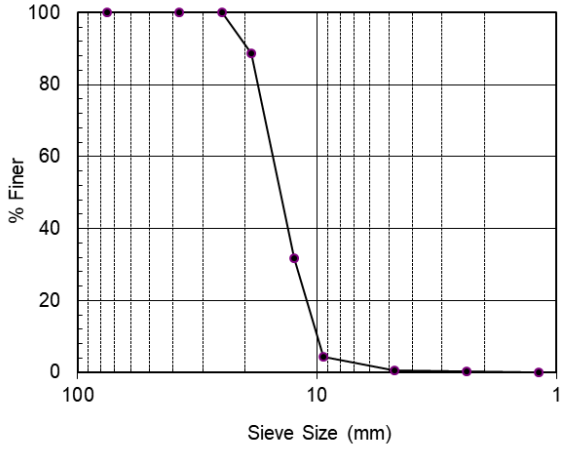

Figure 2: Gradation curve for stone chips

2.1.3 Fibers

Two types of fibers such as polypropylene fibers and steel fibers were utilized in this study to fabricate hybrid fibers. Appearances of polypropylene fibers and steel fibers are displayed in Figure 2. Polypropylene is partially crystalline and non-polar and possesses good abrasion and fatigue resistance, chemical resistance and electrical insulation (Alwesabi, Bakar, Alshaikh & Akil, 2020). However, existence of steel fibers in concrete is a cause of change in physical properties, resistance against cracking, fatigue, durability, impact, and bending. The polypropylene used in this study is the commodity plastic with the lowest density of 853 kg/m^3. Polypropylene fibers (length = 25 mm, width = 10 mm and thickness = 1.3 mm) possesses a tensile strength of 38 MPa, whereas, mill cut steel fibres (25.4 mm in length and 1.15 mm in diameter with an aspect ratio of 22) contains the tensile strength of 358 MPa. Table 2 depicts the physical and engineering properties of polypropylene and steel fiber.

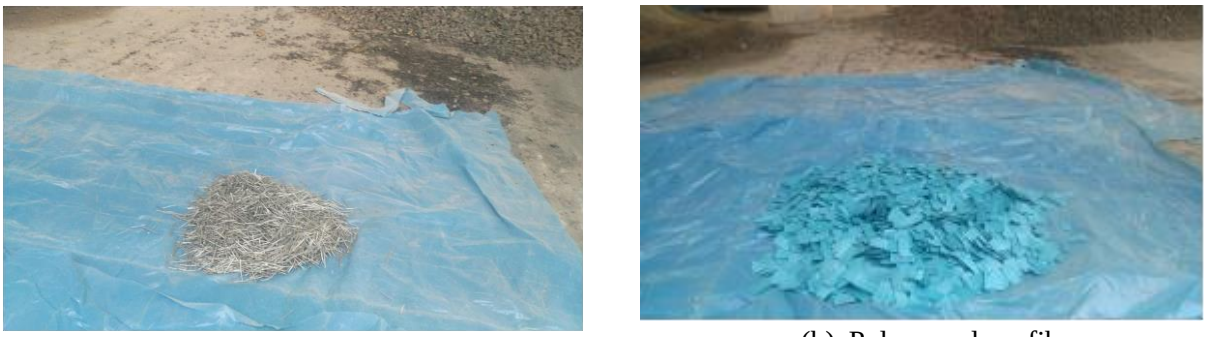

(a) Steel fibers (b) Polypropylene fibers

Figure 2: Appearances of polypropylene fibers and steel fibers

Table 2: Physical and engineering properties of polypropylene and steel fiber

Parameter	Polypropylene fiber	Steel fiber
Length (mm)	25	25.4
Thickness/diameter (mm)	1.3	1.15
width (mm)	10	--
Density (Kg/m^3)	853	7346
Tensile strength (MPa)	38	358

2.2 Mix Proportioning

The strength of concrete prominently depend on mix ratio of concrete. It is the ratio of binding material: fine aggregate: coarse aggregate. Three (03) controlled reinforced concrete beams and nine (09) reinforced concrete beams were constructed with a number of fibre combinations as provided in Table 3. It should be mentioned that three samples were prepared for each batch of concrete mixing. Each batch of concrete mixing used the identical water-cement ratio of 0.45 with the ratio of cement: sylhet sand: black stone chips of 1:2:4. In this study, the utilized volume fraction of three fibre combinations were 1.5% steel fiber alone, 2% polypropylene fiber alone and 0.5% steel fiber-1.5% polypropylene fiber. The workability for each batch of concrete mixing was determined compliant with ASTM C143 and obtained the slump value in the range of 75 to 100 mm.

Table 3: Details of fiber content in different reinforced concrete beams.

Sl. No.	Specimen designation	% of fiber (by volume)		Total fibre volume (%)
		Steel fiber	Polypropylene fiber	
1.	NRB	0	0	0
2.	SFRB	1.5	0	1.5
3.	PFRB	0	2	2.0
4.	SPRB	0.5	1.5	2.0

2.3 Preparation of specimen

In this study a total of 12 reinforced concrete beam specimens were prepared. Each mix had three beam specimens. The dimensions of each beam specimen was 1200 x 150 x 150 mm (length x width x depth). For simplicity, 10 mm deformed bars were used as main bar, whereas, 8 mm deformed bars were used as shear reinforcement to prepare beam specimen. In order to prepare concrete mix at first fine and coarse aggregates were put to the rotating mixer and mixed for 2 minutes. After that, cement was inserted to the mixer using the dry mixing and maintained for another 1.5 minutes. Then, 70% of required water was provided into the rotating mixer and sustained mixing for further 2 minutes. Afterward, the rest of the water was poured into the mixture and mixed for 1.5 minutes up to obtaining homogeneity. Thereafter, the fibers were disperse into the rotating mixer and continued mixing for 3 to 4 minutes until homogeneity of concrete. The beam specimens were cast into steel moulds. Once casting accomplished, each beam specimens were enclosed by polythene sheet at ambient temperature for 24 hours. Finally, each reinforced concrete beams were detached from the steel moulds and provided in a water chamber for curing up to 28 days.

2.4 Test Method

Slump test was performed according to provisions specified by ASTM C143. The slump value for each batch of concrete mixing was obtained by determining the difference of vertical distance between the uppermost of the overturned mould and the center of the upper surface of the concrete mix. Flexural strength test was carried out according to ASTM C78 on each reinforced concrete beams using a calibrated hydraulic jack with the capacity of 500 kN. An axial displacement was implemented at the mid-point of beams at a constant rate of 0.1 mm/min according to the requirements recommended by ASTM C78. The typical test setup for the flexural strength of reinforced concrete beams is presented in Figure 4. The axial displacement was applied until the failure of samples.

Figure 4: Typical test setup for flexural strength of reinforced concrete beam

3 RESULTS AND DISCUSSIONS

3.1 Flexural Strength

The ultimate Load, deflection, failure patterns are analyzed and discussed in this section. This study discusses the comparative effect of using additional fiber materials on flexural behavior of concrete. To analyze the load and deflection relationship, deflection of beams under corresponding loading were recorded. The failure load for each beam was noted for finding flexural strength. The load-deflection behavior for each mixes of reinforced concrete beams at 28 days is demonstrated in Figure 5. Table 4 and Figure 6 demonstrates the results of flexural strength tests for such reinforced concrete beams. It should be noted that the obtained results are the average of the results of three samples. From Figure 5 it has been found that the maximum load carrying capacity of RCC beam without containing any fiber is 70 kN whereas, beams containing 1.5% steel fibers, 2% polypropylene fibers and combination of 0.5% steel fibers and 1.5 % polypropylene fibers carrying maximum load of 81 kN, 85 kN, and 90 kN respectively. While the polypropylene fibers enhance the strain capacity as well as toughness of the post-crack region, the robust and harder steel fibers increase the ultimate strength of concrete (Komloš, Babal, & Nürnbergerova, 1995).

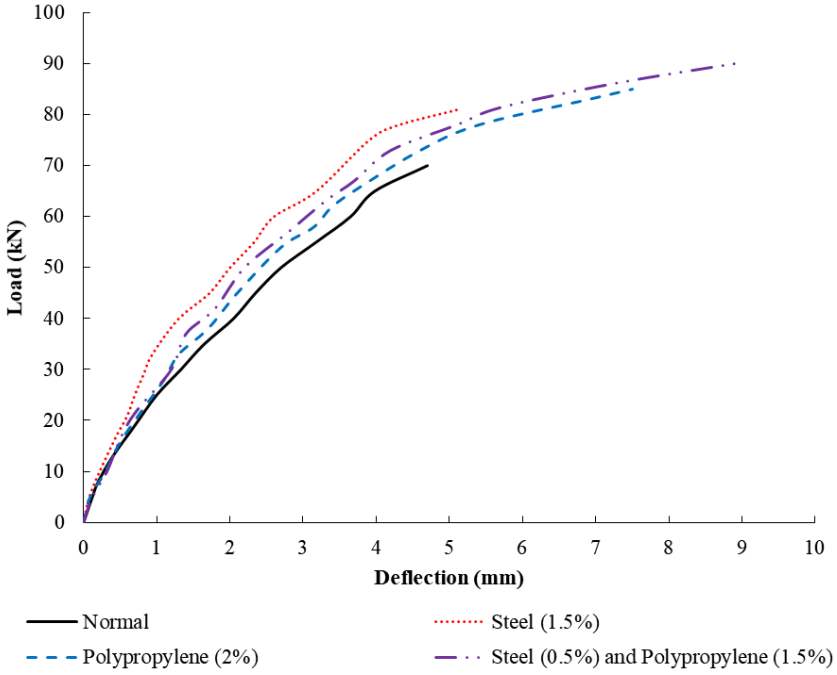

Figure 5: Comparison of load-deflection behavior of different reinforced concrete beams

The integration of fibers in concrete also enlarges the ductility in addition to toughness of the RCC beam as presented in Figure 5. The flexural strength for each beam was calculated according to specified formula. The flexural strength of RCC beam without containing any fiber was 36.2 MPa. Meanwhile, SFRB, PFRB and SPRB produced flexural strengths of 41.9 MPa, 43.9 MPa and 46.5 MPa correspondingly. The flexural strength of RCC beam increases with the increase of fiber content. The percentage increase of flexural strength were found 15.7%, 21.4% and 28.5% with the incorporation of 1.5% steel fibers, 2% polypropylene fiber and combination of 0.5% steel fiber and 1.5 % polypropylene fiber, respectively. The uppermost flexural strength of RCC beam was observed in SPRB mix reinforced with hybrid fiber (combination of 0.5% steel fiber and 1.5 % polypropylene fiber). Therefore, the combination of steel fibers and polypropylene fibers have positive effect on the flexural strength of reinforced concrete.

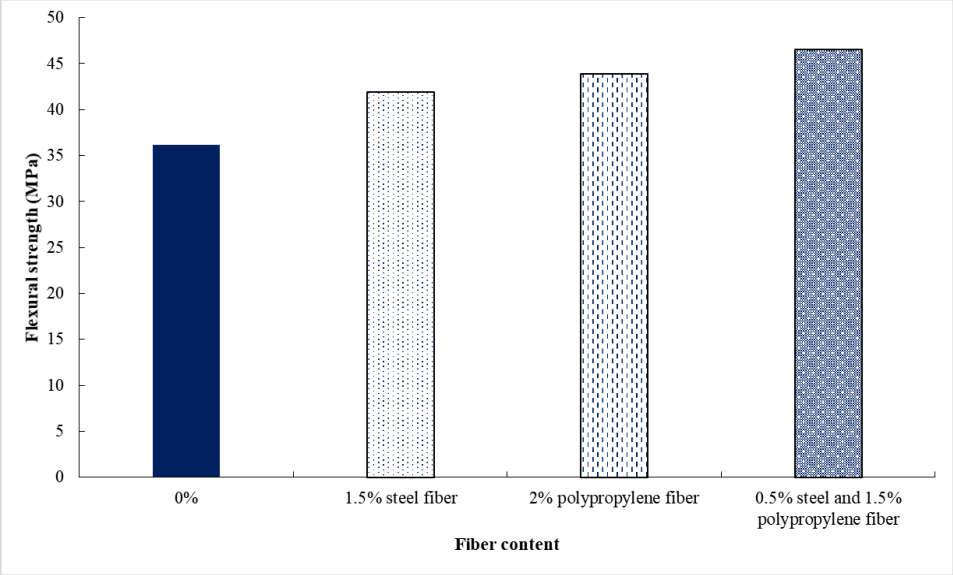

Figure 6: Effect of fiber content on the flexural behavior of reinforced concrete beams

Table 4: Load carrying capacity and flexural strength of different reinforced concrete beams

Specimen designation	Combination	Ultimate load (kN)	Maximum deflection (mm)	Flexural strength (MPa)	Increased flexural strength (%)
NRB	Normal RCC beam	70	4.7	36.2	-
SFRB	1.5% steel fiber	81	5.1	41.9	15.7
PFRB	2% polypropylene fiber	85	7.5	43.9	21.4
SPRB	0.5% steel fiber and 1.5% polypropylene fiber	90	8.9	46.5	28.5

3.2 Failure Patterns

Fiber reinforcement has extensive been understood to enhance the mechanical properties of concrete through restraining the development of cracks (Chi, Xu & Zhang, 2014).The failure modes for each mixes of reinforced concrete beams under mid-point loading conditions at 28 days is presented in Figure 7. For RCC beam without containing any fiber, the propagation of cracks occurrence is presented in Figure 7(a). There were some vertical and diagonal cracks observed in the beam. Crack Propagation can't be controlled under flexure. As there is no fiber, so the rigidity and load carrying capacity of the beam is less and there is a number of crack. In this case, crack pattern is brittle in manner. The cracking behavior of beam is changed from brittle manner when there was inclusion of 1.5% steel fiber in concrete (shown in Figure 7b). Flexural strength is moderately higher than normal RCC beam, but slightly lower than polypropylene fiber containing beam. Steel fiber imparts ductility. The commencement and propagation of cracks in concrete can be postponed due to incorporation of steel fibers (Chen et al. 2016).

(a) Cracks in normal RCC beam

(b) Cracks in 1.5% steel fiber beam

(c) Cracks in 2% polypropylene fiber beam

(d) Cracks in hybrid fiber beam

Figure 7: Failure patterns for each mixes of reinforced concrete beams

Cracks are brittle in manner which were observed in the beam containing 2% polypropylene fiber. There is shear crack under the ultimate load for which crack occurs (shown in Figure 7c). Although incorporation of 2% polypropylene fiber increased the flexural strength compared to normal RCC beam, but this fiber has insignificant effect on cracking. Macro polypropylene fibers can modify the characteristics of concrete as soon as the matrix has fractured and the fibers enhance the ductility as well as energy absorption capability of concrete (Koniki & Prasad, 2019). The inclusion of steel fibres in concrete is not only an extremely cost-effective but also time-effective approach as it permits prohibiting of reinforcement bars throughout the manufacture and design processes. Polypropylene fiber-reinforced concrete has been focus on now-a-days research due to their remarkable toughness, low cost as well as good shrinkage cracking resistance (Afroughsabet & Ozbakkaloglu, 2015). Reinforcement with one category of fiber in concrete improves the mechanical properties within a rationed assortment. On the other hand, hybrid concrete with the incorporation of different types of fibers exhibit the combined interfaces of all fiber and therefore, possess outstanding properties. In this study, the cracks produced in the surface of beam is more ductile in manner due to addition of 0.5% steel fiber and 1.5% polypropylene fiber (shown in Figure 7d). The integrated utilization of steel fibers and polypropylene fibers in reinforced concrete beams can be observed as enormously advantageous as it not only enhances the flexural strength of concrete but also resolves the concern of brittle failure to a considerable amount. Polypropylene fiber resist the cracking in earlier stage and steel fiber resist the crack propagation in later stage (Yap, Bu, Alengaram, Mo & Jumaat, 2014). Therefore, the incorporation of various fibers with different lengths and sizes is a possible strategy to inhibit the cracks problem taking place at different phases in concrete.

4. SUMMARY AND CONCLUSIONS

This study predominatly investigates the flexural performance of reinforced concrete beam (RCC) using polypropylene and steel fibers separately as well as combination of both fibers. In this research, four categories of RCC beam specimens were constructed encompassing normal RCC beam (control); addition of 1.5% steel fiber; 2% polypropylene fiber; and combination of 0.5% steel fiber and 1.5% polypropylene fiber in volume of concrete. Based on the experimental study, the following conclusions have been sorted out:

- The flexural strength of RCC beam increases due to addition fiber content. Compared to RCC beam without containing any fiber, flexural strength increases by 15.7%, 21.4% and 28.5% due to the incorporation of 1.5% steel fibers, 2% polypropylene fiber and combination of 0.5% steel fiber and 1.5 % polypropylene fiber, respectively.
- The initiation and propagation of cracks in RCC beam can be controlled due to incorporation of steel fibers by 1.5% in volume of concrete.
- The incorporation of polypropylene fiber by 2% in volume of concrete in RCC beam not only increases the flexural strength compared to normal RCC beam, but also enhance the ductility in considerable extent.
- The combined use of 0.5% steel fiber and 1.5% polypropylene fiber have positive effect on the flexural strength of reinforced concrete. The hybrid fiber in reinforced concrete beams can be observed as enormously advantageous as it not only enhances the flexural strength of concrete but also resolves the concern of brittle failure to a considerable amount. Therefore, the incorporation of a number of fibers with different lengths and sizes is a possible strategy to inhibit the cracks problem taking place at different phases in concrete.

ACKNOWLEDGMENT

We want to express our acknowledgements to all of the employees of Engineering Materials Laboratory, Department of Civil Engineering, Khulna University of Engineering & Technology for their valuable cooperation during the course of the research period.

References

Afroughsabet, V., & Ozbakkaloglu, T. (2015). Mechanical and durability properties of high-strength concrete containing steel and polypropylene fibers. *Construction and building materials*, *94*, 73-82.

Ahmadi, M., Farzin, S., Hassani, A., & Motamedi, M. (2017). Mechanical properties of the concrete containing recycled fibers and aggregates. *Construction and Building Materials*, *144*, 392-398.

Al-Hadidy, A. I., & Yi-Qiu, T. (2009). Mechanistic approach for polypropylene-modified flexible pavements. *Materials & Design*, *30*(4), 1133-1140.

Alwesabi, E. A., Bakar, B. A., Alshaikh, I. M., & Akil, H. M. (2020). Experimental investigation on mechanical properties of plain and rubberised concretes with steel–polypropylene hybrid fibre. *Construction and Building Materials*, *233*, 117194.

Aslani, F., & Nejadi, S. (2012). Bond characteristics of steel fiber and deformed reinforcing steel bar embedded in steel fiber reinforced self-compacting concrete (SFRSCC). *Open Engineering*, *2*(3), 445-470.

Armandei, M., & de Souza Sanchez Filho, E. (2017). Correlation between fracture roughness and material strength parameters in SFRCs using 2D image analysis. *Construction and Building Materials*, *140*, 82-90.

ASTM C150 (2011). Standard Specification for Portland Cement, ASTM International, West Conshohocken, PA, United States.

ASTM C136 (2019). Standard Test Method for Sieve Analysis of Fine and Coarse Aggregates, ASTM International, West Conshohocken, PA, United States.

ASTM C143 (2015). Standard Test Method for Slump of Hydraulic-Cement Concrete, ASTM International, ASTM International, West Conshohocken, PA, United States.

ASTM C78 (2015). Standard Test Method for Flexural Strength of Concrete (Using Simple Beam with Central-Point Loading), ASTM International, West Conshohocken, PA, United States.

Behfarnia, K., & Behravan, A. (2014). Application of high performance polypropylene fibers in concrete lining of water tunnels. *Materials & Design*, *55*, 274-279.

Chen, G. M., Yang, H., Lin, C. J., Chen, J. F., He, Y. H., & Zhang, H. Z. (2016). Fracture behaviour of steel fibre reinforced recycled aggregate concrete after exposure to elevated temperatures. *Construction and Building Materials*, *128*, 272-286.

Chi, Y., Xu, L., & Zhang, Y. (2014). Experimental study on hybrid fiber–reinforced concrete subjected to uniaxial compression. *Journal of Materials in Civil Engineering*, *26*(2), 211-218.

Ding, Y., Li, D., Zhang, Y., & Azevedo, C. (2017). Experimental investigation on the composite effect of steel rebars and macro fibers on the impact behavior of high performance self-compacting concrete. *Construction and Building Materials*, *136*, 495-505.

Fathima, K. M. A., & Varghese, S. (2014). Behavioural Study of Steel Fibre & Polypropylene FRC. *Impact: International Journal of Research in Engineering & Technology*, *2*(10), 17-24.

Ganesan, N., Indira, P. V., & Sabeena, M. V. (2014). Bond stress slip response of bars embedded in hybrid fibre reinforced high performance concrete. *Construction and Building Materials*, *50*, 108-115.

Gao, D., & Zhang, L. (2018). Flexural performance and evaluation method of steel fiber reinforced recycled coarse aggregate concrete. *Construction and Building Materials*, *159*, 126-136.

Gao, D., Zhang, L., & Nokken, M. (2017). Compressive behavior of steel fiber reinforced recycled coarse aggregate concrete designed with equivalent cubic compressive strength. *Construction and Building Materials*, *141*, 235-244.

Hameed, R., Turatsinze, A., Duprat, F., & Sellier, A. (2013). Bond stress-slip behaviour of steel reinforcing bar embedded in hybrid fiber-reinforced concrete. *KSCE Journal of Civil Engineering*, *17*(7), 1700-1707.

Hanumesh, B. M., Harish, B. A., & Ramana, N. V. (2018). Influence of Polypropylene Fibres on Recycled Aggregate Concrete. *Materials Today: Proceedings*, *5*(1), 1147-1155.

Huang, L., Xu, L., Chi, Y., Deng, F., & Zhang, A. (2019). Bond strength of deformed bar embedded in steel-polypropylene hybrid fiber reinforced concrete. *Construction and Building Materials*, *218*, 176-192.

Kassimi, F., El-Sayed, A. K., & Khayat, K. H. (2014). Performance of fiber-reinforced self-consolidating concrete for repair of reinforced concrete beams. *ACI Structural Journal*, *111*(6), 1277-1286.

Khan, M., & Ali, M. (2016). Use of glass and nylon fibers in concrete for controlling early age micro cracking in bridge decks. *Construction and Building Materials*, *125*, 800-808.

Komloš, K., Babal, B., & Nürnbergerova, T. (1995). Hybrid fibre-reinforced concrete under repeated loading. *Nuclear Engineering and Design*, *156*(1-2), 195-200.

Koniki, S., & Prasad, D. R. (2019). Influence of hybrid fibres on strength and stress-strain behaviour of concrete under uni-axial stresses. *Construction and Building Materials*, *207*, 238-248.

Lawler, J. S. (2002). Hybrid fiber-reinforcement in mortar and concrete. PhD thesis. Northwestern University

Mohseni, E., Saadati, R., Kordbacheh, N., Parpinchi, Z. S., & Tang, W. (2017). Engineering and microstructural assessment of fibre-reinforced self-compacting concrete containing recycled coarse aggregate. *Journal of Cleaner Production*, *168*, 605-613.

Rapoport, J., Aldea, C. M., Shah, S. P., Ankenman, B., & Karr, A. (2002). Permeability of cracked steel fiber-reinforced concrete. *Journal of materials in civil engineering*, *14*(4), 355-358.

Usman, M., Farooq, S. H., Umair, M., & Hanif, A. (2020). Axial compressive behavior of confined steel fiber reinforced high strength concrete. *Construction and Building Materials*, *230*, 117043.

Wang, P., Huang, Z., Jiang, J., & Wu, Y. (2012). Performance of hybrid fiber reinforced concrete with steel fibers and polypropylene fibers. In *Civil Engineering and Urban Planning 2012* (pp. 458-461).

Yap, S. P., Bu, C. H., Alengaram, U. J., Mo, K. H., & Jumaat, M. Z. (2014). Flexural toughness characteristics of steel–polypropylene hybrid fibre-reinforced oil palm shell concrete. *Materials & Design*, *57*, 652-659.

Zhao, G. F. (1999). Structure of steel fiber reinforced concrete. China Architecture & Building Press, Beijing.

Zollo, R. F. (1984). Collated fibrillated polypropylene fibers in FRC. In *Publication SP-American Concrete Institute* (pp. 397-409). American Concrete Institute.

IMPACT ON PHYSICAL, MECHANICAL AND FUNCTIONAL PROPERTIES OF AUTOCLAVED AERATED CONCRETE WITH ALUMINIUM AND AUTOCLAVING TEMPERATURE

Mohei Menul Islam*[1], Muhammad Harunur Rashid[2] and Md. Aqib Muntasir[3]

[1]Post-graduate student, Department of Civil Engineering, Khulna University of Engineering & Technology, Bangladesh, e-mail: mmahir116267@gmail.com
[2]Professor, Department of Civil Engineering, Khulna University of Engineering & Technology, Bangladesh, e-mail: mhrashid@ce.kuet.ac.bd
[3]Graduate, Department of Civil Engineering, Khulna University of Engineering & Technology, Bangladesh, e-mail: amraktim20@gmail.com

***Corresponding Author**

ABSTRACT

Autoclaved aerated concrete is prepared by the mixture of ordinary portland cement, lime powder, sand, aluminium powder and water. AAC is commonly used in building structures as infill or partition wall. To use AAC as building material, it is necessary to assess its various physical, mechanical and functional properties. These properties of AAC depend on the type, quality and amount of cement, sand, lime, aluminium and water. Autoclaving temperature, pressure and curing period also effect the properties of AAC. This study covers the variation of physical, mechanical and functional properties of autoclaved aerated concrete with autoclaving temperature and aluminium content. These properties are compared with the conventional or normal weight cement mortar sample. To fulfill this work, a total of 72 blocks and 18 briquettes both of AAC and controlled samples were prepared. For each property 03 numbers of AAC and normal weight cement mortar were prepared for a specific aluminium content and autoclaving temperature. The size of mortat blocks was 50x50x50 mm according to the size stated in ASTM C109 and the size for briquettes was taken from ASTM C307. In this work, two amount of aluminium content of 0.4% and 0.8% of the dry weight of OPC and three different autoclaving temperature of 160^{o}C, 180^{o}C and 200^{o}C were used. AAC sample with 0.8% aluminium and 160^{o}C temperature had unit weight of 1490kg/m^3 which was lowest among all samples including the controlled or normal weight of cement blocks. Weight reduction of that AAC sample was 31.53% which was higher with respect to normal weight concrete. AAC sample with 0.4% aluminium and 200^{o}C autoclaving temperature gave maximum compressive and tensile strength of 19.4 and 1.81Mpa respectively which were quite close to that of normal weight concrete and it was seen, strength of AAC increases with autoclaving temperature and decreasing of aluminium content. In this research, the functional properties of AAC, water and surface absorption were much higher than normal weight concrete. Absorption capacity of AAC increased with aluminium content and with decreasing autoclaving temperature and unit weight of AAC for this research. For AAC with 0.8% aluminium and 160^{o}C temperature gave maximum water absorption capacity of 9.93%. Again, surface absorption rate was higher for 1st 12hours and with time it would be constant because of its saturated position.

Keywords: *Autoclaved aerated concrete, Autoclaving temperature, Aluminium, Mechanical and functional properties.*

1. INTRODUCTION

Autoclaved aerated concrete is a structural material which is generated by mixing of ordinary Portland cement, fine aggregate, lime powder, aluminium powder with small amount and water and by the steam curing in autoclaved at constant high autoclaving temperature and pressure. AAC is actually a light-weight concrete which is commonly used around world specially in Asia and Europe, particularly as it combines ease of construction with excellent combination of mechanical and thermal properties (Narayanan & Ramamurthy, 2000). Autoclaved aerated concrete, an environmentally friendly material may have considerable potential for further applications (Robert, Jerman, Keppert, & Vy, 2013). Before use AAC, it should be known about its various physical, mechanical and functional properties. Physical properties are shape, size, microstructure, dry unit weight, moist unit weight etc. Mechanical properties are compressive, tensile, flexural strength, modulus of elasticity, shrinkage, creep etc. Functional properties are water and surface absorption capacity, fire resisting capacity etc.

Autoclaved aerated concrete (AAC) gains its light-weight property by a mechanism that consist of a chemical reaction between $Ca(OH)_2$ and aluminium powder (Al). Through this reaction, hydrogen gas (H_2) is produced that makes pores in the AAC. For that reason, AAC is porous and has less self-weight than normal weight concrete. The chemical reaction is (Holt & Raivio, 2005) :

$$2Al + 3Ca(OH)_2 + 6H_2O = 3CaO.Al_2O_3.6H_2O + 3H_2\,(gas)$$

Autoclaved aerated concrete is prepared by steam cured at autoclaved at high temperature and pressure. This temperature and pressure vary from 180°C to 210°C and 4 to 16MPa. The curing period is within 8h to 18h continuously. This steam curing of AAC in autoclaved is done at constant temperature, pressure and curing period (Hauser, Eggenberger, & Mumenthaler, 1999).

The unit weight of AAC can be in the range of 400 to 800kg/m^3 and has less thermal conductivity than normal weight concrete (0.16-0.18W/m-k) (Anon, 1970). For light-weight (aerated) concrete this bulk density varies from 300 to 1850kg/m^3 (Neville, 1995).

In the previous year, Robert, Jerman, Keppert, & Vy, (2013) studied about hygric, thermal properties of AAC with unit weight and compressive strength of AAC and also discusses about durability and various physical properties of AAC. Wakili, Hugi, Karvonen, Schnewlin, & Winnefeld, (2015) studied about thermal characteristics of autoclaved aerated concrete when it was expounded to fire. They analysed the thermal conductivity of autoclaved aerated concrete at temperature of 120°C to 720°C and showed how AAC lost its mass with increasing temperature. Leyla Tanaçan, Yas, & Arpacıog, (2009) investigated the effect of increased temperature and different cooling regime on behaviour of aerated concrete. L Tanaçan, Ersoy, & Arpac, (2005) investigated for the cellular gas concrete, impact on various mechanical properties and velocity of ultrasound due to elevated temperature. They applied temperature with the range of 100°C to 965°C. Kumar & Ramamurthy, (2015) showed impact on various properties of aerated concrete with moist-cured due to various aluminium content and its fineness. Sanjayan, Nazari, Chen, & Nguyen, (2015) investigated effect of various aluminium content on different properties of geopolymer aerated concrete.

As other physical properties of AAC are related with the unit weight (300±1800kg/m^3). For the calculation, the moisture condition is needed to be indicated. The unit weight of autoclaved aerated concrete cured from autoclaved immediately is 15±25% up to 45% heavier than the oven-dried AAC concrete (Narayanan & Ramamurthy, 2000). The density of aerated concrete decreases with the fineness of aluminium powder for a specific dosage of it. High w/c ratio (0.4 to 0.6) gives more weight reduction (30% to 35%) of aerated concrete when the aluminium content is in the range of 0.25 to 0.50% of the weight of binding material respectively. Dry density and compressive strength decreases with aluminium content and water absorption capacity increases with aluminium content (Kumar & Ramamurthy, 2015).

The range of moisture content of autoclaved aerated concrete (AAC) is termed as water absorption of AAC. The capacity of water absorption varies with different dosage of aluminium powder (Koronthalyova, 2011). The overall surface absorption is explained as the combination of 02 processes: a surface absorption through aerated pores of AAC that quickly gains gravitational equilibrium and surface absorption with slow rate through the matrix pores that follows the criterion $t^{1/2}$ law. The capillary or surface absorption of AAC may be presented by 03 parameters, such as: the capillarity of matrix, the capillarity of aerated pores and the aeration pore capillary rise cumulative absorption (Ioannou, Hamilton, & Hall, 2008).

In this research work, effect of various autoclaving temperature producing by heater and aluminium powder content on various physical, mechanical and functional properties of AAC has been investigated and compared these properties with that of normal weight concrete.

2. METHODOLOGY

2.1 Materials for samples

The materials used in this research were OPC, sand with 1.25FM, 20% lime powder of OPC, aluminium powder of 0.4% and 0.8% of total dry weight of OPC. These materials' pastes were prepared by hand mix with sufficient water according to w/c ratio to make the mixture with suitable workability and homogeneity. Table 1 and table 2 are given to show the sieve analysis of sand with 1.25 FM and properties of this sand respectively.

Table 1: Sieve analysis of sand with 1.25FM

Sieve number	Retained weight (gm)	Retained cumulative weight (gm)	Cumulative percent retained (%)	FM
#4	0.0	0.0	0.0	1.25
#8	0.0	0.0	0.0	
#16	0.0	0.0	0.0	
#30	0.0	0.0	0.0	
#50	125.3	125.3	25.32	
#100	369.5	494.8	100.00	
Total=	494.8		125.32	

Table 2: Properties of sand with 1.25FM

FM of sand	Unit weight (kg/m^3)		Specific gravity		Water absorption capacity (%)
	Loose condition	Compact condition	Oven dry	SSD	
1.25	1487	1612	2.35	2.43	3.65

2.2 Experimental program

2.2.1 Kneading and readiness of samples

The experimental samples were prepared according to ASTM C109. Mix proportion of AAC by weight for OPC cement: sand: aluminium powder: lime is 1:2.2:0.004:0.2 and 1:2.2:0.008:0.2 for aluminium content with 0.4% and 0.8% respectively. W/c ratio was 0.5 for both mix proportion of AAC. In table-3 the amount of ingredients for each six 50x50x50 mm AAC blocks are indicated below.

Table 3: Amount of ingredients for each six 50x50x50 mm AAC blocks

Ingredients	Sample type-1 (0.4% Al)	Sample type-2 (0.8% Al)
OPC (gm)	500	500
Sand with 1.25FM (gm)	1100	1100
Aluminium powder (gm)	2	4
Lime powder (gm)	100	100

All the ingredients of amount indicated in table-3 without aluminium powder were mixed by hand for 3 minutes so that the mixture might be homogeneous and have uniform colour. Then aluminium powder with desired amount was subtracted to that composition and compounded thoroughly about 30 sec. After that required amount water was added to the mixture to make homogeneous paste. That paste was poured in the moulds and tamped the paste by a tamping bar according to ASTM C109 standard. The surface of the paste was levelled with the straight edge and this levelling process was continued to 120 minutes due to volume increasing of that paste. Then the moulds with paste were kept in the room at room temperature and 75% relative humidity. By this process 36 numbers of 50x50x50 mm blocks and 9 numbers of briquettes with standard size were prepared for each sample type.

Conventional or normal weight concrete blocks and briquettes with same amount and size stated above were prepared with same amount of ingredients indicated in table-3 without adding lime and aluminium powder.

2.2.2 Steam curing of AAC (Autoclaving process)

After 24 hours from casting of the samples, they were demoulded and then kept in the autoclave chamber. These blocks were cured in the autoclave for 8h continuously at constant high temperature 160^{o}C, 180^{o}C and 200^{o}C separately and 8atm pressure with each temperature. Each sample type was introduced to autoclaving processes at three different temperatures and each time temperature and pressure were constant throughout the curing period. 36 numbers of blocks and 9 numbers of briquettes with standard size were autoclaved together.

After autoclaving, the samples were cooled and stored in the laboratory at room temperature and 75% relative humidity.

2.2.3 Physical properties

2.2.3.1 Unit weight

The three 50x50x50mm AAC blocks were weighted by balance. Volume of the blocks were determined. By dividing the weight with the volume of sample, the unit weight of AAC would be calculated. Same procedure was applied for conventional blocks.

2.2.4 Mechanical properties of samples

2.2.4.1 Compressive and tensile strength test

Compressive strength test of the three AAC blocks were determined by compressive strength testing machine according to ASTM C109 standard. This test was performed after 7days from casting of blocks. Tensile strength of 7days was tested for three AAC briquettes by tensile strength testing machine according to ASTM C307.

Compressive and tensile strength of conventional blocks and briquettes were determined in the same procedure stated above and the result of AAC samples were compared with that of conventional concrete.

2.2.5 Functional properties

2.2.5.1 Water absorption test

Water absorption capacity of AAC blocks were determined according to BS 1881-122 standard. Three AAC blocks after 7 days from its casting were kept in the electric oven at 105°C for 72h in such a way that these blocks were far at distance 25mm from each other. After that, the AAC blocks were dispelled from the oven and block samples were gentled in the airtight pot for 24±0.5h. Then each block was weighed by a balance and all the blocks were immersed in a bowl with water depth 25±5mm from the upper surface of sample blocks. The blocks were removed from the bowl after 30±0.5min. Each block was dried with cloth as soon as possible after taking from bowl with water. Then each block was weighed by the balance. The increased of weight as the percentage of its full dry weight and by which water absorption capacity of AAC blocks were calculated.

2.2.5.2 Surface absorption test

Surface absorption test or capillary test of AAC blocks were determined by standard test (Ioannou et al., 2008). After 7days from casting of AAC blocks, these blocks were sealed with wax except one surface which would be contacted to water. Sealed blocks were weighed by balance and they were kept in a narrow tray with water of 50mm depth. Weight of each block was weighed at regular interval of 12h for the total time 60h.

3. RESULTS AND DISCUSSION

There were six sets of AAC sample with two different amount of aluminium (0.4% & 0.8% of weight of OPC) and three high temperature (160°C, 180°C & 200°C).

3.1 Unit weight of AAC and conventional block

Unit weight is the physical property of a concrete block both for AAC and normal block. Unit weight of concrete varies with the different cement, various material characteristics of sand, amount of entrained air etc. In Figure-1, it is showed the variation of unit weight with different amount of aluminium and autoclaving temperature.

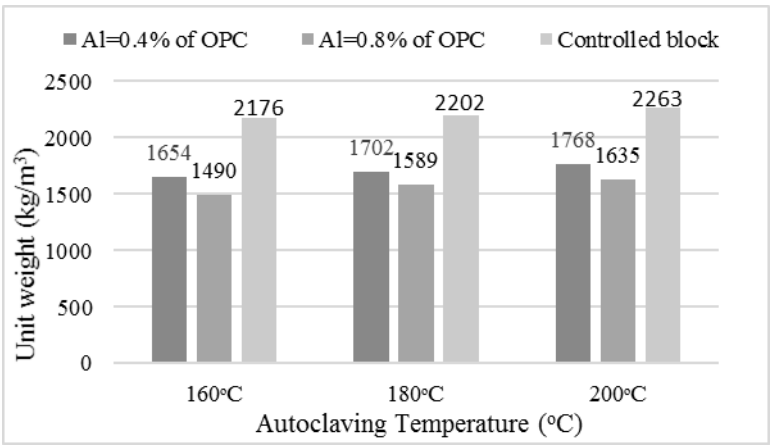

Figure 1: Variation of unit weight of AAC and controlled block

From figure-1 it is seen that, unit weight of AAC blocks increases with decreasing aluminium content and increasing autoclaving temperature. For AAC sample with aluminium content 0.8% of OPC and 160°C autoclaving temperature shows less unit weight (1490kg/m^3) and this sample is more light weight. Again, unit weight of AAC is less than controlled blocks (normal weight concrete). Aluminium powder is used as a foaming agent. Aluminium powder reacts with $Ca(OH)_2$ and

hydrogen gas (H_2) is produced that makes concrete porous. So, if aluminium content is increased, more porosity will be produced in the concrete and it becomes more light weight. Unit weight of AAC and controlled block is lower at autoclaving temperature of 160°C due to the change of chemical composition. From figure-1, the more weight reduction of AAC with respect to controlled block is 31.53%. Dry density or unit weight of aerated concrete decreases with aluminium content (Kumar & Ramamurthy, 2015). Again, unit weight of AAC increases with temperature and pressure significantly (Neville, 1995). The experimental result follows the trend from previous research works.

3.2 Strength of AAC and conventional concrete

The strength of AAC is less than that of conventional concrete. The compressive and tensile strength both for autoclaved aerated concrete and conventional or normal weight concrete were determined to compare the results between this two.

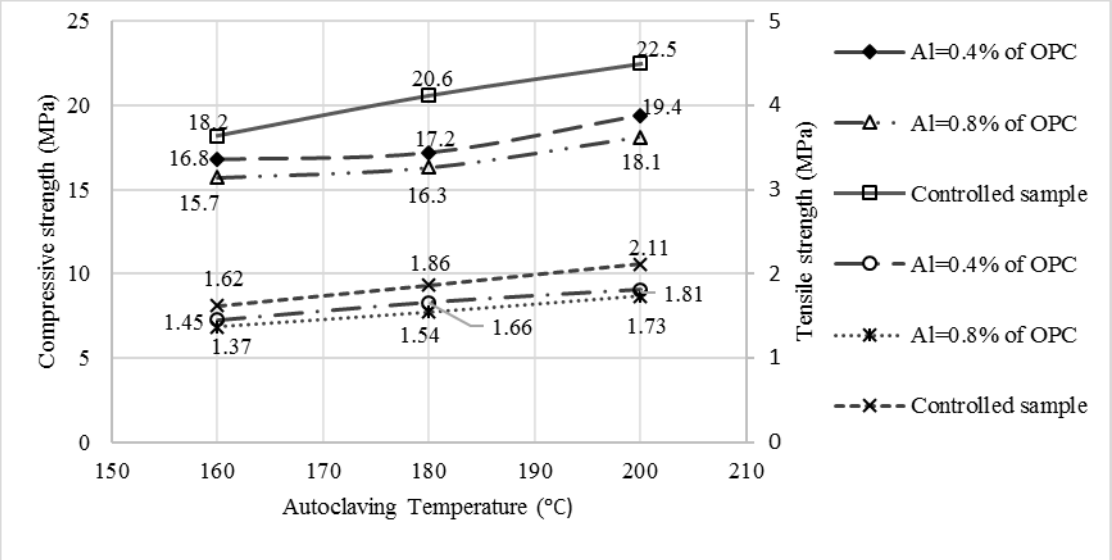

Figure 2: Variation of strength of AAC and controlled sample

From figure-2, strength of autoclaved aerated concrete increases with decreasing aluminium content and increasing autoclaving temperature. For controlled block, this strength increases with autoclaving temperature. There is little difference of strength between AAC and controlled sample. Strength of controlled sample is higher than AAC because of its porosity and less unit weight with respect to normal weight (controlled sample). The maximum compressive and tensile strength of normal weight concrete are 22.5MPa and 2.11MPa respectively and for AAC they are 19.4MPa and 1.81MPa respectively at aluminium=0.4% of OPC and 200°C autoclaving temperature. The lowest strength is seen at aluminium=0.8% of OPC and 160°C among all the criterions in this research work. Because of lower unit weight, concrete has lower strength. At lower temperature and higher aluminium content unit weight of AAC was less.

The strength of aerated concrete varies linearly with density of that type of concrete (Mirza & Ainoury, 1986).Strength of AAC increases with autoclaving temperature at high pressure (Shabbar, Nedwell, & Wu, 2016). The experimental result follows the trend of previous works.

3.3 Water and surface absorption of AAC and conventional concrete

The capacity of water absorption of concrete is functional property of concrete. The capacity of water absorption of concrete is presented as the percentage of the fully dried weight of concrete. Extremely good concrete might have up to 5% water absorption capacity, very good concrete might be 5 or 6%

by mass, typical commercial concrete might be 6 or 7%, ordinary concrete may have greater than 6% water absorption capacity with mass.

The capacity of water absorption of autoclaved aerated concrete generally lies in the range of more than 8% to 11.1% of its dry unit weight (Shabbar, Nedwell, & Wu, 2018). Water absorption capacity of AAC depends on autoclaving temperature, pressure, aluminium content, unit weight of AAC etc. Concrete is more durable when water absorption capacity is less.

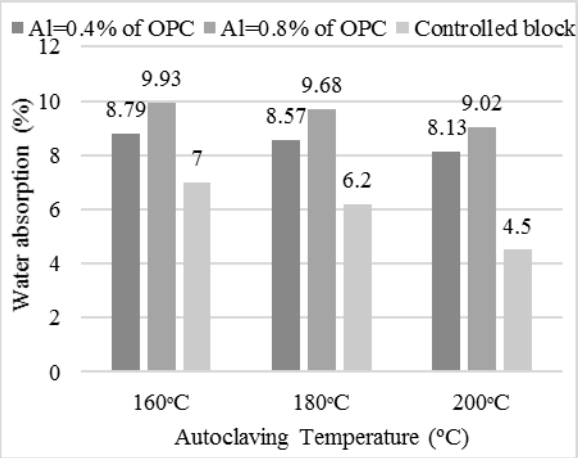

Figure 3: Water absorption of AAC and controlled block.

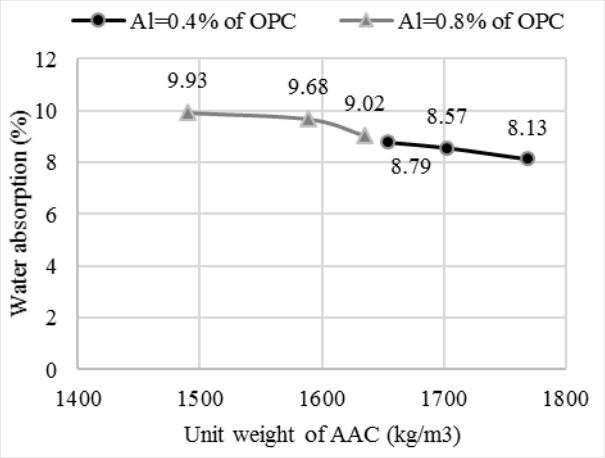

Figure 4: Change of water absorption with unit weight of AAC.

From figure-3, water absorption capacity of autoclaved aerated concrete increases with aluminium content and this capacity both for AAC and controlled block decreases with autoclaving temperature. Capacity of water absorption of AAC is higher than that of controlled block because of porosity properties of AAC. When aluminium content is higher, more H_2 gas is produced and more pore will be created. At higher autoclaving temperature (200°C) and pressure (8atm), samples gave higher unit weight. From figure-4, water absorption capacity of AAC decreases almost linearly with unit weight of AAC. Number of pores of sample reduces with unit weight and that's why water absorption capacity is reduced with unit weight.

Aerated concrete (foamed concrete) with less dry density or unit weight absorbs more water and these type of samples are less durable for structural work (Kearsley & Wainwright, 2017). So, the above results obey the previous research work.

Surface absorption test of concrete also known as the capillary test of concrete. In the surface absorption test, wax was used as the sealing agent. The amount of surface absorption of concrete block will be decreased with time. Initially the surface absorption rate is high. With the time this rate will be decreased.

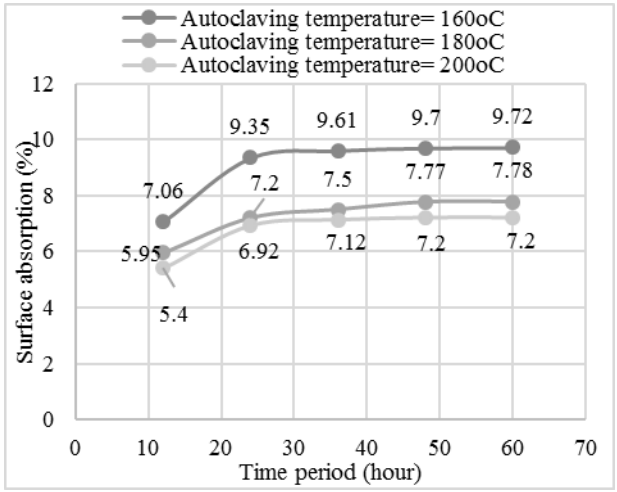

Figure 5: Changing of surface absorption with time for aluminium=0.4% of OPC

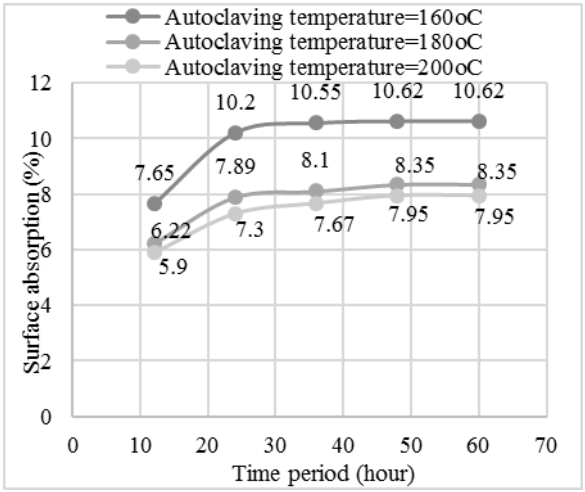

Figure 6: Changing of surface absorption with time for aluminium=0.8% of OPC

From figure-5 and figure-6, surface absorption capacity of AAC blocks decreases with autoclaving temperature. This is happened for the same reason stated above for water absorption capacity of AAC. At initial time absorption rate is higher, so the slope of the graph is steeper for 1st 12 hours. At that time there are small pores and these are filled with water quickly. After 12 hours, the block is getting its saturation position and absorption rate is decreased and after 60 hours rate is almost constant and graph is linear. Then no amount of water is absorbed by the capillary action.

Surface absorption capacity of aerated concrete increases with aluminium content and initially absorption rate is high and at the final time rate will be constant (Shabbar et al., 2018). So, the experimental result follows the trend of previous research work.

4. CONCLUSIONS

The physical, mechanical and functional properties of AAC were determined at two aluminium content and three high autoclaving temperature in this research work. These properties were compared with that of conventional or normal weight concrete. These properties vary with different aluminium content and autoclaving temperature. Unit weight of AAC was less than conventional concrete. Unit weight of AAC decreases with aluminium content and with decreasing autoclaving temperature. The more light- weight AAC sample was one with 0.8% aluminium of OPC and 160^{o}C autoclaving temperature and unit weight was 1490kg/m^3 and here the weight reduction of that AAC sample was 31.53% with respect to conventional concrete.

The strength (compressive and tensile) of AAC for 7days was almost near to that of conventional concrete block. Strength of AAC decreases with aluminium content and strength increases with autoclaving temperature. Maximum compressive and tensile strength for AAC with 0.4% aluminium and 200^{o}C autoclaving temperature were 19.4MPa and 1.81MPa respectively where as for conventional concrete block, they were 22.5MPa and 2.11MPa respectively at same autoclaving temperature.

Water and surface absorption capacity of AAC as its functional properties increases with aluminium content and decreases with temperature. Maximum water absorption capacity of AAC with 0.8% aluminium content and 160^{o}C autoclaving temperature was 9.93%. Capacity of water absorption of AAC was much greater than that of conventional concrete or normal weight concrete (controlled block) because of porosity. Water absorption capacity was almost linearly decreased with unit weight of AAC.

Surface absorption rate of AAC was higher at initial time. For 1st 12hours block absorbed more water by capillary action. After 60hours, this rate was almost constant due to its saturated condition.

ACKNOWLEDGEMENTS

The authors would like to express praise and gratitude to the Almighty and would like to thank the Strength of Materials and Concrete laboratory personals of the Department of Civil Engineering, Khulna University of Engineering & Technology, Khulna, for their helping hand to fulfil this work.

REFERENCES

Anon. (1970). ACI Committee Report 213, Guide for Structural Lightweight Aggregate Concrete. American Concrete Institute.

ASTM C109, "Standard Test Method for Compressive Strength of Hydraulic Cement Mortars".

ASTM C307, "Standard Test Method for Tensile Strength of Chemical-Resistant Mortar, Grouts, and Monolithic Surfacings".

BS 1881-122 (1983). "Method for determination of water absorption".

Hauser, A., Eggenberger, U., & Mumenthaler, T. (1999). Fly ash from cellulose industry as secondary raw material in autoclaved aerated concrete, *29*, 297–302.

Holt, E., & Raivio, P. (2005). Use of gasification residues in aerated autoclaved concrete, *35*, 796–802. https://doi.org/10.1016/j.cemconres.2004.05.005

Ioannou, I., Hamilton, A., & Hall, C. (2008). Capillary absorption of water and n -decane by autoclaved aerated concrete, *38*, 766–771. https://doi.org/10.1016/j.cemconres.2008.01.013

Kearsley, E. P., & Wainwright, P. J. (2017). Porosity and permeability of foamed concrete, *8846*(May 2001). https://doi.org/10.1016/S0008-8846(01)00490-2

Koronthalyova, O. (2011). Moisture storage capacity and microstructure of ceramic brick and autoclaved aerated concrete. *Construction and Building Materials*, *25*(2), 879–885. https://doi.org/10.1016/j.conbuildmat.2010.06.098

Kumar, E. M., & Ramamurthy, K. (2015). Effect of fineness and dosage of aluminium powder on the properties of moist-cured aerated concrete. *Construction & Building Materials*, *95*, 486–496. https://doi.org/10.1016/j.conbuildmat.2015.07.122

Mirza, W. H., & Ai-noury, S. I. (1986). Utilisation of Saudi sands for aerated concrete production, *8*(May), 81–85.

Narayanan, N., & Ramamurthy, K. (2000). Structure and properties of aerated concrete : a review, *22*, 321–329.

Neville, A. M. (1995). Properties of Concrete AM NEVILLE.pdf (5th ed.).

Robert, C., Jerman, M., Keppert, M., & Vy, J. (2013). Hygric , thermal and durability properties of autoclaved aerated concrete, *41*, 352–359. https://doi.org/10.1016/j.conbuildmat.2012.12.036

Sanjayan, J. G., Nazari, A., Chen, L., & Nguyen, G. H. (2015). Physical and mechanical properties of lightweight aerated geopolymer. *Construction & Building Materials*, *79*, 236–244. https://doi.org/10.1016/j.conbuildmat.2015.01.043

Shabbar, R., Nedwell, P., & Wu, Z. (2016). Influence of temperature and curing method on strength of autoclaved aerated concrete, *7833*, 9–11.

Shabbar, R., Nedwell, P., & Wu, Z. (2018). Porosity and Water Absorption of Aerated Concrete with Varying Aluminium Powder Content, *10*(3), 3–7. https://doi.org/10.7763/IJET.2018.V10.1065

Tanaçan, L., Ersoy, H. Y., & Arpac, Ü. (2005). Effect of High Temperature on the Mechanical Properties and Ultrasound Velocity of Cellular Gas Concrete, (April).

Tanaçan, L., Yas, H., & Arpacıog, Ü. (2009). Effect of high temperature and cooling conditions on aerated concrete properties, *23*, 1240–1248. https://doi.org/10.1016/j.conbuildmat.2008.08.007

Wakili, K. G., Hugi, E., Karvonen, L., Schnewlin, P., & Winnefeld, F. (2015). Cement & Concrete Composites Thermal behaviour of autoclaved aerated concrete exposed to fire. *Cement And Concrete Composites*, *62*, 52–58. https://doi.org/10.1016/j.cemconcomp.2015.04.018